# THE REDOXOMICS OF PTEN: WALKING A FINE LINE BETWEEN DAMAGE AND SIGNALING

**Mass spectrometry-based approaches to study the effect of oxidation on PTEN function, structure, and protein-protein interactions**

IVAN VERRASTRO

Doctor of Philosophy

ASTON UNIVERSITY

June 2015

# Thesis Summary

**Aston University**
**The redoxomics of PTEN: walking a fine line between damage and signaling**
**Mass spectrometry-based approaches to study the effect of oxidation on PTEN function, structure, and protein-protein interactions**
**Ivan Verrastro**
**Doctor of Philosophy in Health Sciences**
**2015**

The research described in this PhD thesis focuses on proteomics approaches to study the effect of oxidation on the modification status and protein-protein interactions of PTEN, a redox-sensitive phosphatase involved in a number of cellular processes including metabolism, apoptosis, cell proliferation, and survival. While direct evidence of a redox regulation of PTEN and its downstream signaling has been reported, the effect of cellular oxidative stress or direct PTEN oxidation on PTEN structure and interactome is still poorly defined.

In a first study, GST-tagged PTEN was directly oxidized over a range of hypochlorous acid (HOCl) concentration, assayed for phosphatase activity, and oxidative post-translational modifications (oxPTMs) were quantified using LC-MS/MS-based label-free methods. In a second study, GST-tagged PTEN was prepared in a reduced and reversibly $H_2O_2$-oxidized form, immobilized on a resin support and incubated with HCT116 cell lysate to capture PTEN interacting proteins, which were analyzed by LC-MS/MS and comparatively quantified using label-free methods. In parallel experiments, HCT116 cells transfected with a GFP-tagged PTEN were treated with $H_2O_2$ and PTEN-interacting proteins immunoprecipitated using standard methods.

Several high abundance HOCl-induced oxPTMs were mapped, including those taking place at amino acids known to be important for PTEN phosphatase activity and protein-protein interactions, such as Met35, Tyr155, Tyr240 and Tyr315. A PTEN redox interactome was also characterized, which identified a number of PTEN-interacting proteins that vary with the reversible inactivation of PTEN caused by $H_2O_2$ oxidation. These included new PTEN interactors as well as the redox proteins peroxiredoxin-1 (Prdx1) and thioredoxin (Trx), which are known to be involved in the recycling of PTEN active site following $H_2O_2$-induced reversible inactivation. The results suggest that the oxidative modification of PTEN causes functional alterations in PTEN structure and interactome, with fundamental implications for the PTEN signaling role in many cellular processes, such as those involved in the pathophysiology of disease and ageing.

Keywords: functional proteomics, oxidative stress, protein tyrosine phosphatases, ROS signaling, thiol/disulfide switches

# The Proxomics project

The work presented in this thesis is part of the Proxomics project (http://www.proxomics.ac.uk), a collaboration between Imperial College London, Aston University and the University of Glasgow that has been funded by the Engineering and Physical Sciences Research Council (EPSRC). The aim of the Proxomics project is to develop new technology platforms to study oxidative damage occurring to proteins due to free radicals and ROS (reactive oxygen species) and its relationship to ageing. The Proxomics project has been recently selected by the Royal Society of London to exhibit at the Royal Society Summer Science Exhibition 2015 (30 June - 5 July 2015, London).

# Acknowledgements

First and foremost, I would like to thank my supervisor Prof. Andrew Pitt and co-supervisor Dr. Corinne Spickett for having me onboard as PhD student in the Oxidative Stress group and as part of the Proxomics Project. Andy's excellent supervisory skills and radial–thinking approach to science made him the go-to person during my PhD, and I am extremely grateful to him for helping me crank out this thesis, and for the insightful discussions and scientific advice which inspired me to progress in my research. I am indebted to Corinne for her useful suggestions and continuous support which helped me through the many challenges that I had to face to complete this thesis, and that, ultimately, made me a better researcher than I was three and half years ago when I first started.

The list of people without whom I wouldn't have survived these PhD years is way too long for me to remember everyone, and I apologize in advance for narrowing it down to include only those that played a massive role.

The workplace would have been boring and the science (even more) difficult without Karina (Dr. Karina Tveen-Jensen). Karina has been immensely supportive on so many levels, and I am sincerely grateful to her for being the primary source of answers to my science and non-science questions. Karina is someone you can instantly love and that will make you laugh, and I hope she keeps up her friendly and outgoing spirit.

Minor challenges in the lab such as instrumental troubleshooting would have been a major problem without Sabah (Sabah Pasha), with whom I also had the chance to engage in interesting conversations during the time we shared in the lab or in the office. I am indebted to Sabah for the unconditional assistance and support that she offered me on a daily basis, and I wish her the best of luck for her future career.

Thanks go to Dr. Gemma Warren, which joined our group only for a relatively short time, but her assistance and support has been invaluable for me, and I wish her lots of happiness with her new little one!

I would also like to thank all the other - past and present - members of the Oxidative Stress group and lab MB358 for their help both inside and outside the lab, and for making me feel always welcome from day one.

My last thanks go to the Proxomics Group, in particular to Dr. Rudiger Woscholski (donation of the plasmid used for protein expression and purification), Dr. Lok Hang Mak (knowledge transfer for protein phosphatase assay), and to the former project manager Wing-Chau Tung and current project manager Natalia Goehring for their great work and contribution to the project's success and impact.

*This genuine excitement when exploring the unknown will hold you back for a while just to prolong the experience.*

# List of contents


**Thesis Summary** 2

**The Proxomics project** 3

**Acknowledgements** 4

**List of contents** 7

**List of abbreviations** 11

**List of figures** 17

**List of tables** 20

**Chapter 1. General Introduction** 22

**1.1 Ageing and disease** 23
1.1.1 Ageing in human societies 23
1.1.2 Age-related diseases 26
1.1.3 Theories of biological ageing 28
1.1.4 The pathways of ageing 30
1.1.5 Innovative therapy solutions 32
**1.2 Protein oxidation** 34
1.2.1 Oxidative stress 34
1.2.2 Reactive species 34
1.2.3 Protein oxidation and oxidative post-translational modifications (oxPTMs) 38
1.2.4 Redox signaling 44
1.2.5 Measurement of oxidative stress 46
**1.3 Mass spectrometry** 48
1.3.1 Introduction 48
1.3.2 Sample preparation for mass spectrometry 48
1.3.3 Instrumentation 51
1.3.5 Mass spectrometry approaches in proteomics 59
1.3.6 Quantification of protein oxidative products using MS 62
1.3.7 MS-based detection of protein oxPTMs in disease 68
**1.4 The phosphatase PTEN** 74
1.4.1 Introduction 74
1.4.2 The structure of PTEN: functional and regulatory implications 75
1.4.3 The role of PTEN in cell signaling 82
1.4.4 Aims of the work presented in this thesis 88

**Chapter 2. General Material and Methods** 89

**2.1 Introduction** 90
2.1.1 Chapter contents 90
**2.2 General information** 91
2.2.1 Health and Safety 91
2.2.2 Sterility measures 91
2.2.3 Reagents 91

**2.3 Cell Culture** **93**
2.3.1 Cells propagation 93
2.3.2 Sterility measures 93
2.3.3 Cells growth and maintenance 93
2.3.4 Cell counting 94
2.3.5 Cell storage and recovery 94
**2.4 Molecular Biology** **95**
2.4.1 Sterility measures 95
2.4.2 Source of Plasmid expression systems 95
2.4.3 Preparation of Calcium competent E.coli DH5α cells 95
2.4.4 Transformation of competent DH5α E.coli cells 96
2.4.5 Preculture 97
2.4.6 Plasmid DNA preparation 97
**2.5 Protein expression and purification** **98**
2.5.1 PTEN-GST expression 98
2.5.2 PTEN-GST protein purification 99
**2.6 Biochemistry techniques** **100**
2.6.1 SDS-PAGE gel electrophoresis 100
2.6.2 Coomassie-staining of proteins 100
2.6.3 Protein phosphatase activity assay 101
**2.7 Mass spectrometry** **103**
2.7.1 In-gel digestion for mass spectrometry 103
2.7.2 LC-MS 103
2.7.3 Label-free quantification with Progenesis QI for proteomics 104
2.7.4 Database search 105
**2.8 Bioinformatics tools** **106**
2.8.1 UCSF Chimera Molecular Modeling System 106
2.8.2 Expasy 106

**Chapter 3. Functional proteomics analysis of PTEN oxidative post-translational modifications 107**

**3.1 Summary** **108**
**3.2 Introduction** **109**
**3.3 Materials and Methods** **114**
3.3.1 HOCl concentration assay 114
3.3.2 Buffer exchange optimization 114
3.3.3 Oxidation and activity assay 115
3.3.4 SDS-PAGE and protein in-gel digestion 115
3.3.5 Image processing 115
3.3.6 LC-MS 116
3.3.7 Label-free quantification using Progenesis QI for Proteomics 116
3.3.8 Database Search 116
3.3.9 Statistical analysis 117
3.3.10 *De novo* peptide sequencing 117
3.3.11 NetSurfP 118
**3.4 Results** **119**
3.4.1 Transformation of *E. coli* DH5α PTEN-GST 119
3.4.2 PTEN-GST purification 119
3.4.3 OMFP activity assay of the purified PTEN-GST 122
3.4.4 Optimization of PTEN buffer exchange 123
3.4.5 Effect of HOCl oxidation on PTEN phosphatase activity 126
3.4.6 SDS-PAGE and densitometry analysis of HOCl-oxidized PTEN 127
3.4.7 Identification and quantification of HOCl-oxidized PTEN peptides 130
3.4.8 Validation of HOCl-induced modifications by *de novo* sequencing of MS/MS data 135
3.4.10 Quantitative mapping of HOCl-induced oxPTMs to PTEN 137
**3.5 Discussion** **149**

**Chapter 4. The redox interactome of PTEN analyzed by affinity-capture and label-free MS quantitation 157**

**4.1 Summary 158**
**4.2 Introduction 159**
**4.3 Materials and Methods 163**
4.3.1 Reagents 163
4.3.2 Cell culture 163
4.3.3 Buffer exchange 163
4.3.4 PTEN oxidation and activity assay 164
4.3.5 Preparation of PTEN affinity-capture column and protein capture 164
4.3.6 Protein digestion 165
4.3.7 LC-MS 165
4.3.8 Label-free quantification with Progenesis QI for proteomics 165
4.3.9 Database Search 166
4.3.10 Relative quantification of bait modification 166
4.3.11 Western Blotting 167
**4.4 Results 168**
4.4.1 Buffer exchange of PTEN-GST 168
4.4.2 Reversible oxidation of PTEN after $H_2O_2$ treatment 169
4.4.3 GSH affinity enrichment affinity-captured PTEN-interacting proteins 170
4.4.4 MS-based quantitative analysis of PTEN affinity-captured interactions 172
4.4.5 Validation of selected interactions with Western Blotting 176
4.4.6 Relative quantification of the oxPTMs revealed extent of Met oxidation in the oxidized PTEN-GST bait 178
**4.5 Discussion 180**

**Chapter 5. Validation and profiling of PTEN protein-protein interactions under cellular oxidative stress 187**

**5.1 Summary 188**
**5.2 Introduction 189**
**5.3 Materials and methods 192**
5.3.1 Optimization of transfection conditions 192
5.3.2 Transfection of HCT116 cells and protein capture 193
5.3.3 Protein digestion 193
5.3.4 LC-MS 194
5.3.5 MS-based proteomics analysis 194
5.3.6 Oxidation and XTT assay 194
5.3.7 Oxidation treatment 194
5.3.8 Western blotting 195
5.3.9 Image processing and protein quantification 195
**5.4 Results 196**
5.4.1 Optimization of transfection conditions and comparison of different transfection reagents 196
5.4.2 Immunoprecipitation of PTEN from HCT116 transfected cells 198
5.4.3 MS-based validation of PTEN-interacting proteins 199
5.4.4 Effect of oxidation on cell viability 202
5.4.5 Validation and redox profiling of interacting proteins 204
**5.5 Discussion 207**

**Chapter 6. Conclusion 213**

**6.1 Introduction 214**
**6.2 General discussion 215**
6.2.1 Oxidation of PTEN in vitro 215
6.2.2 Methods of Protein-protein interactions identification 216
6.2.3 Model for PTEN/Prdx1 and PTEN/Trx interactions under oxidative stress 219
**6.3 Future directions 223**

**Chapter 7. References 227**

**Chapter 8. Appendix 260**

**8.1 Plasmid Constructs 261**
8.1.1 PGEX4-T1–PTEN-GST plasmid DNA sequence 261
8.1.2 PEGFP-C1-PTEN-EGFP Plasmid DNA sequence 265
8.1.3 Plasmid maps 269
**8.2 PTEN fusion proteins sequence 271**
8.2.1 PTEN-GST 271
8.2.2 PTEN-EGFP 271
**8.3 PTEN surface accessibility 272**
**8.4 PTEN known interactors summary 281**
**8.5 All identified PTEN-interacting proteins 285**
**8.6 Uncropped Western blot scans 303**
8.6.1 Uncropped scans of Western blots presented in Figure 4.6 303
8.6.2 Uncropped scans of Western blots presented in Figure 5.2 and Figure 5.4 308

# List of abbreviations

| | |
|---|---|
| 1D | One dimensional |
| 2D | Two dimensional |
| AKAP12 | A-kinase anchor protein 12 |
| Ala | Alanine |
| AMP | Adenosine monophosphate |
| AMPK | Amp-activated protein kinase |
| ANOVA | Analysis of variance |
| Anxa2 | Annexin A2 |
| APEX | Absolute protein expression index |
| APS | Ammonium persulfate |
| AQUA | Absolute quantification |
| Arg | Arginine |
| ARP | Aldehyde reactive probe |
| ASA | Absolute surface accessibility |
| Asn | Asparagine |
| Asp | Aspartic acid |
| AtpA | ATP synthase subunit alpha |
| ATPase | Adenosine triphosphatase |
| BAD | Bcl-2-associated death promoter |
| BSA | Bovine serum albumin |
| Ca | Calcium |
| CBR | $Ca^{2+}$- binding regions |
| cDNA | Complementary DNA |
| CE | Capillary electrophoresis |
| CHLOR | Chlorination |
| CID | Collision induced dissociation |
| CK2 | Casein kinase 2 |
| CK2 | Casein kinase 2 glycogen synthase 3 |
| Cl | Chlorine |
| $CO_2$ | Carbon dioxide |
| Co-IP | Co-immunoprecipitation |
| COSHH | Control of substances hazardous to health |
| CR | Calorie restriction |
| CRM | Calorie restriction mimetics |
| CTCF | Corrected total cell fluorescence |
| CuZn-SOD, | Copper/zinc superoxide dismutase |

| | |
|---|---|
| Cys | Cysteine |
| DDA | Data dependent acquisition |
| DDB1 | DNA damage-binding protein 1 |
| DFLE | Disability-free life expectancy |
| DICHL | Dichlorination |
| DIOX | Dioxidation |
| DMEM | Dulbecco's modified eagle medium |
| DMSO | Dimethyl sulfoxide |
| DNA | Deoxyribonucleic acid |
| DNPH | 2,4-dinitrophenylhydrazine |
| Dreb | Drebrin |
| Dsp | Desmoplakin |
| DTT | Dithiothreitol |
| ECL | Electrochemiluminescence |
| EC-SOD | Extracellular superoxide dismutase |
| EDTA | Ethylenediaminetetraacetic acid |
| EGF | Epidermal growth factor |
| EGFP | Enhanced green fluorescent protein |
| emPAI | Exponentially modified protein abundance index |
| ERK | Extracellular-signal-regulated kinase |
| ESI | Electrospray ionization |
| ETC | Electron transfer chain |
| FAS | Fatty acid synthase |
| FBS | Fetal bovine serum |
| FC | Fold change |
| FTC | Fluorescein-5-thiosemicarbazide |
| FTRA | Free radical theory of ageing |
| GC | Gas chromatography |
| GFP | Green fluorescent protein |
| Gln | Glutamine |
| Glu | Glutamic acid |
| Gly | Glycine |
| GNAI1 | Guanine nucleotide-binding protein g (i) subunit alpha 1 |
| GNAI2 | Guanine nucleotide-binding protein g (i) subunit alpha 2 |
| GNAIα/β | Guanine nucleotide-binding protein g (i) subunit alpha and/or beta |
| GR | Glutathione reductase |
| Grb2 | Growth factor receptor-bound protein 2 |
| GSH | Glutathione |
| GSH-Px | Glutathione peroxidase |

| | |
|---|---|
| GSK3 | Glycogen synthase 3 |
| GSK-3β | Glycogen synthase kinase 3β |
| GSSG | Glutathione disulfide |
| GST | Glutathione-S-transferase |
| GTPase | Guanosine triphosphatase |
| $H_2O$ | Water |
| $H_2O_2$ | Hydrogen peroxide |
| HCC | Hepatocellular carcinoma |
| HER2 | Human epidermal growth factor receptor 2 |
| His | Histidine |
| HOCl | Hypochlorous acid |
| HPLC | High-performance liquid chromatography |
| HRP | Horseradish peroxidase |
| IAM | Iodoacetamide |
| ICAT | Isotope-coded affinity tags |
| ID | Identification |
| IDA | Information-dependent acquisition |
| IGF-1 | Insulin-like growth factor 1 |
| IgG | Immunoglobulin G |
| IIS | Insulin/insulin-like growth factor signaling pathway |
| Ile | Isoleucine |
| iNOS | Inducible nitric oxide synthase |
| IP | Immunoprecipitation |
| iTRAQ | Isobaric tags for relative and absolute quantification |
| KCl | Potassium chloride |
| LB | Luria broth |
| LC | Liquid chromatography |
| Ldbh | L-lactate dehydrogenase b chain (ldhb) |
| LEB | Life expectancy at birth |
| Leu | Leucine |
| Lys | Lysine |
| MAGI | Membrane-associated guanylate kinase with inverted orientation |
| MALDI | Matrix-assisted laser desorption ionization |
| MAN2C1 | A-mannosidase 2c1 |
| MAPK | Mitogen-activated protein kinase |
| MC1R | Melanocortin-1 receptor |
| MCO | Metal-catalyzed oxidation |
| MDM2 | Mouse double minute 2 homolog |
| Met | Methionine |

| | |
|---|---|
| Mn-SOD | Manganese superxide dismutase |
| MPO | Myeloperoxidase |
| MPRIP | Myosin phosphatase rho-interacting protein |
| MRM | Multiple reaction monitoring |
| MS | Mass spectrometry |
| MS/MS | Tandem mass spectrometry |
| MSDS | Material safety data sheet |
| MTA | Mitochondrial theory of ageing |
| mtDNA | Mitochondrial DNA |
| mTOR | Mammalian target of rapamycin |
| Na,K-ATPase | Sodium-potassium adenosine triphosphatase |
| NaCl | Sodium chloride |
| NADPH | Nicotinamide adenine dinucleotide phosphate |
| NaOH | Sodium hydroxide |
| NdkA | Nucleoside diphosphate kinase A |
| $NH_4HCO_3$ | Ammonium bicarbonate |
| NLS | Nuclear localization site |
| NLS | Neutral loss scan |
| Nox | NADPH oxidase |
| Nrf2 | Nuclear factor erythroid 2 [NF-E2]-related factor 2 |
| OD | Optical density |
| OMF | 3-*O*-methylfluorescein |
| OMFP | 3-*O*-methylfluorescein phosphate |
| OX | Oxidation |
| oxPTEN | Oxidized PTEN |
| OxPTMs | Oxidative post-translational modifications |
| p130CAS | P130 Crk-associated substrate |
| p53 | Tumour protein 53 |
| PAC | Pten-associated complex |
| PARK7 | Parkinson disease protein 7 |
| PBN | Ptdins (4,5)$P_2$-binding N-terminal module |
| PBS | Phosphate buffered saline |
| PCAF | P300/cbp-associated factor |
| PCC | Protein carbonyl content |
| PD | Phosphatase domain |
| PDB | Protein data bank |
| PDGF | Platelet-derived growth factor |
| PDZ | Pds-95/disc-large/zo-1 |
| PEGFP | Plasmid-enhanced green fluorescent protein |

| | |
|---|---|
| Pelo | Protein pelota homolog |
| PI3K | Phosphoinositide 3-kinase |
| PICT-1 | Protein interacting with carboxyl terminus 1 |
| PIS | Precursor ion scanning |
| PKB | Protein kinase b |
| PKM | Pyruvate kinase M |
| Poldip2 | Polymerase delta-interacting protein 2 |
| PPIs | Protein-protein interactions |
| Prdx1 | Peroxiredoxin-1 |
| P-REX2a | Phosphatidylinositol-(3,4,5)$P_3$-dependent RAC exchange factor 2a |
| Pro | Proline |
| PtdIns(3,4,5)$P_3$ | Phosphatidylinositol-(3,4,5)-trisphosphate |
| PtdIns(4,5)$P_2$ | Phosphatidylinositol-(4,5)-bisphosphate |
| PTEN | Phosphatase and tensin homolog (deleted on chromosome ten) |
| PTMs | Post-translational modifications |
| PTPs | Protein tyrosine phosphatases |
| PVDF | Polyvinylidene difluoride |
| QMS | Quadrupole mass analyzer |
| qTOF | Quadrupole time-of-flight mass spectrometer |
| RFU | Relative fluorescence units |
| RICTOR | Rapamycin-insensitive companion of mammalian target of rapamycin |
| RNS | Reactive nitrogen species |
| ROCK | RhoA-associated kinase |
| ROS | Reactive oxygen species |
| RP | Reverse phase |
| RS | Reactive species |
| RSA | Relative surface accessibility |
| SD | Standard deviation |
| SDS-PAGE | Sodium dodecyl sulphate-polyacrylamide gel electrophoresis |
| Ser | Serine |
| SILAC | Stable isotope labeling with amino acids in cell culture |
| SILAM | Stable isotope labeling with amino acids in mammals |
| SIPL1 | Shank-interacting protein–like 1 |
| Sirt1 | Sirtuin-1 |
| SNO | S-nitrosylation |
| SOD | Superoxide dismutase |
| SOH | S-sulfenylation |
| Sos | Son of sevenless |
| Spta1 | Spectrin α-chain |

| | |
|---|---|
| SRM | Selective reaction monitoring |
| SUMO | Small ubiquitin-related modifier |
| T3PQ | Top 3 protein quantification |
| TBS | Tris-buffered saline |
| TEMED | N,N,N’,N’-tetramethylethylenediamine |
| Thio | Thioredoxin |
| Thr | Threonine |
| TMT | Tandem mass tags |
| TOF | Time-of-flight |
| TOR | Target of rapamycin |
| TRIOX | Trioxidation |
| Tris | Tris(hydroxymethyl)aminomethane |
| Trp | Tryptophan |
| Trx | Thioredoxin |
| TrxR | Thioredoxin reductase |
| Tyr | Tyrosine |
| Utro | Utrophin |
| UV/Vis | Ultraviolet–visible spectroscopy |
| Val | Valine |
| VHR | Vaccinia H1-related phosphatase |
| XIC | Extracted ion chromatogram |
| XTT | 2,3-bis-(2-methoxy-4-nitro-5-sulfophenyl)-2H-tetrazolium-5-carboxanilide |

# List of figures

Figure 1.1 “Where Do We Come From? What Are We? Where Are We Going?” .....23

Figure 1.2 Life expectancy at birth over time in England and Wales .....25

Figure 1.3 The incidence of breast cancer increases with age. .....27

Figure 1.4 Schematic of caloric restriction-induced pathways that modulate ageing .....32

Figure 1.5 The three stages of free radical chain reaction typical of biological systems .....36

Figure 1.6 Commonly oxidized forms of cysteine .....41

Figure 1.7 Oxidative products of methionine .....42

Figure 1.8 Examples of tyrosine oxidative products induced by different reactive species .....44

Figure 1.9 Basic components of a typical mass spectrometry system .....51

Figure 1.10 The process of laser-assisted desorption and ionization in MALDI .....54

Figure 1.11 Ionization mechanism in ESI .....56

Figure 1.12 Ion filtering by quadrupole mass analyzers .....58

Figure 1.13 Representation of various proteomics strategies based on tandem MS .....62

Figure 1.14 Domain structure and organization of PTEN .....76

Figure 1.15 Cellular networks involving PTEN tumour suppression activity .....84

Figure 3.1 Phagocytosis and oxygen-dependent destruction of pathogens .....109

Figure 3.2 SDS-PAGE tracking of the purification of PTEN-GST from the cell lysate of transformed *E. coli* DH5α .....120

Figure 3.3 Representative OMFP phosphatase activity assay of expressed and purified PTEN-GST in reducing buffer conditions .....122

Figure 3.4 Effect of different buffer exchange conditions on PTEN phosphatase activity .....125

Figure 3.5 HOCl irreversibly inactivates PTEN. .....127

Figure 3.6 SDS-PAGE/densitometry analysis versus phosphatase activity of HOCl-oxidized PTEN-GST .....129

Figure 3.7 PTEN sequence coverage and oxidation sites identified from LC-MS/MS data .....133

Figure 3.8 Representative 3D montage zoomed into the feature corresponding to the chlorinated peptide AQEALDFYGEVR matched across the HOCl-oxidized PTEN samples .....134

Figure 3.9 MS/MS spectrum of the doubly-charged ion at m/z 716.33 identified as a chlorinated PTEN peptide....136
Figure 3.10 Quantitative mapping of PTEN oxPTMs upon HOCl treatment....140
Figure 3.11 Comparison of maximum fold change and percentage modification abundance of HOCl-induced PTEN oxPTMs....146
Figure 3.12 HOCl modified residues mapped on PTEN 3D structure....147
Figure 4.1 Interplay between $H_2O_2$ signaling and PTEN reversible inactivation....161
Figure 4.2 Effect of buffer exchange on purified PTEN phosphatase activity....168
Figure 4.3 Effect of 1 mM $H_2O_2$ oxidation on PTEN-GST phosphatase activity....169
Figure 4.4 Representative Coomassie-stained gel showing isolation of putative PTEN-GST binding proteins by GSH-affinity enrichment following 1 mM $H_2O_2$ oxidation....171
Figure 4.5 Representative 3D montages of the comparative MS-based label-free quantification for the peroxiredoxin-1 peptide TIAQDYGVLK and the thioredoxin-1 peptide TAFQEALDAAGDK detected following elution of the proteins bound to the reduced and oxidized PTEN-GST....175
Figure 4.6 Western blots showing validation of proteomics data in comparing selected affinity-captured PTEN interactions across the samples eluted from untreated, oxidized and DTT-recovered PTEN-GST....177
Figure 4.7 Proposed model for PTEN reactivation through interaction with peroxiredoxin-1 and thioredoxin-1....182
Figure 5.1 Transfection efficiency comparison of GeneJuice versus Lipofectamine 2000 on HCT116 cells with the PEGFP-C1 PTEN-EGFP vector....197
Figure 5.2 Co-immunoprecipitation of PTEN from PTEN-EGFP transfected HCT116 cells....199
Figure 5.3 Effect of hydrogen peroxide oxidation on HCT116 cells....203
Figure 5.4 Validation of selected PTEN-interacting proteins following Co-IP from control versus peroxide-oxidized cells....205
Figure 6.1 Proposed model for the regulation of PTEN/Prdx1 and PTEN/Trx interaction under oxidative stress....221
Figure 8.1 Map of the PGEX-4T1 expression plasmid....269
Figure 8.2 Map of the PEGFP-C1 expression plasmid....270

Figure 8.3 Uncropped scans of the Western Blots presented in Figure 4.6 (A).....304
Figure 8.4 Uncropped scans of the Western Blots presented in Figure 4.6 (B).....305
Figure 8.5 Uncropped scans of the Western Blots presented in Figure 4.6 (C).....306
Figure 8.6 Uncropped scans of the Western Blots presented in Figure 4.6 (D).....307
Figure 8.7 Uncropped scan of the Western blot presented in Figure 5.2.....308
Figure 8.8 Uncropped scans of Western blots presented in Figure 5.4 (A).....309
Figure 8.9 Uncropped scans of Western blots presented in Figure 5.4 (B).....310
Figure 8.10 Uncropped scans of Western blots presented in Figure 5.4 (B, continued).....311

# List of tables

Table 1.1 Some of the most important reactive oxygen and nitrogen species .....37

Table 1.2 The most common oxidative products due to oxPTMs .....39

Table 1.3 Identification of protein oxidation biomarkers in biological samples of clinical interest using mass spectrometry techniques.....71

Table 3.1 PTEN-GST indicative purification yields.....121

Table 3.2 Identification and quantification of PTEN oxidative modifications in the PTEN-GST intact band and aggregates following HOCl oxidizing treatment.....142

Table 3.3 Surface accessibility of HOCl modified residues .....148

Table 4.1 Identification and LC-MS based label-free quantification of the binding partners that interact differently with reduced and oxidized PTEN-GST.....173

Table 4.2 Identification and quantification of PTEN and GST oxidative modifications in comparing untreated versus 1 mM oxidized PTEN-GST following GSH-affinity enrichment.....179

Table 5.1 Identification and LC-MS based label-free quantification of PTEN-binding proteins affinity-captured by Co-IP from HCT116 cell lysate matching proteins detected in the *in vitro* interactome generated as described in Chapter 4.....201

Table 8.1 Surface accessibility of PTEN residues .....272

Table 8.2 Known PTEN interactors determined with both high throughput and low throughput experimental systems .....281

Table 8.3 Identification and LC-MS based label-free quantification of the binding partners of reduced and 1 mM $H_2O_2$ oxidized PTEN following GSH affinity enrichment showing the protein hits with confidence score >50 and 2 unique peptides but q-values for quantification below 0.05.....285

Table 8.4 Identification and LC-MS based label-free quantification of the binding partners of reduced and 1mM $H_2O_2$ oxidized PTEN following GSH affinity enrichment showing the protein hits for which the number of unique peptides used for quantification was below 2 .....288

Table 8.5 Identification and LC-MS based label-free quantification of the proteins bound to the untreated and oxidized PTEN-GST that were also identified in the sample eluted from the GST control and the GSH beads alone .....291

Table 8.6 Identification and LC-MS based label-free quantification of PTEN-EGFP binding proteins affinity-captured by Co-IP from HCT116 cell lysate showing the protein hits with more than 2 unique peptides .....292
Table 8.7 Identification and LC-MS based label-free quantification of PTEN-EGFP binding proteins affinity-captured by Co-IP from HCT116 cell lysate showing the protein hits with less than 2 unique peptides .....299

# Chapter 1. General Introduction

# 1.1 Ageing and disease

### 1.1.1 Ageing in human societies

A constant, gradual and inevitable change occurs in living organisms over their entire life, leading to increased risk of disease and worsened health. This phenomenon goes by the name of *ageing*, and is a process that spans many different aspects of a person's life, reflecting physical, psychological and social changes. Over the centuries, many artists have been fascinated by the different features of ageing, and have tried to capture them on canvases, or through other forms of art like music, poetry or prose (Figure 1.1).


**Figure 1.1 "Where Do We Come From? What Are We? Where Are We Going?"**
The painting is the masterpiece of the French post-impressionist artist Paul Gauguin (1848-1903). Read from right to left, this canvas illustrates various stages of life from birth to death.

Ageing plays an important role in human societies from a cultural, economic, and social point of view. Considering the high complexity and the multidimensionality of this phenomenon, it is challenging to study the effects of ageing and its impact on human societies on a global scale. As far as the social impact goes, significant cross-cultural variations have been observed in the views of ageing, particularly when looking at a wide range of cultures. That is, depending on educational, religious or personal values, the effects of ageing – and ageing itself – may be interpreted as symbols of different characteristics, indicating different concepts of time and death across cultures [1].

However, recent studies on the psychology of ageing also suggest a cross-cultural consensus in relation to certain views of ageing and its impact on human societies [2]. For example, several cultures recognize ageing as a process leading to increased knowledge, wisdom or respect, therefore helping individuals in achieving favorable outcomes, such as better wealth and life satisfaction [3]. In a similar way, negative age-related perceptions such as decreased attractiveness or impaired ability to perform certain tasks, were also found to be consistent across different cultures [2,3]. Some of those undesirable effects are typically linked to socio-cultural implications, and may be responsible for fueling the depiction of the ageing body as something that has to be "cured" in the pursuit of a younger or healthier appearance [4]. While a great deal of scientific effort is being made in the field of cosmetic surgery and pharmaceutical sciences to lessen the aesthetic effects of ageing, most of the modern research into ageing is focused on the biological connection between ageing and health. This is because a number of serious health problems become more prominent when people age, including mental health conditions as well as diseases such as cancer and cardiovascular conditions, for which a definitive cure does not yet exist. The negative impact of age-related morbidity on human society is such that a great deal of research effort on this phenomenon has been expended in the last few years by several different field of study, in particular the life sciences.

Much of the current biomedical research into ageing has addressed the cellular and molecular changes that are associated with old age, aiming to increase human life expectancy and reduce the impact of age-related diseases. The life expectancy at birth (LEB) is defined as "the average number of years that a newborn could expect to live if he or she were to pass through life subject to the age-specific mortality rates of a given period" [5]. The LEB is influenced by infant mortality, proneness to disease, accident, and should not be confused with lifespan (or maximum life span), which is a measure of the maximum amount of time that a person lives [6]. As shown in Figure 1.2, the life expectancy at birth (LEB) has almost doubled in England and Wales since 1841 and it is currently at almost 80 years. The increasing LEB in the developed world over the past century has been mainly attributed to improvements in the public health, medical care and diet [7], suggesting a fundamental role for health research in reducing mortality and increasing the quality of life. It has been argued that a consequence of prolonged life is the generation of an ever more aged population, which currently presents a significant financial challenge as the increased number of elderly can slow economic

growth by increasing benefit demand and decreasing the labor-force [8]. In addition, as the number of elderly people increases, the healthcare costs are also rising because of the increasing incidence of age-related conditions [9]. It is clear, though, that by tackling the issue of age-related morbidity the economic burdens can be significantly reduced and the general level of health and, consequently, the quality of life of the ageing population can be improved.

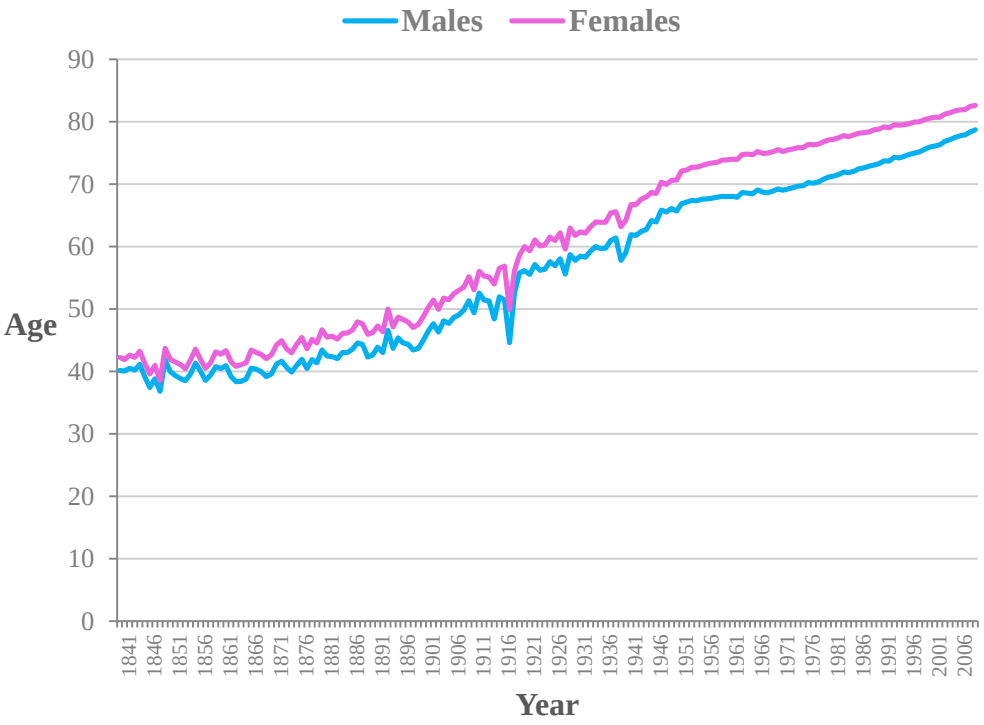


**Figure 1.2 Life expectancy at birth over time in England and Wales**

In general, available data show a higher LEB in recent times, reflecting a significant improvement in human health over the years. Office for National Statistics (2012): Mortality in England and Wales: Average Life Span, 2010.

While the LEB is a direct measure of mortality conditions, it is not a good indicator of the actual level of health of the ageing population. To answer the question as to whether a prolonged life is accompanied by a change in morbidity, the concept of disability-free life expectancy (DFLE) has been introduced [10]. The DFLE, also known as healthy life expectancy, can be defined as "an estimation of the length of time that an individual can expect to live free from a limiting long-standing illness or disability" [11]. This indicator can be useful to predict a ranking for age-related diseases the suppression of which is most correlated with increased LEB and DFLE [12]. According to the Office

for National Statistics, the current healthy life expectancy in England is only 63.4 years for males and 64.1 years for females, significantly lower than the current LEB (78.7 years for males and 82.6 for females in 2010). These figures suggest that while advances in medical care have prolonged life, age-related diseases are significantly reducing the proportion of these additional years that are spent in favorable health conditions.

It is important for modern biomedical research to take on the challenge of improving the health of the ageing population in order to add the dimension of quality to the increasingly longer life expectancy. A healthier population will result in the extension of the social function of the elderly, which in turn would benefit human societies by accelerating the economic growth (e.g. by delaying the retirement age), thus reducing the burden of disability and disease.

### 1.1.2 Age-related diseases

Age-related conditions are responsible for approximately 100.000 deaths every day across the globe accounting for two thirds of the total number of people (150,000) who die every day worldwide, and for about 90% of the total deaths in the developed world [13]. Examples of age-related disease are: Alzheimer's and Parkinson's disease, arthritis, type 2 diabetes, cancer, and cardiovascular diseases. Much of the modern biomedical research into ageing is focused on those age-related diseases, mainly because they represent the most important cause of mortality in many developed countries. Cardiovascular diseases are the biggest cause of death worldwide, although the mortality induced by those conditions has been reducing in developed countries over the past few decades [14]. Age is one of the main risk factors for cardiovascular disease: in the US, over 40% of deaths in those aged 65 years and above was caused by cardiovascular diseases (e.g. hypertension, atherosclerosis) [15]. Following cardiovascular diseases, cancer is the second leading cause of death in the US [16]. Cancer incidence is increasing due to the fact that people live to an older age then they did years ago [17], which makes age a major risk factor for this disease. For example, a woman aged 60 years is more than 40 times more likely to develop breast cancer than a woman aged 25 years (Figure 1.3). However, cancer survival rates are increasing in developed countries due to improving therapeutic interventions [18]. Neurodegenerative diseases (including Alzheimer's, Parkinson's, Huntington's

diseases and amyotrophic lateral sclerosis) represent another relevant group of age-related conditions for which ageing is considered the greatest risk factor [19-25]. In the US, the age-standardized mortality from Alzheimer's disease has increased in the past decade [26], likely as a result of higher survival rates for cancer and heart disease [27]. In addition, Alzheimer's and Parkinson's disease can be a contributing cause of mortality from other conditions, including pneumonia, cerebrovascular disease, and cardiovascular disease [28,29].

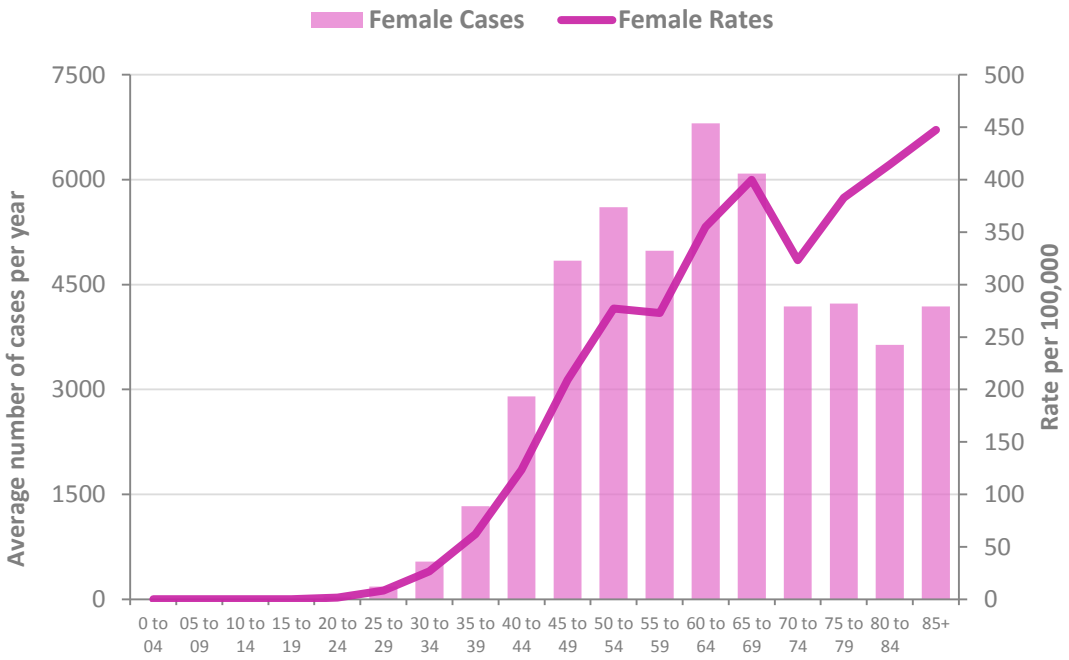


**Figure 1.3 The incidence of breast cancer increases with age.**

Average number of new cases per year and age-specific incidence rates per 100,000 population, females, UK. Cancer Research UK (2014), Breast Cancer (C50): 2009-2011, Cancer Research UK.

Many studies have shown a close relationship between the above conditions and human age, but the degree by which this correlation occurs is yet to be understood [30]. In addition, there is a profound disagreement in the gerontology community about whether ageing is itself a disease, rather than a process separate from age-related diseases [31]. However, if ageing is to be treated as the progressive accumulation of changes over time, it should be noted that those changes happen continuously over the course of the entire life of an individual, from birth to death. Therefore, biological ageing could not be considered as a disease per se (unless, controversially, it is regarded as a "congenital condition"), and it should rather be treated as the common risk factor for age-associated conditions [32].

### 1.1.3 Theories of biological ageing

Biogerontologists distinguish chronological ageing (the number of years a person has lived) from biological ageing, also known as senescence [33]. Because of its intrinsic multi-factor nature, and of its yet-to-be determined biological cause, it is extraordinarily difficult to define ageing. If a comprehensive and modern definition of biological ageing has to be found, as far as it is possible, it may be useful to refer to that reported by Bowen *et al* [34], where ageing is defined as "any change in an organism over time". The concept of biological ageing refers to the changes that take place at the cellular and molecular level in the body of a given organism. Those changes progressively cumulate over time [35] and can occur both at the organismal level (organismal senescence) and at the individual cell level (cellular senescence) [36]. Biological ageing is usually further divided between primary and secondary ageing [37]: primary ageing represents the gradual and inevitable deterioration of cellular structure and function and is independent of environmental factors and disease [38], while secondary ageing is the result of disease and environmental causes including poor diet, radiation, smoking and other factors that are often preventable. Despite advances in cellular and molecular biology, the causes underlying ageing are not completely understood, and multiple theories have been proposed to explain this phenomenon [39,40]. Traditionally, these theories have been divided between programmed and stochastic theories [41]. Programmed theories consider ageing as a process resulting from predetermined genetic factors [42], while stochastic theories (otherwise known as damage-based theories or "wear and tear" theories) argue that ageing is result of a continuous build-up of damage at various levels in the body, encompassing damage to tissue, cells, proteins, and nucleotides [43]. However, these models are often complementary and interact with each other [44,45], thus many contemporary authors consider this division between programmed and stochastic theories to be obsolete [46,47].

One of the most credited theories over the past decade that has been proposed to explain ageing is the free radical theory of ageing (FRTA), developed by Denham Harman in 1956. This theory states that organisms age because cells accumulate free radicals-induced damage over time [48]. Excess free radicals may cause tissue and cell damage, resulting in further radical generation through a series of chain reactions, leading to increased level of reactive species in the body [49]. The increasing amount of free radicals results in oxidative stress, which according to the FTRA is a major factor for the

development of age-related conditions and is driving the ageing process [50,51]. The FRTA has been extensively discussed and reviewed, and is the center of today's debate on the role of free radicals in ageing. In 1972, Harman also proposed the mitochondrial theory of ageing (MTA), which can be considered as an extension of the free radical hypothesis [52]. This theory has also received much attention, although like the FTRA it is widely debated [53]. The MTA maintains that electrons leaking from the electron transfer chain (ETC) can lead to production of reactive oxygen species (ROS) that can damage the mitochondrial DNA (mtDNA). This results in the accumulation of mutations in the mitochondrial DNA, which are responsible for the generation of additional ROS, triggering oxidative stress and tissue damage owing to the production of dysfunctional ETC proteins [54]. According to the MTA, both mitochondrial DNA mutations and free radicals present in the body can contribute to the process of ageing. MTA and FRTA are two similar aspects of the same generally accepted hypothesis, which is now known as the free radical mitochondrial theory of ageing [55]. Significant evidence has been found to support Harman's theories, even though their validity still needs to be fully established [56]. On the other hand, several authors have shown that reactive species also have a beneficial effect, and might even be associated to increased lifespan [57]. Aside from the FTRA, other possible hypotheses explaining the causes of ageing are also being explored. These include, but are by no means limited to: the evolutionary theory of ageing, which explains ageing as a result of a decline in the force of natural selection that acts to reduce mortality [58,59]; the telomere theory, which relies on the experimental evidence showing the shortening of telomeres with each successive cell division [60,61], and a strong correlation between telomeres length and realized lifespan [62]; the reproductive-cell cycle theory of ageing, which implies that a dysregulation in the reproductive hormones is driving the senescence process and it is also a key element in the development of age-related diseases [34,63]; and the DNA damage theory of ageing, which states that accumulating damage to DNA and/or DNA mutations/alterations are the main cause of the functional decline associated with ageing [64].

While in many cases these theories are interconnected (e.g. the DNA damage theory of ageing and the mitochondrial theory of ageing), a complete picture of the biological basis of ageing is still far from being described [39]. Because ageing is a complex and multidimensional phenomenon, it is likely to result from the interaction of several different biological and cellular processes. Therefore, the different theories of ageing should not be treated as unrelated or contradictory models, but rather

as complementary hypotheses explaining various aspects of the same process [40]. By collecting increasing amount of experimental evidence, it may be possible to connect the dots between the proposed explanations, to generate a holistic model including the different biological processes underlying ageing.

### 1.1.4 The pathways of ageing

Research into the cellular and molecular biology of ageing has uncovered a number of metabolic pathways that are able to modulate the rate of ageing, challenging the theories maintaining ageing as a stochastic, irreversible process. Among those, three main independent metabolic pathways were found to extend lifespan and are thought to hold a great potential for therapeutic intervention to combat age-related diseases and promote health in humans [65,66].

The first is caloric restriction (CR), which has been shown to be very effective in prolonging the lifespan in various different species [67-70]. In addition, lifespan extension induced by caloric restriction has been found to reduce the effects of oxidative damage in mammals [71]. The molecular mechanism by which CR affects lifespan is currently under evaluation [70], although evidence is accumulating showing that signaling by the serine/threonine kinase target of rapamycin (TOR) is related to this process (Figure 1.4). Rapamycin-induced inhibition of the mTOR (mammalian target of rapamycin) signaling pathway was found to be associated with extended median lifespan in mice [72]. The AMP-activated protein kinase (AMPK), the activation of which results in mTOR inhibition [73], was also required for lifespan extension in both worms [74] and mice [75] on a caloric restriction regimen. Similar CR-induced positive effects on lifespan have been found for a class of protein deacetylases called sirtuins [76,77]. Sirtuin 1 (Sirt1), activated by caloric restriction, has been found to negatively regulate the mTOR/IGF-1 pathways [78] and to increase mitochondrial biogenesis and function [79]. Sirt1 has also been reported to be activated by resveratrol [80], although the relationship between resveratrol, sirtuins and increased lifespan is currently at the center of an animated debate with multiple authors reporting contradictory findings [76,81]. In addition, there is significant

evidence that the deacetylase activity of sirt1 is associated to cancer, which challenges the alleged tumour suppressor role of this protein [82].

Another promising pathway the study of which holds great potential for the understanding of ageing is the insulin/IGF-1-like signaling pathway (IIS). Inhibition of IIS activity has been associated with extended lifespan in mice [83], although the exact relationship between the molecules involved and the increased longevity is uncertain due the complexity of this pathway [84]. Calorie restriction has been also reported to have an inhibitory effect on the IIS activity in human skeletal muscle [66], suggesting an interplay between the two pathways in regulating longevity [85].

The third metabolic pathway that has been found to affect ageing is related to the mitochondrial electron transfer chain (ETC) activity. There is increasing attention on the signaling effects of mitochondria-generated ROS and their relationship with mitochondrial energy metabolism in the pathophysiology of many age related diseases [86]. A decreased function of the mitochondrial respiratory chain, also linked to reduced endogenous ROS production, has been reported to increase lifespan in worms [87,88]. Moreover, mutations in key mitochondrial genes was reported to increase the protection from oxidative stress and damage to DNA in worms [89] and mice [90], leading to increased cellular fitness and lifespan. However, in humans many mtDNA mutations are associated with shorter lifespan, age associated phenotypes and age-related diseases [91,92], although the implicated causative effect of these mutations on the ageing process is currently debated [93]. In addition, mitochondrial function and respiratory chain activity have been shown to decline with age in mammals including humans [94], but it is not clear whether these changes are secondary to other cellular or metabolic mechanisms [92]. Recent work has also addressed the investigation of the relationship between mitochondrial function, caloric restriction [95] and insulin signaling [96], implicating a fundamental role for mitochondrial metabolism in modulating ageing and lifespan.

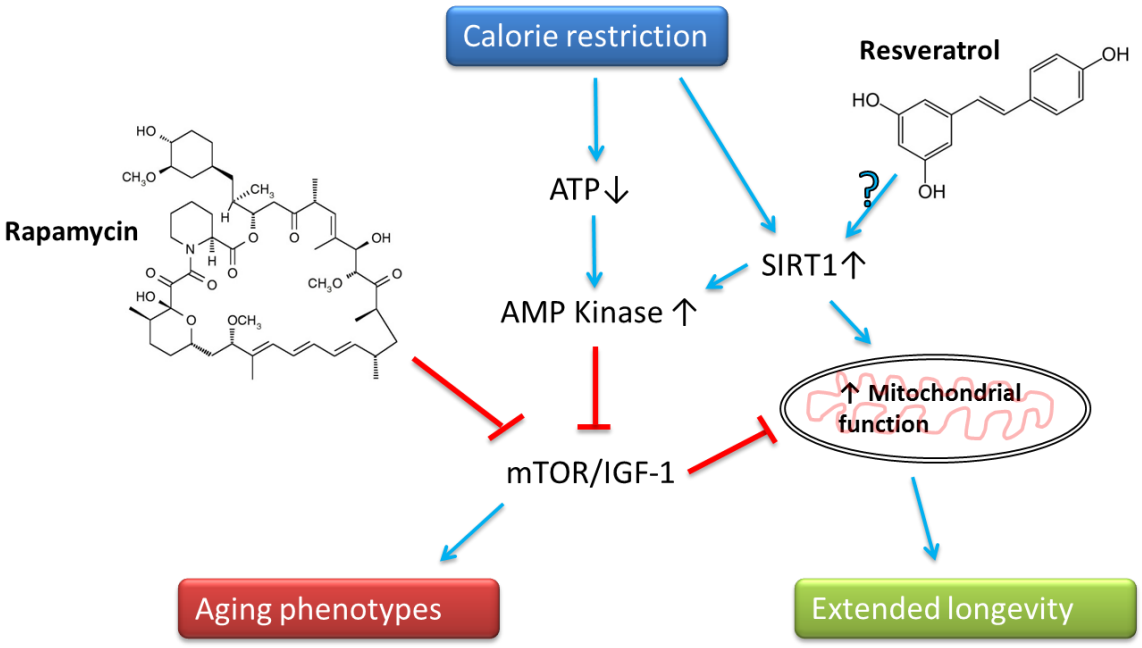


**Figure 1.4 Schematic of caloric restriction-induced pathways that modulate ageing**

Caloric restriction is involved in the activation of metabolic pathways such as those controlled by Sirt1 and AMP Kinase resulting in extended longevity and decreased ageing-associated phenotypes.

### 1.1.5 Innovative therapy solutions

It is hoped that scientific research efforts will soon be able to address the issue of ageing and age related diseases, especially by means of innovative therapy solutions along with new generation high throughput technologies for the treatment of age-related diseases such as cancer, cardiovascular diseases, and neurodegenerative diseases. While a great deal of research is still needed to overcome numerous biological and medical challenges in these growing areas of ageing research, most of the proposed strategies do show great promise for the modulation of ageing-associated phenotypes and age-related conditions.

With an increasing number of research studies uncovering metabolic pathways able to modulate ageing, there is growing interest for the development of pharmacological solutions that can "mimic" the health effect of specific biomolecules, thus delay or prevent the occurrence of age-related diseases. In the light of promising findings showing their positive effect on the lifespan of model organisms,

rapamycin and resveratrol are currently being tested as caloric restriction mimetics (CRM) and represent an attractive target for the discovery and development of anti-ageing drugs [97-99]. Even so, research studying the effect of caloric restriction on humans is at a very early stage, also because of the intrinsic time constraints of performing long term CR studies (and difficulties of finding volunteers) [65,100]. In addition, the beneficial effects of resveratrol on life span and their potential effects on human health are under debate [101].

One promising approach currently being tested to treat age-related conditions involves genetic modification-based strategies such as gene therapy (or gene replacement therapy), which are showing promising results in animal models, also highlighting a fundamental role for DNA damage in mediating age-related phenotypes [102]. Clinical and preclinical studies implementing gene therapy solutions have shown encouraging results for the treatment of Parkinson's disease [103-105], and preclinical studies have shown positive results for the treatment of other age-related conditions such as age-related macular degeneration [106], and cardiovascular disease [107]. However, current gene therapy techniques still present a number of issues that are considerably limiting their application in clinical trials, including unwelcome immune response against the transgene or virus used to deliver the genetic information and other adverse effects [108,109].

Another group of new generation biomedical technologies holding great potential for the treatment of age-related diseases include regenerative medicine solutions such as the transplantation of stem cells [110]. Telomerase-transduced human bone marrow stem cells showed increased lifespan due to increased telomere length, and could be used for in vivo transplants to reduce ageing-associated phenotypes [111]. Recently, mesenchymal stem cells from young donors were transplanted in aged mice showing reduction of age-related bone density loss along with increased lifespan [112]. The transplantation of hematopoietic stem cells is currently widely practiced to replace the heathy cells lost following chemotherapy-based treatment of cancers such as leukemia and lymphoma [113]. Stem cells have also been successfully used for the treatment of age related conditions including cardiovascular diseases [114] and other non-malignant diseases [115]. As of yet, though, a number of ethical concerns and technical difficulties are holding back the clinical application of stem cells-based therapeutic solutions [115].

# 1.2 Protein oxidation

## 1.2.1 Oxidative stress

At the present time, oxidative damage has been recognized as one of the most common feature of several inflammatory and age-related human diseases such as cancer, atherosclerosis, rheumatoid arthritis and neurodegenerative diseases, among others [116]. Oxidative stress is the result of a disequilibrium between the production of oxidizing agents and the cellular antioxidant defences that act to eliminate them [117]. Under normal redox conditions most cellular compartments are a reducing environment, as cytoplasmic antioxidants response readily detoxify excess oxidants [118]. Circumstances of altered redox status, such as those found in disease, reflect a disturbance in this pro-/anti-oxidant balance, due to a decrease in effectiveness of antioxidant response and/or an increase in oxidizing agents exposure [119]. Whether oxidative stress is the cause or the consequence of disease is not yet clear, although increasing evidence suggests that oxidizing molecules exacerbate the pathological state of many conditions [120]. Nonetheless, while oxidative stress has been associated with disease onset and progression, recent studies suggest that minor levels of oxidative stress, such as those generated by regular exercise, have systemic beneficial effects [121]. Research into oxidative stress has also uncovered an important role for oxygen-derived species in intracellular and extracellular signaling networks [122]. A relatively new field of study, called redox biology, has emerged in the past few years to answer key questions pertaining the coordination of redox changes in the cell, their relationship to disease onset and progression, and their physiological significance more generally [123].

## 1.2.2 Reactive species

Much of the redox process in biological systems involves an electron flow moving from a donor molecule to a final acceptor molecule, which for aerobic organisms is ultimately molecular oxygen. Four electrons are normally required to completely reduce molecular oxygen to water. Occasionally, though, oxygen undergoes an incomplete reduction, thereby leading to the formation of reactive

intermediates, also known as reactive oxygen species (ROS). ROS are typically divided between radicals and non-radicals. Radical reactive species (or free radicals) are atoms, molecules or ions that possess at least one unpaired electron, many of which are highly reactive [124]. Non-radical reactive species do not possess any unpaired electron(s), but are also relatively chemically reactive and can be converted into free radicals [125]. Because of their high reactivity, free radicals are chemically unstable, and have a natural tendency to react with other molecules by donating or accepting an electron in order to form more stable chemical species [126]. This results in the propagation of free radicals species by means of chain reactions. Free radical chain reaction processes can be broken down in three different stages: initiation, propagation and termination (Figure 1.5) [127]. During the initiation phase, the radical species can be formed essentially in three different ways: by homolytic covalent bond cleavage of a neutral molecule (homolytic fission); by the transfer of a single electron from a radical to a stable molecule; by the loss of a single electron from a stable molecule (typically as result of abstraction of an hydrogen atom in lipid and protein oxidation) [124]. In general, homolytic fission requires a considerable amount of bond dissociation energy, such as that of high temperatures, UV light, ionizing radiations or radical initiators such as peroxides [128]. Under normal conditions, single electron transfer or loss are a much more common process of radical formation in biological systems than homolytic fission [129]. Most radicals have a very short *in vivo* lifetime. For example, highly reactive oxygen radicals such as the hydroxyl radical ($OH^{\bullet}$) have half-lives in the millisecond to nanosecond range [130]. Once formed, the free radicals react with other stable molecules in the propagation phase of the chain reaction resulting in the generation of new reactive species. It is worth mentioning that after the initiation step, the chain reactions do not increase the net amount of radical species, which stays the same throughout the propagation phase [131]. Finally, the termination phase takes place when two radical species react with each other generating a stable molecule, thus decreasing the number of free radicals. However, this is regarded as a rather rare event, because the concentration of free radicals in the cellular environment is never high enough for two radical species to frequently collide [132]. Compounds known as antioxidants are also capable of terminating the free radical chain reaction by stabilizing free radical intermediates and inhibiting further oxidation [126]. These molecules include reducing agents such thiols, ascorbic acid and polyphenols, among others [133].

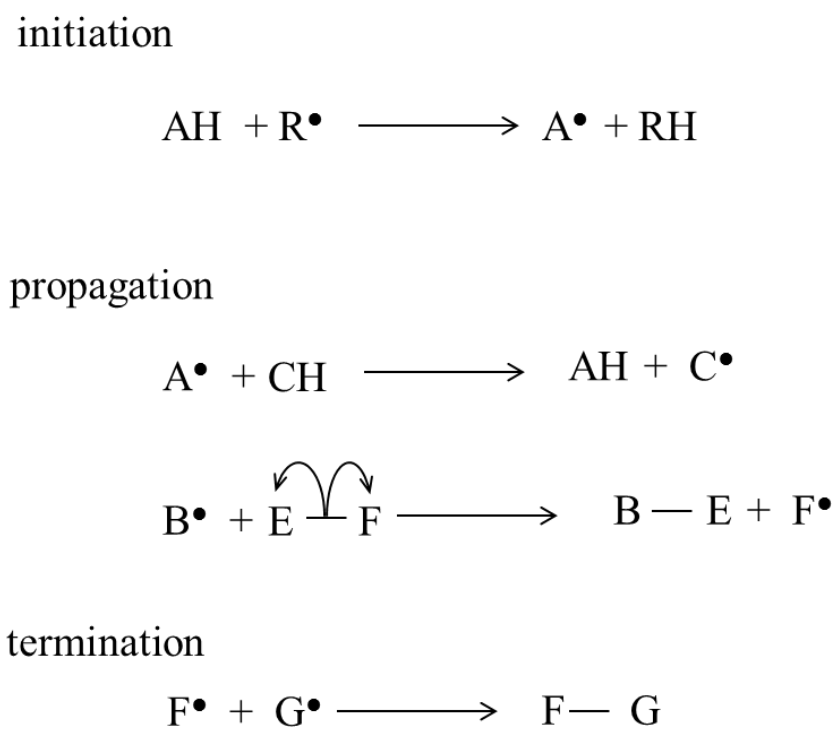


**Figure 1.5 The three stages of free radical chain reaction typical of biological systems**

In the initiation phase, a reactive molecule ($R^{\bullet}$) removes a hydrogen atom from a normal molecule (A) generating an unstable radical. In the propagation phase, newly formed radical species react readily with other non-radicals in order to generate more stable products. The propagation continues until the chain process is terminated by a collision event between two radicals or other biochemical events.

Reactive species (RS) including reactive oxygen species (ROS), and reactive nitrogen species (RNS) that are generated intracellularly (endogenous) or that enter the body from the environment (exogenous) are known to contribute to oxidative stress and function as signaling intermediates in many cellular pathways [51,134]. Endogenous sources consist of free radicals species that are generated intracellularly and that are subsequently released both within and outside the cell [135]. Intracellularly generated, endogenous free radicals can be formed in a number of ways, including autoxidation, enzymatic activity, and respiratory burst. Autoxidation is a free radical chain process that can be originated by the action of various radical initiators [127]. Molecules inside the cells that undergo autoxidation include catecholamine, thiols, flavins, and quinones [136,137]. A number of cellular enzymatic systems are also capable of mediating intracellular free radical generation. These include enzymes involved in various cellular processes including the mitochondrial respiratory chain

(such as oxidases), inflammation (such as myeloperoxidase generated by activated phagocytic cells) [138], biosynthesis of certain biomolecules (such as prostaglandin synthase and lipoxygenase) [139], and in the redox cycling of xenobiotics [140] or estrogens [141]. Oxygen-derived reactive species such as superoxide radical ($O_2^{\bullet -}$) and hydrogen peroxide ($H_2O_2$) are also produced by the NADPH oxidase during the respiratory burst in phagocytic cells [142]. Nitrogen-derived radicals are generated via a series of reactions catalyzed by nitric oxide synthases (NOSs) such as the inducible form iNOS expressed in macrophages during inflammation [143]. ROS can also be generated in non-phagocytic cells by stimulated growth factors, such as PDGF (platelet-derived growth factor), EGF (epidermal growth factor), and insulin [144,145]. Exogenous sources of reactive species include tobacco smoke, drugs, radiation, dust particles and pollutants present in the environment [135]. The lungs are the organs in the body that are most exposed to environmental free radicals, as most of these exogenous sources are found in the ambient air [146]. Ionizing radiation is also responsible for the generation of reactive species in the body by a mechanism of water radiolysis resulting in the formation of oxygen-containing reactive molecules including hydrogen peroxide and superoxide radical [147]. Table 1.1 shows some of the most important reactive species that are responsible for oxidative stress.

**Table 1.1** Some of the most important reactive oxygen and nitrogen species

| **Reactive oxygen species (ROS)** | | | | **Reactive Nitrogen species (RNS)** | | | |
|---|---|---|---|---|---|---|---|
| **Radical** | | **Non-radical** | | **Radical** | | **Non-radical** | |
| $O_2^{\bullet -}$ | Superoxide | $H_2O_2$ | Hydrogen Peroxide | $NO^{\bullet}$ | Nitric Oxide | $ONOO^-$ | Peroxynitrite |
| $OH^{\bullet}$ | Hydroxyl | HOCl | Hypochlorous acid | $NO_2^{\bullet}$ | Nitrogen dioxide | ROONO | Alkyl peroxynitrite |
| $RO_2^{\bullet}$ | Peroxyl | $O_3$ | Ozone | | | $N_2O_3$ | Dinitrogen trioxide |
| $RO^{\bullet}$ | Alkoxyl | ONOO- | Peroxynitrite | | | $N_2O_4$ | Dinitrogen tetraoxide |
| | | | | | | $HNO_2$ | Nitrous acid |
| | | | | | | $NO_2^+$ | Nitronium anion |
| | | | | | | $NO^-$ | Nitrosyl anion |
| | | | | | | $NO^+$ | Nitrosyl cation |
| | | | | | | $NO_2Cl$ | Nitryl chloride |

### 1.2.3 Protein oxidation and oxidative post-translational modifications (oxPTMs)

In the redox biology field there is increasing interest in the oxidation processes that involve proteins and affect their folding, function and interactivity [148]. Protein oxidation has been implicated as one of the contributing factors to the onset and progression of many age-related diseases such as neurodegeneration [149], Alzheimer's disease [150,151], Parkinson's disease [152], cancer [153], cardiovascular diseases [154] and inflammatory diseases [155]. The accumulation of oxidized proteins in human cells has been linked to several ageing-related changes including increases in rates of ROS generation, decreases in antioxidant activities and decreased cellular stress response, that would act to reduce the level of oxidized proteins [156]. Recently, oxidized proteins have also been implicated in intracellular and extracellular signaling pathways, indicating their involvement in modulating the cellular response to stress induced by disease or environmental triggers [157,158].

When exposed to oxidizing agents such as ROS and RNS, proteins may undergo a number of intermolecular and intramolecular changes that affect their structure and folding and, ultimately, their activity and function. Among these functionally relevant alterations, oxidative post-translational modifications (oxPTMs) are of great interest in current research in redox biology. Generally, the majority of human proteins undergo a number of post-translational modifications (PTMs) during their life cycle, reflected in the great level of complexity of the proteomes in comparison to the genome and the transcriptome [159]. PTMs are involved in many aspects of cell biology, including protein biosynthesis [160], enzymatic activity [161], localization [162], degradation [163] and protein-protein interactions [164]. As most of these cellular functions are likely to be altered in disease states, understanding PTMs is crucial to gain insight into the molecular mechanisms behind the pathophysiology of many conditions. Specifically, the study of oxPTMs appears critical to elucidate the role of oxidizing species in the signaling networks involving age-related diseases, as recent studies have exposed an existing correlation between those conditions and protein oxidative damage [165].

A number of oxPTM mechanisms that involve both intermolecular and intramolecular protein dynamics have been reported to date, including oxidation of amino acid residue side chains, formation of protein-protein cross-linkages (via intermolecular disulfide bonds or dityrosine formation), oxidation of the protein backbone resulting in protein fragmentation and/or aggregation, and oxidation

of amino acid residues near to metal-binding sites via metal-catalyzed oxidation (MCO) [166,167]. Generally, the oxidizing action of ROS and RNS has been shown to cause protein inactivation and loss of function, although there is increasing evidence showing that ROS have also regulatory/signaling role function on specific redox-regulated and redox-sensitive proteins [168,169]. Table 1.2 lists the some of the amino acids that are most susceptible to redox reactive species-mediated oxidation along with their corresponding oxidation products.

**Table 1.2** The most common oxidative products due to oxPTMs

| Amino acids | Modification | Oxidative product |
|---|---|---|
| Cysteine | Oxidation | Cysteine sulfenic acid, cysteine sulfonic acid, cysteine sulfinic acid, cystine |
| Cysteine | S-glutathionylation | S-glutathionyl cysteine |
| Cysteine | S-nitrosylation | S-nitrosocysteine |
| Methionine | Oxidation | Methionine sulfoxide, methionine sulfone |
| Tyrosine | Chlorination | 3-chlorotyrosine |
| Tyrosine | Nitration | 3-nitrotyrosine |
| Tyrosine | Oxidation | Dityrosine, 3,4-dihydroxyphenylalanine |
| Tryptophan | Oxidation | 5-hydroxy-tryptophan |
| Phenylalanine | Oxidation | 2,3-dihydroxyphenylalanine, 2-, 3-, and 4-hydroxyphenylalanine |
| Arginine | Oxidation | Glutamic semialdehyde |
| Lysine | Oxidation | α-Aminoadipic semialdehyde |
| Histidine | Oxidation | 2-Oxohistidine |
| Threonine | Oxidation | 2-Amino-3-butyric acid |
| Proline | Oxidation | Glutamic semialdehyde, 5-oxoproline |

As oxPTMs emerge as one of the common feature of many age-related diseases, their potential as predictive biomarkers for the early screening and diagnosis of these conditions also becomes of great importance in both research and clinical settings. Among the many different types of protein oxidative products identified so far, those that have been associated with human disease onset include protein carbonyls [170], cysteic acid [171,172], cysteine disulfide bonds [173], cysteine S-glutathionylation [174], cysteine S-nitrosylation [175], methionine sulfoxide and methionine sulfone [152], 3-nitrotyrosine, 3-chlorotyrosine and dityrosine [176].

### *1.2.3.1 Protein carbonyl formation*

A broad range of amino acids oxidative products can result from the formation of primary protein carbonyls. This occurs presumably by means of a metal-catalyzed oxidation (MCO) of the side chain of a number of amino acids [177]. Protein carbonyl formation is an irreversible oxidative process, which has been linked to protein degradation and function loss, thereby contributing to cellular damage and disease state [178]. Preferential amino acid targets of protein carbonyl formation include: histidine, oxidized to 2-oxohistidine, lysine to α-aminoadipic semialdehyde, threonine to 2-amino-3-oxo-butyric acid, proline to glutamic semialdehyde or 5-oxoproline, and arginine to glutamate semialdehyde. Alternatively, protein carbonyls can be generated by the Michael addition reaction of lipid oxidation products with the side chains of lysine, histidine or cysteine residues [179]. Protein carbonyl formation is one of the most well-studied and widely established biomarkers of oxidative stress-related human diseases [170]. Evidence has been detected for protein carbonyls in the clinical samples of patients affected by several disease states, including Alzheimer's disease [152,180,181], cancer [182], and diabetes [183,184] as well as in the biological samples obtained from animal models of ageing [185-187] and ischemia/reperfusion [188].

### *1.2.3.2 Oxidative products of cysteine*

The thiols groups of cysteine residues in proteins are among the most susceptible targets of ROS-induced oxidation in cells [189]. Moreover, they often play a very important role in the stabilization of protein structure by forming covalent disulfide bonds as well as in the regulation of protein function and activity in response to oxidative stress. Cysteines are often found in the active sites of several enzymes where they directly participate in catalysis [190]. Hence, modifications occurring at the level of the active site cysteines of proteins have the potential to affect activity and function dramatically. The reaction of cysteinyl thiolates with ROS results in the formation of three different oxidized forms of cysteines: cysteine-sulfenic (-SOH), -sulfinic ($-SO_2H$), and -sulfonic ($-SO_3H$) acid. Cysteine sulfenic acid is an unstable product and is usually further oxidized to cysteine sulfinic and/or cysteine sulfonic acid [191]. Alternatively, cysteine sulfenic acid modifications have been shown to be an intermediate in the formation of intermolecular and intramolecular cysteine disulfide bonds [192] (Figure 1.6). The oxidation of cysteine to cysteine sulfenic acid has been shown to be reversible as well as the formation of the cysteine disulfide bridges [169,193]. The formation of cysteine sulfinic

acid has also recently been suggested to be reversible [194], although it is commonly considered to be an irreversible process [195]. Conversely, the formation of cysteine sulfonic acid has been shown to be irreversible [169,196,197]. The redox processes of cysteine, both reversible and irreversible, are of emerging clinical interest [173,198]. The formation of oxidized cysteines has been associated with inflammatory conditions and age-related neurodegenerative diseases [195,199]. Both reversible and irreversible oxidized forms of cysteines have been reported in the clinical samples of patients affected by Alzheimer's and Parkinson's disease [152,171,172,200] and in animal models of ageing [201] and ischemia/reperfusion [202,203].

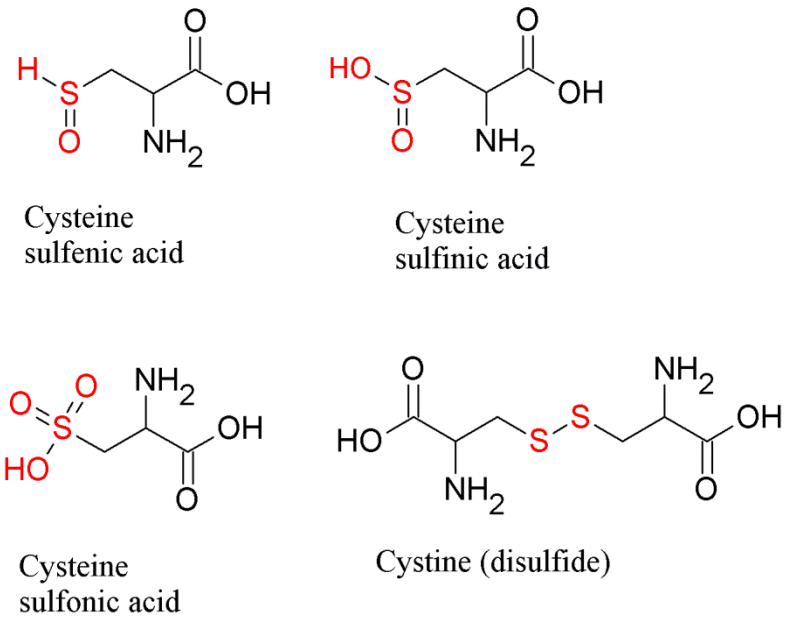


**Figure 1.6 Commonly oxidized forms of cysteine**

Redox-sensitive cysteine residues of proteins play a major role in the regulation of protein properties in response to changes in the cellular redox status [204].

### *1.2.3.3 Oxidative products of methionine*

Alongside cysteine, methionine residues are by far the most sensitive residues to oxidation mediated by several kinds of ROS [156], and the occurrence of methionine oxidation has been shown to affect protein function and stability [205,206]. Figure 1.7 shows the two most common protein-bound methionine oxidative products. Many reactive species are capable of oxidizing methionine readily to methionine sulfoxide, which can be further oxidized to methionine sulfone, although this

happens to a much lesser extent [207]. However, in most biological systems it is possible to convert methionine sulfoxide, but not methionine sulfone back to their unmodified forms. This normally happens via the action of specific enzymes such as methionine sulfoxide reductases [197]. Methionine oxidative products are apparent in age-related conditions in which oxidative stress is involved, such as Alzheimer's [150], Parkinson's disease [152,208], type2 diabetes [209] and ageing [210].

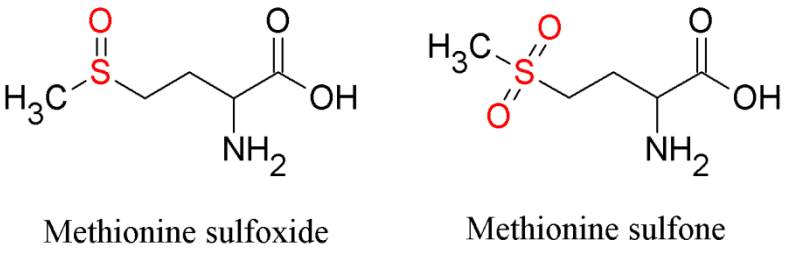


Methionine sulfoxide Methionine sulfone

**Figure 1.7 Oxidative products of methionine**

Methionine residues are among the most vulnerable to oxidation by many reactive species. The oxidation of methionine into methionine sulfoxide occurs easily in biological systems under the conditions of oxidative stress, as in disease states or ageing.

### *1.2.3.4 Oxidative products of tyrosine*

Tyrosine oxidative-induced modifications have also attracted the interest of biomedical research in recent times. Depending on the type of reactive species involved, tyrosine residues of proteins undergo different types of oxPTMs pathways, the most common being chlorination (formation of 3-chlorotyrosine), nitration (formation of 3-nitrotyrosine) and dityrosine formation [189,211-213] (Figure 1.8). The 3-chlorotyrosine modification is regarded as a specific marker of oxidative damage induced by the haem enzyme myeloperoxidase (MPO) secreted by phagocytes activated during the inflammatory response [155]. MPO converts chloride ions ($Cl^-$) and $H_2O_2$ produced during the neutrophils respiratory burst into the reactive intermediate HOCl, which reacts with tyrosine residues generating 3-chlorotyrosine [214]. Multiple oxidative pathways have been proposed for the formation of the nitrotyrosine modification, including peroxynitrite ($ONOO^-$), nitrogen-dioxide ($NO_2^{\bullet}$), and nitric oxide ($NO^{\bullet}$) induced oxidative damage [215]. Peroxynitrite ($ONOO^-$) is generated following

reaction of superoxide radical ($O_2^{\bullet-}$) with nitric oxide radical ($NO^{\bullet}$) produced by inducible nitric oxide synthase, and is capable of inducing protein-bound nitrotyrosine although the mechanism also requires free radical attack [216,217]. Alternatively, nitrogen dioxide radicals ($NO_2^{\bullet}$), generated via MPO-mediated oxidation of nitrite [218], react with tyrosyl radical leading to the formation of 3-nitrotyrosine [219]. Nitric oxide ($NO^{\bullet}$) may also react with tyrosine residues generating nitrosotyrosine, which can be subsequently converted to nitrotyrosine via a further oxidation step [220]. Various types of oxidants including hydrogen peroxide, myeloperoxidase (MPO), nitrogen dioxide and peroxynitrite have been also shown to cause the formation of dityrosine by cross-linking of two spatially close tyrosyl radicals [221,222].

While initially thought to be irreversible, increasing evidence suggests that both protein chlorination and nitration are, in fact, reversible by means of either enzymatic or non-enzymatic processes in biological systems. It has been suggested that nitrotyrosine can be reduced to aminotyrosine in a non-enzymatic process involving haem and thiols [223], or even converted back to tyrosine via a mitochondrial oxygen-dependent denitration system [224]. Likewise, recent studies have worked towards the determination of enzymatic pathways involved in the reduction of chlorination *in vivo*, which is most likely accomplished by means of a reductive deiodinase promoting dehalogenation of both chlorotyrosine and bromotyrosine [225,226]. In contrast, the formation of the dityrosine cross-link is currently considered irreversible [227].

Oxidatively modified tyrosines have also been proposed as biomarkers of several age-related and inflammatory diseases [228]. Elevated levels of protein-bound 3-chlorotyrosine have been recently detected in mouse models of influenza [229], as well as in the clinical samples of inflammatory bowel disease [230], atherosclerosis [231], systemic lupus erythematosus [232] and post-myocardial infarction [233]. Elevated levels of protein-bound 3-nitrotyrosine have been detected in proteins obtained from the biological samples of patients affected by arthritis, atherosclerosis [234], cancer [235], inflammatory bowel disease [230], systemic lupus erythematosus [232], and Alzheimer's disease [236]. Increased dityrosine formation has been associated with a number of age-related conditions, including eye cataract, acute inflammation, Alzheimer's disease, and atherosclerosis [215,222]. Besides nitration, chlorination and dityrosine formation, inflammatory and age-related conditions also seem to be related to other oxidative modifications on tyrosine such as bromination,

and hydroxylation [237]. Other than protein-bound modification, the occurrence of free tyrosine oxidative products in the blood and urine have been reported as promising biomarkers of several human conditions such as diabetes [238], obstructive sleep apnea patients [239], Fabry's disease [240] and low birth weight [241].

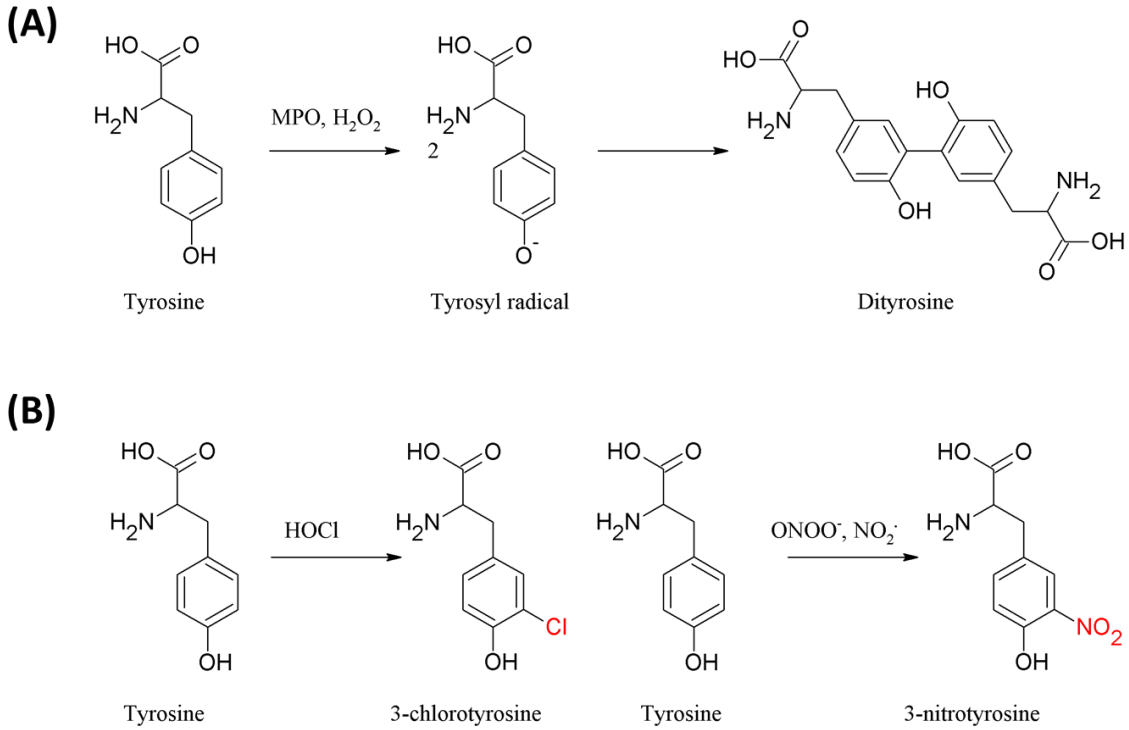


**Figure 1.8 Examples of tyrosine oxidative products induced by different reactive species**

(A) Tyrosine residues exposed to myeloperoxidase (MPO) or $H_2O_2$ are oxidized to tyrosyl radicals that can cross-link to generate a stable dityrosine. (B) Different oxidizing agents (HOCl, peroxinitrite, nitrogen dioxide radical) can generate specific oxidative products of tyrosine such as 3-chlorotyrosine and 3-nitrotyrosine.

### 1.2.4 Redox signaling

Biological organisms continuously rely on the cellular ability to counter the action of oxidizing agents in order to maintain redox homeostasis. Some endogenous reactive species act as second messengers for the activation of a complex array of stress response systems, mediated by various processes including receptor agonists, transcription factors and novel signaling patterns [242]. Thiol groups have shown redox-sensing capacity because of the propensity of cysteine residue to undergo

reversible oxidation states (such as disulfide bonds), which function as a switch for the transmission of the signal via proteins intra and extracellularly. Two main redox signaling mechanisms involving the thiol groups of cysteines have been proposed so far that have a key role in cellular redox regulation.

One major mechanism of redox signaling is based on the ability of protein thiols to maintain a normal cellular redox potential when cells are challenged in oxidative stress conditions [242]. This happens via a number of oxidoreductase systems that act as a buffer for the restoration of a thiol/disulfide equilibrium in cells. Cellular systems exhibiting such mechanism include the glutathione reduced/disulfide (GSH/GSSG) system, the thioredoxin (Trx) system and the glutaredoxin system. The tripeptide glutathione in its reduced form plays a key antioxidant role by donating an electron to reactive species [243]. This process results in the formation of glutathione disulfide (GSSG), which can be re-reduced to GSH by the NADPH-dependent enzyme glutathione reductase (GR), thus restoring the cellular antioxidant defences [244]. In healthy cells, more than 90% of total glutathione is in the reduced form (GSH), which suggest that the action of the GR is very efficient in reducing GSSG [245]. The thioredoxin system, consisting of NADPH, NADPH-dependent thioredoxin reductase (TrxR), and thioredoxin (Trx) is another important oxidoreductase system involved in the regulation of cellular redox balance [246]. Trx uses electrons from NADPH to reduce with a thiol-disulfide exchange mechanisms thioredoxin peroxidase, which acts as a ROS scavenger, while NADPH-dependent TrxR catalyzes the re-reduction of Trx disulfide. The glutaredoxin system, consisting of glutaredoxin (Grx), glutathione (GSH), and NADPH-dependent GSH reductase (GR) acts as an antioxidant by catalyzing the reduction of cysteine oxidative products such as S-glutathionylcysteine and disulfides, with a mechanism similar to that of thioredoxin [247,248].

Another important mechanism of redox regulation involves a number of redox-sensing target proteins, the thiol groups of which are transiently oxidized in the active site and are responsible for the modulation of key cellular pathways via direct signal transmission or protein protein-interactions, in response to activation of receptors such as growth factors. The oxidation of target proteins that initiate the signal transmission can occur directly or indirectly through thiol-disulfide transfer or other reversible cysteine oxidation mechanisms initiated by other sensor proteins [249,250]. Members of the Trx family (including thioredoxins, peroxiredoxins and glutaredoxin), protein tyrosine phosphatases such as PTEN and PTP1B, and other proteins such as caspases have been shown to be regulated by

reversible oxidation of their active site thiolates, with effects on various cellular process such as their subcellular localization, activation of specific signaling pathways, or selective protein-protein interactions [242,251-254].

Increasing evidence suggests that the thiol redox balance is shifted toward oxidation (both reversible and irreversible) with age and disease, although little is known about the exact mechanisms controlling redox balance in cells in response to oxidative stress. With cumulative knowledge of the thiol switches dynamics and their pleiotropic implication in signaling pathways, it will be possible to characterize disease-specific antioxidant pathways, potentially leading to new clinical solutions for the treatment of age-related conditions.

### 1.2.5 Measurement of oxidative stress

The increasing volume of clinically-relevant findings pertaining to oxidative stress has driven research efforts toward the development of methods for the detection and the characterization of protein oxidation products in a wide range of *in vitro* and *in vivo* settings. A large number of methodologies are available for the analysis of protein oxidation products, including immunological, spectrophotometric, and mass spectrometry (MS)-based techniques, often used in combination for increased accuracy, sensitivity or to suit different research needs.

Immunological methods are typically based on antibodies that recognize specific tags reacting with protein oxidative products [255], or raised against a specific peptide containing an oxidized residue [256], or against a specific modification such as nitrotyrosine [257], chlorotyrosine [258], or thiol oxidation states [259]. Among those methods, protein carbonyl content-(PCC) based techniques have been extensively used to screen both biological and *in vitro* samples for protein oxidative products and shed light on the involvement of oxidative stress in several diseases [170,182,183,186,187,260-264]. Carbonyl-containing proteins can be identified by immunological methods after labeling with reactive hydrazines, most notably 2,4-dinitrophenylhydrazine (DNPH). DNPH specifically reacts with protein carbonyls group forming adducts that can be determined by immunodetection with anti-DNP antibodies in a Western blotting (oxy-blotting) and enzyme-linked immuno sorbent assay (ELISA).

Spectrophotometric methods (based on measuring the absorption of specific oxidative products or their tags) have been also widely used for the detection and quantification of oxidative products. PCC-based assays can be performed with spectrophotometric methods by recording the absorbance of DNPH at 365 nm following carbonyls labeling at 365 nm. Alternatively, carbonyls can be derivatized with a number of fluorescent tags [265], which generally represent a valid, timesaving and multiplexable alternative to DNPH labeling [262]. In addition, protein oxidative products such as oxidatively modified tyrosine absorbing at specific wavelengths have been measured with spectrophotometric methods both as free and protein-bound oxPTMs [266]. Similar strategies have been also used to quantify thiol reversible and irreversible oxidative products by means of fluorescence and colorimetric methods based on specific probes or affinity tags [259].

The main disadvantage of immunological and spectrophotometric methods is that, when used on their own, they do not provide information on the oxidized protein identity nor the spatial location of the oxidative modifications. To answer increasingly complex biological questions with regards to the redox regulation of signaling pathways by or via specific redox-sensor proteins, better technologies have been developed for the in-depth investigation of protein oxidative products and their cell-wide implications. When investigating biological problems at the protein level, few analytical techniques, if any, possess the sensitivity and the throughput offered by mass spectrometry (MS). Using mass spectrometry-based analysis, it is possible to obtain detailed and wide-ranging information about the identity and the abundance of the oxidized proteins present in a given sample. MS can be used on its own or in combination with immunological, spectrophotometry based, or gel-based methods, in order to increase the resolution power of the analysis. This offers the potential of analyzing the effect of protein oxidation in a given sample with a high degree of resolution and sensitivity, at the multidimensional levels of identity and quantity, both within and between samples.

# 1.3 Mass spectrometry

## 1.3.1 Introduction

Mass spectrometry (MS)-based methodologies are currently among the state-of-the-art of the available analytical techniques used in the "omics" fields of research, including proteomics [267], lipidomics [268], and metabolomics [269]. The resolution and sensitivity offered by modern MS systems is such that an unprecedented level of detail is achievable these days when investigating by mass spectrometry the structure, modification status, and dynamics of the different cellular components at the molecular level. Because of their resolving power and broad range of application, MS methodologies have widened the scope of many research sceneries, holding a great potential for gaining further insight into the mechanism of life-threatening human diseases. In addition, increasingly automatable and rapid analysis procedures are making MS one of the most promising tools in the field of drug discovery, drug development and for the screening of predictive biomarkers in biological samples of clinical interest.

Several types of mass spectrometry systems are currently available in different configurations, each of them having strengths and limitations that affect the range and type of biomolecules capable of being analyzed, as well as the level and quality of information that can be obtained from the analysis. A number of quantification strategies have also been developed to determine the relative or absolute abundance in MS data, with a broad range of applications in proteomics and clinically relevant research settings.

## 1.3.2 Sample preparation for mass spectrometry

Many biospecimens of research interest, such as biological samples, are complex matrices containing a large number of different macromolecules. Moreover, many buffers used for the extraction of the proteins from biological materials such as cells, tissue or biological samples contain high salt concentration and detergents, which can interfere with the ionization of the analyte (which is necessary for mass spectrometric analysis e.g. by competing for charges), therefore reducing the

sensitivity and accuracy of the analysis. Hence, before undertaking MS analysis, it is generally necessary to perform a number of preliminary steps in order to solubilize and purify the protein(s) of interest from the raw sample and to reduce the detrimental effects of interfering molecules on the MS analysis.

Depending on sample composition, analytical needs and type of instrumentation, a great variety of methods are available for the preparation of protein and peptide mixtures for mass spectrometry analysis. These methods can be generally divided between protein pre-fractionation/separation and protein digestion.

#### *1.3.2.1 Protein pre-fractionation and separation*

In MS workflows, cell/tissue extracts or biological samples containing the protein(s) of interest are first pre-fractionated with different methods depending on the focus of the analysis and the sample composition. Pre-fractionation techniques are generally adopted for the multiple (and sometimes simultaneous) purposes of purifying and/or concentrating the protein(s) of interest, performing a selective affinity-based enrichment (e.g. to study protein complexes), or removing specific molecules (such as detergents or salts used in protein extraction buffers) that may interfere with the MS-based detection [270]. Protein fractionation techniques are typically based on protein physiochemical properties such as size/mass, charge, isoelectric point, hydrophobicity or specific molecular interactions, such as with antibodies. These methods include chromatographic-based methods (such as affinity, ion-exchange, size-exclusion, and hydrophobic interaction chromatography), antibody-based methods (such as immunoprecipitation, and co-immunoprecipitation), and precipitation-based methods (such ionic precipitation with ammonium sulfate or sodium chloride) [271].

After protein purification and/or enrichment, the sample may be further separated by polyacrylamide gel electrophoresis (PAGE), which is one of the most universally used methods for the isolation of proteins prior to mass spectrometry analysis. Depending on sample composition and research needs, PAGE can be also used for the separation of proteins from crude lysates, without previous sample preparation with pre-fractionation methods. Different PAGE methods are available that are capable of separating proteins according to different physical properties: native (non-denaturing) PAGE separates proteins upon both their mass and charge. Denaturing and reducing one-dimensional (1D) SDS-PAGE separates proteins largely according to their mass. Two-dimensional

(2D) PAGE separates proteins based on isoelectric point in the first dimension and mass in the second dimension. PAGE is particularly efficient for both protein separation and contaminant (e.g. salts) removal, and is often the ideal solution for the MS-based proteomics analysis of biological samples or other complex materials.

#### *1.3.2.2 Protein digestion*

Following pre-fractionation and separation, protein samples are further prepared for MS analysis by in-gel or in-solution proteolytic (usually tryptic) digestion of proteins into small peptides (0.1-10 kDa), a strategy known as "bottom-up" proteomic approach. In-gel digestion requires protein pre-fractionation and/or separation performed with PAGE-based methods, while in-solution digestion can be performed on fractionated or even crude extracts [272]. These methods offer great resolving power and sensitivity, because peptides exhibit better front-end separation than intact proteins, and are more amenable to MS analysis [273]. However, digestion-based methods present a number of limitations due to the incomplete recovery of the peptides after trypsin digestion, which results in partial protein sequence coverage. This can be a major drawback for PTMs studies because of the loss of information on any modification present in the uncovered portion of the identified protein [274]. Nonetheless, bottom-up methods are well-suited to large-scale proteomics studies, as only a small portion of the sequence (10-20 amino acids) is often necessary to identify protein IDs from search engine databases (even though one challenge is the ambiguity of identified proteins due to redundant peptide sequences).

Alternatively, intact proteins can be directly analyzed by MS without proteolytic digestion, in the so-called "top-down" approach. This strategy offers the advantage of preserving the protein primary structure, which translates in increased throughput for the analysis of labile protein PTMs, amino acid polymorphism, mutants and protein isoforms resulting from alternative splicing [270,275]. However, the universal implementation of top-down approaches in proteomics research is currently held back by a number of technical and intrinsic challenges, including protein chromatography issues, low sensitivity, and limited availability of bioinformatics tools [276].

### 1.3.3 Instrumentation

Mass spectrometry (MS) is used to obtain information about the identity and abundance of the molecules present in a given sample. The mass-to-charge (*m/z*) ratio of ionized molecules is used to produce a mass spectrum, which is then analyzed for molecule identification and quantification.

Most mass spectrometers are equipped with four different basic components: a sample inlet, an ionization source, a mass analyzer and a detector (Figure 1.9). In a typical mass spectrometry (MS) experiment a solid, liquid or gaseous sample is first introduced into the mass spectrometry system via a sample inlet through which the analytes are converted to ions in the gas. The ionization process can be achieved in a variety of ways (Section 1.3.2.2), and can be completed within or outside the vacuum system of the mass spectrometer. Once formed, the ions enter the mass analyzer where their paths are deflected by electric and/or magnetic fields, which separate and/or filter the ions according to their *m/z* ratio. This part of the analysis is performed under vacuum as collision with other molecules reduces the effectiveness of the analysis. Individual ions hit the ion detector (commonly an electron multiplier) that converts the impact of the ions into an electric signal, which is processed via specific software controlled from computers connected to the mass spectrometer. Data recorded by the ion detector are plotted as a mass spectrum for further analyzing and/or processing via additional software tools or database search engines.

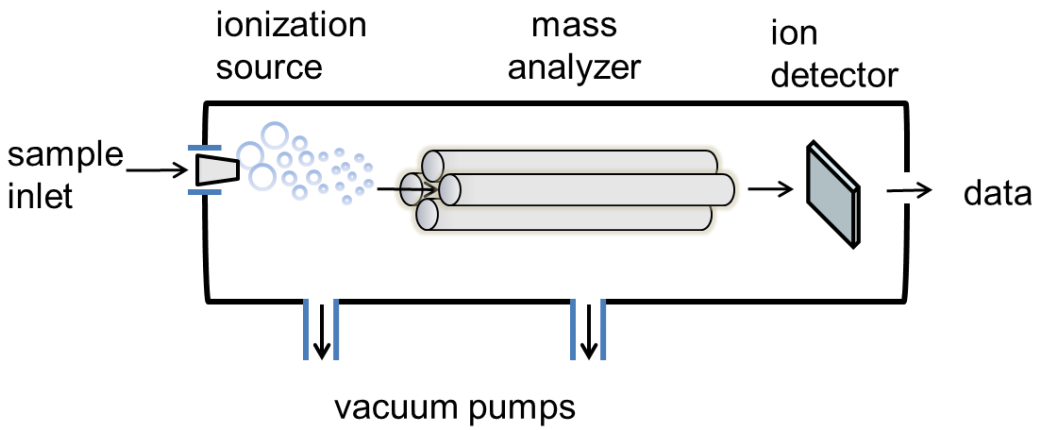


**Figure 1.9 Basic components of a typical mass spectrometry system**

The ionization source can operate at atmospheric pressure or within the vacuum of the mass spectrometer. Mass analyzers separate and/or filter ions formed in the ion source according to their m/z ratio by deflecting their path using electric and magnetic fields. Ions passing through the mass analyzer reach the ion detector that converts them into a digitized output.

#### *1.3.3.1 Sample introduction*

The main purpose of inlet systems in mass spectrometry is to provide an interface to transfer sample molecules at atmospheric pressure to the much lower pressure conditions operating in the mass spectrometer with minimal loss of vacuum. Modern mass spectrometers allow the introduction of a great variety of samples through different types of interface systems. In proteomics applications, the most commonly used sample introduction systems are from chromatographic and capillary electrophoresis systems.

Chromatography-based sample introduction involves coupling of the mass spectrometer to high performance liquid chromatography (HPLC-MS or simply LC-MS) or gas-chromatography (GC-MS) columns. These configurations are also used for the purpose of separating the analytes present in a sample before mass spectrometry, in order to enhance the sensitivity and resolving power of the analysis.

Because of its great sensitivity and specificity, for several years gas chromatography (GC) has been considered the most suitable chromatographic platform to couple with MS for the detection of volatile metabolites in complex samples. However, GC-MS based equipment suffers a number of intrinsic limitations that have considerably hampered its attractiveness to life sciences in recent times. For example, GC-based platforms are only suitable for volatile or vaporizable compounds, and most biomolecules are likely to break down at the high temperature required for vaporization in these systems. High performance liquid chromatography (HPLC), on the other hand, can be conveniently coupled with MS ionization systems that allow a better retention of the original features of many biomolecules (discussed in Section 1.3.2.2). Most HPLC columns used in combination with MS for proteomics applications are reverse-phase (RP) columns. That is, the protein of interest binds to a hydrophobic (non-polar) stationary phase in the presence of an aqueous (polar) mobile phase, and is eluted from the column using a gradient of organic solvent. Reverse-phase columns are particularly advantageous to MS analysis as they offer broad applicability to varied analysis, compatibility with vaporization/ionization systems, and high reproducibility and separation efficiency [277]. In LC-MS configuration, the sample is directly introduced into the mass spectrometer by feeding the liquid eluting from the HPLC column directly to the ionization source, which typically operates at atmospheric pressure.

Alternatively, mass spectrometers can be also interfaced with capillary electrophoresis systems (CE-MS), which are based on the separation of molecules according to their charge and size. CE can be considered a complementary technique to LC-MS [278], as it offers unique advantages over HPLC such as different selectivity, separation of highly polar compounds (which are not retained by standard RP columns), high speed, being inexpensive, and a relatively small amount of sample required. CE is also used online with MS, by connecting the CE capillary directly to the MS ion source with appropriate interface systems [279]. However, CE-MS analytical techniques present a number of difficulties that have been limiting its widespread use in biological applications over the last decade. The major drawback of CE-MS has been the low sensitivity of detection, which makes this technology not ideal for the study of low abundant proteins [280]. Another problem is the incompatibility of MS with sodium phosphate or borate buffers usually used as running buffer in CE [281]. Nonetheless, recent improvement in MS technologies have contributed to reduce the impact of these issues, and CE-MS is currently considered a valid alternative to LC-MS for different biological applications in proteomics [282].

#### *1.3.3.2 Ionization*

The most commonly used ionization methods in proteomics application are: matrix assisted laser desorption ionization (MALDI) and electrospray ionization (ESI). Both these approaches are considered "soft" ionization methods, which are able to transfer the analyte into the gas phase with little or no fragmentation (without breaking chemical bonds), allowing the molecules to remain relatively intact for the MS analysis, and preserving covalent interactions.

In MALDI, a non-volatile sample is co-crystalized with a large excess of an organic matrix in aqueous or organic solvents, and deposited onto a stainless steel target plate, which is then introduced in the MS vacuum ($10^{-2}$-$10^{-3}$ Torr). MALDI matrix materials are typically highly conjugated organic acids capable of absorbing energy at the wavelength of a pulsed laser beam (typically 337 nm), used to irradiate the target plate. The matrix absorbs the laser energy in form of heat, and sublimes forming a gas cloud (known as MALDI plume) carrying the analyte in the gas phase (Figure 1.10). As a result of the collision between the analyte containing the sample (M) and the matrix, which acts as a proton ($H^+$) donor or acceptor, pseudo-molecular ions such as $[M+H]^+$(in positive ion mode) or $[M-H]^-$ (in

negative ion mode) as well as other adducts such as $[M+Na]^+$ or $[M+K]^+$ are formed (in positive ion mode). MALDI is well-suited for the ionization of peptides and proteins with a molecular mass ranging from 1 to 300 kDa, and offers several advantages such as high speed of analysis as well as high sensitivity and specificity. As most ions formed are monocharged molecular species, the MALDI analysis is relatively straightforward in terms of spectral data interpretation, as usually there is only one molecular specie having a specific *m/z* value for each analyte in the sample. However, this can also be a disadvantage as multiply charged ions are better analyzed than large single charged ions in high-resolution mass spectrometers.

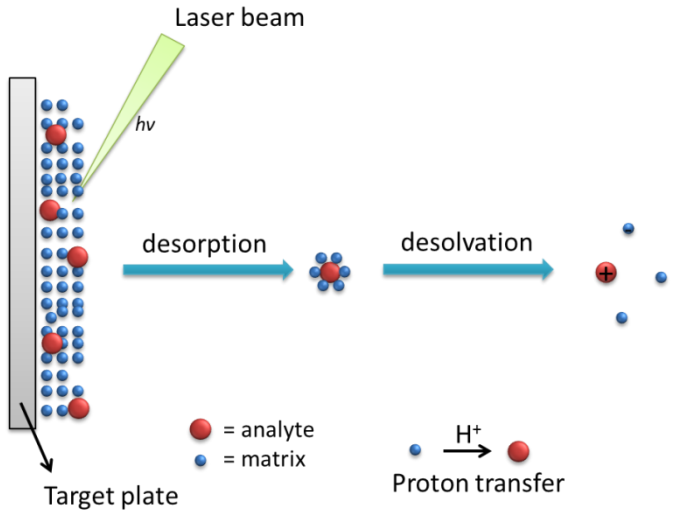


**Figure 1.10 The process of laser-assisted desorption and ionization in MALDI**

The sample and the matrix spotted on the MALDI target plate form co-crystals, which sublime following irradiation with a laser beam. This process triggers the generation of molecular ions by proton transfer from the excited matrix ions to the neutral analyte.

Electrospray (ESI) is a soft ionization method that is performed at atmospheric pressure and involves the nebulization of a liquid sample by applying high electric voltage, resulting in the production of ion species [283]. The process of ionization by ESI is not a process of ion formation per se, but rather a method for releasing analyte ions already present in the sample, the formation of which is achieved prior to MS analysis. This is accomplished by modulating the pH of the sample solution (in case of batch introduction or direct infusion, in which a liquid sample is introduced into the mass spectrometer without LC separation), or by modulating the pH of mobile phase (in case of LC-MS

configuration). The sample is dissolved in a polar volatile solvent, which is typically water mixed with volatile organic compounds such as acetonitrile or methanol that facilitate nebulization, as well as acetic acid or formic acid to increase the conductivity and protonate the molecules. The liquid is pumped through a capillary or needle at a controlled flow rate into the ion source, and a voltage of approximately 3kV is applied between the analyte solution and the mass spectrometer. The potential difference causes the liquid droplet at the tip of the capillary to assume a conic form, a process known as Taylor cone formation, which eventually results in the dispersion of the sample into a fine aerosol containing charged droplets (Figure 1.11). This process is assisted by the addition of an inert gas (such as nitrogen), which is applied both around the outside of the capillary (the nebulizing gas, which assists the nebulization), and across the front of the ionization source (the drying gas, which promotes desolvation) [284]. As the liquid evaporates, the charged droplets shrink in size until the charge density becomes too great on the droplet (a threshold referred to as the Rayleigh limit), and the electrostatic repulsion force becomes stronger than the surface tension. At this point, the droplets are subjected to Coulombic fission, whereby single droplets explode into smaller and more stable droplets (as a result of the increased surface area), and the process repeats until solvent-free ions are released. Once formed, the ion species are directed through the sampling orifice into an intermediate vacuum section, before entering the mass analyzer, which operates under high vacuum, where any residual solvent associated with the ion is removed.

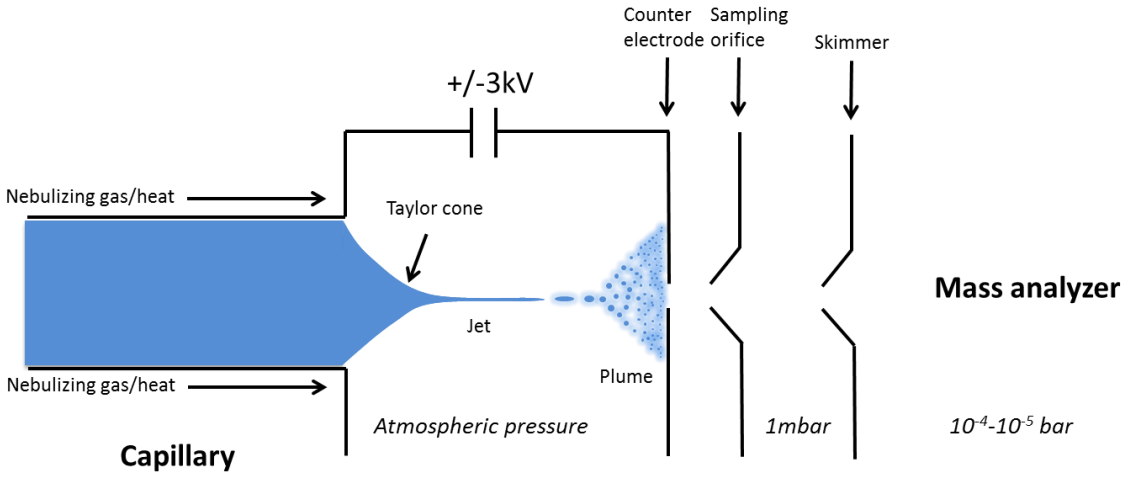


**Figure 1.11 Ionization mechanism in ESI**

At the tip of the capillary, the liquid containing the sample is subjected to high voltage and assumes a conical shape (the Taylor cone) resulting in a fine jet of liquid, which becomes unstable and breaks up into a plume of small, highly charged droplets. The droplets are directed toward the counter electrode orifice of the ionization source, while the solvent evaporates. Solvent-free ions accelerated by the counter electrode enter an intermediate vacuum region through a sampling orifice, before being allowed into the mass analyzer.

Ion species generated by the ESI ionization process include single protonated pseudo-molecular ions $[M+H]^+$ (in positive ion mode) and single deprotonated pseudo-molecular ions $[M-H]^-$ (in negative ion mode). In addition, a number of additional cation species such as $[M+Na]^+$, $[M+K]^+$ and $[M+NH_4]^+$ can be formed in positive ion mode [285]. Ions entering the mass analyzer following ionization can be multiply charged pseudo-molecular ion species such as $[M+nH]^{n+}$ in positive ion mode, and $[M-nH]^{n-}$ in negative ion mode, with the number of charges (n) increasing with the molecular weight of the analyte. In general, multiple charging represents an advantage of ESI over MALDI ionization, as it allows the analysis of high molecular weight analytes, which in MALDI would produce *m/z* values beyond the limit of most modern high-resolution analyzers. However, multiple charging results in a complex ion series for a single compound, which requires mathematic transformation for the interpretation of ESI-derived mass spectra, making the analysis more difficult [286,287]. Moreover, ESI is more susceptible than MALDI to the presence of charge-competing non-

volatile salts and detergents, which can form cluster or spread an ion's signal over several adducts, thus causing signal suppression, increased background noise, and reduced sensitivity [288].

### *1.3.4.1 Mass analysis and analyzers*

Many types of mass analyzers are implemented for the mass-to-charge based separation of the ions formed in the ionization source, all of them operating according to the Lorentz force law and Newton's second law of motion:

$$F = qE + qvxB \text{ (Lorentz force law)}$$

$$F = ma \text{ (Newton's second law of motion)}$$

These can be combined in the differential equation:

$$\frac{m}{q}a = qE + qvxB$$

where *F* is the force applied to the ion, *q* the ion charge, *E* the electric field, *v* the ion velocity, *B* the magnetic field, m the mass of the ion, and a the acceleration. This equation describes the motion of charged particles as function of their mass-to-charge ratio (m/q in the equation) [289]. Many mass analyzers separate the ions by applying electric and/or magnetic fields under vacuum that accelerate the ions toward the detector of the mass spectrometer.

The simplest mass analyzer used in proteomics applications is the Time of Flight (TOF), which offers very rapid analysis times, high sensitivity, high resolution, and a wide mass-to-charge range (20 to 20,000 m/z). The TOF analyzer is a field-free drift tube of known length in which the ions are accelerated by a fixed potential (20-30kV). As a result, same-charge ions obtain the same overall kinetic energy (k) and lower mass ions will travel down the tube with a higher velocity (v) than higher mass ions of the same charge (as kinetic energy equals $0.5mv^2$). The TOF measures the ions velocity by recording the time required by the accelerated ions to cover the distance between the introduction of the ions and the detector (time-of-flight), so that m/z values for each ion can be determined.

Another type of mass analyzer extensively used in proteomics applications (and perhaps the most widely used in MS applications) is the quadrupole mass analyzer (QMS), which is commonly coupled to ESI ionization, and can be used both alone or in tandem, for increased analysis throughput and sensitivity. QMS consists of two pairs of parallel cylindrical rods in a vacuum chamber, equally distant from each other, and electrically connected so that a positive potential is applied to one diagonal pair and a negative potential to the other pair. Ions entering the mass analyzer from the ionization source travel along the axis of the quadrupole. A combination of alternating radio frequency (RF) and fixed direct current (DC) voltage are applied to each quadrupole rod pair. By varying the magnitude of the applied voltages, the quadrupole operates as an ion filter that can be set to pass only resonant ions having a certain *m/z* value, while all other ions will collide into the tube and disappear [290]. Performing MS analysis using a quadrupole has multiple advantages such as good reproducibility, excellent linear dynamic range, and low cost, in spite of the limited working mass range (1-4000Da) and relatively modest mass resolving power in comparison with TOF analyzers [291].

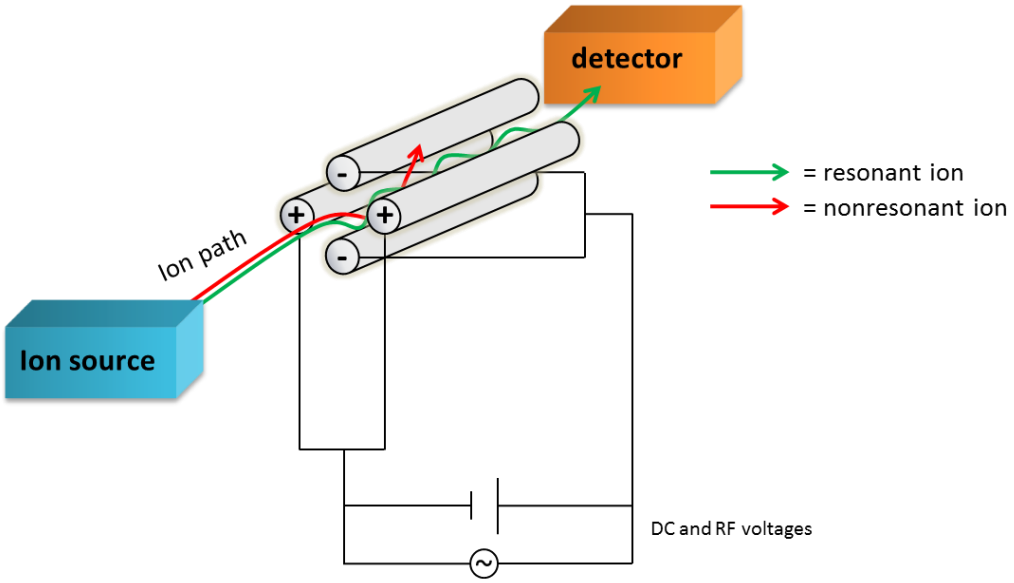


**Figure 1.12 Ion filtering by quadrupole mass analyzers**

Depending on the magnitude of the applied voltage, only resonant ions with a certain mass-to-charge ratio have a stable trajectory while traveling the quadrupole mass filter. Non-resonant ions drift away from the center of the quadrupole and never reach the detector.

Two quadrupoles mass filters can be arranged in series, separated by a RF-only quadrupole functioning as a collision cell, to operate in tandem mass spectrometers (tandem MS), with a number of research applications in proteomics (such as protein sequencing). A mass spectrometer equipped with this quadrupole configuration is known as triple-quadrupole mass spectrometer (TQMS), usually denoted as QqQ or Q1q2Q3. While both Q1 and Q3 operate as mass filters, q2 is responsible for producing fragments of molecular ions selected by Q1 through a mechanism known as CID (collision-induced dissociation). This is accomplished by allowing the molecular ion selected in Q1 (called the parent ion) to collide with neutral molecules of an inert gas (Ar, He, or $N_2$) in the collision cell in order to induce bond breakage and consequent fragmentation of precursor ions into smaller product ions [292]. Different degrees of fragmentation can be achieved by varying the collision energy, with effects on reproducibility and sensitivity of the analysis. The selection of the appropriate collision energy can be crucial for sequence coverage in peptide fragmentation [293]. Tandem mass spectrometers can also use a combination of quadrupoles with other mass analyzers. The final quadrupole (Q3) in the triple quadrupole mass analyzer can be replaced by a TOF analyzer, a configuration known as qTOF (or QqTOF), which has been also used in MS-based proteomics, with better resolving power [294]. Alternatively, the third quadrupole in a triple quadrupole mass analyzer can be operated as a linear ion trap (a mass analyzer that captures and stores ions using a combination of RC and DC fields), a configuration known as QTrap, offering improved sensitivity and choice of additional fragmentation stages [295].

### 1.3.5 Mass spectrometry approaches in proteomics

In the proteomics field, tandem mass spectrometers such as TQMS, qTOF and qTRAP can be operated in a number of different tandem MS (MS/MS) modes, to perform multiple steps of ion selection in order to fit different analytical needs in protein identification and quantification. Depending on which MS acquisition mode is used, several different approaches have been implemented in modern proteomics applications, including discovery (or shotgun), directed, semi-targeted, and targeted approaches [296] (Figure 1.13).

In a discovery (or shotgun) experiment, a series of peptide ions (called precursor ions) obtained from a proteolytic digest ("bottom-up" approach) are automatically selected from a survey scan by the mass spectrometer according to their signal intensity and subsequently fragmented and in the fragment MS recorded. This process, commonly called a 'product ion scan', is typically used in a LC-MS/MS configuration, with the mass spectrometer operating in a data dependent analysis (DDA) mode. Because protein identification and protein quantification in shotgun proteomics are performed in the same experiment, quantification will only be limited to those features corresponding to the selected precursor ions (typically from 3 to 10), which are characteristically the most abundant within a mass spectrum. The obvious resulting limitation of this method is that the quantitative analysis will be restricted to a certain set of ions that exhibit similar abundance values, therefore potentially excluding from the analysis biologically relevant changes in protein abundance. Moreover, the process of the selection of the precursor ions can be biased, particularly when dealing with complex samples, because at times during the analysis the number of analytes of interest exceeds the maximum number of selectable precursor ions. Overall, shotgun strategies offer great power to discover new proteins, but they do need to operate on small or fractionated datasets in order to maximize protein identification and quantification inputs.

In a directed proteomics approach, precursor ions of interest can be selected from a pre-recorded survey scan obtained from a LC-MS or LC-MS/MS run, and are collected into an inclusion list along with their m/z, charge and retention time. A second LC-MS/MS run will then be performed in 'product ion scan' mode fragmenting only the selected precursor ions present in the previously recorded list. With this method protein quantification and identification are performed separately. The analytes are first quantified in the first LC-MS full spectrum survey scan, and the selected precursors are identified with the second LC-MS run. Same sets of precursor ion can be selected across repeated experiments, which results in higher reliability and reproducibility comparing to shotgun strategies. Moreover, because the selection of the precursor is not based upon signal abundance, low abundance features (such as oxidatively modified peptides) can be quantified and identified, allowing of a deeper and less biased exploration of the proteome. Directed proteomics approaches can therefore deal with larger data sets than shotgun approaches, and have higher selectivity, sensitivity and reproducibility.

However, as two separate MS acquisition are effectively performed, directed proteomics experiments are more time-consuming and require a larger sample size than shotgun approaches.

Semi-targeted approaches rely on the mass spectrometry-based detection of fragments having specific structural features that are 'diagnostic' for the identification of certain molecular ions[297]. The semi-targeted approach most widely implemented in proteomics applications are precursor ion scanning and neutral loss scanning. In precursor ion scanning (PIS), the second analyzer is set to select only one specific fragment ion having a specific *m/z* value, while the first analyzer scans all the precursor ions over a chosen mass range. Only the precursor ions that after fragmentation generate the pre-selected diagnostic fragment will be detected. In Neutral Loss scan (NLS) both analyzer are set to scan all m/z values, but the second analyzer is offset from the first by a difference in m/z values equal to the m/z of a specific diagnostic fragment of interest that is lost as a neutral species during the fragmentation. Semi-targeted methods are particularly useful for the rapid and highly specific detection of protein modifications such as phosphopeptides [298] and oxPTMs [299-301]. However, when analyzing complex mixtures, these methods can often be limited by poor resolution due to co-elution of unrelated peptides from the online HPLC column [302], loss of sensitivity due to large dynamic range of peptide abundance and signal suppression effects [303]. Due to these limitations, semi-targeted approaches are limited in terms of accurate protein quantification, for which the implementation of label-based techniques is often required [302].

Targeted experiments are based on SRM (selective reaction monitoring), also called MRM (multiple reaction monitoring), in a non-data-dependent acquisition mode, which does not require survey scans at all. Similarly to the directed approach, quantification in targeted experiments is performed on specific fragment ions obtained by the fragmentation of preselected precursor ion. However, in targeted proteomics the precursor ions are selected using prior acquired information about their identity, therefore the only detected product ions are those deriving from the fragmentation of the selected precursor (both mass filters are set to acquire a preselected ion having a specific m/z). This method allows high signal-to-noise ratio and high performances, although requires some optimization of fragmentation parameters for specific precursors. Using either label-based or label-free strategies, very accurate differential quantification can be obtained with targeted-based methods. Although targeted approaches are not a discovery strategy as prior knowledge of analytes is required, they

represent the most accurate available MS-based quantification tool and can be conveniently used in hypothesis-driven studies upon optimization of chromatographic and mass spectrometric features [304].

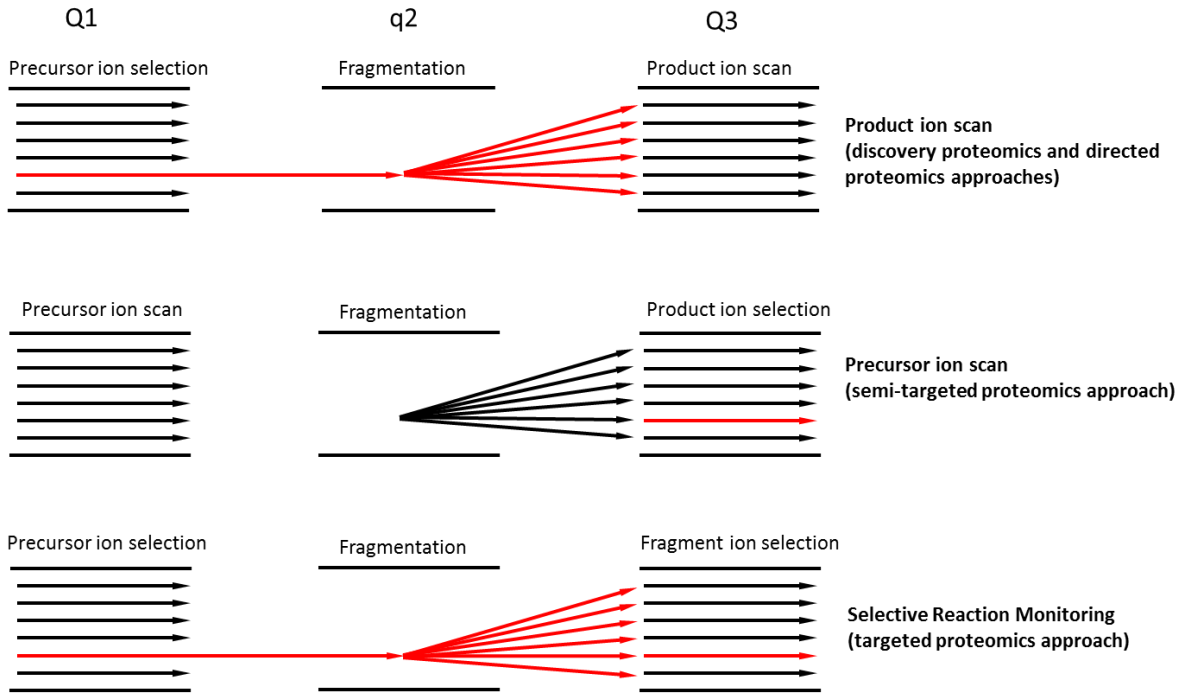


**Figure 1.13 Representation of various proteomics strategies based on tandem MS**

Depending on the proteomics approach used, mass analyzers such as triple quadrupoles can be operated in three different ways: in a shotgun or directed proteomics experiment, a precursor 'parent' molecular ion is selected in the first analyzer (Q1), fragmented in the collision cell (q2) and its product ions are scanned in the third analyzer (Q3) and finally detected (product ion scan); in semi-targeted approach, the precursor ions are scanned in Q1 and only fragments corresponding to a certain m/z value set in the third analyzer Q3 are detected (precursor ion scan); in a targeted proteomics experiment, precursor and product ion are both pre-selected so that only specific fragments selected in Q3 from parent ions pre-selected in Q1 are detected.

### 1.3.6 Quantification of protein oxidative products using MS

Quantitative technologies in mass spectrometry have naturally evolved to face the challenges of the increasingly data-driven outputs in interactomics, functional proteomics, systems biology, redox biology and many other biological applications. Quantitative proteomics strategies can be divided between two major groups: relative and absolute. Relative quantification relies on the measurement of

the fold change in the abundance of peptide ions across two or more samples, whereas absolute quantification delivers direct information about the actual peptide concentration in a given sample. High throughput quantitative proteomics workflows require the combination of mass spectrometry with additional - both MS and non-MS based - methods capable of delivering the most possible unbiased information on the levels of the proteins and peptides detected and identified in a given sample. Several label-based and label-free techniques have been developed and are currently implemented in both absolute and relative MS-based strategies, each of them having strengths and limitations that can affect the analysis to some extent.

#### *1.3.6.1 Label-based methods*

One possible approach in relative quantification is to compare the MS spectra of two or more LC-MS runs (e.g. control versus oxidized sample) to determine the abundance of the modified peptide between different samples. However, this method requires extensive optimization and normalization at all experimental stages, because uncontrolled experimental settings might result in unpredictable fluctuations in peak intensities. A valid solution to this problem is the stable incorporation of isotope labels prior to mass spectrometry analysis. With this method, multiple samples can be labelled with different isotopic reagents, resulting in peptides coded with tags having different mass that can be discriminated in a single mass spectrometry run, eliminating any possible bias in the relative quantification. When approaching the quantification of protein modifications (such as oxPTMs) with this method, the total mass shift of modified peptides compared to control has to be obtained from the total sum of the mass shift due to the isotope label and the mass shift due to the oxidative modification. The isotope labels can be introduced at various stages of the experimental workflow, depending on type of sample and MS approach.

In metabolic labeling, proteins are generally labelled at the cell culture level, implementing growth media modified to contain stable-isotopes containing amino acids. This method was developed in mammalian cell culture under the name of SILAC (stable isotope labeling with amino acids in cell culture), and is currently the metabolic labeling technique of choice in post-translational modifications and protein-protein interaction studies. SILAC approaches have been recently implemented to quantify protein oxidative modifications at the whole proteome level, whereby the proteins of oxidation-stressed and control cells can be labelled with different ‘light’ or ‘heavy’ isotopic variants, and in vivo

versus spontaneously occurring oxidation can also be discriminated [207]. A recent evolution of SILAC is the stable isotope labelling of amino acids in mammals (SILAM), another exciting label-based quantification technology whereby the label is incorporated at the whole animal level and the MS quantitation can be performed one entire tissue-specific proteomes. The clear advantage offered by the SILAM-MS approach is the potential to quantify changes in proteome between diseased versus healthy mammalian tissues, obtained by animal models of certain human pathologies [305]. While offering great isotope incorporation rates (> 90%) with little bias in the quantification, metabolic labeling suffers from some limitations, including issues with cell lines showing altered growth in modified media, formation of labeling-induced artifacts, limited availability of required reagents, among others [306].

Protein oxidative events can be detected with label-based methods adding differential stable isotopes after cell lysis, using chemical or enzymatic methods to place the label after the protein tryptic-digestion. These systems are beneficial in situations whereby metabolic labeling is difficult (e.g. because of the lack of ability of certain cell lines to grow in modified media), as well as in non-tissue culture settings (e.g. non-cell cultured biological samples). Among the chemical methods, those based on amino acid-specific labeling are extensively used to detect oxPTMs. An example of such methods is ICAT (isotope coded affinity tags), which is a gel-free cysteine-specific strategy, based on a iodoacetamide (IAM)-based thiol-reactive group that carries an affinity tag (usually biotin) for the enrichment of labelled peptides, and have been used to quantify evidence of cysteine oxidation in biological samples and complex protein matrixes [307,308]. However, ICAT is applicable to cysteine-containing peptides only and there are potential limitations in terms of number of proteins detected, which have been shown to be considerably less in comparison to gel-based methods (most likely because of the presence of large tags that interfere with database search and consequent mass spectrometry sequencing [309]. Other solutions have been proposed to overcome such problems, including the implementation of isotope-labeled N-ethylmaleimide (NEM) in a targeted MS approach to monitor the redox status of reversibly oxidized cysteines [310,311]. NEM-based technologies have been used for the detection and quantification of cysteine disulfide bonds, using a ‘light’/‘heavy’ ratio as direct measure of reduced/oxidized cysteines [312]. In addition, both IAM and IAM based strategies can be adapted to measure protein S-glutathionylation and such strategies are now being

further developed for the detection and quantification of protein S- nitrosothiols [307]. Promising results in the detection of oxPTMs have also been generated using specific enzymatic reactions to place the isotope tag at specific amino acid groups. Among those approaches, the enzyme-catalyzed $O^{18}$-based labeling has been successfully used in the for the accurate quantification of oxidized methionine, whereby the protein oxidation experiment was carried out using $O^{18}$-enriched $H_2O_2$ to generate differentially labeled oxidized methionine [313]. However, when the biological question requires the simultaneous analysis of several samples (e.g., the analysis of oxPTMs over a range of oxidant concentrations), few available labeling techniques, if any, offer the flexibility and the power of iTRAQ (isobaric tags for relative and absolute quantification). With this approach, primary amino groups in intact or enzyme-digested are labeled by attaching an N-methyl piperazine reporter group linked to a carbonyl group, which functions as a mass balance to generate isobaric-labelled peptides. iTRAQ-based strategies have been used quantify the occurrence of protein S-glutathionylation [314], protein carbonyl formation [264], as well as to selectively label and quantify 3-nitrotyrosine, both on their own [315] or in combination with precursor isotopic labeling [316]. In combination with NEM-based thiol-blockade, iTRAQ has been also used to identify the redox-sensitive reversibly-oxidized cysteines in proteins and to quantitatively assess the oxidation states of individual cysteine residues [317]. Similarly, tandem mass tags (TMT), another type of isobaric mass tags, and their variants are also a popular choice for the analysis of different types of cysteine modification, including S-nitrosylation (SNO) [318] and S-sulfenylation (SOH) [319].

Up-to-date absolute quantification (AQUA) approaches in SRM or MRM mode are also benefiting from of the multiplexing potential of novel isotope- and isobaric tags-based tools for the analysis of protein oxPTMs. For example, absolute quantitation of glutathione-disulfide in erythrocytes was obtained using a multiple-label isotope-based method by spiking differentially labeled standard solutions of glutathione-disulfide and glutathione-sulfonic acid against control [320]. iTRAQ-labeled internal standards have been recently used in combination with targeted MS approaches to quantify evidence of proteolytic post translational modifications such as proteolytic cleavage [321] or phosphorylation [322] as well as to validate candidate biomarkers of clinical interest [323]. However, despite their proven high accuracy and reliability, absolute label-based quantification techniques are

costly and time-consuming compared to relative counterparts, which are therefore preferred for multiplexed proteome-wide studies.

#### *1.3.6.2 Label-free quantification and software based analysis.*

Label-free methods represent a fast, easy-to-use alternative to label-based approaches. The main advantage of label-free based quantification strategies is that no additional sample manipulation step is required before the mass spectrometric analysis. In addition, there is virtually no limit to the number of samples that can be processed in a single experimental analysis, which represents a significant advantage over label-based strategies that are limited by the availability of labeling reagents to be used in an individual experiment. The two fundamental strategies currently used in label-free quantification are spectral counting and feature-based quantification [324].

Methods based on spectral counting rely on the number of identified MS/MS spectra corresponding to a given protein as a measure of protein relative abundance. A high correlation ($R^2 > 0.995$) has been demonstrated between relative protein abundance and number of spectral counts, showing a linear dynamic range higher than that observed with metabolic labeling methods [325,326]. However, spectral counting-based label-free quantification strategies suffer from poor reproducibility for the analysis of low abundance proteins, thus they are not appropriate for the specific analysis of oxPTMs. In fact, because a limited number of MS/MS spectra are detected for low abundance proteins, some proteins and their PTMs may not be detected across all samples, causing misleading results. A number of algorithm-based solutions have been recently developed to optimize the performances spectral counting technologies, including emPAI (exponentially modified protein abundance index) [327,328] and APEX (absolute protein expression index) [329,330], both implementing an algorithm based upon the ratio between observed and observable peptides. These platforms have been used in discovery-driven proteomics investigations [331] as well as to monitor protein expression changes such as those induced by oxidative stress [332]. Nonetheless, critical evaluation of label-free methods did show that emPAI and APEX generated values suffer from concentration-dependent saturation effect among other limitations, compared to more robust feature-based software solutions [333].

Feature-based quantification methods rely on the summed measurement of the peak intensities of peptide ions contributing to a given protein. In a given mass spectrum, each peptide ion that gives rise to a peak represents a feature that is detected by the feature-finding algorithm and plotted in a heat

map showing m/z value, retention time and intensity. The software then aligns the heat maps generated by different LC-MS runs so that the same features are assigned to each other for quantitation and the protein abundance is measured by summing up the peak intensities corresponding to the same area corresponding to the feature. With emerging interest in label-free methods, a new generation of feature-based software solutions capable of processing large amount of high resolution data has been made available for the analysis of LC-MS data, including Progenesis QI for proteomics (Non Linear Dynamics, UK), msInspect/AMT [334], MAXQuant [335], Rosetta Elucidator (Rosetta Biosoftware, Seattle, WA), OpenMS [336], and Superhirn [337], among others. Several recent articles have portrayed a positive picture for the implementation of label-free software based technologies in biomarker discovery in biological samples [338-343], but few studies have reported the use of label-free software based methods for the quantitative determination of specific oxPTMs. This is mainly because software solutions do not offer rigorous analysis tools for the analysis of peptide modifications, and would not be appropriate for a discovery approach in the specific analysis of oxPTMs without implementing a proper downstream validation strategy. Nonetheless, both commercial and open-source modern software packages do include statistical tests tools in order to threshold false positives and significant results over a large amount of features [344]. Recently, reversibly oxidized cysteines in the membrane proteins of human erythrocytes have been quantified using a robust computational software-based approach and validated by matching the modified peptides against Protein Data Bank (PDB) entries [345]. However, higher quality outputs with low false positive rates can be achieved using label-free, narrow-mass window XIC to detect and quantify low abundance oxPTMs in targeted MS approach [346]. Such strategy can be used to validate the oxPTMs discovered with software-based technologies or on its own for the quantitative determination of specific oxPTMs in targeted proteomics (with prior knowledge of peptides and modifications of interest).

The core drawback of label-free methods is that they require highly reproducible experimental techniques, as well as careful control of LC and MS machines performances, much more so than label-based method [347]. In addition, changes in peptide charge state due to oxPTMs affect both peptide ionization efficiency and MS/MS fragmentation pattern, which can alter the feature intensity in a non-controllable way. Therefore, stringent analysis criteria have to be followed using label-free strategies

to ensure a high level confidence in both protein identification (features representative of identified proteins have to be carefully selected) and quantification (a sufficient number of replicate experiments have to be performed to evaluate statistical significance and biological variability). When the above-mentioned conditions are satisfied, label-free software based quantification can be a robust, inexpensive and timesaving alternative to label-based methods, also holding a great potential for the transition of MS proteomics platforms in clinical applications.

### 1.3.7 MS-based detection of protein oxPTMs in disease

The last decade of proteomics research has witnessed increasing evidence that mass spectrometry can be successfully applied to several scientific problems, including biomarker discovery, biomarker validation, and analysis of clinical samples [348,349]. The identification of novel biomarkers in disease is expected to open new doors for the screening of life-threatening diseases like diabetes, cardiovascular diseases, and chronic inflammatory diseases. Many studies have exposed an existing correlation between those conditions and protein oxidative damage [165]; hence, there is increasing attention to the identification of oxPTMs in clinical and animal samples for the characterization of disease-specific modifications. The measurement of amino acid oxidative products has been successfully demonstrated in biological samples using several MS- and non-MS-based techniques [350], yet it remains a challenging task. Critical factors including sample complexity, low abundance of the modifications and pre-analysis spontaneous oxidation during sample handling, often represent a serious problem for a clinically-translatable measure of protein oxidative products [351].

Among the biological samples usable for the detection of oxPTMs, the main sources of proteins are body fluids and tissue extracts. Blood plasma and urine samples are by far the most widely examined body fluids to profile systemic oxidative damage in clinical settings with MS techniques [241,352-354]. However, blood collection is not the preferred method from a patient's perspective, especially for newborn screening, and large amount of sample would be required to detect low abundance proteins. Urine samples are easy to obtain in large volumes, and can be collected non-invasively, but the protein concentration is too low to allow extensive detection of protein-bound oxidative

modifications. In addition, the presence of protein oxidative products in the urine can be also due to the physiological excretory process, since oxidation is a common process in phase 1 metabolism. Alternatively, specific body fluids have been also used as sources of protein samples for the MS-based identification of oxPTMs in certain diseases, such as cerebrospinal fluids for the detection of oxPTMs in patients affected by Alzheimer's disease [355,356], and synovial fluids for the detection of free and protein-bound 3-nitrotyrosine in patients affected by osteoarthritis [357]. Clinically relevant protein oxidative products were also detected in saliva [358], seminal fluid [359], and amniotic fluid [360]. To profile local oxidative damage, the MS determination of oxPTMs in diseased human tissues has been performed using surgical biopsies of human tissue, such as heart [361] or skeletal muscle [362]. However, the invasiveness and the proneness to cause infection of surgical biopsies represent a major limitation for the analysis of protein oxidation events in human patients. Therefore, there is great interest on non-invasive methods to interface MS for the analysis of oxPTMs in human biological samples. These include tissue microarrays of needle-core biopsied tissues [363] and analysis of exhaled breath condensate [364-367].

In spite of several challenges, the application of both label-free and label-based mass spectrometry methods to the detection of oxPTMs in clinical samples has progressed exponentially in recent times. Label-free targeted mass spectrometry approaches (SRM-based) have been used for the identification and quantification of free and protein-bound oxidized amino acids in the clinical samples of patients affected by several different diseases [238,368,369]. The specificity of the targeted approached used in these studies offers a great deal of accuracy for the quantification of oxPTMs in healthy versus diseased sample. Yet, since most of these studies do not provide protein identification data, it is impossible to assess the distribution of the protein-bound modifications within the proteomes, which is critical for a deeper understanding of the effect of reactive species on specific proteins in a well-defined disease status.

Among label-based methods, those based on protein carbonyl content (PCC) have been extensively used in combination with MS techniques to identify oxidized proteins in clinical samples. Several studies have reported the determination of protein carbonyls in biological samples of clinical interest using gel spots obtained by 2D-electrophoresis of DNPH-derivatized proteins in combination with non-tandem MS [180,181] and tandem MS [185,263]. The first high throughput protein carbonylation

profile in human plasma was recently generated using a combination of carbonyl derivatization and MS/MS techniques [370], opening new doors for the study of blood biomarkers in clinical proteomics settings to investigate the relationship between oxidation and certain conditions that are linked to the formation of protein carbonyls. Alongside PCC-MS-based methods, isotope labels based techniques including ICAT and iTRAQ are one of the most promising tool for the clinical application of mass spectrometry techniques to identify oxPTMs for biomarker discovery in disease, despite relatively few studies have implemented them for such purpose so far [182,183,187,203,371,372].

Using MS-based methods, many oxPTMs have been found elevated in diseased samples, including carbonylation, [152,180-188], protein-bound 3-chlorotyrosine [229-233], protein-bound 3-nitrotyrosine [230,232,234-236], cysteine oxidation (both reversible and irreversible) [152,171-173,198,200-203] and methionine oxidation [150,152,208,209] (Table 1.3). With such an increasing amount of published work, it is evident that MS-based strategies represent the cutting-edge technology to measure evidence of oxidative damage to proteins in disease. Yet, new generation proteomics approaches for the detection of oxPTMs still struggle to break into early diagnosis routines. Factors including the lack of a well-established validation protocol for protein oxidation products, the great variety of methodologies, and the relatively time-consuming data analysis times are still a considerable shortcoming that limits the application of mass spectrometry into clinical settings [373]. Nonetheless, the recent advances discussed in this thesis, together with the knowledge that they generate, are having an undeniable impact on the analysis of biological samples of clinical interest. Proteomics applications based on MS methods are going to be prominent in the near future of clinical research whereby early diagnosis becomes essential for the prompt treatment and management of life-threatening human diseases.

**Table 1.3** Identification of protein oxidation biomarkers in biological samples of clinical interest using mass spectrometry techniques

| **Modification type** | **Disease** | **Method** | **Sample type** | **Protein type** | **OX sites identif. ?** | **Reference** |
|---|---|---|---|---|---|---|
| Carbonyl formation | Alzheimer's disease | DNPH, MALDI-TOF/MS | Blood (human) | Fibrinogen γ-chain precursor protein, α-1-Antitrypsin precursor | no | Choi *et al*., 2002 [180] |
| Carbonyl formation | Ageing | Avidin affinity, LC-MS/MS | Brain tissue (mouse) | Brain proteins | yes | Soreghan *et al*., 2003 [263] |
| Carbonyl formation | Ageing | FTC-labeling; 2D PAGE-MS | Liver tissue (mouse) | Cytosolic liver proteins | no | Chaudhuri *et al*., 2006 [186] |
| Carbonyl formation | Ageing | iTRAQ/LC-MS/MS | Skeletal muscle (rat) | Mitochondrial muscle proteins | no | Feng *et al*., 2008 [187] |
| Carbonyl formation | Mild Cognitive impairment and Early Alzheimer's disease | DNPH, MALDI-TOF/MS | Inferior parietal lobule (human) | CA II, Syntaxin binding protein I, Hsp70, MAPK kinase I, FBA-C, PM-1, GFAP | no | Sultana & Perluigi, 2010 [181] |
| Carbonyl formation | Ageing | ARP-labeling, MS/MS | Heart (rat) | Cardiac mitochondrial proteins | yes | Chavez *et al*., 2011 [185] |
| Carbonyl formation | Diabetes | LC-MS/MS, SRM | Plasma (rat) | Plasma proteins | yes | Madian *et al*., 2011 [183] |
| Carbonyl formation | Obesity-induced diabetes mellitus | ARP-labeling, RPC-MS/MS | Plasma (human) | Plasma proteins | yes | Bollineni *et al*., 2014 [184] |
| Carbonyl formation | Breast cancer | iTRAQ/LC-MS/MS | Plasma (human) | Plasma proteins | yes | Madian *et al*., 2011 [182] |
| Carbonyl formation | Ischemia/ reperfusion | 2D-PAGE-MALDI-TOF/TOF/MS/MS | Hippocampus (monkey) | Hsp70-1, DRP2 isoform 2, GFAP, β-actin | yes | Oikawa *et al*., 2009 [188] |
| Carbonyl formation, cysteic acid, MetO, Met O2 | Alzheimer's disease, Parkinson's disease | 2D-PAGE, MALDI-TOF/MS, MALDI-TOF/TOF/MS/MS, HPLC-ESI/MS/MS MALDI-MS/MS | Brain (human) | DJ-1 | yes | Choi *et al*., 2006 [152] |
| 3-$NO_2$Y | Cancer | NTAC (nitrotyrosine affinity column) based MALDI–LTQ MS/MS | Nonfunctional pituitary adenoma tissue (human) | NTAC-enriched proteins | yes | Zhan & Desiderio, 2006 [235] |

| | | | | | | |
|---|---|---|---|---|---|---|
| 3-$NO_2$Y, 3-ClY | Influenza | LC-MS/MS | Serum (mouse) | Serum proteins | yes | Kumar *et al*., 2014 [229] |
| 3-$NO_2$Y, 3-ClY | Inflammatory bowel disease | LC-MS/MS | Serum, colon tissue (human) Serum, colon tissue(mouse) | Serum proteins | no | Knutson *et al*., 2013 [230] |
| 3-$NO_2$Y, 3-ClY | Systemic lupus erythematosus | LC-MS/MS (MRM) | Plasma (human) | HDL | yes | Smith *et al*., 2014 [232] |
| 3-$NO_2$Y | Alzheimer's disease | LC-MS/MS | Brain tissue (human) | α-enolase, Triosephosphate isomerase, Neuropolypeptide h3 | no | Castegna *et al*., 2003[236] |
| 3-ClY | atherosclerosis | LC-MS/MS (SRM) | Plasma (human) | ApoA-1 | yes | Shao *et al*., 2012 [231] |
| 3-ClY, carbonyl formation | Patients post myocardial infection | Stable isotope dilution GC/MS; LC-MS/MS | Plasma (human) | fibrinogen | no | Paton *et al*., 2010 [233] |
| MetO | Type 1 diabetes | LC-MS | Blood (human) | Apo a1 | yes | Brock *et al*., 2008 [209] |
| Cysteine reversible oxidation | Ageing | Fluorescent labeling, LC-MS/MS | Skeletal muscle (rat) | SERCA | yes | Sharov *et al*., 2006 [201] |
| Cysteine-SNO | Ischemia/ reperfusion | Affinity-capture, LC-MS/MS (label-free) | Heart (mouse) | Mouse heart tissue proteins | yes | Kohr *et al*., 2011 [202] |
| Cysteine-SNO | Ageing, Alzheimer's disease | 2D-PAGE, MALDI-MS/MS | Brain tissue (human) | Glial fibrillary proteins | yes | Riederer *et al*., 2009 [200] |
| Cysteine reversible oxidation | Ischemia/ reperfusion | ICAT, LC-MS/MS | Heart (mouse) | Mouse heart tissue proteins | Yes | Kumar *et al*., 2013 [203] |
| Cysteic acid, MetO | Alzheimer's disease and Parkinson's disease | LC-MS/MS and MALDI-TOF | Brain tissue (human) | Ubiquitin Carboxyl-terminal Hydrolase L1 | Yes | Choi *et al*., 2004 [171] |
| Cysteic acid, carbonyl formation | Alzheimer's disease and Parkinson's disease | 2D-PAGE, LC-MS/MS | Brain tissue (human) | SOD | Yes | Choi *et al*., 2005 [172] |
| Free 3-$NO_2$Y | Circulating sleep apnea | LC-MS/MS (MRM) | Plasma (human) | | | Svatikova & Wolk, 2004 [239] |
| Free 3-$NO_2$Y, free 3-BrY, free di-BrY, free di-Y | Diabetes | LC-MS/MS (MRM) | Urine (human) | | | Kato *et al*., 2009 [238] |

| | | | | |
|---|---|---|---|---|
| Free 3-$NO_2$Y, Free 3-ClY | Premature birth | LC-MS/MS (MRM) | Urine (human) | Kuligowski *et al*., 2014 [241] |
| free 3-$NO_2$Y, total 3-$NO_2$Y | Vasculopathy in Fabry disease | Isotope-labeled standards, LC/MS/MS (MRM) | Plasma (human), plasma (rat) | Shu *et al*., 2014 [240] |
| free 3-$NO_2$Y total 3-$NO_2$Y | Arthritis | LC-MS/MS (MRM) | plasma (rat) | Nemirovskiy *et al*., 2009 [368] |

For each modification type in the referenced study, the table above shows the implicated disease, the MS method, the sample type, the protein type, and whether the referenced study reported oxidation sites. SNO = S-nitrosylation; MetO = methionine sulfoxide; MetO2 = methionine sulfone; 3-$NO_2$Y=3-nitrotyrosine; 3-ClY= 3-chlorotyrosine; 3-BrY = 3-bromotyrosine; di-BrY = dibromotyrosine; di-Y = dityrosine.

# 1.4 The phosphatase PTEN

## 1.4.1 Introduction

PTEN (phosphatase and tensin homolog deleted on chromosome 10) is a lipid and protein phosphatase that has attracted significant interest from the biomedical research community over the last two decades. The *PTEN* gene has been found mutated or deleted in many cancers, and its phosphatase product has been implicated as tumour suppressor by many authors over time [374-382].

Functionally, PTEN is a dual-specificity phosphatase that can dephosphorylate both lipids and proteins. As a lipid phosphatase, PTEN dephosphorylates phosphatidylinositol (3,4,5)-trisphosphate (PtdIns(3,4,5)$P_3$) resulting in the production of PtdIns(4,5)$P_2$ [383], while as a protein phosphatase PTEN dephosphorylates Ser, Thr and Tyr phosphoproteins [384]. Given the importance of PTEN in tumour suppression, a great deal of research effort has been expended to characterize PTEN structure, function, signaling networks, and regulation, in order to understand the mechanisms underlying cancer and design therapeutic strategies [385].

PTEN belongs to the protein tyrosine phosphatases (PTPs) family, a structurally diverse group of enzymes that share a highly conserved signature motif in their active site, which contains a reactive cysteine residue. PTPs dephosphorylate phosphoproteins with a common catalytic mechanism, based on a two-stage phosphate monoester hydrolysis involving the active site reactive cysteine [386]. Studies have shown that the thiolate anion of the active site cysteine is essential for the catalytic activity of these proteins, and it is susceptible to oxidation [387]. Together with tyrosine kinases, PTPs control tyrosine phosphorylation, which is one of the key mechanisms in signal transduction, and are therefore implicated in the modulation of many fundamental cellular processes, including cell cycle control, gene regulation, cell migration, cell adhesion, cell differentiation and cell proliferation [388-391]. Because of their importance in cell signaling, there is increasing interest in the study of the regulatory mechanisms of PTPs. The reversible ROS-induced oxidation of the active site cysteine thiolate has emerged as a putative regulatory mechanism of PTPs activity, and accumulating lines of evidence are proposing ROS as important mediators in the signaling pathways controlled by PTPs [392]. As PTEN is a central element of many signaling processes in disease, investigating its redox

regulation has critical implication for understanding the mechanisms underlying certain conditions and developing novel therapeutic intervention.

### 1.4.2 The structure of PTEN: functional and regulatory implications

PTEN is made up of 403 amino acids and consists of two major structural domains: a phosphatase domain (PD), which contains the active site pocket of the protein with the catalytic cysteine (Cys124); a C2 domain, which binds the phospholipid membrane in an electrostatic ($Ca^{2+}$-independent) manner, exposing the active site to the substrate PtdIns(3,4,5)$P_3$. Additionally, PTEN includes a PtdIns (4,5)$P_2$-binding N-terminal module (PBM), and a C-terminal region (or tail) containing a PDZ (PDS-95/Disc-large/Zo-1)-binding motif corresponding to the protein C-terminus.

PTEN exists in mammalian cells either as a monomer or as part of multiple high molecular weight complexes (> 600 kDa), often referred to as PTEN-associated complexes (PAC) [393]. The recruitment of PTEN into PAC appears to be important for PTEN subcellular localization and downstream signaling regulation, although the biological significance of PAC is still under investigation [393-396].

The crystallographic structure of PTEN was solved by Lee *et al* in 1999, and it is the only one available to date [383]. The resolved residues (amino acids 7-353) include both the phosphatase domain (amino acids 14-185), and the C2 domain (amino acids 190-350) [383,397]. Residue 1-6, 286–309, and 354-403 represent unstructured or loosely folded regions, that have been deleted to allow crystallization and are yet to be crystallized [383,398]. Additionally, residues 7–13, 282–285, 310-312, and 352-353 are believed to be disordered and are not yet resolved [383,399]. Figure 1.14 shows the truncated PTEN crystal structure (residues 7-353) with highlighted key regions referred to in the text, and the linear domain map including both crystalized and unresolved regions.

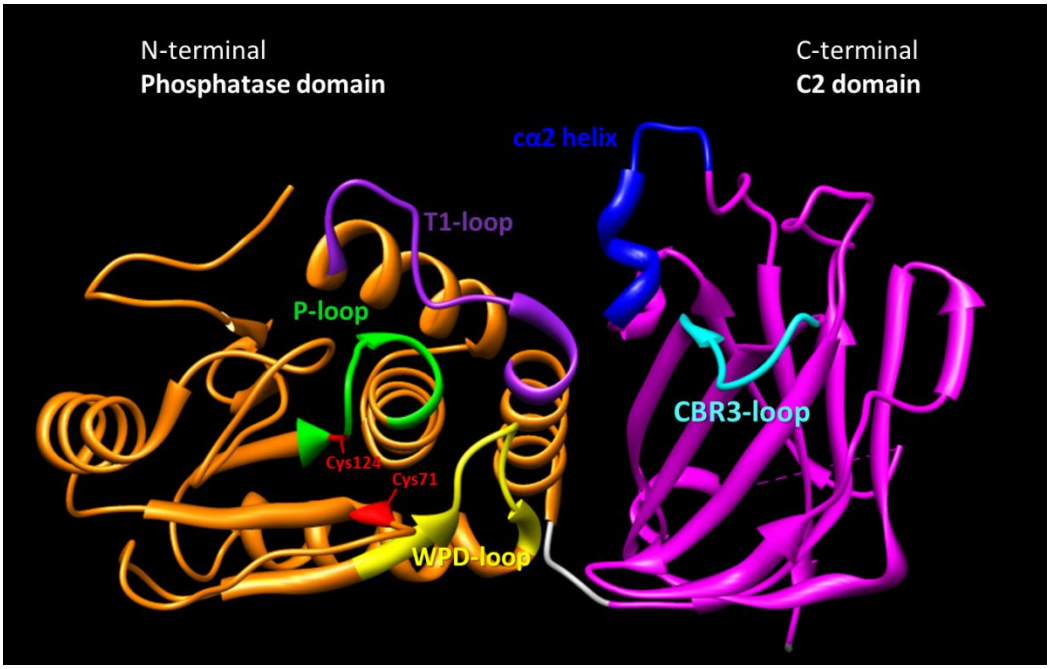


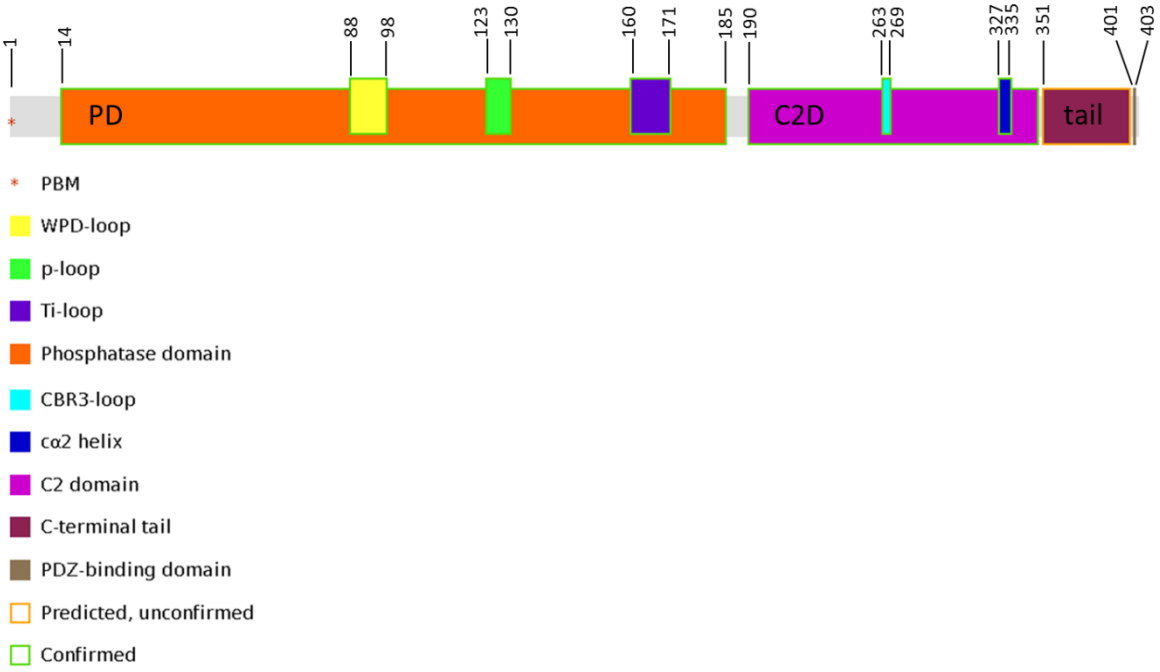


**Figure 1.14 Domain structure and organization of PTEN**

The phosphatase PTEN consists of two core domains: the phosphatase domain (amino acids 14-185, in orange), and the C2 domain (amino acid 190-350, in magenta). The phosphatase domain includes the active site pocket of PTEN, which consists of: the WPD-loop (amino acids 88-98, in yellow), the p-loop (amino acids 123-130, in green), and the T1-loop (amino acids 160-171, in purple). Cys124 in the p-loop and the nearby Cys71 (both shown in red in the 3D crystal structure) form a disulfide bond that reversibly inactivates PTEN upon reaction with $H_2O_2$. The C2 domain includes the CBR3-loop (amino acid 263-269, in cyan) and the cα2 helix (amino acids 327-335, in blue). Additionally, PTEN includes

a PBM region, a C-terminal tail and a PDZ-binding motif which are yet to be resolved. The linear domain map was drawn using the visualization program DomainDraw, available as a webserver at http://domaindraw.imb.uq.edu.au [400]. The truncated PTEN crystal structure (lacking residues 1-13, 282-312 and 351-403)-was obtained by fetching the Protein Data Bank (PDB) ID 1D5R.

#### *1.4.2.1 The N-terminal module*

The PtdIns(4,5)$P_2$-binding N-terminal module (PBM, amino acids 1-13), which includes not yet resolved and disordered residues, is a short regulatory region that contains a conserved phosphoinositide-binding motif.

The PBM region plays a fundamental role in regulating PTEN intracellular localization as it selectively binds PtdIns(4,5)$P_2$ molecules, allowing PTEN to anchor the plasma membrane, which is the site of PTEN phosphatase activity [401]. Accumulating lines of evidence also suggest a role for the PBM region in regulating PTEN phosphatase activity. This is supposedly achieved via an intramolecular interaction between the PBM and PTEN active site [402,403], although other authors have also proposed that PtdIns(4,5)$P_2$ allosterically regulates PTEN conformation (therefore controlling its phosphatase activity) upon PBM binding [402,404].

The N terminal module is also important for PTEN subcellular localization as it contains residues that are part of a nuclear localization signal (NLS, residue 8-32), essential for the nuclear-cytoplasmic shutting of PTEN [405,406] and cationic residues Arg11 and Lys13 required for phospholipid membrane binding [407]. In addition, Lys13, which is required for the PtdIns(4,5)$P_2$-mediated activation of PTEN [408], was also found mutated in cancer [409].

#### *1.4.2.2 The phosphatase domain*

The phosphatase domain (PD, amino acids 14-185) consists of five stranded β-sheets surrounded by six α-helices (two on one side and four on the other), a structure similar to that of the dual specificity phosphatase VHR (vaccinia H1-related phosphatase) [410]. The PD is primarily responsible for PTEN catalytic activity, but is also required for PTEN subcellular localization.

The PD includes the active site pocket of PTEN, at the bottom of which is mapped the highly conserved PTPs signature motif H-C-X-X-G-X-X-R (amino acids 123-130), that forms a loop known

as p-loop or p-catalytic loop [411]. When at neutral pH, this motif exists as a thiolate anion and contributes to the formation of a thiol-phosphate intermediate, which is essential for PTEN catalytic activity [412]. Compared to other PTPs, the p-loop sequence of PTEN (H-C-K/R-A-G-K-G-R) is unique because it contains two lysines (Lys125 and Lys128) that give a positive charge to the active site pocket, explaining the selectivity of PTEN for extremely acidic substrates such as PtdIns(3,4,5)$P_3$ [413]. Moreover, the active site pocket is larger than that of similar PTPs, a feature that could be important for accommodating phosphoinositide substrates [383]. Residues Cys124 and Arg130 in the p-loop are essential for PTEN phosphatase activity [383], while His123 and Gly127 are important for the conformation of the loop [414]. More recently, mutagenesis studies have shown that tumour-related mutations of each one of the p-loop residues is capable of causing a complete loss of PTEN activity (except for Ala126 and Lys128, the mutation of which that are associated with a partial inactivation) [415]. In addition, tumour-related mutation of His123 to Tyr produced an inactive PTEN mutant that was also incapable of tumour suppression [416]. It has also been shown that the histone acetyltransferase PCAF (p300/CBP-associated factor) is responsible for the acetylation of PTEN on Lys125 and Lys128 in the p-loop, and this results in decreased PTEN activity, Akt activation, and increased cell cycle progression [417].

The walls of the active site pocket are delimited by the "WPD" loop (or pβ4-α3 loop, amino acids 88–98) and the "T1" loop (or pα5-α6 loop, amino acids 160–171), which are less conserved than the p-loop [415]. The residue Asp92 in the WPD loop seems to be important for PTEN catalytic activity as it might function as a general acid in the catalysis process, although this is currently under debate [415,418]. WPD-loop residues that were found mutated in tumours include Asp92 and His93, which were found to cause a dramatic loss of PTEN function [409,415], as well as Pro95 and Pro96, which are reported to cause a partial [415] or complete [409] inactivation of PTEN. T1 loop residues Asp162, Gly165, Val166, Thr167, Ser170 and Gln171, which were also found mutated in cancer, are associated with partial or full inactivation [383,409,415].

Other key residues mapped in the phosphatase domain of PTEN were found mutated in tumours and are required for PTEN catalytic activity. These include Ala34, Met35, Gly36, Leu42, Gly44, Asn48, Tyr68, Arg121, Ile122, Thr131, and Leu181 which are associated with a complete loss of PTEN catalytic activity [409,415], and Tyr16, Ile33, His61, Pro96, Tyr155, which are required for

PTEN activity and also thought to be important for PTEN stability [409]. Additional mutational hotspots in PTEN phosphatase domain that are associated with cancer include Arg173, which, together with the p-loop residue Arg130, is the most frequently mutated residue of PTEN [419,420].

Some key residues in the phosphatase domain of PTEN are also important for PTEN membrane association, which occurs via an electrostatic interaction with the phosphatidylserine (PS), which is an abundant lipid component in the plasma membrane [421]. Residues Lys161, Arg162, Lys163 and Arg164 in the TI loop make up a cationic motif (KRKR) that has been shown to be required for PTEN membrane binding [407]. In addition, Arg15, which has been repeatedly reported to be essential for PTEN catalytic activity and tumour suppression [406,409,422], forms a cationic patch (with Arg11 and Lys13 on PBM region and Arg14 on the PD), which is also implicated as required for PTEN membrane binding [407].

Finally, in studying the effect of altered redox conditions on PTEN, it was revealed that Cys124 in the p-loop of the active site pocket forms a disulfide bond with Cys71 (located near the active site pocket), typically upon $H_2O_2$ oxidation, causing reversible inactivation of the phosphatase [423]. These findings have a number of important implications for PTEN redox regulation and signaling pathways, and are further discussed in Section 1.4.3.3.

#### *1.4.2.3 The C2 domain*

The C2 domain (amino acids 190-350) consists of two antiparallel β-sheets linked by two short α-helices. The main function of the C2 domain of PTEN is to bind the plasma membrane, transporting the active site of PTEN to the membrane-bound PtdIns(3,4,5)$P_3$, where PTEN can dephosphorylate it.

The C2 domain of PTEN differs from that of other membrane-interacting proteins because it does not have calcium-binding activity [383]. The C2 domain lacks the $Ca^{2+}$-binding regions CBR1 and CBR2 that are typically found in other C2 domains, but includes the CBR3 loop (amino acids 263-269), that is required for is $Ca^{2+}$-independent membrane binding [383,403]. The C2 domain binds the membrane by associating with phosphatidylserine (PS) in the plasma membrane via the CBR3 loop [421]. CBR3 contains a series of positively charged residues (Lys260, Lys263, Lys266, Lys267, Lys269) that give an overall positive charge to the region and are required for the phospholipid membrane binding[422]. Along with the CBR3, another motif included in the C2 domain of PTEN

that is required for membrane binding is the cα2 helix (amino acids 327-335). Positively charged residues of the cα2 helix (Lys327, Lys330, Lys332, and Arg335) are involved in the stabilization of the PTEN interaction with the plasma membrane [402]. In addition, Lys266 and Lys289 of the C2 domain are modified by the small ubiquitin-like proteins, small ubiquitin-related modifier 1 (SUMO1) and SUMO2, which induce a post-translational modification known as SUMOylation, which controls PTEN membrane association [424] and nuclear localization [425].

A number of mutagenesis studies revealed an essential role for key residues within the C2 domain in PTEN growth suppression and/or phosphatase activity. These include: cα2 helix residues, which are associated with decreased affinity of PTEN for phospholipid vesicle and reduced tumour suppression, although the mutants retained phosphatase activity [383]; Tyr240 and Tyr 315, which decreased both PTEN tumour suppression and phosphatase activity [426]; Asp252, which was found mutated in cancer, and is implicated as important for PTEN activity and stability [409]; Lys289, which plays an important role in PTEN tumour suppression, stability and nuclear localization [427], and was found mutated in tumours [409]; Val343, which was found mutated in cancer and generated a total loss of function [415]; and Leu345,which reduced both the growth suppression and the phosphatase activity of PTEN [416].

#### *1.4.2.4 The C-terminal tail*

The C terminal region or tail (amino acids 351-400), which contains residues that are yet to be crystallized, and is important for PTEN phosphatase activity, stability, tumour suppression function, membrane association and protein-protein interactions [397,428,429]. Compared to any other 50-amino acid stretch within PTEN, the C-terminal tail shows lower mutability, suggesting a critical biological function that is evolutionarily conserved [397].

Many studies have revealed that the C-terminal tail is required for the regulation of PTEN stability and phosphatase activity via phosphorylation of its residues Ser362, Thr366, Ser370, Ser380, Thr382, Thr383, and Ser385 [430-433]. Phosphorylation of Ser370 and the cluster Ser380-Ser385 is catalyzed by the casein kinase 2 (CK2), while glycogen synthase kinase 3 (GSK3) is responsible for the phosphorylation of Ser362 and Thr366 [429]. Phosphorylation of the cluster Ser380-385 has been shown to reduce PTEN activity and in general is associated with loss of PTEN function [428,429],

while phosphorylation of Thr366 negatively regulates protein stability and tumour suppressing phenotypes [429,434]. In addition, the tail contains two tandem PEST (rich in Pro, Glu, Ser and Thr) motifs (amino acids 350-375 and 379-386), which have been shown to be involved in the proteolytic degradation, protein stabilization, phosphatase activity, and subcellular localization [416,435].

The C-terminal tail is also important for the dynamic regulation of PTEN membrane association. There is evidence showing that the tail acts as an auto inhibitory domain controlling PTEN membrane binding with an open/closed conformation model controlled by phosphorylation [435,436]. According to this model, an intramolecular interaction between the C-terminal tail and the phosphatase and the C2 domain of PTEN when C-terminal tail is phosphorylated (likely at Ser380, Thr382, Thr383, and Ser 385 in the second PEST motif), induces a closed conformation that inhibits PTEN catalytic activity and membrane binding [403,436]. It was also reported that the recruitment of PTEN into high molecular weight complexes (PTEN-associated complexes) is inhibited by the phosphorylation of the tail, with effects on PTEN membrane translocation and function [394-396]. Phosphatase activity and protein-membrane interaction are restored by dephosphorylation of the tail residues. This results in the C-terminal tail being released from the phosphatase and C2 domains, which can bind the plasma membrane by means of electrostatic interactions.

#### *1.4.2.5 The PDZ motif*

Another interesting feature of the C-terminal tail of PTEN is the functional PDZ-binding motif, a three-amino acids unresolved sequence located at the far C-terminus of the protein (residues Thr401-Lys402-Val403).

The PDZ-binding motif of PTEN controls the association of PTEN proteins containing PDZ domains such as membrane-associated guanylate kinase with inverted orientation (MAGI) proteins [437,438], and proteins constituting the PTEN-associated complexes [394].

The phosphorylation-induced intramolecular interaction between the C-terminal tail and the phosphatase and C2 domains seems to masks the PDZ-binding motif due to the closed conformation induced, which supposedly prevents PDZ-mediated protein interactions, such as those implicated in PTEN function and subcellular localization [395]. However, the deletion of PDZ-domain did not show a significant effect on either PTEN membrane targeting [407] or PAC complex assembly [393], which suggests that the phosphorylation-mediated regulation of PTEN membrane recruitment does not

involve the PDZ domain. In addition, it has been shown that CREB-binding protein (CBP) is responsible for the acetylation of PTEN at Lys402 in the PDZ-binding motif, and that such mechanism is associated to increased binding of PDZ domain-containing proteins [438]. Deacetylation of PTEN is primarily operated by Sirt1, which appears to play a tumour promoting role, despite being implicated in extended longevity [439].

### 1.4.3 The role of PTEN in cell signaling

#### *1.4.3.1 Cancer -related pathways*

PTEN has been identified as central regulatory element in many cellular processes, including cell growth, migration, apoptosis, adhesion and DNA repair [440,441]. Much of the research into the cellular role of PTEN has been focused on its tumour suppression function that takes place via inhibition of the PI3K/Akt pathway [382]. Important studies have shown that the PI3K/Akt pathway is associated with both apoptosis and cancer cells proliferation and survival [442,443]. The intracellular protein Akt (also known as protein kinase B, PKB) plays a central role in this pathway as it controls the signal responsible for the modulation of many cellular functions, including cell cycle regulation, cell growth, apoptosis, angiogenesis, protein synthesis, transcription and proliferation among others [444,445]. The activation of Akt is achieved through a multistage process, involving the recruitment of the protein to the plasma membrane and its activation via phosphorylation operated by specific protein kinases. Initially, Class IA phosphoinositide 3-kinases (PI3Ks) catalyze the formation of PtdIns(3,4,5)$P_3$ upon activation of specific growth factors receptors tyrosine kinases (RTKs) [445]. The PtdIns(3,4,5)$P_3$ binds to Akt at the plasma membrane, and this activates the phosphoinositide-dependent kinase PDK1 to phosphorylate Akt at Thr308 on the catalytic domain of the protein [444,446]. The phosphorylation of the Ser473 residue in the C-terminal is also required for the full kinase activation [447]. There is evidence suggesting that the mTOR-RICTOR complex is the major kinase responsible for the phosphorylation of Akt at Ser473, but other kinases might be involved as well [448,449]. The activation of Akt results in increased kinase activity towards pro-apoptotic factors, including the Bcl-2 family member BAD (Bcl-2-associated death promoter) [450], caspase-9, GSK-3, and many others [428]. In addition, Akt activates mammalian target of rapamycin (mTOR) [451],

which promotes translation initiation, a process linked to cancer [452]. Extensive work has been done to demonstrate the involvement of PTEN in the Akt pathway and to elucidate the mechanism through which PTEN exerts its anti-tumorigenic function [453,454]. PTEN specifically dephosphorylates the signaling intermediate PtdIns(3,4,5)$P_3$ to PtdIns (4,5)$P_2$, therefore suppressing the PI3K-dependent signaling cascade that leads to the activation of Akt (Figure 1.15).

Furthermore, many studies have shown a close relationship between the Akt/PI3K/PTEN pathway and the signaling pathways of p53 (tumour protein 53, TP53), another tumour suppressor [455]. Growth factor-activated Akt promotes MDM2 (mouse double minute 2 homolog) translocation to the nucleus, where MDM2 interacts with p53 and initiate its proteasomal degradation [456,457]. There is evidence suggesting that by antagonizing the Akt/PI3K pathway, PTEN protects p53 from MDM2-mediated proteosomal degradation, therefore promoting p53 tumour suppressing function [457].

While the tumour suppression function of PTEN has been mainly associated with its lipid phosphatase activity, accumulating lines of evidence suggest that PTEN protein phosphatase activity plays an important role in cell cycle regulation [458]. PTEN can dephosphorylate the integrin-signaling protein FAK (focal adhesion kinase), thereby reducing focal adhesion formation and blocking the downstream activation of the p130 Crk-associated substrate (p130CAS), which promotes cell migration and growth [459]. In addition, PTEN dephosphorylates the integrin Shc/Grb2/Sos complex, blocking the activation of the MAPK/ERK pathway [460], which regulates cell motility and migration [461] and is implicated in cell growth and cycle progression [462,463]. There is also evidence that PTEN may autodephosphorylate its C-terminal tail at Thr366, with important implications for PTEN-mediated tumour suppressing phenotypes [434].

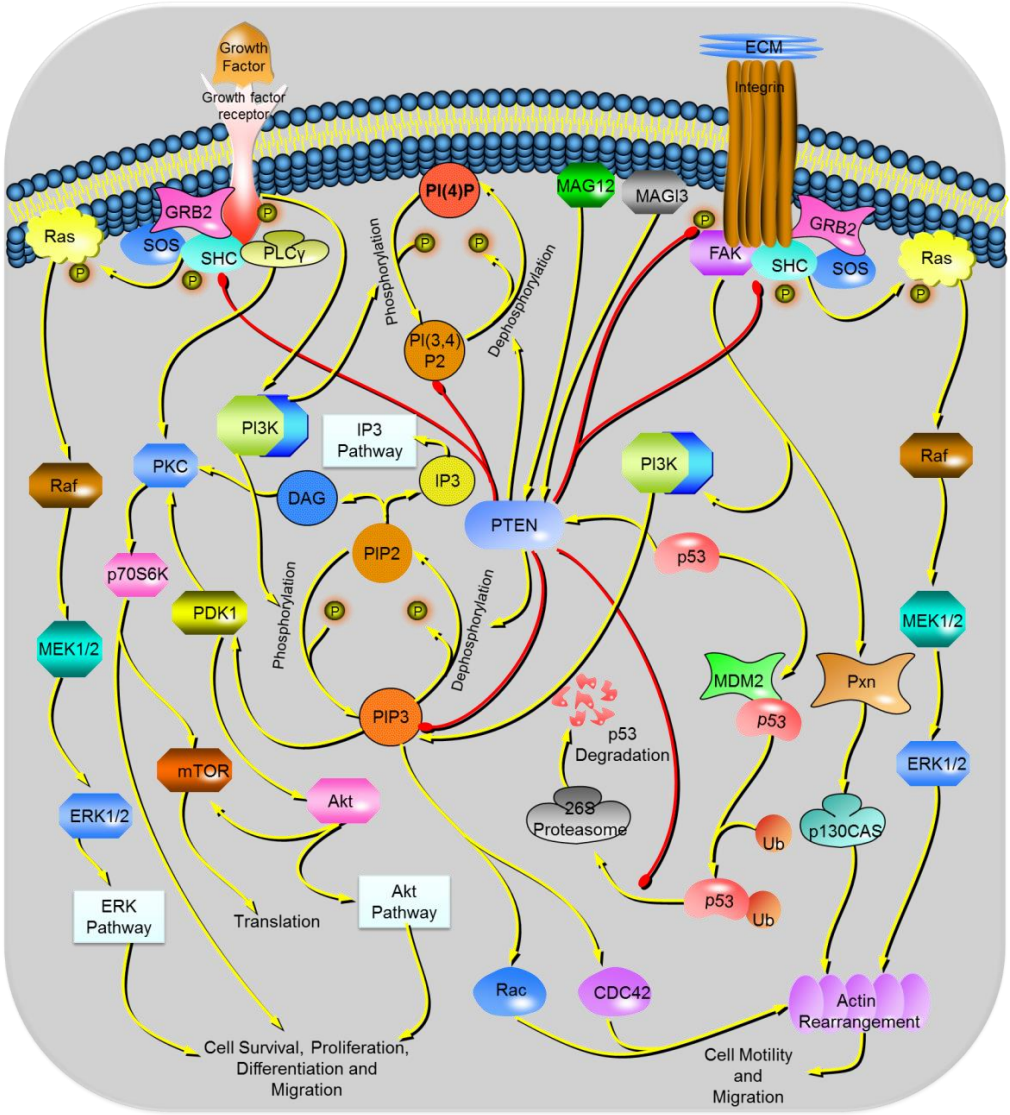


**Figure 1.15 Cellular networks involving PTEN tumour suppression activity**

PTEN is involved in a number of cancer-related signal transduction pathways by means of both its lipid phosphatase and protein phosphatase activity. Picture modified from editable pathway map obtained from SABiosciences.

### *1.4.3.2 Regulation of PTEN by protein-protein interactions*

Many PTEN protein-protein interactions (PPIs) have been identified and characterized in *Homo sapiens* (Appendix, Section 8.4). There is growing evidence that PPIs play a relevant role in the regulation of PTEN function, stability and subcellular localization, and it is likely that the molecular dynamics controlling these interactions are modulated in altered cellular conditions such as those found in disease states [445].

Many PTEN-interacting proteins have been shown to activate PTEN by controlling its subcellular localization, regulating its stability and preventing its degradation. PTEN interacts with RhoA-

associated kinase (ROCK) which can exert positive modulation of PTEN enzymatic activity and promote its recruitment to leukocytes membrane by phosphorylating its C2 domain [427,464]. PTEN has been shown to interact with melanocortin-1 receptor (MC1R) and Rak kinase (also known as Fyn-related kinase, FRK), which are both involved in preventing PTEN degradation by antagonizing its polyubiquitination mediated by E3 ligases [465,466]. PTEN has also been shown to interact with PICT-1 (protein interacting with carboxyl terminus 1) which plays a role in the regulation of PTEN C-terminal tail phosphorylation and degradation [467]. PICT-1 binds the C-terminus of PTEN and promotes its phosphorylation by CK2 (casein kinase 2) and GSK3β (glycogen synthase kinase 3β), which has been shown to be associated with increased protein stability [432]. PTEN also interacts with members of the membrane guanylate-kinase inverted (MAGI) family, such as MAGI-2, which can prevent PTEN degradation by favoring its recruitment into high molecular complexes [468]. Other studies have further demonstrated that PTEN-MAGI-2 interaction also results in PTEN stabilization, and leads to the inhibition of cell proliferation and migration [469]. Another important PTEN direct interaction having a significant effect on PTEN activity is he EGF-dependent association with the PI3 kinase regulatory subunit p85a, which appears to promote a positive regulation of PTEN lipid phosphatase activity [470]. PTEN has also been shown to bind the tumour suppressor p53 at its C2 domain, resulting in to increased p53 levels, which in turn leads to up-regulation of PTEN own expression, as p53 can also regulates PTEN transcription [471,472].

A number of proteins were found to interfere with PTEN phosphatase activity and tumour suppressing function by direct interaction. Among those, PtdIns(3,4,5)$P_3$-dependent RAC exchange factor 2a (P-REX2a), a component of the PI3K/Akt pathway which is overexpressed in cancer cells, has been shown to bind PTEN inhibiting its lipid phosphatase activity increasing Akt phosphorylation and tumour growth [473]. Likewise, the shank-interacting protein–like 1 (SIPL1) was also found to abrogate PTEN-mediated tumour suppression and inhibiting its lipid phosphatase activity by direct interaction, although no concomitant Akt activation was reported [474]. Another PTEN-interacting protein involved in inhibition of PTEN activity is α-mannosidase 2C1 (MAN2C1), which is also upregulated in cancer, and appears to negatively regulate PTEN phosphatase activity and disturb its subcellular localization [429]. In addition, PTEN is negatively regulated by its interaction with DJ-1 (also known as Parkinson protein 7, PARK7), a tumour-promoting protein that is capable of inhibiting

PTEN catalytic activity, resulting in increased cell proliferation and apoptosis due to enhanced Akt phosphorylation [475].

#### *1.4.3.3 Redox regulation of PTEN*

The effect of ROS-mediated oxidation on PTEN catalytic activity has important implications for both PTEN tumour suppressing function and signaling role in the cell. Many peptide growth factors that are responsible for the activation of Akt such as insulin, the platelet-derived growth factor (PDGF) receptor (PDGFR) and epidermal growth factor (EGF) receptor (EGFR), also trigger the generation of ROS, which can inactivate cytosolic PTEN, therefore blocking its tumour suppression activity [144]. The transmembrane NADPH oxidase Nox4 (or Nox1), has been identified as the main source of $H_2O_2$ production in non-phagocytic cells initiated by growth factors stimulation [476]. Nox4 has been shown to be activated by PtdIns(3,4,5)$P_3$, which triggers the increased generation of $H_2O_2$ resulting in the oxidation of PTEN [144]. As the disulfide bond between Cys71 and Cys124 is formed in PTEN active site upon oxidation, the lipid phosphatase activity of PTEN is inhibited, resulting in the accumulation of PI3K-generated PtdIns(3,4,5)$P_3$ and consequent Akt activation. PtdIns(3,4,5)$P_3$ can be dephosphorylated by both PTEN and 5-phosphatases, but it is likely that accumulating PtdIns(3,4,5)$P_3$ in oxidizing cellular conditions is primarily due to PTEN inactivation [144].

The reversible character of the oxidative-induced disulfide bond in the active site of PTEN is particularly important for the redox regulation of the phosphatase and may be critical as a redox-sensing mechanism for the regulation of various cellular processes, including those linked to its tumour suppressing function. Important publications have shown that PTEN is inactivated when treated with oxidizing agents *in vitro*, as well as in cells exposed to oxidative stress conditions [423,477]. Reversible inactivation of PTEN has been shown upon hydrogen peroxide oxidation, and results in the formation of a disulfide bond between Cys71 and the active site Cys124, in the N-terminal PD of the protein [144]. It has been reported that the thioredoxin system is responsible for the re-reduction of the $H_2O_2$-induced Cys71-Cys124 disulfide with a NADPH-dependent thiol-disulfide exchange mechanism. The antioxidant thioredoxin-1 (Trx) binds the C2 domain of PTEN and is capable of completely restoring its activity following $H_2O_2$-mediated inactivation [144,423]. Interestingly, other authors have shown that in cells treated with $H_2O_2$, oxidized thioredoxin-1 forms a

disulfide bond with Cys212 in the C2 domain of PTEN, causing PTEN inactivation and promoting tumorigenesis due to increased Akt activation [478]. The interaction between PTEN and the thioredoxin peroxidase peroxiredoxin-1 (Prdx1) has also been proposed as a possible mechanism to protect PTEN from hydrogen peroxide-induced reversible inactivation, therefore preserving its tumour suppressing function [479]. Conversely, with high concentration of $H_2O_2$ the interaction PTEN/Prdx1 was reduced, possibly due to oxidative damage to Cys51 of Prdx1, resulting in the dissociation of the complex, as this residue may be exposed to further oxidation when Prdx1 interacts with PTEN [480]. Other authors have investigated the interaction between PTEN and its negative regulator and tumour promoter PARK7, which was found increased in mammalian cells treated with $H_2O_2$, in accordance with other lines of evidence showing an existing relationship between tumorigenesis and excess ROS production [481].

Additionally, S-nitrosylation of Cys83 was also reported in PTEN following NO-mediated oxidation, with inhibition of PTEN activity, activation of Akt and increased cell survival [482]. Unlike $H_2O_2$, NO has not been shown to induce the formation of Cys71-Cys124 disulfide bond in the active site of PTEN, suggesting different redox-regulation mechanisms depending on the reactive molecules involved [482].

### 1.4.4 Aims of the work presented in this thesis

With growing interest for the role of ROS in the onset and progression of age-related diseases such as cancer [168], it is becoming increasingly important to understand the structural and signaling dynamics of redox-sensing proteins such as PTEN. Although PTEN structure, function and role in signaling pathways have already been characterized to some extent, few studies have addressed its signaling role and modification status under oxidative stress conditions.

The research elaborated in this PhD thesis focuses on the analysis of the functional effect of ROS-mediated oxidation on PTEN structure and interacting partners. The experimental strategies implemented have been designed to investigate a signaling and damaging role of reactive species in relationship to PTEN protein function. Three research studies are described in this thesis and are summarized below:

1) **Mass spectrometry generated quantitative mapping and functional proteomics of PTEN oxidative post-translational modifications (Chapter 3).** In this *in vitro* study is described the oxPTMs mapping of irreversibly oxidized PTEN and its relationship to its drop in catalytic activity. The aim of the research elaborated in this study was to investigate the effect of inflammation-mimicking HOCl oxidizing conditions on the modification state of the protein, in order to identify key residues that are best correlated with PTEN phosphatase activity.
2) **Analysis of PTEN protein-protein interactions in its reduced and oxidized form by GSH-affinity enrichment and label-free MS quantitation (Chapter 4).** This *in vitro* study addressed the investigation of the effect of $H_2O_2$-mediated reversible oxidation on PTEN protein-protein interactions and oxPTMs. The aim of the study was to characterize and compare the protein-protein interaction of an active (reduced) and inactive (disulfide) PTEN in order to elucidate the role of ROS in modulating the signaling pathways involving PTEN.
3) **Validation and in vivo profiling of PTEN protein-protein interactions in proteomics workflows (Chapter 5).** This chapter contains *in vivo* experimental work carried out to follow up on the *in vitro* study described in Chapter 4. The aim of the study was to perform an *in vivo* validation of selective PTEN interactors detected with the method described in Chapter 4, and to analyze the interaction profile of those PTEN-binding proteins under oxidative stress conditions *in cellulo*.

# Chapter 2. General Material and Methods

# 2.1 Introduction

### 2.1.1 Chapter contents

This chapter describes the general procedures carried out for the experimental work presented in this thesis, including molecular biology techniques, protein expression and purification, biochemistry techniques, mass spectrometry, and bioinformatics tools. Experimental methods specific to individual chapters (Chapter 3, 4 and 5) are described separately in the appropriate Materials and Methods section (Sections 3.3, 4.3, and 5.3).

# 2.2 General information

## 2.2.1 Health and Safety

Risk assessment forms COSHH (Control of substances hazardous to health) and/or MSDS (material safety data sheet) form have been used as reference for all the health and safety implications for every reagents and protocols used in the laboratory, including commercial kits and stock chemicals. For every experiment performed, the corresponding COSHH form was carefully read and signed before commencing any laboratory work.

Biological waste such as tissue culture waste and bacterial cultures waste was disinfected with 1% Virkon before disposal. All laboratory equipment used with all kind of biological samples was disposed for incineration. Chlorinated and non-chlorinated solvent waste was disposed via the appropriate route.

Ethical implication were also considered regarding samples, protocols and reagents implemented and assessed alongside health and safety matters.

## 2.2.2 Sterility measures

All reagents, glassware, pipet tips, tubes, and other material used for sterile applications were autoclaved using the Aston University autoclave service. Large laboratory equipment and laboratory furniture used for sterile applications were sterilized with 70% ethanol.

## 2.2.3 Reagents

All reagents were stored at recommended temperature and conditions. All reagents were purchased from Fisher Scientific (Loughborough, UK), unless otherwise indicated. All solvents used were of LC-MS grade and Milli-Q water was used at all times. All solutions where solvent is not specified were prepared in Milli-Q water.

All described reactions and experimental procedures were carried out under normal atmospheric conditions and at room temperature unless otherwise specified. All laboratory equipment was operated under normal atmospheric conditions and at room temperature unless otherwise specified.

# 2.3 Cell Culture

### 2.3.1 Cells propagation

HCT116 cells (wild-type) were obtained by Rudiger Woscholski's lab at ICL (Imperial College London).

### 2.3.2 Sterility measures

All tissue culture operations were performed strictly under a Class 2 Microbiological Safety cabinet (MSC advantage, Thermo Fisher Scientific, Hemel Hempstead, UK) under laminar flow conditions. The work surface inside the cabinet was sprayed with 70% ethanol before use. Water baths were sanitized using AQUASAN sanitizing tablets (Guest Medical Limited, UK). All laboratory equipment, reagents, and tissue culture vessels to be used inside the cabinet were sprayed with 70% ethanol before use.

### 2.3.3 Cells growth and maintenance

Tissue culture operations were performed using disposable sterile Serological pipettes (Appleton Woods, Birmingham, UK) controlled by a motorized pipetting controller (Fisherbrand, UK). HCT116 cells were cultured in canted neck, tissue culture-treated, nonpyrogenic, sterile flasks (Appleton Woods, Birmingham, UK), grown in Dulbecco's modified Eagle medium (DMEM, 41966, Life technologies, Paisley, UK) supplemented with 10% fetal bovine serum (Life technologies, Paisley UK) and maintained at 37ºC, 5% $CO_2$ in the controlled incubator Sanyo MCO-18AIC (Sanyo, UK), equipped with vapor withdrawal $CO_2$ cylinders (BOC, UK). Cell confluency and health were observed using the inverted microscope Olympus CK2 (Olympus Optical Co., Japan). Phosphate buffered saline (PBS) tablets (Sigma-Aldrich Chemical Co., Poole, UK) were used to prepare 0.01 M phosphate buffer pH 7.4, 0.0027 M potassium chloride and 0.137 M sodium chloride, used to wash the cell layer. For harvesting, 0.25% Trypsin EDTA phenol red (25200-056, Life technologies, Paisley, UK) was

added to the cell layer, incubated for 10 minutes with occasional shaking. Next, the cells were resuspended in fresh medium for sub-culturing. Before use, Growth Medium, Trypsin EDTA and fetal bovine serum were warmed in a water bath (Jb Nova Water Bath, Grant, UK) set at 37 ºC.

### 2.3.4 Cell counting

50 µL of cell suspension were mixed with 100µl PBS and 50µL 0.4% Trypan Blue (Sigma-Aldrich Chemical Co., Poole, UK). 20µL of this mixture was added onto haemocytometer (Superior, Germany), and the live cells counted with a tally counter (Uniwise group, China).

### 2.3.5 Cell storage and recovery

The cell suspension was spun down at 500xg at room temperature in an Eppendorf 5810R (Eppendorf UK Ltd, Stevenage, UK) centrifuge, the medium removed and replaced with FBS (Life technologies, Paisley UK), supplemented with 10% DMSO and pre-warmed to 37 ºC. Next, the cell suspension was aliquoted in sterile cryogenic vials (Fisher, US), transferred to -80°C overnight, and stored in liquid nitrogen. For thawing, cryovials were removed from the liquid nitrogen, quickly placed in 37ºC water bath while swirling the tube, and the cell suspension pipetted out into tissue culture flask containing pre-warmed DMEM medium, supplemented with 10% FBS. The cell vessel was placed in the controlled incubator, and the culture medium was changed after 24 hours.

# 2.4 Molecular Biology

### 2.4.1 Sterility measures

All microbiology work that needed sterile conditions was performed close to a Bunsen burner flame.

### 2.4.2 Source of Plasmid expression systems

The plasmid vector systems PGEX-4T1 containing the Glutathione S-transferase (GST)-PTEN cDNA and PEGFP-C1 containing the Enhanced Green Fluorescent protein (EGFP) PTEN cDNA were obtained from Rudiger Woscholski's lab at ICL (Imperial College London). The plasmid sequences and maps are shown in the Appendix (Section 8.1).

### 2.4.3 Preparation of Calcium competent E.coli DH5α cells

1L of bacterial growth medium Luria Broth (LB) was prepared using 5g of yeast extract, (Fisher Scientific, UK), 10g of bacto-tryptone (Fisher Scientific, UK), 10g NaCl (Sigma-Aldrich Chemical Co., Poole, UK), pH 7.5, made up to 1L with Milli-Q water. A 5 mL overnight *E.coli* cell culture was set up and grown at 37°C in a shaking incubator (Infors AG, Bottmingen, Switzerland) at 180 rpm. 1 mL of this culture was used to inoculate 2 x 100 mL LB and further grown at 37 °C in the shaking incubator at 180 rpm for 3 hours. The absorbance was monitored the OD at 600 nm using a UV/Vis spectrophotometer (PerkinElmer™ instruments, PTP-6 Peltier System, Lambda 35 UV/Vis Spectrophotometer, Llantrisant, UK). When the cultures reached approximately OD = 0.6, the cells were harvested by centrifugation at 2000xg, 20min using Sorvall Legend XTR centrifuge (Thermo Fisher Scientific, Hemel Hempstead, UK) equipped with TX-750 Swinging Bucket. The supernatant was discarded and the pellet resuspended in 10 mL of ice-cold 0.1M $CaCl_2$ (Sigma-Aldrich Chemical Co., Poole, UK). The suspension was left on ice for 20 minutes and the cells harvested again by

centrifugation at 2000xg, 20min using the Sorvall Legend XTR centrifuge. The supernatant was discarded and the cell pellet resuspended in 3 mL of ice-cold 0.1M $CaCl_2$ 15% glycerol. Cells were then aliquoted by dispensing 100 µL into microcentrifuge tubes, frozen on dry ice/ethanol and stored at -80°C for later use.

### 2.4.4 Transformation of competent DH5α E.coli cells

1L of bacterial growth medium Luria Broth (LB) was prepared using 5g of yeast extract, 10g of bacto-tryptone,10g NaCl, pH 7.5, made up to 1L with high quality distilled water. The LB broth was autoclaved and stored at 4°C. Selective additives were added immediately before inoculation: 100x Ampicillin sodium salt (Sigma-Aldrich Chemical Co., Poole, UK) was added to LB media to a final concentration of 100 µg/mL; 100x Kanamycin sulphate (Sigma-Aldrich Chemical Co., Poole, UK) was added to LB media to a final concentration of 30 µg/mL. LB Agar used to prepare plates was made using LB medium with the addition of 1.5% of bacto-agar, (DIFCO, US). LB Agar was autoclaved, cooled down at 55°C, and then additives were added right before pouring into petri dishes: 100x ampicillin sodium salt was added to LB agar to a final concentration of 100 µg/mL; 100x kanamycin sulphate was added to LB agar to a final concentration of 30 µg/mL.

*E. coli* DH5α Calcium chloride-competent cells competent cells were taken from the -80°C freezer and kept on ice. *E. coli* calcium-competent cells (100µL) were transformed by incubating on ice with 1µL of either PGEX-4T1-GST-PTEN or PEGFP-C1-EGFP-PTEN plasmid DNA for 30 minutes, heat shocking at 42°C for exact 90 seconds, followed by incubation on ice for 2 minutes. The cells suspension was pre-incubated at 37°C in a shaking incubator (Infors AG, Bottmingen, Switzerland) at 180 rpm for 1 hour, and then plated in petri dishes onto sterile LB-agar containing fresh 100 µg/mL ampicillin or 30µg/mL kanamycin. A glass spreader dripped with 100% ethanol was used to spread cells on the plates under a blue Bunsen burner flame. The plates were sealed with laboratory film (Pechiney Plastic Package, US) and incubated at 37°C for 16-21 hours in a plate incubator (Lenton Thermal Design, UK).

### 2.4.5 Preculture

Isolated bacterial colonies obtained from the transformation of *E. coli* DH5α Calcium chloride-competent cells were picked up from the agar plate, and pre-cultured in 10 mL of LB Broth medium supplemented with 100 µg/mL ampicillin or 30 µg/mL kanamycin at 180 rpm for 16 hours at 37°C.

### 2.4.6 Plasmid DNA preparation

Precultures of *E. coli* DH5α transformed with PGEX-4T1-GST-PTEN or PEFGP-C1-EGFP-PTEN expression plasmid were further grown in 100 mL of LB broth medium supplemented with 100 µg/mL ampicillin or 30 µg/mL kanamycin at 37 ºC and at 180 rpm in a shaking incubator (MAXQ 8000, Thermo Fisher Scientific, Hemel Hempstead, UK). DNA midipreparation (Midiprep) or maxipreparation (Maxiprep) was performed with the PureYield™ Plasmid Midiprep (Promega, US), and the PureYield™ Plasmid Maxiprep System (Promega, US), following the recommended protocol. All the centrifugation steps were performed using a Sorvall Legend XTR centrifuge (Thermo Fisher Scientific, Hemel Hempstead, UK) equipped with TX-750 Swinging Bucket. Once the plasmid DNAs were eluted, the concentration and the purity were checked monitoring absorbance ratios at 260/280 nm and 260/230 nm using Nanodrop 2000c UV-Vis Spectrophotometer (Thermo Fisher Scientific, Hemel Hempstead, UK). The obtained DNA concentration values were compared with reference values provided by the manufacturer.

# 2.5 Protein expression and purification

## 2.5.1 PTEN-GST expression

Precultures of *E. coli* DH5α transformed with PGEX-4T1-GST-PTEN expression plasmid were further grown in 1L LB Broth medium supplemented with 100 µg/mL ampicillin at 37 ºC and at 180 rpm in a shaking incubator (MAXQ 8000, Thermo Fisher Scientific, Hemel Hempstead, UK), while measuring the optical density at 600 nm ($OD_{600}$) with a MultiScan GO Microplate Spectrophotometer (Thermo Fisher Scientific, Hemel Hempstead, UK). When the $OD_{600}$ reached 0.5-0.6, isopropyl beta-D-1-thiogalactopyranoside (IPTG) was added to a final concentration of 1 mM to induce protein expression, and the cultures grown for a further 24 hours at 23 ºC. The cells were harvested by centrifugation at 4600 rpm for 20 minutes at 4 ºC in a Sorvall EVOLUTION RC centrifuge (Thermo Fisher Scientific, Hemel Hempstead, UK) equipped with FIBERLite® F8-6x1000y rotor (Piramoon Technologies Inc, USA). Pellets were resuspended in 50 mM Tris pH 7.4 (Trizma base, Sigma-Aldrich Chemical Co., Poole, UK); supplemented with EDTA-free protease inhibitor cocktail (Catalog no.11 873 580 001, Roche Diagnostics GmbH, Mannheim, Germany), the suspension was centrifuged at at 4700 rpm for 20 minutes at 4 ºC in a Sorvall Legend XTR centrifuge (Thermo Fisher Scientific, Hemel Hempstead, UK) equipped with TX-750 Swinging Bucket Rotor for 20 min at 4°C and stored at -20ºC. Cells were lysed in 50 mM Tris pH 7.4, 2 mg/mL lysozyme, 2 mM EDTA (BDH limited, UK), 2 mM DTT, 1% Triton, supplemented with EDTA-free protease inhibitor cocktail by ultrasonication (UP50H, Ultrasonic processor, Hielscher ultrasound technology) for 5 cycles of 1 minute pulsing and 2 minutes of rest on ice, and finally with a Potter homogenizer until the suspension no longer appeared viscous. The homogenized suspension was centrifuged at 4°C for 45 minutes at 14,780xg in a Jouan Gr2022 centrifuge (Thermo Fisher Scientific, Hemel Hempstead, UK), the pellet discarded and the supernatant filtered through a 0.45 µM syringe filter (Millex® Syringe-driven filter unit, Millipore Ltd, Feltham UK).

### 2.5.2 PTEN-GST protein purification

All purification steps were performed at 4ºC. A 10 mL chromatography column (Econopack, BioRad, US) was mounted on a suspension clamp stand, secured with a cap and equipped with a valve. The column was packed with Glutathione Sepharose 4B beads (GE Healthcare, Little Chalfont, UK) added to a final bed volume of approximately 5 mL, and pre-equilibrated with 50 mM Tris pH 7.4, 140 mM NaCl, 2.7 mM KCl (Tris column buffer). The filtered cell extract was loaded onto the column and allowed to flow through by gravity. A series of reducing saline wash buffers were then loaded onto the column and allowed to flow through in the following order: 25 mL of Tris column buffer containing 1% Triton X-100 and 2 mM DTT; 40 mL of Tris column buffer containing 2 mM DTT; 40 mL of 50 mM Tris pH 7.4, 500 mM NaCl, 2.7 mM KCl, 2 mM DTT. Next, 10 mL 50 mM Tris pH 7.4, 20 mM reduced L-Glutathione, 250 mM NaCl, 2 mM DTT (elution buffer) were added, 2 mL were allowed to flow through, at which point the valve was closed and the beads incubated with elution buffer overnight. The valve was then opened, and the flow-through collected while pouring additional elution buffer (10 mL) onto the column. The protein solution was then concentrated in the Amicon® Ultra-15 centrifugal filter device (Millipore Ltd, Feltham UK), according to the manufacturer's instruction by centrifugation at 4ºC in the Sorvall Legend XTR centrifuge (Thermo Fisher Scientific, Hemel Hempstead, UK) equipped with TX-750 Swinging Bucket Rotor. Bradford protein assay was used to determine the concentration of the purified PTEN-GST. Serial dilution of Bovine Serum Albumin standards (Thermo Fisher Scientific, Hemel Hempstead, UK) were used to plot a standard curve from which to obtain the sample protein concentration. Both the standard and the samples were loaded in triplicates on a 96-well clear plate (Nunc, Thermo Fisher Scientific, Hemel Hempstead, UK). The assays were performed using Coomassie Stain Plus Bradford Assay (Thermo Fisher Scientific, Hemel Hempstead, UK) according to the manufacturer's instruction. A BioTek® plate reader (Biotek, UK) and was used to measure absorbance at 570 nm. Next, purified PTEN was prepared in 50% glycerol (Analytic reagent grade, Fisher Chemical, UK), aliquoted out in single vials, and stored at -80°C.

# 2.6 Biochemistry techniques

## 2.6.1 SDS-PAGE gel electrophoresis

SDS-PAGE was performed using an X-Cell Sure Lock ® module (Life technologies) connected to a BioRad powerpack (BioRad, US). A 12% acrylamide gel was made by adding 3.4 mL of water, 2.5 mL of 1.5M Tris pH 8.8 (gel resolving buffer), 4.0 mL of 40% acrylamide/bis acrylamide 37.5:1 (Sigma-Aldrich Chemical Co., Poole, UK), 100 µL of 10% Sodium dodecyl sulphate (Sigma-Aldrich Chemical Co., Poole, UK) , 90 µL of 10% ammonium persulfate (APS, Sigma-Aldrich Chemical Co., Poole, UK), 12µL of TEMED (NNN'-N' Tetramethylethylenediamine, BDH Limited, UK). The 4% stacking gel was prepared by adding 2.0 mL of water, 830µL of 1.0M Tris pH 6.8 (Stacking buffer), 440µL of 40% acrylamide/bis-acrylamide 37.5:1, 33 µL of 10% SDS, 20 µL of APS, 5 µL of TEMED. Running Buffer for the gel was prepared as a 10X solution with 30g Tris, 144g Glycine (Fisher Scientific, Loughborough, UK), 10g of SDS, pH 8.3, made up to 1L with water. Protein samples were mixed with 2x SDS-PAGE Sample Buffer (Laemmli 2X Concentrate, Sigma-Aldrich Chemical Co., Poole, UK) in a 1:1 ratio and loaded with gel loading tips into wells. 5µL of PageRuler™ Plus Prestained Protein Ladder (Thermo Fisher Scientific, Hemel Hempstead, UK) was loaded as protein visible marker. The gels were run at 80V for 15min, before increasing to 120V when the visible dye front reached the resolving gel.

## 2.6.2 Coomassie-staining of proteins

After the electrophoresis run, the gels were taken out of the tank module and stained with Coomassie Brilliant Blue stain solution prepared by adding 0.5g Coomassie dye to 100 mL of 45% methanol, 45% $H_2O$ and 10% acetic acid. The gels were then immersed for 12-16 hours in the staining solution with gentle shaking on the Stuart SS-M1 orbital mini shaker (Bibby Scientific, Stone, UK). The following day the gels were destained using a destain solution made of 45% methanol, 45% $H_2O$ and 10% acetic acid. The gels was placed in the destain solution and left on the rotational shaker until clear bands were visible on the gel. The destain solution was renewed twice over time. Alternatively,

gels were also stained using Coomassie Instant Blue (Expedeon, Cambridge, UK), by immersing for 1 hour in the staining solution. No destaining procedure was necessary after staining with this system. To obtain images of gels displayed in this work, a G:BOX system (Syngene, Cambridge, UK) running the GeneSys software (Syngene, Cambridge, UK).

### 2.6.3 Protein phosphatase activity assay

The phosphatase activity of PTEN was measured by monitoring the hydrolysis of the artificial substrate 3-*O*-methylfluorescein phosphate (OMFP) to 3-*O*-methylfluorescein (OMF). 3-*O*-methylfluorescein phosphate cyclohexylammonium salt (Sigma-Aldrich Chemical Co., Poole, UK) was prepared in dimethyl sulfoxide (DMSO) to a final concentration of 20 mM. After vigorous vortexing, sonication in a water bath (Ultrawave limited, Cardiff, UK) for 30 minutes was used to complete the solubilization. Each sample analyzed with the OMFP assay was prepared mixing 10x Assay Buffer (150 mM Tris, 10 mM EDTA, 750 mM NaCl, pH 7.4) with an aliquot of the purified protein sample (usually 60µg), and made up to 600 µL with water. 600 µL 1X Assay buffer was prepared as a negative control. Each sample was used to load three technical replicates (200 µl each) onto a black 96-well plate (Nunc, Thermo Fisher Scientific, Hemel Hempstead, UK). The 20 mM OMFP solution previously prepared was diluted in a 2:48 molar ratio with 1 M Tris pH 7.4, and 50 µL of the resulting substrate mix was pipetted into each of the well of the 96-well plate containing the samples. The change in relative fluorescence units (RFUs) due to released OMF was determined with at excitation 485 nm and emission at 525 nm and cutoff at 515 nm continuously over 20 minutes using a Spectra MAX GEMINI XS Fluorescence plate reader (Molecular Devices Ltd, Wokingham, UK) controlled with the Softmax Pro® software. The settings of the Spectra MAX GEMINI XS device were as follows. Temperature: 25ºC. Mode: Kinetic. Read mode: Fluorescence (RFUs). Wavelengths: 1; Excitation 485; Emission 525; Cutoff 515. Sensitivity: readings sensitivity 30 (precise); PMT sensitivity medium. Timing: Run time 20:00; interval 15 sec. Automix: before first read 10 sec; between reads 3 sec; Autocalibrate: on (calibrate once). Autoread: on, delay 0 sec. Reduction settings were as follows. Wavelength combination:!Lm1. Kinetic Reduction: Onset time; Onset RFU 10. Limits: RFU min 0; RFU max 400000; Lag time 0:00; End Time 20:00. An OMF calibration curve

was produced by dissolving OMF (Apollo Scientific, Denton, UK) in dimethyl sulfoxide to a final concentration of 20μM. Serial dilutions of this solution were assayed using the standard conditions against a DMSO blank. The nmol of OMF were plotted against net RFU to generate the calibration curve. The protein specific activity was calculated as follows:

$$\frac{end\ RFU\ (protein-blank) - start\ RFU\ (protein-blank)}{time\ lenght\ of\ the\ assay\ (\mathrm{min})}$$

to give the amount of RFU/min which was converted in nmol(OMF)/min using the slope-intercept of the OMF calibration curve.

# 2.7 Mass spectrometry

## 2.7.1 In-gel digestion for mass spectrometry

The gel pieces were washed twice with 500 µL 100 mM $NH_4HCO_3$ and twice with 100 mM $NH_4HCO_3$/50% Acetonitrile. Reduction was performed adding 10 µL of 45 mM DTT (Sigma-Aldrich Chemical Co., Poole, UK) to 150 µL $NH_4HCO_3$ and incubating at 60ºC for 30 mins. Cysteine alkylation was performed by adding 10 µL of 100 mM iodoacetamide (Sigma-Aldrich Chemical Co., Poole, UK) to 150 and incubating at room temperature for 30 mins in the dark. The gel pieces were washed in 100 mM $NH_4HCO_3$/50% acetonitrile and incubated in 50 µL of 100% acetonitrile for 10 min. The gel pieces were then dried completely in a centrifugal evaporator and resuspended in 25 µL of 0.1 µg/µL trypsin (Trypsin Gold, Mass Spectrometry Grade, Promega, Southampton, UK) in 50 mM acetic acid. 100 µL 40 mM $NH_4HCO_3$/10% acetonitrile was added to the gel pieces, which were incubated overnight at 37 ºC. The gel pieces were pelleted by centrifugation and the supernatant was collected in a fresh tube. Peptide extraction from the gel pieces was performed by adding 20 µL 5% formic acid and incubating at 37 ºC for 20 mins, followed by addition of 40 µL acetonitrile and incubation for 20 mins at 37 ºC. The gel pieces were pelleted by centrifugation, and the supernatant was combined with the first extract; this procedure was repeated twice. The peptide extracts were dried completely in a vacuum centrifuge and resuspended in a volume up to 50 µl of 98% $H_2O$, 2% acetonitrile, 0.1% formic acid (HPLC solvent A) and loaded into screw top glass autosampler vials (Chromacol, Speck and Burke analytical, Clackmannanshire, UK).

## 2.7.2 LC-MS

Peptides were separated and analyzed using an Ultimate 3000 system (Dionex, Camberley, UK) coupled to a 5600 TripleTOF (ABSciex, Warrington, UK) controlled by Chromeleon Xpress and Analyst software (TF1.5.1, ABSciex, Warrington, UK). Enrichment and desalting of the peptides was achieved using a C18 pre-column (C18 PepMap™, 5 µm, 5 mm × 0.3 mm i.d. Dionex, Bellefonte, PA,

US) washing for 4 min with aq. 2% acetonitrile, 0.1% formic acid at 30 µL/min. The peptides were then separated on a C18 nano-HPLC column (C18 PepMap™, 5 µm, 75 µm i.d. × 150 mm, Dionex, Dionex, Camberley, UK) at 300 nL/min using a gradient elution running from 2% to 45% aqueous acetonitrile (0.1% formic acid) over 45 min followed by a washing gradient from 45% to 90% aq. acetonitrile (0.1% formic acid) in 1 min. The system was washed with 90% aq. acetonitrile (0.1% formic acid) for 5 min and then re-equilibrated to the starting solvent. Ionization of the peptides was achieved with spray voltage set at 2.4 kV, a source temperature of 150°C, declustering potential of 50 V and a curtain gas setting of 15. Survey scans were collected in positive mode from 350 to 1250 Da for 200 ms using the high resolution TOF-MS mode. Information-dependent acquisition (IDA) was used to collect MS/MS data using the following criteria: the 10 most intense ions with + 2 to + 5 charge states and a minimum of intensity of 200 cps were chosen for analysis, using dynamic exclusion for 12s, and a rolling collision energy setting.

### 2.7.3 Label-free quantification with Progenesis QI for proteomics

The LC-MS runs acquired with the 5600 Triple TOF were loaded as .wiff files onto the software Progenesis QI for Proteomics (Non Linear Dynamics, Newcastle upon Tyne, UK), implemented for the label-free quantification of proteins and peptides throughout the research elaborated in this thesis. For each LC-MS run of interest, elution profile and isotope pattern of the analyzed peptides were integrated in a 2D map where m/z is plotted against retention time. Each detected ion that produced a peak across the mass spectrum represents a feature that can be determined by the feature-finding algorithm. 2D maps generated by different LC-MS runs were then aligned for comparison so that features corresponding to the same peptide were assigned to each other. Finally, the abundance of a given feature was measured summing the peak intensities in the feature region and compared across multiple aligned 2D maps. The alignment was performed loading LC-MS runs corresponding to peptides digested from gel bands cut at the same molecular weight across three biological replicates. The alignment reference was chosen by letting the software automatically assess every run in the each of the single fraction experiment for suitability. After manual validation of the alignments, additional vectors were added where necessary. The features normalization was set to normalize to all proteins.

The automatic sensitivity method of the peak picking algorithm was set at default. The maximum allowable ion charge was set at 20. No peptide ion filtering was applied. The experimental design setup was set as Between-subject Design. The spectra were exported in .mgf format for database searching, and the search results were imported in .xml format after Mascot Database search for the identification of matched peptides. Any peptide showing a Mascot ion score below the threshold indicative of identity or extensive homology ($p$ value $< 0.05$) was removed from the feature identification list. Only features that showed zero conflicts were used for quantification. Data obtained from the alignment of LC-MS runs corresponding to single fractions were then pooled into a multi-fraction experiment.

### 2.7.4 Database search

Mascot® probability based search engine (Matrix Science, London, version 2.4.0) was used to perform protein identification tasks on MS data by interrogating SwissProt 2015-03 primary database [483]. The parameters of the software that were controlled to set up the searches method were: Taxonomy; Database; Fixed modifications; Variable modifications; Experimental mass values. Enzyme; Missed cleavages; Peptide Charge Peptide tolerance; Number of 13C; Data format; MS/MS tolerance; Peptide Charge; Error tolerant search; Instrument type; Data format; Quantitation; Experimental mass values.

# 2.8 Bioinformatics tools

### 2.8.1 UCSF Chimera Molecular Modeling System

The UCSF (University of California San Francisco) Chimera Molecular Modeling System software (http://www.cgl.ucsf.edu/chimera) was used to generate all the PTEN 3D structures images displayed in this thesis. The PTEN raw 3D structure was retrieved by searching the PDB (Protein Data Bank) for the PTEN protein ID (15DR), deposited by Lee *et al*. [383], and subsequently processed to highlight specific residues or protein domains.

### 2.8.2 Expasy

PTEN amino acid sequence was obtained by translating with Expasy translate software tool (http://web.expasy.org/translate/) the nucleotide sequence provided by Rudiger Woscholski's Group at Imperial College London. Expasy ProtParam (http://web.expasy.org/protparam/) was used to predict PTEN and GST molecular weight, and extinction molar coefficient; Expasy PeptideCutter (http://web.expasy.org/peptide_cutter/) was used to predict protein fragmentation after enzymatic or chemical cleavage. The obtained sequence was then used to calculate the extinction coefficient using the Expasy ProtParam software. The extinction coefficient of 88130 $M^{-1}$ $cm^{-1}$ was used, assuming that all PTEN cysteine are reduced.

# Chapter 3. Functional proteomics analysis of PTEN oxidative post-translational modifications

# 3.1 Summary

The oxidative action of reactive species causes important changes in protein function and can affect signaling networks and cellular pathways. Protein oxidative post-translational modifications (oxPTMs) are a promising class of biomarkers of inflammatory and age-related diseases including cancer, cardiovascular diseases and neurodegeneration, as well as a target for novel therapeutics.

In the study presented in this chapter, a functional proteomics approach is used for the systematic oxPTMs mapping of the tumour suppressor phosphatase PTEN following oxidative treatment. A purified GST-tagged fusion PTEN was irreversibly oxidized with hypochlorous acid (HOCl) and its phosphatase activity and electrophoretic profile compared across the different HOCl concentrations used. Using mass spectrometry based label-free quantification, PTEN peptides carrying modified residues were identified, and the relative abundance of the oxPTMs was determined in HOCl-treated PTEN samples versus untreated control.

A total of 13 high abundance oxPTMs that were significantly elevated upon HOCl treatment are described, including those taking place at amino acid residues important for PTEN phosphatase activity and protein-protein interactions such as Met35, Tyr155, Tyr240 and Tyr315. The modifications map outlines the patterns of oxPTMs linked to phosphatase inactivation and structural changes in response to *in vitro* oxidation. The systematic characterization of oxPTMs profiles can be used to gain deeper insight in the regulation of cellular pathways linked to inflammation and disease.

# 3.2 Introduction

Hypochlorous acid (HOCl) is a powerful reactive molecule produced by the body to fight infections. The intracellular production of HOCl is triggered by pro-inflammatory stimuli such as those present in various pathophysiological states which activate phagocytic white blood cells such as macrophages and neutrophils [484-486]. Activated phagocytes kill pathogens such as bacteria either extracellularly or by ingesting them into intracellular compartments called phagosomes [487]. When ingested into phagosomes, the invader can be destroyed via mechanisms including the production of large quantities of superoxide via a membrane associated NADPH oxidase (Figure 3.1) [488]. The enzyme superoxide dismutase converts superoxide into $H_2O_2$, which is involved in the formation of secondary hydroxyl radicals that assist the destruction of pathogens [489]. In neutrophils, azurophilic granules can fuse with phagosomes and release myeloperoxidase (MPO), a haem-containing lysosomal peroxidase enzyme [490,491]. MPO oxidizes $Cl^-$ ions in the presence of $H_2O_2$ producing HOCl, which functions as an efficient microbicide, and can also act as a natural adjuvant of adaptive immunity [492]. However, because of its significant oxidizing capacity, the production of HOCl can also result in oxidative damage to biomolecules of the host tissue including proteins.

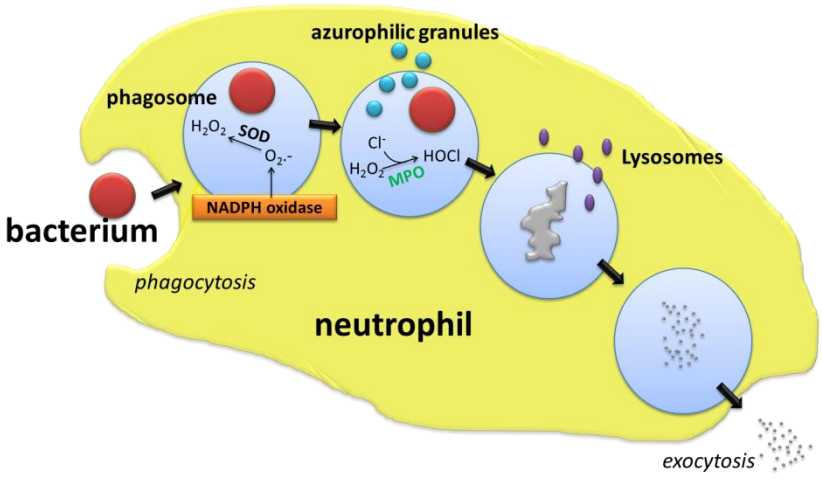


**Figure 3.1 Phagocytosis and oxygen-dependent destruction of pathogens**

Pathogens such as bacteria are ingested by the neutrophil and kept in intracellular compartments called phagosomes. A membrane-associated NADPH oxidase generates superoxide, which is converted into

$H_2O_2$ by superoxide dismutases (SOD) inside the phagosome. Azurophilic granules that fuse with the phagosome release myeloperoxidase (MPO), which uses $Cl^-$ to produce HOCl from $H_2O_2$. The oxidative action of HOCl and $H_2O_2$ kills the pathogen, which is further degraded by lysosomal hydrolases, and expelled by exocytosis into the extracellular environment.

Protein oxidative damage due to the MPO/HOCl system can result in tissue injury, and has been associated with several conditions such as cancer, neurodegenerative disease and cardiovascular disease [493,494]. HOCl attacks mainly free amino groups ($-NH_2$) and sulfhydryl groups (-SH) in proteins [51]. When oxidizing thiol groups, HOCl-mediated oxidation can cause the formation of reversible disulfide bonds that result in protein crosslinking and can result in complete inactivation [495], or other non-specific thiol oxidative products such as methionine sulfoxide and sulfone as well as cysteine sulfinic and sulfonic acid [485,496]. When reacting with the amino groups of proteins, HOCl damage results in the formation of unstable chloramines, which are rapidly reduced back to their unmodified form or broken down to aldehydes [496]. Both thiol oxidative products and chloramines are major products of HOCl-induced protein damage, but they are unlikely to be useful as biomarkers of HOCl production, as thiol oxidative products may be caused by a range of oxidants and are often reversible by the cellular antioxidant system, while chloramines are highly unstable and therefore difficult to detect. Aside from thiols and amine groups, HOCl also reacts with tyrosyl groups of proteins to form 3-chlorotyrosine and 3,5-dichlorotyrosine [497]. The reactions that result in tyrosine chlorination are less favored than those with amine groups and protein thiols; however, chlorinated tyrosine is a much more stable end product of HOCl oxidation than chloramines, and a more specific marker of HOCl-induced damage than thiol oxidative products [496]. In the past two decades, 3-chlorotyrosine and 3,5-dichlorotyrosine have emerged as reliable biomarkers of protein damage by myeloperoxidase, and have been identified in the clinical samples of patients affected by various inflammatory conditions [496,498,499]. It has also been reported that HOCl-induced oxidative damage can cause the irreversible formation of protein aggregates *in vivo* [227]. HOCl-induced protein aggregation has attracted interest as a possible factor contributing to the pathophysiology of certain conditions such as atherosclerosis [500], but the biochemical processes triggering the oxidation-mediated formation of protein aggregates are not completely understood. It has been suggested that the

alteration of protein folding responsible for protein aggregation upon HOCl-induced oxidation could be due to strong, non-covalent interactions between protein chains, rather than intermolecular covalent cross-linking [500]. An alternative mechanism that has been proposed involves intermolecular Schiff-base formation and requires lysine residues modification to reactive carbonyl [501]. HOCl-modified proteins have been detected in different diseased tissue, including atherosclerotic tissue, [155] bowel tissue obtained from patients affected by inflammatory bowel disease [502], and in the glomeruli of patients affected by membranous glomerulonephritis [503].

Besides evidence showing an association between HOCl and molecular and cellular damage, an increasing number of studies indicates that HOCl is also involved in the modulation of redox-sensitive intracellular signaling pathways, though less attention has been given to this aspect [504]. For example, both MPO and HOCl have been implicated in the regulation of cancer-related cellular processes [504] and it has been reported that HOCl is involved in the selective elimination of transformed fibroblast through the induction of apoptosis [505]. Moreover, HOCl has been shown to promote the activation of several cellular pathways via the activation of key proteins such as the tumour suppressor p53 [506], members of the MAP kinase pathway [507] and the iron-regulatory protein 1 [504].

The identification of HOCl-specific modifications to proteins is, therefore, a critical task for the investigation into the effects of myeloperoxidase production on tissue damage as well as for the in-depth analysis of HOCl-mediated regulation of cellular networks [485]. The cutting-edge analytical technique for the analysis of post-translational modifications such as oxPTMs (oxidative post-translational modifications) is mass spectrometry [508]. Modern mass spectrometry instruments allow high levels of selectivity and reproducibility for the detection of oxPTMs such as tyrosine chlorination, and are now emerging as a powerful tool for the discovery and validation of clinical biomarkers. In identifying biomarkers of myeloperoxidase activity, many MS-based studies have reported the identification of free 3-chlorotyrosine in biological samples such as urine [238,241] and blood plasma [509,510]. However, the detection of free modified amino acids does not provide any information on the identity of the oxidized protein, which is essential for understanding the processes and mechanisms of signal transduction in response to oxidation. With growing interest in the signaling role of reactive species such as HOCl, obtaining information on the identity of oxidized proteins and

their oxidation sites has become increasingly essential to answer oxidation-related biological questions, in both clinical and *in vitro* settings. Using MS and MS/MS methods, the detection of protein bound 3-chlorotyrosine and the corresponding chlorination sites within the oxidized protein has been shown to be important for understanding the mechanisms of myeloperoxidase-related protein damage and alteration of protein folding status [511,512], and protein-bound chlorotyrosine has been found elevated in the biological samples of patients affected by several conditions, including inflammatory and cardiovascular disease [229-233].

This PhD thesis focuses on the redox regulation of the dual specificity phosphatase (PTEN), which is a negative regulator of the PI3K/Akt pathway and is involved in a number of cellular processes, including metabolism, apoptosis, cell cycle regulation and cell proliferation and survival [445,455]. Much of the research into the oxPTMs of PTEN has been focused on the redox status of the Cys71 and Cys124 thiols in the active site of the phosphatase, which form a reversible disulfide bond upon low concentration $H_2O_2$-mediated oxidation [144,423,477] that inactivates the protein. However, no study to date has addressed the correlation between oxidation-induced inactivation and oxPTMs at PTEN amino acid residues other than the active site cysteines. As HOCl has been shown to form protein modifications other than reversible thiol oxidative products, it is likely that HOCl-specific modifications such as tyrosine chlorination are associated with a permanent alteration of PTEN phosphatase activity and folding status.

This chapter describes the LC/MS-based quantitative mapping of HOCl-induced oxidative post-translational modifications (oxPTMs) of PTEN. The GST-tagged purified protein was treated with increasing HOCl concentrations and its phosphatase activity measured by monitoring the hydrolysis of the fluorescent substrate 3-*O*-methylfluorescein phosphate. The effect of HOCl on the thiol/disulfide dynamics of PTEN active site was tested by comparing the phosphatase activity before and after incubating the HOCl-oxidized protein in reducing conditions, and the modification status of the protein was compared to the rate of inactivation and folding status upon HOCl oxidation. The functional proteomics approach identified HOCl-specific oxPTMs that were associated with irreversible PTEN inactivation and alteration of PTEN folding status. Specific residues were mapped onto the PTEN structure, and changes that could be important for understanding HOCl damaging and

signaling role in cells identified, thereby gaining potential insights into the molecular mechanisms of disease.

# 3.3 Materials and Methods

### 3.3.1 HOCl concentration assay

The sodium hypochlorite stock solution (Sigma-Aldrich Chemical Co., Poole, UK) was first assayed to determine its molar concentration. A Lambda 35 UV/Vis Spectrophotometer (PerkinElmer™ instruments, Seer Green, UK) fitted with a PTP-6 Peltier System was used to measure the absorbance at 292 nm of HOCl serial dilutions prepared in 0.1 mM NaOH against blank 0.1 mM NaOH and the concentration obtained using a molar extinction coefficient of 350 $M^{-1}$ $cm^{-1}$. HOCl stock solution was then diluted in 50 mM Phosphate buffer pH 7.4 to prepare the solutions for the oxidation experiment.

### 3.3.2 Buffer exchange optimization

Purified PTEN-GST was buffer exchanged using either Slide-A-Lyzer dialysis cassette 10,000 MWCO (Thermo Fisher Scientific, Hemel Hempstead, UK) or Microcon® 10 kDa centrifugal filter unit (Millipore Ltd, Feltham UK), according to the manufacturer's recommendations. The buffers of choice were tested using the Slide-A-Lyzer dialysis cassette were 50 mM phosphate buffer pH 7.4, prepared using sodium phosphate monobasic and dibasic (both obtained from Sigma-Aldrich Chemical Co., Poole, UK), and 20 mM diethylmalonic acid (Sigma-Aldrich Chemical Co., Poole, UK), pH 7.4, and dialysis was performed overnight at 4ºC. When using the centrifugal filter unit, PTEN was buffer-exchanged in 50 mM phosphate buffer, and all centrifugation steps were performed at 14,000xg in a 5417R Eppendorf microcentrifuge (Eppendorf UK Ltd, Stevenage, UK) for 10 min at 4 ºC. All buffer exchange conditions were optimized testing 60 µg of buffer exchanged-protein with the OMFP phosphatase assay as described in Section 2.6.3. A Nanodrop c2000 UV-Vis Spectrophotometer (Thermo Fisher Scientific, Hemel Hempstead, UK) was used to determine the concentration of buffer-exchanged PTEN-GST using the absorbance at 280 nm. The field "protein type" was set to "other protein", the predicted molecular weight was set at 73.5 kDa, and an extinction coefficient of 88,130 $M^{-1}$ $cm^{-1}$ was used, assuming that all PTEN cysteine are reduced.

### 3.3.3 Oxidation and activity assay

Purified, buffer-exchanged PTEN-GST was oxidized with 0, 0.5, 1, 2, 5 and 10 mM HOCl for 1 hour at room temperature. The HOCl to PTEN-GST molar ratios were 15:1 (0.5 mM HOCl), 30:1 (1 mM HOCl), 60:1 (2 mM HOCl), 150:1 (5 mM HOCl), and 300:1 (10 mM HOCl). A 60 µg aliquot of each sample was incubated in 100 mM DTT for 15 min. Next, the phosphatase activity of PTEN was measured by assaying 60 µg of HOCl-oxidized and DTT-incubated HOCl-oxidized PTEN-GST with the OMFP phosphatase assay as described in Section 2.6.3.

### 3.3.4 SDS-PAGE and protein in-gel digestion

50 µg of HOCl-oxidized PTEN-GST samples were analyzed by SDS-PAGE as described in Section 2.6.1. The Coomassie-stained bands corresponding to the intact protein and the protein aggregates across the range of HOCl treatment were cut out from the polyacrylamide gel and digested as described in Section 2.7.1.

### 3.3.5 Image processing

Gel densitometry was performed with the Java-based image processing ImageJ [513]. For the full lane gel densitometry, the gel images were first imported into Microsoft Powerpoint® and cropped so that white space was left between lanes corresponding to different experimental conditions. The images were saved as .png and opened in ImageJ. All images were converted to 8-bit, background subtracted using a rolling ball radius of 50 pixels and light background, and contrast enhanced by 0.4% of saturated pixels. The stacking gel was included in the crop selection of the full lanes. For the densitometry analysis of the single PTEN band, the gel images were first imported into Microsoft Powerpoint® and cropped so that white space was left between lanes corresponding to different experimental conditions. Next, the lanes were further cropped to include only the protein band at 73kDa corresponding to PTEN, cropping the image along the edge of the gel band. The images were then saved as .png and opened in ImageJ. All images were converted to 8-bit, and no background subtraction or contrast enhancing was performed.

### 3.3.6 LC-MS

Peptides were separated and analyzed as described in Section 2.7.2.

### 3.3.7 Label-free quantification using Progenesis QI for Proteomics

LC-MS runs obtained from the HOCl oxidation experiments were used to generate a total of 2 separate Progenesis QI experiments, one for gel bands excised from the area corresponding to the intact PTEN-GST band, and one for the gel areas corresponding to protein aggregates. Each of the two Progenesis QI experiments was generated using a total of 18 LC-MS runs (three independent experiments across six different experimental conditions). The Progenesis analysis was performed as described in Section 2.7.3. The protein identification list was filtered to include only peptides corresponding to PTEN. To analyze PTEN modification, the conflicts between the detected modified peptides were handled as follows: firstly, the MS/MS fragmentation pattern of each conflicting peptide was analyzed by *de novo* sequencing. Where the *de novo* sequencing was not sufficient to resolve the conflicts, the peptide showing the highest Mascot Ion score among the conflicting detected peptides was selected. In the event of conflicting peptides showing equal Mascot Ion score, the peptide showing the highest number of hits was selected.

### 3.3.8 Database Search

Progenesis-generated .mgf files for both the intact PTEN-GST band and the protein aggregates LC-MS runs were searched with Mascot. Variable modifications were searched for in groups of 3-5 modifications at a time. Tyrosine chlorination and dichlorination, cysteine dioxidation and trioxidation, methionine oxidation and dioxidation, proline oxidation, tyrosine oxidation, lysine oxidation, tryptophan oxidation, and histidine oxidation were specifically searched for as variable modifications. Carbamidomethyl cysteine was used as a fixed modification. The peptide tolerance used was +/- 0.8 Da, peptide charges of 2+, 3+ and 4+ was used, MS/MS ion search was selected. Other parameters for the searches were as follows: Enzyme: Trypsin; Peptide tolerance: ±0.8 Da; MS/MS tolerance: ±0.8 Da; Peptide charge state: +2, +3 and +4; Max Missed cleavages: 1; #13C: 1;

Quantitation: None; Instrument: ESI-QUAD-TOF; Data format: Mascot Generic; Experimental mass values: Monoisotopic; Taxonomy *Homo Sapiens* (Human).

### 3.3.9 Statistical analysis

Graph Pad Prism was used for the statistical analysis performed on all data presented in this chapter. Activity, densitometry and modifications data were analyzed using one-way ANOVA with Dunnett's multiple comparisons test, comparing the mean values of each treated sample to the mean of the untreated control. Correlation between activity and densitometry data was performed using Pearson's correlation analysis. To compare retained activity between two treated samples before and after reducing wash, two-tailed unpaired Student's t-test was used. $P < 0.05$ was considered significant.

### 3.3.10 *De novo* peptide sequencing

Tryptic peptides containing modified residues for which the relative modification abundance was significantly higher in the HOCl-treated samples than controls were manually sequenced by viewing the spectra in Peakview® software (AB Sciex Ltd, Warrington, UK). For each modified peptide detected by Progenesis QI HOCl concentrations, the m/z, retention time and average normalized abundance in each sample treated with different HOCl to PTEN molar ratios were recorded from the peptide identification screen. Next, the LC-MS run containing the modified peptide showing the highest normalized abundance in comparing the samples treated with different HOCl to PTEN molar ratios was imported into Peakview®. The MS/MS spectrum of each modified peptide was retrieved searching the independent data acquisition (IDA) list for the precursor's m/z and retention time. The mass difference between two product ions was used to calculate the mass of each amino acid composing the modified peptide backbone. Product ion series were sequenced by sequentially subtracting higher residue masses from an arginine (m/z 147.113) or lysine (m/z 175.119) y1 ion at the low end of the MS/MS spectrum.

### 3.3.11 NetSurfP

The NetsurfP (ver. 1.1) server (http://www.cbs.dtu.dk/services/NetSurfP) was implemented to predict solvent accessibility of PTEN residues using the PTEN FASTA sequence obtained from Uniprot [514]. The software predicts relative solvent accessibility (RAS), absolute solvent accessibilIty (ASA) for each residue, and regions of the protein are divided between exposed and buried by using a cutoff of 25% exposed accessible surface area based on the $ASA_{max}$ of each given amino acid [514]. The Z-score indicates the reliability of the prediction (data points with high Z-scores have lower predicted error compared to data points with low Z-scores) [514].

# 3.4 Results

## 3.4.1 Transformation of *E. coli* DH5α PTEN-GST

The first stage of the project was the transformation of *E. coli* DH5α bacterial cells with the PGEX-4T1 expression plasmid encoding PTEN-GST. The *E. coli* Bacterial strain (DH5α) was selected to produce the PTEN-GST fusion protein following the work of Dr. Karina Tveen Jensen at Aston University and Dr. Lok Hang Mak and Dr. John Mina at Imperial College London who previously tested three different *E. coli* bacterial strains, BL21, (BL21) DE3 and DH5α for PTEN-GST expression. IPTG-induction temperature (23°C) and incubation time (24 hours) were also chosen after testing a range of conditions in collaboration with Dr Karina Tveen Jensen (data not shown).

Following transformation of $Ca^{2+}$ generated competent *E. coli* DH5α the cell suspension was plated onto agar containing ampicillin as the selection antibiotic, and incubated at 37°C overnight. Bacterial colonies were observed on the agar plates the next day, indicating that the transformation was successful. Single isolated colonies were carefully picked from the edge of the plate, precultured in fresh LB medium, and further grown at 37 ºC until the optical density at 600 nm ($OD_{600}$) reached 0.5-0.6 OD, at which point IPTG was added to a final concentration of 1 mM to induce protein expression.

## 3.4.2 PTEN-GST purification

After IPTG-induced protein expression, harvesting and cell lysis, PTEN-GST was purified from the cell extract with a gravity flow column packed with Glutathione Sepharose beads. The cell lysate was loaded onto the column followed by a series of reducing saline wash buffers, and the beads were incubated overnight incubation at 4°C with the elution buffer. Aliquots of the first 10 mL elution buffer used for the elution of PTEN-GST were collected in 1 mL fractions, a small amount of which (20 µL) was loaded onto a SDS-PAGE gel along with samples representative of critical steps of the cell lysis (such as the centrifugation and filtration step), and the purification (such as the unbound flow-through and the wash), so that the overall efficiency of the procedure could be evaluated. An example of the Coomassie-stained gels displaying a representative PTEN-GST purification process is

shown in Figure 3.2. The SDS-PAGE analysis was useful to visually track the PTEN-GST purification process. The PTEN-GST protein band at ~70kDa became clearly visible from eluted fraction 3, and its intensity increased in the subsequent gel lanes. Samples aliquoted from an additional 10 mL of elution buffer added following the first elution step showed little or no visible PTEN-GST signal (data not shown), but were also pooled together with the first 10 mL and the protein concentrated using an Amicon® Ultra-15 centrifugal filter unit.

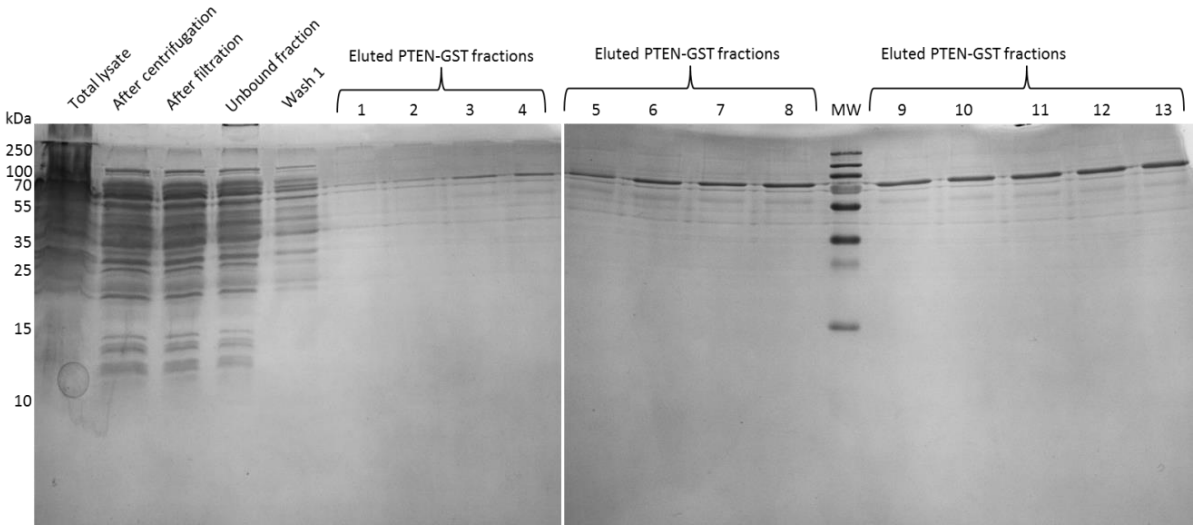


**Figure 3.2 SDS-PAGE tracking of the purification of PTEN-GST from the cell lysate of transformed *E. coli* DH5α**

Samples corresponding to critical steps of the purification of PTEN were analyzed by SDS-PAGE. These include: the total cell extract obtained from the lysis of PTEN-GST-overexpressing *E. coli* DH5α cells; the supernatant obtained from the centrifugation of the total lysate, before and after filtration; the unbound flow-through and the first wash flow-through; fractions of eluted PTEN-GST collected for each mL of elution buffer flowing through the Glutathione-Sepharose column, as annotated on the gels.

Following concentration by ultrafiltration of the eluted PTEN-GST, the protein concentration was measured using a Bradford protein assay. Indicative yields and concentrations for a medium (1 L) and large (6 L) prep are shown in Table 3.1. In general, a higher concentration of PTEN-GST was obtained after purification from larger starting culture volumes, with comparable protein yield per liter of culture.

**Table 3.1** PTEN-GST indicative purification yields

| **Starting *E. coli* culture volume (mL)** | **Purified PTEN-GST concentration (µg/mL)** | **PTEN-GST Yield per liter of culture (µg)** |
|---|---|---|
| 1500 | 313.75 | 2091 |
| 6000 | 1288.88 | 2148 |

### 3.4.3 OMFP activity assay of the purified PTEN-GST

An OMPF assay was performed to check the enzymatic activity of the purified and concentrated PTEN-GST in reducing conditions (elution buffer). An example of the data collected is shown in Figure 3.3. The positive increase in RFUs, after subtraction of the RFU values of the blank, shows that the expressed and purified PTEN-GST is active. The obtained specific activity values over different PTEN-GST preparation were in the 0.5-1 nmol OMF/min/mg protein range, in line with results obtained by other investigators (Lok Hang Mak, Karina Tveen Jensen, unpublished results).

In most cases, repeated freeze-thawing was found to negatively affect protein activity, resulting in a poorly active or inactive protein. For this reason, the purified PTEN-GST was prepared in 50% glycerol and aliquoted out in single vials before storage at - 80°C so that each aliquot contained sufficient amount of protein for individual experimental use.

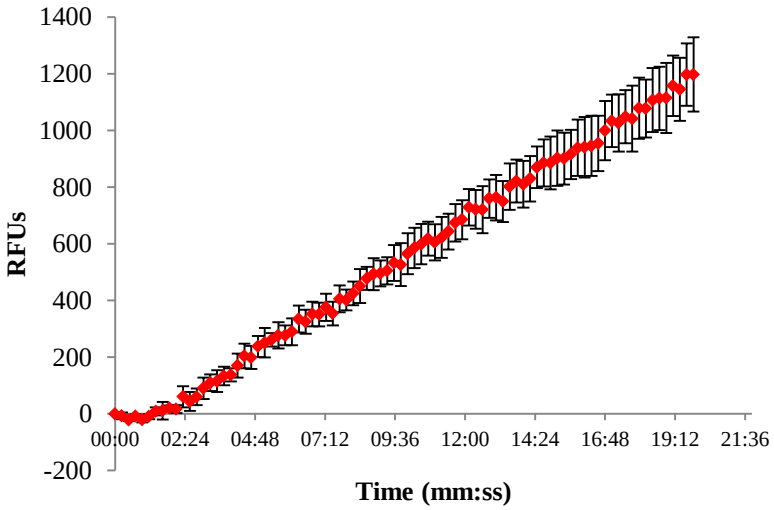


**Figure 3.3 Representative OMFP phosphatase activity assay of expressed and purified PTEN-GST in reducing buffer conditions**

The mean Relative Fluorescence Units values are calculated after subtraction of the blank values and normalization of the curve to start at zero. The calculated specific activity for the OMFP substrate from this experiment was 0.66 ± 0.07 nmol/min/mg protein**.** Data are presented as mean ± SD of three technical replicates.

### 3.4.4 Optimization of PTEN buffer exchange

Prior to any experimental use, the purified PTEN was buffer-exchanged in order to remove the cryoprotectant glycerol, which can interfere with assays used to measure protein concentration, as well as the reducing agents glutathione and DTT, which would interfere with the oxidation studies. Maintaining unaltered protein activity during the buffer exchange process was considered critical for the study, as if PTEN is significantly inactivated in non-reducing buffer conditions, the interpretation of any oxidation-related changes in activity may be more difficult.

Initially, preliminary tests were carried out to assess the effect of different buffer exchange conditions on PTEN phosphatase activity. Three different buffer exchange conditions were tested with the OMFP phosphatase assay to identify the best method for preserving PTEN phosphatase activity before oxidation (Figure 3.4). Using the Slide-A-Lyzer dialysis cassette, PTEN specific activity dropped by approximately 69% when buffer-exchanging in 50 mM phosphate buffer pH 7.4, and by approximately 56% when buffer-exchanging in 20 mM diethylmalonic acid pH 7.4. On the other hand, using a Microcon centrifugal filter unit, PTEN specific phosphatase activity only dropped by approximately 10% in 50 mM phosphate buffer. Generally, the specific activity values of the buffer-exchanged purified PTEN-GST was found to be in the 0.5-1 nmol OMF/min/mg protein range, and protein was considered fully active. These preliminary tests indicated the importance of monitoring the adverse effect of buffer-exchange methods on protein activity, and identified the centrifugal filter unit as the method of choice for protein buffer-exchange, and this device was therefore used to filter PTEN-GST before all oxidation experiments.

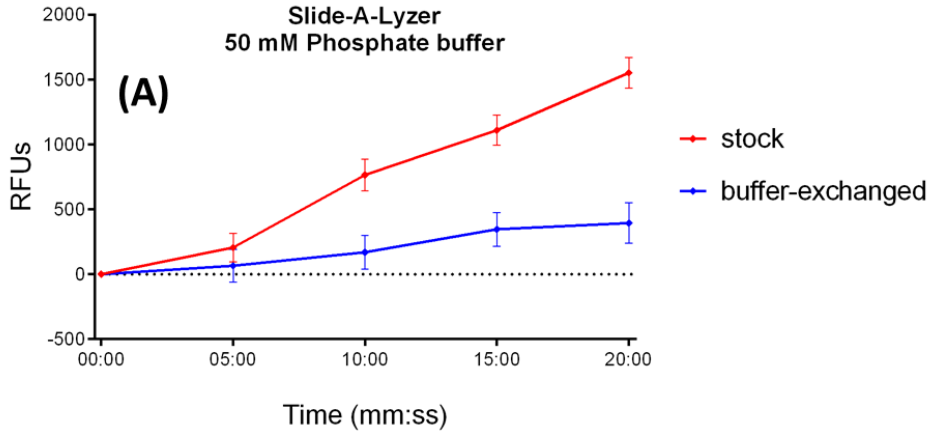


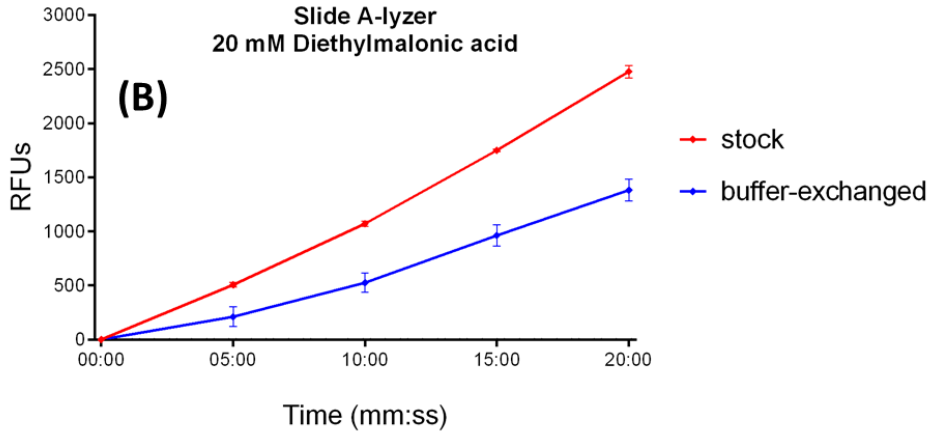


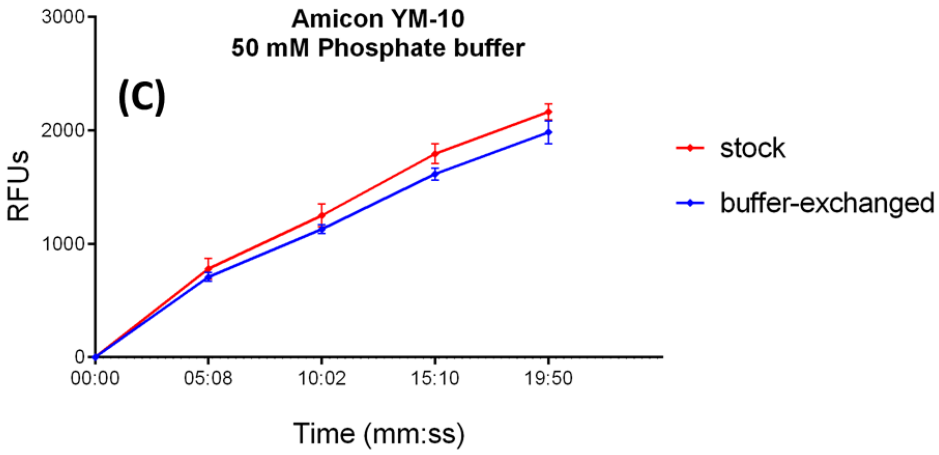


| **Device implemented** | **Buffer of choice** | **Specific activity of buffer-exchanged protein (nmol OMF/min/mg of protein)** | **Specific activity of stock protein (nmol OMF/min/mg of protein)** | **% specific activity loss due to buffer exchange** |
|---|---|---|---|---|
| Slide A-Lyzer | 50 mM Phosphate buffer | 0.20 ± 0.04 | 0.64 ± 0.02 | -69 ± 3.12 |
| Slide A-Lyzer | 20 mM Diethylmalonic acid | 0.31 ± 0.03 | 0.71 ± 0.02 | -56 ± 4.22 |
| Amicon YM-10 | 50 mM Phosphate buffer | 0.61 ± 0.03 | 0.68 ± 0.02 | -10 ± 2.94 |

**Figure 3.4 Effect of different buffer exchange conditions on PTEN phosphatase activity**

The change in RFUs due to the OMF released by stock versus buffer-exchanged PTEN was monitored over 20 min with the OMFP phosphatase assay. (A) When PTEN is dialyzed in 50 mM phosphate buffer pH 7.4 using the Slide-A-Lyzer cassette dialysis device its activity drops significantly (-69%). (B) The experiment was also repeated with the same device, replacing the exchange buffer with 20 mM diethylmalonic pH 7.4 with a minor improvement in retention of activity (-56%). (C) Following buffer exchange in 50 mM phosphate buffer pH 7.4 using the Amicon YM-10 centrifugal filter unit, the activity drop was drastically reduced (-10%). The Relative Fluorescence Units values are calculated after blank subtraction and normalization of the curve to start at zero. Data are presented as mean ± SD of three technical replicates.

### 3.4.5 Effect of HOCl oxidation on PTEN phosphatase activity

Following buffer exchange in 50 mM phosphate buffer pH 7.4 with the centrifugal filter unit, PTEN-GST was treated for 1 hour with a 15:1, 30:1, 60:1, 150:1, or 300:1 molar ratios of HOCl to PTEN-GST. HOCl-oxidized samples and untreated control were assayed for phosphatase activity using the OMFP assay. Increasing molar ratios of HOCl to PTEN-GST were found to correlate with a decrease in PTEN phosphatase activity, as evident from Figure 3.5 (A). A 75% drop in PTEN activity was seen upon treatment with 60:1 molar ratio of HOCl to PTEN-GST, while a 150:1 or a 300:1 molar ratio of HOCl to PTEN-GST caused the phosphatase activity of PTEN to drop by > 90%. 15:1 or 30:1 molar ratios of HOCl to PTEN-GST did not appear to cause significant protein inactivation.

A second phosphatase activity assay was performed after incubation of the HOCl-treated and untreated PTEN-GST sample with 100 mM DTT for 15 min, to test recovery of activity following re-reduction of the disulfide bond between Cys71 and Cys124 in the active site pocket of PTEN. For each molar ratio of HOCl to PTEN-GST, the activity following HOCl oxidation was compared to the activity after DTT incubation. The results of the OMFP activity assay, shown in Figure 3.5 (B), indicate that for each of the HOCl to PTEN-GST molar ratios tested, the DTT incubation was not able to significantly recover activity. This confirmed that the HOCl treatment caused modifications to the protein structure that resulted in irreversible inactivation of PTEN.

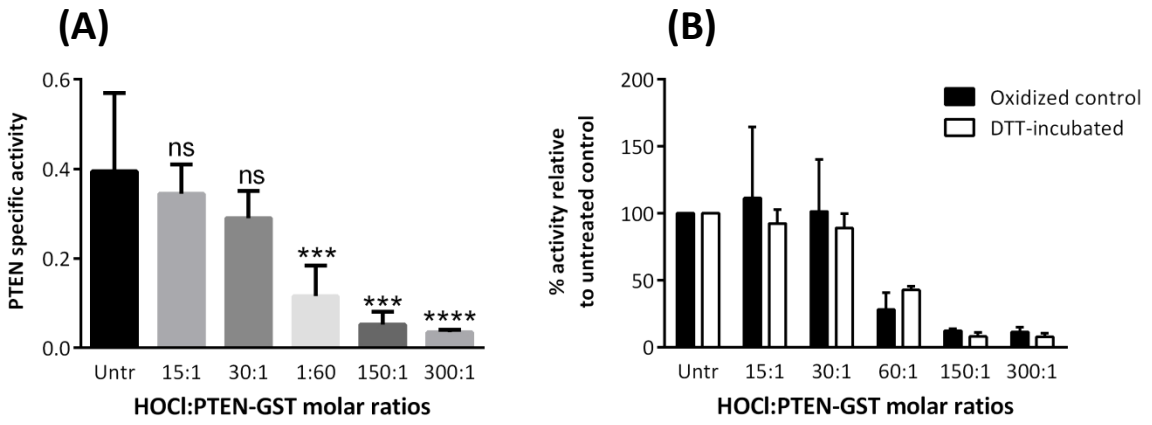


**Figure 3.5 HOCl irreversibly inactivates PTEN.**

(A) The OMFP assay was used to monitor the effect of increasing HOCl to PTEN-GST molar ratios on PTEN specific activity. The results are presented as mean ± SD (N = 4). Statistical significance was assessed by one-way ANOVA followed by Dunnett's correction for multiple comparisons (*** = $p < 0.001$; **** = $p < 0.0001$; ns = not significant). PTEN specific activity is expressed in nmol OMF/min/mg protein. (B) The effect of DTT reduction on the phosphatase activity of HOCl-oxidized PTEN was evaluated by comparing the percentage activity retained by the HOCl oxidized versus 100 mM DTT-incubated PTEN. The results are presented as mean ± SD (N = 3). Statistical significance was assessed by two-tailed unpaired Student's t-test). Untr= untreated.

### 3.4.6 SDS-PAGE and densitometry analysis of HOCl-oxidized PTEN

Aliquots of HOCl-treated and control samples were analyzed by SDS-PAGE, and the resulting gels were Coomassie-stained to visualize the electrophoretic profile of the oxidized protein. After careful consideration, 50 µg of protein was considered the appropriate amount to load on SDS-PAGE gels to generate an interpretable electrophoretic profile of oxidized PTEN-GST without too significant overloading, and to obtain enough material for the MS analysis.

Scans of the Coomassie-stained gels were imported into the software ImageJ to perform densitometry. Three gels obtained from the SDS-PAGE analysis of biological repeats of the HOCl treatment were used. The analysis was performed first by measuring the amount of protein signal corresponding to the PTEN-GST intact band across the different HOCl-treated samples. In addition, the analysis was performed on the full gel lane for each of the samples treated with oxidants, in order

to compare the level of total protein in each gel lane. The densitometry results for both the intact PTEN fusion band and the full gel lane were then plotted against the phosphatase activity data recorded with the OMFP assay (Figure 3.6 A). The percentage of signal intensity corresponding to the PTEN-GST main band dropped following a pattern similar to that of the percentage phosphatase activity relative to the untreated control. Densitometry analysis of the intact PTEN-GST band found statistically significant reduction in signal intensity for the sample treated with a 60:1 (-20%), 150:1 (-80%) and 300:1 (-90%) molar ratio of HOCl to PTEN-GST. As expected, the full lane protein content dropped to a lesser extent due to the dose-dependent increase in aggregation counterbalancing the loss of protein in the main band, and is only significantly lower in the sample treated with a 300:1 molar ratio of HOCl to PTEN-GST, which shows a ~30% reduction in protein Coomassie-staining. Pearson's correlation analysis was performed to measure the relationship between the protein signal on the gel and PTEN phosphatase activity (Figure 3.6 B). A strong positive correlation was found between the PTEN phosphatase activity and the PTEN-GST main band signal, which followed a similar trend of reduction with increasing HOCl to PTEN molar ratios (Pearson's correlation coefficient $r = 0.936$; p-value = 0.006), while correlation between the PTEN phosphatase activity and the full lane protein content was non-statistically significant (Pearson's correlation coefficient $r = 0.685$; p-value = 0.133). In Figure 3.6 (C) is presented a Coomassie-stained gel image, representative of the three that were used for the densitometry analysis. The gel shows an increasing amount of protein signal at kDa > 100 with increasing PTEN-GST to HOCl molar ratios, while the intensity of the PTEN-GST intact band at ~70 kDa decreases. Samples treated with a 60:1 HOCl to PTEN-GST molar ratio generally showed reduced intact PTEN-GST band signal on the gels, while samples treated with a 150:1 and a 300:1 HOCl to PTEN-GST molar ratios showed little or no PTEN-GST band at all. The presence of protein aggregates at > 100 kDa is visible in both the resolving and the stacking gel and it is particularly evident in the gel lanes corresponding to the PTEN-GST samples treated with 60:1, 150:1, and 300:1 PTEN-GST to HOCl molar ratios. The bands observable between 20 and 30 kDa were most probably due to protein degradation products which had formed after the protein purification (as these bands were not visible in the original PTEN-GST preparation shown in Figure 3.2, pg. 120), and that became prominent as the gel shown in Figure 3.6 (C) was overloaded with protein sample. As the PTEN specific activity assayed immediately after purification of the PTEN-

GST protein was comparable to that of the protein samples used for the experiments (both approximately 0.7 nmol OMF/min/mg of protein), it is unlikely that the degradation products observed had a significant effect on protein stability.

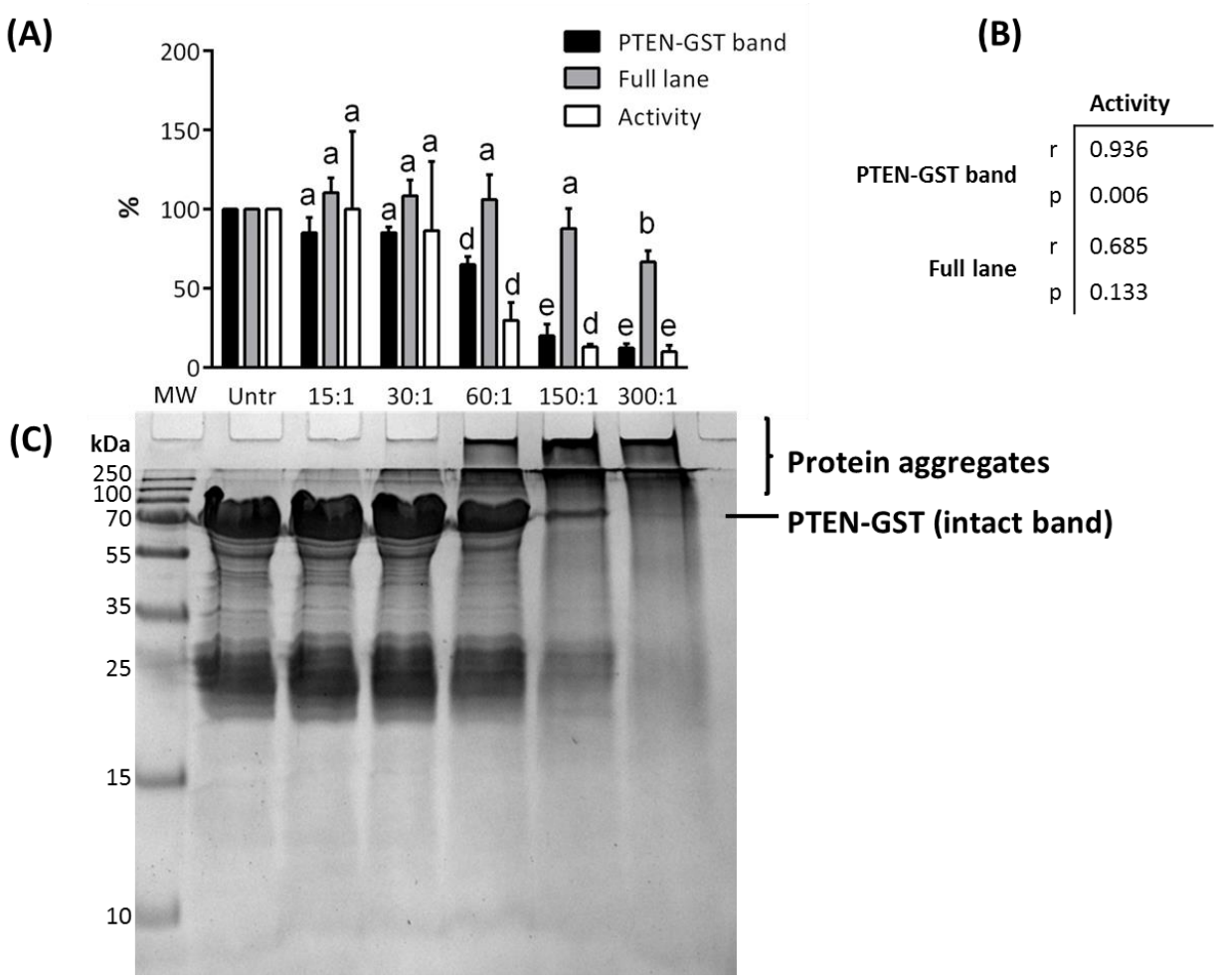


**Figure 3.6 SDS-PAGE/densitometry analysis versus phosphatase activity of HOCl-oxidized PTEN-GST**

(A) The percentage signal intensity of the Coomassie-stained intact PTEN-GST band and the full gel lane analyzed by densitometry were plotted versus the percentage phosphatase activity. Statistical analysis was performed with one-way ANOVA followed by Dunnett's multiple comparisons test before baseline correction. Densitometry data are presented as mean ± SD for N= 3 and activity data are presented as mean ± SD for N = 4 (a = not significant; b = $p < 0.05$; c = $p < 0.01$; d = $p < .001$; e = $p < 0.0001$). (B) Correlation between PTEN phosphatase activity and the protein signal on the gel corresponding to the PTEN-GST band or the full lane. The correlation coefficient r and the p-value were calculated using Pearson's correlation analysis. (C) Representative Coomassie-stained gel of

HOCl-oxidized PTEN-GST. With increasing HOCl molarities, the percentage protein content of the main PTEN-GST bands at ~ 70 kDa drops and protein aggregation builds up in the top section of the gel (kDa > 100). Untr = untreated. MW = molecular weight.

### 3.4.7 Identification and quantification of HOCl-oxidized PTEN peptides

Following in-gel digestion of gel pieces obtained from the excision of the intact GST-fusion protein main band for each of the HOCl treatments, the extracted peptides were analyzed by mass spectrometry and the resulting LC-MS runs were imported onto the label-free quantification software Progenesis QI for Proteomics. Similarly, the gel pieces obtained from the excision of the areas of gel corresponding to protein aggregation (both in the resolving and the stacking gel) for each of the HOCl treatments were digested and the LC-MS runs acquired from the analysis of the extracted peptides were loaded on a separate Progenesis experiment. For the quantification of oxPTMs, the LC-MS runs of both main band and protein aggregates samples of HOCl-treated PTEN-GST were aligned against untreated controls for feature matching and peptide identification. The Mascot Database Searches were performed in multiple rounds on the aligned LC-MS runs searching for no more than 5 modifications at a time. The protein of interest (PTEN) was identified with a high level of confidence in both Progenesis QI experiments created for the main band and the aggregates.

The initial Mascot sequence coverage for PTEN was 81% for the intact band sample and 85% for the protein aggregates sample, and decreased to 67% and 66%, respectively, after peptide score thresholding. Figure 3.7 shows the PTEN amino acid sequence coverage obtained after Mascot database search of MS/MS data and peptide score thresholding for both PTEN intact band and aggregates, along with oxidation sites and modifications detected. In both intact band and aggregates samples many amino acid residues were missing from the final features dataset. No data was available for residues mapped in the PtdIns(4,5)$P_2$-binding N-terminal module (PBM, amino acids 1-13), as residues 1-14 were not covered by any of the identified peptides. In the phosphatase domain, residues 56-62 were not detected, while residues 63-66 were covered only in the intact band sample (in the aggregate sample the peptides containing these residues scored below the threshold used for identification). Residues 75-80 were detected in peptides scoring below the adopted threshold, while

residues 81-84 were not covered by any of the identified peptides. Moreover, residues 85-125 were part of a peptide scoring below the adopted identification threshold, amino acids 126-128 were not covered by any identified peptide, and residues 129-130 were detected in the intact band sample only. As a result of this, the PTEN catalytic WPD-loop (amino acids 88-98) was not covered, while the catalytic p-loop (amino acids 123-130) was only partially covered in the intact band sample and completely uncovered in the aggregates sample, resulting in the catalytic cysteine (Cys124) being excluded from the systematic modification mapping. Additionally, none of the identified peptides contained residues 143-144 or residues 160-172, which include residues mapping in the catalytic T1-loop (amino acids 160-171). In the C2 domain, the PTEN sequence coverage for the intact band sample did not include any peptide that contained amino acid 222-234, while these residues were successfully detected in the aggregates sample. The CBR3-loop (amino acid 263-269) was only partially covered in the intact band sample (residues 261-267 were missing), and completely excluded from the analysis in the aggregates sample (residues 255- 260 and residues 267-269 were detected in peptides scoring below the identification threshold, while residues 261-267 were not detected at all). In addition, no data was available for the cα2 helix (amino acids 327-335), as none of the identified peptide contained amino acid residues 323-345. Finally, Val403 mapping in the PDZ-binding domain (amino acids 401-403) was identified in the intact band sample as part of a tryptic peptide miscleaved at Lys402. This peptide was not detected in the aggregates sample where only the non-miscleaved version (lacking the last residue Val403) was identified.

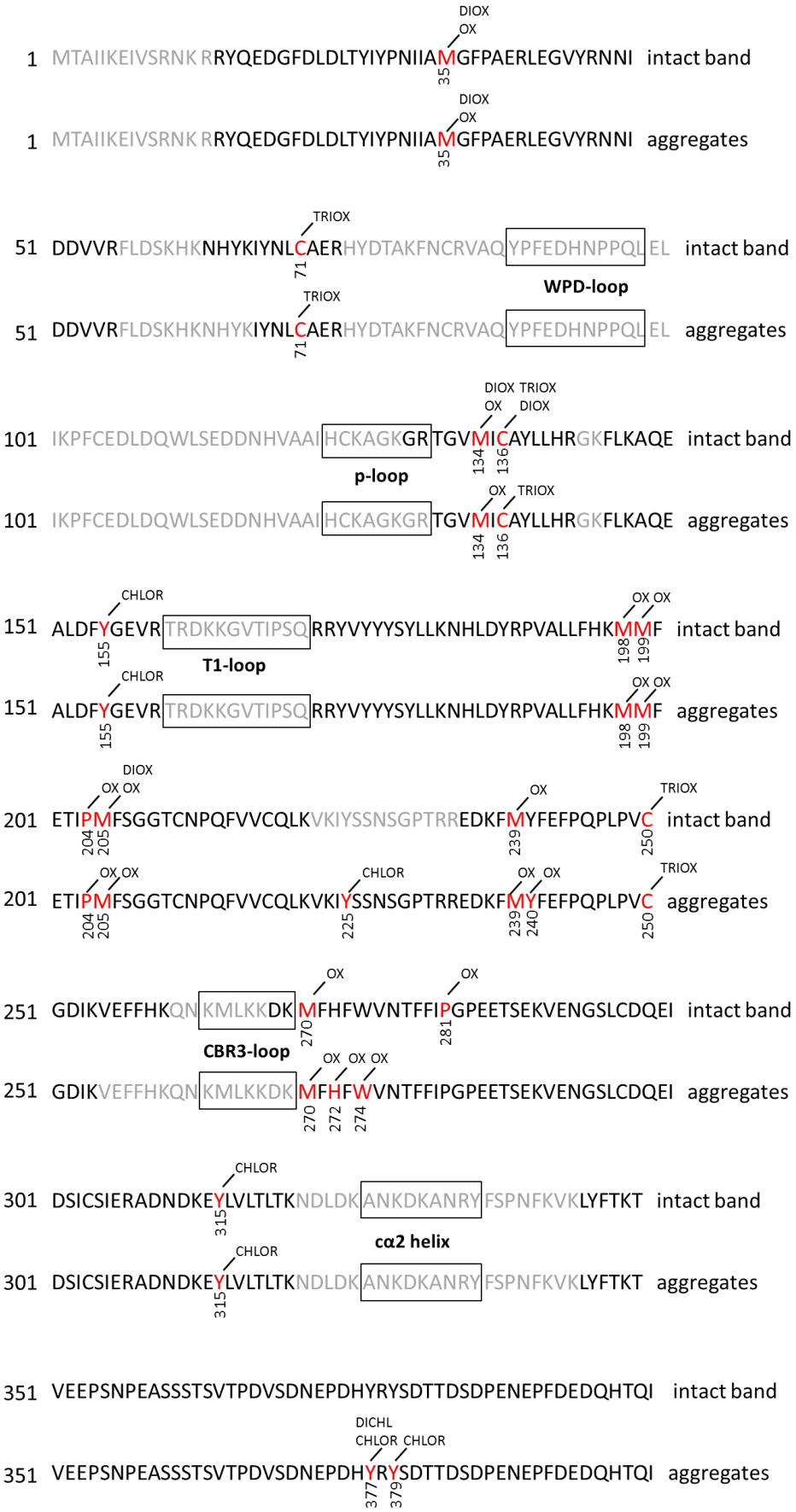
1 MTAIIKEIVSRNK RRYQEDGFDLDLTYIYPNIIAMGFPAERLEGVYRNNI intact band
DIOX
OX
35
1 MTAIIKEIVSRNK RRYQEDGFDLDLTYIYPNIIAMGFPAERLEGVYRNNI aggregates
DIOX
OX
35
51 DDVVRFLDSKHKNHYKIYNLCAERHYDTAKFNCRVAQYPFEDHNPPQLEL intact band
TRIOX
71
WPD-loop
51 DDVVRFLDSKHKNHYKIYNLCAERHYDTAKFNCRVAQYPFEDHNPPQLEL aggregates
TRIOX
71
101 IKPFCEDLDQWLSEDDNHVAAIHCKAGKGRTGVMICAYLLHRGKFLKAQE intact band
DIOX TRIOX
OX DIOX
134 136
p-loop
101 IKPFCEDLDQWLSEDDNHVAAIHCKAGKGRTGVMICAYLLHRGKFLKAQE aggregates
OX TRIOX
134 136
151 ALDFYGEVRTRDKKGVTIPSQRRYVYYYSYLLKNHLDYRPVALLFHKMMF intact band
CHLOR
155
T1-loop
OX OX
198 199
151 ALDFYGEVRTRDKKGVTIPSQRRYVYYYSYLLKNHLDYRPVALLFHKMMF aggregates
CHLOR
155
OX OX
198 199
201 ETIPMFSGGTCNPQFVVCQLKVKIYSSNSGPTRREDKFMYFEFPQPLPVC intact band
DIOX
OX OX
204 205
OX
239
TRIOX
250
201 ETIPMFSGGTCNPQFVVCQLKVKIYSSNSGPTRREDKFMYFEFPQPLPVC aggregates
OX OX
204 205
CHLOR
225
OX OX
239 240
TRIOX
250
251 GDIKVEFFHKQNKMLKKDKMFHFWVNTFFIPGPEETSEKVENGSLCDQEI intact band
OX
270
OX
281
CBR3-loop
251 GDIKVEFFHKQNKMLKKDKMFHFWVNTFFIPGPEETSEKVENGSLCDQEI aggregates
OX OX OX
270 272 274
301 DSICSIERADNDKEYLVLTLTKNDLDKANKDKANRYFSPNFKVKLYFTKT intact band
CHLOR
315
cα2 helix
301 DSICSIERADNDKEYLVLTLTKNDLDKANKDKANRYFSPNFKVKLYFTKT aggregates
CHLOR
315
351 VEEPSNPEASSSTSVTPDVSDNEPDHYRYSDTTDSDPENEPFDEDQHTQI intact band
DICHL
CHLOR CHLOR
377 379
351 VEEPSNPEASSSTSVTPDVSDNEPDHYRYSDTTDSDPENEPFDEDQHTQI aggregates
401 TKV intact band
PDZ-binding motif
401 TKV aggregates

**Figure 3.7 PTEN sequence coverage and oxidation sites identified from LC-MS/MS data**

For both intact band and aggregates samples, PTEN residues which were identified by Mascot database search of LC-MS/MS data are indicated in black, while missing residues are indicated in grey. The amino acid numbers are indicated on the left and the oxidation sites are highlighted in red. The position of each modification detected is indicated below each of the modified amino acid shown in red. The squared boxes highlight key structural and functional domains of the phosphatase. OX= oxidation; DIOX = dioxidation; TRIOX= chlorination; CHLOR = chlorination; DICHL = dichlorination.

Figure 3.8 shows representative 3D images displaying the cross-sample peak picking of the modified peptide AQEALDFYGEVR (m/z = 716.33, charge = +2), carrying a 3-chlorotyrosine modification at Tyr8, corresponding to PTEN Tyr155 chlorination. This peptide was detected in the HOCl-oxidized samples obtained from the digestion of both intact band and aggregates fractions. The Progenesis QI screen view shown in Figure 3.8 can be used to revise the results of the software peak picking, in order to obtain information about the quality of feature matching and differential quantification performed. The peptide abundance for the modified peptide AQEALDFYGEVR was highest in the sample treated with 300:1 HOCl to PTEN-GST molar ratio and showed a HOCl dose-dependent trend in increase. A signal was also detected in the untreated sample, as a result of background noise falling within the borders of the peak picking area used for the peptide quantification. The peptide identification data were reviewed to resolve any conflicts and the raw data exported to a separate Excel worksheet to manually calculate the percentage relative modification.

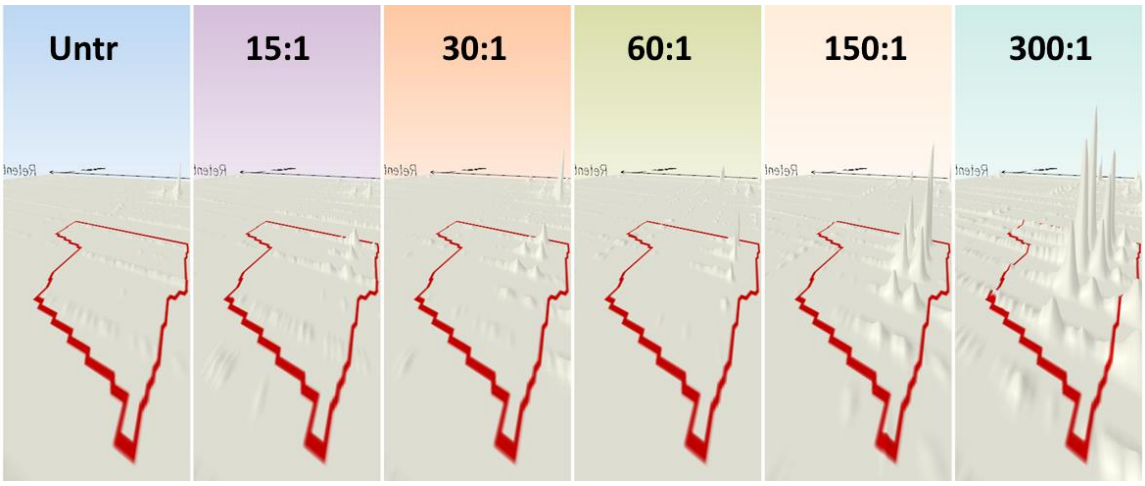


**Figure 3.8 Representative 3D montage zoomed into the feature corresponding to the chlorinated peptide AQEALDFYGEVR matched across the HOCl-oxidized PTEN samples**

Following alignment of the elution profiles, the software matches the feature corresponding to the same ion across multiple samples, and performs the relative quantification after normalization. Highlighted in red is the peak picking area drawn by the software algorithm around the peaks corresponding to the peptide matched across the LC-MS runs aligned for quantification. The modified peptide abundance was highest in the protein sample treated with a 300:1 molar ratio of HOCl to PTEN-GST and lowest in the untreated PTEN-GST sample (maximum fold change = 17.7, ANOVA p-value < 0.0001).

### 3.4.8 Validation of HOCl-induced modifications by *de novo* sequencing of MS/MS data

Following label-free quantification and identification, modified peptides were *de novo* sequenced so that the oxPTM(s) detected could be validated, and any conflicts could be resolved between same-m/z peptides carrying different modified residues. An example of such process is displayed in Figure 3.9, which shows the modified PTEN peptide AQEALDFYGEVR in being *de novo* sequenced to validate the 3-chlorotyrosine modification at Tyr8. As each peptide that is chlorinated when exposed to HOCl gains a chlorine atom (+35 atomic mass units) and loses one hydrogen (-1 atomic mass unit), chlorination events resulted in a +34 net increase in atomic mass unit [511]. For a doubly-charged ion as that shown in Figure 3.9, the net m/z increase relative to the native (unmodified) precursor was 34/2 = 17 m/z (the modified peptide had a m/z of 716.33 and the corresponding native peptide had a m/z of 699.35). The *de novo* sequencing procedure was repeated for all peptide features containing modifications that were found significantly more abundant in the HOCl-treated PTEN-GST versus untreated control. As a result of this, the accuracy of Mascot protein modification assignment could be evaluated. The peptide identification Mascot score cutoff that was adopted when filtering the peptide features identifications in Progenesis QI resulted in 0 false protein modifications assignments by Mascot. In the event of modified peptide conflicts that could not be resolved by *de novo* sequencing (e.g. both same-m/z peptides sequencable in the MS/MS spectrum), the modified peptide with higher Mascot Score was selected. Where the Ion Score was also equal between conflicting same-mass modified peptides, the modified peptide with the highest number of hits would be preferred.

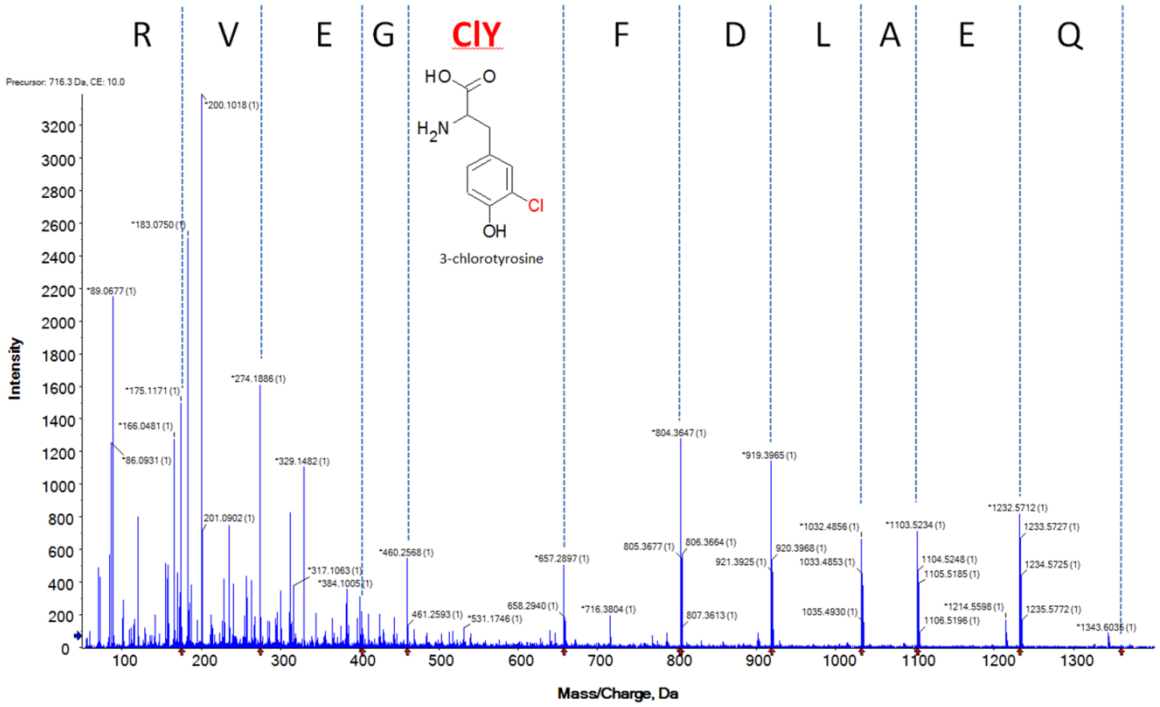


**Figure 3.9 MS/MS spectrum of the doubly-charged ion at m/z 716.33 identified as a chlorinated PTEN peptide**

The PTEN peptide AQEALDFYGEVR was identified in the aggregates fraction and was most abundant in the LC-MS run obtained from the analysis of the sample treated with a 300:1 molar ratio of HOCl to PTEN-GST. The tryptic peptide carried a chlorination at Tyr8, corresponding to Tyr155 in PTEN. The y1 ion observed at m/z 175 was established as the C-terminal residue R, and used to determine the remaining amino acid residues by calculating the mass difference of adjacent y-ions (labeled using red arrows in the software toolbar). By following the y-ion series residues Gln2-Arg12 were sequenced, while Ala1 could not be determined from the above MS/MS spectrum. The chlorinated tyrosine (ClY) corresponded to a mass shift of 197 Da (163 Da for tyrosine + 34 Da due to the addition of one chlorine).

### 3.4.10 Quantitative mapping of HOCl-induced oxPTMs to PTEN

For each modified residue detected, the abundances of all detected peptides containing the modification were added together. To calculate the relative modification, the summed up abundance of the modified peptide was divided by the summed up abundance of every other peptide containing the residue in question in the unmodified form (including peptides carrying other modifications). A total of 18 oxidatively modified amino acids were detected in the peptides generated from the intact PTEN-GST bands and a total of 21 in the peptides extracted from the protein aggregation area of the gel, accounting for 19 different modified residues and 10 different types of identified oxPTMs: methionine sulfoxide and sulfone, cysteine sulfonic and sulfinic acid, 4-hydroxyproline, 5-hydroxytryptophan, 2-oxo-histidine, 3,4-dihydroxyphenylalanine, 3-chlorotyrosine and 3,5-dichlorotyrosine. The percentage relative abundance data for each modification detected across the HOCl treatment used were analyzed using one way ANOVA with Dunnett's multiple comparisons to determine statistical significance.

After statistical analysis, thirteen amino acid residues revealed a significant increase in the level of oxidative modification upon HOCl treatment in at least one HOCl to PTEN-GST molar ratio condition. Those residues were Met35, Met134, Cys136, Tyr155, Met205, Met239, Tyr240, Met270, His272, Trp274, Tyr315, Tyr377 and Tyr379. For most oxPTMs, significant results were found upon a 60:1, 150:1 or 300:1 molar ratio of HOCl to PTEN-GST, while no significant increase in modification abundance was seen for the PTEN-GST samples treated with either a 15:1 or a 30:1 molar ratio of HOCl to PTEN-GST.

Figure 3.10 shows the quantification of oxPTMs found in the intact PTEN-GST band (A) and in the protein aggregates (B) for which a statistical significant difference and a fold change $\geq 2$ was seen in comparing against the untreated control the percentage modification abundance of at least one of the HOCl to PTEN-GST molar ratios used. The full dataset containing the PTEN peptide sequence carrying the modifications, the average relative abundance of all modifications detected in the treated samples, the fold change relative to untreated control and the p-value returned by one-way ANOVA with Dunnett's multiple comparisons test is displayed in Table 3.2. Methionine residues were found extremely susceptible to HOCl-mediated oxidation to both methionine sulfoxide and sulfone, although in many cases a significant extent of high abundance methionine oxidation was also found in the untreated control. A significant increase in the modification level was observed for Met35, which was

found approximately 10% oxidized to methionine sulfone upon 150:1 and 300:1 molar ratios of HOCl to PTEN, in both intact band and aggregates. In the intact PTEN-GST band, methionine sulfoxide was also found significantly more abundant at Met134 and Met239 upon 60:1, 150:1 and 300:1 HOCl to PTEN-GST molar ratios, and at Met270 upon 150:1 and 300:1 HOCl to PTEN-GST molar ratios, with all residues reaching approximately a 70% level of percentage modification in the samples treated with the highest HOCl concentration. Approximately 10-20% level of methionine sulfoxide at Met134, Met 239 and Met270 was found in the untreated control. Met205 was also found up to 38.4% oxidized to sulfoxide in the aggregated protein (but not in the intact PTEN-GST band) in high HOCl concentration, although the level of modification in the untreated control was also relatively high (22.7%). Cysteine was also found to be extensively oxidized. A 150:1 and a 300:1 molar ratio of HOCl to PTEN-GST caused a significant increase in the oxidation of Cys136, which was found 80% oxidized to sulfonic acid in the intact PTEN–GST band. In the aggregates the level of Cys136 sulfonic acid was close to 90% for all samples including untreated control. A significant increase in sulfinic acid was also detected at Cys136 in the intact band, although the maximum level of modification was very low (~2%). Cys250 was found significantly more oxidized to sulfonic acid in both intact band and aggregates upon 60:1, 150:1 and 300:1 HOCl to PTEN-GST molar ratios, with a peak modification level of approximately 60% in the intact band and of 50% in the protein aggregates. The active site Cys71 was also found oxidized to sulfonic acid in both intact band and aggregates, but none of the treated samples showed an increase in modification level that was statistically significant (Table 3.8). Lastly, the HOCl treatment resulted in the chlorination of tyrosine residues in both PTEN-GST intact band and aggregates. A significant increase in the abundance of chlorination was found at Tyr155, for which a 10% level of 3-chlorotyrosine was seen in the intact band upon 150:1 and 300:1 HOCl to PTEN-GST molar ratios, and a 15% in the aggregates upon 300:1 molar ratio of HOCl to PTEN-GST. A significant increase in chlorination level was also seen for Tyr 315 upon 60:1, 150:1 and 300:1 HOCl to PTEN-GST molar ratios in the intact band (with a peak modification level of approximately 10%) and upon 150:1 and 300:1 HOCl to PTEN-GST molar ratios in the aggregates fraction (with a peak modification level of approximately 5%). Moreover, Tyr 377 was found significantly more modified in peptides obtained from the aggregation build-up of HOCl treated samples, but not from the intact PTEN-GST band, showing a 15% level of chlorination upon 300:1

HOCl to PTEN-GST molar ratios, and a 5% and 10% of dichlorination upon 150:1 and 300:1 HOCl to PTEN-GST molar ratios, respectively. In the aggregates fraction, but not in the intact band, significantly higher levels of oxPTMs were seen that were due to hydroxylation of aromatic amino acids, including tyrosine, histidine and tryptophan. Tyrosine was found significantly more oxidized to 3,4-dihydroxyphenylalanine upon 60:1, 150:1 and 300:1 HOCl to PTEN molar ratios compared to the untreated control, although the level of modification only peaked at approximately 6% in the sample treated with the highest HOCl concentration. Conversely, His272 and Trp274 which showed a significant increase in hydroxylation with either 150:1 or 300:1 HOCl to PTEN-GST molar ratios had a modification level equal or greater than 20% in the samples treated more aggressively.

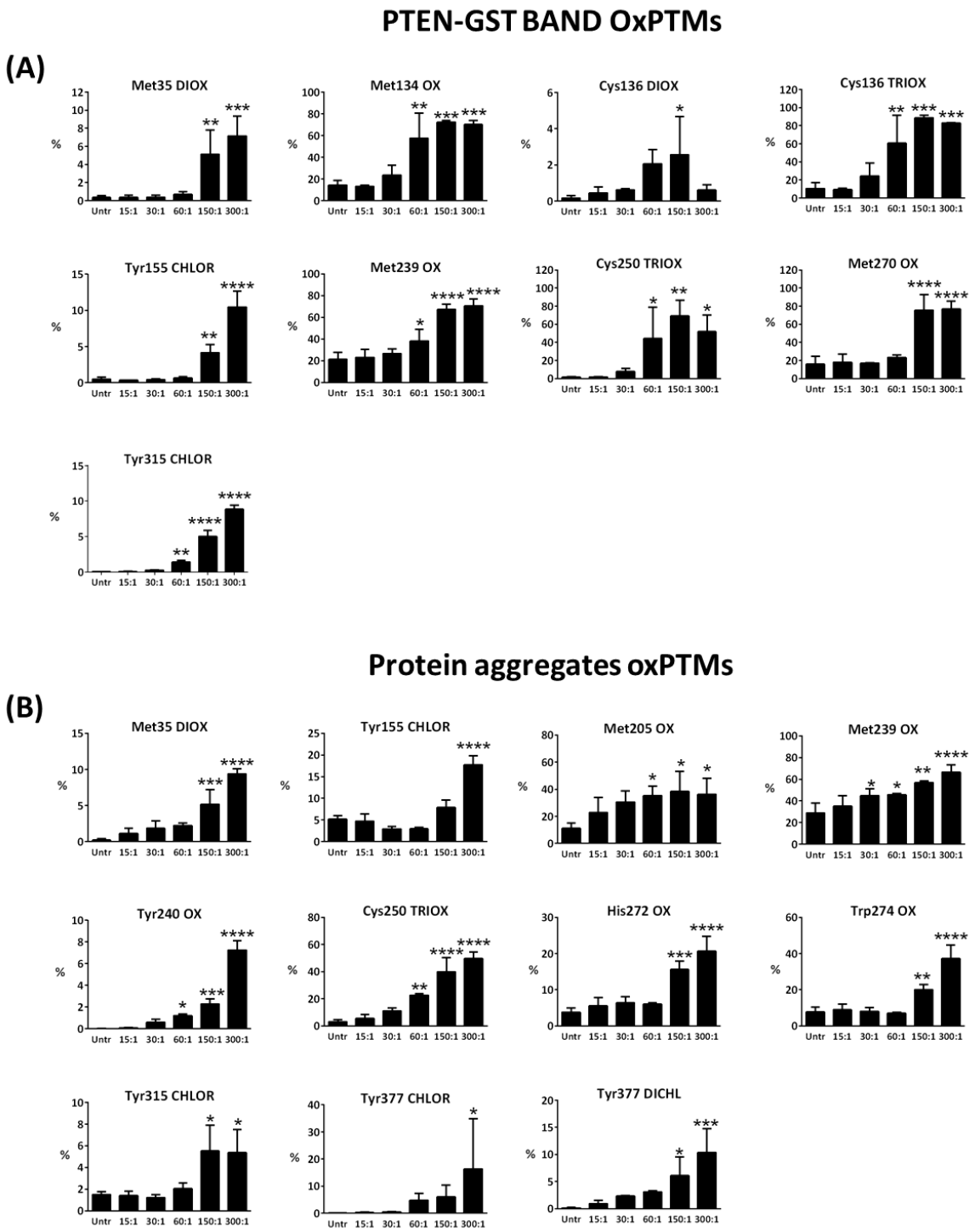


**Figure 3.10 Quantitative mapping of PTEN oxPTMs upon HOCl treatment**

The oxPTMs quantitative map was generated by MS-based label-free-quantitation of the in-gel digests obtained from the gel areas corresponding to the molecular weight of the intact GST-tagged protein (A) and the aggregation build-up area (B). The graph collages show modifications for which a statistical significant difference and a fold change ≥ 2 was seen in comparing against the untreated control the percentage modification abundance of at least one of the HOCl to PTEN-GST molar ratios used. Statistical analysis was performed by one-way ANOVA with Dunnett's multiple comparison

test. Data are presented as mean ± SD (N = 3, * = $p < 0.05$, ** = $p < 0.01$, *** = $p < 0.001$, **** = $p < 0.0001$). OX= Oxidation. DIOX= Dioxidation; TRIOX= Trioxidation; CHLOR= Chlorination; DICHL= Dichlorination. Untr = untreated.

**Table 3.2** Identification and quantification of PTEN oxidative modifications in the PTEN-GST intact band and aggregates following HOCl oxidizing treatment

| Peptide sequence[1] | Mod[2] | Fraction detected[3] | | HOCl:PTEN-GST molar ratios 15:1 | 30:1 | 60:1 | 150:1 | 300:1 |
|---|---|---|---|---|---|---|---|---|
| TVEEPSNPEASSSTSVTPDVSDNEPDHYR | **Tyr377 CHLOR*** | Aggregation | FC | 0 | Infinity | Infinity | Infinity | **Infinity** |
| | | | p-value | > 0.9999 | > 0.9999 | 0.6843 | 0.9908 | **0.0417** |
| | | | % | 0.00 | 0.00 | 0.00 | 0.01 | 0.29 |
| FMYFEFPQPLPVCGDIK | **Tyr240 OX*** | Aggregation | FC | 10.06 | 47.11 | 84.95 | 323.25 | **1031.21** |
| | | | p-value | 0.9997 | 0.3521 | **0.0196** | **0.0001** | **< 0.0001** |
| | | | % | 0.07 | 0.60 | 1.20 | 2.27 | 7.24 |
| ADNDKEYLVLTLTK | **Tyr315 CHLOR*** | PTEN-GST band | FC | 1.22 | 4.82 | 25.45 | 88.76 | **156.24** |
| | | | p-value | > 0.9999 | 0.9568 | **0.0087** | **< 0.0001** | **< 0.0001** |
| | | | % | 0.07 | 0.27 | 1.44 | 5.03 | 8.85 |
| | | Aggregation | FC | 0.92 | 0.86 | 0.80 | 3.66 | 3.56 |
| | | | p-value | 0.9999 | 0.9985 | 0.9801 | **0.0131** | **0.0164** |
| | | | % | 1.39 | 1.21 | 2.06 | 5.52 | 5.38 |
| TVEEPSNPEASSSTSVTPDVSDNEPDHYR | **Tyr377 DICHL*** | Aggregation | FC | 6.31 | 9.78 | 15.99 | 41.92 | **71.31** |
| | | | p-value | 0.9916 | 0.6690 | 0.4131 | **0.0305** | **0.0006** |
| | | | % | 0.92 | 2.32 | 3.10 | 6.09 | 10.35 |
| FMYFEFPQPLPVCGDIK | **Cys250 TRIOX*** | PTEN-GST band | FC | 1.20 | 5.64 | 33.08 | **51.84** | 38.82 |
| | | | p-value | > 0.9999 | 0.9899 | **0.0449** | **0.0022** | **0.0176** |
| | | | % | 1.60 | 7.52 | 44.11 | 69.12 | 51.76 |
| | | Aggregation | FC | 1.77 | 2.26 | 3.66 | 13.20 | 16.48 |
| | | | p-value | 0.9674 | 0.2470 | **0.0020** | **< 0.0001** | **< 0.0001** |
| | | | % | 5.34 | 11.02 | 22.54 | 39.74 | 49.61 |
| YQEDGFDLDLTYIYPNIIAMGFPAER | **Met35 DIOX*** | PTEN-GST band | FC | 1.05 | 1.07 | 1.98 | 14.78 | 20.67 |
| | | | p-value | > 0.9999 | > 0.9999 | 0.9982 | **0.0059** | **0.0003** |
| | | | % | 0.36 | 0.37 | 0.69 | 5.12 | 7.16 |
| | | Aggregation | FC | 5.11 | 7.48 | 8.31 | 23.39 | **42.33** |
| | | | p-value | 0.7291 | 0.2585 | 0.1209 | **0.0003** | **< 0.0001** |
| | | | % | 1.13 | 1.84 | 2.24 | 5.18 | 9.37 |
| AQEALDFYGEVR | **Tyr155 CHLOR*** | PTEN-GST band | FC | 0.68 | 0.84 | 1.34 | 8.91 | **22.48** |
| | | | p-value | 0.9997 | 0.9999 | 0.9997 | **0.0035** | **< 0.0001** |
| | | | % | 0.32 | 0.39 | 0.62 | 4.14 | 10.45 |
| | | Aggregation | FC | 0.91 | 0.77 | 0.57 | 1.52 | 3.42 |
| | | | p-value | 0.9885 | 0.2165 | 0.2214 | 0.1095 | **< 0.0001** |
| | | | % | 4.70 | 2.94 | 2.96 | 7.91 | 17.75 |
| TGVMICAYLLHR | **Cys136 DIOX*** | PTEN-GST band | FC | 2.68 | 3.71 | 12.40 | **15.39** | 3.63 |
| | | | p-value | 0.9952 | 0.9628 | 0.1075 | **0.0352** | 0.9672 |
| | | | % | 0.45 | 0.62 | 2.06 | 2.56 | 0.60 |
| TGVMICAYLLHR | **Cys136 TRIOX*** | PTEN-GST band | FC | 0.87 | 2.31 | 5.75 | **8.41** | 7.85 |
| | | | p-value | 0.9999 | 0.6478 | **0.0040** | **0.0001** | **0.0002** |
| | | | % | 9.22 | 24.41 | 60.64 | 88.72 | 82.82 |
| | | Aggregation | FC | 1.00 | 1.01 | 1.04 | 1.11 | 1.12 |
| | | | p-value | > 0.9999 | 0.5898 | 0.6901 | **0.0064** | **0.0048** |
| | | | % | 87.18 | 90.42 | 90.05 | 97.07 | 97.46 |
| MFHFWVNTFFIPGPEETSEK | **His272 OX*** | Aggregation | FC | 1.46 | 1.68 | 1.68 | 4.13 | **5.47** |
| | | | p-value | 0.8268 | 0.5526 | 0.6474 | **0.0002** | **< 0.0001** |
| | | | % | 5.50 | 6.33 | 6.05 | 15.58 | 20.65 |
| TGVMICAYLLHR | **Met134 OX*** | PTEN-GST band | FC | 0.91 | 1.64 | 4.01 | **5.05** | 4.89 |
| | | | p-value | 0.9998 | 0.7326 | **0.0013** | **0.0001** | **0.0002** |
| | | | % | 13.07 | 23.52 | 57.49 | 72.39 | 70.11 |
| | | Aggregation | FC | 1.03 | 1.07 | 1.00 | 1.10 | 1.19 |
| | | | p-value | 0.9779 | > 0.9999 | 0.5731 | 0.2360 | **0.0138** |
| | | | % | 65.55 | 63.97 | 68.18 | 70.35 | 75.81 |
| MFHFWVNTFFIPGPEETSEK | **Met270 OX*** | PTEN-GST band | FC | 1.13 | 1.08 | 1.47 | 4.78 | **4.86** |
| | | | p-value | 0.9985 | 0.9997 | 0.7986 | **< 0.0001** | **< 0.0001** |
| | | | % | 17.90 | 17.09 | 23.27 | 75.51 | 76.89 |
| | | Aggregation | FC | 1.12 | 1.17 | 1.23 | 1.22 | 1.05 |
| | | | p-value | 0.3084 | **0.0172** | **0.0019** | **0.0227** | 0.8982 |
| | | | % | 58.51 | 64.31 | 68.59 | 63.78 | 55.06 |
| MFHFWVNTFFIPGPEETSEK | **Trp274 OX*** | Aggregation | FC | 1.16 | 1.20 | 1.04 | 2.63 | **4.86** |
| | | | p-value | 0.9926 | 0.9999 | 0.9997 | **0.0065** | **< 0.0001** |
| | | | % | 8.88 | 7.98 | 7.00 | 20.10 | 37.18 |

| | | | | | | | | |
|---|---|---|---|---|---|---|---|---|
| MMFETIP**M**FSG GTCNPQFVVC QLK | **Met205 OX*** | PTEN-GST band | FC | 0.95 | 0.58 | 0.57 | 0.23 | 2.43 |
| | | | p-value | > 0.9999 | 0.9985 | 0.9985 | 0.9799 | 0.8160 |
| | | | % | 0.03 | 0.02 | 0.02 | 0.01 | 0.09 |
| | | Aggregation | FC | 2.02 | 2.64 | 2.72 | **3.41** | 3.22 |
| | | | p-value | 0.5278 | 0.1311 | **0.0493** | **0.0254** | **0.0398** |
| | | | % | 22.71 | 30.59 | 35.29 | 38.40 | 36.30 |
| F**M**YFEFPQPLP VCGDIK | **Met239 OX*** | PTEN-GST band | FC | 1.09 | 1.26 | 1.80 | 3.18 | **3.34** |
| | | | p-value | 0.9968 | 0.8082 | **0.0483** | **< 0.0001** | **< 0.0001** |
| | | | % | 23.06 | 26.67 | 38.17 | 67.24 | 70.65 |
| | | Aggregation | FC | 1.21 | 1.40 | 1.56 | 1.97 | 2.31 |
| | | | p-value | 0.6932 | **0.0457** | **0.0354** | **0.0010** | **< 0.0001** |
| | | | % | 35.0135 | 44.9442 | 45.7299 | 56.9346 | 66.5483 |
| YQEDGFDLDLT YIYPNIIA**M**GFP AER | Met35 OX* | PTEN-GST band | FC | 1.05 | 0.99 | 1.34 | 1.80 | 1.74 |
| | | | p-value | 0.9942 | 0.9999 | 0.0950 | **0.0003** | **0.0006** |
| | | | % | 52.79 | 49.61 | 67.18 | 90.22 | 87.34 |
| | | Aggregation | FC | 0.92 | 0.99 | 1.06 | 1.11 | 1.24 |
| | | | p-value | 0.9433 | 0.9819 | 0.9998 | 0.8455 | 0.2735 |
| | | | % | 62.35 | 72.23 | 66.89 | 75.57 | 84.18 |
| IYNL**C**AER | **Cys71 TRIOX** | PTEN-GST band | FC | 1.20 | 2.62 | 3.58 | 4.20 | 3.42 |
| | | | p-value | 0.9998 | 0.7290 | 0.3467 | 0.1874 | 0.4026 |
| | | | % | 10.43 | 22.85 | 31.23 | 36.62 | 29.79 |
| | | Aggregation | FC | 0.88 | 0.79 | 0.74 | 2.33 | 2.53 |
| | | | p-value | 0.9998 | 0.9971 | 0.9725 | 0.3804 | 0.2653 |
| | | | % | 3.72 | 3.14 | 2.37 | 9.84 | 10.70 |
| TGV**M**ICAYLLH R | Met134 DIOX | PTEN-GST band | FC | 0.85 | 2.59 | 1.20 | 0.38 | 1.01 |
| | | | p-value | 0.9997 | 0.1617 | 0.9985 | 0.8523 | > 0.9999 |
| | | | % | 13.07 | 23.52 | 57.49 | 72.39 | 70.11 |
| **M**MFETIPMFSG GTCNPQFVVC QLK | Met198 OX | PTEN-GST band | FC | 0.96 | 1.32 | 1.27 | 1.09 | 1.36 |
| | | | p-value | 0.9999 | 0.8843 | 0.9388 | 0.9997 | 0.8426 |
| | | | % | 0.35 | 0.48 | 0.46 | 0.40 | 0.49 |
| | | Aggregation | FC | 1.53 | 1.82 | 1.70 | 2.00 | 1.93 |
| | | | p-value | 0.5635 | 0.3338 | 0.2112 | 0.1034 | 0.1328 |
| | | | % | 38.16 | 42.23 | 45.30 | 49.67 | 48.18 |
| M**M**FETIPMFSG GTCNPQFVVC QLK | Met199 OX | PTEN-GST band | FC | 0.96 | 1.32 | 1.26 | 1.09 | 1.42 |
| | | | p-value | 0.9999 | 0.8920 | 0.9484 | 0.9989 | 0.7536 |
| | | | % | 0.35 | 0.48 | 0.46 | 0.40 | 0.52 |
| | | Aggregation | FC | 1.57 | 1.93 | 1.63 | 1.86 | 1.92 |
| | | | p-value | 0.5032 | 0.6319 | 0.1596 | 0.5086 | 0.4257 |
| | | | % | 30.82 | 31.98 | 33.18 | 36.44 | 37.67 |
| MMFETI**P**MFSG GTCNPQFVVC QLK | Pro204 OX | PTEN-GST band | FC | 1.13 | 1.39 | 1.37 | 0.53 | 0.70 |
| | | | p-value | 0.9910 | 0.6105 | 0.6534 | 0.4490 | 0.7928 |
| | | | % | 33.36 | 41.09 | 40.49 | 15.50 | 20.54 |
| | | Aggregation | FC | 0.94 | 0.87 | 0.97 | 0.88 | 0.97 |
| | | | p-value | 0.9965 | 0.9998 | 0.9631 | 0.9543 | 0.9997 |
| | | | % | 29.24 | 30.40 | 34.63 | 27.57 | 30.16 |
| MMFETIP**M**FSG GTCNPQFVVC QLK | Met205 DIOX | PTEN-GST band | FC | 1.10 | 0.63 | 0.37 | 0.39 | 0.85 |
| | | | p-value | 0.9998 | 0.9644 | 0.7835 | 0.8006 | 0.9996 |
| | | | % | 0.09 | 0.05 | 0.03 | 0.03 | 0.07 |
| VKI**Y**SSNSGPT R | Tyr225 CHLOR | Aggregation | FC | 0.99 | 0.96 | 1.14 | 1.35 | 1.40 |
| | | | p-value | > 0.9999 | 0.8106 | 0.5871 | 0.1363 | 0.0780 |
| | | | % | 67.54 | 77.73 | 81.32 | 91.78 | 95.16 |
| MFHFWVNTFFI **P**GPEETSEK | Pro281 OX | PTEN-GST band | FC | 0.37 | 0.77 | 0.65 | 0.00 | 0.00 |
| | | | p-value | 0.8137 | 0.9960 | 0.9770 | 0.4673 | 0.4673 |
| | | | % | 0.12 | 0.25 | 0.21 | 0.00 | 0.00 |
| **Y**SDTTDSDPEN EPFDEDQHTQI TK | **Tyr379 CHLOR** | Aggregation | FC | 7.37 | 12.40 | 14.83 | 170.06 | 459.86 |
| | | | p-value | > 0.9999 | 0.9999 | 0.9107 | 0.8143 | 0.0944 |
| | | | % | 0.26 | 0.53 | 4.80 | 6.03 | 16.31 |

[1] Peptide sequence obtained from the Mascot database search of LC-MS runs aligned on Progenesis QI, carrying the modified residue (in red)

[2] Gel Fraction corresponding to the LC-MS run where the peptide was detected

[3] Modification type and position within the protein amino acid sequence

FC = fold change relative to untreated control; p-value was returned by one-way ANOVA with Dunnett's multiple comparison test for each modification detected following relative quantification. % = average percentage abundance of the modification;

**Bold** indicates more than 2-maximum fold change in abundance of the modification in at least one HOCl to PTEN-GST molar ratio used; * indicates modification with a statistically significant increase in abundance. Infinity indicates FC values obtained when the abundance of the modification in the untreated control was 0.

The data was obtained from the analysis of PTEN-GST intact band and protein aggregates features present in three independent HOCl oxidation experiments.
Ranking of modifications with * is based on maximum FC, highlighted in bold **blue**. Ranking of other modification is based on their position within PTEN structure.

Next, the maximum fold change relative to untreated control was compared to the maximum average percentage modification recorded for each oxPTMs detected (in either intact PTEN-GST band or aggregates) that was significantly more abundant in the treated samples (Figure 3.11). For all oxPTMs detected, the highest level of average modification abundance and fold change relative to untreated control were seen after treatment with either a 150:1 or a 300:1 molar ratio of HOCl to PTEN-GST. In most cases, the maximum percentage modification abundance of residues which were found significantly more oxidized in the HOCl-treated samples depended on both the amino acid residue (shape-coded in Figure 3.11) and the type of modification involved (color-coded in Figure 3.11). Methionine residues that were significantly more oxidized to sulfoxide upon HOCl treatment (Met35, Met134, Met205, Met239, and Met270) usually reached very high levels of maximum modification abundance (38.4-90.2%), but the maximum fold change relative to the untreated control was generally in the low range (1.8-5.0), due to high level of modification in the untreated control. However, the occurrence of methionine sulfone detected at Met35 showed a completely different trend, as a maximum abundance of only 9.3% was reported, while the maximum fold change relative to untreated control was 20.7 for the intact PTEN-GST band and 42.3 for the aggregation area. Conversely, all tyrosine modifications detected showed a similar fold change/abundance pattern. While the maximum detected modification abundance of tyrosine chlorination events (both chlorination and dichlorination) was relatively low (0.3-17.8%), their average fold changes relative to the untreated control are among the highest recorded across the map (22.5-Infinity). The level of hydroxylation at Tyr240 only reached 7.2% in the sample treated with a 300:1 molar ratio of HOCl to PTEN-GST, and the maximum fold change relative to untreated control was 1031.2. Quantification of hydroxylation at both His272 and Trp274 revealed a maximum fold change of only 5, while the percentage modification abundance was 20.7% for 2-oxohistidine and 37.3% for 5-hydroxytryptophan. Cysteine residues were generally found to be extensively oxidized to cysteine sulfonic acid, showing very high level of modification (69.1-97.5%) as well as relatively high maximum fold change relative to the untreated control (8.4-51.8). Cysteine sulfinic acid was also detected with a high fold change (15.4), but the maximum level of modification abundance was below 3% as most of it was further oxidized to the sulfonic form.

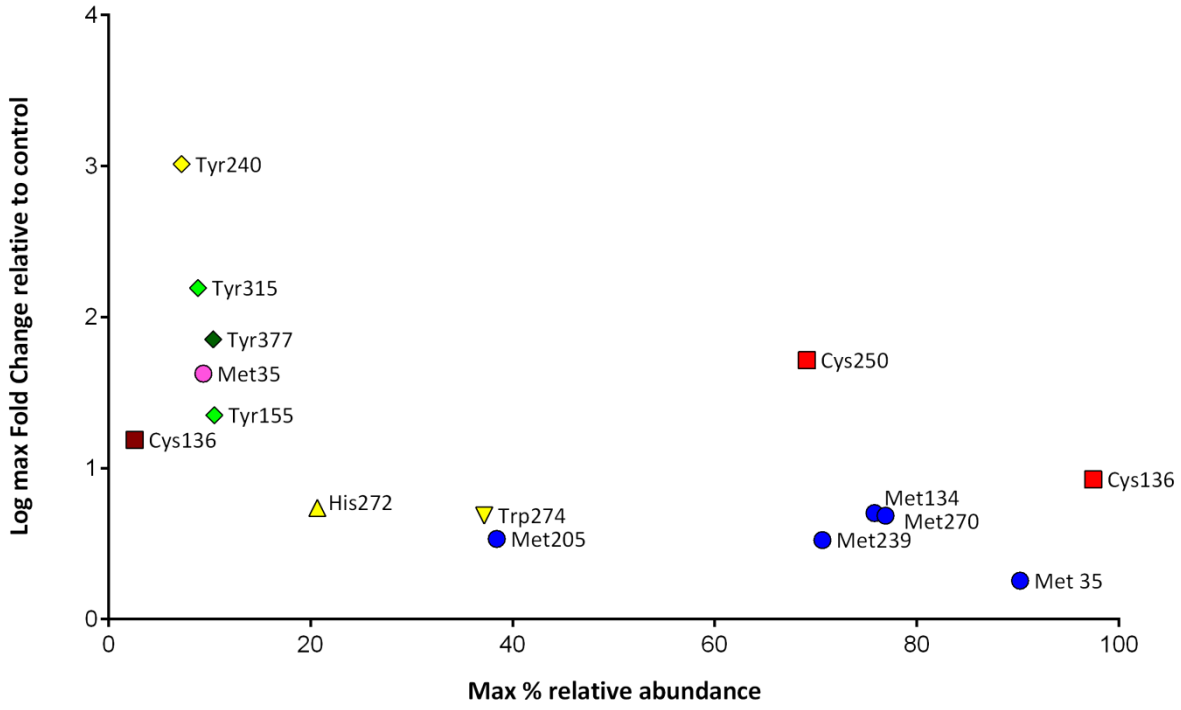


**Figure 3.11 Comparison of maximum fold change and percentage modification abundance of HOCl-induced PTEN oxPTMs**

Different symbols in the scatterplot correspond to different residues: square: cysteine; rhombus: tyrosine; circle: methionine, up-pointing triangle: histidine; down-pointing triangle: tryptophan. Different colors in the scatterplot correspond to different oxPTMs: yellow: hydroxylation; light green: chlorination; dark green: dichlorination; blue: methionine sulfoxidation; pink: methionine sulfonation; brown: cysteine sulfinylation; red: cysteine sulfonylation. Chlorination of Tyr377 (Max F.C = Infinity, Max % abundance = 0.29) was excluded from the scatter plot. Data is presented as the mean of the % maximum relative abundance versus maximum average fold change from three independent experiments for each detected modification that was found significantly elevated in comparing HOCl-treated samples with untreated control.

Lastly, oxidation sites corresponding to the 13 PTEN amino acid residues showing a significant increase in oxPTMs levels were mapped on the PTEN 3D crystal structure obtained from the Protein Data Bank (PDB) ID 1D5R (Figure 3.12) using the UCSF Chimera Molecular Modeling software. The oxPTMs are highlighted with different colors on the PTEN 3D structure depending on whether they were detected exclusively in the intact PTEN-GST band (cyan), in the aggregates (green) or in both (red). Met134 sulfoxide and Cys136 sulfinic acid in the phosphatase domain were significantly more

abundant in the PTEN peptides analyzed in the intact PTEN-GST band, while Cys136 sulfonic was abundant in both intact band and aggregates. With the exception of Tyr377 3-chlorotyrosine and 3,5-dichlorotyrosine which mapped in C-terminal tail, all remaining oxPTMs that were found exclusively in the PTEN aggregates (Met205 sulfoxide, His272 2-oxohistidine, Trp274 5-hydroxytryptophan and Tyr240 3,5-dihydroxyphenylalanine) mapped in the C2 domain.

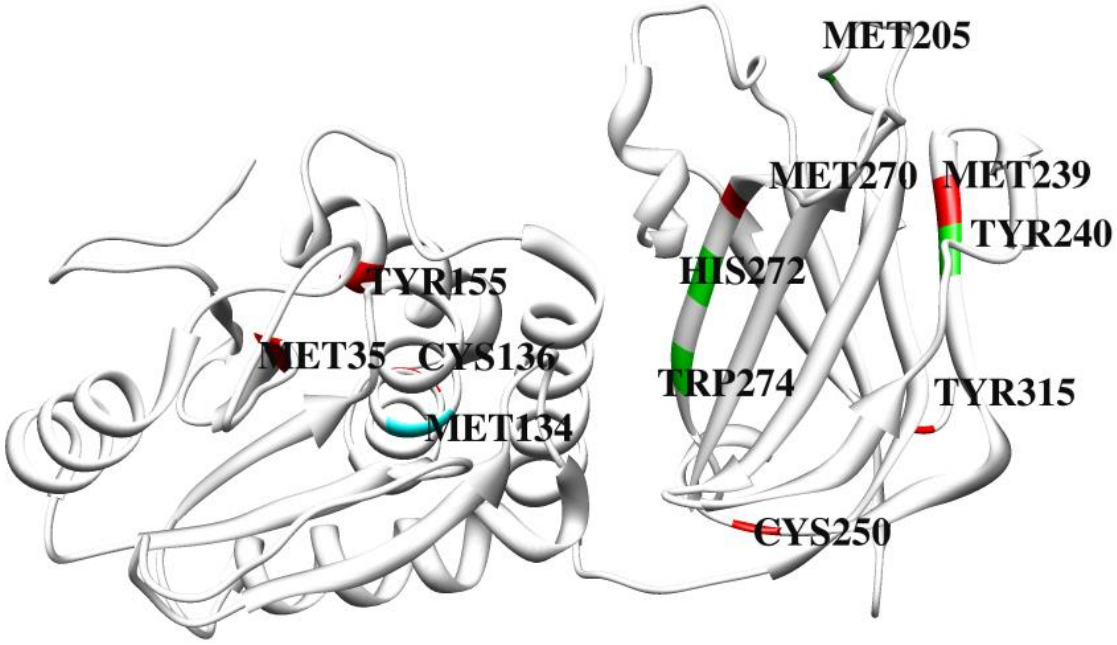


**Figure 3.12 HOCl modified residues mapped on PTEN 3D structure**

The 3D structure map was generated using UCSF Chimera Molecular Modeling System software, highlighting oxidation sites corresponding to a significant increase in modification level for oxPTMs. Residues that were found significantly more modified upon HOCl treatment in both intact PTEN-GST and aggregates are highlighted in red. Met134, which was found to be significantly more oxidized only in the PTEN-GST intact band, is highlighted in cyan; Met205, Tyr240, His272, and Trp274, which only showed a significant increase modification levels in the aggregates fractions are highlighted in green. Tyr 377 was also found significantly more oxidized in the PTEN aggregates upon HOCl treatment, but is not visible in the 3D model as is yet to be crystallized.

Solvent accessibility of PTEN residues was predicted with NetsurfP. Table 3.3 shows the solvent accessibility predicted for all modified residues that were found significantly more modified upon

HOCl treatment, including the uncrystallized residue Tyr377. Solvent accessibility data obtained for all 403 PTEN amino acids are reported in the Appendix (Section 8.3, Table 8.1). Based on their surface accessibility PTEN residues were predicted to be in two classes as either buried or exposed using a cut-off of 25% exposed accessible surface area for each given amino acid. The majority of the oxPTMs detected after HOCl treatment of PTEN mapped in residues that are buried in the protein interior in normal folding conditions (Table 3.3). These included Met134, which was found significantly more oxidized only in the intact PTEN-GST, His272 and Trp274, which were found significantly more oxidized only in the aggregates, and all remaining residues that were found significantly more modified in both intact and aggregates. However, Met205, Tyr240, and the uncrystallized Tyr377, which were detected exclusively in the aggregates fraction, mapped in regions of the proteins that were predicted to be solvent-exposed.

**Table 3.3** Surface accessibility of HOCl modified residues

| **AA[1]** | **AA position[2]** | **RSA[3]** | **ASA[4]** | **Z-Score** | **Class assignment[5]** |
|---|---|---|---|---|---|
| M | 35 | 0.018 | 3.582 | 0.817 | Buried |
| *M* | *134* | *0.022* | *4.422* | *1.041* | *Buried* |
| C | 136 | 0.016 | 2.246 | 1.028 | Buried |
| Y | 155 | 0.04 | 8.505 | 0.173 | Buried |
| **M** | **205** | **0.339** | **67.874** | **-1.508** | **Exposed** |
| M | 239 | 0.066 | 13.287 | 0.097 | Buried |
| **Y** | **240** | **0.271** | **57.977** | **0.743** | **Exposed** |
| C | 250 | 0.235 | 33.022 | 0.221 | Buried |
| M | 270 | 0.03 | 6.003 | 0.395 | Buried |
| **H** | **272** | **0.044** | **7.913** | **0.388** | **Buried** |
| **W** | **274** | **0.022** | **5.219** | **1.212** | **Buried** |
| Y | 315 | 0.177 | 37.932 | 0.048 | Buried |
| **Y** | **377** | **0.325** | **69.41** | **-1.253** | **Exposed** |

[1]AA = Amino acid
[2]Amino acid position
[3]RSA = Relative Surface Accessibility
[4]ASA = Absolute Solvent Accessibility
[5]Class assignment was predicted using a threshold of 25 exposed accessible surface area, based on the $ASA_{max}$ of a given amino acid.
Residues that were found significantly more modified exclusively in the aggregates fraction are indicated in **bold.**
Met134, which was found significantly more modified exclusively in the PTEN-GST intact band is indicated in *italic.*

# 3.5 Discussion

The study presented in this chapter describes the effect of hypochlorous acid-induced oxidative damage to the activity and structure of the dual specificity phosphatase PTEN. A number of oxPTMs has been identified that appear to be related to the irreversible inactivation of PTEN caused by the HOCl treatment.

Prior to any oxidation experiment, the purified PTEN was buffer-exchanged in order to remove reagents present in the elution buffer (such as the antioxidant glutathione and the reducing agent DTT) that would interfere with the controlled oxidation experiment and the cryoprotectant glycerol that interfered with the assays used to measure protein concentration. Maintaining unaltered protein activity during the buffer exchange process was challenging, but also considered critical for the study, as if the protein is inactivated in non-reducing buffer conditions, the interpretation of any oxidation-related changes in activity may be more difficult or incomplete. For this reason some preliminary tests were carried out to compare PTEN-GST enzymatic activity before and after buffer exchange performed with different methods and buffers. The Slide-A-Lyzer dialysis cassette was unsuccessful in retaining PTEN activity after buffer exchange in 50 mM phosphate buffer pH 7.4, which resulted in approximately 69% drop in phosphatase activity. To test the hypothesis that the free phosphate present in phosphate buffers might interfere with the protein activity, the exchange buffer was replaced with 20 mM diethylmalonic acid pH 7.4, but no substantial improvement was seen (-56% activity), suggesting that this dialysis method was not compatible with the protein of interest. The second device tested for dialysis was Microcon centrifugal filter units. Minimal activity losses (-10%) were seen when PTEN-GST was buffer-exchanged in 50 mM phosphate buffer pH 7.4 using this system, which was therefore used throughout the entire experimental described in this thesis. While such system was considered reliable in maintaining PTEN activity for the purpose of this study, care was taken while handling the PTEN-GST protein solutions in order to minimize spontaneous oxidation events (by using the protein immediately after buffer exchange) and loss of stability due to environmental factors such as temperature or contaminants.

The buffer-exchanged GST-tagged PTEN was treated with hypochlorous acid to mimic the effect of myeloperoxidase-induced damage on PTEN phosphatase activity and structure. The maximum level of HOCl concentration used to treat PTEN was chosen after evaluating: 1) the information available on the HOCl concentrations generated by inflammation-stimulated neutrophils *in vivo* (up to 5 mM HOCl) [493]; and 2) the HOCl concentration necessary to fragment proteins *in vivo* (10 mM HOCl) [515]. A maximum concentration of 10 mM HOCl (300:1 HOCl to PTEN-GST molar ratio) and a range of HOCl concentrations were eventually used, so that the protein modifications patterns could be correlated to various degrees of protein inactivation and structural changes due to oxidation. Exposing PTEN to increasing HOCl concentrations for 1 hour caused a relatively linear drop in PTEN activity, assayed by measuring the amount of fluorescent OMF released following hydrolysis of the artificial substrate OMFP. The phosphatase activity was significantly reduced when the phosphatase was treated with 60:1 (2 mM HOCl), 150:1 (5 mM HOCl), and 300:1 (10 mM HOCl) HOCl to PTEN-GST molar ratios. As the reversible formation of a disulfide bond between Cys71 and Cys124 in the active site of PTEN has been previously associated to PTEN $H_2O_2$-induced inactivation [144,423], the hypothesis that the drop in activity could be reversible was tested by assaying the HOCl-treated protein activity after incubation for 15 min in reducing conditions (100 mM DTT). For all the HOCl concentrations tested, the OMFP assay showed no significant difference between the activity of the HOCl-oxidized protein before and after incubation with 100 mM DTT, suggesting that modifications other than the Cys71-Cys124 disulfide bond were responsible for the reduction in activity. However, the formation of the active site disulfide bond could not be ruled out, as HOCl was previously demonstrated to cause the formation of an intramolecular DTT-reversible disulfide bond [227] as well as intermolecular dimers containing a disulfide cross-link [516] in other proteins.

The effects of HOCl oxidation on PTEN structure were further evaluated by analyzing the electrophoretic profile of the oxidized protein. The decrease in PTEN-GST band intensity observed on the gel suggested that increasing HOCl concentrations altered PTEN protein structure substantially. High molecular mass aggregates were observed for all PTEN samples treated with HOCl (but were particularly evident in the samples treated with 60:1, 150:1, and 300:1 HOCl to PTEN-GST molar ratios), and increased following a dose-dependent pattern, in line with that reported for other proteins treated with HOCl *in vitro* [500,517]. The activity data previously recorded were compared to the

densitometry data performed on both the full gel lane and the intact PTEN-GST band visible on the SDS-PAGE used to analyze HOCl-treated PTEN samples. Similar reduction patterns were seen in comparing the protein intact band signal and the phosphatase activity, both of which dropped significantly with HOCl to PTEN-GST molar ratios higher than 60:1. Unsurprisingly, the total protein signal on the gel was unchanged from 15:1 to 150:1 molar ratios of HOCl to PTEN-GST, and dropped by 30% only when the protein was treated with a 300:1 molar ratio HOCl to PTEN-GST (likely due to fragmentation or to larger aggregates that could not enter the resolving gel). This was considered essential to rule out the possibility that less total protein content rather than oxidation-induced damage could be responsible for the reduction of the intact protein signal and for any protein activity loss. PTEN activity showed a strong positive correlation with data obtained from the densitometry of the intact PTEN-GST band ($r = 0.936$; p-value = 0.006), while data obtained from the densitometry of the entire gel lane did not correlate as well ($r = 0.685$; p-value = 0.133). These results suggest a link between PTEN activity and protein structure, which would lead to speculate that aggregates of PTEN are not active upon HOCl oxidation, as full phosphatase activity seems to be present only in the intact form (visible as the 73kDa PTEN-GST band on the gel).

HOCl-induced oxPTMs for both intact band and aggregates were identified and quantified by MS-based label-free quantification using Progenesis QI for Proteomics. The protein sequence coverage after peptide score thresholding was 67%, thereby excluding from the oxPTMs mapping many important amino acid residues, such as Cys124 in the catalytic p-loop, all residues in the catalytic WPD-loop and T1-loop, part of the CBR3-loop and all residues of the cα2 helix.

After peptide quantification with Progenesis and identification with Mascot, the modified peptides were *de novo* sequenced to resolve same-m/z peptides conflicts and to validate the search engine results. The *de novo* sequencing procedure was time-consuming and laborious, but was found useful to gain confidence on the Mascot-identified modifications in peptides that were found significantly more modified in the HOCl-treated protein versus untreated control. However, the process did not reveal any Mascot false assignment, indicating that the score-based threshold was efficient in removing any ambiguous identification from the modified peptides list.

For each of the oxPTMs detected, the relative abundance of each modified peptide(s) obtained from Progenesis QI and validated with *de novo* sequencing was used to calculate the percentage

relative modification accounting for the relative abundance of the corresponding unmodified peptide(s). Obtaining the oxPTMs amount directly from the abundance of each modified peptide was not considered accurate as the level of the peptide in its unmodified form also influenced the total amount of a given residue in each HOCl treated sample.

Among the 19 modified residues that were mapped and quantified, 13 were found to carry oxidative modifications that were significantly more abundant upon HOCl treatment. These oxPTMs included methionine sulfoxide and sulfone, cysteine sulfinic and sulfonic acid, tyrosine hydroxylation, chlorination and dichlorination, histidine hydroxylation and tryptophan hydroxylation.

Methionine sulfoxide was significantly higher at several methionine residues within PTEN, including Met 134, Met205, Met239, and Met270. These residues were expected to reach high level of modification upon HOCl treatment due to their well-known susceptibility to oxidation mediated by reactive species [518]. Instance of methionine sulfoxide was found elevated also in the untreated control for all the residues involved, suggesting that methionine residues underwent spontaneous oxidation regardless of the HOCl treatment. This explains the relatively low fold change range (3-5) that was seen for these modifications in comparing HOCl-treated samples with untreated control. Except for Met134 which was identified as a PTPs mutational hotspot [413], no study to date has investigated the role of Met205, Met239 or Met270 in PTEN structure and function.

Another significant HOCl-induced oxPTM was methionine sulfone, which was found at Met35, a residue previously characterized as important for PTEN phosphatase activity [409]. In contrast to what was observed for methionine sulfoxide, this residue did not show high levels of modifications in the untreated control, and was 20-40 times more abundant in the sample treated with the highest HOCl concentration. Because Met35 was not found to be significantly more oxidized to sulfoxide, it is reasonable to assume that this residue specifically oxidizes to sulfone under strong oxidizing conditions causing inactivation of PTEN (such as high HOCl molarities), in line to previous studies demonstrating its role in maintaining PTEN catalytic activity [409]. As this residue was already extensively modified to sulfoxide in the untreated control, it is likely that that the HOCl oxidation resulted in "saturation" of the sulfoxide modification state. This caused further oxidation of sulfoxide to sulfone, which was, in fact, detected in substantial amount only in the sample treated with the highest HOCl concentration used, while the corresponding sulfoxide did not increase. In addition,

because methionine sulfone, but not sulfoxide, has been shown to be irreversible *in vivo* [519], these results suggest that HOCl-induced PTEN inactivation is also irreversible in cells.

Additional significant changes were seen for the modification status of cysteine residues. Cysteine sulfinic and sulfonic acid modifications were seen upon HOCl treatment at Cys136, a PTEN residue that has been previously found mutated in Cowden's disease [520]. However, only a small percentage of Cys136 was actually sulfinic acid (2%), while the level of sulfonic acid reached 82% in the sample treated with the highest HOCl concentration, as cysteine sulfinic acid easily oxidizes to the corresponding cysteine sulfonic acid under oxidizing conditions [521]. Interestingly, PTEN aggregates corresponding to all the different HOCl concentration used (including the untreated control) showed a level of Cys136 sulfonic acid close to 90%, suggesting a HOCl-induced saturation effect for this modification. High levels of sulfonic acid were also seen at Cys250 (69%), which was found significantly more oxidized upon HOCl treatment, with a max fold change of 52, the highest recorded among cysteine residues. A sulfonic acid modification was also detected at Cys71, which is known to form the reversible disulfide bond with Cys124 upon $H_2O_2$ treatment, resulting in the reversible inactivation of PTEN [144,423]. While the HOCl treatment did not result in a significant increase in sulfonic acid at Cys71, the modification status of this residue is important for investigating the redox status of PTEN active site upon HOCl treatment. A previous study has compared the effect of HOCl and $H_2O_2$ oxidation demonstrating that while HOCl can also induce disulfides, it preferentially oxidizes thiol groups of active site cysteines to sulfinic and sulfonic acid, in contrast to $H_2O_2$ which only generated an intermolecular disulfide bridge [516]. As high abundance irreversible sulfonic acid was detected at Cys71, it could be speculated that the HOCl treatment did not result in the formation of high abundant reversible disulfide bond in the active site of PTEN. Further evidence supporting this hypothesis is provided by activity assay results, which demonstrated the irreversibility of PTEN inactivation upon HOCl treatment, denoting the presence of irreversible modifications such as sulfonic acid in the active site essential cysteines [522]. However, as Cys124 was not detected, care should be taken when relying on this data to draw conclusions on the thiol/disulfide intramolecular dynamics of PTEN active site.

One important group of significant oxPTMs included tyrosine chlorination states, which are a specific marker of myeloperoxidase-induced protein damage [231,523,524]. Among the chlorinated

amino acid was Tyr155, which has been shown by mutagenesis studies to be required for PTEN catalytic activity [409], as well as for the regulation of PTEN interaction with the E3 ubiquitin ligase WWP2, which mediates degradation of PTEN through a ubiquitination-dependent pathway [525]. Another significant increase in the level of chlorination was seen for Tyr315, for which mutagenesis studies have revealed a role in PTEN tumour suppressing function and phosphatase activity [426]. The *in vitro* HOCl oxidation of PTEN resulted in significantly higher levels of 3-chlorotyrosine at Tyr155 (max FC = 22.5) and Tyr 315 (max FC = 156.2), the abundance of which increased with decreasing PTEN activity and increasing aggregation. 3-chlorotyrosine and 3,5-dichlorotyrosine were also found significantly more abundant at Tyr377, mapped in the C-terminal tail of PTEN, a region of the phosphatase that has been demonstrated to be required for protein stability [428,526]. Interestingly, Tyr377 was found excessively modified exclusively in the aggregate fractions of HOCl-treated PTEN, (with a fold change of Infinity for the chlorination and 71 for the dichlorination), suggesting that this residue might be important for the PTEN C-terminal tail role in maintaining protein stability, a function that could be compromised upon HOCl oxidation.

The last group of significant oxPTMs was the hydroxylation of aromatic amino acids in the C2 domain of PTEN. These included Tyr240, the mutation of which has been shown to decrease both PTEN tumour suppressing function and phosphatase activity [426] and Trp274, which has been identified as a cancer-related mutation site in PTEN [527]. High fold change (1031.2) was seen for 3,4-dihydroxyphenylalanine at Tyr240 in the sample treated with the highest HOCl concentration, while a less marked increase in hydroxylation was observed at His272 (Max FC= 4.9) and Trp274 (Max FC 5.5). Similarly to that observed for Tyr377, these oxPTMs were identified exclusively in the PTEN aggregates. As a stabilization role has also been proposed for the C2 domain of PTEN [528], it is possible that these residues are involved in maintaining protein stability and that their oxidation contributed to the increased PTEN aggregation observed upon treatment of the protein with high HOCl concentrations.

Following identification and relative quantification, amino acids that were found significantly more modified upon HOCl treatment were mapped on the available PTEN 3D structure and their surface accessibility predicted using the PTEN FASTA sequence. The results of this analysis were useful to correlate the surface accessibility of the modified residue with whether the modification was

associated with the intact PTEN or the aggregated protein or both. The majority of the oxPTMs that were found significantly more abundant upon HOCl treatment were detected at residues buried within the protein, which are normally inaccessible to the surface and protected from oxidation [529]. Buried residues that carried oxPTMs were detected in the PTEN intact band only (Met136), and in the aggregates fraction only (His272 and Trp274), but the majority was detected in both and included Met35, Cys136, Tyr155, Met239, Cys250, Met270, and Tyr315. This results suggest that the HOCl treatment had destabilized the protein structure exposing more surface area, as HOCl has been previously shown to easily oxidize buried hydrophobic residues such as methionine, likely due to structure alterations caused by the oxidant [227,530]. Nonetheless, Met205, Tyr240, and the uncrystallized Tyr377, which mapped in regions of the protein predicted to be surface-accessible, were also found to be significantly more oxidized upon HOCl treatment. These surface-exposed modified residues were only detected in the aggregate samples, raising interesting questions about their correlation with the HOCl-induced aggregation. Hydroxylation of solvent-exposed Tyr, and oxidation of Met residues has been previously detected in oxidation-inducible protein aggregates, although is unclear whether these modification occur before or after the aggregates formation [531,532]. However, recent studies have shown evidence that oxidation of surface-exposed redox-sensitive amino acids is a primary event that promotes protein misfolding and aggregation [533,534]. It is possible that HOCl-induced modification of Met 205 and Tyr240 of PTEN could initiate a misfolding event by destabilizing nearby residues, therefore increasing the likelihood of secondary oxidative damage and aggregation-proneness.

In conclusion, the study described in this chapter addressed the comprehensive characterization of the effect of HOCl-mediated damage on the structure and function of the phosphatase PTEN. HOCl concentrations of 2 mM, 5 mM, and 10 mM were found to be the most effective in causing significant levels of protein inactivation, protein aggregation and, ultimately, modification status. The LC-MS-based quantitative mapping identified oxPTMs at residues important for PTEN activity and protein-protein interactions as well as at residues for which a functional role has not yet been determined. However, as of today the functional profile of PTEN oxidative modifications patterns is far from being complete. The partial sequence coverage which excluded key amino acid residues from the proteomics analysis is one of the main challenges that still need to be overcome to correlate PTEN oxPTMs to

protein phosphatase activity and folding status. Nevertheless, the proteomics approach described holds a great potential for measuring the effects of oxidation on proteins and could be important for the characterization of oxPTMs biomarkers in inflammation and disease.

# Chapter 4. The redox interactome of PTEN analyzed by affinity-capture and label-free MS quantitation

# 4.1 Summary

Phosphatase and tensin homolog (PTEN) is a redox-sensitive, dual-specificity protein phosphatase that acts as a tumour suppressor by negatively regulating the PI3K/Akt pathway. While direct evidence of a redox regulation of PTEN downstream signaling has been reported, the effect of oxidation on the PTEN interactome is still poorly defined. Here we present a correlation between PTEN redox status and PTEN protein-protein interactions.

PTEN-GST fusion protein was prepared in its reduced and $H_2O_2$-oxidized form and immobilized on a Glutathione Sepharose-based support. The immobilized protein was incubated with a HCT116 cell lysate to capture interacting proteins. Captured proteins were eluted from the beads, analyzed by LC-MS/MS and comparatively quantified using label-free methods.

Thirteen PTEN-interacting proteins were identified that showed a significantly increased interaction with oxidized over reduced PTEN. These included new PTEN interactors as well as the redox proteins Prdx1 (peroxiredoxin-1) and Trx (thioredoxin), which are known to be involved in the recycling of the PTEN disulfide bond. The results of this study suggest that the redox status of PTEN causes a functional variation in the PTEN interactome which is important for the cellular function of PTEN. The resin capture method developed had distinct advantages in that the redox status of PTEN could be directly controlled and measured.

# 4.2 Introduction

The vast majority of cellular processes rely upon the ability of proteins to interact with each other and generate precise networks through which biological signals are transmitted within cells and understanding the dynamics and the functional significance of protein-protein interactions (PPIs) is of vital importance. PPIs have been shown to play a major role in the biological mechanism behind many human diseases and are currently considered a promising target for the discovery and development of new drugs [535,536].

This PhD thesis focuses on the dual specificity tumour suppressor phosphatase PTEN, which is a negative regulator of PI3K/Akt pathway [374], but is also involved in other cellular networks, including the function of the actin cytoskeleton [537,538] as well as DNA damage repair and response pathways [441]. PTEN has been reported to be inactivated when treated with oxidizing agents *in vitro*, as well as in cells exposed to oxidative stress conditions [144,423,477]. Reversible inactivation of PTEN has been shown upon hydrogen peroxide oxidation, resulting from the formation of a disulfide bond between Cys71 and Cys124 in the N-terminal phosphatase domain of the protein [144]. It has been suggested that as well as affecting protein activity, the targeted oxidation of PTEN may possibly modulate its ability to interact with its binding partners, thereby controlling the downstream signaling [193]. However, very few studies to date have described the effect of altered redox conditions directly on the regulation of signaling pathways and the protein-protein interactions of PTEN.

Several different techniques have been used to characterize the PTEN interactome over the last two decades, and have produced both high-throughput and low-throughput data [427,539-541]. An up-to-date list of PTEN-interactions identified in the available published work is reported in the Appendix, Section 8.4 (Table 8.2). Research into the redox regulation of PTEN has shown that in mammalian cells treated with $H_2O_2$ the protein DJ-1 (also known as Parkinson disease 7, PARK7) binds more strongly to PTEN, causing a reduction in PTEN catalytic activity, and enhanced phosphorylation of Akt [481], resulting in increased cell proliferation and apoptosis. Similarly, a number of studies have identified a direct interaction between thioredoxin-1 and PTEN, which has been shown to be redox-regulated [478]. Thioredoxin-1 plays an important role in the re-activation of PTEN *in vivo* after $H_2O_2$

treatment and has been demonstrated to be even more efficient than glutathione or glutaredoxin in the reduction of oxidized PTEN [423]. The signaling implications of the PTEN/Trx interaction are important for the tumour suppressing role of PTEN (Figure 4.1). In growth factor-stimulated non phagocytic cells, PI3K activates the transmembrane NADPH oxidase Nox4 (or Nox1) via the conversion of PtdIns(4,5)$P_2$ to the signaling intermediate PtdIns(3,4,5)$P_3$. Activated NOX results in the increase in intracellular $H_2O_2$ production [476], which causes the oxidative inactivation of PTEN, and consequent activation of Akt by PI3K due to PtdIns(3,4,5)$P_3$ accumulation [144]. This signaling cascade is blocked by the action of Trx that reactivates PTEN with a thiol-disulfide exchange mechanism, therefore restoring the Akt PTEN-mediated deactivation [423]. The reactivation of PTEN by Trx is assisted by the NADPH-dependent thioredoxin reductase (TrxR), which restores Trx thiols to its reduced form after the reduction of PTEN disulfide bond [246]. In addition, Trx regulates the cellular redox state by reducing the thioredoxin peroxidase peroxiredoxin-1, which acts as an antioxidant scavenger by reducing $H_2O_2$ to $H_2O$ [542]. A direct interaction between PTEN and peroxiredoxin-1 has also been proposed as a possible mechanism to protect PTEN from hydrogen peroxide-induced inactivation, thereby preserving its tumour suppressing function [479]. Generally, these studies suggest a correlation between cellular redox status and the regulation of specific PTEN protein-protein interactions. However, very little information on direct, redox-dependent interactions is available, and this relationship needs to be further investigated, as such mechanisms are likely to be involved in the modulation of tumorigenesis- or stress-related cellular processes.

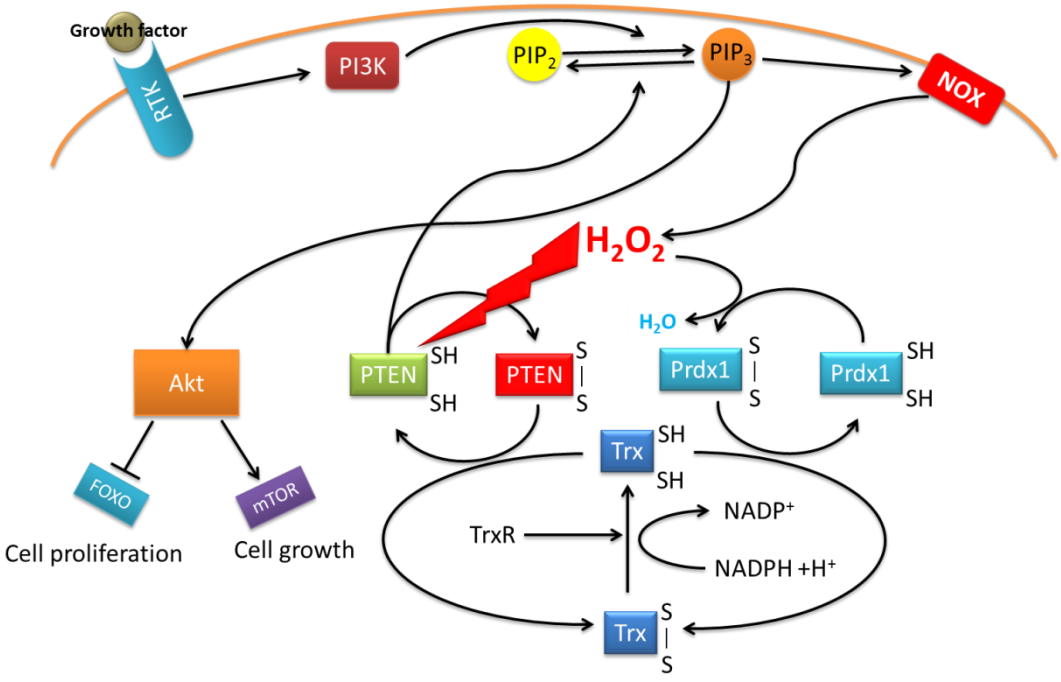


**Figure 4.1 Interplay between $H_2O_2$ signaling and PTEN reversible inactivation**

In growth-factor stimulated cells activated PI 3-kinase (PI3K) converts PtdIns(4,5)$P_2$ to PtdIns(3,4,5)$P_3$, which activates the NADPH oxidase (NOX) complex, resulting in the production of intracellular $H_2O_2$. Sufficient $H_2O_2$ concentrations inactivate PTEN, thereby promoting the activation of Akt due to accumulating PtdIns(4,5)$P_3$. $H_2O_2$ is scavenged by peroxiredoxin-1, while the thioredoxin system (Trx and NADPH-dependent TrxR) restores PTEN activity and regulates the cellular redox state.

Mass spectrometry (MS) methods used in combination with affinity capture-based experiments are a valuable and well-recognized tool to investigate protein-protein interactions [267]. The sensitivity of modern MS technologies is such that increasingly large number of proteins within a given sample can be identified with a high level of selectivity and accuracy. Along with data providing evidence of protein identity, accurate information on protein abundance is also required to generate high-throughput protein-protein interaction datasets. Methodologies based on *in vivo* isotope labeling have been used extensively for this purpose and are currently among the top choices for absolute and relative quantification of protein-protein interaction data [543]. Label-based methods offer the advantage of minimal errors in the final quantification, which significantly lowers the risk of biased conclusions, but present a number of significant limitations, including amenability of certain cell lines

to grow in modified media, labeling-induced artifacts, and limited availability of required reagents [306]. Recently, label-free methods have become more popular in the field of LC-MS-based interactomics [544]. These techniques do not require additional sample manipulation steps, and represent a fast, straightforward, and relatively cost-effective tool to detect and match peptides across multiple LC-MS runs, monitor protein expression levels in complex biological samples, and perform comparative analysis between different protein mixtures. New generation label-free *in silico* solutions rely on accurate feature-intensity-based quantification and are capable of processing large amount of high resolution data [324]. Over the past few years, complex proteome-wide data like those generated from biomarker discovery and protein-protein interactions studies have been analyzed by proteomics researchers using label-free quantification, with accurate and reliable results [545].

In the study described in this chapter it was hypothesized that oxidative-induced inactivation of PTEN would modulate the ability of the protein to bind its interacting partners, thus altering its interactome. To investigate this, a GST-tagged fusion PTEN was immobilized on a glutathione-sepharose resin and challenged with HCT116 cell lysate for the affinity-capture of the interactions. Using label-free quantitative LC-MS/MS, the abundance of the binding proteins was compared between the reduced and oxidized PTEN. The method described identified a number of putative novel protein-protein interactions that can contribute to shed a light on the possible involvement of PTEN in several cellular process of current interest.

# 4.3 Materials and Methods

### 4.3.1 Reagents

Monoclonal antibodies against thioredoxin-1 (ab16965) and annexin A2 (ab54771) were purchased from Abcam (Cambridge, UK). Monoclonal antibodies against Prdx1 (D5G12), DDB1 (D4C8) and PTEN (26H9) were purchased from Cell Signaling Technology (New England Biolabs, Hitchin, UK). HRP-linked anti-mouse IgG secondary antibody was purchased from Santa-Cruz (sc-2031, Wembley, UK) and anti-rabbit IgG was from Cell Signaling Technology (7074S, New England Biolabs, Hitchin, UK). Enhanced chemiluminescence (ECL kit) was from Thermo Scientific (Thermo Fisher Scientific, Hemel Hempstead, UK).

### 4.3.2 Cell culture

Approximately $5x10^7$ HCT116 human colon cancer cells (cultured as described in Section 2.3.3) of passage 4 to 10 were harvested, washed twice with ice cold PBS pH 7.4 with centrifugation at 500xg for 10 minutes between washes, and lysed with ice cold 50 mM Tris pH 7.4 containing 150 mM NaCl, 1 mM EDTA, 0.5% NP-40 (Sigma-Aldrich Chemical Co., Poole, UK) supplemented with EDTA-free protease inhibitor cocktail (Catalog no.11 873 580 001, Roche Diagnostics GmbH, Mannheim, Germany) by incubating for 45 minutes on ice with occasional mixing. The lysate was clarified by spinning at 20,000xg for 15 minutes at 4 ºC.

### 4.3.3 Buffer exchange

Prior to any downstream experiment, purified PTEN-GST was buffer-exchanged in 20 mM Tris pH 7.4, 0.1 mM EDTA, 100 mM NaCl using a Microcon® 10kDa centrifugal filter unit (Millipore Ltd, Feltham UK), and all centrifugation steps were performed at 14,000xg in a 5417R Eppendorf

microcentrifuge (Eppendorf UK Ltd, Stevenage, UK) for 10 min at 4 ºC. Protein concentration was then determined using absorbance at 280 nm using a Nanodrop 2000c UV-Vis Spectrophotometer (Thermo Fisher Scientific, Hemel Hempstead, UK).

### 4.3.4 PTEN oxidation and activity assay

Purified buffer-exchanged PTEN-GST was treated with either 0 or 1 mM $H_2O_2$ for 1 hour at room temperature. The reaction was quenched by the addition of 5 mM methionine (Sigma-Aldrich Chemical Co., Poole, UK). An aliquot of the 1 mM $H_2O_2$ oxidized sample was subsequently incubated in 100 mM DTT for 15 min to assess the reversibility of the oxidation. 60 µg each of untreated, oxidized and DTT-incubated oxidized protein were assayed with the OMFP phosphatase assay as described in Section 2.6.3. Statistical analysis of activity data was performed using GraphPad Prism Software (GraphPad, San Diego, CA, USA) using one-way ANOVA followed by Tukey's multiple comparison test.

### 4.3.5 Preparation of PTEN affinity-capture column and protein capture

The untreated and oxidized/DTT-recovered samples of PTEN-GST (100 µg protein each) were diluted in 500 µL of wash buffer (20 mM Tris pH 7.4, 0.1 mM EDTA, 100 mM NaCl) supplemented with 100 mM DTT; the oxidized PTEN-GST (100 µg) and a GST control (100 µg) were diluted in 500 µL of wash buffer without DTT. 100 µL of Glutathione Sepharose 4B slurry (GE Healthcare, Little Chalfont, UK) was sedimented by centrifugation at 500xg for 5 minutes. The Glutathione Sepharose beads were extensively washed with wash buffer and stored at 4ºC. The bait proteins (PTEN-GST) were immobilized on the Glutathione Sepharose beads by incubation with the protein solutions at 4ºC for 3 hours. The beads were then washed once with wash buffer, and then 1 mL of HCT116 cell lysate derived from approximately 5 x $10^7$ cells was incubated with each of the immobilized bait proteins and a control consisting of Glutathione Sepharose beads only, at 4ºC overnight on an end-over-end mixer (Dynabeads® MX1 Mixer, Life technologies, Paisley, UK). Subsequently, the beads were washed with 20 mM Tris pH 7.4, 0.1 mM EDTA, 300 mM NaCl, 0.5% NP-40 to remove non-bound proteins.

The bound proteins were then eluted by boiling in SDS-PAGE 2× Laemmli sample buffer Concentrate (Sigma-Aldrich Chemical Co., Poole, UK) and analyzed by SDS-polyacrylamide gel electrophoresis followed by staining with Coomassie Brilliant Blue as described in Section 2.6.1.

### 4.3.6 Protein digestion

The gel lanes corresponding to the bead control, the GST control, the untreated (reduced) PTEN-GST and the oxidized PTEN-GST samples were each cut into 12 approximately equal slices, and the gel pieces digested as described in Section 2.7.1.

### 4.3.7 LC-MS

Peptides were separated and analyzed as described in Section 2.7.2. Peptide samples corresponding to same-molecular weight gel bands were acquired back-to-back.

### 4.3.8 Label-free quantification with Progenesis QI for proteomics

Comparative quantification was performed using the Progenesis QI for Protemics software (Non-linear Dynamics, Newcastle upon Tyne, UK) as described in Section 2.7.3. A total of 12 experiments were created, one for gel bands excised from each lane of the Coomassie-stained gel at the same molecular weight. Any peptide showing a Mascot Ion Score below the threshold indicative of identity or extensive homology ($p$-value $< 0.05$) was removed from the feature identification list. Cytoskeletal keratin IDs were removed from the feature identification list. Only features that had zero protein conflicts were used for quantification. Data obtained from the alignment of LC-MS runs corresponding to single fractions were then pooled into a multi-fraction experiment. Statistical analysis was performed using Progenesis QI for Proteomics using a one-factor ANOVA.

### 4.3.9 Database Search

The Mascot® probability based search engine (Matrix Science, London, version 2.4.0) was used to interrogate the SwissProt 2015-03 primary database. For Mascot searches that was not automated through the Progenesis QI analysis, LC-MS .wiff file were converted into .mgf format using Peakview® (AB SCIEX). The 12 .mgf files obtained the Progenesis analysis of each of the samples were searched for protein identification and for bait protein oxidative post-translational modifications (oxPTMs). For protein identification, a variable modification of methionine oxidation and a fixed modification carbamidomethyl cysteine were used. For the analysis of the oxPTMs of the bait, the variable modification lists included: methionine oxidation and dioxidation; cysteine oxidation, dioxidation and trioxidation, and tyrosine oxidation. Other parameters for the searches were as follows: Enzyme: Trypsin; Peptide tolerance: ± 0.8 Da; MS/MS tolerance: ± 0.8 Da; Peptide charge state: +2,+3 and +4; Max Missed cleavages: 1; #13C: 1; Quantitation: None; Instrument: ESI-QUAD-TOF; Data format: Mascot Generic; Experimental mass values: Monoisotopic; Taxonomy *Homo Sapiens* (Human).

### 4.3.10 Relative quantification of bait modification

To calculate the relative abundance of a given modified residue, the individual abundance values of each detected peptides containing the amino acid in both its modified and unmodified form were added together. Next, the abundances of the detected peptides containing the residue solely in its modified form were summed up and divided by the total abundance value to obtain the relative abundance of the modification. Statistical analysis of modification data was performed with GraphPad Prism Software (GraphPad, San Diego, CA, USA) using two-tailed unpaired Student's t test (for multiple comparisons). $P < 0.05$ was considered significant.

### 4.3.11 Western Blotting

Proteins resolved by SDS-PAGE were transferred onto PVDF membrane (Immobilion-P, Millipore Ltd, Feltham UK) in 25 mM Tris, 192 mM glycine, 10% methanol pH 8.3 applying 30V overnight at 4ºC. The membrane was blocked in Tris buffered saline (TBS)-Tveen blocking buffer (20 mM Tris pH 7.6, 137 mM NaCl 0.05% Tveen-20), supplemented with 5% BSA (Bovine Serum Albumin, Sigma-Aldrich Chemical Co., Poole, UK) for 1 hour, incubated in blocking buffer with monoclonal primary antibodies for Trx, Prdx1, Anxa2, or DDB1 at the working dilution of 1:1000 overnight at 4ºC, washed extensively for 30 minutes (3 washes of 10 minutes each) with Tris buffered saline (TBS)-Tween (20 mM Tris pH 7.6,), 137 mM NaCl, 0.05% Tween-20) and incubated with either HRP-linked anti-mouse or HRP-linked anti-rabbit secondary antibodies (working dilution 1:1000) for 1 hour at room temperature. The membrane was washed again as described above and HRP-linked anti-mouse or HRP-linked anti-rabbit were detected using enhanced chemiluminescence (ECL kit, Thermo Fisher Scientific, Hemel Hempstead, UK) according to the manufacturer's instructions. The membrane was scanned using a G:BOX system (Syngene, Cambridge, UK) running the GeneSys software (Syngene, Cambridge, UK). Next, the membrane was stripped in Restore Plus Stripping buffer (Thermo Fisher Scientific, Hemel Hempstead, UK) for 15 minutes, washed as described above and reblocked in TBS-Tween plus 5% BSA. The monoclonal primary antibodies for PTEN was incubated with the stripped membrane in blocking buffer at the working dilution of 1:2500 for 1 hour at room temperature, the membrane washed, and incubated with HRP-linked secondary antibody for 1 hour at room temperature at the working dilution of 1:2500. After washing, HRP-linked antibody detection and scanning procedures were repeated as described above.

# 4.4 Results

### 4.4.1 Buffer exchange of PTEN-GST

As described in the previous chapter, before any oxidation experiment the purified PTEN-GST was buffer-exchanged in order to remove reagents in the storing buffer that could interfere with concentration assays (glycerol) and oxidation experiments (glutathione and DTT) using a Microcon Centrifugal Filter unit (Section 3.4.4). Purified PTEN was buffer exchanged into 20 mM Tris pH 7.4, 0.1 mM EDTA, 100 mM NaCl, which was the buffer of choice for PTEN oxidation and protein interactions capture. PTEN activity before and after buffer exchange was monitored using the OMFP phosphatase assay (Figure 4.2). The phosphatase retained full activity following buffer exchange.

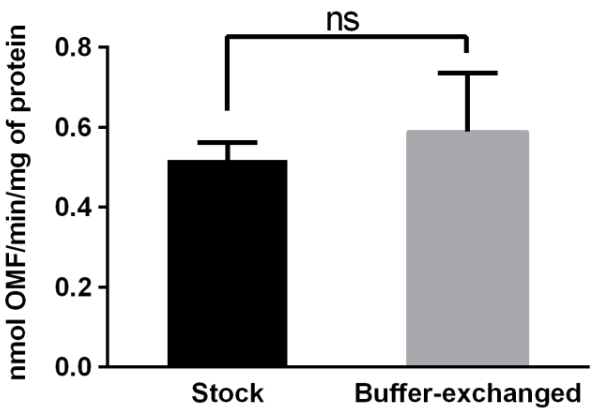


**Figure 4.2 Effect of buffer exchange on purified PTEN phosphatase activity**

The activity of the stock protein in elution buffer (50 mM Tris pH 7.4, 20 mM reduced L-Glutathione, 250 mM NaCl, 2 mM DTT in 50% glycerol) was compared to the activity of the untreated protein following buffer exchange in 20 mM Tris pH 7.4, 0.1 mM EDTA, 100 mM NaCl, in order to assess whether activity loss had taken place before the oxidative treatment. The results are presented as mean ± SD (N= 3) of PTEN specific activity. No significant difference was found in the specific activity of the protein before and after buffer exchange (two-tailed unpaired Student's t test, $p = 0.4745$). The calculated specific activity values are: 0.5184 ± 0.0424 nmol OMF/min/mg protein for the stock PTEN-GST and 0.5881 ± 0.1473 nmol OMF/min/mg protein for the buffer-exchanged PTEN-GST.

### 4.4.2 Reversible oxidation of PTEN after $H_2O_2$ treatment

Initially, the effect of 1 mM $H_2O_2$ *in vitro* oxidation on PTEN activity was monitored using the OMFP phosphatase assay immediately before the immobilization of the reduced and oxidized PTEN-GST protein onto the Glutathione Sepharose beads. When PTEN was treated with 1 mM $H_2O_2$ for 1 hour, the phosphatase activity dropped dramatically (Figure 4.3). Treatment with 1 mM $H_2O_2$ causes a loss of catalytic activity mainly through the formation of a intramolecular disulfide bond between the catalytic cysteine Cys124 and regulatory cysteine Cys71 in the active site of the enzyme [423]. Because no significant activity loss was detected following buffer exchange in non-reducing buffer conditions, it can be reasonably assumed that the oxidizing treatment is the only event responsible for the inactivation of PTEN. After the treatment, the protein activity was restored to its original values by incubating the 1 mM $H_2O_2$-oxidized protein in reducing conditions (100 mM DTT), thereby suggesting the presence of the disulfide bond between Cys71 and Cys124 in the active site of the inactivated PTEN.

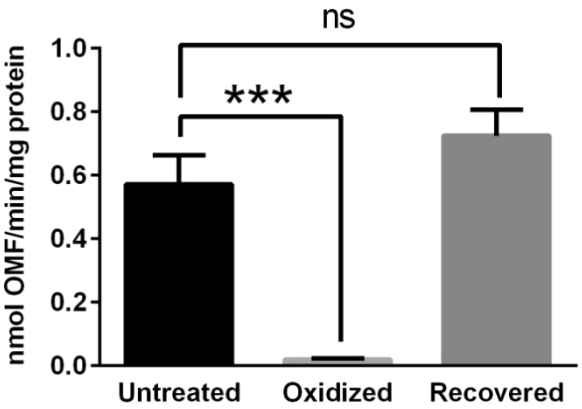


**Figure 4.3 Effect of 1 mM $H_2O_2$ oxidation on PTEN-GST phosphatase activity**

The untreated, oxidized and DTT-incubated PTEN-GST were assayed for phosphatase activity using the *O*-methyl fluorescein phosphate assay, immediately before the immobilization step. The results are presented as mean ± SD (N= 3) of PTEN specific activity. Statistical significance was assessed by one-way ANOVA followed by Tukey's multiple comparison test. The enzymatic activity of PTEN-GST following 1 mM $H_2O_2$ oxidation is significantly different to that of the untreated PTEN-GST ($p = 0.0002$). The enzymatic activity of the untreated protein is not significantly different to that obtained

following incubation of the oxidized PTEN-GST with 100 mM DTT ($p = 0.0861$). The calculated specific activity values are: 0.5720 ± 0.0917 nmol OMF/min/mg protein for the untreated PTEN-GST; 0.0206 ± 0.0031 nmol OMF/min/mg protein for the $H_2O_2$-oxidized PTEN-GST and 0.7249 ± 0.0819 nmol OMF/min/mg protein for the PTEN-GST following 15 minutes incubation with 100 mM DTT. *** = $p < 0.001$; ns = not significant

### 4.4.3 GSH affinity enrichment affinity-captured PTEN-interacting proteins

HCT116 (wild-type) were chosen as a source of prey proteins for the affinity-capture because this cell line has been previously used to study the protein-protein interactions of PTEN [546,547]. In addition, the HCT116 cell line contains two wild-type alleles for PTEN and has been used as an *in vivo* model to study ROS cellular levels and activation of protein signaling pathways related to the loss of the PTEN phenotype [548,549].

The untreated PTEN bait protein was maintained in constant reducing conditions (100 mM DTT) during the immobilization step to prevent any spontaneously occurring oxidation, and to avoid any inter and intramolecular disulfide bonds. Such conditions were considered necessary to ensure direct correlation between PTEN redox status (reduced versus oxidized) and the results of the protein interaction analysis. However, no reducing agent was added to the HCT116 cell lysate used for the affinity-capture, in order to avoid further alteration of the redox dynamics between the immobilized proteins and their interactors. Care was taken to keep the amount of immobilized proteins consistent across the different baits used. Proteins captured by the reduced and oxidized PTEN-GST bait were analyzed by SDS-PAGE against GST control (Figure 4.4). The Glutathione Sepharose beads were also incubated with HCT116 lysate as a negative control. Comparing the observed gel bands, unique bands were detected in the oxidized PTEN-GST sample (Lane 4) over reduced PTEN-GST (Lane 3), as well as over GST (Lane 2) and beads controls (Lane 1). The wash buffer after bait immobilization was also analyzed in order to assess the binding efficiency of the reduced and the oxidized PTEN-GST to the Glutathione Sepharose beads. The results shown in Figure 4.4 suggest that the resin was fully saturated for the affinity-capture, as traces of PTEN-GST are still visible in the gel lanes loaded with

the supernatant obtained after the immobilization of both reduced PTEN-GST (Lane 5) and oxidized PTEN-GST (Lane 6).

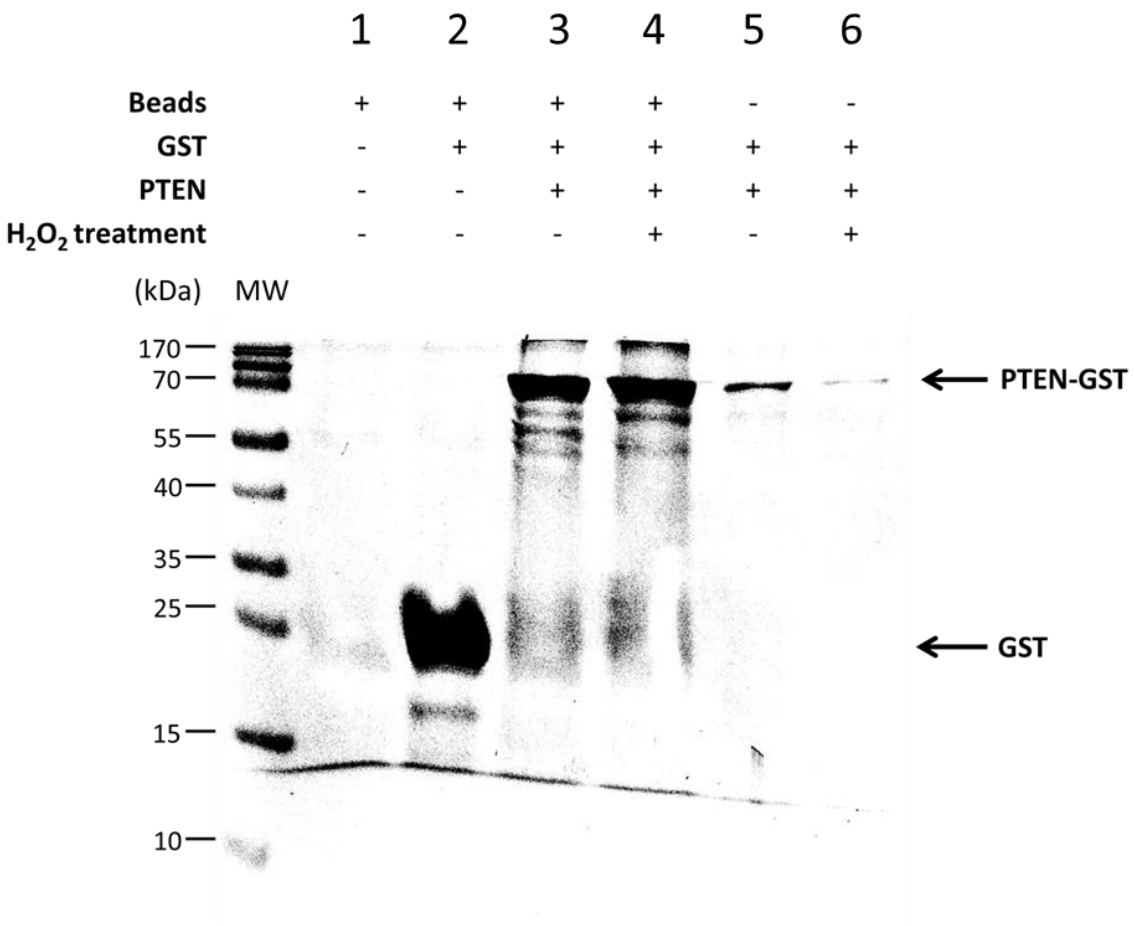


**Figure 4.4 Representative Coomassie-stained gel showing isolation of putative PTEN-GST binding proteins by GSH-affinity enrichment following 1 mM $H_2O_2$ oxidation**

The Glutathione Sepharose beads resin was tested for non-specific binding by eluting the bound proteins after incubation with HCT116 cell extract. The observable gel bands were compared after elution of the bound proteins following incubation of HCT116 cell extract with the bait proteins Glutathione-S-Transferase, untreated PTEN-GST and PTEN-GST treated with 1 mM $H_2O_2$. The binding efficiency of the PTEN-GST baits to the Glutathione Sepharose beads was tested by loading 15 µL of the wash buffer after the immobilization step of the control PTEN-GST and the PTEN-GST treated with 1 mM $H_2O_2$.

### 4.4.4 MS-based quantitative analysis of PTEN affinity-captured interactions

#### *4.4.4.1 Overview of the identified PTEN-interacting proteins*

The peptides obtained from the in-gel digestion of the gel fractions cut from the lanes loaded with the beads, the GST, the reduced and oxidized PTEN-GST were analyzed by mass spectrometry. For the MS-based label-free quantification, the LC-MS runs corresponding to the tryptic digest of the proteins bound to the reduced and the oxidized PTEN-GST samples were used.

The Mascot database search engine (v. 2.4.0) and Progenesis QI for proteomics software were used to identify and quantify the putative PTEN-interacting proteins detected after LC-MS/MS analysis of the tryptic peptides. A total of 237 different proteins were identified after Mascot database search of each of the aligned LC-MS runs processed by Progenesis and pooled in the multi-fraction experiment. Initially, identified proteins that were also detected in the beads and GST controls were removed from the list. Of the remaining proteins, 97 proteins showed a confidence score above 50 and a number of unique peptides greater than or equal to 2. Of those 97, 27 proteins had q-values < 0.05 for the quantification (Table 4.2). Section 8.5 in the Appendix reports the remaining 70 proteins showing a q-value > 0.05 (Table 8.3), proteins that were below the cutoff criteria of confidence score and abundance (Table 8.4) and proteins that were also found in the beads and GST controls (Table 8.5).

The bait protein PTEN and its Glutathione-Transferase protein tag were identified with a high level of confidence in both reduced and oxidized fractions. A relatively substantial portion of the putative PTEN interactors detected are highly abundant within cells and may have bound non-specifically to the Glutathione Sepharose beads, despite not being detected in the controls. However, these proteins included elongation factors, tubulin, myosins, histones, 60S and 40S ribosomal proteins, and heat-shock proteins, all of which have been reported in previous proteomics studies of PTEN interacting proteins [550,551].

**Table 4.1** Identification and LC-MS based label-free quantification of the binding partners that interact differently with reduced and oxidized PTEN-GST

| Accession[1] | Peptide count[2] | Confidence score[3] | p-value[4] | q-value[4] | Fold change[4] | Highest mean condition | Protein Description |
|---|---|---|---|---|---|---|---|
| **PDIP2_HUMAN** | **4 (4)** | **190.31** | **<0.0001** | **0.0005** | **10.8** | **Oxidized** | **Polymerase delta-interacting protein 2 *** |
| **PELO_HUMAN** | **2 (2)** | **110.35** | **0.0018** | **0.0212** | **2.7** | **Oxidized** | **Protein pelota homolog *** |
| RS2_HUMAN | 2 (2) | 97.3 | 0.0021 | 0.0212 | 1.9 | Oxidized | 40S ribosomal protein S2 ‡ |
| **RL10A_HUMAN** | **2 (2)** | **71.19** | **0.0014** | **0.0212** | **5.3** | **Reduced** | **60S ribosomal protein L10a** ‡ |
| RLA0_HUMAN | 3 (3) | 159.13 | 0.0052 | 0.0261 | 2.4 | Oxidized | 60S acidic ribosomal protein P0 ‡ |
| **THIO_HUMAN** | **2 (2)** | **150.69** | **0.0065** | **0.0299** | **6.2** | **Oxidized** | **Thioredoxin** |
| SSRD_HUMAN | 2 (2) | 153.39 | 0.0075 | 0.0301 | 1.7 | Reduced | Translocon-associated protein subunit delta * |
| **ANXA2_HUMAN** | **3 (3)** | **195.41** | **0.0118** | **0.0374** | **6.8** | **Oxidized** | **Annexin A2** |
| FAS_HUMAN | 3 (3) | 163.01 | 0.0144 | 0.0387 | 1.7 | Oxidized | Fatty acid synthase * |
| AKA12_HUMAN | 4 (4) | 180.42 | 0.0181 | 0.0415 | 1.3 | Oxidized | A-kinase anchor protein 12 * |
| **DREB_HUMAN** | **2 (2)** | **83.3** | **0.018** | **0.0415** | **4.9** | **Oxidized** | **Drebrin** |
| **PRDX1_HUMAN** | **6 (5)** | **316.76** | **0.0233** | **0.0437** | **4.1** | **Oxidized** | **Peroxiredoxin-1** |
| DESP_HUMAN | 4 (4) | 165.62 | 0.0221 | 0.0437 | 1.6 | Oxidized | Desmoplakin * |
| NDKA_HUMAN | 3 (3) | 131.93 | 0.026 | 0.0448 | 1.5 | Oxidized | Nucleoside diphosphate kinase A * |
| **DHB8_HUMAN** | **2 (2)** | **110.35** | **0.0258** | **0.0448** | **6.4** | **Oxidized** | **Estradiol 17-beta-dehydrogenase 8 *** |
| UTRO_HUMAN | 2 (2) | 101.72 | 0.0306 | 0.0454 | 2.2 | Oxidized | Utrophin * |
| **SPTN1_HUMAN** | **4 (4)** | **188.58** | **0.0361** | **0.0456** | **2.9** | **Oxidized** | **Spectrin alpha chain, non-erythrocytic 1 *** |
| RS9_HUMAN | 4 (4) | 172.02 | 0.0331 | 0.0456 | 1.5 | Oxidized | 40S ribosomal protein S9 ‡ |
| RL38_HUMAN | 5 (5) | 405.89 | 0.0389 | 0.0463 | 1.6 | Oxidized | 60S ribosomal protein L38 ‡ |
| **GNAI1_HUMAN** | **6 (4)** | **343.46** | **0.0462** | **0.0463** | **3.6** | **Oxidized** | **Guanine nucleotide-binding protein G(i) subunit alpha-1 *** |
| **GNAI2_HUMAN** | **5 (2)** | **300.5** | **0.0488** | **0.0463** | **6.9** | **Oxidized** | **Guanine nucleotide-binding protein G(i) subunit alpha-2 *** |
| MPRIP_HUMAN | 4 (4) | 164.53 | 0.0423 | 0.0463 | 2.1 | Oxidized | Myosin phosphatase Rho-interacting protein * |
| **RS15A_HUMAN** | **3 (2)** | **135.35** | **0.0449** | **0.0463** | **0.7** | **Oxidized** | **40S ribosomal protein S15a** ‡ |
| GSTM2_HUMAN | 2 (2) | 130.8 | 0.0495 | 0.0463 | 1.4 | Reduced | Glutathione S-transferase Mu 2 * |
| **SKP1_HUMAN** | **2 (2)** | **112.83** | **0.0413** | **0.0463** | **8.6** | **Oxidized** | **S-phase kinase-associated protein 1** |
| **HSP7C_HUMAN** | **2 (2)** | **107.77** | **0.0413** | **0.0463** | **3.0** | **Oxidized** | **Heat shock cognate 71 kDa protein** |
| EF2_HUMAN | 2 (2) | 101.61 | 0.0428 | 0.0463 | 1.3 | Oxidized | Elongation factor 2 ‡ |

[1]Accession = SwissProt Protein ID

[2]Peptide count = the number of detected peptides (the number of unique peptides) used for quantification

[3]The protein confidence score was generated using Mascot as described in the experimental.

[4]The p-value, q-value and fold change were generated by Progenesis QI for proteomics as described in the experimental.

**Bold** indicates more than 2.5-fold change in abundance depending on PTEN redox status.
* indicates proteins not previously identified as PTEN interactors.
‡ indicates proteins that appeared to be PTEN interactors (i.e. were not found in controls) but have also been found as common non-specific interactors in bead-based affinity enrichments.
The data were obtained from the analysis of three independent GSH-affinity experiments. The list was restricted to the protein hits showing a confidence score ≥ 50, a number of unique peptides ≥ 2 and a q-value < 0.05. Ranking is based on q-values.

#### *4.4.4.2 Putative novel PTEN interactors*

The majority of the proteins detected corresponded to previously unidentified PTEN-binding proteins and are indicated by a * in Table 4.1. Other interacting proteins that were not previously identified but are commonly associated with beads are indicated by ‡ in Table 4.1. While no direct interaction with PTEN has been shown to date, a number of the identified putative novel interactors have been linked with cellular pathways in which PTEN is involved. These proteins include: the multi-enzyme fatty acid synthase (FAS), A-kinase anchor protein 12 (AKAP12) and guanine nucleotide-binding protein G (i) subunit α and/or β (GNAIα/β). In addition, there are proteins involved in DNA replication and DNA repair such as protein pelota homolog (Pelo), and Polymerase delta-interacting protein 2 (PDIP2 or PolDIP2) as well as proteins associated with cytoskeleton structure and regulation such as spectrin α-chain (Spta1), myosin phosphatase Rho-interacting protein (MPRIP) and desmoplakin (Dsp).

#### *4.4.4.3 PTEN-interacting proteins showing a significant change*

Of the 27 significantly changing proteins reported in Table 4.1, **14** showed significant fold change differences upon oxidative inactivation of the PTEN-GST bait (fold change greater than 2.5), and are indicated in **bold**. All differentially binding proteins were manually validated to confirm the quality of the identification and between-sample quantification. Significantly changing proteins included previously identified PTEN-binding proteins such as annexin A2 (Anxa2, F.C 6.8, p-value = 0.0118), and the actin-binding protein drebrin (Dreb, FC = 4.8, p-value = 0.0180) as well as potential novel interactors such as Poldip2 (F.C=10.8, p-value < 0.0001), which also showed increased abundance in the interaction with the oxidized PTEN-GST.

Two interesting proteins that showed a significant change were the redox proteins peroxiredoxin-1 (Prdx1) and thioredoxin-1 (Trx). Peroxiredoxin-1 (Prdx1) is a non-seleno peroxidase that is known to catalyze the reduction of $H_2O_2$, protecting the cells from oxidative damage to DNA, lipids and proteins

[552]. A total of 6 Prdx1 peptides were detected, of which 5 unique peptides were used for quantification. Prdx1 was found significantly more abundant in the sample eluted from the oxidized PTEN-GST than in the sample eluted from the reduced PTEN-GST (FC=4.1, p-value=0.0233). Another identified redox protein was the antioxidant protein thioredoxin-1 (Trx), which is believed to play a major role in the recycling of PTEN disulfide [423]. 2 unique thioredoxin-1 peptides were detected, and the protein was found significantly more abundant (FC = 6.2, p-value = 0.0065) in the protein fraction eluted from the oxidized PTEN-GST. Using the Progenesis software we were able to verify the presence of the peptide features corresponding to the identified proteins listed in Table 1. Figure 4.5 shows the three-dimensional maps zoomed into the features corresponding to the Prdx1 and the Trx peptides detected following elution of the proteins bound to the oxidized and reduced PTEN-GST.

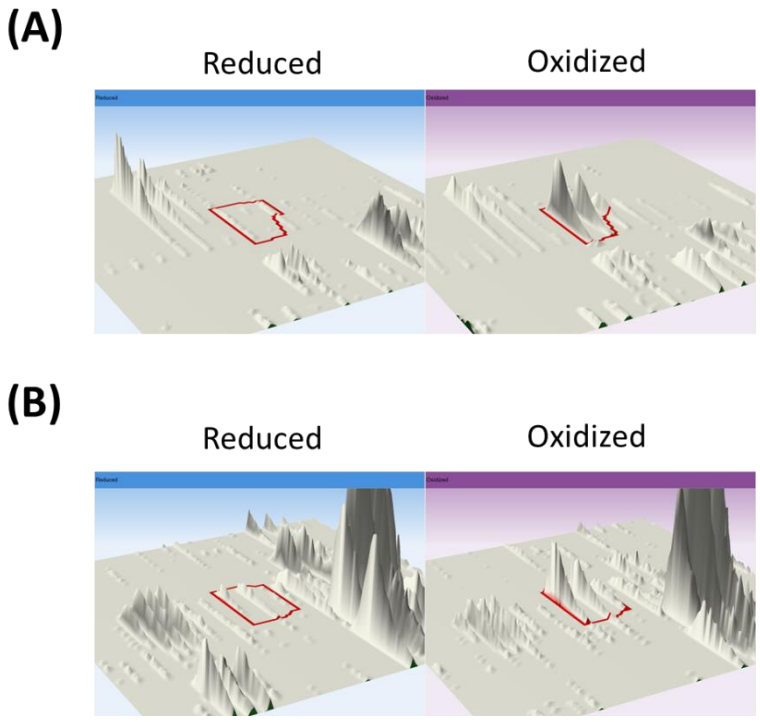


**Figure 4.5 Representative 3D montages of the comparative MS-based label-free quantification for the peroxiredoxin-1 peptide TIAQDYGVLK and the thioredoxin-1 peptide TAFQEALDAAGDK detected following elution of the proteins bound to the reduced and oxidized PTEN-GST**

The montages are representative of three independent experiments. (A) The Prdx1 peptide TIAQDYGVLK (m/z = 554.30, 2+; RT = 22.24 min) was found to be 4.23 times more abundant in

the sample obtained from the oxidized PTEN GST than in the sample obtained from the reduced PTEN-GST (one-factor ANOVA, p-value = 0.0358, n= 3). (B) The Trx peptide TAFQEALDAAGDK (m/z = 668.83, 2+; RT = 24.45 min) was found to be 7.33 times more abundant in the sample obtained from the oxidized PTEN GST than in the sample obtained from the reduced PTEN-GST (one-factor ANOVA, p-value = 0.0107, n= 3).

### 4.4.5 Validation of selected interactions with Western Blotting

Following screening of the identified proteins and their abundance profile between the sample eluted from the reduced and oxidized bait, a number of interactors were selected to be taken forward onto a Western Blot-based validation. This analysis was considered essential to confirm the validity of the interactors identification as well as the between reduced versus oxidized PTEN-GST. The GSH affinity-capture was performed with the DTT-recovered oxidized PTEN-GST as additional control for the interactors validation. The selection of the proteins for validation was mainly based upon their quantitative profile between the reduced and oxidized PTEN-GST as well as upon their relevance to the present study. Ultimately, Prdx1, Trx, Anxa2 and DDB1 were chosen among the identified interactors, and their levels compared across the protein samples eluted from the reduced, oxidized and DTT-recovered PTEN-GST against PTEN loading control (Figure 4.6). For all the proteins selected, the Western blot results were in agreement with the proteomics data and confirmed the comparative quantitative analysis between the oxidized and reduced sample. As expected, the interacting protein levels were comparable between reduced (untreated) and DTT- recovered samples. The levels of Prdx1 (Figure 4.6 A), Trx (Figure 4.6 B) and Anxa2 (Figure 4.6 C) were visibly increased in the sample eluted from the $H_2O_2$-oxidized PTEN. Little or no signal was observed for those proteins in the samples corresponding to the reduced (untreated) and DTT-recovered PTEN, confirming, at a qualitative level, the significant difference observed by MS-based label-free quantitation. No significant change in the levels of DDB1 were observed on the blot shown in (Figure 4.6 D), again in agreement with the proteomics-based analysis. None of the chosen interaction was detected in the samples eluted neither from the immobilized GST control nor from the Glutathione Sepharose beads alone.

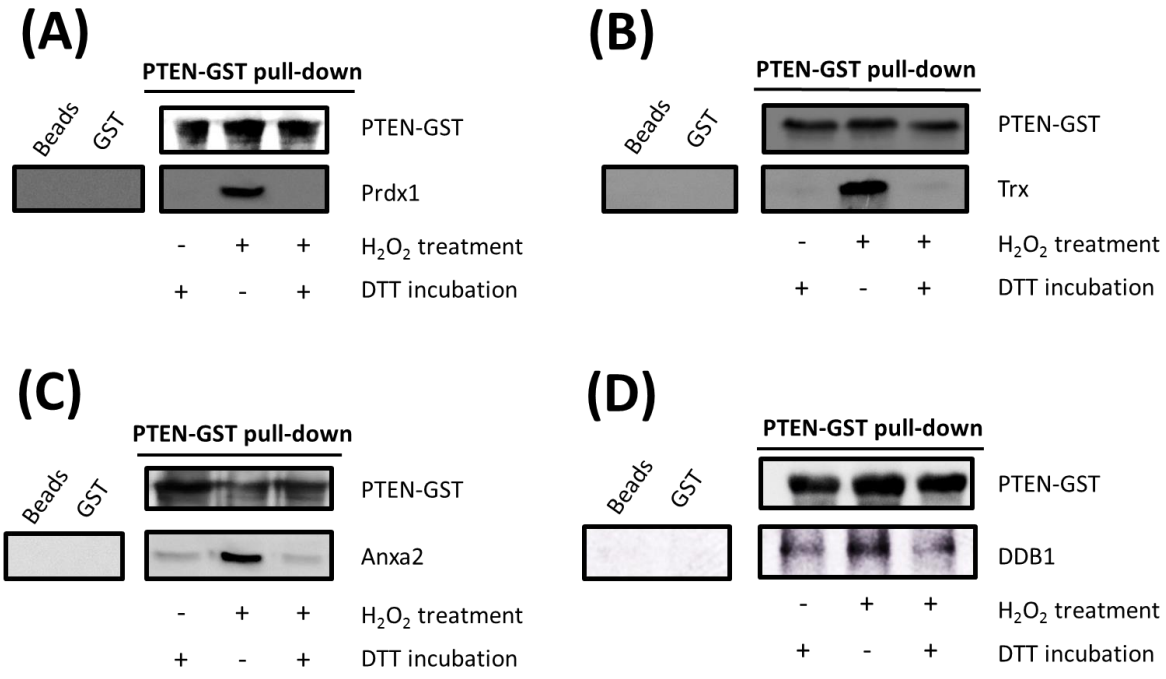


**Figure 4.6 Western blots showing validation of proteomics data in comparing selected affinity-captured PTEN interactions across the samples eluted from untreated, oxidized and DTT-recovered PTEN-GST**

Each panel shows: PTEN-GST loading control; expression of selected PTEN-interactor in the $H_2O_2$-treated, untreated and recovered PTEN-GST pull down compared to the sample eluted from GST and beads alone; whether the bait PTEN-GST protein was treated with 1 mM $H_2O_2$ and/or incubated with 100 mM DTT. Both untreated and recovered samples were kept in constant reducing conditions (100 mM DTT incubation) during the bait immobilization and showed similar interaction profiles. The $H_2O_2$-treated PTEN-GST pull down showed increased level of Prdx1 (A), Trx (B) and Anxa2 (C) and comparable levels of DDB1 (D) when compared to the reduced controls. The results are representative of two replicate experiments for each interactor shown. The uncropped Western blots used to generate this figure are shown in the Appendix (Sect. 8.6.1).

### 4.4.6 Relative quantification of the oxPTMs revealed extent of Met oxidation in the oxidized PTEN-GST bait

After quantification and validation of the affinity-captured interactors, a Mascot Database search was performed on the aligned LC-MS runs to check for any oxidative post-translational modifications (oxPTMs) that occurred to the PTEN-GST bait following oxidation with hydrogen peroxide. Given the concentration of hydrogen peroxide used to inactivate PTEN (1 mM), we did not expect the oxidation event to generate major modifications other than the Cys71-Cys124 disulfide bond. The aligned features identified as PTEN and GST peptides across three independent GSH-affinity enrichment experiments were searched for: methionine oxidation and dioxidation, cysteine oxidation, dioxidation and trioxidation, and tyrosine oxidation. A total of 4 PTEN peptides and a total of 6 GST oxidatively modified peptides were found in both untreated and 1 mM $H_2O_2$ oxidized sample (Table 4.2). PTEN was found oxidatively modified at Met35, Met134, Cys136 and Met239, while GST was found oxidatively modified at Met1, Tyr4, Met20, Cys48 and Met92. All of the identified features shown in Table 4.2 were matched to high Mascot score PTEN and GST peptides. Interestingly, Met134 of PTEN was substantially oxidized (more than 30%) in both untreated and oxidized PTEN-GST, but there was no significant difference between the two. Met20 and Met92 of GST also showed significant extent of oxidation in both samples, but again no significant difference was observed in comparing the untreated and oxidized PTEN-GST. The only significant change in oxidation was seen for Met35 in the PTEN peptide YQEDGFDLDLTYIYPNIIAMGFPAE, which oxidized to approximately 14% methionine sulfoxide upon $H_2O_2$ treatment. Overall, these results are indicative of the fact that while generating the intramolecular disulfide bond between Cys71 and Cys124 in the active site, the oxidative treatment caused minimal additional oxidative modifications to the immobilized PTEN-GST.

**Table 4.2** Identification and quantification of PTEN and GST oxidative modifications in comparing untreated versus 1 mM oxidized PTEN-GST following GSH-affinity enrichment

| Protein | Peptide Sequence[1] | Fraction detected[2] | m/z (charge) | Modifications[3] | p-value[4] | % Relative modification | |
|---|---|---|---|---|---|---|---|
| | | | | | | Reduced | Oxidized |
| PTEN | YQEDGFDL DLTYIYPNII AMGFPAER | 5 | 1023.2028 (3) | Met 35 OX | **0.0004** | 1.01 ± 1.74 | 14.48 ± 1.28 |
| PTEN | TGVMICAY LLHR | 3 | 470.2714 (3) | Cys 136 DIOX | 0.4207 | 2.31 ± 0.60 | 1.63 ± 1.17 |
| PTEN | TGVMICAY LLHR | 2,3,4 | 483.9500 (3) | Met 134 OX | 0.6963 | 34.05 ± 3.61 | 30.64 ± 13.64 |
| PTEN | FMYFEFPQP LPVCGDIK | 3 | 1052.5630 (2) | Met 239 OX | 0.9593 | 1.76 ± 3.05 | 1.65 ± 1.61 |
| GST | MLLADQGQ SWK | 6,7,8,9,10,11 | 646.8266 (2) | Met 20 OX | **0.0333** | 24.59 ± 3.69 | 17.79 ± 0.19 |
| GST | MLLADQGQ SWK | 7,10 | 431.5445 (3) | Met 20 OX | **0.0487** | 24.33 ± 2.01 | 21.00 ± 0.46 |
| GST | MLLADQGQ SWK | 7 | 654.8150 (2) | Met 20 DIOX | 0.0681 | 0.39 ± 0.12 | 0.21 ± 0.03 |
| GST | ASCLYGQL PK | 7 | 556.2746 (2) | Cys 48 DIOX | 0.0705 | 1.80 ± 0.69 | 0.65 ± 0.44 |
| GST | ASCLYGQL PK | 7 | 564.2732 (2) | Cys 48 TRIOX | 0.2220 | 0.89 ± 0.42 | 1.59 ± 0.73 |
| GST | PPYTVVYFP VR | 7 | 677.3622 (2) | Tyr 4 OX | 0.2590 | 0.76 ± 0.26 | 0.55 ± 0.05 |
| GST | DQQEAALV DMVNDGVE DLR | 7,8,9,10 | 1067.0113 (2) | Met 92 OX | 0.3008 | 30.14 ±11.34 | 22.27 ± 1.78 |
| GST | MLLADQGQ SWKEEVVT VETWQEGS LK | 10 | 752.6226 (4) | Met 20 OX | 0.5333 | 13.07 ± 3.68 | 14.88 ± 2.78 |
| GST | MLLADQGQ SWKEEVVT VETWQEGS LK | 9,10 | 1003.1702 (3) | Met 20 OX | 0.5981 | 18.41 ± 1.64 | 19.83 ± 3.96 |
| GST | DQQEAALV DMVNDGVE DLR | 7,8,9,10 | 711.6659 (3) | Met 92 OX | 0.6981 | 26.70 ± 6.68 | 25.03 ± 1.97 |
| GST | MPPYTVVY FPVR | 7 | 495.5891 (3) | Met 1 OX | 0.7441 | 19.89 ± 4.56 | 18.93 ± 1.39 |
| GST | DQQEAALV DMVNDGVE DLR | 7 | 533.9936 (4) | Met 92 OX | 0.9933 | 44.85 ± 21.58 | 44.97 ± 9.42 |

[1]Peptide sequence obtained from the Mascot database search of LC-MS runs aligned on Progenesis QI, carrying the modified amino acid (in red)

[2]Gel slice Fraction(s) corresponding to the LC-MS run where the peptide was detected

[3]Modification type and position within the protein amino acid sequence

[4]p-value returned by two-tailed unpaired Student's t test, following relative quantification of the modifications (significant p-values are indicated in **bold)**

The data was obtained from the analysis of PTEN and GST peptide features present in three independent GSH-affinity experiments. Ranking is based on p-values returned by Two-tailed unpaired Student's t test.

# 4.5 Discussion

The study presented in this chapter describes for the first time a correlation between the targeted oxidative inactivation of the tumour suppressor phosphatase PTEN and changes in its binding proteins. Several proteins were detected whose interaction with PTEN changes upon $H_2O_2$ treatment of PTEN, and a number of novel PTEN interactions has also been discovered.

As the aim of the study was to compare the interactions captured by an active versus inactive bait protein, the oxidative treatment was designed to promote the formation of the regulatory disulfide bond between Cys71 and Cys124 in the active site of PTEN while minimizing other oxidations. The observed level of oxidative-induced inactivation of the bait protein was in agreement with previous studies reporting the effect of 1 mM $H_2O_2$ on PTEN phosphatase activity [477]. The DTT-induced reversibility of the inhibitory effect was considered satisfactory evidence of the involvement of the regulatory disulfide in PTEN-GST inactivation, as previously shown by Lee *et al* [423]. The oxidant type and concentration were chosen to maximize the generation of the regulatory disulfide bond between Cys71 and Cys124 while reducing the risk of significant oxidation of other amino acids. Treatment with 1 mM $H_2O_2$ caused little change in the modification status of PTEN or GST, except for Met35 of PTEN which was found 13% more oxidized to sulfoxide in the oxidized PTEN-GST sample. Given the fact that the activity of the oxidized protein was fully restored upon DTT incubation, it is reasonable to assume that the modification at Met35 of PTEN was not responsible for major protein function loss. Whether this modification had a significant effect on the observed changes in PTEN interacting proteins is not completely clear at this stage, and additional studies would be necessary to address this question. However, this hypothesis also seems unlikely, as the observed changes in interactions were reversible by DTT, as shown by the Western-blotting based validation.

One significant finding reported in this study is the significant increase in the abundance of the redox proteins peroxiredoxin-1 (Prdx1, FC=4.1, p-value = 0.0437) and thioredoxin-1 (Thio, FC = 6.2, p-value = 0.0065) interacting with the oxidized (inactive) PTEN-GST. A study published by Cao *et al*. showed that Prdx1 fully restores PTEN activity in the presence of hydrogen peroxide [479]. Prdx1

seems to bind PTEN through interaction with its C2 domain (amino acids 190-350), although the exact amino acid residues where the binding occurs have not been established yet [479]. Interestingly, the authors have shown a decreased binding of Prdx1 to PTEN by co-immunoprecipitation when cells were treated with high concentration of $H_2O_2$ [479]. However, it has been proposed that the oxidative damage to Cys51 in Prdx1 is responsible for the dissociation of PTEN/Prdx1 complex, as this residue may be exposed to further oxidation when Prdx1 interacts with PTEN [480]. Besides, the experimental system described in this study did not involve direct oxidative damage to Prdx1, but rather the targeted *in vitro* inactivation of PTEN, which suggests that the Prdx1/PTEN was unlikely to dissociate once formed in the conditions described. A second significant increase was seen for the antioxidant thioredoxin-1. It is generally accepted that Trx is responsible for the reactivation of PTEN via reduction of the disulfide bond between Cys71 and Cys124 of PTEN with a thiol-disulfide exchange mechanism [144,423,553]. The increased abundance of Trx affinity captured with the oxidized PTEN-GST bait suggests that the formation of the PTEN:Trx complex is strictly dependent on the redox status of PTEN. On the other hand, another study showed that the redox status of Trx is also important in the PTEN/Trx interaction. The authors showed that reduced Trx, but not oxidized Trx, binds the C2 domain of PTEN via a disulfide bond with PTEN Cys212 causing inhibition of the phosphatase resulting in increased tumorigenesis [478]. Overall, these findings imply that the redox status of Trx is an important factor in the regulation of the interaction and additional studies would be required to fully understand the dynamics of Trx-mediated PTEN reactivation *in vivo*.

The results observed in this study suggest that both Prdx1 and Trx are involved in the recycling of PTEN active site when the protein is targetedly oxidized with $H_2O_2$. It could be speculated that PTEN reactivation requires the binding of both proteins at the C2 domain of PTEN, consistent with other published work [423,479,480]. In this model, Prdx1 is responsible for scavenging $H_2O_2$ molecules in the proximity of oxidized PTEN molecules, whilst Trx restores the protein to its active form by reducing the Cys71-Cys124 disulfide back to the reduced (free thiol) form (Figure 4.7). However, numerous questions remain unresolved though, and further studies are required to elucidate the relationship between ROS-signaling and the PTEN/Prdx1/Trx system. For example, it is not clear whether Trx and Prdx1 bind PTEN at the same time, exclusively or independently following PTEN inactivation. It is likely that the oxidation-generated disulfide bond in the PTEN active site triggers the

increased binding of Prdx1 and Trx, but the exact sequence of events that leads to the reactivation of the phosphatase remains unclear. It is also possible that Trx and Prdx1 became trapped to oxidized PTEN via intermolecular disulfide bonds which remains during the capture, thereby explaining their increased binding to the $H_2O_2$-oxidized purified PTEN compared to the untreated and recovered samples which were in the thiols form. Most importantly, the studies conducted to date imply that the mechanism by which the PTEN/Prdx1 and PTEN/Trx interactions are modulated by oxidative stress *in vivo* is not dependent solely on the inactivation of PTEN, and that other oxidative stress-induced events might be involved.

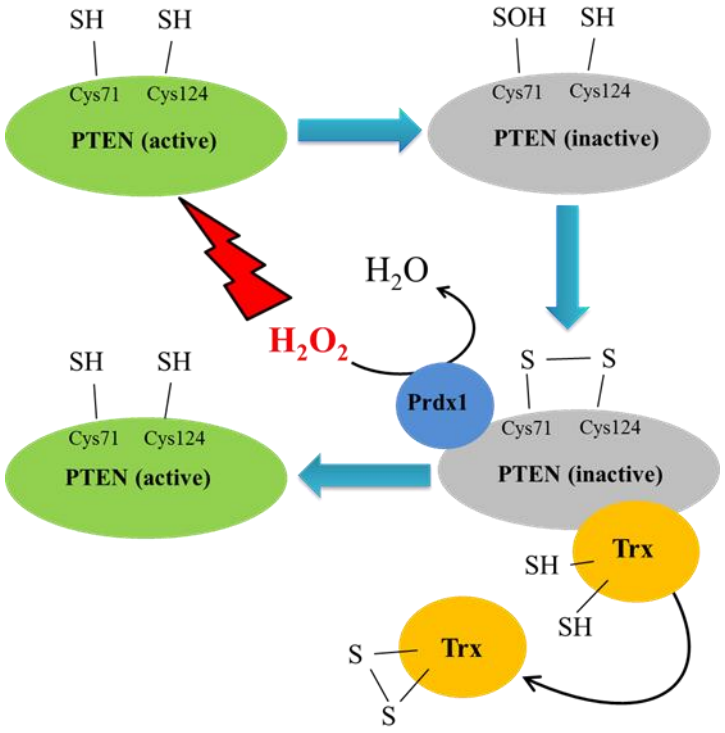


**Figure 4.7 Proposed model for PTEN reactivation through interaction with peroxiredoxin-1 and thioredoxin-1**

When PTEN is exposed to hydrogen peroxide, the Cys124 and Cys71 thiols are oxidized to form a disulfide bond (through the formation of a cysteine sulfenic acid intermediate). This series of events, in combination with the ROS-mediated signal transduction, is likely responsible for the increased Prdx1 and Trx binding to the oxidized PTEN. Prdx1 scavenges $H_2O_2$ molecules around PTEN, protecting the phosphatase from oxidative damage. Trx converts PTEN back to the active (reduced) form in a thiol-disulfide exchange-like mechanism.

An interesting group of proteins among the PTEN interactors detected were those associated with the control of the actin cytoskeleton pathway, for which PTEN phosphatase activity was identified as a key regulator [537,538]. One actin-binding proteins detected in this study was the actin-binding protein Drebrin (Dreb), which was found significantly more associated to the oxidized PTEN-GST bait (FC=4.9, p-value=0.0180), and has been identified as PTEN interactor in a previous study [554]. PTEN has been proposed as a negative regulator of the phosphorylation of Dreb at Ser647, and the formation of the complex PTEN:Dreb seems to be inversely correlated to neuronal activity [554]. Nonetheless, a relationship between the redox status of PTEN and the molecular dynamics of the PTEN:Dreb complex has not yet been studied, and the mechanism by which PTEN binds Dreb seems to be independent of PI3K signaling. Another actin-binding protein identified among the PTEN-binding partners was annexin A2 (Anxa2), which appeared to bind more strongly to the oxidized PTEN-GST (FC=6.8, p-value=0.0118), and which was also previously described as a PTEN binding protein [541]. Anxa2 has been recently implicated as a redox-sensitive protein, as it contains a reactive cysteine residue (Cys8) which is susceptible to oxidation and is reduced by the thioredoxin system *in vitro* [555]. Anxa2 depleted cells have shown increased levels of ROS, ROS-induced pro-apoptotic kinases, and increased susceptibility, suggesting the involvement of Anxa2 in the cellular response to oxidative stress associated with tumorigenesis [555,556]. Overexpression of annexin A2 has been associated with cancer metastasis [557] and there is evidence of a PI3K-dependent regulation of the interaction between Anxa2 and the Na,K-ATPase β1-subunit (Na,K-β), involved in the suppression of cell motility [558]. Interestingly, it has been shown that PTEN co-localizes on the apical surface of polarized cells along with Anxa2 and the small GTPase Cdc42 and plays a role in regulating epithelial morphogenesis [559]. The authors also showed that Anxa2 binds PtdIns(4,5)$P_2$ at the apical surface, assuming the involvement of PTEN in the depletion of PtdIns(4,5)$P_2$ from PtdIns(3,4,5)$P_3$. However, this conclusion requires further investigation, as the PtdIns(4,5)$P_2$ is in large excess and generally converted into PtdIns(3,4,5)$P_3$ by PI3 kinases [560]. The exact molecular mechanism responsible for the PTEN/PtdIns(4,5)$P_2$/Anxa2 network is therefore still unclear and may involve a direct association between annexin A2 and PTEN in the apical domain for the recruitment of PtdIns(4,5)$P_2$ to the apical surface. Another actin-binding protein detected among the PTEN interactors was spectrin alpha chain (non-erythrocytic 1, Spta1), which is a putative novel PTEN interactors that was also found to bind

more intensely to oxPTEN (FC=2.9, p-value=0.0361). Spta1 is a cytoskeletal protein that act as scaffold protein stabilizing the plasma membrane and organizing intracellular organelles [561]. Other actin-binding proteins identified as novel PTEN interactors were myosin phosphatase Rho-interacting protein (MPRIP), involved in shuttling myosin phosphatase to the actin cytoskeleton [562], and Utrophin (Utro), which plays an important role in the cytoskeleton during neuromuscular junction formation [563]. Only a slight difference in binding was detected in comparing oxidized and reduced PTEN-GST for binding to MPRIP (FC=2.1, p-value= 0.0423) or Utro (FC = 2.2, p-value= 0.0306).

Another key group of PTEN-interacting proteins were those involved in DNA repair, chromosomal segregation and genomic stability. Among those, one potential novel PTEN interactor was Polymerase delta-interacting protein 2 (PDIP2 or Poldip2), which showed stronger association with oxidized PTEN (FC=10.8, p-value <0.0001). Poldip2 has been shown to interact with DNA polymerase delta (p50) and is involved in DNA repair, cell cycle regulation and chromosomal replication [564]. In addition, Poldip2 might have a signaling role in the oxidative inactivation of PTEN as it was reported to increase the activity of the transmembrane protein Nox4 (or Nox1), a NADPH oxidase that has been identified as the main source of $H_2O_2$ production in non-phagocytic cells [476,565]. Nox4 has been shown to be activated by PtdIns(3,4,5)$P_3$, which triggers the increased generation of $H_2O_2$ resulting in the oxidation of PTEN [144]. Interestingly, this study has shown a 10.8 fold increase in binding of Poldip2 to the oxidized PTEN-GST, suggesting that this protein might be involved in the ROS-mediated signaling cascade responsible for PTEN inactivation. Protein pelota homolog (PELO), a protein required for cell cycle control, chromosomal segregation and meiotic cell division [566], was also identified as novel PTEN interactor and showed significantly increased binding to oxidized PTEN (FC=2.7, p-value=0.0018). Pelo has also been shown to control the HER2 (human epidermal growth factor receptor 2) signaling through the PI3K/Akt pathway [567]. DNA-damage binding protein1 (DDB1), a protein involved in DNA repair [568], was also identified as a putative novel PTEN interactor. No significant change was found in comparing the abundance of DDB1 captured from the reduced and the oxidized PTEN-GST (FC=1.0, p-value=0.8942). The interplay between the PI3K/Akt pathway and the excision nucleotide pathway, of which DDB1 is a member, has been shown in human epithelial cells [569]. Moreover, a role in DNA damage repair and response has also been proposed for PTEN, although the knowledge of the molecular mechanism is currently limited [441].

Some other interesting proteins were also identified as putative novel PTEN interactors. Among those was the multi-enzyme fatty acid synthase (FAS). Because of its demonstrated link to the PI3K/Akt pathway, fatty acid synthase (FAS) can also be considered as putative PTEN direct interaction. A close correlation has been demonstrated between the overexpression of FAS and the loss of PTEN in HCC tissue [544], and PTEN seems involved in the regulation of FAS through the inhibition of Akt [570]. Neither of the mentioned studies investigated the effect of PTEN oxidative inactivation on FAS regulation. However, only a little variation in abundance was detected when comparing the levels of FAS in the sample eluted from the reduced to the oxidized PTEN-GST (FC=1.7, p-value=0.0144). Two other putative novel PTEN interactors proteins that were found to bind oxPTEN significantly more strongly were Guanine nucleotide-binding protein G (i) subunit alpha1 (GNAI1, FC=3.6, -p-value = 0.0462) and alpha-2 (GNAI2, FC= 6.9, p-value=0.0488). These are members of the Gαi family, and are adenylate cyclase inhibitors that are involved in the control of cellular proliferation and differentiation [571], processes in which PTEN also plays an important role [572]. Another interesting new interaction was A-kinase anchor protein-12 (AKA12 orAKAP12) a tumour suppressing scaffold protein involved in the regulation of PKA (Protein Kinase A) and PKC (Protein Kinase C) in G-protein coupled receptor signaling [573,574]. The interaction of AKA12 with PTEN-GST did not appear to be redox-sensitive (FC = 1.3, p-value= 0.0181), there is evidence of a cross-talk between the PTEN-mediated inhibition of the PI3/Akt pathway and AKAP12 in the suppression of prostate cancer (CaP) progression [574].

Protein-protein interactions (PPIs) have been shown to play a major role in the biological mechanism behind many human diseases and are currently considered a promising target for the discovery and development of new drugs [535,536]. The data presented in this study showed that the oxidative treatment had influenced the ability of PTEN to capture proteins from the cell lysate, which might be important to understand how the oxidative-induced inactivation affects PTEN protein-protein interactions. The *in vitro* affinity-capture of proteins from cell lysates by reduced and oxidized PTEN in combination with label-free quantitative mass spectrometry has provided a valuable tool for studying PTEN signaling networks under oxidative stress and for the discovery of novel protein-protein interactions. This method can be usefully implemented to measure the protein levels in

complex biological mixtures in order to accurately interpret MS-based proteomics datasets and has identified a new mechanism by which protein-protein interactions are regulated.

# Chapter 5. Validation and profiling of PTEN protein-protein interactions under cellular oxidative stress

# 5.1 Summary

Oxidative stress caused by reactive oxygen species is a common feature of many diseases and results in oxidative damage toward cellular biomolecules such as proteins, DNA and lipids. One of the biological mechanisms by which cells respond to oxidative stress involves the activation of signaling pathways linked to cell survival and apoptosis. These pathways are controlled by intracellular redox-sensing proteins such as the phosphatase PTEN, the function of which can be regulated by specific protein-protein interactions that can be activated in response to oxidative stress.

In the study presented in this chapter, PTEN-interacting proteins that showed a differential abundance profile upon targeted inactivation of purified PTEN were validated with an *in vivo* method. PTEN was overexpressed as an EGFP-tagged fusion protein by transfection in HCT116 cells, and PTEN-interactors were captured by Co-IP, identified by LC-MS, and matched against PTEN interactions data generated previously with the *in vitro* method. HCT116 cell survival following treatment with 1 and 5 mM $H_2O_2$ was monitored by XTT viability assay and four preselected PTEN interactions (Prdx1, Trx, Anxa2 and DDB1) were quantitatively analyzed by immunoblotting following Co-IP from untreated versus oxidized PTEN-EGFP transfected cells.

33 PTEN-interactors identified by LC-MS were found to be common between the *in vitro* and *in vivo* datasets, and three out of four preselected proteins were validated by immunoblotting. A $H_2O_2$ concentration of 5 mM, but not of 1 mM, induced a significant increase in the association of selected interactors to PTEN, and both treatments affected HCT116 cell survival to a similar degree. The study presented confirms the importance of validation procedures in complex proteome-wide datasets and highlights the complexity of protein dynamics in redox-sensitive signaling pathways.

# 5.2 Introduction

Free radicals and other reactive molecules that are generated intracellularly as a result of normal cell metabolism or enter the body from the environment can overwhelm the cellular antioxidant defenses and cause oxidative stress. Cellular redox imbalance has been linked to many diseases, including neurodegeneration, cancer, inflammatory diseases, and cardiovascular diseases [56,120,153,165,361,575].

Healthy cells are equipped with powerful antioxidant defenses that control the removal of reactive molecules such as ROS (Reactive oxygen species) and can prevent damage to proteins, DNA and other biomolecules. However, in pathological conditions, the antioxidant systems can be overwhelmed by the action of ROS, resulting in cell and tissue injury which may cause important damage to cellular biomolecules. Based on their mechanism of action, cellular antioxidants can be divided between enzymatic and non-enzymatic. The major cellular enzymatic antioxidants include superoxide dismutases (SOD), Glutathione Peroxidase (GSH-Px), and catalase. SODs in the cell exist in three main forms (CuZn-SOD, Mn-SOD, and EC-SOD), all of which catalyze the reduction of superoxide anion ($O_2^{-\cdot}$) to hydrogen peroxide ($H_2O_2$) [576]. This is particularly important for the cellular antioxidant defense as superoxide is the primary ROS produced within the mitochondria [576], and if not removed may accumulate and be converted into highly toxic species such as hydroxyl radicals [577]. $H_2O_2$ produced by SODs or generated by the mitochondria during the respiratory burst can be converted into water by the action of catalases and GSH-Px, which are both dependent on NAPDH for their function [578]. Additionally, a number of thiol-containing redox-sensing proteins such as thioredoxin, thioredoxin reductase, thioredoxin peroxidase (also known as peroxiredoxins) and glutaredoxin are involved in scavenging of $H_2O_2$ and have an important role in determining peroxide response signals [579]. Non-enzymatic antioxidants are also involved in maintaining cellular redox balance and include low molecular weight compounds such as the tripeptide glutathione (GSH), vitamins (vitamins A, C and E), and uric acid, among others [576].

While initially regarded as toxic metabolites, ROS are now considered important signaling intermediate that play a central role in cell proliferation and survival, although the exact mechanism

through which ROS interact with signaling molecules is unclear [580,581]. Many of the enzymatic antioxidants involved in detoxifying the cells by ROS scavenging are also involved in ROS-sensing and ROS homeostasis through oxido-reductase systems such as those based on thiol-disulfide exchange mechanisms [580]. These proteins include thioredoxins, peroxiredoxins, and protein tyrosine phosphatases such as PTEN, all which are central regulatory element of cellular networks linked to disease such as the PI3K/Akt Pathway [144,445,479].

One of the most commonly used approaches in cell biology to investigate the molecular mechanisms regulating signaling pathways is by analyzing protein-protein interactions. As shown in the previous chapter, studying the redox interactome of PTEN is important to identify molecular mechanisms that regulate PTEN function and activity under oxidative stress. By coupling affinity-capture methods with mass spectrometry, a number of PTEN-interacting proteins were identified that are modulated upon reversible $H_2O_2$-induced oxidation of purified PTEN-GST, including thioredoxin (Trx), peroxiredoxin-1 (Prdx1) and annexin A2 (Anxa2). These proteins were found to associate more strongly with the oxidized PTEN-GST immobilized onto a GSH-based resin, suggesting a role for these proteins in the regulation of the ROS-mediated signaling associated with the downstream pathways of PTEN, most notably the PI3/Akt pathway. However, the redox interactome generated in Chapter 4 is not a good indicator of the PTEN protein-protein interactions dynamics under physiological oxidative stress, since the oxidation-induced changes observed in PTEN-interacting proteins were only due to the targeted oxidation of PTEN, which is unlikely to take place in cells. It was therefore considered important to further investigate the redox interactome of PTEN by analyzing PTEN protein-protein interactions in $H_2O_2$-oxidized versus untreated cells overexpressing PTEN. In this fashion, the entire set of PTEN-interacting "prey" proteins, rather than just the PTEN "bait" are exposed to the oxidizing action of $H_2O_2$, therefore the molecular dynamics involved in the intracellular ROS-regulation of PTEN downstream signaling pathways can be studied.

The *in vivo* study presented in this chapter represents an attempt to validate the *in vitro* findings reported in Chapter 4 with a complementary approach and to further investigate the difference in abundance in the association of binding proteins with PTEN in oxidizing versus normal cellular redox conditions. A PTEN interactome generated analyzing with MS the proteins captured by the overexpressed recombinant PTEN was matched against the dataset obtained from the *in vitro* study

and identified 33 common proteins, including Prdx1 and Anxa2, which were previously described as PTEN interactors and showed an increased abundance in the presence of oxidized PTEN. Preselected PTEN interactors Anxa2, Prdx1 and Trx were detected by immunoblotting and their association with PTEN quantitatively compared between oxidized versus untreated cells. The results of this study showed that the cellular redox dynamics that regulate PTEN protein-protein interactions are complex and opened different perspectives on the molecular mechanisms of interplay between ROS signaling and oxidative stress.

# 5.3 Materials and methods

### 5.3.1 Optimization of transfection conditions

Confluent HCT116 cells were cultured as described in Section 2.3.3 and 0.4, 0.6, 0.8 and 1 x $10^5$ cells/mL were seeded in a tissue-culture treated 24-well plate with DMEM) supplemented with 10% FBS. Transfection conditions were optimized by testing GeneJuice (Novagen, Millipore Ltd, Feltham UK) and Lipofectamine 2000 (Life technologies, Paisley, UK) reagents. For GeneJuice, the transfection reagent was diluted in serum-free DMEM according to the manufacturer's instructions. The plasmid DNA with the vector containing PTEN-EGFP (prepared as described in Section 2.4.6) was mixed with the GeneJuice solution (3 µL GeneJuice reagent per 1 µg DNA), allowed to sit at room temperature for 15 min, and then added drop-wise to each well of the 24-well plate containing 0.4, 0.6, 0.8 and 1 x $10^5$ HCT116 cells/mL. For Lipofectamine 2000, both the transfection reagent and the PEGFP-C1 plasmid DNA containing PTEN-EGFP were diluted in Opti-MEM® I Reduced Serum Medium (31985-062, Life technologies, Paisley, UK) in two separate tubes according to the manufacturer's instructions. The two solutions were then mixed in a 1:1 ratio and allowed to sit at room temperature for 20 min. Next, the DNA-Lipofectamine complex was added to each well of the 24-well plate containing 0.4, 0.6, 0.8 and 1 x $10^5$ HCT116 cells/mL. 24-well plates containing transfected HCT-116 cells were placed at 37C°, 5% $CO_2$ and observed under the Olympus CK2 inverted microscope after 4-6 hours to check cell viability, and placed back at 37C°, 5% $CO_2$ in the controlled incubator for a total of 24, 48 or 72 hours as required.

Fluorescent cells were observed under an inverted Fluorescence microscope (DMI400B, Leica Microsystems), controlled using the Leica Application suite software. Transfection efficiency (% GFP-positive cells) and fluorescence intensity were measured using ImageJ. Transfection efficiency was determined by manually counting GFP-positive and total bright-field cells using the Cell Counter plugin in Image J. Fluorescence intensity was determined by selecting single cells and background areas from images of transfected cells, and calculating the corrected total cell fluorescence (CTCF) using the formula: CTCF = Integrated Density - (Area of selected cell X Mean fluorescence of background).

### 5.3.2 Transfection of HCT116 cells and protein capture

Approximately 30 million HCT116 confluent cells were transfected with the PEGFP-C1 vector containing PTEN-EGFP using Lipofectamine 2000 as described in the previous section. Tissue culture flasks containing PTEN-EGFP transfected HCT-116 cells were incubated at 37C°, 5% $CO_2$ for a total of 48 hours. HCT116 PTEN-EGFP transfected cells were harvested, washed twice with ice cold PBS pH 7.4 by spinning at 500g for 10 minutes at 4°C in an Eppendorf 5810R (Eppendorf UK Ltd, Stevenage, UK), and lysed for 30 min on ice with ice-cold 10 mM Tris pH 7.5, 150 mM NaCl, 0.5 mM EDTA, 0.5% NP-40 (GFP trap kit, Chromotek, Martinsried, Germany) with occasional shaking. GFP trap magnetic beads (Chromotek, Martinsried, Germany) were used for the co-immunoprecipitation of PTEN interacting proteins. The bead slurry was briefly vortexed and 30 µL were diluted in 500 µL of ice-cold mM Tris pH 7.5, 150 mM NaCl, 0.5 mM EDTA (GFP trap kit, Chromotek, Martinsried, Germany). Beads were magnetically separated by placing micro-centrifuge tubes in a magnetic separation rack for 1-2 minutes (Millipore Ltd, Feltham UK), until the supernatant was clear. The supernatant was removed and the wash was repeated twice. The entire volume of cell lysate of 30 million cells from above was added to micro-centrifuge tubes containing the GFP-Trap beads, and rotated horizontally using a Dynabeads® MX1 Mixer (Life technologies, Paisley, UK), overnight at $4^0$C. The beads were isolated by placing the tube in a magnetic separation rack for 1-2 minutes, a 30 µL aliquot of the supernatant from both a control and oxidized micro-centrifuge tube was saved for the SDS-PAGE, and the rest of the supernatant was discarded. The beads were re-suspended in 500 µL dilution buffer, and magnetically separated three times to wash away any non-specifically bound proteins. The beads were then re-suspended in 50 µL of 2x SDS-sample buffer and the mixture was heated for 10 minutes at $95^0$C. 25 µL of the supernatant were loaded on a SDS-PAGE, and electrophoretic run was performed as described in Section 2.6.1.

### 5.3.3 Protein digestion

The gel lane corresponding to the protein eluted from the GFP antibody after incubation with PTEN-EGFP transfected HCT116 cells were each cut into 12 approximately equal slices, and the gel pieces digested as described in Section 2.7.1.

### 5.3.4 LC-MS

Peptides were separated and analyzed as described in Section 2.7.2.

### 5.3.5 MS-based proteomics analysis

A total of 12 experiments were created, one for gel bands excised from each lane of the Coomassie-stained gel at the same molecular weight. Any peptide showing a Mascot Ion Score below the threshold indicative of identity or extensive homology ($p$ value $< 0.05$) was removed from the feature identification list. Cytoskeletal keratin IDs were removed from the feature identification list. Only features that had zero protein conflicts were used for quantification. Data obtained from the alignment of LC-MS runs corresponding to single fractions were then pooled into a multi-fraction experiment

### 5.3.6 Oxidation and XTT assay

Confluent HCT116 human colon cancer cells (cultured as described in Section 2.3.3) of passage 4 to 10 were harvested, washed twice with ice PBS pH 7.4 by spinning at 500g for 10 minutes and 100 µL contained approximately 100,000 cells were added to each well of a tissue-culture treated 96 well plate (Appleton Woods, Birmingham, UK). 100 µL growth medium was added as negative control. The 96-well plate was incubated overnight at 37°C, 5% $CO_2$ in the controlled incubator Sanyo MCO-18AIC (Sanyo, UK). Next, the electron coupling solution and the XTT detection solutions (XTT assay kit, New England Biolabs, Hitchin, UK) were thawed, mixed in a 1:50 volume ratio, and added to each well of the 96-well plate. To induce oxidative stress 150 µL $H_2O_2$ was added to each well in a row to a final concentration of 0, 1, 2, or 5 mM. Cell viability was checked by monitoring the absorbance at 450 nm in a BioTek® plate reader (Biotek, Potton, UK) every hour.

### 5.3.7 Oxidation treatment

Oxidative stress was induced in PTEN-EGFP overexpressing HCT116 cells after 48 hours transfection with the DNA-Lipofectamine complex by adding 0, 1, 2 or 5 mM $H_2O_2$ in DMEM

medium supplemented with 10% FBS, and incubating for 1 hour at 37C°, 5% $CO_2$ in the controlled incubator.

### 5.3.8 Western blotting

The Western blotting analysis was performed as described in Section 4.3.11

### 5.3.9 Image processing and protein quantification

Gel densitometry was performed with the Java-based image processing ImageJ [513]. Images of Western blot scans were first imported into Microsoft Powerpoint® and cropped so that white space was left between lanes corresponding to different replicates and/or experimental conditions. Next, the lanes were further cropped to include only the protein band corresponding to PTEN-EGFP, Anxa2, Prdx1 or Trx, cropping the image along the edge of the gel band. The images were then saved as .png and opened in ImageJ. All images were converted to 8-bit, and no background subtraction or contrast enhancing was performed. Relative proteins levels for Anxa2, Prdx1 and Trx were normalized against PTEN-EGFP densitometry and plotted as fold change relative to PTEN-EGFP loading control.

# 5.4 Results

## 5.4.1 Optimization of transfection conditions and comparison of different transfection reagents

To achieve optimum levels of PTEN overexpression in HCT116 cells, two available transfection reagents, GeneJuice and Lipofectamine 2000, were tested for transfection efficiency of the PTEN-EGFP plasmid DNA. For both reagents used, the fluorescence emitted by the PTEN-EGFP-transfected HCT116 cells was evaluated using a fluorescence microscope (ARCHA microscope facility at Aston University). The GFP-positive cells and the total cells were manually counted from representative images acquired from the microscope software using the Cell Counter function in ImageJ to determine the transfection efficiency. For each of the two reagents, a range of different cell densities (0.4, 0.6, 0.8 and 1.0 x $10^5$ cells/mL) and transfection times (24, 48 and 72 hours) were tested in order to identify the conditions that were associated with best transfection rates For a 24-well plate, a cell density of 0.6 or 0.8 x $10^5$ HCT116 cells/mL and a transfection time of 48 hours were found to be associated with the highest number of GFP-positive cells with minimum cell death. Figure 5.1 (A) shows representative fluorescent and corresponding bright-field images comparing the GFP-positive and total cells after transfection of HCT116 cells with the PEGFP-C1-PTEN-EGFP plasmid DNA with GeneJuice and Lipofectamine 2000 reagents. The images were acquired from wells containing PTEN-EGFP transfected HCT116 cells which were seeded at an initial cell density of 0.6 x $10^5$ cells/mL and incubated with the DNA-reagent complex for 48 hours. As evident from the images, Lipofectamine2000 clearly outperformed GeneJuice for number of viable GFP-positive cells when HCT116 are transfected with the PTEN-EGFP plasmid DNA. The average percentage transfection efficiency after 48 hours of incubation with the DNA-reagent complex was 11% for GeneJuice and 73% for Lipofectamine 2000. The intensity of the fluorescent signals corresponding to the GFP-positive cells transfected with Lipofectamine 2000 was also higher (+25%) than that detected after transfection with GeneJuice. Generally, the number of live cells observed using bright field illumination was comparable between the two transfection reagents.

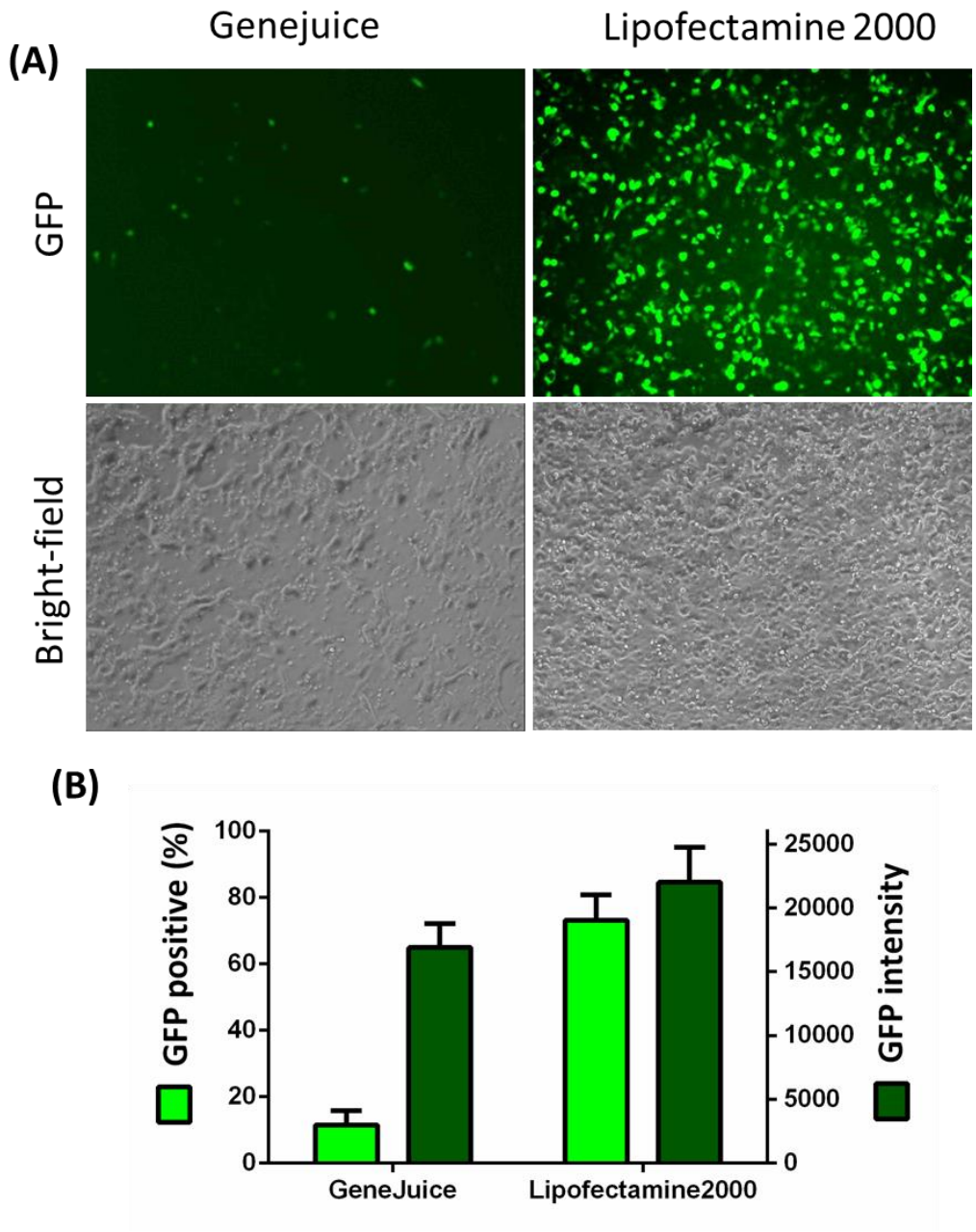


**Figure 5.1 Transfection efficiency comparison of GeneJuice versus Lipofectamine 2000 on HCT116 cells with the PEGFP-C1 PTEN-EGFP vector.**

(A) HCT116 cells were visualized by Leica fluorescence microscope following 48h incubation with the DNA-reagent complex The GFP fluorescence images captured after transfection with each of the two reagents are shown with the corresponding bright-field image. The number of observable GFP – positive cells after transfection with Lipofectamine 2000 was significantly higher than that detected after transfection with GeneJuice, while the number of live cells observable under bright-field illumination was similar (B) GFP positive (%) cells and fluorescence intensity were compared between GeneJuice and Lipofectamine. The percentage of GFP positive cells was calculated from the ratio of fluorescent cells to total bright-field cells and was approximately 11% using GeneJuice and

approximately 73% using Lipofectamine2000. The fluorescence intensity corresponds to the background-corrected measurement of single GFP-positive cells for each transfection reagent used. The results are presented of mean ± SD of three independent transfection experiments performed on HCT116 cells seeded at the same initial cell density (0.6 x $10^5$ cells/ mL).

### 5.4.2 Immunoprecipitation of PTEN from HCT116 transfected cells

After transfection with the PTEN-EGFP plasmid DNA, HCT116 cells were grown for the required length of time, harvested, lysed, and the cell extract was incubated with the anti-GFP antibody immobilized onto the GFP trap magnetic particles. Proteins eluted from the GFP-trap beads were loaded on a SDS-PAGE gel along with a small sample of the cell lysate retained after incubation with the GFP trap beads and cell lysate from untransfected HCT116 cells (used as a negative control). The proteins were then transferred onto a PVDF membrane, which was probed with an anti- PTEN antibody to confirm PTEN immunoprecipitation from the PTEN-EGFP overexpressing-HCT116 cells. The Western blot results are shown in Figure 5.2 (A). A strong signal that corresponded to PTEN-EGFP was detected in the sample corresponding to the proteins immunoprecipitated from the PTEN-EGFP- transfected HCT116 cells. A PTEN-EGFP band was also detected in the unbound cell lysate, although the signal was not as intense as in the immunoprecipitation sample. As expected, no signal for the fusion protein PTEN-EGFP was detected in the negative control. In addition, a protein band likely corresponding to the endogenous PTEN was also detectable in all samples, and the signal was higher in the negative control than in the IP and the input sample.

In a parallel experiment, proteins eluted from the GFP trap were once again loaded onto an SDS-PAGE, and the gel was stained with Coomassie brilliant blue (Figure 5.2 B). Protein bands were observed in the gel that corresponded to PTEN-EGFP fusion protein (at around 80 kDa) and putative interacting partners co-immunoprecipitated from the HCT116 transfected cells. The entire resolving gel lane was cut into 12 equally sized slices, which were digested with trypsin and the peptides extracted were analyzed by LC-MS.

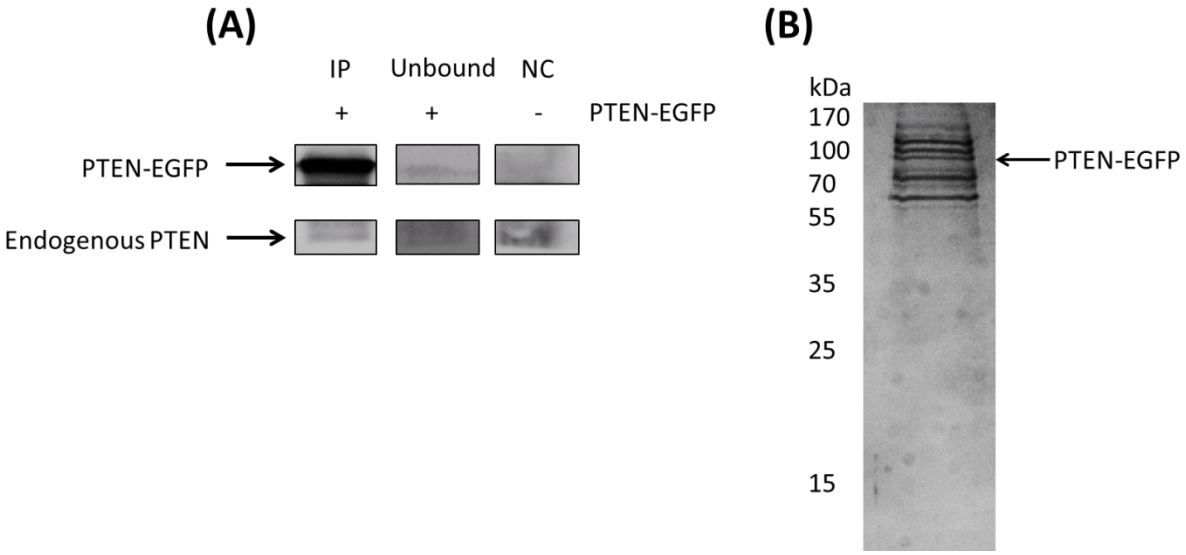


**Figure 5.2 Co-immunoprecipitation of PTEN from PTEN-EGFP transfected HCT116 cells**

(A) Following incubation with the HCT116 cell lysate, 25 µL of proteins eluted from the GFP trap magnetic beads were loaded on a SDS-PAGE and transferred onto a PVDF membrane along 20 µL of supernatant collected after incubation with the GFP trap beads (referred to as "Unbound") and 20 µL of whole cell lysate from untransfected HCT116 cells (referred to as negative control, "NC"). The Western blot results confirmed the immunoprecipitation of PTEN-EGFP fusion protein from transfected HCT116 cells as a strong band is visible that corresponded to the fusion protein in the IP sample. Endogenous PTEN was also detected in all samples and appeared to be more intense in the negative control. The uncropped Western blot used to generate this figure is shown in the Appendix (sect. 8.6.2, Figure 8.7). In a parallel experiment, the PTEN IP sample was loaded on the SDS-PAGE gel and Coomassie-stained. The protein bands visualized included bands corresponding to the molecular weight of the fusion protein PTEN-EGFP (around 80 kDa) as well as additional signals corresponding to putative PTEN-interacting proteins co-immunoprecipitated from the HCT116 cell lysate.

### 5.4.3 MS-based validation of PTEN-interacting proteins

The first part of the validation of potential PTEN interactors addressed the MS-based identification of PTEN-interacting proteins after co-immunoprecipitation of PTEN from PTEN-EGFP

overexpressing HCT-116 cells under normal redox conditions. This experiment was performed so that the resulting PTEN MS-generated interactome could be matched against the interactome generated with the *in vitro* study previously described in Chapter 4 in order to identify any common proteins. LC-MS runs obtained from the "bottom-up" MS analysis of peptides extracted from each of the 12 gel slices were loaded onto Progenesis QI for proteomics as 12 separate experiments, and the software was used in combination with Mascot dataset search engine to obtain protein identification and quantification data. Once the analysis was completed, the individual experiments corresponding to each of the 12 LC-MS runs were pooled into a multi-fraction experiment. A total of 371 putative PTEN interacting proteins were detected by the MS-based analysis. Of these 371 proteins, 214 showed confidence score above 50 and a number of unique peptides greater than or equal to 2. Table 5.1 shows 33 proteins among these 214 that had been detected also in the *in vitro* interactome generated by GSH-affinity enrichment as described in Chapter 4. In the Appendix (Section 8.5) are reported all 214 identified proteins (Table 8.6) and the remaining 157 that were below the cutoff criteria (Table 8.7). Protein IDs in the *in vivo* interactome that matched those found in the *in vitro* interactome described in Chapter 4 included peroxiredoxin-1 (Prdx1), annexin A2 (Anxa2), pyruvate kinase PKM (Kpym or Pkm), L-lactate dehydrogenase B chain, ATP synthase subunit alpha (mitochondrial, AtpA), and nucleoside diphosphate kinase A (NdkA). Proteins that were assumed to be non-specific interactors included 40S and 60S ribosomal proteins, heat shock proteins, tubulin, histones and elongation factors, although all of these have been reported in previous PTEN interactors data sets [541]. PTEN peptides that belonged to the PTEN-EGFP fusion protein bait were identified in the IP sample with a high confidence score (1253) and 16 unique peptides among those were used for quantification. Neither thioredoxin-1 (Trx) nor DNA-damage binding protein 1 (DDB1) were detected among the PTEN interacting proteins identified by MS in combination with the GFP-trap-based affinity-capture from the *in vivo* experiment.

**Table 5.1** Identification and LC-MS based label-free quantification of PTEN-binding proteins affinity-captured by Co-IP from HCT116 cell lysate matching proteins detected in the *in vitro* interactome generated as described in Chapter 4

| **Accession**[1] | **Peptides count**[2] | **Confidence Score**[3] | **Description** | **Average Normalized Abundance**[4] |
|---|---|---|---|---|
| HS90B_HUMAN | 20 (9) | 1440.25 | Heat shock protein HSP 90-beta | 12200 |
| PTEN_HUMAN (bait) | 16 (16) | 1252.96 | Phosphatidylinositol 3,4,5-trisphosphate 3-phosphatase and dual-specificity protein phosphatase PTEN | 233000 |
| TBB5_HUMAN | 16 (2) | 1045.15 | Tubulin beta chain | 7057.32 |
| CH60_HUMAN | 13 (13) | 1016.71 | 60 kDa heat shock protein, mitochondrial | 18800 |
| HSP7C_HUMAN | 13 (11) | 809.93 | Heat shock cognate 71 kDa protein | 9336.89 |
| RS4X_HUMAN | 11 (11) | 625.81 | 40S ribosomal protein S4, X isoform | 8836.6 |
| RS3_HUMAN | 12 (12) | 542.64 | 40S ribosomal protein S3 | 9871.58 |
| RS2_HUMAN | 10 (10) | 462.57 | 40S ribosomal protein S2 | 6503.36 |
| LDHB_HUMAN | 6 (4) | 392.69 | L-lactate dehydrogenase B chain | 2189.7 |
| KPYM_HUMAN | 6 (6) | 390.12 | Pyruvate kinase PKM | 9366.31 |
| RS13_HUMAN | 5 (5) | 343.18 | 40S ribosomal protein S13 | 11200 |
| ANXA2_HUMAN | 6 (6) | 320.89 | Annexin A2 | 5482.44 |
| ATPA_HUMAN | 3 (3) | 237.85 | ATP synthase subunit alpha, mitochondrial | 1023.53 |
| RL31_HUMAN | 4 (4) | 235.43 | 60S ribosomal protein L31 1 | 8672.43 |
| RL22L_HUMAN | 2 (2) | 225.37 | 60S ribosomal protein L22-like 1 | 2308.21 |
| RS27_HUMAN | 4 (4) | 213.66 | 40S ribosomal protein S27 | 2608.79 |
| NDKA_HUMAN | 4 (4) | 203.91 | Nucleoside diphosphate kinase A | 2765.63 |
| RS9_HUMAN | 5 (5) | 198.54 | 40S ribosomal protein S9 | 6700.77 |
| RL12_HUMAN | 3 (3) | 192.92 | 60S ribosomal protein L12 | 3199.86 |
| RLA0_HUMAN | 4 (4) | 181.26 | 60S acidic ribosomal protein P0 | 3571.97 |
| RL23_HUMAN | 2 (2) | 180.3 | 60S ribosomal protein L23 | 2284.74 |
| RS15A_HUMAN | 4 (4) | 180.29 | 40S ribosomal protein S15a | 12000 |
| PRDX1_HUMAN | 4 (4) | 173.27 | Peroxiredoxin-1 | 3012.07 |
| RL13_HUMAN | 2 (2) | 170.55 | 60S ribosomal protein L13 | 2201.69 |
| RS25_HUMAN | 3 (3) | 160.46 | 40S ribosomal protein S25 | 5004.7 |
| RS17L_HUMAN | 3 (3) | 158.9 | 40S ribosomal protein S17-like | 3100.06 |
| RS6_HUMAN | 2 (2) | 152.91 | 40S ribosomal protein S6 | 2371.51 |
| EFTU_HUMAN | 2 (2) | 123.01 | Elongation factor Tu, mitochondrial | 1190.6 |
| RL7_HUMAN | 3 (3) | 121.45 | 60S ribosomal protein L7 | 2622.87 |
| RS26_HUMAN | 2 (2) | 116.95 | 40S ribosomal protein S26 | 2290.79 |
| EF2_HUMAN | 2 (2) | 104.32 | Elongation factor 2 | 125.38 |
| RL13A_HUMAN | 2 (2) | 99.28 | 60S ribosomal protein L13a | 1881.3 |
| H2A1B_HUMAN | 2 (2) | 95.17 | Histone H2A type 1-B/E | 2908.23 |
| RL27_HUMAN | 2 (2) | 89.54 | 60S ribosomal protein L27 | 1182 |

[1]Accession = SwissProt Protein ID
[2]Peptide count = the number of detected peptides (the number of unique peptides) used for quantification
[3]The protein confidence score was generated using Mascot as described in the experimental.
[4]Average normalized abundance of the protein calculated by label-free quantification
Ranking is based on Confidence score.

### 5.4.4 Effect of oxidation on cell viability

Following MS-identification of PTEN protein-protein interactions under normal redox conditions, HCT116 cells were treated with different concentrations of $H_2O_2$ for the analysis of the PTEN interaction profile under oxidative stress. The effect of oxidative stress on HCT116 cells was investigated by monitoring the cell viability of $H_2O_2$-oxidized cells using the XTT colorimetric assay to identify the highest concentration that could be used while still maintaining a sufficient number of viable cells. Confluent HCT116 cells were seeded in a 96-well plate, treated with 1 mM $H_2O_2$ to induce oxidative stress and incubated with the XTT reagent mix to measure cell viability. Metabolically active cells cleave the XTT by reducing it to a formazan dye that can be measured by its absorbance at 450 nm in a plate reader [582]. Figure 5.1 (A) shows the absorbance curves for HCT116 cells treated with either 0 or 1 mM $H_2O_2$ over 5 hours of incubation time. As evident from the graph, a concentration of 1 mM $H_2O_2$ resulted in a significant reduction in cell viability after 1 hour of incubation with $H_2O_2$, and the effect was also observed for longer peroxide incubation times. In addition, the absorbance of $H_2O_2$-oxidized cells increased at a slower rate than untreated cells over time. The effect of higher peroxide concentrations on cell viability was also tested with the XTT assay following treatment of HCT116 with 1, 2 and 5 mM and monitoring the absorbance at 450 nm with the XTT reagents, plotted as percentage of cell survival relative to untreated control in Figure 5.2. No significant difference was seen in comparing HCT116 cell viability between the three different peroxide concentrations used, and the percentage cell survival seemed to decrease at similar rates. In general, after 1 hour of incubation with $H_2O_2$, the number of metabolically active cells decreased by approximately 20% for all peroxide concentration used. However, further peroxide incubation time did not result in additional viability loss as the percentage cell survival relative to untreated control decreased at a much slower rate over time. Concentrations higher than 5 mM $H_2O_2$ could not be tested with this viability assay method, as reproducible absorbance values could not be obtained due to possible interference of high oxidant concentrations with the XTT reagents. Because of this, it is also likely that the viability level observed upon 5 mM $H_2O_2$ treatment could have been overestimated by the XTT assay.

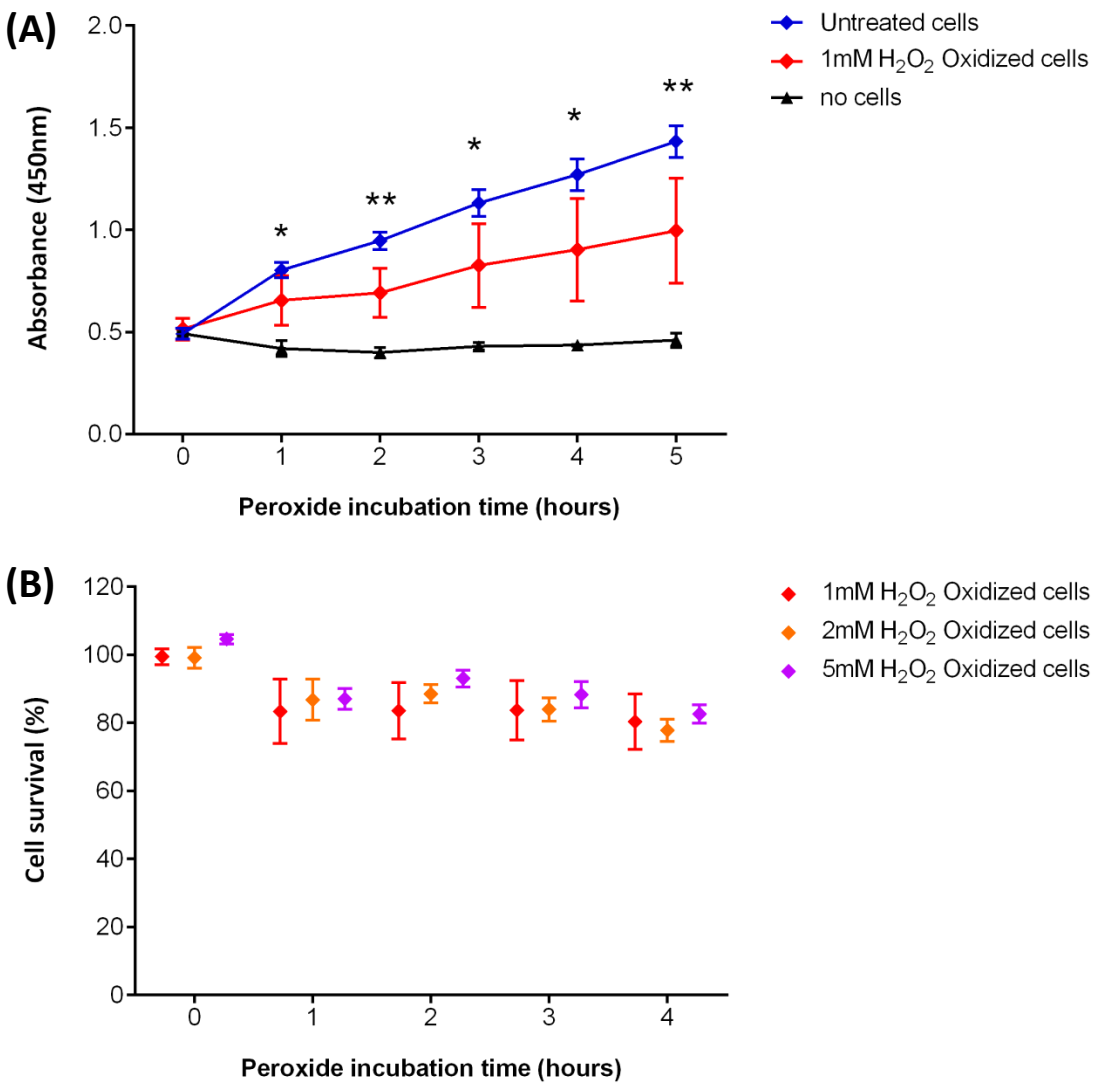


**Figure 5.3 Effect of hydrogen peroxide oxidation on HCT116 cells**

HCT116 cells were oxidized with 0, 1, 2 or 5 mM $H_2O_2$ and the cell viability monitored spectrophotometrically with the XTT assay by measuring the absorbance at 450 nm every hour for 4 hours. (A) The absorbance corresponding to the 1 mM $H_2O_2$ oxidized cells increases at a slower rate and is significantly lower than the absorbance corresponding to the untreated cells for each time point of the XTT assay (Two tailed unpaired Student's t test, N=6). Data are presented as mean ± SD (N=6). (B) The % cell survival relative to untreated control for HCT116 cells treated with 1, 2 and 5 mM was plotted against peroxide incubation time. No significant difference was seen in comparing the effect of the peroxide concentration tested on the cell survival for each of the assay time points shown. (Two-way ANOVA followed by Tukey's multiple comparisons test, N=3). Data are presented as mean ± SD (N=3).

### 5.4.5 Validation and redox profiling of interacting proteins

In the light of the viability assay results, a 1 mM and a 5 mM final concentration of hydrogen peroxide and an incubation time of 1 hour were eventually chosen as the treatment conditions to oxidatively stress the cells for the Co-IP of PTEN interacting proteins.

Given the fact that the MS-generated PTEN *in vivo* interactome was found to be significantly different from the *in vitro* dataset (as described in Section 5.4.3), a MS-based proteomics approach was not undertaken at this stage to cross-validate the proteins redox profiles reported in the previous chapter. Instead, the same four PTEN interacting proteins (Prdx1, Trx, Anxa2 and DDB1) that were originally selected to validate the *in vitro* data (as described in Section 4.4.7) were validated in *in vivo* experiment. Following 1 mM and 5 mM $H_2O_2$ oxidative treatment, PTEN-interacting proteins were co-immunoprecipitated as described in Section 5.4.2. Proteins eluted from the GFP trap magnetic beads following incubation with the cell lysate of control and $H_2O_2$-oxidized cells were loaded onto a SDS-PAGE and transferred on a PVDF membrane, which was probed with primary monoclonal antibodies recognizing the four proteins selected along the PTEN-EGFP. Secondary antibodies detected by ECL confirmed the presence of specific protein bands for Anxa2, Prdx1 as well as Trx (which could not be detected by LC-MS). DDB1 did not produce a reproducible signal on the Western blot scans, and several non-specific bands were observed upon ECL detection due to antibody cross-reactivity. Consequently, the redox profile for this protein could not be analyzed by Western blotting at this stage. Signals on the Western blots membrane were quantified by densitometry using ImageJ, and relative protein quantification was calculated as ratio to PTEN-EGFP. The Western blot images and quantification results for the three proteins co-immunoprecipitated after 1 mM and 5 mM $H_2O_2$ treatment in HCT116 cells are shown in Figure 5.4. When HCT116 cells were treated with 1 mM $H_2O_2$, no significant difference was observed when comparing the signal intensity for Anxa1, Prdx1 or Trx between the untreated and oxidized sample. These results showed a different profile from that described in Chapter 4 where a concentration of 1 mM $H_2O_2$ was found to induce a significant change in PTEN interactions *in vitro*. However, increasing the $H_2O_2$ concentration to 5 mM resulted in a significant difference in the levels of all three PTEN-interacting proteins, which were found elevated after co-IP from oxidized cells. This effect was particularly evident for Trx, which was found to

associate with PTEN approximately 4 times more strongly when HCT116 treated with 5 mM $H_2O_2$, while Anxa2 and Prdx1 levels were less than doubled.

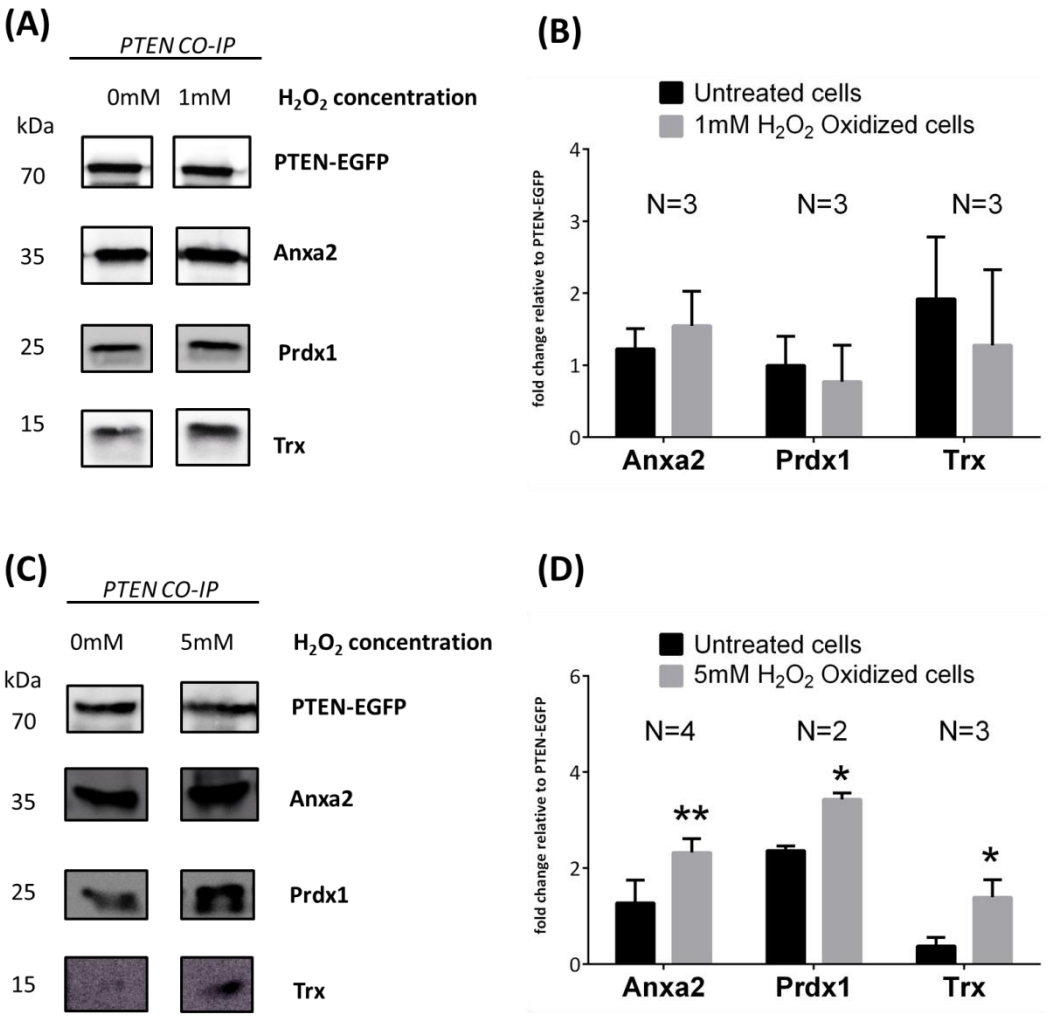


**Figure 5.4 Validation of selected PTEN-interacting proteins following Co-IP from control versus peroxide-oxidized cells**

HCT116 were treated with either 1 or 5 mM hydrogen peroxide for 1 hour, and PTEN interacting partners were captured by Co-IP using the GFP trap magnetic beads. Anxa2, Prdx1, and Trx were detected by Western blotting and their relative intensity corrected against the loading control PTEN-EGFP. Representative Western Blots and data analysis are shown for Anxa2, Prdx1, and Trx captured by Co-IP upon treatment of HCT116 cells with 1 mM hydrogen peroxide (A and B, top panel) and 5 mM hydrogen peroxide (C and D, bottom panel) versus untreated control. Treating the cells with 1 mM did not result in a significant change in protein level for the three selected interactors, while upon treatment with 5 mM $H_2O_2$ all proteins showed a statistical trend toward an increase compared to untreated control (Two tailed Unpaired Student's t test, * = $p < 0.01$, ** = $p < 0.001$). The uncropped

Western blots used to generate this figure are shown in the Appendix (Sect. 8.6.2, Figures 8.8, 8.9, and 8.10).

# 5.5 Discussion

The study presented in this chapter addressed the *in vivo* validation and redox profiling of the PTEN protein-protein interactions that were previously studied upon targeted PTEN inactivation as described in Chapter 4.

Before investigating the interaction profiles, overexpression of PTEN in HCT116 cells was induced by transfecting the cells with the PEGFP-C1 plasmid vector containing the PTEN-EGFP, which resulted in the expression of recombinant PTEN as EGFP-tagged fusion protein. The transfection conditions were optimized by testing two different available reagents (GeneJuice and Lipofectamine2000) for transfection efficiency post transfection in HCT116 cells. While the two reagents generally were associated with comparable levels of live cells and GFP fluorescence intensity, Lipofectamine2000 delivered the PTEN-EGFP Plasmid DNA with transfection efficiency ~7 times higher than GeneJuice. It seems unlikely that this substantial difference in transfection efficiency could be a result of the intrinsic nature of the reagents (as both reagents rely on cationic lipids for DNA delivery), and it would rather be related to the HCT116 cell line used, which may or may not be compatible with specific transfection formulations.

The first part of the validation process was focused on the determination of PTEN- protein-protein interaction by Co-IP and LC-MS under normal redox conditions, in order to match the results against the interaction dataset generated with the same method in the *in vitro* study described in Chapter 4. The LC-MS results identified 214 proteins above the cutoff criteria, of which only 33 proteins were common between the two datasets. These results are in some ways unsurprising, since the two methods differed greatly in the affinity-capture system used, one using a GST-tagged purified protein immobilized onto a GSH-based resin and the other based on a GFP antibody used to immunoprecipitate an overexpressed EGFP-tagged protein *in vivo*. However, while thioredoxin-1 (Trx) was absent in the proteomics dataset generated by LC-MS (Section 5.4.3, Table 5.1), it did show a band on the Western blotting (Section 5.3.7, Figure 5.4), indicating that Trx was, in fact, co-immunoprecipitated from the cells with the affinity-capture method, but was not detected by the MS. This suggests that although the “bottom-up” LC-MS approach using data dependent acquisition is a

powerful discovery tool in proteomics, it still often lacks the sensitivity required to identify low abundance proteins in complex datasets (as only the most abundant precursor ions are selected for the analysis). It also highlights the importance of using targeted or antibody-based techniques to validate MS-based protein identifications, and even as a complementary discovery tool to increase the power of the analysis. Among the 33 PTEN-interacting proteins common between the two datasets were peroxiredoxin-1 (Prdx1) and annexin A2 (Anxa2), both of which were identified with a high confidence score and number of unique peptides using the Co-IP method described in this chapter. However, the majority of the remaining protein IDs that were identified in both studies corresponded to proteins such as tubulin, elongation factors, heat shock proteins and ribosomal proteins, which have commonly been found as non-specific interactors in other bead-based affinity datasets [541]. While these proteins cannot be ruled as false positives (especially as being present in two separate interactomes generated with complementary affinity-capture techniques), are commonly regarded as contaminants that routinely bind to matrixes used for affinity-capture [583].

The second part of the validation involved studying the effect of $H_2O_2$ oxidation of HCT116 on selected PTEN interactors. One key experiment performed in this direction was the XTT viability assay that was used to test the effect of $H_2O_2$ concentrations on HCT116 cells viability. When choosing the $H_2O_2$ concentrations, the aim of the study was to achieve partial cell damage that could induce a change in the association levels of PTEN with its interacting partner, without causing complete cytotoxicity. Equally important for the purpose of the validation was to treat the cells with a final concentration of $H_2O_2$ that was likely to result in significant inactivation of the PTEN-EGFP due to disulfide bond formation in the active site of PTEN, for direct comparison with the *in vitro* study described in Chapter 4, where the inactive (disulfide) form of PTEN showed significant changes in the level of association of key PTEN-interacting proteins in comparison with the active (reduced) PTEN. Previous studies reporting inactivation of PTEN upon $H_2O_2$ treatment in mammalian cells were also considered when identifying the ideal $H_2O_2$ concentration to induce PTEN inactivation and modulation of downstream signaling pathways. Leslie *et al.* described the reversible inactivation of both endogenous and recombinant PTEN upon 1 mM $H_2O_2$ oxidation in cells, which in turn resulted in the activation of the PI3K/Akt pathway [477]. Based on this, a concentration of 1 mM $H_2O_2$ was initially used to test the cell survival response in HCT116. 1 mM $H_2O_2$ was found to cause approximately 20%

significant decrease in cell viability after 1 hour of treatment, in agreement with previous studies [584]. In addition, HCT116 were also treated with 2 and 5 mM $H_2O_2$ to see if a higher peroxide concentration would result in higher cytotoxicity. Interestingly, the cell survival after 1h-incubation with 2 or 5 mM $H_2O_2$ was not significantly different to that observed after 1h-incubation with 1 mM $H_2O_2$. However, these results could be misleading due to a cross-reaction between the XTT reagents and the $H_2O_2$ which was clearly observed at higher $H_2O_2$ concentrations. Hence, a 1 mM and a 5 mM $H_2O_2$ treatment for 1 hour were eventually chosen to induce oxidative stress in HCT116 cells for the affinity-capture of PTEN-interacting proteins.

The redox interaction profile of the PTEN-interacting proteins Prdx1, Anxa2 and Trx was analyzed by Western blotting following 1 mM and 5 mM $H_2O_2$ treatment in HCT116 cells and affinity-capture with the GFP trap magnetic beads. These three proteins were selected for this validation study as they were found to associate more strongly with oxidized purified PTEN-GST upon targeted 1 mM $H_2O_2$ treatment as described in Chapter 4. The abundance of the selected PTEN interactors was determined by densitometry and normalized against the levels of PTEN-EGFP loading control. No significant difference was seen in comparing the levels of PTEN associated Anxa2, Prdx1 and Trx between untreated and 1 mM $H_2O_2$-oxidized cells. Interestingly, treatment with 5 mM resulted in a significant change in the levels of Trx, which associated with PTEN, with 4 times more in the sample immunoprecipitated from oxidized cells versus untreated cells. A statistically significant increase was also seen for Anxa2 and Prdx1, but the fold change in abundance of oxidized versus control was less than 2 for these proteins.

In order to interpret these data it is important to consider the redox dynamics of the different proteins that associate with PTEN, especially Prdx1 and Trx. Prdx1 has been shown to act as a $H_2O_2$ scavenger, and is believed to protect PTEN from oxidative induced inactivation via a direct interaction with PTEN [479,480]. High peroxide concentrations such as those used in this validation study have been previously reported to induce dissociation of the PTEN/Prdx1 complex because of oxidative damage to Prdx1 Cys51, which forms a disulfide bond with the resolving cysteine Cys172 and is required for the $H_2O_2$-mediated regulation of the PTEN/Prdx1 interaction [479,480]. However, it has also been proposed that Trx acts as an electron donor to Prdx1 and reduces the oxidized Cys51 in Prdx1 back to its thiol form under hyper-oxidizing conditions [479,585]. In addition, it has been

recently demonstrated that the hyper-oxidation and consequent inactivation of Prdx1 is required to allow Trx to act on other substrates to effect the repair of oxidized proteins and cell survival following exposure to toxic levels of hydrogen peroxide [585]. This could, in fact, result in the restoring of the PTEN/Prdx1 interaction by Trx under severe oxidative stress, and would also explain the increase in PTEN/Trx interaction upon 5 mM $H_2O_2$ treatment (as more Trx would be required to reduce a more oxidized Prdx1), as well as the presence of PTEN/Prdx1 complex under high peroxide concentrations (in order to maintain Prdx1 $H_2O_2$-scavenging activity and its protective effect against oxidative induced PTEN inactivation). Nonetheless, the exact sequence of events for the Trx-mediated protection of the Prdx1/PTEN interaction upon oxidation is not clear and further studies would be required to address this question. Another important point to consider is the levels of PTEN/Prdx1 and PTEN/Trx interactions under normal (reducing) conditions. Very low levels of interactions with Trx and Prdx1 were seen for the untreated and DTT-recovered purified PTEN-GST *in vitro* (Section 4.4.7), while both proteins were found to bind PTEN-EGFP in control (untreated) cells in the *in vivo* experiment. This suggests that PTEN constantly binds Prdx1 and Trx under homeostatic redox conditions so that the phosphatase is protected from physiological levels of oxidation that naturally occur as a result of cellular respiration. Therefore, it is possible that under relatively mild oxidative stress (1 mM $H_2O_2$) *in vivo*, PTEN reactivation does not require an increase in the level of these interactions. Conversely, in the *in vitro* experiments in Chapter 4 PTEN-GST was not protected by the interaction with Trx or Prdx1, so the treatment with 1 mM $H_2O_2$ caused oxidative damage to the unprotected protein that triggered the increased binding of both of the two redox proteins. This would explain why treating PTEN-GST with 1 mM $H_2O_2$ in the *in vitro* study caused a significant increase in both PTEN/Prdx1 and PTEN/Trx interactions, while in cells treated with 1 mM $H_2O_2$ the levels of PTEN/Prdx1 and PTEN/Trx were unchanged, and a modulation in the interactions could only be seen by increasing the $H_2O_2$ concentration.

Finally, the present study suggests that the PTEN/Anxa2 interaction might also be regulated by $H_2O_2$ oxidation *in vivo*, as a 5 mM $H_2O_2$ treatment resulted in a moderate increase in the levels of association between PTEN-EGFP and Anxa2. PTEN and Anxa2 exhibit common characteristics that suggest that these two proteins could act synergically to protect the cells from oxidative damage by regulating the cellular pathways involved in oxidative stress response. Similarly to PTEN, Anxa2 is a

redox-sensitive protein, as it contains a reactive cysteine which is target for oxidation by $H_2O_2$ oxidation and appears to be reduced by the thioredoxin system [556]. In addition, it has been shown that Anxa2 depleted cells exhibit higher levels of ROS, increased Akt activation, and increased susceptibility to ROS-induced cell death, suggesting that Anxa2 is also a redox-regulatory protein involved in ROS signaling [555,556]. Previous studies have shown that up-regulation of the reduced form of Anxa2 is associated with protection of oxidative stress responsive signaling proteins from $H_2O_2$-induced damage in cancer cells [556]. Hence, it could be speculated that Anxa2 associates to PTEN more strongly under oxidative stress in order to protect PTEN from inactivation caused by $H_2O_2$. In the *in vitro* study presented in Chapter 4, the inactivation of PTEN due to targeted 1 mM $H_2O_2$ oxidation was associated with a 6.8-fold increase in the PTEN/Anxa2 interaction, whereas in the present *in vivo* study the PTEN/Anxa2 association levels were unchanged upon 1 mM $H_2O_2$ treatment of HCT116 cells, and only moderately increased (< 2 fold change) upon 5 mM $H_2O_2$. This suggests that the $H_2O_2$ treatment of the cells resulted in more Anxa2 present in the oxidized form, which led to a less marked oxidation-induced increase in the PTEN/Anxa2 interaction compared to the *in vitro* experiments, where Anxa2 was likely in the reduced form (as the cell lysate used for the affinity-capture was not treated with $H_2O_2$). Generally, these data indicate that the redox status of both PTEN and Anxa2 are important in regulating the association between PTEN and Anxa2 *in vivo* and, consequently, in the ROS-mediated signaling response involving this interaction under oxidative stress.

Overall, these results suggest that while a 1 mM $H_2O_2$ was sufficient to induce a significant reduction in cell survival, and inactivation of PTEN as shown by previous studies [144,477], the reversible disulfide bond that is presumably formed between Cys71 and Cys124 in PTEN active site upon 1 mM $H_2O_2$ treatment in cells would not be directly involved in the modulation of the selected PTEN-interacting proteins. This would implicate that other molecular mechanisms that are susceptible to peroxide concentrations higher than 1 mM $H_2O_2$ (such as 5 mM) could be responsible for the redox-sensitive regulation of the selected PTEN interactions *in vivo*. These regulatory mechanisms of interaction regulation could involve other structural or modification status changes to PTEN or to its binding proteins that would be required to induce a redox-sensitive modulation of PTEN protein-protein interactions and a corresponding signaling response in cells. Alternatively, it is also possible

that while a PTEN-related signaling response was, in fact, induced by 1 mM $H_2O_2$ and potentially caused by the disulfide bond in PTEN active site, it could not be measured by analyzing the three interactors selected and that other PTEN-interacting proteins are involved.

In conclusion, the study presented in this chapter validated the PTEN interactors described previously and opened interesting perspectives on the cellular redox dynamics that affect PTEN interactions networks and signaling pathways. Proteins that were detected with the *in vitro* method were confirmed *in vivo* by MS-based identification and immunoblotting after affinity-capture using a Co-IP based method. A final concentration of 5 mM, but not 1 mM $H_2O_2$, was associated with significant increase in the association of PTEN to selected PTEN interactors, especially with respect to Trx, although both treatments induced a similar significant reduction in HCT116 cell viability. The findings reported in this study highlight the importance of validation procedures in MS-based proteomics data and contributed to gain deeper insight into the redox regulation of PTEN and its association with redox-sensitive interacting proteins.

# Chapter 6. Conclusion

# 6.1 Introduction

The research work presented in this PhD thesis has aimed to further the knowledge of the effect of oxidation and redox regulation of PTEN, using a combination of functional assays, mass spectrometry and software-based analysis. The research aimed to answer the following questions:

1) What happens to PTEN structure when the protein is exposed to ROS?
2) In which way is PTEN modification status correlated to PTEN phosphatase activity?
3) Does the reversible oxidation of PTEN affect PTEN protein-protein interactions?
4) Is the cellular redox status important in determining PTEN association with its binding proteins?

The three proteomics studies presented in the thesis approached the investigation of PTEN "redoxomics" from different angles, leading to a body of research work that produced interconnected results, with respect to both PTEN modification status and interactome. In this chapter, the research findings reported in the different studies are brought together along with the challenges and limitations of the approaches described. Moreover, a model for the dynamics of the PTEN interactions with Prdx1 and Trx under oxidative stress based on the results presented in this thesis is discussed.

# 6.2 General discussion

### 6.2.1 Oxidation of PTEN in vitro

One recurring theme in this PhD thesis was the analysis of the effect of oxidation on PTEN phosphatase activity, monitored with the OMFP phosphatase assay after treating purified PTEN-GST with either HOCl (Chapter 3, Section 3.4.3) or $H_2O_2$ (Chapter 4, Section 4.4.2).

The activity assay results obtained varied greatly depending on which oxidant was used to treat PTEN-GST. When treating PTEN-GST with 1 mM $H_2O_2$, its phosphatase activity dropped dramatically, most probably due to the formation of a reversible disulfide bond between the essential cysteines Cys124 and Cys71 in the active site pocket of PTEN. This intramolecular disulfide bond was likely responsible for the full inactivation of the protein, as the protein activity was fully restored by DTT incubation, in line with previous studies on $H_2O_2$-oxidized PTEN [477]. Surprisingly, a 1 mM concentration of HOCl, a biological oxidant generated by myeloperoxidase under inflammatory conditions [155], did not cause a reduction in PTEN-GST phosphatase activity. Higher concentrations (>2 mM) were required to induce significant protein inactivation, despite HOCl generally being considered a more aggressive oxidizing agent than $H_2O_2$ both *in vivo* and *in vitro* [586]. While no study to date has previously reported the phosphatase activity of PTEN following HOCl treatment, it could be speculated that the HOCl oxidation did not induce the formation of the disulfide bond in PTEN active site as readily as $H_2O_2$ treatment; this is supported by both the activity and modification data as described in Chapter 3. Firstly, when treating PTEN with HOCl PTEN phosphatase activity was not recoverable by DTT, unlike for $H_2O_2$ treatment [144,423]. Secondly, the MS-based modification mapping revealed that the essential cysteine Cys71 was found abundantly modified to sulfonic acid upon treatment with HOCl although the increase in oxidation was not statistically significant, whereas treatment with $H_2O_2$ did not result in any observable $oxPTM_S$ at Cys71. This result is in agreement with previous studies that have reported when the essential active site cysteines of protein tyrosine phosphatases are oxidized to sulfonic acid the catalytic activity is irreversibly inhibited [522,587,588], and that HOCl, but not $H_2O_2$ oxidizes active site cysteines of proteins to sulfonic acid [516]. However,

as Cys124 could not be detected by LC-MS in either of the two studies, definitive conclusions cannot be drawn at this stage about the redox state of the PTEN active site catalytic cysteine upon oxidative treatment.

Another important aspect of the studies addressing the oxidation of purified PTEN-GST was the overall modification status of the protein determined by LC-MS/MS, and its correlation with PTEN phosphatase activity. The HOCl treatment resulted in a much more extensive range of oxidation than $H_2O_2$, producing 13 different oxPTMs distributed at different sites within the protein, while the only one significant oxPTM that was associated with $H_2O_2$ oxidation was at Met35 (excluding the active site disulfide bond). Because the $H_2O_2$ treatment caused complete protein inactivation at a concentration of 1 mM due to the active site disulfide bond, it is difficult to evaluate the contribution of the modified Met35 to the drop in activity, and further studies would be required to address this question. However, this result clearly indicates that the overall extent of protein post-translational modification does not correlate directly with PTEN enzymatic activity, and that specific oxPTMs rather than number of oxPTMs are associated with oxidation-induced protein inactivation. That being said, the vast majority of HOCl-induced oxPTMs detected increased in abundance with increasing HOCl concentrations and decreasing phosphatase activity, suggesting that a correlation exists between the level of modification of individual residues and enzyme activity. Nonetheless, assessing the contribution of each HOCl-modified residue to PTEN activity would be challenging, especially because the occurrence of certain oxPTMs could be dependent on other oxidative events that act as initiator for secondary oxidative damage [533].

### 6.2.2 Methods of Protein-protein interactions identification

In Chapter 4 and 5, the same LC-MS label-free-based method was combined with two different affinity-capture methods for the identification and quantification of PTEN protein interactions (Section 4.4.6 and Section 5.4.3), one *in vitro* the other *in vivo*. The two studies were conducted using two different PTEN fusions proteins as bait for the affinity-capture, one purified *in vitro* and the other overexpressed *in vivo*. Both affinity-capture methods had advantages and disadvantages and complemented one another for the detection of PTEN interacting proteins. In the study presented in

Chapter 4, the purified PTEN-GST was immobilized onto a GSH-based resin and challenged with HCT116 cell lysate for the capture. While this system is fast, inexpensive and had the advantage in that the enzymatic activity and oxidation status of the bait protein can be directly measured, it can only "simulate" the protein-protein interaction environment that exists physiologically. In the validation study presented in Chapter 5, the fusion protein PTEN-EGFP was overexpressed in HCT116 cells and co-immunoprecipitated with its interacting proteins using a GFP antibody pre-immobilized onto a resin. With this method, the overexpressed PTEN-EGFP binds its interacting partners while still under what is hoped to be close to physiological conditions; therefore, the captured proteins should be generally representative of the protein interaction dynamics present inside the cell. However, this method presents a number of significant limitations such as possible cross-reactivity and poor performance of antibodies used for the Co-IP giving low yields of material. In addition, it is likely that the overexpression of PTEN-EGFP could, in fact, modify the normal cellular environment and significantly alter the interactome. The *in vitro* experiment will also decouple the effect of PTEN oxidation form other effects of cellular oxidation, such as altered PTM or oxidative status of interacting proteins, which should allow the direct effects of PTEN oxidation on the interactome to be identified.

Another important point to discuss with regards to the methods of protein-protein interactions analysis is the LC-MS-based proteomics approach used for the interactions identification. Both studies generated a PTEN interactome with a "shotgun" (or discovery) proteomics approach. As explained in detail in Section 1.3.4, this method presents limitations inherent to the process of precursor ion selection, which is automatically performed by the mass spectrometer and limited to the most intense ions of the spectrum. When the LC-MS runs that are acquired using these settings are analyzed by the quantification software (Progenesis QI for Proteomics), the peak-picking algorithm will only analyze the features corresponding to the preselected set of precursor ions, therefore limiting the number of identified peptides to those exhibiting similar abundance values in the spectrum. Consequently, as the number of proteins in affinity-enriched samples, such as those analyzed in Chapter 4 and 5, may exceed the maximum number of selectable precursor ions in the more congested parts of the chromatogram, the analysis can be biased toward the most abundant proteins in the samples, and can exclude biologically significant changes relevant to non-abundant proteins, and also make it difficult

to identify PTMs in the interacting proteins. The maximum number of ions that mass spectrometer can be controlled by the user and was set at 10 for all the LC-MS analysis performed in this thesis. Further increasing the amount of selected precursor ion could have increased the power of the analysis (and, theoretically, the number of identified proteins), but the necessarily decreased acquisition times usually results in lower quality fragmentation spectra which would have likely resulted in a higher number of false negatives or lower scoring peptide matches [483]. However, as the LC-MS analysis in both studies was performed on fractionated samples (separated by SDS-PAGE, and each gel lane sliced in 12 slices), the protein identification and quantification performance were maximized. The two LC-MS generated PTEN interactomes described in the two studies contained a similar number of total proteins (234 proteins for GSH-based affinity capture, and 214 for the Co-IP-based method), but were largely different, with only 33 proteins in common. This indicates that the affinity-capture method used had a great impact on the proteins captured, and possibly that the two techniques are complementary and can be used together to increase the power of the protein-protein interactions discovery, but that they might not be appropriate to validate each other. However, because of the limitations of the proteomics approach discussed above, it is also likely that the two interactomes had, in fact, many more proteins in common which were not detected because of low abundance in either of the two affinity-enriched samples. This was the case for Trx, which was detected by LC-MS and immunoblotting in the study presented in Chapter 4, but only by immunoblotting in the study presented in Chapter 5. Overall, these results highlighted the importance of a validation-oriented approach both within and between studies when exploring complex proteomics datasets such as interactomes. While immunoblotting would not be feasibile to screen all protein-interactions with a discovery approach, it can be more sensitive than shotgun MS-based approaches for the detection of low abundant proteins in complex samples, hence can be used both as a validation method and as a method of detection of target proteins with prior knowledge of a direct interaction.

Alternatively, other MS-based identification and quantification methods that can be used in directed proteomics approaches could have been implemented in combination with the shotgun approach described to increase the power of the analysis. Among those, the T3PQ (Top 3 Protein Quantification), is ideally suited for protein identification and absolute quantification in complex mixtures such as the affinity-enriched lysates that have been analyzed in this thesis [589]. This method

uses the average MS signal response of the three most intense precursor ions to calculate the abundance of each identified protein [590], and can be used to fragment pre-selected precursor ions obtained from a LC-MS run analyzed with a shotgun approach. As the number of ion detections is restricted to the three best ionizing peptides for each identified protein, the instrument can be set to acquire a higher number of precursors in the first LC-MS run, allowing for the identification of a larger number of proteins with high sequence coverage and accuracy with the second LC-MS run [589,590]. However, T3PQ is based on the assumption that for each protein identified by at least three peptides, the average of the three most intensive precursor ions directly correlates with the protein abundance in the sample, therefore excluding the contribution of any additional peptides corresponding to the protein (even those that are only marginally less abundant than the selected three). Moreover, the method can still limit protein identification outputs to the most abundant proteins in the sample, as all proteins identified by less than three peptides will be excluded a priori from the analysis [591].

### 6.2.3 Model for PTEN/Prdx1 and PTEN/Trx interactions under oxidative stress

The effect of altered redox conditions on PTEN protein interactions was investigated in Chapter 4 by analyzing the redox interactome of the oxidized versus untreated protein *in vitro* and in Chapter 5 by validating selected interactions *in vivo* under cellular oxidative stress.

The results overall showed that the redox status of both purified PTEN and cells influences the ability of PTEN to bind its interacting proteins. In the *in vitro* study presented in Chapter 4, 13 proteins were detected that bound significantly more strongly to the 1 mM oxidized PTEN-GST than to the untreated control. Among those 13, the redox proteins Trx and Prdx1, the phospholipid-binding protein Anxa2 and the DNA binding protein DDB1 were selected for further investigation and their association with PTEN studied in oxidized cells in Chapter 5, and except for DDB1 (for which a reproducible signal could not be detected by immunoblotting in the in *vivo* study) were found to associate more strongly to the overexpressed PTEN-EGFP when HCT116 cells were treated with 5 mM $H_2O_2$ (but not with 1 mM $H_2O_2$). Particularly interesting for the research questions addressed in this PhD thesis were the PTEN/Prdx1 and PTEN/Trx interactions and the interplay between them

under oxidative stress. It is worth bearing in mind that the nature of the interactions has not been demonstrated, and this may be non-covalent, or possibly could be covalent by formation of mixed disulfides between the proteins. The latter has already been proposed as a potential mechanism for interaction between Trx and PTEN [478]. However, given that the formation of the interactions is selective for the 13 proteins described, and many interactors show no differential binding, if mixed disulfide formation is the cause then it is a selective process and still has validity and interest.

Based on the results described in Chapter 4 and 5 and on previous studies on the redox regulation of PTEN, it is possible to propose a model for the protein interactions dynamics between PTEN, Prdx1 and Trx, and their modulation under mild and severe oxidative stress (Figure 6.1). Both Trx and Prdx1 are required to maintain PTEN phosphatase activity, and interact with overexpressed PTEN-EGFP in normal (reducing) redox conditions as shown in the immunoblotting results presented in Chapter 5 (Section 5.4.6). In mild oxidizing conditions (1 mM $H_2O_2$), a disulfide bond is formed in the active site of PTEN between Cys71 and Cys124 and PTEN is inactivated [423], and Prdx1 scavenges $H_2O_2$ molecules from around PTEN protecting it from further oxidative damage, while Trx reduces PTEN active site disulfide back to the thiols form, as also previously proposed by Lee *et al* [423]. While Prdx1 is scavenging $H_2O_2$ during mild oxidative stress, Cys51 in Prdx1 might also be oxidized to a sulfenic intermediate (not shown in the model), which is also reduced by Trx via the formation of a mixed disulfide intermediate [585]. In severe oxidative stress conditions (e.g. 5 mM $H_2O_2$), most Prdx1 is inactivated and dissociates from PTEN due to the intermolecular disulfide bond formation between Cys51 and the Cys172 of a neighboring Prdx1 molecule [479,585]. As a result of this, higher levels of Trx are required for the reduction of Prdx1, in agreement with previous studies showing that the over-oxidation of Prdx1 is associated with a corresponding increase in cellular Trx upon $H_2O_2$-induced oxidative stress [585,592]. In addition, it has been shown that oxidative stress induces the gene expression of Trx, via binding of the Nrf2/small Maf complex to antioxidant responsive elements (AREs) in the upstream promoter region of the *Trx* gene [593,594]. Therefore, the increased Trx activity due to oxidative stress and Prdx1 inactivation is likely responsible for maintaining the PTEN/Prdx1 interaction under severe oxidative stress, as shown in the immunoblotting results presented in Chapter 5 (Section 5.4.6). Consequently, according to this model, the increased binding of Trx to inactive PTEN could be also due to the increased activity of Trx as a result of the

inactivation of Prdx1 and temporary dissociation of PTEN/Prdx1 interaction under severe oxidative stress, which has been previously shown to lead to even higher levels of cellular Trx [594]. In both mild and severe oxidative stress conditions, oxidized Trx is formed due to oxidoreductase activity of Trx on both PTEN and Prdx1 and results in the temporary dissociation of the PTEN:Trx complex. The disulfide between Cys32 and Cys35 in active site of oxidized Trx is reduced by the NADPH-dependent thioredoxin reductase (TrxR), which is essential to maintain the antioxidant capacity of the thioredoxin system under oxidative stress [595].

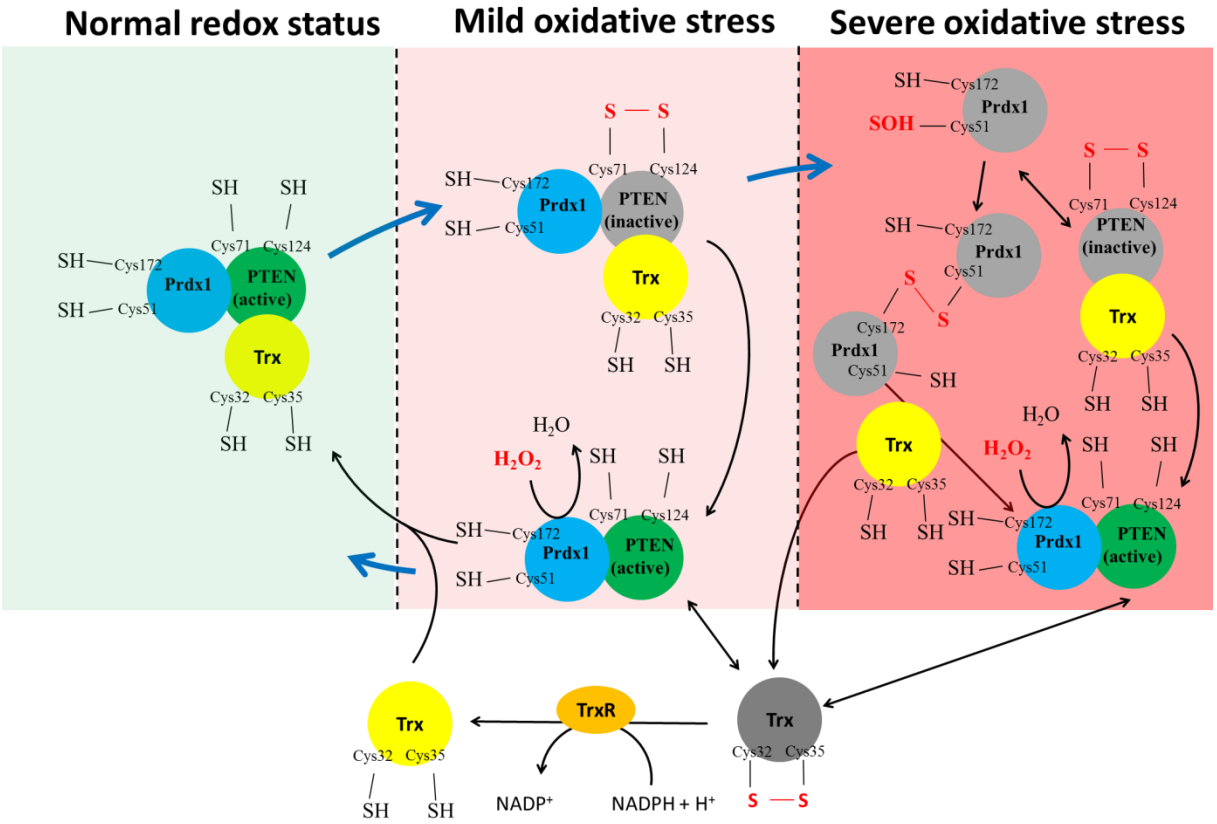


**Figure 6.1 Proposed model for the regulation of PTEN/Prdx1 and PTEN/Trx interaction under oxidative stress**

In normal redox conditions such as those found in healthy cells, Prdx1 and Trx interact with PTEN protecting it from physiological levels of free radicals and ROS. In mild oxidative stress, Trx readily reduces the disulfide bond in PTEN active site thereby reactivating the phosphatase, while Prdx1 scavenges $H_2O_2$ molecules protecting PTEN from further oxidative damage. In severe oxidative stress conditions, such as those found in disease states, Prdx1 dissociates from PTEN due to oxidative damage to Cys51 in Prdx1 which forms an intermolecular disulfide bond with the Cys172 of another

Prdx1 molecule. More Trx supply is required to reduce Prdx1 and restore the PTEN/Prdx1 interaction, and thus an increased amount of Trx binds the inactive PTEN in order to reactivate the phosphatase via reduction of the active site disulfide in PTEN active site. The disulfide bond between the catalytic cysteines Cys32 and Cys35 in Trx is reduced by the NADPH-dependent TrxR, which restores Trx oxidoreductase activity.

## 6.3 Future directions

The research presented here has highlighted the importance of analyzing the structure and protein interactions of PTEN to gain further insight in the role of ROS signaling in the pathophysiology of ageing and disease. However, there still remains much to be studied about the mechanisms of PTEN redox regulation.

The incomplete PTEN sequence coverage detected by LC-MS represents a major challenge to overcome in order to obtain detailed information on the modification status of Cys124 in the active site of PTEN, as well as of other residues which were also excluded. Promising results are currently being generated to tackle this issue on both native and HOCl-oxidized PTEN by implementing an alternative peptide digestion method based on the in-gel digestion with the endoproteinase Lys-C, in line to that previously reported by Lee *et al*, which successfully detected the active site of PTEN using this enzyme with an in-solution digestion protocol [423]. Other methods for increasing sequence coverage are also considered for this purpose, and include the implementation of multienzymatic and limited proteolytic digestions (MELD), which use a combination of different proteases (such as Trypsin and Lys-C) to digest proteins under strictly controlled incubation conditions [596,597]. These methods can generate in a single digestion experiment many overlapping miscleaved peptides (due to the combinatory action of the different proteases cleaving at different sites of the same protein), therefore increasing the chance of obtaining the complete sequence coverage for a given protein. In addition to MELD methods, "top-down" approaches (in which intact proteins are analyzed by MS without previous proteolytic digestion) are also considered as a possible future alternative and/or complementary technique to the "bottom-up" approach for improving the analysis of PTEN oxPTMs. Top down approaches have the advantage in that the full protein sequence coverage is obtained and the protein primary structure is usually preserved, leading to the in-depth characterization of modification patterns, including labile oxPTMs [270,275,598]. It is hoped that by uncovering the active site cysteine and other important residues by implementing the above described methods, the intramolecular dynamics of PTEN upon oxidative stress both *in vivo* and *in vitro* can be correlated to

PTEN phosphatase activity and secondary structure, to better understand the role of specific amino acids residues in PTEN redox regulation and ROS-mediated signaling.

Interesting perspectives have also been opened by the analysis of PTEN redox interactome. Work is currently underway to assess using non-reducing SDS-PAGE whether redox-sensing PTEN-interacting proteins such as Trx and Prdx1 associate to oxidized PTEN by trapping via intermolecular disulfide bonds during both *in vitro* and *in vivo* affinity-capture, or bind PTEN as a result of other molecular mechanisms. In this fashion, the exact molecular mechanisms involved in the regulation of these PTEN interactions and their dynamic interplay under oxidative stress can be determined.

Much of the future work on the analysis of PTEN redox interactome also includes further design of the *in vivo* methodologies aiming to determine the correlation between cellular oxidative stress and the ROS-mediated signaling networks involving PTEN and its binding partners. Firstly, it might be important to test a broader range of $H_2O_2$ concentrations for the cellular oxidation, with the purpose of further characterizing the role of severe oxidative stress on PTEN interactions dynamics and to identify the $H_2O_2$ concentrations at which the PTEN interactions may be disrupted (due to the level of ROS exceeding the cellular antioxidant capacity). This would help determining the effect of over-oxidation on the redox-sensing mechanisms that regulate the PTEN/Trx/Prdx1 system as well as other redox-regulated PTEN interactions, and can contribute to gain further insight into the cellular pathways involved in oxidative stress response. Another important point to bear in mind is that the overexpressed PTEN-EGFP levels likely exceed the endogenous levels of PTEN-interacting proteins, and thus any ROS-induced increase in the cellular expression of these proteins translates in their increased interaction with PTEN-EGFP, affecting the levels of interaction detected in the affinity-capture. Based on this, for each PTEN interactor studied under $H_2O_2$-induced cellular oxidative stress, the protein levels in the total and unbound lysates could be compared across the different $H_2O_2$ concentrations used and against the corresponding levels observed in the affinity-capture. With this adjustment, it would be possible to assess the contribution of ROS-induced changes in protein expression (or ROS-induced protein damage) to the variation observed in the levels of association of these proteins with PTEN-EGFP. In addition, further analyses that will be incorporated in the *in vivo* study include the MS-based identification of the proteins captured by the overexpressed EGFP tag (following transfection of HCT116 cells with an empty PEGFP-C1 vector) and by the GFP-trap resin

alone, in order to filter EGFP-binding proteins out of the PTEN interactome, to characterize non-specifically bound proteins, and to detect possible contaminants that could interfere with the LC-MS analysis.

Finally, additional experiments involving mutagenesis approaches are also considered as part of the follow-up work on the research presented in this thesis. The study of PTEN mutants could be crucial in clarifying the role of key amino acid residues in determining the oxidation-mediated effects on PTEN function, structure and protein-protein interactions described in this work. PTEN fusion proteins carrying mutations in either one or both of the two the active site cysteines (Cys71 and Cys124) can be used in the various experimental systems described to block the disulfide bond formation upon oxidation of PTEN. This would be important to investigate whether the disulfide bond in the active site of wild-type PTEN contributes to: 1) the HOCl-induced drop in PTEN phosphatase activity; 2) the significant changes observed in the levels of PTEN-interacting proteins upon $H_2O_2$ oxidation *in vitro*; 3) the redox-regulation of PTEN-interacting proteins upon cellular oxidation, especially with regards to the PTEN/Prdx1 and the PTEN/Trx interactions. The mutations of other PTEN amino acids for which a functional role has been proposed in this thesis would also be decisive to gain further insight into PTEN redox-regulation. These include Met35, which was the only residue that was found significantly more modified upon $H_2O_2$ treatment of purified PTEN-GST, and that previous mutagenesis studies described as essential for PTEN phosphatase activity [409]. Met35 mutants could be used for the interactions capture (both *in vitro* and *in vivo*) to assess whether this residue plays a significant role in modulating the levels of PTEN binding proteins, and, ultimately, the redox-regulated networks involving PTEN protein-protein interactions. Along these lines, PTEN-EGFP carrying mutations at Met205, Tyr240, His272, Trp274 orTyr377 (all of which were found significantly more modified exclusively in HOCl-induced PTEN-GST aggregates) could be used to confirm the role of these residues in the oxidation-mediated PTEN aggregation (e.g. by live cell imaging studies using HOCl-treated cells).

Exciting prospects are also offered by PTEN-deficient mammalian cell lines for the analysis of the cellular signals and phenotypes associated with the oxidative sensitive PTEN-interactions that were identified in this thesis, especially those involved in the processes of disease (such as cytoskeleton control and DNA damage). In parallel workflows, mammalian cell lines genetically engineered to

express mutant forms of PTEN that carry mutations in oxidative-sensitive residues could be used to further characterize the molecular systems regulating PTEN function in altered redox conditions. These experiments would result in the identification of the exact molecular mechanisms responsible for protein-specific, cellular and phenotypic changes under oxidative stress, and could be important for the development of novel therapeutics.

In summary, the work presented in this thesis has contributed to the current knowledge of PTEN "redoxomics", opening new perspectives on its redox regulation and interaction dynamics under oxidative stress. Amino acid modifications associated with functional loss and structural alteration have been determined, and it has been demonstrated that PTEN interacts differently with its binding partners depending on the redox conditions in which it is challenged. While much work is still needed to fully characterize the molecular mechanism of PTEN redox regulation, the research presented in this thesis is an important and original contribution toward a more complete understanding of the signaling role of reactive molecules in the processes of ageing and disease.

# Chapter 7. References

1. Helman, C.G., Cultural aspects of time and ageing. Time is not the same in every culture and every circumstance; our views of aging also differ. *EMBO Rep* **2005**, *6 Spec No*, S54-58.
2. Kotter-Gruhn, D.; Hess, T.M., The impact of age stereotypes on self-perceptions of aging across the adult lifespan. *J Gerontol B Psychol Sci Soc Sci* **2012**, *67*, 563-571.
3. Lockenhoff, C.E.; De Fruyt, F.; Terracciano, A.; McCrae, R.R.; De Bolle, M.; Costa, P.T., Jr.; Aguilar-Vafaie, M.E.; Ahn, C.K.; Ahn, H.N.; Alcalay, L., *et al.*, Perceptions of aging across 26 cultures and their culture-level associates. *Psychol Aging* **2009**, *24*, 941-954.
4. Bayer, K., Cosmetic surgery and cosmetics: Redefining the appearance of age. *Generations* **2005**, *29*, 13-18.
5. Division., U.N.D.o.E.a.S.A.P., *Charting the progress of populations*. United Nations: New York, 2000; p x, 95 p., 9789211513448.
6. Speakman, J.R.; Selman, C.; McLaren, J.S.; Harper, E.J., Living fast, dying when? The link between aging and energetics. *J Nutr* **2002**, *132*, 1583s-1597s.
7. Ikeda, N.; Saito, E.; Kondo, N.; Inoue, M.; Ikeda, S.; Satoh, T.; Wada, K.; Stickley, A.; Katanoda, K.; Mizoue, T., *et al.*, What has made the population of Japan healthy? *The Lancet* **2011**, *378*, 1094-1105.
8. Bloom, D.E.; Canning, D.; Fink, G., Implications of population ageing for economic growth. *Oxford Rev Econ Pol* **2010**, *26*, 583-612.
9. Karasek, M., Melatonin, human aging, and age-related diseases. *Exp Gerontol* **2004**, *39*, 1723-1729.
10. Sullivan, D.F., A single index of mortality and morbidity. *HSMHA Health Rep* **1971**, *86*, 347-354.
11. Smith, M.P.; Olatunde, O.; White, C., Disability-free life expectancy: comparison of sources and small area estimates in England, 2006-08. *Health Stat Q* **2011**, 40-78.
12. Robine, J.M.; Ritchie, K., Healthy life expectancy: evaluation of global indicator of change in population health. *BMJ* **1991**, *302*, 457-460.
13. Lopez, A.D.; Mathers, C.D.; Ezzati, M.; Jamison, D.T.; Murray, C.J.L., Global and regional burden of disease and risk factors, 2001: systematic analysis of population health data. *Lancet* **2006**, *367*, 1747-1757.
14. Berg, J.; Bjorck, L.; Lappas, G.; O'Flaherty, M.; Capewell, S.; Rosengren, A., Continuing decrease in coronary heart disease mortality in Sweden. *BMC Cardiovasc Disord* **2014**, *14*, 9.
15. Lakatta, E.G., Age-associated cardiovascular changes in health: impact on cardiovascular disease in older persons. *Heart Fail Rev* **2002**, *7*, 29-49.
16. Siegel, R.; Ma, J.; Zou, Z.; Jemal, A., Cancer statistics, 2014. *CA Cancer J Clin* **2014**, *64*, 9-29.
17. Jemal, A.; Bray, F.; Center, M.M.; Ferlay, J.; Ward, E.; Forman, D., Global cancer statistics. *CA Cancer J Clin* **2011**, *61*, 69-90.
18. Coleman, M.P.; Forman, D.; Bryant, H.; Butler, J.; Rachet, B.; Maringe, C.; Nur, U.; Tracey, E.; Coory, M.; Hatcher, J., *et al.*, Cancer survival in Australia, Canada, Denmark, Norway, Sweden, and the UK, 1995-2007 (the International Cancer Benchmarking Partnership): an analysis of population-based cancer registry data. *Lancet* **2011**, *377*, 127-138.
19. Hung, C.W.; Chen, Y.C.; Hsieh, W.L.; Chiou, S.H.; Kao, C.L., Ageing and neurodegenerative diseases. *Ageing Res Rev* **2010**, *9*, S36-S46.
20. Playfer, J.R., Ageing and Parkinson's disease. *Pract Neurol* **2007**, *7*, 4-5.
21. Reeve, A.; Simcox, E.; Turnbull, D., Ageing and Parkinson's disease: why is advancing age the biggest risk factor? *Ageing Res Rev* **2014**, *14*, 19-30.
22. Collier, T.J.; Kanaan, N.M.; Kordower, J.H., Ageing as a primary risk factor for Parkinson's disease: evidence from studies of non-human primates. *Nat Rev Neurosci* **2011**, *12*, 359-366.

23. Bugiani, O., Alzheimer's disease: ageing-related or age-related? New hypotheses from an old debate. *Neurol Sci* **2011**, *32*, 1241-1247.
24. Field, E.J., Amyloidosis, Alzheimer's disease, and ageing. *Lancet* **1970**, *2*, 780-781.
25. Tedeschi, G.; Trojsi, F.; Tessitore, A.; Corbo, D.; Sagnelli, A.; Paccone, A.; D'Ambrosio, A.; Piccirillo, G.; Cirillo, M.; Cirillo, S., *et al.*, Interaction between aging and neurodegeneration in amyotrophic lateral sclerosis. *Neurobiol Aging* **2012**, *33*, 886-898.
26. Tejada-Vera, B., Mortality from Alzheimer's disease in the United States: data for 2000 and 2010. *NCHS Data Brief* **2013**, 1-8.
27. Griffiths, C.; Rooney, C., Trends in mortality from Alzheimer's disease, Parkinson's disease and dementia, England and Wales, 1979-2004. *Health Stat Q* **2006**, 6-14.
28. Pinter, B.; Diem-Zangerl, A.; Wenning, G.K.; Scherfler, C.; Oberaigner, W.; Seppi, K.; Poewe, W., Mortality in Parkinson's disease: a 38-year follow-up study. *Mov Disord* **2015**, *30*, 266-269.
29. Desesquelles, A.; Demuru, E.; Salvatore, M.A.; Pappagallo, M.; Frova, L.; Mesle, F.; Egidi, V., Mortality from Alzheimer's disease, Parkinson's disease, and dementias in France and Italy: a comparison using the multiple cause-of-death approach. *J Aging Health* **2014**, *26*, 283-315.
30. Hayflick, L., The not-so-close relationship between biological aging and age-associated pathologies in humans. *J Gerontol A Biol Sci Med Sci* **2004**, *59*, 547-550.
31. de Grey, A.D., The desperate need for a biomedically useful definition of "aging". *Rejuvenation Res* **2013**, *16*, 89-90.
32. Rattan, S.I., Aging is not a disease: implications for intervention. *Aging Dis* **2014**, *5*, 196-202.
33. Karasik, D.; Demissie, S.; Cupples, L.A.; Kiel, D.P., Disentangling the genetic determinants of human aging: Biological age as an alternative to the use of survival measures. *J Gerontol A Biol Sci Med Sci* **2005**, *60*, 574-587.
34. Bowen, R.L.; Atwood, C.S., Living and dying for sex. A theory of aging based on the modulation of cell cycle signaling by reproductive hormones. *Gerontology* **2004**, *50*, 265-290.
35. Harman, D., The aging process. *Proc Natl Acad Sci U S A* **1981**, *78*, 7124-7128.
36. Chen, J.H.; Hales, C.N.; Ozanne, S.E., DNA damage, cellular senescence and organismal ageing: causal or correlative? *Nucleic Acids Res* **2007**, *35*, 7417-7428.
37. Anstey, K.; Stankov, L.; Lord, S., Primary aging, secondary aging, and intelligence. *Psychol Aging* **1993**, *8*, 562-570.
38. Booth, F.W.; Laye, M.J.; Roberts, M.D., Lifetime sedentary living accelerates some aspects of secondary aging. *J Appl Physiol* **2011**, *111*, 1497-1504.
39. Jin, K., Modern biological theories of aging. *Aging Dis* **2010**, *1*, 72-74.
40. Tosato, M.; Zamboni, V.; Ferrini, A.; Cesari, M., The aging process and potential interventions to extend life expectancy. *Clin Interv Aging* **2007**, *2*, 401-412.
41. Gavrilova, N.S.; Gavrilov, L.A.; Severin, F.F.; Skulachev, V.P., Testing predictions of the programmed and stochastic theories of aging: comparison of variation in age at death, menopause, and sexual maturation. *Biochemistry (Mosc)* **2012**, *77*, 754-760.
42. Prinzinger, R., Programmed ageing: the theory of maximal metabolic scope. How does the biological clock tick? *EMBO Rep* **2005**, *6 Spec No*, S14-19.
43. Holliday, R., The multiple and irreversible causes of aging. *J Gerontol A Biol Sci Med Sci* **2004**, *59*, B568-572.
44. Kirkwood, T.B.L.; Austad, S.N., Why do we age? *Nature* **2000**, *408*, 233-238.
45. Papaconstantinou, J., Unifying model of the programmed (intrinsic) and stochastic (extrinsic) theories of aging. The stress response genes, signal transduction-redox pathways and aging. *Ann N Y Acad Sci* **1994**, *719*, 195-211.
46. Rattan, S.I., Theories of biological aging: genes, proteins, and free radicals. *Free Radic Res* **2006**, *40*, 1230-1238.

47. Hedge, J.W.; Borman, W.C., *The Oxford handbook of work and aging*. Oxford University Press: Oxford; New York, 2012; p xvii, 717 p., 9780195385052.
48. Harman, D., Aging: a theory based on free radical and radiation chemistry. *J Gerontol* **1956**, *11*, 298-300.
49. March, J., *Advanced organic chemistry: reactions, mechanisms, and structure*. McGraw-Hill: New York, 1968; p ix, 1098 p., 9780470084960.
50. Floyd, R.A., Neuroinflammatory processes are important in neurodegenerative diseases: an hypothesis to explain the increased formation of reactive oxygen and nitrogen species as major factors involved in neurodegenerative disease development. *Free Radic Biol Med* **1999**, *26*, 1346-1355.
51. Aruoma, O.I., Free radicals, oxidative stress, and antioxidants in human health and disease. *J Am Oil Chem Soc* **1998**, *75*, 199-212.
52. Harman, D., The biologic clock: the mitochondria? *J Am Geriatr Soc* **1972**, *20*, 145-147.
53. Jacobs, H.T., The mitochondrial theory of aging: dead or alive? *Aging Cell* **2003**, *2*, 11-17.
54. Jang, Y.C.; Van Remmen, H., The mitochondrial theory of aging: insight from transgenic and knockout mouse models. *Exp Gerontol* **2009**, *44*, 256-260.
55. Loeb, L.A.; Wallace, D.C.; Martin, G.M., The mitochondrial theory of aging and its relationship to reactive oxygen species damage and somatic mtDNA mutations. *Proc Natl Acad Sci U S A* **2005**, *102*, 18769-18770.
56. Gianni, P.; Jan, K.J.; Douglas, M.J.; Stuart, P.M.; Tarnopolsky, M.A., Oxidative stress and the mitochondrial theory of aging in human skeletal muscle. *Exp Gerontol* **2004**, *39*, 1391-1400.
57. Liochev, S.I., Reactive oxygen species and the free radical theory of aging. *Free Radic Biol Med* **2013**, *60*, 1-4.
58. Lee, R.D., Rethinking the evolutionary theory of aging: transfers, not births, shape senescence in social species. *Proc Natl Acad Sci U S A* **2003**, *100*, 9637-9642.
59. Hamilton, W.D., The moulding of senescence by natural selection. *J Theor Biol* **1966**, *12*, 12-45.
60. Olovnikov, A.M., Telomeres, telomerase, and aging: origin of the theory. *Exp Gerontol* **1996**, *31*, 443-448.
61. Mikhelson, V.M.; Gamaley, I.A., Telomere shortening is a sole mechanism of aging in mammals. *Curr Aging Sci* **2012**, *5*, 203-208.
62. Heidinger, B.J.; Blount, J.D.; Boner, W.; Griffiths, K.; Metcalfe, N.B.; Monaghan, P., Telomere length in early life predicts lifespan. *Proc Natl Acad Sci U S A* **2012**, *109*, 1743-1748.
63. Atwood, C.S.; Bowen, R.L., The reproductive-cell cycle theory of aging: an update. *Exp Gerontol* **2011**, *46*, 100-107.
64. Freitas, A.A.; de Magalhaes, J.P., A review and appraisal of the DNA damage theory of ageing. *Mutat Res* **2011**, *728*, 12-22.
65. Taylor, R.C.; Dillin, A., Aging as an event of proteostasis collapse. *Cold Spring Harb Perspect Biol* **2011**, *3*.
66. Mercken, E.M.; Crosby, S.D.; Lamming, D.W.; JeBailey, L.; Krzysik-Walker, S.; Villareal, D.T.; Capri, M.; Franceschi, C.; Zhang, Y.; Becker, K., *et al.*, Calorie restriction in humans inhibits the PI3K/AKT pathway and induces a younger transcription profile. *Aging Cell* **2013**, *12*, 645-651.
67. Mair, W.; Dillin, A., Aging and survival: the genetics of life span extension by dietary restriction. *Annu Rev Biochem* **2008**, *77*, 727-754.
68. Wolff, S.; Dillin, A., The trifecta of aging in Caenorhabditis elegans. *Exp Gerontol* **2006**, *41*, 894-903.
69. Yu, B.P., Dietary restriction and life-span extension. *Methods Mol Med* **2000**, *38*, 353-359.

70. Heilbronn, L.K.; Ravussin, E., Calorie restriction and aging: review of the literature and implications for studies in humans. *Am J Clin Nutr* **2003**, *78*, 361-369.
71. Sohal, R.S.; Weindruch, R., Oxidative stress, caloric restriction, and aging. *Science* **1996**, *273*, 59-63.
72. Harrison, D.E.; Strong, R.; Sharp, Z.D.; Nelson, J.F.; Astle, C.M.; Flurkey, K.; Nadon, N.L.; Wilkinson, J.E.; Frenkel, K.; Carter, C.S., *et al.*, Rapamycin fed late in life extends lifespan in genetically heterogeneous mice. *Nature* **2009**, *460*, 392-395.
73. Liu, X.; Chhipa, R.R.; Pooya, S.; Wortman, M.; Yachyshin, S.; Chow, L.M.; Kumar, A.; Zhou, X.; Sun, Y.; Quinn, B., *et al.*, Discrete mechanisms of mTOR and cell cycle regulation by AMPK agonists independent of AMPK. *Proc Natl Acad Sci U S A* **2014**, *111*, E435-444.
74. Schulz, T.J.; Zarse, K.; Voigt, A.; Urban, N.; Birringer, M.; Ristow, M., Glucose restriction extends Caenorhabditis elegans life span by inducing mitochondrial respiration and increasing oxidative stress. *Cell Metab* **2007**, *6*, 280-293.
75. Chen, K.; Kobayashi, S.; Xu, X.; Viollet, B.; Liang, Q., AMP activated protein kinase is indispensable for myocardial adaptation to caloric restriction in mice. *PLoS One* **2013**, *8*, e59682.
76. Guarente, L., Calorie restriction and sirtuins revisited. *Genes Dev* **2013**, *27*, 2072-2085.
77. Schmeisser, K.; Mansfeld, J.; Kuhlow, D.; Weimer, S.; Priebe, S.; Heiland, I.; Birringer, M.; Groth, M.; Segref, A.; Kanfi, Y., *et al.*, Role of sirtuins in lifespan regulation is linked to methylation of nicotinamide. *Nat Chem Biol* **2013**, *9*, 693-+.
78. Ghosh, H.S.; McBurney, M.; Robbins, P.D., SIRT1 negatively regulates the mammalian target of rapamycin. *PLoS One* **2010**, *5*, e9199.
79. Price, N.L.; Gomes, A.P.; Ling, A.J.; Duarte, F.V.; Martin-Montalvo, A.; North, B.J.; Agarwal, B.; Ye, L.; Ramadori, G.; Teodoro, J.S., *et al.*, SIRT1 is required for AMPK activation and the beneficial effects of resveratrol on mitochondrial function. *Cell Metab* **2012**, *15*, 675-690.
80. Gertz, M.; Nguyen, G.T.; Fischer, F.; Suenkel, B.; Schlicker, C.; Franzel, B.; Tomaschewski, J.; Aladini, F.; Becker, C.; Wolters, D., *et al.*, A molecular mechanism for direct sirtuin activation by resveratrol. *PLoS One* **2012**, *7*, e49761.
81. Hu, Y.; Liu, J.; Wang, J.; Liu, Q., The controversial links among calorie restriction, SIRT1, and resveratrol. *Free Radic Biol Med* **2011**, *51*, 250-256.
82. Deng, C.X., Sirt1, is it a tumor promoter or tumor suppressor? *Int J Biol Sci* **2009**, *5*, 147-152.
83. Bartke, A., Insulin and aging. *Cell Cycle* **2008**, *7*, 3338-3343.
84. van Heemst, D., Insulin, IGF-1 and longevity. *Aging Dis* **2010**, *1*, 147-157.
85. Everitt, A.V., *Calorie restriction, aging, and longevity*. Springer: Dordrecht ; New York, 2010; p xvi, 323 p., 9789048185559 (alk. paper).
86. Murphy, M.P., How mitochondria produce reactive oxygen species. *Biochem J* **2009**, *417*, 1-13.
87. Feng, J.L.; Bussiere, F.; Hekimi, S., Mitochondrial electron transport is a key determinant of life span in Caenorhabditis elegans. *Dev Cell* **2001**, *1*, 633-644.
88. Lee, S.S.; Lee, R.Y.; Fraser, A.G.; Kamath, R.S.; Ahringer, J.; Ruvkun, G., A systematic RNAi screen identifies a critical role for mitochondria in C. elegans longevity. *Nat Genet* **2003**, *33*, 40-48.
89. Shibata, Y.; Branicky, R.; Landaverde, I.O.; Hekimi, S., Redox regulation of germline and vulval development in Caenorhabditis elegans. *Science* **2003**, *302*, 1779-1782.
90. Liu, X.; Jiang, N.; Hughes, B.; Bigras, E.; Shoubridge, E.; Hekimi, S., Evolutionary conservation of the clk-1-dependent mechanism of longevity: loss of mclk1 increases cellular fitness and lifespan in mice. *Genes Dev* **2005**, *19*, 2424-2434.

91. Wallace, D.C., A mitochondrial paradigm of metabolic and degenerative diseases, aging, and cancer: a dawn for evolutionary medicine. *Annu Rev Genet* **2005**, *39*, 359-407.
92. Bratic, A.; Larsson, N.G., The role of mitochondria in aging. *J Clin Invest* **2013**, *123*, 951-957.
93. Bratic, I.; Trifunovic, A., Mitochondrial energy metabolism and ageing. *Biochim Biophys Acta* **2010**, *1797*, 961-967.
94. Short, K.R.; Bigelow, M.L.; Kahl, J.; Singh, R.; Coenen-Schimke, J.; Raghavakaimal, S.; Nair, K.S., Decline in skeletal muscle mitochondrial function with aging in humans. *Proc Natl Acad Sci U S A* **2005**, *102*, 5618-5623.
95. Choi, J.S.; Choi, K.M.; Lee, C.K., Caloric restriction improves efficiency and capacity of the mitochondrial electron transport chain in Saccharomyces cerevisiae. *Biochem Biophys Res Commun* **2011**, *409*, 308-314.
96. Holzenberger, M.; Dupont, J.; Ducos, B.; Leneuve, P.; Geloen, A.; Even, P.C.; Cervera, P.; Le Bouc, Y., IGF-1 receptor regulates lifespan and resistance to oxidative stress in mice. *Nature* **2003**, *421*, 182-187.
97. Barger, J.L.; Kayo, T.; Vann, J.M.; Arias, E.B.; Wang, J.; Hacker, T.A.; Wang, Y.; Raederstorff, D.; Morrow, J.D.; Leeuwenburgh, C., *et al.*, A low dose of dietary resveratrol partially mimics caloric restriction and retards aging parameters in mice. *PLoS One* **2008**, *3*, e2264.
98. Dhahbi, J.M.; Mote, P.L.; Fahy, G.M.; Spindler, S.R., Identification of potential caloric restriction mimetics by microarray profiling. *Physiol Genomics* **2005**, *23*, 343-350.
99. Kaeberlein, M., Resveratrol and rapamycin: are they anti-aging drugs? *Bioessays* **2010**, *32*, 96-99.
100. Holloszy, J.O.; Fontana, L., Caloric restriction in humans. *Exp Gerontol* **2007**, *42*, 709-712.
101. Bhullar, K.S.; Hubbard, B.P., Lifespan and healthspan extension by resveratrol. *Biochim Biophys Acta* **2015**.
102. Bernardes de Jesus, B.; Vera, E.; Schneeberger, K.; Tejera, A.M.; Ayuso, E.; Bosch, F.; Blasco, M.A., Telomerase gene therapy in adult and old mice delays aging and increases longevity without increasing cancer. *EMBO Mol Med* **2012**, *4*, 691-704.
103. Isacson, O.; Kordower, J.H., Future of cell and gene therapies for Parkinson's disease. *Ann Neurol* **2008**, *64 Suppl 2*, S122-138.
104. Allen, P.J.; Feigin, A., Gene-based therapies in Parkinson's disease. *Neurotherapeutics* **2014**, *11*, 60-67.
105. Coune, P.G.; Schneider, B.L.; Aebischer, P., Parkinson's disease: gene therapies. *Cold Spring Harb Perspect Med* **2012**, *2*, a009431.
106. Askou, A.L., Development of gene therapy for treatment of age-related macular degeneration. *Acta Ophthalmol* **2014**, *92 Thesis3*, 1-38.
107. Wolfram, J.A.; Donahue, J.K., Gene therapy to treat cardiovascular disease. *J Am Heart Assoc* **2013**, *2*, e000119.
108. Kay, M.A., State-of-the-art gene-based therapies: the road ahead. *Nat Rev Genet* **2011**, *12*, 316-328.
109. Kaplitt, M.G.; Feigin, A.; Tang, C.; Fitzsimons, H.L.; Mattis, P.; Lawlor, P.A.; Bland, R.J.; Young, D.; Strybing, K.; Eidelberg, D., *et al.*, Safety and tolerability of gene therapy with an adeno-associated virus (AAV) borne GAD gene for Parkinson's disease: an open label, phase I trial. *Lancet* **2007**, *369*, 2097-2105.
110. Kassem, M., Stem cells: potential therapy for age-related diseases. *Ann N Y Acad Sci* **2006**, *1067*, 436-442.
111. Simonsen, J.L.; Rosada, C.; Serakinci, N.; Justesen, J.; Stenderup, K.; Rattan, S.I.; Jensen, T.G.; Kassem, M., Telomerase expression extends the proliferative life-span

and maintains the osteogenic potential of human bone marrow stromal cells. *Nat Biotechnol* **2002**, *20*, 592-596.
112. Shen, J.; Tsai, Y.T.; Dimarco, N.M.; Long, M.A.; Sun, X.; Tang, L., Transplantation of mesenchymal stem cells from young donors delays aging in mice. *Sci Rep* **2011**, *1*, 67.
113. Karanes, C.; Nelson, G.O.; Chitphakdithai, P.; Agura, E.; Ballen, K.K.; Bolan, C.D.; Porter, D.L.; Uberti, J.P.; King, R.J.; Confer, D.L., Twenty years of unrelated donor hematopoietic cell transplantation for adult recipients facilitated by the National Marrow Donor Program. *Biol Blood Marrow Transplant* **2008**, *14*, 8-15.
114. Cohen, T.J.; Hwang, A.W.; Unger, T.; Trojanowski, J.Q.; Lee, V.M., Redox signalling directly regulates TDP-43 via cysteine oxidation and disulphide cross-linking. *EMBO J* **2012**, *31*, 1241-1252.
115. Burt, R.K.; Loh, Y.; Pearce, W.; Beohar, N.; Barr, W.G.; Craig, R.; Wen, Y.; Rapp, J.A.; Kessler, J., Clinical applications of blood-derived and marrow-derived stem cells for nonmalignant diseases. *JAMA* **2008**, *299*, 925-936.
116. Mendoza-Nunez, V.M.; Ruiz-Ramos, M.; Sanchez-Rodriguez, M.A.; Retana-Ugalde, R.; Munoz-Sanchez, J.L., Aging-related oxidative stress in healthy humans. *Tohoku J Exp Med* **2007**, *213*, 261-268.
117. Xia, T.; Kovochich, M.; Brant, J.; Hotze, M.; Sempf, J.; Oberley, T.; Sioutas, C.; Yeh, J.I.; Wiesner, M.R.; Nel, A.E., Comparison of the abilities of ambient and manufactured nanoparticles to induce cellular toxicity according to an oxidative stress paradigm. *Nano Lett* **2006**, *6*, 1794-1807.
118. Chaves, F.J.; Mansego, M.L.; Blesa, S.; Gonzalez-Albert, V.; Jimenez, J.; Tormos, M.C.; Espinosa, O.; Giner, V.; Iradi, A.; Saez, G., *et al.*, Inadequate cytoplasmic antioxidant enzymes response contributes to the oxidative stress in human hypertension. *Am J Hypertens* **2007**, *20*, 62-69.
119. Kelly, F.J., Oxidative stress: its role in air pollution and adverse health effects. *Occup Environ Med* **2003**, *60*, 612-616.
120. Andersen, J.K., Oxidative stress in neurodegeneration: cause or consequence? *Nat Med* **2004**, *10 Suppl*, S18-25.
121. Radak, Z.; Chung, H.Y.; Koltai, E.; Taylor, A.W.; Goto, S., Exercise, oxidative stress and hormesis. *Ageing Res Rev* **2008**, *7*, 34-42.
122. Bartz, R.R.; Piantadosi, C.A., Clinical review: oxygen as a signaling molecule. *Critical Care* **2010**, *14*.
123. Herrmann, J.M.; Dick, T.P., Redox Biology on the rise. *Biol Chem* **2012**, *393*, 999-1004.
124. Cheeseman, K.H.; Slater, T.F., An introduction to free radical biochemistry. *Br Med Bull* **1993**, *49*, 481-493.
125. Trachootham, D.; Alexandre, J.; Huang, P., Targeting cancer cells by ROS-mediated mechanisms: a radical therapeutic approach? *Nat Rev Drug Discov* **2009**, *8*, 579-591.
126. Lobo, V.; Patil, A.; Phatak, A.; Chandra, N., Free radicals, antioxidants and functional foods: Impact on human health. *Pharmacogn Rev* **2010**, *4*, 118-126.
127. Simic, M.G., Free-radical mechanisms in autoxidation processes. *J Chem Educ* **1981**, *58*, 125-131.
128. Crowe, J.; Bradshaw, T., *Chemistry for the biosciences : the essential concepts*. 2nd ed.; Oxford University Press: Oxford; New York, 2010; p xxv, 678 p., 9780199570874 (acid-free paper).
129. Bondy, S.C.; Maiese, K., *Aging and age-related disorders*. Humana: New York, 2010; p xv, 471 p., 9781607616016 (alk. paper).
130. Sies, H., Strategies of antioxidant defense. *Eur J Biochem* **1993**, *215*, 213-219.
131. Nauman, E.B., *Chemical reactor design, optimization, and scaleup*. 2nd ed.; Wiley: Hoboken, N.J., 2008; p xxxii, 608 p., 9780470105252 (cloth).

132. Turk, A., *Introduction to chemistry*. Academic Press: New York, 1968; p xii, 577 p., 9780127038308.
133. Sies, H., Oxidative stress: oxidants and antioxidants. *Exp Physiol* **1997**, *82*, 291-295.
134. D'Autreaux, B.; Toledano, M.B., ROS as signalling molecules: mechanisms that generate specificity in ROS homeostasis. *Nat Rev Mol Cell Biol* **2007**, *8*, 813-824.
135. Machlin, L.J.; Bendich, A., Free radical tissue damage: protective role of antioxidant nutrients. *FASEB J* **1987**, *1*, 441-445.
136. Miller, D.M.; Buettner, G.R.; Aust, S.D., Transition-metals as catalysts of autoxidation reactions. *Free Radic Bio Med* **1990**, *8*, 95-108.
137. Xi, L.; Serebrovskaya, T.V., *Intermittent hypoxia and human diseases*. Springer: Dordrecht, Netherlands, 2012; p xi, 316 p., 9781447129059 (hbk. alk. paper).
138. Nicholls, S.J.; Hazen, S.L., Myeloperoxidase, modified lipoproteins, and atherogenesis. *J Lipid Res* **2009**, *50 Suppl*, S346-351.
139. Rice-Evans, C.; Burdon, R.H., *Free radical damage and its control*. Elsevier: Amsterdam ; New York, 1994; p xvi, 392 p., 9780444897169 (alk. paper).
140. Livertoux, M.H.; Lagrange, P.; Minn, A., The superoxide production mediated by the redox cycling of xenobiotics in rat brain microsomes is dependent on their reduction potential. *Brain Res* **1996**, *725*, 207-216.
141. Tsuchiya, Y.; Nakajima, M.; Yokoi, T., Cytochrome P450-mediated metabolism of estrogens and its regulation in human. *Cancer Lett* **2005**, *227*, 115-124.
142. Segal, A.W., How neutrophils kill microbes. *Annu Rev Immunol* **2005**, *23*, 197-223.
143. Sunil, V.R.; Shen, J.; Patel-Vayas, K.; Gow, A.J.; Laskin, J.D.; Laskin, D.L., Role of reactive nitrogen species generated via inducible nitric oxide synthase in vesicant-induced lung injury, inflammation and altered lung functioning. *Toxicol Appl Pharmacol* **2012**, *261*, 22-30.
144. Kwon, J.; Lee, S.R.; Yang, K.S.; Ahn, Y.; Kim, Y.J.; Stadtman, E.R.; Rhee, S.G., Reversible oxidation and inactivation of the tumor suppressor PTEN in cells stimulated with peptide growth factors. *Proc Natl Acad Sci U S A* **2004**, *101*, 16419-16424.
145. Finkel, T., Signal transduction by reactive oxygen species in non-phagocytic cells. *J Leukoc Biol* **1999**, *65*, 337-340.
146. Vallyathan, V.; Shi, X., The role of oxygen free radicals in occupational and environmental lung diseases. *Environ Health Perspect* **1997**, *105 Suppl 1*, 165-177.
147. Yamamori, T.; Yasui, H.; Yamazumi, M.; Wada, Y.; Nakamura, Y.; Nakamura, H.; Inanami, O., Ionizing radiation induces mitochondrial reactive oxygen species production accompanied by upregulation of mitochondrial electron transport chain function and mitochondrial content under control of the cell cycle checkpoint. *Free Radic Biol Med* **2012**, *53*, 260-270.
148. Hayflick, L., Biological aging is no longer an unsolved problem. *Ann Ny Acad Sci* **2007**, *1100*, 1-13.
149. Butterfield, D.A.; Kanski, J., Brain protein oxidation in age-related neurodegenerative disorders that are associated with aggregated proteins. *Mech Ageing Dev* **2001**, *122*, 945-962.
150. Schoneich, C., Methionine oxidation by reactive oxygen species: reaction mechanisms and relevance to Alzheimer's disease. *Biochim Biophys Acta* **2005**, *1703*, 111-119.
151. Smith, C.D.; Carney, J.M.; Starke-Reed, P.E.; Oliver, C.N.; Stadtman, E.R.; Floyd, R.A.; Markesbery, W.R., Excess brain protein oxidation and enzyme dysfunction in normal aging and in Alzheimer disease. *Proc Natl Acad Sci U S A* **1991**, *88*, 10540-10543.
152. Choi, J.; Sullards, M.C.; Olzmann, J.A.; Rees, H.D.; Weintraub, S.T.; Bostwick, D.E.; Gearing, M.; Levey, A.I.; Chin, L.S.; Li, L., Oxidative damage of DJ-1 is linked to sporadic Parkinson and Alzheimer diseases. *J Biol Chem* **2006**, *281*, 10816-10824.
153. Oberley, T.D., Oxidative damage and cancer. *Am J Pathol* **2002**, *160*, 403-408.

154. Brennan, M.L.; Hazen, S.L., Amino acid and protein oxidation in cardiovascular disease. *Amino Acids* **2003**, *25*, 365-374.
155. Hazen, S.L.; Heinecke, J.W., 3-Chlorotyrosine, a specific marker of myeloperoxidase-catalyzed oxidation, is markedly elevated in low density lipoprotein isolated from human atherosclerotic intima. *J Clin Invest* **1997**, *99*, 2075-2081.
156. Stadtman, E.R., Protein oxidation in aging and age-related diseases. *Ann N Y Acad Sci* **2001**, *928*, 22-38.
157. Bigelow, D.J.; Squier, T.C., Thioredoxin-dependent redox regulation of cellular signaling and stress response through reversible oxidation of methionines. *Molecular Biosystems* **2011**, *7*, 2101-2109.
158. Rose, S.; Melnyk, S.; Trusty, T.A.; Pavliv, O.; Seidel, L.; Li, J.; Nick, T.; James, S.J., Intracellular and extracellular redox status and free radical generation in primary immune cells from children with autism. *Autism Res Treat* **2012**, *2012*, 986519.
159. Mann, M.; Jensen, O.N., Proteomic analysis of post-translational modifications. *Nat Biotechnol* **2003**, *21*, 255-261.
160. Tokmakov, A.A.; Kurotani, A.; Takagi, T.; Toyama, M.; Shirouzu, M.; Fukami, Y.; Yokoyama, S., Multiple post-translational modifications affect heterologous protein synthesis. *J Biol Chem* **2012**, *287*, 27106-27116.
161. Oliveira, A.P.; Sauer, U., The importance of post-translational modifications in regulating Saccharomyces cerevisiae metabolism. *FEMS Yeast Res* **2012**, *12*, 104-117.
162. Borgese, N.; Aggujaro, D.; Carrera, P.; Pietrini, G.; Bassetti, M., A role for N-myristoylation in protein targeting: NADH-cytochrome b5 reductase requires myristic acid for association with outer mitochondrial but not ER membranes. *J Cell Biol* **1996**, *135*, 1501-1513.
163. Lecker, S.H.; Goldberg, A.L.; Mitch, W.E., Protein degradation by the ubiquitin-proteasome pathway in normal and disease states. *J Am Soc Nephrol* **2006**, *17*, 1807-1819.
164. Li, X.; Foley, E.A.; Kawashima, S.A.; Molloy, K.R.; Li, Y.; Chait, B.T.; Kapoor, T.M., Examining post-translational modification-mediated protein-protein interactions using a chemical proteomics approach. *Protein Sci* **2013**, *22*, 287-295.
165. Reuter, S.; Gupta, S.C.; Chaturvedi, M.M.; Aggarwal, B.B., Oxidative stress, inflammation, and cancer: how are they linked? *Free Radic Biol Med* **2010**, *49*, 1603-1616.
166. Trachootham, D.; Lu, W.; Ogasawara, M.A.; Nilsa, R.D.; Huang, P., Redox regulation of cell survival. *Antioxid Redox Signal* **2008**, *10*, 1343-1374.
167. Cabiscol, E.; Tamarit, J.; Ros, J., Oxidative stress in bacteria and protein damage by reactive oxygen species. *Int Microbiol* **2000**, *3*, 3-8.
168. Liou, G.Y.; Storz, P., Reactive oxygen species in cancer. *Free Radic Res* **2010**, *44*, 479-496.
169. Meng, T.C.; Fukada, T.; Tonks, N.K., Reversible oxidation and inactivation of protein tyrosine phosphatases in vivo. *Mol Cell* **2002**, *9*, 387-399.
170. Dalle-Donne, I.; Aldini, G.; Carini, M.; Colombo, R.; Rossi, R.; Milzani, A., Protein carbonylation, cellular dysfunction, and disease progression. *J Cell Mol Med* **2006**, *10*, 389-406.
171. Choi, J.; Levey, A.I.; Weintraub, S.T.; Rees, H.D.; Gearing, M.; Chin, L.S.; Li, L., Oxidative modifications and down-regulation of ubiquitin carboxyl-terminal hydrolase L1 associated with idiopathic Parkinson's and Alzheimer's diseases. *J Biol Chem* **2004**, *279*, 13256-13264.
172. Choi, J.; Rees, H.D.; Weintraub, S.T.; Levey, A.I.; Chin, L.S.; Li, L., Oxidative modifications and aggregation of Cu,Zn-superoxide dismutase associated with Alzheimer and Parkinson diseases. *J Biol Chem* **2005**, *280*, 11648-11655.
173. Go, Y.M.; Jones, D.P., Cysteine/cystine redox signaling in cardiovascular disease. *Free Radic Biol Med* **2011**, *50*, 495-509.

174. Mieyal, J.J.; Gallogly, M.M.; Qanungo, S.; Sabens, E.A.; Shelton, M.D., Molecular mechanisms and clinical implications of reversible protein S-glutathionylation. *Antioxid Redox Signal* **2008**, *10*, 1941-1988.
175. Zahid, S.; Khan, R.; Oellerich, M.; Ahmed, N.; Asif, A.R., Differential S-Nitrosylation of Proteins in Alzheimer's Disease. *Neuroscience* **2014**, *256*, 126-136.
176. Mohiuddin, I.; Chai, H.; Lin, P.H.; Lumsden, A.B.; Yao, Q.; Chen, C., Nitrotyrosine and chlorotyrosine: clinical significance and biological functions in the vascular system. *J Surg Res* **2006**, *133*, 143-149.
177. Maisonneuve, E.; Ducret, A.; Khoueiry, P.; Lignon, S.; Longhi, S.; Talla, E.; Dukan, S., Rules governing selective protein carbonylation. *PLoS One* **2009**, *4*, e7269.
178. Moller, I.M.; Rogowska-Wrzesinska, A.; Rao, R.S., Protein carbonylation and metal-catalyzed protein oxidation in a cellular perspective. *J Proteomics* **2011**, *74*, 2228-2242.
179. Grimsrud, P.A.; Xie, H.; Griffin, T.J.; Bernlohr, D.A., Oxidative stress and covalent modification of protein with bioactive aldehydes. *J Biol Chem* **2008**, *283*, 21837-21841.
180. Choi, J.; Malakowsky, C.A.; Talent, J.M.; Conrad, C.C.; Gracy, R.W., Identification of oxidized plasma proteins in Alzheimer's disease. *Biochem Biophys Res Commun* **2002**, *293*, 1566-1570.
181. Sultana, R.; Perluigi, M.; Newman, S.F.; Pierce, W.M.; Cini, C.; Coccia, R.; Butterfield, D.A., Redox proteomic analysis of carbonylated brain proteins in mild cognitive impairment and early Alzheimer's disease. *Antioxid Redox Signal* **2010**, *12*, 327-336.
182. Madian, A.G.; Diaz-Maldonado, N.; Gao, Q.; Regnier, F.E., Oxidative stress induced carbonylation in human plasma. *J Proteomics* **2011**, *74*, 2395-2416.
183. Madian, A.G.; Myracle, A.D.; Diaz-Maldonado, N.; Rochelle, N.S.; Janle, E.M.; Regnier, F.E., Differential carbonylation of proteins as a function of in vivo oxidative stress. *J Proteome Res* **2011**, *10*, 3959-3972.
184. Bollineni, R.C.; Fedorova, M.; Bluher, M.; Hoffmann, R., Carbonylated plasma proteins as potential biomarkers of obesity induced type 2 diabetes mellitus. *J Proteome Res* **2014**, *13*, 5081-5093.
185. Chavez, J.D.; Wu, J.; Bisson, W.; Maier, C.S., Site-specific proteomic analysis of lipoxidation adducts in cardiac mitochondria reveals chemical diversity of 2-alkenal adduction. *J Proteomics* **2011**, *74*, 2417-2429.
186. Chaudhuri, A.R.; de Waal, E.M.; Pierce, A.; Van Remmen, H.; Ward, W.F.; Richardson, A., Detection of protein carbonyls in aging liver tissue: A fluorescence-based proteomic approach. *Mech Ageing Dev* **2006**, *127*, 849-861.
187. Feng, J.; Xie, H.; Meany, D.L.; Thompson, L.V.; Arriaga, E.A.; Griffin, T.J., Quantitative proteomic profiling of muscle type-dependent and age-dependent protein carbonylation in rat skeletal muscle mitochondria. *J Gerontol A Biol Sci Med Sci* **2008**, *63*, 1137-1152.
188. Oikawa, S.; Yamada, T.; Minohata, T.; Kobayashi, H.; Furukawa, A.; Tada-Oikawa, S.; Hiraku, Y.; Murata, M.; Kikuchi, M.; Yamashima, T., Proteomic identification of carbonylated proteins in the monkey hippocampus after ischemia-reperfusion. *Free Radic Biol Med* **2009**, *46*, 1472-1477.
189. Berlett, B.S.; Stadtman, E.R., Protein oxidation in aging, disease, and oxidative stress. *J Biol Chem* **1997**, *272*, 20313-20316.
190. Fomenko, D.E.; Marino, S.M.; Gladyshev, V.N., Functional diversity of cysteine residues in proteins and unique features of catalytic redox-active cysteines in thiol oxidoreductases. *Mol Cells* **2008**, *26*, 228-235.
191. Halliwell, B.; Poulsen, H.E., *Cigarette smoke and oxidative stress*. Springer: Berlin; New York, 2006; p xi, 407 p., 9783540314103.

192. Rehder, D.S.; Borges, C.R., Cysteine sulfenic acid as an intermediate in disulfide bond formation and nonenzymatic protein folding. *Biochemistry* **2010**, *49*, 7748-7755.
193. Piotukh, K.; Kosslick, D.; Zimmermann, J.; Krause, E.; Freund, C., Reversible disulfide bond formation of intracellular proteins probed by NMR spectroscopy. *Free Radic Biol Med* **2007**, *43*, 1263-1270.
194. Das, D.K., *Methods in redox signaling*. Mary Ann Liebert: New Rochelle, NY, 2010; p xix, 264 p., 9781934854068.
195. Danielson, S.R.; Held, J.M.; Oo, M.; Riley, R.; Gibson, B.W.; Andersen, J.K., Quantitative mapping of reversible mitochondrial Complex I cysteine oxidation in a Parkinson disease mouse model. *J Biol Chem* **2011**, *286*, 7601-7608.
196. Cho, S.H.; Lee, C.H.; Ahn, Y.; Kim, H.; Kim, H.; Ahn, C.Y.; Yang, K.S.; Lee, S.R., Redox regulation of PTEN and protein tyrosine phosphatases in H2O2-mediated cell signaling. *FEBS Lett* **2004**, *560*, 7-13.
197. Denu, J.M.; Tanner, K.G., Specific and reversible inactivation of protein tyrosine phosphatases by hydrogen peroxide: Evidence for a sulfenic acid intermediate and implications for redox regulation. *Biochemistry* **1998**, *37*, 5633-5642.
198. Sanders, L.H.; Greenamyre, J.T., Oxidative damage to macromolecules in human Parkinson disease and the rotenone model. *Free Radic Biol Med* **2013**, *62*, 111-120.
199. Spickett, C.M.; Pitt, A.R., Protein oxidation: role in signalling and detection by mass spectrometry. *Amino Acids* **2012**, *42*, 5-21.
200. Riederer, I.M.; Schiffrin, M.; Kovari, E.; Bouras, C.; Riederer, B.M., Ubiquitination and cysteine nitrosylation during aging and Alzheimer's disease. *Brain Res Bull* **2009**, *80*, 233-241.
201. Sharov, V.S.; Dremina, E.S.; Galeva, N.A.; Williams, T.D.; Schoneich, C., Quantitative mapping of oxidation-sensitive cysteine residues in SERCA in vivo and in vitro by HPLC-electrospray-tandem MS: selective protein oxidation during biological aging. *Biochem J* **2006**, *394*, 605-615.
202. Kohr, M.J.; Sun, J.; Aponte, A.; Wang, G.; Gucek, M.; Murphy, E.; Steenbergen, C., Simultaneous measurement of protein oxidation and S-nitrosylation during preconditioning and ischemia/reperfusion injury with resin-assisted capture. *Circ Res* **2011**, *108*, 418-426.
203. Kumar, V.; Kleffmann, T.; Hampton, M.B.; Cannell, M.B.; Winterbourn, C.C., Redox proteomics of thiol proteins in mouse heart during ischemia/reperfusion using ICAT reagents and mass spectrometry. *Free Radic Biol Med* **2013**, *58*, 109-117.
204. Brandes, N.; Schmitt, S.; Jakob, U., Thiol-based redox switches in eukaryotic proteins. *Antioxid Redox Signal* **2009**, *11*, 997-1014.
205. Chen, J.M.; Fu, X.Y.; Wang, Y.; Ling, M.H.; McMullen, B.; Kulman, J.; Chung, D.W.; Lopez, J.A., Oxidative modification of von Willebrand factor by neutrophil oxidants inhibits its cleavage by ADAMTS13. *Blood* **2010**, *115*, 706-712.
206. Kim, Y.H.; Berry, A.H.; Spencer, D.S.; Stites, W.E., Comparing the effect on protein stability of methionine oxidation versus mutagenesis: steps toward engineering oxidative resistance in proteins. *Protein Eng* **2001**, *14*, 343-347.
207. Ghesquiere, B.; Jonckheere, V.; Colaert, N.; Van Durme, J.; Timmerman, E.; Goethals, M.; Schymkowitz, J.; Rousseau, F.; Vandekerckhove, J.; Gevaert, K., Redox proteomics of protein-bound methionine oxidation. *Mol Cell Proteomics* **2011**, *10*, M110 006866.
208. Glaser, C.B.; Yamin, G.; Uversky, V.N.; Fink, A.L., Methionine oxidation, alpha-synuclein and Parkinson's disease. *Biochim Biophys Acta* **2005**, *1703*, 157-169.
209. Brock, J.W.; Jenkins, A.J.; Lyons, T.J.; Klein, R.L.; Yim, E.; Lopes-Virella, M.; Carter, R.E.; Research, G.; Thorpe, S.R.; Baynes, J.W., Increased methionine sulfoxide content of apoA-I in type 1 diabetes. *J Lipid Res* **2008**, *49*, 847-855.
210. Stadtman, E.R.; Van Remmen, H.; Richardson, A.; Wehr, N.B.; Levine, R.L., Methionine oxidation and aging. *Biochim Biophys Acta* **2005**, *1703*, 135-140.

211. Takakura, K.; Beckman, J.S.; MacMillan-Crow, L.A.; Crow, J.P., Rapid and irreversible inactivation of protein tyrosine phosphatases PTP1B, CD45, and LAR by peroxynitrite. *Arch Biochem Biophys* **1999**, *369*, 197-207.
212. Stadtman, E.R., Role of oxidant species in aging. *Curr Med Chem* **2004**, *11*, 1105-1112.
213. van der Vliet, A.; Hristova, M.; Cross, C.E.; Eiserich, J.P.; Goldkorn, T., Peroxynitrite induces covalent dimerization of epidermal growth factor receptors in A431 epidermoid carcinoma cells. *J Biol Chem* **1998**, *273*, 31860-31866.
214. Gaut, J.P.; Yeh, G.C.; Tran, H.D.; Byun, J.; Henderson, J.P.; Richter, G.M.; Brennan, M.L.; Lusis, A.J.; Belaaouaj, A.; Hotchkiss, R.S., *et al.*, Neutrophils employ the myeloperoxidase system to generate antimicrobial brominating and chlorinating oxidants during sepsis. *Proc Natl Acad Sci U S A* **2001**, *98*, 11961-11966.
215. Radi, R., Nitric oxide, oxidants, and protein tyrosine nitration. *Proc Natl Acad Sci U S A* **2004**, *101*, 4003-4008.
216. Vanderheyden, M.; Bartunek, J.; Knaapen, M.; Kockx, M.; De Bruyne, B.; Goethals, M., Hemodynamic effects of inducible nitric oxide synthase and nitrotyrosine generation in heart failure. *J Heart Lung Transplant* **2004**, *23*, 723-728.
217. Halliwell, B., What nitrates tyrosine? Is nitrotyrosine specific as a biomarker of peroxynitrite formation in vivo? *FEBS Lett* **1997**, *411*, 157-160.
218. Lamas, S.; Cadenas, E., *Nitric oxide, cell signaling, and gene expression*. CRC/Taylor & Francis: Boca Raton, FL, 2006; p 430 p., 9780824729608 (alk. paper).
219. Byun, J.; Mueller, D.M.; Fabjan, J.S.; Heinecke, J.W., Nitrogen dioxide radical generated by the myeloperoxidase-hydrogen peroxide-nitrite system promotes lipid peroxidation of low density lipoprotein. *FEBS Lett* **1999**, *455*, 243-246.
220. Nakai, K.; Mason, R.P., Immunochemical detection of nitric oxide and nitrogen dioxide trapping of the tyrosyl radical and the resulting nitrotyrosine in sperm whale myoglobin. *Free Radic Biol Med* **2005**, *39*, 1050-1058.
221. Aeschbach, R.; Amado, R.; Neukom, H., Formation of dityrosine cross-links in proteins by oxidation of tyrosine residues. *Biochim Biophys Acta* **1976**, *439*, 292-301.
222. DiMarco, T.; Giulivi, C., Current analytical methods for the detection of dityrosine, a biomarker of oxidative stress, in biological samples. *Mass Spectrom Rev* **2007**, *26*, 108-120.
223. Balabanli, B.; Kamisaki, Y.; Martin, E.; Murad, F., Requirements for heme and thiols for the nonenzymatic modification of nitrotyrosine. *Proc Natl Acad Sci U S A* **1999**, *96*, 13136-13141.
224. Abello, N.; Kerstjens, H.A.; Postma, D.S.; Bischoff, R., Protein tyrosine nitration: selectivity, physicochemical and biological consequences, denitration, and proteomics methods for the identification of tyrosine-nitrated proteins. *J Proteome Res* **2009**, *8*, 3222-3238.
225. Mani, A.R.; Ippolito, S.; Moreno, J.C.; Visser, T.J.; Moore, K.P., The metabolism and dechlorination of chlorotyrosine in vivo. *J Biol Chem* **2007**, *282*, 29114-29121.
226. McTamney, P.M.; Rokita, S.E., A mammalian reductive deiodinase has broad power to dehalogenate chlorinated and brominated substrates. *J Am Chem Soc* **2009**, *131*, 14212-14213.
227. Winter, J.; Ilbert, M.; Graf, P.C.; Ozcelik, D.; Jakob, U., Bleach activates a redox-regulated chaperone by oxidative protein unfolding. *Cell* **2008**, *135*, 691-701.
228. Tsimikas, S., In vivo markers of oxidative stress and therapeutic interventions. *Am J Cardiol* **2008**, *101*, 34D-42D.
229. Kumar, Y.; Liang, C.; Limmon, G.V.; Liang, L.; Engelward, B.P.; Ooi, E.E.; Chen, J.; Tannenbaum, S.R., Molecular analysis of serum and bronchoalveolar lavage in a mouse model of influenza reveals markers of disease severity that can be clinically useful in humans. *PLoS One* **2014**, *9*, e86912.

230. Knutson, C.G.; Mangerich, A.; Zeng, Y.; Raczynski, A.R.; Liberman, R.G.; Kang, P.; Ye, W.; Prestwich, E.G.; Lu, K.; Wishnok, J.S., *et al.*, Chemical and cytokine features of innate immunity characterize serum and tissue profiles in inflammatory bowel disease. *Proc Natl Acad Sci U S A* **2013**, *110*, E2332-2341.
231. Shao, B.; Pennathur, S.; Heinecke, J.W., Myeloperoxidase targets apolipoprotein A-I, the major high density lipoprotein protein, for site-specific oxidation in human atherosclerotic lesions. *J Biol Chem* **2012**, *287*, 6375-6386.
232. Smith, C.K.; Vivekanandan-Giri, A.; Tang, C.; Knight, J.S.; Mathew, A.; Padilla, R.L.; Gillespie, B.W.; Carmona-Rivera, C.; Liu, X.; Subramanian, V., *et al.*, Neutrophil extracellular trap-derived enzymes oxidize high-density lipoprotein: an additional proatherogenic mechanism in systemic lupus erythematosus. *Arthritis Rheumatol* **2014**, *66*, 2532-2544.
233. Paton, L.N.; Mocatta, T.J.; Richards, A.M.; Winterbourn, C.C., Increased thrombin-induced polymerization of fibrinogen associated with high protein carbonyl levels in plasma from patients post myocardial infarction. *Free Radic Biol Med* **2010**, *48*, 223-229.
234. Pennathur, S.; Bergt, C.; Shao, B.; Byun, J.; Kassim, S.Y.; Singh, P.; Green, P.S.; McDonald, T.O.; Brunzell, J.; Chait, A., *et al.*, Human atherosclerotic intima and blood of patients with established coronary artery disease contain high density lipoprotein damaged by reactive nitrogen species. *J Biol Chem* **2004**, *279*, 42977-42983.
235. Zhan, X.; Desiderio, D.M., Nitroproteins from a human pituitary adenoma tissue discovered with a nitrotyrosine affinity column and tandem mass spectrometry. *Anal Biochem* **2006**, *354*, 279-289.
236. Castegna, A.; Thongboonkerd, V.; Klein, J.B.; Lynn, B.; Markesbery, W.R.; Butterfield, D.A., Proteomic identification of nitrated proteins in Alzheimer's disease brain. *J Neurochem* **2003**, *85*, 1394-1401.
237. Kambayashi, Y.; Ogino, K.; Takemoto, K.; Imagama, T.; Takigawa, T.; Kimura, S.; Hibino, Y.; Hitomi, Y.; Nakamura, H., Preparation and characterization of a polyclonal antibody against brominated protein. *J Clin Biochem Nutr* **2009**, *44*, 95-103.
238. Kato, Y.; Dozaki, N.; Nakamura, T.; Kitamoto, N.; Yoshida, A.; Naito, M.; Kitamura, M.; Osawa, T., Quantification of modified tyrosines in healthy and diabetic human urine using liquid chromatography/tandem mass spectrometry. *J Clin Biochem Nutr* **2009**, *44*, 67-78.
239. Svatikova, A.; Wolk, R.; Wang, H.H.; Otto, M.E.; Bybee, K.A.; Singh, R.J.; Somers, V.K., Circulating free nitrotyrosine in obstructive sleep apnea. *Am J Physiol Regul Integr Comp Physiol* **2004**, *287*, R284-287.
240. Shu, L.; Vivekanandan-Giri, A.; Pennathur, S.; Smid, B.E.; Aerts, J.M.; Hollak, C.E.; Shayman, J.A., Establishing 3-nitrotyrosine as a biomarker for the vasculopathy of Fabry disease. *Kidney Int* **2014**, *86*, 58-66.
241. Kuligowski, J.; Torres-Cuevas, I.; Quintas, G.; Rook, D.; van Goudoever, J.B.; Cubells, E.; Asensi, M.; Lliso, I.; Nunez, A.; Vento, M., *et al.*, Assessment of oxidative damage to proteins and DNA in urine of newborn infants by a validated UPLC-MS/MS approach. *PLoS One* **2014**, *9*, e93703.
242. Winterbourn, C.C.; Hampton, M.B., Thiol chemistry and specificity in redox signaling. *Free Radic Biol Med* **2008**, *45*, 549-561.
243. Townsend, D.M.; Tew, K.D.; Tapiero, H., The importance of glutathione in human disease. *Biomed Pharmacother* **2003**, *57*, 145-155.
244. Couto, N.; Malys, N.; Gaskell, S.J.; Barber, J., Partition and turnover of glutathione reductase from Saccharomyces cerevisiae: a proteomic approach. *J Proteome Res* **2013**, *12*, 2885-2894.

245. Halprin, K.M.; Ohkawara, A., The measurement of glutathione in human epidermis using glutathione reductase 1. *J Invest Dermatol* **1967**, *48*, 149-152.
246. Berndt, C.; Lillig, C.H.; Holmgren, A., Thiol-based mechanisms of the thioredoxin and glutaredoxin systems: implications for diseases in the cardiovascular system. *Am J Physiol Heart Circ Physiol* **2007**, *292*, H1227-1236.
247. Mukwevho, E.; Ferreira, Z.; Ayeleso, A., Potential role of sulfur-containing antioxidant systems in highly oxidative environments. *Molecules* **2014**, *19*, 19376-19389.
248. Shelton, M.D.; Chock, P.B.; Mieyal, J.J., Glutaredoxin: role in reversible protein s-glutathionylation and regulation of redox signal transduction and protein translocation. *Antioxid Redox Signal* **2005**, *7*, 348-366.
249. Knoefler, D.; Leicher, L.I.O.; Thamsen, M.; Cremers, C.M.; Reichmann, D.; Gray, M.J.; Wholey, W.Y.; Jakob, U., About the dangers, costs and benefits of living an aerobic lifestyle. *Biochem Soc Trans* **2014**, *42*, 917-921.
250. Forman, H.J.; Ursini, F.; Maiorino, M., An overview of mechanisms of redox signaling. *J Mol Cell Cardiol* **2014**, *73*, 2-9.
251. Forman, H.J.; Fukuto, J.M.; Torres, M., Redox signaling: thiol chemistry defines which reactive oxygen and nitrogen species can act as second messengers. *Am J Physiol Cell Physiol* **2004**, *287*, C246-256.
252. Karplus, P.A., A primer on peroxiredoxin biochemistry. *Free Radic Biol Med* **2014**.
253. Giles, N.M.; Watts, A.B.; Giles, G.I.; Fry, F.H.; Littlechild, J.A.; Jacob, C., Metal and redox modulation of cysteine protein function. *Chem Biol* **2003**, *10*, 677-693.
254. Jones, D.P., Redox sensing: orthogonal control in cell cycle and apoptosis signalling. *J Intern Med* **2010**, *268*, 432-448.
255. Ruiz, M.C.; Portero-Otin, M.; Pamplona, R.; Requena, J.R.; Prat, J.; Lafarga, M.A.; Borras, M.; Bellmunt, M.J., Chemical and immunological characterization of oxidative nonenzymatic protein modifications in dialysis fluids. *Perit Dial Int* **2003**, *23*, 23-32.
256. Persson, C.; Kappert, K.; Engstrom, U.; Ostman, A.; Sjoblom, T., An antibody-based method for monitoring in vivo oxidation of protein tyrosine phosphatases. *Methods* **2005**, *35*, 37-43.
257. Petre, B.A.; Dragusanu, M.; Przybylski, M., Molecular recognition specificity of anti-3-nitrotyrosine antibodies revealed by affinity - mass spectrometry and immunoanalytical methods. In *Applications of Mass Spectrometry in Life Safety*, Springer, Ed. Springer: Dusseldorf, Germany, 2008; pp 55-67.
258. Gujral, J.S.; Hinson, J.A.; Jaeschke, H., Chlorotyrosine protein adducts are reliable biomarkers of neutrophil-induced cytotoxicity in vivo. *Comp Hepatol* **2004**, *3 Suppl 1*, S48.
259. Rudyk, O.; Eaton, P., Biochemical methods for monitoring protein thiol redox states in biological systems. *Redox Biol* **2014**, *2*, 803-813.
260. Oberg, B.P.; McMenamin, E.; Lucas, F.L.; McMonagle, E.; Morrow, J.; Ikizler, T.A.; Himmelfarb, J., Increased prevalence of oxidant stress and inflammation in patients with moderate to severe chronic kidney disease. *Kidney Int* **2004**, *65*, 1009-1016.
261. Kadiiska, M.B.; Gladen, B.C.; Baird, D.D.; Germolec, D.; Graham, L.B.; Parker, C.E.; Nyska, A.; Wachsman, J.T.; Ames, B.N.; Basu, S., *et al.*, Biomarkers of oxidative stress study II: are oxidation products of lipids, proteins, and DNA markers of CCl4 poisoning? *Free Radic Biol Med* **2005**, *38*, 698-710.
262. Tamarit, J.; de Hoogh, A.; Obis, E.; Alsina, D.; Cabiscol, E.; Ros, J., Analysis of oxidative stress-induced protein carbonylation using fluorescent hydrazides. *J Proteomics* **2012**, *75*, 3778-3788.
263. Soreghan, B.A.; Yang, F.; Thomas, S.N.; Hsu, J.; Yang, A.J., High-throughput proteomic-based identification of oxidatively induced protein carbonylation in mouse brain. *Pharm Res* **2003**, *20*, 1713-1720.

264. Palmese, A.; De Rosa, C.; Chiappetta, G.; Marino, G.; Amoresano, A., Novel method to investigate protein carbonylation by iTRAQ strategy. *Anal Bioanal Chem* **2012**, *404*, 1631-1635.
265. Potthast, A.; Rohrling, J.; Rosenau, T.; Borgards, A.; Sixta, H.; Kosma, P., A novel method for the determination of carbonyl groups in cellulosics by fluorescence labeling. 3. Monitoring oxidative processes. *Biomacromolecules* **2003**, *4*, 743-749.
266. WitkoSarsat, V.; Friedlander, M.; CapeillereBlandin, C.; NguyenKhoa, T.; Nguyen, N.T.; Zingraff, J.; Jungers, P.; DescampsLatscha, B., Advanced oxidation protein products as a novel marker of oxidative stress in uremia. *Kidney Int* **1996**, *49*, 1304-1313.
267. Aebersold, R.; Mann, M., Mass spectrometry-based proteomics. *Nature* **2003**, *422*, 198-207.
268. Blanksby, S.J.; Mitchell, T.W., Advances in mass spectrometry for lipidomics. *Annu Rev Anal Chem (Palo Alto Calif)* **2010**, *3*, 433-465.
269. Dettmer, K.; Aronov, P.A.; Hammock, B.D., Mass spectrometry-based metabolomics. *Mass Spectrom Rev* **2007**, *26*, 51-78.
270. Zhang, H.; Ge, Y., Comprehensive analysis of protein modifications by top-down mass spectrometry. *Circ Cardiovasc Genet* **2011**, *4*, 711.
271. Issaq, H.J.; Conrads, T.P.; Janini, G.M.; Veenstra, T.D., Methods for fractionation, separation and profiling of proteins and peptides. *Electrophoresis* **2002**, *23*, 3048-3061.
272. Wolters, D.A.; Washburn, M.P.; Yates, J.R., An automated multidimensional protein identification technology for shotgun proteomics. *Anal Chem* **2001**, *73*, 5683-5690.
273. Zhou, J., *Microbial functional genomics*. Wiley-Liss: Hoboken, N.J., 2004; p xxi, 590 p., 9780471071907 (cloth alk. paper).
274. Yates, J.R.; Ruse, C.I.; Nakorchevsky, A., Proteomics by mass spectrometry: approaches, advances, and applications. *Annu Rev Biomed Eng* **2009**, *11*, 49-79.
275. Siuti, N.; Kelleher, N.L., Decoding protein modifications using top-down mass spectrometry. *Nat Methods* **2007**, *4*, 817-821.
276. Armirotti, A.; Damonte, G., Achievements and perspectives of top-down proteomics. *Proteomics* **2010**, *10*, 3566-3576.
277. Ahuja, S., *Chiral separation methods for pharmaceutical and biotechnological products*. Wiley: Hoboken, N.J., 2011; p 491 p., 9780470406915 (cloth).
278. Klein, J.; Papadopoulos, T.; Mischak, H.; Mullen, W., Comparison of CE-MS/MS and LC-MS/MS sequencing demonstrates significant complementarity in natural peptide identification in human urine. *Electrophoresis* **2014**, *35*, 1060-1064.
279. Whitt, J.T.; Moini, M., Capillary electrophoresis to mass spectrometry interface using a porous junction. *Anal Chem* **2003**, *75*, 2188-2191.
280. Landers, J.P., *Handbook of capillary and microchip electrophoresis and associated microtechniques*. 3rd ed.; CRC Press: Boca Raton, 2008; p xxi, 1567 p., 1566 p. of plates, 9780849333293 (hbk.).
281. Petersen, J.R.; Mohammad, A.A., *Clinical and forensic applications of capillary electrophoresis*. Humana Press: Totowa, N.J., 2001; p x, 453 p., 9780896036451 (alk. paper).
282. Moini, M., Capillary electrophoresis mass spectrometry and its application to the analysis of biological mixtures. *Anal Bioanal Chem* **2002**, *373*, 466-480.
283. Yamashita, M.; Fenn, J.B., Electrospray ion-source - another variation on the free-jet theme. *J Phys Chem* **1984**, *88*, 4451-4459.
284. Kruve, A.; Herodes, K.; Leito, I., Optimization of electrospray interface and quadrupole ion trap mass spectrometer parameters in pesticide liquid chromatography/electrospray ionization mass spectrometry analysis. *Rapid Commun Mass Spectrom* **2010**, *24*, 919-926.
285. Mass spectrometry of nucleosides and nucleic acids. *Sci-Tech News* **2010**, *64*, 91-91.

286. Silberring, J.; Ekman, R., *Mass spectrometry and hyphenated techniques in neuropeptide research*. Wiley-Interscience: New York, 2002; p xii, 558 p., 9780471354932 (cloth alk. paper).
287. Banerjee, S.; Mazumdar, S., Electrospray ionization mass spectrometry: a technique to access the information beyond the molecular weight of the analyte. *Int J Anal Chem* **2012**, *2012*, 282574.
288. Sterling, H.J.; Batchelor, J.D.; Wemmer, D.E.; Williams, E.R., Effects of buffer loading for electrospray ionization mass spectrometry of a noncovalent protein complex that requires high concentrations of essential salts. *J Am Soc Mass Spectrom* **2010**, *21*, 1045-1049.
289. Boyd, B.; Basic, C.; Bethem, R., *Trace quantitative analysis by mass spectrometry*. John Wiley & Sons: Chichester, West Sussex, England; Hoboken, N.J., 2008; p xxi, 724 p., 9780470057711 (hbk. alk. paper).
290. Sudakov, M.; Konenkov, N.; Douglas, D.J.; Glebova, T., Excitation frequencies of ions confined in a quadrupole field with quadrupole excitation. *J Am Soc Mass Spectrom* **2000**, *11*, 10-18.
291. Barner-Kowollik, C., *Mass spectrometry in polymer chemistry*. Wiley-VCH: Weinheim, 2012; p xv, 483 p., 9783527329243 (cased).
292. Wells, J.M.; McLuckey, S.A., Collision-induced dissociation (CID) of peptides and proteins. *Methods Enzymol* **2005**, *402*, 148-185.
293. Dayon, L.; Pasquarello, C.; Hoogland, C.; Sanchez, J.C.; Scherl, A., Combining low- and high-energy tandem mass spectra for optimized peptide quantification with isobaric tags. *J Proteomics* **2010**, *73*, 769-777.
294. Steen, H.; Kuster, B.; Mann, M., Quadrupole time-of-flight versus triple-quadrupole mass spectrometry for the determination of phosphopeptides by precursor ion scanning. *J Mass Spectrom* **2001**, *36*, 782-790.
295. Pitt, J.J., Principles and applications of liquid chromatography-mass spectrometry in clinical biochemistry. *Clin Biochem Rev* **2009**, *30*, 19-34.
296. Domon, B.; Aebersold, R., Options and considerations when selecting a quantitative proteomics strategy. *Nat Biotechnol* **2010**, *28*, 710-721.
297. Louris, J.N.; Wright, L.G.; Cooks, R.G.; Schoen, A.E., New scan modes accessed with a hybrid mass-spectrometer. *Anal Chem* **1985**, *57*, 2918-2924.
298. Steen, H.; Mann, M., A new derivatization strategy for the analysis of phosphopeptides by precursor ion scanning in positive ion mode. *J Am Soc Mass Spectrom* **2002**, *13*, 996-1003.
299. Petersson, A.S.; Steen, H.; Kalume, D.E.; Caidahl, K.; Roepstorff, P., Investigation of tyrosine nitration in proteins by mass spectrometry. *J Mass Spectrom* **2001**, *36*, 616-625.
300. Mouls, L.; Silajdzic, E.; Haroune, N.; Spickett, C.M.; Pitt, A.R., Development of novel mass spectrometric methods for identifying HOCl-induced modifications to proteins. *Proteomics* **2009**, *9*, 1617-1631.
301. Galeva, N.A.; Esch, S.W.; Williams, T.D.; Markille, L.M.; Squier, T.C., Rapid method for quantifying the extent of methionine oxidation in intact calmodulin. *J Am Soc Mass Spectrom* **2005**, *16*, 1470-1480.
302. Ducheyne, P., *Comprehensive biomaterials*. Elsevier: Amsterdam ; Boston, 2011, 9780080553023 (set).
303. Trajanoski, Z., *Computational medicine : tools and challenges*. Springer: Wien; New York, 2012; p ix, 203 p., 9783709109465 (alk. paper).
304. Deutsch, E.W.; Lam, H.; Aebersold, R., PeptideAtlas: a resource for target selection for emerging targeted proteomics workflows. *EMBO Rep* **2008**, *9*, 429-434.
305. McClatchy, D.B.; Liao, L.; Park, S.K.; Xu, T.; Lu, B.; Yates Iii, J.R., Differential proteomic analysis of mammalian tissues using SILAM. *PLoS One* **2011**, *6*, e16039.

306. Nakamura, T.; Oda, Y., Mass spectrometry-based quantitative proteomics. *Biotechnol Genet Eng Rev* **2007**, *24*, 147-163.
307. Leonard, S.E.; Carroll, K.S., Chemical 'omics' approaches for understanding protein cysteine oxidation in biology. *Curr Opin Chem Biol* **2011**, *15*, 88-102.
308. Sethuraman, M.; McComb, M.E.; Huang, H.; Huang, S.; Heibeck, T.; Costello, C.E.; Cohen, R.A., Isotope-coded affinity tag (ICAT) approach to redox proteomics: identification and quantitation of oxidant-sensitive cysteine thiols in complex protein mixtures. *J Proteome Res* **2004**, *3*, 1228-1233.
309. Zhao, Y.; Lee, W.N.; Xiao, G.G., Quantitative proteomics and biomarker discovery in human cancer. *Expert Rev Proteomics* **2009**, *6*, 115-118.
310. Victor, K.G.; Rady, J.M.; Cross, J.V.; Templeton, D.J., Proteomic profile of reversible protein oxidation using PROP, purification of reversibly oxidized proteins. *PLoS One* **2012**, *7*, e32527.
311. Held, J.M.; Danielson, S.R.; Behring, J.B.; Atsriku, C.; Britton, D.J.; Puckett, R.L.; Schilling, B.; Campisi, J.; Benz, C.C.; Gibson, B.W., Targeted quantitation of site-specific cysteine oxidation in endogenous proteins using a differential alkylation and multiple reaction monitoring mass spectrometry approach. *Mol Cell Proteomics* **2010**, *9*, 1400-1410.
312. Scotcher, J.; Bythell, B.J.; Marshall, A.G., Unequivocal determination of site-specific protein disulfide bond reduction potentials by top-down FTICR MS: characterization of the N- and C-terminal redox-active sites in human thioredoxin 1. *Anal Chem* **2013**, *85*, 9164-9172.
313. Liu, H.; Ponniah, G.; Neill, A.; Patel, R.; Andrien, B., Accurate determination of protein methionine oxidation by stable isotope labeling and LC-MS analysis. *Anal Chem* **2013**, *85*, 11705-11709.
314. Su, D.; Gaffrey, M.J.; Guo, J.; Hatchell, K.E.; Chu, R.K.; Clauss, T.R.; Aldrich, J.T.; Wu, S.; Purvine, S.; Camp, D.G., *et al.*, Proteomic identification and quantification of S-glutathionylation in mouse macrophages using resin-assisted enrichment and isobaric labeling. *Free Radic Biol Med* **2014**, *67*, 460-470.
315. Chiappetta, G.; Corbo, C.; Palmese, A.; Galli, F.; Piroddi, M.; Marino, G.; Amoresano, A., Quantitative identification of protein nitration sites. *Proteomics* **2009**, *9*, 1524-1537.
316. Robinson, R.A.; Evans, A.R., Enhanced sample multiplexing for nitrotyrosine-modified proteins using combined precursor isotopic labeling and isobaric tagging. *Anal Chem* **2012**, *84*, 4677-4686.
317. McDonagh, B.; Martinez-Acedo, P.; Vazquez, J.; Padilla, C.A.; Sheehan, D.; Barcena, J.A., Application of iTRAQ reagents to relatively quantify the reversible redox state of cysteine residues. *Int J Proteomics* **2012**, *2012*, 514847.
318. Kohr, M.J.; Aponte, A.; Sun, J.; Gucek, M.; Steenbergen, C.; Murphy, E., Measurement of S-nitrosylation occupancy in the myocardium with cysteine-reactive tandem mass tags: short communication. *Circ Res* **2012**, *111*, 1308-1312.
319. Wojdyla, K.; Williamson, J.; Roepstorff, P.; Rogowska-Wrzesinska, A., The SNO/SOH TMT strategy for combinatorial analysis of reversible cysteine oxidations. *J Proteomics* **2015**, *113*, 415-434.
320. Reinbold, J.; Koehler, P.; Rychlik, M., Quantitation of glutathione and its oxidation products in erythrocytes by multiple-label stable-isotope dilution. *Anal Biochem* **2014**, *445*, 41-48.
321. Fahlman, R.P.; Chen, W.; Overall, C.M., Absolute proteomic quantification of the activity state of proteases and proteolytic cleavages using proteolytic signature peptides and isobaric tags. *J Proteomics* **2014**, *100*, 79-91.
322. Pflieger, D.; Junger, M.A.; Muller, M.; Rinner, O.; Lee, H.; Gehrig, P.M.; Gstaiger, M.; Aebersold, R., Quantitative proteomic analysis of protein complexes: concurrent

identification of interactors and their state of phosphorylation. *Mol Cell Proteomics* **2008**, *7*, 326-346.

323. Percy, A.J.; Yang, J.; Chambers, A.G.; Simon, R.; Hardie, D.B.; Borchers, C.H., Multiplexed MRM with Internal Standards for Cerebrospinal Fluid Candidate Protein Biomarker Quantitation. *J Proteome Res* **2014**.
324. Nahnsen, S.; Bielow, C.; Reinert, K.; Kohlbacher, O., Tools for label-free peptide quantification. *Mol Cell Proteomics* **2013**, *12*, 549-556.
325. Liu, H.; Sadygov, R.G.; Yates, J.R., 3rd, A model for random sampling and estimation of relative protein abundance in shotgun proteomics. *Anal Chem* **2004**, *76*, 4193-4201.
326. Washburn, M.P.; Ulaszek, R.; Deciu, C.; Schieltz, D.M.; Yates, J.R., 3rd, Analysis of quantitative proteomic data generated via multidimensional protein identification technology. *Anal Chem* **2002**, *74*, 1650-1657.
327. Ishihama, Y.; Oda, Y.; Tabata, T.; Sato, T.; Nagasu, T.; Rappsilber, J.; Mann, M., Exponentially modified protein abundance index (emPAI) for estimation of absolute protein amount in proteomics by the number of sequenced peptides per protein. *Mol Cell Proteomics* **2005**, *4*, 1265-1272.
328. Shinoda, K.; Tomita, M.; Ishihama, Y., emPAI Calc--for the estimation of protein abundance from large-scale identification data by liquid chromatography-tandem mass spectrometry. *Bioinformatics* **2010**, *26*, 576-577.
329. Lu, P.; Vogel, C.; Wang, R.; Yao, X.; Marcotte, E.M., Absolute protein expression profiling estimates the relative contributions of transcriptional and translational regulation. *Nat Biotechnol* **2007**, *25*, 117-124.
330. Braisted, J.C.; Kuntumalla, S.; Vogel, C.; Marcotte, E.M.; Rodrigues, A.R.; Wang, R.; Huang, S.T.; Ferlanti, E.S.; Saeed, A.I.; Fleischmann, R.D., *et al.*, The APEX Quantitative Proteomics Tool: generating protein quantitation estimates from LC-MS/MS proteomics results. *BMC Bioinformatics* **2008**, *9*, 529.
331. Turk, R.; Piras, C.; Kovacic, M.; Samardzija, M.; Ahmed, H.; De Canio, M.; Urbani, A.; Mestric, Z.F.; Soggiu, A.; Bonizzi, L., *et al.*, Proteomics of inflammatory and oxidative stress response in cows with subclinical and clinical mastitis. *J Proteomics* **2012**, *75*, 4412-4428.
332. Vogel, C.; Silva, G.M.; Marcotte, E.M., Protein expression regulation under oxidative stress. *Mol Cell Proteomics* **2011**, *10*, M111 009217.
333. Grossmann, J.; Roschitzki, B.; Panse, C.; Fortes, C.; Barkow-Oesterreicher, S.; Rutishauser, D.; Schlapbach, R., Implementation and evaluation of relative and absolute quantification in shotgun proteomics with label-free methods. *J Proteomics* **2010**, *73*, 1740-1746.
334. May, D.; Fitzgibbon, M.; Liu, Y.; Holzman, T.; Eng, J.; Kemp, C.J.; Whiteaker, J.; Paulovich, A.; McIntosh, M., A platform for accurate mass and time analyses of mass spectrometry data. *J Proteome Res* **2007**, *6*, 2685-2694.
335. Cox, J.; Mann, M., MaxQuant enables high peptide identification rates, individualized p.p.b.-range mass accuracies and proteome-wide protein quantification. *Nat Biotechnol* **2008**, *26*, 1367-1372.
336. Sturm, M.; Bertsch, A.; Gropl, C.; Hildebrandt, A.; Hussong, R.; Lange, E.; Pfeifer, N.; Schulz-Trieglaff, O.; Zerck, A.; Reinert, K., *et al.*, OpenMS - an open-source software framework for mass spectrometry. *BMC Bioinformatics* **2008**, *9*, 163.
337. Mueller, L.N.; Rinner, O.; Schmidt, A.; Letarte, S.; Bodenmiller, B.; Brusniak, M.Y.; Vitek, O.; Aebersold, R.; Muller, M., SuperHirn - a novel tool for high resolution LC-MS-based peptide/protein profiling. *Proteomics* **2007**, *7*, 3470-3480.
338. Quintana, L.F.; Campistol, J.M.; Alcolea, M.P.; Banon-Maneus, E.; Sol-Gonzalez, A.; Cutillas, P.R., Application of label-free quantitative peptidomics for the identification of urinary biomarkers of kidney chronic allograft dysfunction. *Mol Cell Proteomics* **2009**, *8*, 1658-1673.

339. Fischer, R.; Trudgian, D.C.; Wright, C.; Thomas, G.; Bradbury, L.A.; Brown, M.A.; Bowness, P.; Kessler, B.M., Discovery of candidate serum proteomic and metabolomic biomarkers in ankylosing spondylitis. *Mol Cell Proteomics* **2012**, *11*, M111 013904.
340. Yang, N.; Feng, S.; Shedden, K.; Xie, X.; Liu, Y.; Rosser, C.J.; Lubman, D.M.; Goodison, S., Urinary glycoprotein biomarker discovery for bladder cancer detection using LC/MS-MS and label-free quantification. *Clin Cancer Res* **2011**, *17*, 3349-3359.
341. Zeng, X.; Hood, B.L.; Zhao, T.; Conrads, T.P.; Sun, M.; Gopalakrishnan, V.; Grover, H.; Day, R.S.; Weissfeld, J.L.; Wilson, D.O., *et al.*, Lung cancer serum biomarker discovery using label-free liquid chromatography-tandem mass spectrometry. *J Thorac Oncol* **2011**, *6*, 725-734.
342. Perrin, R.J.; Payton, J.E.; Malone, J.P.; Gilmore, P.; Davis, A.E.; Xiong, C.; Fagan, A.M.; Townsend, R.R.; Holtzman, D.M., Quantitative label-free proteomics for discovery of biomarkers in cerebrospinal fluid: assessment of technical and inter-individual variation. *PLoS One* **2013**, *8*, e64314.
343. Sandin, M.; Chawade, A.; Levander, F., Is label-free LC-MS/MS ready for biomarker discovery? *Proteomics Clin Appl* **2015**, *9*, 289-294.
344. Lemeer, S.; Hahne, H.; Pachl, F.; Kuster, B., Software tools for MS-based quantitative proteomics: a brief overview. *Methods Mol Biol* **2012**, *893*, 489-499.
345. Zaccarin, M.; Falda, M.; Roveri, A.; Bosello-Travain, V.; Bordin, L.; Maiorino, M.; Ursini, F.; Toppo, S., Quantitative label-free redox proteomics of reversible cysteine oxidation in red blood cell membranes. *Free Radic Biol Med* **2014**, *71*, 90-98.
346. Spickett, C.M.; Reis, A.; Pitt, A.R., Use of narrow mass-window, high-resolution extracted product ion chromatograms for the sensitive and selective identification of protein modifications. *Anal Chem* **2013**.
347. Zhu, W.; Smith, J.W.; Huang, C.M., Mass spectrometry-based label-free quantitative proteomics. *J Biomed Biotechnol* **2010**, *2010*, 840518.
348. Hawkridge, A.M.; Muddiman, D.C., Mass spectrometry-based biomarker discovery: toward a global proteome index of individuality. *Annu Rev Anal Chem (Palo Alto Calif)* **2009**, *2*, 265-277.
349. Street, J.M.; Dear, J.W., The application of mass-spectrometry-based protein biomarker discovery to theragnostics. *Br J Clin Pharmacol* **2010**, *69*, 367-378.
350. Winyard, P.G.; Ryan, B.; Eggleton, P.; Nissim, A.; Taylor, E.; Lo Faro, M.L.; Burkholz, T.; Szabo-Taylor, K.E.; Fox, B.; Viner, N., *et al.*, Measurement and meaning of markers of reactive species of oxygen, nitrogen and sulfur in healthy human subjects and patients with inflammatory joint disease. *Biochem Soc Trans* **2011**, *39*, 1226-1232.
351. Thornalley, P.J.; Rabbani, N., Detection of oxidized and glycated proteins in clinical samples using mass spectrometry--a user's perspective. *Biochim Biophys Acta* **2014**, *1840*, 818-829.
352. Colombo, G.; Clerici, M.; Giustarini, D.; Rossi, R.; Milzani, A.; Dalle-Donne, I., Redox albuminomics: oxidized albumin in human diseases. *Antioxid Redox Signal* **2012**, *17*, 1515-1527.
353. Martinez, M.; Weisel, J.W.; Ischiropoulos, H., Functional impact of oxidative posttranslational modifications on fibrinogen and fibrin clots. *Free Radic Biol Med* **2013**, *65*, 411-418.
354. Hui, Y.; Wong, M.; Zhao, S.S.; Love, J.A.; Ansley, D.M.; Chen, D.D., A simple and robust LC-MS/MS method for quantification of free 3-nitrotyrosine in human plasma from patients receiving on-pump CABG surgery. *Electrophoresis* **2012**, *33*, 697-704.
355. Korolainen, M.A.; Nyman, T.A.; Nyyssonen, P.; Hartikainen, E.S.; Pirttila, T., Multiplexed proteomic analysis of oxidation and concentrations of cerebrospinal fluid proteins in Alzheimer disease. *Clin Chem* **2007**, *53*, 657-665.

356. Ahmed, N.; Ahmed, U.; Thornalley, P.J.; Hager, K.; Fleischer, G.; Munch, G., Protein glycation, oxidation and nitration adduct residues and free adducts of cerebrospinal fluid in Alzheimer's disease and link to cognitive impairment. *J Neurochem* **2005**, *92*, 255-263.
357. Radabaugh, M.R.; Nemirovskiy, O.V.; Misko, T.P.; Aggarwal, P.; Mathews, W.R., Immunoaffinity liquid chromatography-tandem mass spectrometry detection of nitrotyrosine in biological fluids: development of a clinically translatable biomarker. *Anal Biochem* **2008**, *380*, 68-76.
358. Bahar, G.; Feinmesser, R.; Shpitzer, T.; Popovtzer, A.; Nagler, R.M., Salivary analysis in oral cancer patients: DNA and protein oxidation, reactive nitrogen species, and antioxidant profile. *Cancer* **2007**, *109*, 54-59.
359. Aydemir, B.; Onaran, I.; Kiziler, A.R.; Alici, B.; Akyolcu, M.C., The influence of oxidative damage on viscosity of seminal fluid in infertile men. *J Androl* **2008**, *29*, 41-46.
360. Perluigi, M.; di Domenico, F.; Fiorini, A.; Cocciolo, A.; Giorgi, A.; Foppoli, C.; Butterfield, D.A.; Giorlandino, M.; Giorlandino, C.; Schinina, M.E., *et al.*, Oxidative stress occurs early in Down syndrome pregnancy: A redox proteomics analysis of amniotic fluid. *Proteomics Clin Appl* **2011**, *5*, 167-178.
361. Canton, M.; Menazza, S.; Sheeran, F.L.; Polverino de Laureto, P.; Di Lisa, F.; Pepe, S., Oxidation of myofibrillar proteins in human heart failure. *J Am Coll Cardiol* **2011**, *57*, 300-309.
362. Lourenco Dos Santos, S.; Baraibar, M.A.; Lundberg, S.; Eeg-Olofsson, O.; Larsson, L.; Friguet, B., Oxidative proteome alterations during skeletal muscle ageing. *Redox Biol* **2015**, *5*, 267-274.
363. Djidja, M.C.; Claude, E.; Snel, M.F.; Francese, S.; Scriven, P.; Carolan, V.; Clench, M.R., Novel molecular tumour classification using MALDI-mass spectrometry imaging of tissue micro-array. *Anal Bioanal Chem* **2010**, *397*, 587-601.
364. Tsikas, D., Analytical methods for 3-nitrotyrosine quantification in biological samples: the unique role of tandem mass spectrometry. *Amino Acids* **2012**, *42*, 45-63.
365. Larstad, M.; Soderling, A.S.; Caidahl, K.; Olin, A.C., Selective quantification of free 3-nitrotyrosine in exhaled breath condensate in asthma using gas chromatography/tandem mass spectrometry. *Nitric Oxide* **2005**, *13*, 134-144.
366. Bajtarevic, A.; Ager, C.; Pienz, M.; Klieber, M.; Schwarz, K.; Ligor, M.; Ligor, T.; Filipiak, W.; Denz, H.; Fiegl, M., *et al.*, Noninvasive detection of lung cancer by analysis of exhaled breath. *BMC Cancer* **2009**, *9*, 348.
367. Pelclova, D.; Fenclova, Z.; Kacer, P.; Kuzma, M.; Navratil, T.; Lebedova, J., Increased 8-isoprostane, a marker of oxidative stress in exhaled breath condensate in subjects with asbestos exposure. *Ind Health* **2008**, *46*, 484-489.
368. Nemirovskiy, O.V.; Radabaugh, M.R.; Aggarwal, P.; Funckes-Shippy, C.L.; Mnich, S.J.; Meyer, D.M.; Sunyer, T.; Rodney Mathews, W.; Misko, T.P., Plasma 3-nitrotyrosine is a biomarker in animal models of arthritis: Pharmacological dissection of iNOS' role in disease. *Nitric Oxide* **2009**, *20*, 150-156.
369. Murdaugh, L.S.; Wang, Z.; Del Priore, L.V.; Dillon, J.; Gaillard, E.R., Age-related accumulation of 3-nitrotyrosine and nitro-A2E in human Bruch's membrane. *Exp Eye Res* **2010**, *90*, 564-571.
370. Madian, A.G.; Regnier, F.E., Profiling carbonylated proteins in human plasma. *J Proteome Res* **2010**, *9*, 1330-1343.
371. Go, Y.M.; Roede, J.R.; Orr, M.; Liang, Y.; Jones, D.P., Integrated redox proteomics and metabolomics of mitochondria to identify mechanisms of cd toxicity. *Toxicol Sci* **2014**, *139*, 59-73.
372. Johnson, J.M.; Strobel, F.H.; Reed, M.; Pohl, J.; Jones, D.P., A rapid LC-FTMS method for the analysis of cysteine, cystine and cysteine/cystine steady-state redox potential in human plasma. *Clin Chim Acta* **2008**, *396*, 43-48.

373. Coon, J.J.; Zurbig, P.; Dakna, M.; Dominiczak, A.F.; Decramer, S.; Fliser, D.; Frommberger, M.; Golovko, I.; Good, D.M.; Herget-Rosenthal, S., *et al.*, CE-MS analysis of the human urinary proteome for biomarker discovery and disease diagnostics. *Proteomics Clin Appl* **2008**, *2*, 964.
374. Li, J.; Yen, C.; Liaw, D.; Podsypanina, K.; Bose, S.; Wang, S.I.; Puc, J.; Miliaresis, C.; Rodgers, L.; McCombie, R., *et al.*, PTEN, a putative protein tyrosine phosphatase gene mutated in human brain, breast, and prostate cancer. *Science* **1997**, *275*, 1943-1947.
375. Furnari, F.B.; Huang, H.J.; Cavenee, W.K., The phosphoinositol phosphatase activity of PTEN mediates a serum-sensitive G1 growth arrest in glioma cells. *Cancer Res* **1998**, *58*, 5002-5008.
376. Song, M.S.; Carracedo, A.; Salmena, L.; Song, S.J.; Egia, A.; Malumbres, M.; Pandolfi, P.P., Nuclear PTEN regulates the APC-CDH1 tumor-suppressive complex in a phosphatase-independent manner. *Cell* **2011**, *144*, 187-199.
377. Delgado-Esteban, M.; Martin-Zanca, D.; Andres-Martin, L.; Almeida, A.; Bolanos, J.P., Inhibition of PTEN by peroxynitrite activates the phosphoinositide-3-kinase/Akt neuroprotective signaling pathway. *J Neurochem* **2007**, *102*, 194-205.
378. Ramaswamy, S.; Nakamura, N.; Vazquez, F.; Batt, D.B.; Perera, S.; Roberts, T.M.; Sellers, W.R., Regulation of G1 progression by the PTEN tumor suppressor protein is linked to inhibition of the phosphatidylinositol 3-kinase/Akt pathway. *Proc Natl Acad Sci U S A* **1999**, *96*, 2110-2115.
379. Wang, S.; Gao, J.; Lei, Q.; Rozengurt, N.; Pritchard, C.; Jiao, J.; Thomas, G.V.; Li, G.; Roy-Burman, P.; Nelson, P.S., *et al.*, Prostate-specific deletion of the murine Pten tumor suppressor gene leads to metastatic prostate cancer. *Cancer Cell* **2003**, *4*, 209-221.
380. Groszer, M.; Erickson, R.; Scripture-Adams, D.D.; Lesche, R.; Trumpp, A.; Zack, J.A.; Kornblum, H.I.; Liu, X.; Wu, H., Negative regulation of neural stem/progenitor cell proliferation by the Pten tumor suppressor gene in vivo. *Science* **2001**, *294*, 2186-2189.
381. Chen, Z.; Trotman, L.C.; Shaffer, D.; Lin, H.K.; Dotan, Z.A.; Niki, M.; Koutcher, J.A.; Scher, H.I.; Ludwig, T.; Gerald, W., *et al.*, Crucial role of p53-dependent cellular senescence in suppression of Pten-deficient tumorigenesis. *Nature* **2005**, *436*, 725-730.
382. Myers, M.P.; Pass, I.; Batty, I.H.; Van der Kaay, J.; Stolarov, J.P.; Hemmings, B.A.; Wigler, M.H.; Downes, C.P.; Tonks, N.K., The lipid phosphatase activity of PTEN is critical for its tumor supressor function. *Proc Natl Acad Sci U S A* **1998**, *95*, 13513-13518.
383. Lee, J.O.; Yang, H.; Georgescu, M.M.; Di Cristofano, A.; Maehama, T.; Shi, Y.; Dixon, J.E.; Pandolfi, P.; Pavletich, N.P., Crystal structure of the PTEN tumor suppressor: implications for its phosphoinositide phosphatase activity and membrane association. *Cell* **1999**, *99*, 323-334.
384. Besson, A.; Robbins, S.M.; Yong, V.W., PTEN/MMAC1/TEP1 in signal transduction and tumorigenesis. *Eur J Biochem* **1999**, *263*, 605-611.
385. Dillon, L.M.; Miller, T.W., Therapeutic targeting of cancers with loss of PTEN function. *Curr Drug Targets* **2014**, *15*, 65-79.
386. Kolmodin, K.; Aqvist, J., The catalytic mechanism of protein tyrosine phosphatases revisited. *FEBS Lett* **2001**, *498*, 208-213.
387. Weibrecht, I.; Bohmer, S.A.; Dagnell, M.; Kappert, K.; Ostman, A.; Bohmer, F.D., Oxidation sensitivity of the catalytic cysteine of the protein-tyrosine phosphatases SHP-1 and SHP-2. *Free Radic Biol Med* **2007**, *43*, 100-110.
388. Di Stefano, P.; Cabodi, S.; Boeri Erba, E.; Margaria, V.; Bergatto, E.; Giuffrida, M.G.; Silengo, L.; Tarone, G.; Turco, E.; Defilippi, P., P130Cas-associated protein

(p140Cap) as a new tyrosine-phosphorylated protein involved in cell spreading. *Mol Biol Cell* **2004**, *15*, 787-800.
389. Lin, M.; Lee, Y.H.; Xu, W.; Baker, M.A.; Aitken, R.J., Ontogeny of tyrosine phosphorylation-signaling pathways during spermatogenesis and epididymal maturation in the mouse. *Biol Reprod* **2006**, *75*, 588-597.
390. Meijer, L.; Azzi, L.; Wang, J.Y., Cyclin B targets p34cdc2 for tyrosine phosphorylation. *EMBO J* **1991**, *10*, 1545-1554.
391. Atherton-Fessler, S.; Hannig, G.; Piwnica-Worms, H., Reversible tyrosine phosphorylation and cell cycle control. *Semin Cell Biol* **1993**, *4*, 433-442.
392. Tonks, N.K., Redox redux: revisiting PTPs and the control of cell signaling. *Cell* **2005**, *121*, 667-670.
393. Mosessian, S.; Avliyakulov, N.K.; Mulholland, D.J.; Boontheung, P.; Loo, J.A.; Wu, H., Analysis of PTEN complex assembly and identification of heterogeneous nuclear ribonucleoprotein C as a component of the PTEN-associated complex. *J Biol Chem* **2009**, *284*, 30159-30166.
394. Mosessian, S.; Wu, H., PTEN-associated complexes: An overview. *Curr Top Biochem Res* **2010**, *12*, 37-42.
395. Vazquez, F.; Grossman, S.R.; Takahashi, Y.; Rokas, M.V.; Nakamura, N.; Sellers, W.R., Phosphorylation of the PTEN tail acts as an inhibitory switch by preventing its recruitment into a protein complex. *J Biol Chem* **2001**, *276*, 48627-48630.
396. Rabinovsky, R.; Pochanard, P.; McNear, C.; Brachmann, S.M.; Duke-Cohan, J.S.; Garraway, L.A.; Sellers, W.R., p85 Associates with unphosphorylated PTEN and the PTEN-associated complex. *Mol Cell Biol* **2009**, *29*, 5377-5388.
397. Malaney, P.; Pathak, R.R.; Xue, B.; Uversky, V.N.; Dave, V., Intrinsic disorder in PTEN and its interactome confers structural plasticity and functional versatility. *Sci Rep* **2013**, *3*, 2035.
398. Shenoy, S.; Shekhar, P.; Heinrich, F.; Daou, M.C.; Gericke, A.; Ross, A.H.; Losche, M., Membrane association of the PTEN tumor suppressor: molecular details of the protein-membrane complex from SPR binding studies and neutron reflection. *PLoS One* **2012**, *7*, e32591.
399. Gericke, A.; Leslie, N.R.; Losche, M.; Ross, A.H., PtdIns(4,5)P2-mediated cell signaling: emerging principles and PTEN as a paradigm for regulatory mechanism. *Adv Exp Med Biol* **2013**, *991*, 85-104.
400. Fink, J.L.; Hamilton, N., DomainDraw: a macromolecular feature drawing program. *In Silico Biol* **2007**, *7*, 145-150.
401. Malaney, P.; Uversky, V.N.; Dave, V., The PTEN Long N-tail is intrinsically disordered: increased viability for PTEN therapy. *Molecular Biosystems* **2013**, *9*, 2877-2888.
402. Yasui, M.; Matsuoka, S.; Ueda, M., PTEN hopping on the cell membrane is regulated via a positively-charged C2 domain. *PLoS Comput Biol* **2014**, *10*, e1003817.
403. Rahdar, M.; Inoue, T.; Meyer, T.; Zhang, J.; Vazquez, F.; Devreotes, P.N., A phosphorylation-dependent intramolecular interaction regulates the membrane association and activity of the tumor suppressor PTEN. *Proc Natl Acad Sci U S A* **2009**, *106*, 480-485.
404. Redfern, R.E.; Redfern, D.; Furgason, M.L.M.; Munson, M.; Ross, A.H.; Gericke, A., PTEN phosphatase selectively binds phosphoinositides and undergoes structural changes. *Biochemistry* **2008**, *47*, 2162-2171.
405. Gil, A.; Andres-Pons, A.; Fernandez, E.; Valiente, M.; Torres, J.; Cervera, J.; Pulido, R., Nuclear localization of PTEN by a Ran-dependent mechanism enhances apoptosis: Involvement of an N-terminal nuclear localization domain and multiple nuclear exclusion motifs. *Mol Biol Cell* **2006**, *17*, 4002-4013.

406. Gil, A.; Rodriguez-Escudero, I.; Stumpf, M.; Molina, M.; Cid, V.J.; Pulido, R., A functional dissection of PTEN N-terminus: implications in PTEN subcellular targeting and tumor suppressor activity. *PLoS One* **2015**, *10*, e0119287.
407. Das, S.; Dixon, J.E.; Cho, W., Membrane-binding and activation mechanism of PTEN. *Proc Natl Acad Sci U S A* **2003**, *100*, 7491-7496.
408. Wei, Y.; Stec, B.; Redfield, A.G.; Weerapana, E.; Roberts, M.F., Phospholipid-binding sites of phosphatase and tensin homolog (PTEN): exploring the mechanism of phosphatidylinositol 4,5-bisphosphate activation. *J Biol Chem* **2015**, *290*, 1592-1606.
409. Andres-Pons, A.; Rodriguez-Escudero, I.; Gil, A.; Blanco, A.; Vega, A.; Molina, M.; Pulido, R.; Cid, V.J., In vivo functional analysis of the counterbalance of hyperactive phosphatidylinositol 3-kinase p110 catalytic oncoproteins by the tumor suppressor PTEN. *Cancer Res* **2007**, *67*, 9731-9739.
410. Yuvaniyama, J.; Denu, J.M.; Dixon, J.E.; Saper, M.A., Crystal structure of the dual specificity protein phosphatase VHR. *Science* **1996**, *272*, 1328-1331.
411. Hlobilkova, A.; Knillova, J.; Bartek, J.; Lukas, J.; Kolar, Z., The mechanism of action of the tumour suppressor gene PTEN. *Biomed Pap Med Fac Univ Palacky Olomouc Czech Repub* **2003**, *147*, 19-25.
412. Denu, J.M.; Dixon, J.E., Protein tyrosine phosphatases: mechanisms of catalysis and regulation. *Curr Opin Chem Biol* **1998**, *2*, 633-641.
413. Myers, M.P.; Stolarov, J.P.; Eng, C.; Li, J.; Wang, S.I.; Wigler, M.H.; Parsons, R.; Tonks, N.K., P-TEN, the tumor suppressor from human chromosome 10q23, is a dual-specificity phosphatase. *Proc Natl Acad Sci U S A* **1997**, *94*, 9052-9057.
414. Barford, D.; Flint, A.J.; Tonks, N.K., Crystal structure of human protein tyrosine phosphatase 1B. *Science* **1994**, *263*, 1397-1404.
415. Rodriguez-Escudero, I.; Oliver, M.D.; Andres-Pons, A.; Molina, M.; Cid, V.J.; Pulido, R., A comprehensive functional analysis of PTEN mutations: implications in tumor- and autism-related syndromes. *Hum Mol Genet* **2011**, *20*, 4132-4142.
416. Georgescu, M.M.; Kirsch, K.H.; Akagi, T.; Shishido, T.; Hanafusa, H., The tumor-suppressor activity of PTEN is regulated by its carboxyl-terminal region. *Proc Natl Acad Sci U S A* **1999**, *96*, 10182-10187.
417. Okumura, K.; Mendoza, M.; Bachoo, R.M.; DePinho, R.A.; Cavenee, W.K.; Furnari, F.B., PCAF modulates PTEN activity. *J Biol Chem* **2006**, *281*, 26562-26568.
418. Jia, Z.; Barford, D.; Flint, A.J.; Tonks, N.K., Structural basis for phosphotyrosine peptide recognition by protein tyrosine phosphatase 1B. *Science* **1995**, *268*, 1754-1758.
419. Hollander, M.C.; Blumenthal, G.M.; Dennis, P.A., PTEN loss in the continuum of common cancers, rare syndromes and mouse models (vol 11, pg 289, 2011). *Nat Rev Cancer* **2011**, *11*, 458-458.
420. Xu, J.; Li, Z.; Wang, J.; Chen, H.; Fang, J.Y., Combined PTEN mutation and protein expression associate with overall and disease-free survival of glioblastoma patients. *Transl Oncol* **2014**, *7*, 196-205 e191.
421. Shenoy, S.S.; Nanda, H.; Losche, M., Membrane association of the PTEN tumor suppressor: electrostatic interaction with phosphatidylserine-containing bilayers and regulatory role of the C-terminal tail. *J Struct Biol* **2012**, *180*, 394-408.
422. Campbell, R.B.; Liu, F.; Ross, A.H., Allosteric activation of PTEN phosphatase by phosphatidylinositol 4,5-bisphosphate. *J Biol Chem* **2003**, *278*, 33617-33620.
423. Lee, S.R.; Yang, K.S.; Kwon, J.; Lee, C.; Jeong, W.; Rhee, S.G., Reversible inactivation of the tumor suppressor PTEN by H2O2. *J Biol Chem* **2002**, *277*, 20336-20342.
424. Gonzalez-Santamaria, J.; Campagna, M.; Ortega-Molina, A.; Marcos-Villar, L.; de la Cruz-Herrera, C.F.; Gonzalez, D.; Gallego, P.; Lopitz-Otsoa, F.; Esteban, M.; Rodriguez, M.S., *et al.*, Regulation of the tumor suppressor PTEN by SUMO. *Cell Death Dis* **2012**, *3*, e393.

425. Bassi, C., Nuclear PTEN controls DNA repair and sensitivity to genotoxic stress (vol 341, pg 395, 2013). *Science* **2013**, *341*, 1064-1064.
426. Koul, D.; Jasser, S.A.; Lu, Y.L.; Davies, M.A.; Shen, R.J.; Shi, Y.X.; Mills, G.B.; Yung, W.K.A., Motif analysis of the tumor suppressor gene MMAC/PTEN identifies tyrosines critical for tumor suppression and lipid phosphatase activity. *Oncogene* **2002**, *21*, 2357-2364.
427. Salmena, L.; Carracedo, A.; Pandolfi, P.P., Tenets of PTEN tumor suppression. *Cell* **2008**, *133*, 403-414.
428. Vazquez, F.; Ramaswamy, S.; Nakamura, N.; Sellers, W.R., Phosphorylation of the PTEN tail regulates protein stability and function. *Mol Cell Biol* **2000**, *20*, 5010-5018.
429. Hopkins, B.D.; Hodakoski, C.; Barrows, D.; Mense, S.M.; Parsons, R.E., PTEN function: the long and the short of it. *Trends Biochem Sci* **2014**, *39*, 183-190.
430. Maccario, H.; Perera, N.M.; Davidson, L.; Downes, C.P.; Leslie, N.R., PTEN is destabilized by phosphorylation on Thr366. *Biochem J* **2007**, *405*, 439-444.
431. Xu, D.; Yao, Y.; Jiang, X.; Lu, L.; Dai, W., Regulation of PTEN stability and activity by Plk3. *J Biol Chem* **2010**, *285*, 39935-39942.
432. Torres, J.; Pulido, R., The tumor suppressor PTEN is phosphorylated by the protein kinase CK2 at its C terminus. Implications for PTEN stability to proteasome-mediated degradation. *J Biol Chem* **2001**, *276*, 993-998.
433. Bolduc, D.; Rahdar, M.; Tu-Sekine, B.; Sivakumaren, S.C.; Raben, D.; Amzel, L.M.; Devreotes, P.; Gabelli, S.B.; Cole, P., Phosphorylation-mediated PTEN conformational closure and deactivation revealed with protein semisynthesis. *Elife* **2013**, *2*, e00691.
434. Tibarewal, P.; Zilidis, G.; Spinelli, L.; Schurch, N.; Maccario, H.; Gray, A.; Perera, N.M.; Davidson, L.; Barton, G.J.; Leslie, N.R., PTEN protein phosphatase activity correlates with control of gene expression and invasion, a tumor-suppressing phenotype, but not with AKT activity. *Sci Signal* **2012**, *5*, ra18.
435. Odriozola, L.; Singh, G.; Hoang, T.; Chan, A.M., Regulation of PTEN activity by its carboxyl-terminal autoinhibitory domain. *J Biol Chem* **2007**, *282*, 23306-23315.
436. Ross, A.H.; Gericke, A., Phosphorylation keeps PTEN phosphatase closed for business. *Proc Natl Acad Sci U S A* **2009**, *106*, 1297-1298.
437. Subauste, M.C.; Nalbant, P.; Adamson, E.D.; Hahn, K.M., Vinculin controls PTEN protein level by maintaining the interaction of the adherens junction protein beta-catenin with the scaffolding protein MAGI-2. *J Biol Chem* **2005**, *280*, 5676-5681.
438. Ikenoue, T.; Inoki, K.; Zhao, B.; Guan, K.L., PTEN acetylation modulates its interaction with PDZ domain. *Cancer Res* **2008**, *68*, 6908-6912.
439. Kitagishi, Y.; Matsuda, S., Redox regulation of tumor suppressor PTEN in cancer and aging (Review). *Int J Mol Med* **2013**, *31*, 511-515.
440. Yamada, K.M.; Araki, M., Tumor suppressor PTEN: modulator of cell signaling, growth, migration and apoptosis. *J Cell Sci* **2001**, *114*, 2375-2382.
441. Ming, M.; He, Y.Y., PTEN in DNA damage repair. *Cancer Lett* **2012**, *319*, 125-129.
442. DeFeo-Jones, D.; Barnett, S.F.; Fu, S.; Hancock, P.J.; Haskell, K.M.; Leander, K.R.; McAvoy, E.; Robinson, R.G.; Duggan, M.E.; Lindsley, C.W., *et al.*, Tumor cell sensitization to apoptotic stimuli by selective inhibition of specific Akt/PKB family members. *Mol Cancer Ther* **2005**, *4*, 271-279.
443. Whiteman, E.L.; Cho, H.; Birnbaum, M.J., Role of Akt/protein kinase B in metabolism. *Trends Endocrinol Metab* **2002**, *13*, 444-451.
444. Hemmings, B.A.; Restuccia, D.F., PI3K-PKB/Akt pathway. *Cold Spring Harb Perspect Biol* **2012**, *4*, a011189.
445. Georgescu, M.M., PTEN tumor suppressor network in PI3K-Akt pathway control. *Genes Cancer* **2010**, *1*, 1170-1177.

446. Ma, K.; Cheung, S.M.; Marshall, A.J.; Duronio, V., PI(3,4,5)P3 and PI(3,4)P2 levels correlate with PKB/akt phosphorylation at Thr308 and Ser473, respectively; PI(3,4)P2 levels determine PKB activity. *Cell Signal* **2008**, *20*, 684-694.
447. Persad, S.; Attwell, S.; Gray, V.; Mawji, N.; Deng, J.T.; Leung, D.; Yan, J.; Sanghera, J.; Walsh, M.P.; Dedhar, S., Regulation of protein kinase B/Akt-serine 473 phosphorylation by integrin-linked kinase: critical roles for kinase activity and amino acids arginine 211 and serine 343. *J Biol Chem* **2001**, *276*, 27462-27469.
448. Hresko, R.C.; Mueckler, M., mTOR.RICTOR is the Ser473 kinase for Akt/protein kinase B in 3T3-L1 adipocytes. *J Biol Chem* **2005**, *280*, 40406-40416.
449. Lee, S.L.; Chou, C.C.; Chuang, H.C.; Hsu, E.C.; Chiu, P.C.; Kulp, S.K.; Byrd, J.C.; Chen, C.S., Functional role of mTORC2 versus integrin-linked kinase in mediating Ser473-Akt phosphorylation in PTEN-negative prostate and breast cancer cell lines. *PLoS One* **2013**, *8*, e67149.
450. Datta, S.R.; Brunet, A.; Greenberg, M.E., Cellular survival: a play in three Akts. *Genes Dev* **1999**, *13*, 2905-2927.
451. Hahn-Windgassen, A.; Nogueira, V.; Chen, C.C.; Skeen, J.E.; Sonenberg, N.; Hay, N., Akt activates the mammalian target of rapamycin by regulating cellular ATP level and AMPK activity. *J Biol Chem* **2005**, *280*, 32081-32089.
452. Mamane, Y.; Petroulakis, E.; LeBacquer, O.; Sonenberg, N., MTOR, translation initiation and cancer. *Oncogene* **2006**, *25*, 6416-6422.
453. Cantley, L.C.; Neel, B.G., New insights into tumor suppression: PTEN suppresses tumor formation by restraining the phosphoinositide 3-kinase/AKT pathway. *Proc Natl Acad Sci U S A* **1999**, *96*, 4240-4245.
454. Tamguney, T.; Stokoe, D., New insights into PTEN. *J Cell Sci* **2007**, *120*, 4071-4079.
455. Yin, Y.; Shen, W.H., PTEN: a new guardian of the genome. *Oncogene* **2008**, *27*, 5443-5453.
456. Freeman, D.J.; Li, A.G.; Wei, G.; Li, H.H.; Kertesz, N.; Lesche, R.; Whale, A.D.; Martinez-Diaz, H.; Rozengurt, N.; Cardiff, R.D., *et al.*, PTEN tumor suppressor regulates p53 protein levels and activity through phosphatase-dependent and -independent mechanisms. *Cancer Cell* **2003**, *3*, 117-130.
457. Mayo, L.D.; Donner, D.B., The PTEN, Mdm2, p53 tumor suppressor-oncoprotein network. *Trends Biochem Sci* **2002**, *27*, 462-467.
458. Wu, H.; Goel, V.; Haluska, F.G., PTEN signaling pathways in melanoma. *Oncogene* **2003**, *22*, 3113-3122.
459. Tamura, M.; Gu, J.; Takino, T.; Yamada, K.M., Tumor suppressor PTEN inhibition of cell invasion, migration, and growth: differential involvement of focal adhesion kinase and p130Cas. *Cancer Res* **1999**, *59*, 442-449.
460. Teresi, R.E.; Waite, K.A., PPAR gamma, PTEN, and the fight against cancer. *Ppar Research* **2008**.
461. Krueger, J.S.; Keshamouni, V.G.; Atanaskova, N.; Reddy, K.B., Temporal and quantitative regulation of mitogen-activated protein kinase (MAPK) modulates cell motility and invasion. *Oncogene* **2001**, *20*, 4209-4218.
462. McCubrey, J.A.; Steelman, L.S.; Chappell, W.H.; Abrams, S.L.; Wong, E.W.; Chang, F.; Lehmann, B.; Terrian, D.M.; Milella, M.; Tafuri, A., *et al.*, Roles of the Raf/MEK/ERK pathway in cell growth, malignant transformation and drug resistance. *Biochim Biophys Acta* **2007**, *1773*, 1263-1284.
463. Weng, L.P.; Smith, W.M.; Brown, J.L.; Eng, C., PTEN inhibits insulin-stimulated MEK/MAPK activation and cell growth by blocking IRS-1 phosphorylation and IRS-1/Grb-2/Sos complex formation in a breast cancer model. *Hum Mol Genet* **2001**, *10*, 605-616.
464. Papakonstanti, E.A.; Ridley, A.J.; Vanhaesebroeck, B., The p110delta isoform of PI 3-kinase negatively controls RhoA and PTEN. *EMBO J* **2007**, *26*, 3050-3061.

465. Cao, J.X.; Wan, L.X.; Hacker, E.; Dai, X.P.; Lenna, S.; Jimenez-Cervantes, C.; Wang, Y.J.; Leslie, N.R.; Xu, G.X.; Widlund, H.R., *et al.*, MC1R Is a potent regulator of PTEN after UV exposure in melanocytes. *Mol Cell* **2013**, *51*, 409-422.
466. Yim, E.K.; Peng, G.; Dai, H.; Hu, R.Z.; Li, K.Y.; Lu, W.; Mills, G.B.; Meric-Bernstam, F.; Hennessy, B.T.; Craven, R.J., *et al.*, Rak functions as a tumor suppressor by regulating pten protein stability and function. *Cancer Cell* **2009**, *15*, 304-314.
467. Okahara, F.; Ikawa, H.; Kanaho, Y.; Maehama, T., Regulation of PTEN phosphorylation and stability by a tumor suppressor candidate protein. *J Biol Chem* **2004**, *279*, 45300-45303.
468. Wu, X.; Hepner, K.; Castelino-Prabhu, S.; Do, D.; Kaye, M.B.; Yuan, X.J.; Wood, J.; Ross, C.; Sawyers, C.L.; Whang, Y.E., Evidence for regulation of the PTEN tumor suppressor by a membrane-localized multi-PDZ domain containing scaffold protein MAGI-2. *Proc Natl Acad Sci U S A* **2000**, *97*, 4233-4238.
469. Hu, Y.; Li, Z.; Guo, L.; Wang, L.; Zhang, L.; Cai, X.; Zhao, H.; Zha, X., MAGI-2 Inhibits cell migration and proliferation via PTEN in human hepatocarcinoma cells. *Arch Biochem Biophys* **2007**, *467*, 1-9.
470. Chagpar, R.B.; Links, P.H.; Pastor, M.C.; Furber, L.A.; Hawrysh, A.D.; Chamberlain, M.D.; Anderson, D.H., Direct positive regulation of PTEN by the p85 subunit of phosphatidylinositol 3-kinase. *Proc Natl Acad Sci U S A* **2010**, *107*, 5471-5476.
471. Tang, Y.; Eng, C., PTEN autoregulates its expression by stabilization of p53 in a phosphatase-independent manner. *Cancer Res* **2006**, *66*, 736-742.
472. Stambolic, V.; MacPherson, D.; Sas, D.; Lin, Y.; Snow, B.; Jang, Y.; Benchimol, S.; Mak, T.W., Regulation of PTEN transcription by p53. *Mol Cell* **2001**, *8*, 317-325.
473. Fine, B.; Hodakoski, C.; Koujak, S.; Su, T.; Saal, L.H.; Maurer, M.; Hopkins, B.; Keniry, M.; Sulis, M.L.; Mense, S., *et al.*, Activation of the PI3K pathway in cancer through inhibition of PTEN by exchange factor P-REX2a. *Science* **2009**, *325*, 1261-1265.
474. He, L.; Ingram, A.; Rybak, A.P.; Tang, D., Shank-interacting protein-like 1 promotes tumorigenesis via PTEN inhibition in human tumor cells. *J Clin Invest* **2010**, *120*, 2094-2108.
475. Kim, R.H.; Peters, M.; Jang, Y.J.; Shi, W.; Pintilie, M.; Fletcher, G.C.; DeLuca, C.; Liepa, J.; Zhou, L.; Snow, B., *et al.*, DJ-1, a novel regulator of the tumor suppressor PTEN. *Cancer Cell* **2005**, *7*, 263-273.
476. Miller, F.J., Jr., NADPH oxidase 4: walking the walk with Poldip2. *Circ Res* **2009**, *105*, 209-210.
477. Leslie, N.R.; Bennett, D.; Lindsay, Y.E.; Stewart, H.; Gray, A.; Downes, C.P., Redox regulation of PI 3-kinase signalling via inactivation of PTEN. *EMBO J* **2003**, *22*, 5501-5510.
478. Meuillet, E.J.; Mahadevan, D.; Berggren, M.; Coon, A.; Powis, G., Thioredoxin-1 binds to the C2 domain of PTEN inhibiting PTEN's lipid phosphatase activity and membrane binding: a mechanism for the functional loss of PTEN's tumor suppressor activity. *Arch Biochem Biophys* **2004**, *429*, 123-133.
479. Cao, J.; Schulte, J.; Knight, A.; Leslie, N.R.; Zagozdzon, A.; Bronson, R.; Manevich, Y.; Beeson, C.; Neumann, C.A., Prdx1 inhibits tumorigenesis via regulating PTEN/AKT activity. *EMBO J* **2009**, *28*, 1505-1517.
480. Neumann, C.A.; Cao, J.; Manevich, Y., Peroxiredoxin 1 and its role in cell signaling. *Cell Cycle* **2009**, *8*, 4072-4078.
481. Kim, Y.C.; Kitaura, H.; Taira, T.; Iguchi-Ariga, S.M.; Ariga, H., Oxidation of DJ-1-dependent cell transformation through direct binding of DJ-1 to PTEN. *Int J Oncol* **2009**, *35*, 1331-1341.
482. Numajiri, N.; Takasawa, K.; Nishiya, T.; Tanaka, H.; Ohno, K.; Hayakawa, W.; Asada, M.; Matsuda, H.; Azumi, K.; Kamata, H., *et al.*, On-off system for PI3-kinase-

Akt signaling through S-nitrosylation of phosphatase with sequence homology to tensin (PTEN). *Proc Natl Acad Sci U S A* **2011**, *108*, 10349-10354.

483. Perkins, D.N.; Pappin, D.J.; Creasy, D.M.; Cottrell, J.S., Probability-based protein identification by searching sequence databases using mass spectrometry data. *Electrophoresis* **1999**, *20*, 3551-3567.
484. Sugiyama, S.; Okada, Y.; Sukhova, G.K.; Virmani, R.; Heinecke, J.W.; Libby, P., Macrophage myeloperoxidase regulation by granulocyte macrophage colony-stimulating factor in human atherosclerosis and implications in acute coronary syndromes. *Am J Pathol* **2001**, *158*, 879-891.
485. Pitt, A.R.; Spickett, C.M., Mass spectrometric analysis of HOCl- and free-radical-induced damage to lipids and proteins. *Biochem Soc Trans* **2008**, *36*, 1077-1082.
486. Whiteman, M.; Hooper, D.C.; Scott, G.S.; Koprowski, H.; Halliwell, B., Inhibition of hypochlorous acid-induced cellular toxicity by nitrite. *Proc Natl Acad Sci U S A* **2002**, *99*, 12061-12066.
487. Hampton, M.B.; Kettle, A.J.; Winterbourn, C.C., Inside the neutrophil phagosome: oxidants, myeloperoxidase, and bacterial killing. *Blood* **1998**, *92*, 3007-3017.
488. Mutze, S.; Hebling, U.; Stremmel, W.; Wang, J.; Arnhold, J.; Pantopoulos, K.; Mueller, S., Myeloperoxidase-derived hypochlorous acid antagonizes the oxidative stress-mediated activation of iron regulatory protein 1. *J Biol Chem* **2003**, *278*, 40542-40549.
489. Winterbourn, C.C.; Hampton, M.B.; Livesey, J.H.; Kettle, A.J., Modeling the reactions of superoxide and myeloperoxidase in the neutrophil phagosome: implications for microbial killing. *J Biol Chem* **2006**, *281*, 39860-39869.
490. Frei, B., *Natural antioxidants in human health and disease*. Academic Press: San Diego, 1994; p xxviii, 588 p., 9780122669750 (alk. paper).
491. Harrison, J.E.; Schultz, J., Studies on the chlorinating activity of myeloperoxidase. *J Biol Chem* **1976**, *251*, 1371-1374.
492. Prokopowicz, Z.M.; Arce, F.; Biedron, R.; Chiang, C.L.; Ciszek, M.; Katz, D.R.; Nowakowska, M.; Zapotoczny, S.; Marcinkiewicz, J.; Chain, B.M., Hypochlorous acid: a natural adjuvant that facilitates antigen processing, cross-priming, and the induction of adaptive immunity. *J Immunol* **2010**, *184*, 824-835.
493. Zhu, L.X.; Pi, J.B.; Wachi, S.; Andersen, M.E.; Wu, R.E.; Chen, Y., Identification of Nrf2-dependent airway epithelial adaptive response to proinflammatory oxidant-hypochlorous acid challenge by transcription profiling. *Am J Physiol* **2008**, *294*, L469-L477.
494. Curtis, M.P.; Hicks, A.J.; Neidigh, J.W., Kinetics of 3-chlorotyrosine formation and loss due to hypochlorous acid and chloramines. *Chem Res Toxicol* **2011**, *24*, 418-428.
495. Pattison, D.I.; Davies, M.J., Absolute rate constants for the reaction of hypochlorous acid with protein side chains and peptide bonds. *Chem Res Toxicol* **2001**, *14*, 1453-1464.
496. Pryor, W.A., *Bio-assays for oxidative stress status (BOSS)*. 1st ed.; Elsevier: New York, 2001; p ix, 286 p., 9780444509574.
497. Kang, J.I., Jr.; Neidigh, J.W., Hypochlorous acid damages histone proteins forming 3-chlorotyrosine and 3,5-dichlorotyrosine. *Chem Res Toxicol* **2008**, *21*, 1028-1038.
498. Sochaski, M.A.; Jarabek, A.M.; Murphy, J.; Andersen, M.E., 3-chlorotyrosine and 3,5-dichlorotyrosine as biomarkers of respiratory tract exposure to chlorine gas. *J Anal Toxicol* **2008**, *32*, 99-105.
499. Westman, E.; Lundberg, K.; Erlandsson Harris, H., Arthritogenicity of collagen type II is increased by chlorination. *Clin Exp Immunol* **2006**, *145*, 339-345.
500. Chapman, A.L.; Winterbourn, C.C.; Brennan, S.O.; Jordan, T.W.; Kettle, A.J., Characterization of non-covalent oligomers of proteins treated with hypochlorous acid. *Biochem J* **2003**, *375*, 33-40.

501. Hazell, L.J.; Vandenberg, J.J.M.; Stocker, R., Oxidation of low-density-lipoprotein by hypochlorite causes aggregation that is mediated by modification of lysine residues rather than lipid oxidation. *Biochem J* **1994**, *302*, 297-304.
502. McKenzie, S.J.; Baker, M.S.; Buffinton, G.D.; Doe, W.F., Evidence of oxidant-induced injury to epithelial cells during inflammatory bowel disease. *J Clin Invest* **1996**, *98*, 136-141.
503. Grone, H.J.; Grone, E.F.; Malle, E., Immunohistochemical detection of hypochlorite-modified proteins in glomeruli of human membranous glomerulonephritis. *Lab Invest* **2002**, *82*, 5-14.
504. Mutze, S.; Hebling, U.; Stremmel, W.; Wang, J.; Arnhold, J.; Pantopoulos, K.; Mueller, S., Myeloperoxidase-derived hypochlorous acid antagonizes the oxidative stress-mediated activation of iron regulatory protein 1 (vol 278, pg 40542, 2003). *J Biol Chem* **2003**, *278*, 49662-49662.
505. Herdener, M.; Heigold, S.; Saran, M.; Bauer, G., Target cell-derived superoxide anions cause efficiency and selectivity of intercellular induction of apoptosis. *Free Radic Biol Med* **2000**, *29*, 1260-1271.
506. Vile, G.F.; Rothwell, L.A.; Kettle, A.J., Hypochlorous acid activates the tumor suppressor protein p53 in cultured human skin fibroblasts. *Arch Biochem Biophys* **1998**, *359*, 51-56.
507. Midwinter, R.G.; Vissers, M.C.; Winterbourn, C.C., Hypochlorous acid stimulation of the mitogen-activated protein kinase pathway enhances cell survival. *Arch Biochem Biophys* **2001**, *394*, 13-20.
508. Witze, E.S.; Old, W.M.; Resing, K.A.; Ahn, N.G., Mapping protein post-translational modifications with mass spectrometry. *Nat Methods* **2007**, *4*, 798-806.
509. Kumar, Y.; Liang, C.; Bo, Z.; Rajapakse, J.C.; Ooi, E.E.; Tannenbaum, S.R., Serum proteome and cytokine analysis in a longitudinal cohort of adults with primary dengue infection reveals predictive markers of DHF. *PLoS Negl Trop Dis* **2012**, *6*, e1887.
510. Mocatta, T.J.; Pilbrow, A.P.; Cameron, V.A.; Senthilmohan, R.; Frampton, C.M.; Richards, A.M.; Winterbourn, C.C., Plasma concentrations of myeloperoxidase predict mortality after myocardial infarction. *J Am Coll Cardiol* **2007**, *49*, 1993-2000.
511. Bergt, C.; Fu, X.; Huq, N.P.; Kao, J.; Heinecke, J.W., Lysine residues direct the chlorination of tyrosines in YXXK motifs of apolipoprotein A-I when hypochlorous acid oxidizes high density lipoprotein. *J Biol Chem* **2004**, *279*, 7856-7866.
512. Khor, H.K.; Fisher, M.T.; Schoneich, C., Potential role of methionine sulfoxide in the inactivation of the chaperone GroEL by hypochlorous acid (HOCl) and peroxynitrite (ONOO-). *J Biol Chem* **2004**, *279*, 19486-19493.
513. Schneider, C.A.; Rasband, W.S.; Eliceiri, K.W., NIH Image to ImageJ: 25 years of image analysis. *Nat Methods* **2012**, *9*, 671-675.
514. Petersen, B.; Petersen, T.N.; Andersen, P.; Nielsen, M.; Lundegaard, C., A generic method for assignment of reliability scores applied to solvent accessibility predictions. *BMC Struct Biol* **2009**, *9*, 51.
515. McKenna, S.M.; Davies, K.J., The inhibition of bacterial growth by hypochlorous acid. Possible role in the bactericidal activity of phagocytes. *Biochem J* **1988**, *254*, 685-692.
516. Fu, X.; Kassim, S.Y.; Parks, W.C.; Heinecke, J.W., Hypochlorous acid oxygenates the cysteine switch domain of pro-matrilysin (MMP-7). A mechanism for matrix metalloproteinase activation and atherosclerotic plaque rupture by myeloperoxidase. *J Biol Chem* **2001**, *276*, 41279-41287.
517. Fabjan, J.S.; Abuja, P.M.; Schaur, R.J.; Sevanian, A., Hypochlorite induces the formation of LDL-, a potentially atherogenic low density lipoprotein subspecies. *FEBS Lett* **2001**, *499*, 69-72.
518. Hoshi, T.; Heinemann, S., Regulation of cell function by methionine oxidation and reduction. *J Physiol* **2001**, *531*, 1-11.

519. Levine, R.L.; Moskovitz, J.; Stadtman, E.R., Oxidation of methionine in proteins: Roles in antioxidant defense and cellular regulation. *Iubmb Life* **2000**, *50*, 301-307.
520. Scala, S.; Bruni, P.; Lo Muzio, L.; Mignogna, M.; Viglietto, G.; Fusco, A., Novel mutation of the PTEN gene in an Italian Cowden's disease kindred. *Int J Oncol* **1998**, *13*, 665-668.
521. Bindoli, A.; Fukuto, J.M.; Forman, H.J., Thiol chemistry in peroxidase catalysis and redox signaling. *Antioxid Redox Signal* **2008**, *10*, 1549-1564.
522. Conte, M.; Carroll, K., The chemistry of thiol oxidation and detection. In *Oxidative Stress and Redox Regulation*, Jakob, U.; Reichmann, D., Eds. Springer: New York 2013; pp 1-42.
523. Steinbeck, M.J.; Nesti, L.J.; Sharkey, P.F.; Parvizi, J., Myeloperoxidase and chlorinated-peptides in osteoarthritis: Potential biomarkers of the disease. *J Bone Miner Res* **2006**, *21*, S144-S144.
524. Buss, I.H.; Senthilmohan, R.; Darlow, B.A.; Mogridge, N.; Kettle, A.J.; Winterbourn, C.C., 3-Chlorotyrosine as a marker of protein damage by myeloperoxidase in tracheal aspirates from preterm infants: association with adverse respiratory outcome. *Pediatr Res* **2003**, *53*, 455-462.
525. Maddika, S.; Kavela, S.; Rani, N.; Palicharla, V.R.; Pokorny, J.L.; Sarkaria, J.N.; Chen, J., WWP2 is an E3 ubiquitin ligase for PTEN. *Nat Cell Biol* **2011**, *13*, 728-733.
526. Valiente, M.; Andres-Pons, A.; Gomar, B.; Torres, J.; Gil, A.; Tapparel, C.; Antonarakis, S.E.; Pulido, R., Binding of PTEN to specific PDZ domains contributes to PTEN protein stability and phosphorylation by microtubule-associated serine/threonine kinases. *J Biol Chem* **2005**, *280*, 28936-28943.
527. Naguib, A.; Bencze, G.; Cho, H.; Zheng, W.; Tocilj, A.; Elkayam, E.; Faehnle, C.R.; Jaber, N.; Pratt, C.P.; Chen, M.H., *et al.*, PTEN functions by recruitment to cytoplasmic vesicles. *Mol Cell* **2015**, *58*, 255-268.
528. Georgescu, M.M.; Kirsch, K.H.; Kaloudis, P.; Yang, H.; Pavletich, N.P.; Hanafusa, H., Stabilization and productive positioning roles of the C2 domain of PTEN tumor suppressor. *Cancer Res* **2000**, *60*, 7033-7038.
529. Levine, R.L.; Berlett, B.S.; Moskovitz, J.; Mosoni, L.; Stadtman, E.R., Methionine residues may protect proteins from critical oxidative damage. *Mech Ageing Dev* **1999**, *107*, 323-332.
530. Fu, X.; Chen, J.; Gallagher, R.; Zheng, Y.; Chung, D.W.; Lopez, J.A., Shear stress-induced unfolding of VWF accelerates oxidation of key methionine residues in the A1A2A3 region. *Blood* **2011**, *118*, 5283-5291.
531. Torosantucci, R.; Mozziconacci, O.; Sharov, V.; Schoneich, C.; Jiskoot, W., Chemical modifications in aggregates of recombinant human insulin induced by metal-catalyzed oxidation: covalent cross-linking via michael addition to tyrosine oxidation products. *Pharm Res* **2012**, *29*, 2276-2293.
532. Luo, Q.; Joubert, M.K.; Stevenson, R.; Ketchem, R.R.; Narhi, L.O.; Wypych, J., Chemical modifications in therapeutic protein aggregates generated under different stress conditions. *J Biol Chem* **2011**, *286*, 25134-25144.
533. Samson, A.L.; Knaupp, A.S.; Kass, I.; Kleifeld, O.; Marijanovic, E.M.; Hughes, V.A.; Lupton, C.J.; Buckle, A.M.; Bottomley, S.P.; Medcalf, R.L., Oxidation of an exposed methionine instigates the aggregation of glyceraldehyde-3-phosphate dehydrogenase. *J Biol Chem* **2014**, *289*, 26922-26936.
534. Tornvall, U., Pinpointing oxidative modifications in proteins-recent advances in analytical methods. *Anal Methods* **2010**, *2*, 1638-1650.
535. Archakov, A.I.; Govorun, V.M.; Dubanov, A.V.; Ivanov, Y.D.; Veselovsky, A.V.; Lewi, P.; Janssen, P., Protein-protein interactions as a target for drugs in proteomics. *Proteomics* **2003**, *3*, 380-391.
536. Ryan, D.P.; Matthews, J.M., Protein-protein interactions in human disease. *Curr Opin Struct Biol* **2005**, *15*, 441-446.

537. Li, J.; Tanhehco, E.J.; Russell, B., Actin dynamics is rapidly regulated by the PTEN and PIP2 signaling pathways leading to myocyte hypertrophy. *Am J Physiol Heart Circ Physiol* **2014**, *307*, H1618-1625.
538. Kolsch, V.; Charest, P.G.; Firtel, R.A., The regulation of cell motility and chemotaxis by phospholipid signaling. *J Cell Sci* **2008**, *121*, 551-559.
539. Tamura, M.; Gu, J.; Danen, E.H.; Takino, T.; Miyamoto, S.; Yamada, K.M., PTEN interactions with focal adhesion kinase and suppression of the extracellular matrix-dependent phosphatidylinositol 3-kinase/Akt cell survival pathway. *J Biol Chem* **1999**, *274*, 20693-20703.
540. Gorbenko, O.; Panayotou, G.; Zhyvoloup, A.; Volkova, D.; Gout, I.; Filonenko, V., Identification of novel PTEN-binding partners: PTEN interaction with fatty acid binding protein FABP4. *Mol Cell Biochem* **2010**, *337*, 299-305.
541. Gunaratne, J.; Goh, M.X.; Swa, H.L.; Lee, F.Y.; Sanford, E.; Wong, L.M.; Hogue, K.A.; Blackstock, W.P.; Okumura, K., Protein interactions of phosphatase and tensin homologue (PTEN) and its cancer-associated G20E mutant compared by using stable isotope labeling by amino acids in cell culture-based parallel affinity purification. *J Biol Chem* **2011**, *286*, 18093-18103.
542. Rawat, S.J.; Creasy, C.L.; Peterson, J.R.; Chernoff, J., The tumor suppressor Mst1 promotes changes in the cellular redox state by phosphorylation and inactivation of peroxiredoxin-1 protein. *J Biol Chem* **2013**, *288*, 8762-8771.
543. Vermeulen, M.; Hubner, N.C.; Mann, M., High confidence determination of specific protein-protein interactions using quantitative mass spectrometry. *Curr Opin Biotechnol* **2008**, *19*, 331-337.
544. Zhu, X.; Qin, X.; Fei, M.; Hou, W.; Greshock, J.; Bachman, K.E.; Wooster, R.; Kang, J.; Qin, C.Y., Combined phosphatase and tensin homolog (PTEN) loss and fatty acid synthase (FAS) overexpression worsens the prognosis of chinese patients with hepatocellular carcinoma. *Int J Mol Sci* **2012**, *13*, 9980-9991.
545. Kumar, C.; Mann, M., Bioinformatics analysis of mass spectrometry-based proteomics data sets. *FEBS Lett* **2009**, *583*, 1703-1712.
546. Nguyen, H.N.; Yang, J.M.; Miyamoto, T.; Itoh, K.; Rho, E.; Zhang, Q.; Inoue, T.; Devreotes, P.N.; Sesaki, H.; Iijima, M., Opening the conformation is a master switch for the dual localization and phosphatase activity of PTEN. *Sci Rep* **2015**, *5*, 12600.
547. Kim, J.S.; Xu, X.; Li, H.; Solomon, D.; Lane, W.S.; Jin, T.; Waldman, T., Mechanistic analysis of a DNA damage-induced, PTEN-dependent size checkpoint in human cells. *Mol Cell Biol* **2011**, *31*, 2756-2771.
548. McCabe, N.; Hanna, C.; Walker, S.M.; Gonda, D.; Li, J.; Wikstrom, K.; Savage, K.I.; Butterworth, K.T.; Chen, C.; Harkin, D.P., *et al.*, Mechanistic rationale to target PTEN-deficient tumor cells with inhibitors of the DNA damage response kinase ATM. *Cancer Res* **2015**, *75*, 2159-2165.
549. Mereniuk, T.R.; El Gendy, M.A.; Mendes-Pereira, A.M.; Lord, C.J.; Ghosh, S.; Foley, E.; Ashworth, A.; Weinfeld, M., Synthetic lethal targeting of PTEN-deficient cancer cells using selective disruption of polynucleotide kinase/phosphatase. *Mol Cancer Ther* **2013**, *12*, 2135-2144.
550. Crockett, D.K.; Fillmore, G.C.; Elenitoba-Johnson, K.S.; Lim, M.S., Analysis of phosphatase and tensin homolog tumor suppressor interacting proteins by in vitro and in silico proteomics. *Proteomics* **2005**, *5*, 1250-1262.
551. Ahn, Y.; Hwang, C.Y.; Lee, S.R.; Kwon, K.S.; Lee, C., The tumour suppressor PTEN mediates a negative regulation of the E3 ubiquitin-protein ligase Nedd4. *Biochem J* **2008**, *412*, 331-338.
552. Berggren, M.I.; Husbeck, B.; Samulitis, B.; Baker, A.F.; Gallegos, A.; Powis, G., Thioredoxin peroxidase-1 (peroxiredoxin-1) is increased in thioredoxin-1 transfected cells and results in enhanced protection against apoptosis caused by hydrogen

peroxide but not by other agents including dexamethasone, etoposide, and doxorubicin. *Arch Biochem Biophys* **2001**, *392*, 103-109.
553. Schwertassek, U.; Haque, A.; Krishnan, N.; Greiner, R.; Weingarten, L.; Dick, T.P.; Tonks, N.K., Reactivation of oxidized PTP1B and PTEN by thioredoxin 1. *FEBS J* **2014**, *281*, 3545-3558.
554. Kreis, P.; Hendricusdottir, R.; Kay, L.; Papageorgiou, I.E.; van Diepen, M.; Mack, T.; Ryves, J.; Harwood, A.; Leslie, N.R.; Kann, O., *et al.*, Phosphorylation of the actin binding protein Drebrin at S647 is regulated by neuronal activity and PTEN. *PLoS One* **2013**, *8*, e71957.
555. Madureira, P.A.; Waisman, D.M., Annexin A2: the importance of being redox sensitive. *Int J Mol Sci* **2013**, *14*, 3568-3594.
556. Madureira, P.A.; Hill, R.; Miller, V.A.; Giacomantonio, C.; Lee, P.W.K.; Waisman, D.M., Annexin A2 is a novel cellular redox regulatory protein involved in tumorigenesis. *Oncotarget* **2011**, *2*, 1075-1093.
557. Wang, C.Y.; Lin, Y.S.; Su, W.C.; Chen, C.L.; Lin, C.F., Glycogen synthase kinase-3 and Omi/HtrA2 induce annexin A2 cleavage followed by cell cycle inhibition and apoptosis. *Mol Biol Cell* **2009**, *20*, 4153-4161.
558. Barwe, S.P.; Anilkumar, G.; Moon, S.Y.; Zheng, Y.; Whitelegge, J.P.; Rajasekaran, S.A.; Rajasekaran, A.K., Novel role for Na,K-ATPase in phosphatidylinositol 3-kinase signaling and suppression of cell motility. *Mol Biol Cell* **2005**, *16*, 1082-1094.
559. Martin-Belmonte, F.; Gassama, A.; Datta, A.; Yu, W.; Rescher, U.; Gerke, V.; Mostov, K., PTEN-mediated apical segregation of phosphoinositides controls epithelial morphogenesis through Cdc42. *Cell* **2007**, *128*, 383-397.
560. Leslie, N.R.; Batty, I.H.; Maccario, H.; Davidson, L.; Downes, C.P., Understanding PTEN regulation: PIP2, polarity and protein stability. *Oncogene* **2008**, *27*, 5464-5476.
561. Chakrabarti, A.; Kelkar, D.A.; Chattopadhyay, A., Spectrin organization and dynamics: new insights. *Biosci Rep* **2006**, *26*, 369-386.
562. Surks, H.K.; Richards, C.T.; Mendelsohn, M.E., Myosin phosphatase-Rho interacting protein. A new member of the myosin phosphatase complex that directly binds RhoA. *J Biol Chem* **2003**, *278*, 51484-51493.
563. Dobbins, G.C.; Zhang, B.; Xiong, W.C.; Mei, L., The role of the cytoskeleton in neuromuscular junction formation. *J Mol Neurosci* **2006**, *30*, 115-118.
564. Liu, L.; Rodriguez-Belmonte, E.M.; Mazloum, N.; Xie, B.; Lee, M.Y.W.T., Identification of a novel protein, PDIP38, that interacts with the p50 subunit of DNA polymerase delta and proliferating cell nuclear antigen. *J Biol Chem* **2003**, *278*, 10041-10047.
565. Yan, F.; Wang, Y.; Wu, X.; Peshavariya, H.M.; Dusting, G.J.; Zhang, M.; Jiang, F., Nox4 and redox signaling mediate TGF-beta-induced endothelial cell apoptosis and phenotypic switch. *Cell Death Dis* **2014**, *5*, e1010.
566. Shamsadin, R.; Adham, I.M.; von Beust, G.; Engel, W., Molecular cloning, expression and chromosome location of the human pelota gene PELO. *Cytogenet Cell Genet* **2000**, *90*, 75-78.
567. Pedersen, K.; Canals, F.; Prat, A.; Tabernero, J.; Arribas, J., PELO negatively regulates HER receptor signalling and metastasis. *Oncogene* **2014**, *33*, 1190-1197.
568. Dualan, R.; Brody, T.; Keeney, S.; Nichols, A.F.; Admon, A.; Linn, S., Chromosomal localization and cDNA cloning of the genes (DDB1 and DDB2) for the p127 and p48 subunits of a human damage-specific DNA binding protein. *Genomics* **1995**, *29*, 62-69.
569. Chen, Y.R.; Liu, M.T.; Chang, Y.T.; Wu, C.C.; Hu, C.Y.; Chen, J.Y., Epstein-Barr virus latent membrane protein 1 represses DNA repair through the PI3K/Akt/FOXO3a pathway in human epithelial cells. *J Virol* **2008**, *82*, 8124-8137.

570. Van de Sande, T.; De Schrijver, E.; Heyns, W.; Verhoeven, G.; Swinnen, J.V., Role of the phosphatidylinositol 3'-kinase/PTEN/Akt kinase pathway in the overexpression of fatty acid synthase in LNCaP prostate cancer cells. *Cancer Res* **2002**, *62*, 642-646.
571. Yao, J.; Liang, L.H.; Zhang, Y.; Ding, J.; Tian, Q.; Li, J.J.; He, X.H., GNAI1 Suppresses Tumor Cell Migration and Invasion and is Post-Transcriptionally Regulated by Mir-320a/c/d in Hepatocellular Carcinoma. *Cancer Biol Med* **2012**, *9*, 234-241.
572. Choorapoikayil, S.; Kers, R.; Herbomel, P.; Kissa, K.; den Hertog, J., Pivotal role of Pten in the balance between proliferation and differentiation of hematopoietic stem cells in zebrafish. *Blood* **2014**, *123*, 184-190.
573. Chen, M.H.; Malbon, C.C., G-protein-coupled receptor-associated A-kinase anchoring proteins AKAP5 and AKAP12: differential trafficking and distribution. *Cell Signal* **2009**, *21*, 136-142.
574. Akakura, S.; Huang, C.; Nelson, P.J.; Foster, B.; Gelman, I.H., Loss of the SSeCKS/Gravin/AKAP12 gene results in prostatic hyperplasia. *Cancer Res* **2008**, *68*, 5096-5103.
575. Chinta, S.J.; Andersen, J.K., Redox imbalance in Parkinson's disease. *Biochim Biophys Acta* **2008**, *1780*, 1362-1367.
576. Birben, E.; Sahiner, U.M.; Sackesen, C.; Erzurum, S.; Kalayci, O., Oxidative stress and antioxidant defense. *World Allergy Organ J* **2012**, *5*, 9-19.
577. Dhar, S.K.; Tangpong, J.; Chaiswing, L.; Oberley, T.D.; St Clair, D.K., Manganese superoxide dismutase is a p53-regulated gene that switches cancers between early and advanced stages. *Cancer Res* **2011**, *71*, 6684-6695.
578. Gaetani, G.F.; Galiano, S.; Canepa, L.; Ferraris, A.M.; Kirkman, H.N., Catalase and glutathione peroxidase are equally active in detoxification of hydrogen peroxide in human erythrocytes. *Blood* **1989**, *73*, 334-339.
579. Prinz, W.A.; Aslund, F.; Holmgren, A.; Beckwith, J., The role of the thioredoxin and glutaredoxin pathways in reducing protein disulfide bonds in the Escherichia coli cytoplasm. *J Biol Chem* **1997**, *272*, 15661-15667.
580. Ray, P.D.; Huang, B.W.; Tsuji, Y., Reactive oxygen species (ROS) homeostasis and redox regulation in cellular signaling. *Cell Signal* **2012**, *24*, 981-990.
581. Mittler, R.; Vanderauwera, S.; Suzuki, N.; Miller, G.; Tognetti, V.B.; Vandepoele, K.; Gollery, M.; Shulaev, V.; Van Breusegem, F., ROS signaling: the new wave? *Trends Plant Sci* **2011**, *16*, 300-309.
582. Kuhn, D.M.; Balkis, M.; Chandra, J.; Mukherjee, P.K.; Ghannoum, M.A., Uses and limitations of the XTT assay in studies of Candida growth and metabolism. *J Clin Microbiol* **2003**, *41*, 506-508.
583. Trinkle-Mulcahy, L.; Boulon, S.; Lam, Y.W.; Urcia, R.; Boisvert, F.M.; Vandermoere, F.; Morrice, N.A.; Swift, S.; Rothbauer, U.; Leonhardt, H., *et al.*, Identifying specific protein interaction partners using quantitative mass spectrometry and bead proteomes. *J Cell Biol* **2008**, *183*, 223-239.
584. Gasche, C.; Chang, C.L.; Rhees, J.; Goel, A.; Boland, C.R., Oxidative stress increases frameshift mutations in human colorectal cancer cells. *Cancer Res* **2001**, *61*, 7444-7448.
585. Day, A.M.; Brown, J.D.; Taylor, S.R.; Rand, J.D.; Morgan, B.A.; Veal, E.A., Inactivation of a peroxiredoxin by hydrogen peroxide is critical for thioredoxin-mediated repair of oxidized proteins and cell survival. *Mol Cell* **2012**, *45*, 398-408.
586. Jacob, C.; Doering, M.; Burkholz, T., The chemical basis of biological redox control. In *Redox Signaling and Regulation in Biology and Medicine*, Wiley-VCH Verlag GmbH & Co. KGaA: Weinheim, Germany, 2009; pp 63-122.
587. van Montfort, R.L.; Congreve, M.; Tisi, D.; Carr, R.; Jhoti, H., Oxidation state of the active-site cysteine in protein tyrosine phosphatase 1B. *Nature* **2003**, *423*, 773-777.

588. den Hertog, J., Protein tyrosine phosphatases as mediators of redox signaling. In *Redox Signaling and Regulation in Biology and Medicine*, Wiley-VCH Verlag GmbH & Co. KGaA: Weinheim, Germany, 2009; pp 197-206.
589. Grossmann, J.; Roschitzki, B.; Panse, C.; Fortes, C.; Barkow-Oesterreicher, S.; Rutishauser, D.; Schlapbach, R., Implementation and evaluation of relative and absolute quantification in shotgun proteomics with label-free methods. *Journal of Proteomics* **2010**, *73*, 1740-1746.
590. Silva, J.C.; Gorenstein, M.V.; Li, G.Z.; Vissers, J.P.C.; Geromanos, S.J., Absolute quantification of proteins by LCMSE - A virtue of parallel MS acquisition. *Molecular & Cellular Proteomics* **2006**, *5*, 144-156.
591. Vanderschuren, H.; Nyaboga, E.; Poon, J.S.; Baerenfaller, K.; Grossmann, J.; Hirsch-Hoffmann, M.; Kirchgessner, N.; Nanni, P.; Gruissem, W., Large-scale proteomics of the cassava storage root and identification of a target gene to reduce postharvest deterioration. *Plant Cell* **2014**, *26*, 1913-1924.
592. Yang, K.S.; Kang, S.W.; Woo, H.A.; Hwang, S.C.; Chae, H.Z.; Kim, K.; Rhee, S.G., Inactivation of human peroxiredoxin I during catalysis as the result of the oxidation of the catalytic site cysteine to cysteine-sulfinic acid. *J Biol Chem* **2002**, *277*, 38029-38036.
593. Kim, Y.C.; Masutani, H.; Yamaguchi, Y.; Itoh, K.; Yamamoto, M.; Yodoi, J., Hemin-induced activation of the thioredoxin gene by Nrf2. A differential regulation of the antioxidant responsive element by a switch of its binding factors. *J Biol Chem* **2001**, *276*, 18399-18406.
594. Karlenius, T.C.; Tonissen, K.F., Thioredoxin and cancer: a role for thioredoxin in all states of tumor oxygenation. *Cancers (Basel)* **2010**, *2*, 209-232.
595. Hashemy, S.I.; Holmgren, A., Regulation of the catalytic activity and structure of human thioredoxin 1 via oxidation and S-nitrosylation of cysteine residues. *J Biol Chem* **2008**, *283*, 21890-21898.
596. Choudhary, G.; Wu, S.L.; Shieh, P.; Hancock, W.S., Multiple enzymatic digestion for enhanced sequence coverage of proteins in complex proteomic mixtures using capillary LC with ion trap MS/MS. *J Proteome Res* **2003**, *2*, 59-67.
597. Dator, R.P.; Gaston, K.W.; Limbach, P.A., Multiple enzymatic digestions and ion mobility separation improve quantification of bacterial ribosomal proteins by data independent acquisition liquid chromatography-mass spectrometry. *Anal Chem* **2014**, *86*, 4264-4270.
598. Zhao, C.; Sethuraman, M.; Clavreul, N.; Kaur, P.; Cohen, R.A.; O'Connor, P.B., Detailed map of oxidative post-translational modifications of human p21ras using Fourier transform mass spectrometry. *Anal Chem* **2006**, *78*, 5134-5142.

# Chapter 8. Appendix

# 8.1 Plasmid Constructs

### 8.1.1 PGEX4-T1–PTEN-GST plasmid DNA sequence

The GST tag encoding sequence is in italic, the PTEN encoding sequence is in bold. The construct includes a thrombin cleavage linker (sequence underlined).

AATGAGCTGTTGACAATTAATCATCGGCTCGTATAATGTGTGGAATTGTGAGCGGATAAC

AATTTCACACAGGAAACAGTATTC*ATGTCCCCTATACTAGGTTATTGGAAAATTAAGGGCCTT*

*GTGCAACCCACTCGACTTCTTTTGGAATATCTTGAAGAAAAATATGAAGAGCATTTGTATGAGCG*

*CGATGAAGGTGATAAATGGCGAAACAAAAAGTTTGAATTGGGTTTGGAGTTTCCCAATCTTCCTT*

*ATTATATTGATGGTGATGTTAAATTAACACAGTCTATGGCCATCATACGTTATATAGCTGACAAGC*

*ACAACATGTTGGGTGGTTGTCCAAAAGAGCGTGCAGAGATTTCAATGCTTGAAGGAGCGGTTTT*

*GGATATTAGATACGGTGTTTCGAGAATTGCATATAGTAAAGACTTTGAAACTCTCAAAGTTGATTT*

*TCTTAGCAAGCTACCTGAAATGCTGAAAATGTTCGAAGATCGTTTATGTCATAAAACATATTTAAA*

*TGGTGATCATGTAACCCATCCTGACTTCATGTTGTATGACGCTCTTGATGTTGTTTTATACATGGA*

*CCCAATGTGCCTGGATGCGTTCCCAAAATTAGTTTGTTTTAAAAAACGTATTGAAGCTATCCCAC*

*AAATTGATAAGTACTTGAAATCCAGCAAGTATATAGCATGGCCTTTGCAGGGCTGGCAAGCCAC*

*GTTTGGTGGTGGCGACCATCCTCCAAAATCGGAT*<u>CTGGTTCCGCGTGGATCC</u>CCGGAATTC**A**

**CAGCCATCATCAAAGAGATCGTTAGCAGAAACAAAAGGAGATATCAAGAGGATGGA**

**TTCGACTTAGACTTGACCTATATTTATCCAAACATTATTGCTATGGGATTTCCTGCAG**

**AAAGACTTGAAGGCGTATACAGGAACAATATTGATGATGTAGTAAGGTTTTTGGATT**

**CAAAGCATAAAAACCATTACAAGATATACAATCTTTGTGCTGAAAGACATTATGACA**

**CCGCCAAATTTAATTGCAGAGTTGCACAATATCCTTTTGAAGACCATAACCCACCAC**

**AGCTAGAACTTATCAAACCCTTTTGTGAAGATCTTGACCAATGGCTAAGTGAAGATG**

**ACAATCATGTTGCAGCAATTCACTGTAAAGCTGGAAAGGGACGAACTGGTGTAATG**

**ATATGTGCATATTTATTACATCGGGGCAAATTTTTAAAGGCACAAGAGGCCCTAGAT**

**TTCTATGGGGAAGTAAGGACCAGAGACAAAAAGGGAGTAACTATTCCCAGTCAGAG**

**GCGCTATGTGTATTATTATAGCTACCTGTTAAAGAATCATCTGGATTATAGACCAGT**

**GGCACTGTTGTTTCACAAGATGATGTTTGAAACTATTCCAATGTTCAGTGGCGGAAC**

**TTGCAATCCTCAGTTTGTGGTCTGCCAGCTAAAGGTGAAGATATATTCCTCCAATTC**

**AGGACCCACACGACGGGAAGACAAGTTCATGTACTTTGAGTTCCCTCAGCCGTTACC**

**TGTGTGTGGTGATATCAAAGTAGAGTTCTTCCACAAACAGAACAAGATGCTAAAAAA**

**GGACAAAATGTTTCACTTTTGGGTAAATACATTCTTCATACCAGGACCAGAGGAAAC**

**CTCAGAAAAAGTAGAAAATGGAAGTCTATGTGATCAAGAAATCGATAGCATTTGCAG**

**TATAGAGCGTGCAGATAATGACAAGGAATATCTAGTACTTACTTTAACAAAAAATGA**

**TCTTGACAAAGCAAATAAAGACAAAGCCAACCGATACTTTTCTCCAAATTTTAAGGT**

**GAAGCTGTACTTCACAAAAACAGTAGAGGAGCCGTCAAATCCAGAGGCTAGCAGTT**

**CAACTTCTGTAACACCAGATGTTAGTGACAATGAACCTGATCATTATAGATATTCTG**

**ACACCACTGACTCTGATCCAGAGAATGAACCTTTTGATGAAGATCAGCATACACAAA**

**TTACAAAAGTCTGA**CTCGAGCGGCCGCATCGTGACTGACTGACGATCTGCCTCGCGCGTT

TCGGTGATGACGGTGAAAACCTCTGACACATGCAGCTCCCGGAGACGGTCACAGCTTGTC

TGTAAGCGGATGCCGGGAGCAGACAAGCCCGTCAGGGCGCGTCAGCGGGTGTTGGCGGG

TGTCGGGGCGCAGCCATGACCCAGTCACGTAGCGATAGCGGAGTGTATAATTCTTGAAGA

CGAAAGGGCCTCGTGATACGCCTATTTTTATAGGTTAATGTCATGATAATAATGGTTTCTT

AGACGTCAGGTGGCACTTTTCGGGGAAATGTGCGCGGAACCCCTATTTGTTTATTTTTCTA

AATACATTCAAATATGTATCCGCTCATGAGACAATAACCCTGATAAATGCTTCAATAATA

TTGAAAAAGGAAGAGTATGAGTATTCAACATTTCCGTGTCGCCCTTATTCCCTTTTTTGCG

GCATTTTGCCTTCCTGTTTTTGCTCACCCAGAAACGCTGGTGAAAGTAAAAGATGCTGAA

GATCAGTTGGGTGCACGAGTGGGTTACATCGAACTGGATCTCAACAGCGGTAAGATCCTT

GAGAGTTTTCGCCCCGAAGAACGTTTTCCAATGATGAGCACTTTTAAAGTTCTGCTATGTG

GCGCGGTATTATCCCGTGTTGACGCCGGGCAAGAGCAACTCGGTCGCCGCATACACTATT

CTCAGAATGACTTGGTTGAGTACTCACCAGTCACAGAAAAGCATCTTACGGATGGCATGA

CAGTAAGAGAATTATGCAGTGCTGCCATAACCATGAGTGATAACACTGCGGCCAACTTAC

TTCTGACAACGATCGGAGGACCGAAGGAGCTAACCGCTTTTTTGCACAACATGGGGGATC

ATGTAACTCGCCTTGATCGTTGGGAACCGGAGCTGAATGAAGCCATACCAAACGACGAG

CGTGACACCACGATGCCTGCAGCAATGGCAACAACGTTGCGCAAACTATTAACTGGCGA

ACTACTTACTCTAGCTTCCCGGCAACAATTAATAGACTGGATGGAGGCGGATAAAGTTGC

AGGACCACTTCTGCGCTCGGCCCTTCCGGCTGGCTGGTTTATTGCTGATAAATCTGGAGCC

GGTGAGCGTGGGTCTCGCGGTATCATTGCAGCACTGGGGCCAGATGGTAAGCCCTCCCGT

ATCGTAGTTATCTACACGACGGGGAGTCAGGCAACTATGGATGAACGAAATAGACAGAT

CGCTGAGATAGGTGCCTCACTGATTAAGCATTGGTAACTGTCAGACCAAGTTTACTCATA

TATACTTTAGATTGATTTAAAACTTCATTTTTAATTTAAAAGGATCTAGGTGAAGATCCTT

TTTGATAATCTCATGACCAAAATCCCTTAACGTGAGTTTTCGTTCCACTGAGCGTCAGACC

CCGTAGAAAAGATCAAAGGATCTTCTTGAGATCCTTTTTTTCTGCGCGTAATCTGCTGCTT

GCAAACAAAAAAACCACCGCTACCAGCGGTGGTTTGTTTGCCGGATCAAGAGCTACCAA

CTCTTTTTCCGAAGGTAACTGGCTTCAGCAGAGCGCAGATACCAAATACTGTCCTTCTAGT

GTAGCCGTAGTTAGGCCACCACTTCAAGAACTCTGTAGCACCGCCTACATACCTCGCTCT

GCTAATCCTGTTACCAGTGGCTGCTGCCAGTGGCGATAAGTCGTGTCTTACCGGGTTGGA

CTCAAGACGATAGTTACCGGATAAGGCGCAGCGGTCGGGCTGAACGGGGGGTTCGTGCA

CACAGCCCAGCTTGGAGCGAACGACCTACACCGAACTGAGATACCTACAGCGTGAGCTA

TGAGAAAGCGCCACGCTTCCCGAAGGGAGAAAGGCGGACAGGTATCCGGTAAGCGGCAG

GGTCGGAACAGGAGAGCGCACGAGGGAGCTTCCAGGGGGAAACGCCTGGTATCTTTATA

GTCCTGTCGGGTTTCGCCACCTCTGACTTGAGCGTCGATTTTTGTGATGCTCGTCAGGGGG

GCGGAGCCTATGGAAAAACGCCAGCAACGCGGCCTTTTTACGGTTCCTGGCCTTTTGCTG

GCCTTTTGCTCACATGTTCTTTCCTGCGTTATCCCCTGATTCTGTGGATAACCGTATTACCG

CCTTTGAGTGAGCTGATACCGCTCGCCGCAGCCGAACGACCGAGCGCAGCGAGTCAGTG

AGCGAGGAAGCGGAAGAGCGCCTGATGCGGTATTTTCTCCTTACGCATCTGTGCGGTATT

TCACACCGCATAAATTCCGACACCATCGAATGGTGCAAAACCTTTCGCGGTATGGCATGA

TAGCGCCCGGAAGAGAGTCAATTCAGGGTGGTGAATGTGAAACCAGTAACGTTATACGA

TGTCGCAGAGTATGCCGGTGTCTCTTATCAGACCGTTTCCCGCGTGGTGAACCAGGCCAG

CCACGTTTCTGCGAAAACGCGGGAAAAAGTGGAAGCGGCGATGGCGGAGCTGAATTACA

TTCCCAACCGCGTGGCACAACAACTGGCGGGCAAACAGTCGTTGCTGATTGGCGTTGCCA

CCTCCAGTCTGGCCCTGCACGCGCCGTCGCAAATTGTCGCGGCGATTAAATCTCGCGCCG

ATCAACTGGGTGCCAGCGTGGTGGTGTCGATGGTAGAACGAAGCGGCGTCGAAGCCTGT

AAAGCGGCGGTGCACAATCTTCTCGCGCAACGCGTCAGTGGGCTGATCATTAACTATCCG

CTGGATGACCAGGATGCCATTGCTGTGGAAGCTGCCTGCACTAATGTTCCGGCGTTATTTC

TTGATGTCTCTGACCAGACACCCATCAACAGTATTATTTTCTCCCATGAAGACGGTACGCG

ACTGGGCGTGGAGCATCTGGTCGCATTGGGTCACCAGCAAATCGCGCTGTTAGCGGGCCC

ATTAAGTTCTGTCTCGGCGCGTCTGCGTCTGGCTGGCTGGCATAAATATCTCACTCGCAAT

CAAATTCAGCCGATAGCGGAACGGGAAGGCGACTGGAGTGCCATGTCCGGTTTTCAACA

AACCATGCAAATGCTGAATGAGGGCATCGTTCCCACTGCGATGCTGGTTGCCAACGATCA

GATGGCGCTGGGCGCAATGCGCGCCATTACCGAGTCCGGGCTGCGCGTTGGTGCGGATAT

CTCGGTAGTGGGATACGACGATACCGAAGACAGCTCATGTTATATCCCGCCGTTAACCAC

CATCAAACAGGATTTTCGCCTGCTGGGGCAAACCAGCGTGGACCGCTTGCTGCAACTCTC

TCAGGGCCAGGCGGTGAAGGGCAATCAGCTGTTGCCCGTCTCACTGGTGAAAAGAAAAA

CCACCCTGGCGCCCAATACGCAAACCGCCTCTCCCCGCGCGTTGGCCGATTCATTAATGC

AGCTGGCACGACAGGTTTCCCGACTGGAAAGCGGGCAGTGAGCGCAACGCAATTAATGT

GAGTTAGCTCACTCATTAGGCACCCCAGGCTTTACACTTTATGCTTCCGGCTCGTATGTTG

TGTGGAATTGTGAGCGGATAACAATTTCACACAGGAAACAGCTATGACCATGATTACGGA

TTCACTGGCCGTCGTTTTACAACGTCGTGACTGGGAAAACCCTGGCGTTACCCAACTTAAT

CGCCTTGCAGCACATCCCCCTTTCGCCAGCTGGCGTAATAGCGAAGAGGCCCGCACCGAT

CGCCCTTCCCAACAGTTGCGCAGCCTGAATGGCGAATGGCGCTTTGCCTGGTTTCCGGCA

CCAGAAGCGGTGCCGGAAAGCTGGCTGGAGTGCGATCTTCCTGAGGCCGATACTGTCGTC

GTCCCCTCAAACTGGCAGATGCACGGTTACGATGCGCCCATCTACACCAACGTAACCTAT

CCCATTACGGTCAATCCGCCGTTTGTTCCCACGGAGAATCCGACGGGTTGTTACTCGCTCA

CATTTAATGTTGATGAAAGCTGGCTACAGGAAGGCCAGACGCGAATTATTTTTGATGGCG

TTGGAATTACGTTATCGACTGCACGGTGCACCAATGCTTCTGGCGTCAGGCAGCCATCGG

AAGCTGTGGTATGGCTGTGCAGGTCGTAAATCACTGCATAATTCGTGTCGCTCAAGGCGC

ACTCCCGTTCTGGATAATGTTTTTTGCGCCGACATCATAACGGTTCTGGCAAATATTCTGA

### 8.1.2 PEGFP-C1-PTEN-EGFP Plasmid DNA sequence

The EGGP tag encoding sequence is in italic, the PTEN encoding sequence is in bold.

TTTGTTTTGGCACCAAAATCAACGGGACTTTCCAAAATGTCGTAACAACTCCGCCCCATTG

ACGCAAATGGGCGGTAGGCGTGTACGGTGGGAGGTCTATATAAGCAGAGCTGGTTTAGT

GAACCGTCAGATCCGCTAGCGCTACCGGTCGCCACC*ATGGTGAGCAAGGGCGAGGAGCTGT*

*TCACCGGGGTGGTGCCCATCCTGGTCGAGCTGGACGGCGACGTAAACGGCCACAAGTTCAGC*

*GTGTCCGGCGAGGGCGAGGGCGATGCCACCTACGGCAAGCTGACCCTGAAGTTCATCTGCAC*

*CACCGGCAAGCTGCCCGTGCCCTGGCCCACCCTCGTGACCACCCTGACCTACGGCGTGCAGT*

*GCTTCAGCCGCTACCCCGACCACATGAAGCAGCACGACTTCTTCAAGTCCGCCATGCCCGAAG*

*GCTACGTCCAGGAGCGCACCATCTTCTTCAAGGACGACGGCAACTACAAGACCCGCGCCGAGG*

*TGAAGTTCGAGGGCGACACCCTGGTGAACCGCATCGAGCTGAAGGGCATCGACTTCAAGGAG*

*GACGGCAACATCCTGGGGCACAAGCTGGAGTACAACTACAACAGCCACAACGTCTATATCATG*

*GCCGACAAGCAGAAGAACGGCATCAAGGTGAACTTCAAGATCCGCCACAACATCGAGGACGGC*

*AGCGTGCAGCTCGCCGACCACTACCAGCAGAACACCCCCATCGGCGACGGCCCCGTGCTGCT*

*GCCCGACAACCACTACCTGAGCACCCAGTCCGCCCTGAGCAAAGACCCCAACGAGAAGCGCG*

*ATCACATGGTCCTGCTGGAGTTCGTGACCGCCGCCGGGATCACTCTCGGCATGGACGAGCTGT*

*ACAAG*TCCGGACTCAGATCTCGAGCTCAAGCTTCGAATTCTGCAGTCGACGGTACCGCGG

GCCCGGGATCC**ATGACAGCCATCATCAAAGAGATCGTTAGCAGAAACAAAAGGAGAT**

**ATCAAGAGGATGGATTCGACTTAGACTTGACCTATATTTATCCAAACATTATTGCTA**

**TGGGATTTCCTGCAGAAAGACTTGAAGGCGTATACAGGAACAATATTGATGATGTAG**

**TAAGGTTTTTGGATTCAAAGCATAAAAACCATTACAAGATATACAATCTTTGTGCTG**

**AAAGACATTATGACACCGCCAAATTTAATTGCAGAGTTGCACAATATCCTTTTGAAG**

**ACCATAACCCACCACAGCTAGAACTTATCAAACCCTTTTGTGAAGATCTTGACCAAT**

**GGCTAAGTGAAGATGACAATCATGTTGCAGCAATTCACTGTAAAGCTGGAAAGGGA**

**CGAACTGGTGTAATGATATGTGCATATTTATTACATCGGGGCAAATTTTTAAAGGCA**

**CAAGAGGCCCTAGATTTCTATGGGGAAGTAAGGACCAGAGACAAAAAGGGAGTAAC**

**TATTCCCAGTCAGAGGCGCTATGTGTATTATTATAGCTACCTGTTAAAGAATCATCT**

**GGATTATAGACCAGTGGCACTGTTGTTTCACAAGATGATGTTTGAAACTATTCCAAT**

**GTTCAGTGGCGGAACTTGCAATCCTCAGTTTGTGGTCTGCCAGCTAAAGGTGAAGAT**

**ATATTCCTCCAATTCAGGACCCACACGACGGGAAGACAAGTTCATGTACTTTGAGTT**

**CCCTCAGCCGTTACCTGTGTGTGGTGATATCAAAGTAGAGTTCTTCCACAAACAGAA**

**CAAGATGCTAAAAAAGGACAAAATGTTTCACTTTTGGGTAAATACATTCTTCATACC**

**AGGACCAGAGGAAACCTCAGAAAAAGTAGAAAATGGAAGTCTATGTGATCAAGAAA**

**TCGATAGCATTTGCAGTATAGAGCGTGCAGATAATGACAAGGAATATCTAGTACTTA**

**CTTTAACAAAAAATGATCTTGACAAAGCAAATAAAGACAAAGCCAACCGATACTTTT**

**CTCCAAATTTTAAGGTGAAGCTGTACTTCACAAAAACAGTAGAGGAGCCGTCAAATC**

**CAGAGGCTAGCAGTTCAACTTCTGTAACACCAGATGTTAGTGACAATGAACCTGATC**

**ATTATAGATATTCTGACACCACTGACTCTGATCCAGAGAATGAACCTTTTGATGAAG**

**ATCAGCATACACAAATTACAAAAGTCTGA**GAGGGATCCACCGGATCTAGATAACTGAT

CATAATCAGCCATACCACATTTGTAGAGGTTTTACTTGCTTTAAAAAACCTCCCACACCTC

CCCCTGAACCTGAAACATAAAATGAATGCAATTGTTGTTGTTAACTTGTTTATTGCAGCTT

ATAATGGTTACAAATAAAGCAATAGCATCACAAATTTCACAAATAAAGCATTTTTTTCAC

TGCATTCTAGTTGTGGTTTGTCCAAACTCATCAATGTATCTTAACGCGTAAATTGTAAGCG

TTAATATTTTGTTAAAATTCGCGTTAAATTTTTGTTAAATCAGCTCATTTTTTAACCAATAG

GCCGAAATCGGCAAAATCCCTTATAAATCAAAAGAATAGACCGAGATAGGGTTGAGTGT

TGTTCCAGTTTGGAACAAGAGTCCACTATTAAAGAACGTGGACTCCAACGTCAAAGGGCG

AAAAACCGTCTATCAGGGCGATGGCCCACTACGTGAACCATCACCCTAATCAAGTTTTTT

GGGGTCGAGGTGCCGTAAAGCACTAAATCGGAACCCTAAAGGGAGCCCCCGATTTAGAG

CTTGACGGGGAAAGCCGGCGAACGTGGCGAGAAAGGAAGGGAAGAAAGCGAAAGGAGC

GGGCGCTAGGGCGCTGGCAAGTGTAGCGGTCACGCTGCGCGTAACCACCACACCCGCCG

CGCTTAATGCGCCGCTACAGGGCGCGTCAGGTGGCACTTTTCGGGGAAATGTGCGCGGAA

CCCCTATTTGTTTATTTTTCTAAATACATTCAAATATGTATCCGCTCATGAGACAATAACC

CTGATAAATGCTTCAATAATATTGAAAAAGGAAGAGTCCTGAGGCGGAAAGAACCAGCT

GTGGAATGTGTGTCAGTTAGGGTGTGGAAAGTCCCCAGGCTCCCCAGCAGGCAGAAGTAT

GCAAAGCATGCATCTCAATTAGTCAGCAACCAGGTGTGGAAAGTCCCCAGGCTCCCCAGC

AGGCAGAAGTATGCAAAGCATGCATCTCAATTAGTCAGCAACCATAGTCCCGCCCCTAAC

TCCGCCCATCCCGCCCCTAACTCCGCCCAGTTCCGCCCATTCTCCGCCCCATGGCTGACTA

ATTTTTTTTATTTATGCAGAGGCCGAGGCCGCCTCGGCCTCTGAGCTATTCCAGAAGTAGT

GAGGAGGCTTTTTTGGAGGCCTAGGCTTTTGCAAAGATCGATCAAGAGACAGGATGAGG

ATCGTTTCGCATGATTGAACAAGATGGATTGCACGCAGGTTCTCCGGCCGCTTGGGTGGA

GAGGCTATTCGGCTATGACTGGGCACAACAGACAATCGGCTGCTCTGATGCCGCCGTGTT

CCGGCTGTCAGCGCAGGGGCGCCCGGTTCTTTTTGTCAAGACCGACCTGTCCGGTGCCCT

GAATGAACTGCAAGACGAGGCAGCGCGGCTATCGTGGCTGGCCACGACGGGCGTTCCTT

GCGCAGCTGTGCTCGACGTTGTCACTGAAGCGGGAAGGGACTGGCTGCTATTGGGCGAA

GTGCCGGGGCAGGATCTCCTGTCATCTCACCTTGCTCCTGCCGAGAAAGTATCCATCATG

GCTGATGCAATGCGGCGGCTGCATACGCTTGATCCGGCTACCTGCCCATTCGACCACCAA

GCGAAACATCGCATCGAGCGAGCACGTACTCGGATGGAAGCCGGTCTTGTCGATCAGGA

TGATCTGGACGAAGAGCATCAGGGGCTCGCGCCAGCCGAACTGTTCGCCAGGCTCAAGG

CGAGCATGCCCGACGGCGAGGATCTCGTCGTGACCCATGGCGATGCCTGCTTGCCGAATA

TCATGGTGGAAAATGGCCGCTTTTCTGGATTCATCGACTGTGGCCGGCTGGGTGTGGCGG

ACCGCTATCAGGACATAGCGTTGGCTACCCGTGATATTGCTGAAGAGCTTGGCGGCGAAT

GGGCTGACCGCTTCCTCGTGCTTTACGGTATCGCCGCTCCCGATTCGCAGCGCATCGCCTT

CTATCGCCTTCTTGACGAGTTCTTCTGAGCGGGACTCTGGGGTTCGAAATGACCGACCAA

GCGACGCCCAACCTGCCATCACGAGATTTCGATTCCACCGCCGCCTTCTATGAAAGGTTG

GGCTTCGGAATCGTTTTCCGGGACGCCGGCTGGATGATCCTCCAGCGCGGGGATCTCATG

CTGGAGTTCTTCGCCCACCCTAGGGGGAGGCTAACTGAAACACGGAAGGAGACAATACC

GGAAGGAACCCGCGCTATGACGGCAATAAAAAGACAGAATAAAACGCACGGTGTTGGGT

CGTTTGTTCATAAACGCGGGGTTCGGTCCCAGGGCTGGCACTCTGTCGATACCCCACCGA

GACCCCATTGGGGCCAATACGCCCGCGTTTCTTCCTTTTCCCCACCCCACCCCCCAAGTTC

GGGTGAAGGCCCAGGGCTCGCAGCCAACGTCGGGGCGGCAGGCCCTGCCATAGCCTCAG

GTTACTCATATATACTTTAGATTGATTTAAAACTTCATTTTTAATTTAAAAGGATCTAGGT

GAAGATCCTTTTTGATAATCTCATGACCAAAATCCCTTAACGTGAGTTTTCGTTCCACTGA

GCGTCAGACCCCGTAGAAAAGATCAAAGGATCTTCTTGAGATCCTTTTTTTCTGCGCGTA

ATCTGCTGCTTGCAAACAAAAAAACCACCGCTACCAGCGGTGGTTTGTTTGCCGGATCAA

GAGCTACCAACTCTTTTTCCGAAGGTAACTGGCTTCAGCAGAGCGCAGATACCAAATACT

GTCCTTCTAGTGTAGCCGTAGTTAGGCCACCACTTCAAGAACTCTGTAGCACCGCCTACAT

ACCTCGCTCTGCTAATCCTGTTACCAGTGGCTGCTGCCAGTGGCGATAAGTCGTGTCTTAC

CGGGTTGGACTCAAGACGATAGTTACCGGATAAGGCGCAGCGGTCGGGCTGAACGGGGG

GTTCGTGCACACAGCCCAGCTTGGAGCGAACGACCTACACCGAACTGAGATACCTACAGC

GTGAGCTATGAGAAAGCGCCACGCTTCCCGAAGGGAGAAAGGCGGACAGGTATCCGGTA

AGCGGCAGGGTCGGAACAGGAGAGCGCACGAGGGAGCTTCCAGGGGGAAACGCCTGGT

ATCTTTATAGTCCTGTCGGGTTTCGCCACCTCTGACTTGAGCGTCGATTTTTGTGATGCTC

GTCAGGGGGGCGGAGCCTATGGAAAAACGCCAGCAACGCGGCCTTTTTACGGTTCCTGGC

CTTTTGCTGGCCTTTTGCTCACATGTTCTTTCCTGCGTTATCCCCTGATTCTGTGGATAACC

GTATTACCGCCATGCATTAGTTATTAATAGTAATCAATTACGGGGTCATTAGTTCATAGCC

CATATATGGAGTTCCGCGTTACATAACTTACGGTAAATGGCCCGCCTGGCTGACCGCCCA

ACGACCCCCGCCCATTGACGTCAATAATGACGTATGTTCCCATAGTAACGCCAATAGGGA

CTTTCCATTGACGTCAATGGGTGGAGTATTTACGGTAAACTGCCCACTTGGCAGTACATC

AAGTGTATCATATGCCAAGTACGCCCCCTATTGACGTCAATGACGGTAAATGGCCCGCCT

GGCATTATGCCCAGTACATGACCTTATGGGACTTTCCTACTTGGCAGTACATCTACGTATT

AGTCATCGCTATTACCATGGTGATGCGGTTTTGGCAGTACATCAATGGGCGTGGATAGCG

GTTTGACTCACGGGGATTTCCAAGTCTCCACCCCATTGACGTCAATGGGAG

### 8.1.3 Plasmid maps

Plasmid maps were generated using Plasmapper (http://wishart.biology.ualberta.ca/PlasMapper) using the DNA sequences reported in sect. 8.1.1 and 8.1.2.

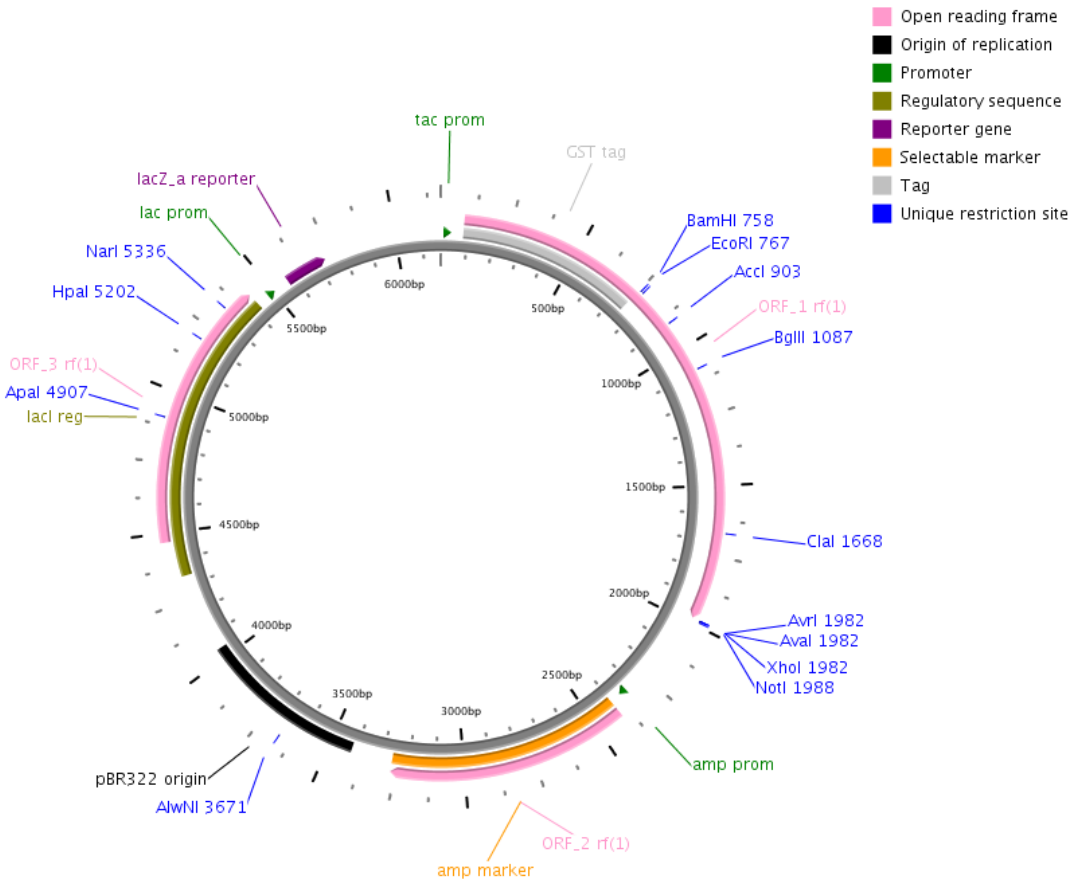


**Figure 8.1 Map of the PGEX-4T1 expression plasmid.**

The gene encoding the GST tagged protein is ligated to the GST tag at ORF 1. The lac operon is sensitive to IPTG-induction.

The PEGFP-C1-PTEN expression plasmid was a gift by Dr. Rudiger Woscholski's group, Imperial College London. The plasmid map shown in fig.8.

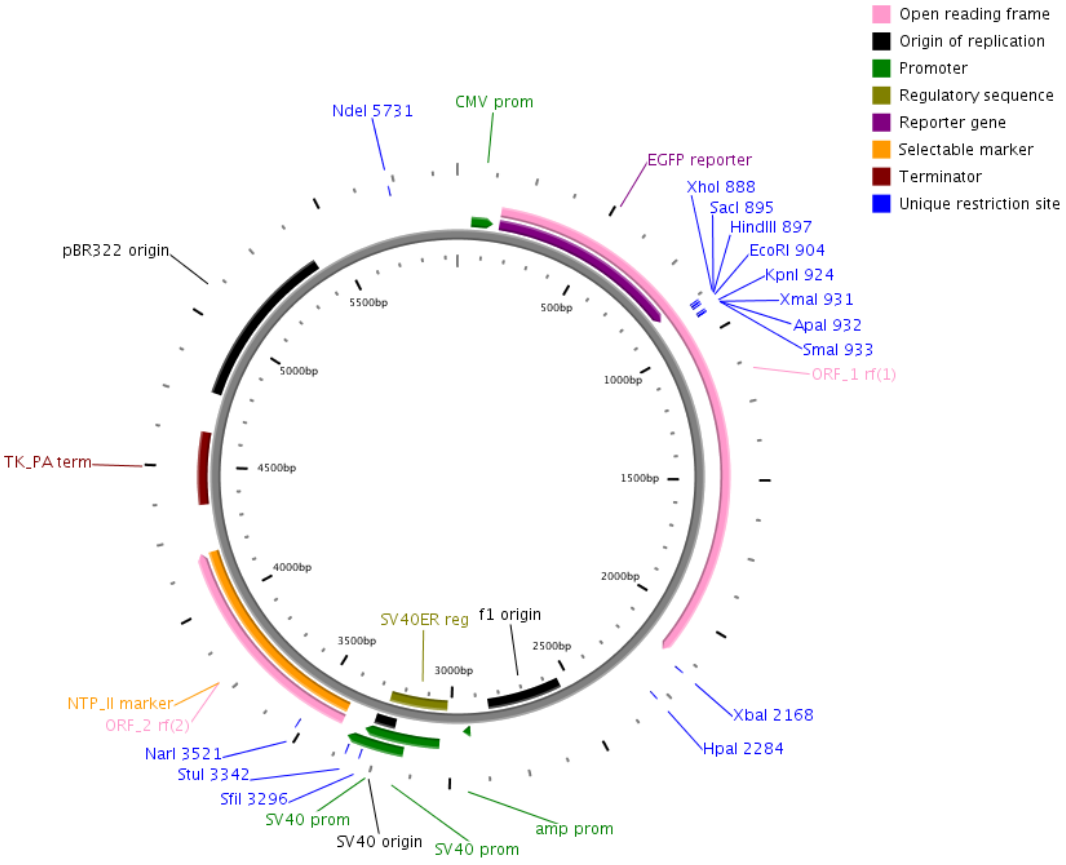


**Figure 8.2 Map of the PEGFP-C1 expression plasmid.**

PTEN was cloned after PCR amplification of its DNA and insertion into the BamHI site of the vector in the multiple cloning side of the plasmid (not visible in the picture).

# 8.2 PTEN fusion proteins sequence

PTEN-GST and PTEN-EGFP amino acid sequence were obtained by translating with the software tool Expasy translate (http://web.expasy.org/translate/) the nucleotide sequences provided by Rudiger Woscholski's Group at Imperial College London, which supplied the plasmid DNAs.

### 8.2.1 PTEN-GST

The PTEN sequence is in bold, the GST tag is in italic. The thrombin cleavage site is underlined.

*MSPILGYWKIKGLVQPTRLLLEYLEEKYEEHLYERDEGDKWRNKKFELGLEFPNLPYYIDGDVKLT*
*QSMAIIRYIADKHNMLGGCPKERAEISMLEGAVLDIRYGVSRIAYSKDFETLKVDFLSKLPEMLKMF*
*EDRLCHKTYLNGDHVTHPDFMLYDALDVVLYMDPMCLDAFPKLVCFKKRIEAIPQIDKYLKSSKYI*
*AWPLQGWQATFGGGDHPPKSD*LVPRGSPEF**TAIIKEIVSRNKRRYQEDGFDLDLTYIYPNIIA**
**MGFPAERLEGVYRNNIDDVVRFLDSKHKNHYKIYNLCAERHYDTAKFNCRVAQYPFED**
**HNPPQLELIKPFCEDLDQWLSEDDNHVAAIHCKAGKGRTGVMICAYLLHRGKFLKAQE**
**ALDFYGEVRTRDKKGVTIPSQRRYVYYYSYLLKNHLDYRPVALLFHKMMFETIPMFSG**
**GTCNPQFVVCQLKVKIYSSNSGPTRREDKFMYFEFPQPLPVCGDIKVEFFHKQNKMLKK**
**DKMFHFWVNTFFIPGPEETSEKVENGSLCDQEIDSICSIERADNDKEYLVLTLTKNDLDK**
**ANKDKANRYFSPNFKVKLYFTKTVEEPSNPEASSSTSVTPDVSDNEPDHYRYSDTTDSDP**
**ENEPFDEDQHTQITKV**

### 8.2.2 PTEN-EGFP

The PTEN sequence is in bold, the EGFP tag is in italic.

*MVSKGEELFTGVVPILVELDGDVNGHKFSVSGEGEGDATYGKLTLKFICTTGKLPVPWPTLVTTLT*
*YGVQCFSRYPDHMKQHDFFKSAMPEGYVQERTIFFKDDGNYKTRAEVKFEGDTLVNRIELKGIDF*
*KEDGNILGHKLEYNYNSHNVYIMADKQKNGIKVNFKIRHNIEDGSVQLADHYQQNTPIGDGPVLLP*
*DNHYLSTQSALSKDPNEKRDHMVLLEFVTAAGITLGMDELYK*SGLRSRAQASNSAVDGTAGPGS
**MTAIIKEIVSRNKRRYQEDGFDLDLTYIYPNIIAMGFPAERLEGVYRNNIDDVVRFLDSKH**
**KNHYKIYNLCAERHYDTAKFNCRVAQYPFEDHNPPQLELIKPFCEDLDQWLSEDDNHV**
**AAIHCKAGKGRTGVMICAYLLHRGKFLKAQEALDFYGEVRTRDKKGVTIPSQRRYVYY**
**YSYLLKNHLDYRPVALLFHKMMFETIPMFSGGTCNPQFVVCQLKVKIYSSNSGPTRRED**
**KFMYFEFPQPLPVCGDIKVEFFHKQNKMLKKDKMFHFWVNTFFIPGPEETSEKVENGSL**
**CDQEIDSICSIERADNDKEYLVLTLTKNDLDKANKDKANRYFSPNFKVKLYFTKTVEEPS**
**NPEASSSTSVTPDVSDNEPDHYRYSDTTDSDPENEPFDEDQHTQITKV**

# 8.3 PTEN surface accessibility

Surface accessibility was calculated using NetsurfP (Ver. 1.1), submitting the FASTA sequence of PTEN obtained from Uniprot (P60484).

**Table 8.1** Surface accessibility of PTEN residues

| **AA[1]** | **AA position[2]** | **RSA[3]** | **ASA[4]** | **Z-Score** | **Class assignment[5]** |
|---|---|---|---|---|---|
| M | 1 | 0.625 | 125.143 | -2.026 | Exposed |
| T | 2 | 0.425 | 58.892 | -0.289 | Exposed |
| A | 3 | 0.495 | 54.582 | -0.833 | Exposed |
| I | 4 | 0.307 | 56.832 | 0.949 | Exposed |
| I | 5 | 0.162 | 30.062 | -0.631 | Buried |
| K | 6 | 0.274 | 56.465 | 0.904 | Buried |
| E | 7 | 0.421 | 73.619 | 0.447 | Exposed |
| I | 8 | 0.103 | 19.073 | 0.663 | Buried |
| V | 9 | 0.098 | 15.124 | -0.324 | Buried |
| S | 10 | 0.416 | 48.708 | -0.458 | Exposed |
| R | 11 | 0.494 | 113.24 | 0.467 | Exposed |
| N | 12 | 0.345 | 50.523 | 0.018 | Exposed |
| K | 13 | 0.441 | 90.631 | -0.405 | Exposed |
| R | 14 | 0.416 | 95.15 | -0.242 | Exposed |
| R | 15 | 0.281 | 64.257 | 0.876 | Exposed |
| Y | 16 | 0.119 | 25.473 | 0.362 | Buried |
| Q | 17 | 0.306 | 54.634 | 0.19 | Exposed |
| E | 18 | 0.449 | 78.405 | -0.320 | Exposed |
| D | 19 | 0.435 | 62.727 | 0.059 | Exposed |
| G | 20 | 0.25 | 19.644 | -1.291 | Buried |
| F | 21 | 0.363 | 72.894 | -0.588 | Exposed |
| D | 22 | 0.382 | 55.118 | -1.393 | Exposed |
| L | 23 | 0.066 | 12.121 | 0.185 | Buried |
| D | 24 | 0.097 | 13.963 | -0.955 | Buried |
| L | 25 | 0.029 | 5.273 | 0.814 | Buried |
| T | 26 | 0.032 | 4.411 | -0.864 | Buried |
| Y | 27 | 0.051 | 10.835 | 1.207 | Buried |
| I | 28 | 0.025 | 4.588 | 0.588 | Buried |
| Y | 29 | 0.046 | 9.787 | 1.126 | Buried |
| P | 30 | 0.343 | 48.615 | 0.128 | Exposed |
| N | 31 | 0.253 | 36.995 | -0.061 | Exposed |
| I | 32 | 0.023 | 4.181 | 0.695 | Buried |
| I | 33 | 0.032 | 5.865 | -0.344 | Buried |
| A | 34 | 0.021 | 2.303 | -0.491 | Buried |
| M | 35 | 0.018 | 3.582 | 0.817 | Buried |
| G | 36 | 0.033 | 2.581 | -1.095 | Buried |

| | | | | | |
|---|---|---|---|---|---|
| F | 37 | 0.086 | 17.3 | -0.711 | Buried |
| P | 38 | 0.063 | 8.883 | -0.979 | Buried |
| A | 39 | 0.167 | 18.392 | -1.790 | Buried |
| E | 40 | 0.226 | 39.482 | -1.333 | Exposed |
| R | 41 | 0.208 | 47.609 | -0.664 | Buried |
| L | 42 | 0.115 | 21.111 | -0.256 | Buried |
| E | 43 | 0.211 | 36.897 | -0.668 | Buried |
| G | 44 | 0.435 | 34.258 | -0.976 | Exposed |
| V | 45 | 0.194 | 29.818 | -1.347 | Buried |
| Y | 46 | 0.119 | 25.516 | 0.047 | Buried |
| R | 47 | 0.338 | 77.448 | -0.346 | Exposed |
| N | 48 | 0.286 | 41.797 | -0.618 | Exposed |
| N | 49 | 0.302 | 44.169 | -0.000 | Exposed |
| I | 50 | 0.041 | 7.529 | -0.352 | Buried |
| D | 51 | 0.551 | 79.385 | 1.023 | Exposed |
| D | 52 | 0.376 | 54.182 | 0.847 | Exposed |
| V | 53 | 0.022 | 3.366 | 0.954 | Buried |
| V | 54 | 0.093 | 14.34 | 0.842 | Buried |
| R | 55 | 0.495 | 113.263 | 1.819 | Exposed |
| F | 56 | 0.125 | 25.027 | 0.912 | Buried |
| L | 57 | 0.021 | 3.882 | 0.984 | Buried |
| D | 58 | 0.504 | 72.698 | 0.999 | Exposed |
| S | 59 | 0.536 | 62.866 | -0.793 | Exposed |
| K | 60 | 0.423 | 87.052 | -0.181 | Exposed |
| H | 61 | 0.25 | 45.493 | -0.154 | Buried |
| K | 62 | 0.548 | 112.826 | -0.826 | Exposed |
| N | 63 | 0.642 | 94.047 | -1.668 | Exposed |
| H | 64 | 0.278 | 50.641 | -0.665 | Buried |
| Y | 65 | 0.151 | 32.226 | -0.694 | Buried |
| K | 66 | 0.193 | 39.762 | 0.008 | Buried |
| I | 67 | 0.094 | 17.427 | -1.580 | Buried |
| Y | 68 | 0.154 | 32.995 | -1.207 | Buried |
| N | 69 | 0.29 | 42.412 | -1.428 | Exposed |
| L | 70 | 0.202 | 37.023 | -0.235 | Buried |
| C | 71 | 0.539 | 75.69 | -1.460 | Exposed |
| A | 72 | 0.508 | 55.949 | -1.715 | Exposed |
| E | 73 | 0.389 | 67.941 | -0.816 | Exposed |
| R | 74 | 0.375 | 85.967 | -0.642 | Exposed |
| H | 75 | 0.504 | 91.605 | -1.172 | Exposed |
| Y | 76 | 0.15 | 32.034 | 0.429 | Buried |
| D | 77 | 0.387 | 55.839 | 0.12 | Exposed |
| T | 78 | 0.384 | 53.247 | -0.892 | Exposed |
| A | 79 | 0.596 | 65.668 | -1.023 | Exposed |
| K | 80 | 0.434 | 89.294 | 1.213 | Exposed |
| F | 81 | 0.121 | 24.285 | -0.499 | Buried |
| N | 82 | 0.519 | 75.952 | -0.247 | Exposed |
| C | 83 | 0.4 | 56.104 | -1.125 | Exposed |

| | | | | | |
|---|---|---|---|---|---|
| R | 84 | 0.406 | 93.02 | 0.854 | Exposed |
| V | 85 | 0.129 | 19.827 | -0.134 | Buried |
| A | 86 | 0.114 | 12.574 | 1.133 | Buried |
| Q | 87 | 0.359 | 64.1 | -0.593 | Exposed |
| Y | 88 | 0.045 | 9.552 | 0.947 | Buried |
| P | 89 | 0.112 | 15.921 | -1.405 | Buried |
| F | 90 | 0.064 | 12.805 | 1.065 | Buried |
| E | 91 | 0.411 | 71.802 | 0.339 | Exposed |
| D | 92 | 0.263 | 37.913 | -2.105 | Buried |
| H | 93 | 0.269 | 49.004 | -1.246 | Buried |
| N | 94 | 0.323 | 47.273 | -1.140 | Exposed |
| P | 95 | 0.064 | 9.053 | -0.810 | Buried |
| P | 96 | 0.038 | 5.449 | -0.233 | Buried |
| Q | 97 | 0.231 | 41.185 | 0.261 | Exposed |
| L | 98 | 0.11 | 20.178 | -0.121 | Buried |
| E | 99 | 0.507 | 88.503 | 0.077 | Exposed |
| L | 100 | 0.161 | 29.479 | 0.454 | Buried |
| I | 101 | 0.009 | 1.721 | 1.847 | Buried |
| K | 102 | 0.222 | 45.707 | 1.277 | Buried |
| P | 103 | 0.442 | 62.791 | 1.768 | Exposed |
| F | 104 | 0.028 | 5.579 | 0.532 | Buried |
| C | 105 | 0.019 | 2.696 | 1.209 | Buried |
| E | 106 | 0.433 | 75.663 | 1.69 | Exposed |
| D | 107 | 0.214 | 30.881 | 1.398 | Buried |
| L | 108 | 0.016 | 2.948 | 1.449 | Buried |
| D | 109 | 0.244 | 35.16 | 0.875 | Buried |
| Q | 110 | 0.437 | 78.102 | 1.554 | Exposed |
| W | 111 | 0.083 | 19.865 | 0.913 | Buried |
| L | 112 | 0.051 | 9.32 | 0.353 | Buried |
| S | 113 | 0.569 | 66.71 | 0.818 | Exposed |
| E | 114 | 0.635 | 110.917 | 0.475 | Exposed |
| D | 115 | 0.443 | 63.836 | -0.226 | Exposed |
| D | 116 | 0.598 | 86.172 | -0.312 | Exposed |
| N | 117 | 0.609 | 89.143 | 0.671 | Exposed |
| H | 118 | 0.137 | 24.92 | 0.395 | Buried |
| V | 119 | 0.039 | 6.025 | 0.374 | Buried |
| A | 120 | 0.018 | 2.017 | 1.131 | Buried |
| A | 121 | 0.018 | 1.951 | 1.198 | Buried |
| I | 122 | 0.013 | 2.497 | 1.538 | Buried |
| H | 123 | 0.034 | 6.239 | 0.722 | Buried |
| C | 124 | 0.02 | 2.836 | 0.917 | Buried |
| K | 125 | 0.274 | 56.28 | 0.85 | Exposed |
| A | 126 | 0.34 | 37.446 | -1.113 | Exposed |
| G | 127 | 0.353 | 27.757 | -1.242 | Exposed |
| K | 128 | 0.165 | 34.002 | 0.335 | Buried |
| G | 129 | 0.197 | 15.496 | -0.515 | Buried |
| R | 130 | 0.062 | 14.267 | 0.326 | Buried |

| | | | | | |
|---|---|---|---|---|---|
| T | 131 | 0.035 | 4.799 | -0.436 | Buried |
| G | 132 | 0.028 | 2.235 | 0.05 | Buried |
| V | 133 | 0.028 | 4.365 | 0.008 | Buried |
| M | 134 | 0.022 | 4.422 | 1.041 | Buried |
| I | 135 | 0.021 | 3.885 | 0.488 | Buried |
| C | 136 | 0.016 | 2.246 | 1.028 | Buried |
| A | 137 | 0.021 | 2.336 | 0.532 | Buried |
| Y | 138 | 0.048 | 10.322 | 0.19 | Buried |
| L | 139 | 0.019 | 3.479 | 1.157 | Buried |
| L | 140 | 0.042 | 7.69 | 0.329 | Buried |
| H | 141 | 0.164 | 29.777 | -0.503 | Buried |
| R | 142 | 0.095 | 21.847 | -0.797 | Buried |
| G | 143 | 0.375 | 29.489 | -1.335 | Exposed |
| K | 144 | 0.413 | 84.975 | -0.639 | Exposed |
| F | 145 | 0.203 | 40.722 | -1.043 | Buried |
| L | 146 | 0.387 | 70.933 | -0.941 | Exposed |
| K | 147 | 0.476 | 97.995 | 0.66 | Exposed |
| A | 148 | 0.122 | 13.411 | -0.268 | Buried |
| Q | 149 | 0.576 | 102.909 | 0.386 | Exposed |
| E | 150 | 0.332 | 58.035 | 1.148 | Exposed |
| A | 151 | 0.016 | 1.719 | 0.972 | Buried |
| L | 152 | 0.076 | 13.989 | 0.677 | Buried |
| D | 153 | 0.44 | 63.418 | 1.415 | Exposed |
| F | 154 | 0.146 | 29.382 | 1.392 | Buried |
| Y | 155 | 0.04 | 8.505 | 0.173 | Buried |
| G | 156 | 0.176 | 13.859 | -0.117 | Buried |
| E | 157 | 0.402 | 70.194 | 0.385 | Exposed |
| V | 158 | 0.178 | 27.374 | 0.443 | Buried |
| R | 159 | 0.125 | 28.648 | -0.485 | Buried |
| T | 160 | 0.442 | 61.25 | -0.552 | Exposed |
| R | 161 | 0.411 | 94.188 | -0.413 | Exposed |
| D | 162 | 0.557 | 80.264 | -1.413 | Exposed |
| K | 163 | 0.567 | 116.694 | -2.772 | Exposed |
| K | 164 | 0.498 | 102.418 | -1.227 | Exposed |
| G | 165 | 0.15 | 11.797 | -2.231 | Buried |
| V | 166 | 0.069 | 10.682 | -1.895 | Buried |
| T | 167 | 0.176 | 24.411 | -1.551 | Buried |
| I | 168 | 0.217 | 40.163 | -0.485 | Buried |
| P | 169 | 0.253 | 35.943 | -0.971 | Buried |
| S | 170 | 0.182 | 21.33 | -1.223 | Buried |
| Q | 171 | 0.039 | 6.983 | -0.611 | Buried |
| R | 172 | 0.185 | 42.479 | 0.308 | Buried |
| R | 173 | 0.346 | 79.257 | 1.077 | Exposed |
| Y | 174 | 0.033 | 6.988 | 0.194 | Buried |
| V | 175 | 0.029 | 4.473 | 0.323 | Buried |
| Y | 176 | 0.364 | 77.744 | 0.786 | Exposed |
| Y | 177 | 0.225 | 48.104 | 0.736 | Buried |

| | | | | | |
|---|---|---|---|---|---|
| Y | 178 | 0.038 | 8.099 | 0.555 | Buried |
| S | 179 | 0.173 | 20.276 | 0.343 | Buried |
| Y | 180 | 0.439 | 93.836 | 0.652 | Exposed |
| L | 181 | 0.135 | 24.755 | 0.378 | Buried |
| L | 182 | 0.078 | 14.19 | -0.591 | Buried |
| K | 183 | 0.486 | 100.032 | 0.306 | Exposed |
| N | 184 | 0.631 | 92.364 | -1.050 | Exposed |
| H | 185 | 0.59 | 107.376 | -1.731 | Exposed |
| L | 186 | 0.241 | 44.127 | -0.923 | Buried |
| D | 187 | 0.579 | 83.434 | -0.639 | Exposed |
| Y | 188 | 0.223 | 47.676 | -1.054 | Buried |
| R | 189 | 0.347 | 79.555 | -0.619 | Exposed |
| P | 190 | 0.527 | 74.71 | -1.057 | Exposed |
| V | 191 | 0.329 | 50.613 | 0.21 | Exposed |
| A | 192 | 0.196 | 21.654 | 0.052 | Buried |
| L | 193 | 0.055 | 10.034 | 0.372 | Buried |
| L | 194 | 0.183 | 33.526 | 0.908 | Buried |
| F | 195 | 0.037 | 7.386 | -0.257 | Buried |
| H | 196 | 0.127 | 23.101 | 0.369 | Buried |
| K | 197 | 0.075 | 15.386 | -0.164 | Buried |
| M | 198 | 0.02 | 3.922 | 0.933 | Buried |
| M | 199 | 0.111 | 22.251 | 0.584 | Buried |
| F | 200 | 0.019 | 3.833 | 0.653 | Buried |
| E | 201 | 0.247 | 43.168 | 0.311 | Buried |
| T | 202 | 0.197 | 27.352 | -1.939 | Buried |
| I | 203 | 0.061 | 11.266 | 0.424 | Buried |
| P | 204 | 0.167 | 23.726 | -2.065 | Buried |
| M | 205 | 0.339 | 67.874 | -1.508 | Exposed |
| F | 206 | 0.138 | 27.777 | -1.078 | Buried |
| S | 207 | 0.509 | 59.69 | -1.128 | Exposed |
| G | 208 | 0.607 | 47.795 | -2.216 | Exposed |
| G | 209 | 0.504 | 39.649 | -3.440 | Exposed |
| T | 210 | 0.383 | 53.15 | -2.272 | Exposed |
| C | 211 | 0.109 | 15.261 | -2.207 | Buried |
| N | 212 | 0.271 | 39.689 | 1.025 | Exposed |
| P | 213 | 0.054 | 7.62 | -1.200 | Buried |
| Q | 214 | 0.133 | 23.772 | 0.118 | Buried |
| F | 215 | 0.03 | 6.101 | -0.250 | Buried |
| V | 216 | 0.166 | 25.453 | 0.961 | Buried |
| V | 217 | 0.017 | 2.644 | 0.573 | Buried |
| C | 218 | 0.15 | 21.102 | -0.463 | Buried |
| Q | 219 | 0.297 | 53.08 | -0.767 | Buried |
| L | 220 | 0.425 | 77.781 | -1.070 | Exposed |
| K | 221 | 0.599 | 123.153 | -0.861 | Exposed |
| V | 222 | 0.514 | 79.048 | -0.163 | Exposed |
| K | 223 | 0.39 | 80.223 | 0.441 | Exposed |
| I | 224 | 0.183 | 33.947 | -0.761 | Buried |

| | | | | | |
|---|---|---|---|---|---|
| Y | 225 | 0.137 | 29.234 | 0.133 | Buried |
| S | 226 | 0.356 | 41.7 | -1.263 | Exposed |
| S | 227 | 0.19 | 22.256 | -2.194 | Buried |
| N | 228 | 0.433 | 63.377 | -1.438 | Exposed |
| S | 229 | 0.528 | 61.882 | -0.241 | Exposed |
| G | 230 | 0.445 | 34.998 | -1.077 | Exposed |
| P | 231 | 0.455 | 64.593 | -1.553 | Exposed |
| T | 232 | 0.378 | 52.387 | -0.593 | Exposed |
| R | 233 | 0.484 | 110.928 | -0.206 | Exposed |
| R | 234 | 0.47 | 107.584 | -0.403 | Exposed |
| E | 235 | 0.62 | 108.314 | -1.391 | Exposed |
| D | 236 | 0.581 | 83.722 | -0.316 | Exposed |
| K | 237 | 0.386 | 79.318 | -0.270 | Exposed |
| F | 238 | 0.308 | 61.775 | -0.048 | Exposed |
| M | 239 | 0.066 | 13.287 | 0.097 | Buried |
| Y | 240 | 0.271 | 57.977 | 0.743 | Exposed |
| F | 241 | 0.026 | 5.278 | 0.062 | Buried |
| E | 242 | 0.391 | 68.238 | 0.555 | Exposed |
| F | 243 | 0.038 | 7.586 | -0.489 | Buried |
| P | 244 | 0.71 | 100.721 | 0.376 | Exposed |
| Q | 245 | 0.521 | 93.051 | -0.953 | Exposed |
| P | 246 | 0.52 | 73.717 | -1.316 | Exposed |
| L | 247 | 0.101 | 18.475 | 0.363 | Buried |
| P | 248 | 0.302 | 42.911 | 1.237 | Exposed |
| V | 249 | 0.034 | 5.287 | -0.204 | Buried |
| C | 250 | 0.235 | 33.022 | 0.221 | Buried |
| G | 251 | 0.117 | 9.192 | -1.585 | Buried |
| D | 252 | 0.128 | 18.416 | -0.761 | Buried |
| I | 253 | 0.025 | 4.68 | 0.762 | Buried |
| K | 254 | 0.125 | 25.815 | 1.257 | Buried |
| V | 255 | 0.017 | 2.628 | 1.63 | Buried |
| E | 256 | 0.146 | 25.471 | 1.811 | Buried |
| F | 257 | 0.015 | 3.111 | 1.464 | Buried |
| F | 258 | 0.114 | 22.9 | 0.728 | Buried |
| H | 259 | 0.073 | 13.351 | -0.322 | Buried |
| K | 260 | 0.235 | 48.36 | 0.254 | Buried |
| Q | 261 | 0.653 | 116.662 | -0.716 | Exposed |
| N | 262 | 0.403 | 58.999 | -0.936 | Exposed |
| K | 263 | 0.639 | 131.381 | -2.104 | Exposed |
| M | 264 | 0.476 | 95.228 | -0.889 | Exposed |
| L | 265 | 0.486 | 89.06 | -1.037 | Exposed |
| K | 266 | 0.362 | 74.443 | -0.646 | Exposed |
| K | 267 | 0.473 | 97.337 | -0.978 | Exposed |
| D | 268 | 0.283 | 40.737 | 0.06 | Exposed |
| K | 269 | 0.057 | 11.663 | 0.641 | Buried |
| M | 270 | 0.03 | 6.003 | 0.395 | Buried |
| F | 271 | 0.015 | 2.93 | 1.063 | Buried |

| | | | | | |
|---|---|---|---|---|---|
| H | 272 | 0.044 | 7.913 | 0.388 | Buried |
| F | 273 | 0.011 | 2.248 | 1.61 | Buried |
| W | 274 | 0.022 | 5.219 | 1.212 | Buried |
| V | 275 | 0.017 | 2.567 | 1.265 | Buried |
| N | 276 | 0.027 | 3.938 | 0.733 | Buried |
| T | 277 | 0.021 | 2.927 | 0.807 | Buried |
| F | 278 | 0.039 | 7.807 | -0.861 | Buried |
| F | 279 | 0.033 | 6.623 | -0.187 | Buried |
| I | 280 | 0.029 | 5.273 | 0.243 | Buried |
| P | 281 | 0.202 | 28.65 | 0.358 | Buried |
| G | 282 | 0.252 | 19.801 | -0.668 | Buried |
| P | 283 | 0.481 | 68.254 | -1.226 | Exposed |
| E | 284 | 0.381 | 66.526 | -0.625 | Exposed |
| E | 285 | 0.283 | 49.475 | -1.564 | Buried |
| T | 286 | 0.271 | 37.574 | -1.179 | Buried |
| S | 287 | 0.246 | 28.784 | -2.017 | Buried |
| E | 288 | 0.422 | 73.758 | -0.941 | Exposed |
| K | 289 | 0.361 | 74.299 | -0.743 | Exposed |
| V | 290 | 0.273 | 42.006 | -1.324 | Buried |
| E | 291 | 0.446 | 77.934 | -1.337 | Exposed |
| N | 292 | 0.405 | 59.233 | -1.190 | Exposed |
| G | 293 | 0.381 | 29.993 | -1.583 | Exposed |
| S | 294 | 0.418 | 48.99 | -1.657 | Exposed |
| L | 295 | 0.291 | 53.282 | -1.967 | Buried |
| C | 296 | 0.376 | 52.79 | -0.861 | Exposed |
| D | 297 | 0.45 | 64.787 | -1.138 | Exposed |
| Q | 298 | 0.434 | 77.602 | -1.540 | Exposed |
| E | 299 | 0.342 | 59.782 | -1.389 | Exposed |
| I | 300 | 0.379 | 70.041 | -1.626 | Exposed |
| D | 301 | 0.504 | 72.612 | -1.939 | Exposed |
| S | 302 | 0.47 | 55.072 | -1.830 | Exposed |
| I | 303 | 0.306 | 56.573 | -1.850 | Buried |
| C | 304 | 0.266 | 37.389 | -2.119 | Buried |
| S | 305 | 0.39 | 45.767 | -1.386 | Exposed |
| I | 306 | 0.4 | 74.056 | -1.400 | Exposed |
| E | 307 | 0.37 | 64.569 | -1.629 | Exposed |
| R | 308 | 0.463 | 106.142 | -1.041 | Exposed |
| A | 309 | 0.341 | 37.534 | -1.415 | Exposed |
| D | 310 | 0.424 | 61.026 | -1.278 | Exposed |
| N | 311 | 0.44 | 64.401 | -2.283 | Exposed |
| D | 312 | 0.369 | 53.216 | -2.157 | Exposed |
| K | 313 | 0.277 | 56.897 | -1.363 | Buried |
| E | 314 | 0.316 | 55.258 | -1.470 | Exposed |
| Y | 315 | 0.177 | 37.932 | 0.048 | Buried |
| L | 316 | 0.092 | 16.809 | -0.174 | Buried |
| V | 317 | 0.097 | 14.863 | 0.417 | Buried |
| L | 318 | 0.041 | 7.58 | -0.148 | Buried |

| | | | | | |
|---|---|---|---|---|---|
| T | 319 | 0.273 | 37.851 | 0.733 | Exposed |
| L | 320 | 0.031 | 5.694 | 0.612 | Buried |
| T | 321 | 0.403 | 55.868 | 0.548 | Exposed |
| K | 322 | 0.227 | 46.714 | 0.052 | Buried |
| N | 323 | 0.517 | 75.689 | -0.953 | Exposed |
| D | 324 | 0.391 | 56.386 | -0.797 | Exposed |
| L | 325 | 0.098 | 17.999 | -0.515 | Buried |
| D | 326 | 0.193 | 27.811 | -0.911 | Buried |
| K | 327 | 0.62 | 127.616 | -0.058 | Exposed |
| A | 328 | 0.316 | 34.867 | -1.196 | Exposed |
| N | 329 | 0.274 | 40.172 | -0.312 | Buried |
| K | 330 | 0.555 | 114.122 | -0.170 | Exposed |
| D | 331 | 0.508 | 73.26 | -0.896 | Exposed |
| K | 332 | 0.59 | 121.363 | 0.184 | Exposed |
| A | 333 | 0.546 | 60.202 | 0.237 | Exposed |
| N | 334 | 0.309 | 45.238 | 0.043 | Exposed |
| R | 335 | 0.682 | 156.178 | 0.613 | Exposed |
| Y | 336 | 0.332 | 71.034 | 0.663 | Exposed |
| F | 337 | 0.061 | 12.323 | 0.919 | Buried |
| S | 338 | 0.319 | 37.363 | 0.887 | Exposed |
| P | 339 | 0.758 | 107.503 | -0.106 | Exposed |
| N | 340 | 0.63 | 92.217 | 0.415 | Exposed |
| F | 341 | 0.043 | 8.59 | -0.172 | Buried |
| K | 342 | 0.427 | 87.875 | 1.712 | Exposed |
| V | 343 | 0.052 | 7.962 | 0.22 | Buried |
| K | 344 | 0.192 | 39.556 | 0.917 | Buried |
| L | 345 | 0.066 | 12.14 | 0.321 | Buried |
| Y | 346 | 0.16 | 34.256 | 0.832 | Buried |
| F | 347 | 0.043 | 8.65 | -0.603 | Buried |
| T | 348 | 0.333 | 46.187 | 0.269 | Exposed |
| K | 349 | 0.555 | 114.225 | 0.06 | Exposed |
| T | 350 | 0.209 | 29.058 | 0.074 | Buried |
| V | 351 | 0.433 | 66.475 | -0.384 | Exposed |
| E | 352 | 0.563 | 98.286 | -0.035 | Exposed |
| E | 353 | 0.622 | 108.646 | 0.17 | Exposed |
| P | 354 | 0.262 | 37.22 | -0.597 | Exposed |
| S | 355 | 0.67 | 78.524 | 0.089 | Exposed |
| N | 356 | 0.578 | 84.605 | -0.571 | Exposed |
| P | 357 | 0.491 | 69.687 | -1.625 | Exposed |
| E | 358 | 0.708 | 123.757 | -0.558 | Exposed |
| A | 359 | 0.272 | 29.93 | -0.330 | Buried |
| S | 360 | 0.536 | 62.772 | -0.547 | Exposed |
| S | 361 | 0.62 | 72.711 | -1.781 | Exposed |
| S | 362 | 0.462 | 54.1 | -0.984 | Exposed |
| T | 363 | 0.543 | 75.342 | -0.723 | Exposed |
| S | 364 | 0.615 | 72.031 | -0.832 | Exposed |
| V | 365 | 0.276 | 42.452 | -0.380 | Exposed |

| | | | | | |
|---|---|---|---|---|---|
| T | 366 | 0.484 | 67.089 | -0.052 | Exposed |
| P | 367 | 0.405 | 57.498 | -1.305 | Exposed |
| D | 368 | 0.566 | 81.546 | -1.095 | Exposed |
| V | 369 | 0.324 | 49.799 | -0.405 | Exposed |
| S | 370 | 0.37 | 43.329 | -0.989 | Exposed |
| D | 371 | 0.625 | 90.077 | -1.035 | Exposed |
| N | 372 | 0.623 | 91.163 | -1.923 | Exposed |
| E | 373 | 0.534 | 93.22 | -0.386 | Exposed |
| P | 374 | 0.287 | 40.754 | -1.197 | Buried |
| D | 375 | 0.54 | 77.785 | -1.074 | Exposed |
| H | 376 | 0.345 | 62.701 | -0.945 | Exposed |
| Y | 377 | 0.325 | 69.41 | -1.253 | Exposed |
| R | 378 | 0.612 | 140.217 | -0.378 | Exposed |
| Y | 379 | 0.419 | 89.626 | -1.669 | Exposed |
| S | 380 | 0.434 | 50.877 | -1.696 | Exposed |
| D | 381 | 0.652 | 93.939 | -1.746 | Exposed |
| T | 382 | 0.386 | 53.483 | -0.547 | Exposed |
| T | 383 | 0.484 | 67.145 | -2.135 | Exposed |
| D | 384 | 0.651 | 93.751 | -1.375 | Exposed |
| S | 385 | 0.577 | 67.624 | -1.643 | Exposed |
| D | 386 | 0.411 | 59.153 | -0.394 | Exposed |
| P | 387 | 0.446 | 63.231 | -0.994 | Exposed |
| E | 388 | 0.595 | 103.859 | -0.758 | Exposed |
| N | 389 | 0.644 | 94.34 | -0.928 | Exposed |
| E | 390 | 0.422 | 73.776 | -0.732 | Exposed |
| P | 391 | 0.604 | 85.651 | -1.141 | Exposed |
| F | 392 | 0.368 | 73.898 | -1.544 | Exposed |
| D | 393 | 0.403 | 58.043 | -0.967 | Exposed |
| E | 394 | 0.475 | 82.948 | -2.052 | Exposed |
| D | 395 | 0.472 | 68.087 | -1.271 | Exposed |
| Q | 396 | 0.289 | 51.633 | -0.103 | Buried |
| H | 397 | 0.241 | 43.82 | 0.088 | Buried |
| T | 398 | 0.166 | 23.094 | -0.150 | Buried |
| Q | 399 | 0.452 | 80.799 | 0.882 | Exposed |
| I | 400 | 0.129 | 23.958 | -0.236 | Buried |
| T | 401 | 0.479 | 66.465 | 0.851 | Exposed |
| K | 402 | 0.562 | 115.645 | 0.516 | Exposed |
| V | 403 | 0.68 | 104.455 | -0.634 | Exposed |

[1] AA=Amino acid
[2] Amino acid position
[3] RSA= Relative Surface Accessibility
[4] ASA= Absolute Solvent Accessibility
[5] Class assignment was predicted using a thresohold 25% surface exposure, based on the $ASA_{max}$ of a given amino acid

# 8.4 PTEN known interactors summary

The table below was generated through database search performed with BioGRID (Biological General Repository for Interaction Datasets): http://thebiogrid.org/

**Table 8.2** Known PTEN interactors determined with both high throughput and low throughput experimental systems

| Interactor | Role | Organism | Experimental Evidence Code | Dataset | Throughput |
|---|---|---|---|---|---|
| AKT1 | HIT | H. sapiens | Affinity Capture-Western | Mistafa O (2010) | Low Throughput |
| AMHR2 | HIT | H. sapiens | Affinity Capture-MS | Crockett DK (2005) | Low Throughput |
| ANAPC4 | HIT | H. sapiens | Affinity Capture-MS | Song MS (2011) | Low Throughput |
| ANAPC4 | HIT | H. sapiens | Affinity Capture-Western | Song MS (2011) | Low Throughput |
| ANAPC5 | HIT | H. sapiens | Affinity Capture-MS | Song MS (2011) | Low Throughput |
| ANAPC5 | HIT | H. sapiens | Affinity Capture-Western | Song MS (2011) | Low Throughput |
| ANAPC7 | HIT | H. sapiens | Affinity Capture-MS | Song MS (2011) | Low Throughput |
| ANAPC7 | HIT | H. sapiens | Affinity Capture-Western | Song MS (2011) | Low Throughput |
| ANG | HIT | H. sapiens | Two-hybrid | Stelzl U (2005) | High Throughput |
| ARHGAP26 | HIT | H. sapiens | Affinity Capture-MS | Crockett DK (2005) | Low Throughput |
| AR | HIT | H. sapiens | Affinity Capture-Western | Lin HK (2004) | Low Throughput |
| AR | HIT | H. sapiens | Reconstituted Complex | Lin HK (2004) | Low Throughput |
| BAP1 | HIT | H. sapiens | Affinity Capture-MS | Crockett DK (2005) | Low Throughput |
| BMI1 | HIT | H. sapiens | Affinity Capture-Western | Fan C (2009) | Low Throughput |
| BMI1 | BAIT | H. sapiens | Affinity Capture-Western | Fan C (2009) | Low Throughput |
| CASP8 | HIT | H. sapiens | Affinity Capture-MS | Crockett DK (2005) | Low Throughput |
| CASP8 | HIT | H. sapiens | Affinity Capture-Western | Crockett DK (2005) | Low Throughput |
| CAV1 | HIT | H. sapiens | Affinity Capture-Western | Caselli A (2002) | Low Throughput |
| CBL | BAIT | H. sapiens | Affinity Capture-Western | Rodriguez S (2013) | Low Throughput |
| CBL | HIT | H. sapiens | Affinity Capture-Western | Rodriguez S (2013) | Low Throughput |
| CCNE2 | HIT | H. sapiens | Affinity Capture-MS | Crockett DK (2005) | Low Throughput |
| CCNE2 | HIT | H. sapiens | Affinity Capture-Western | Crockett DK (2005) | Low Throughput |
| CDC27 | HIT | H. sapiens | Affinity Capture-MS | Song MS (2011) | Low Throughput |
| CDC27 | HIT | H. sapiens | Affinity Capture-Western | Song MS (2011) | Low Throughput |
| CDC27 | BAIT | H. sapiens | Affinity Capture-Western | Song MS (2011) | Low Throughput |
| CDC27 | HIT | H. sapiens | Reconstituted Complex | Song MS (2011) | Low Throughput |
| CDH1 | HIT | H. sapiens | Affinity Capture-Western | Choi BH (2014) | Low Throughput |
| CENPC | HIT | H. sapiens | Affinity Capture-MS | Crockett DK (2005) | Low Throughput |
| CHGB | HIT | H. sapiens | Two-hybrid | Stelzl U (2005) | High Throughput |
| COPS6 | HIT | H. sapiens | Two-hybrid | Stelzl U (2005) | High Throughput |
| CRKL | HIT | H. sapiens | Affinity Capture-MS | Crockett DK (2005) | Low Throughput |
| CSNK2A1 | HIT | H. sapiens | Affinity Capture-MS | Crockett DK (2005) | Low Throughput |
| CSNK2A1 | BAIT | H. sapiens | Biochemical Activity | Miller SJ (2002) | Low Throughput |
| CSNK2A1 | HIT | H. sapiens | Reconstituted Complex | Miller SJ (2002) | Low Throughput |

| | | | | | |
|---|---|---|---|---|---|
| CSNK2A2 | BAIT | H. sapiens | Biochemical Activity | Miller SJ (2002) | Low Throughput |
| CSNK2A2 | HIT | H. sapiens | Reconstituted Complex | Miller SJ (2002) | Low Throughput |
| CTNNB1 | HIT | H. sapiens | Affinity Capture-Western | Li A (2010) | Low Throughput |
| CTNNB1 | BAIT | H. sapiens | Affinity Capture-Western | Li A (2010) | Low Throughput |
| DBF4B | HIT | H. sapiens | Affinity Capture-MS | Crockett DK (2005) | Low Throughput |
| EEF1A2 | HIT | H. sapiens | Affinity Capture-MS | Crockett DK (2005) | Low Throughput |
| EGR1 | BAIT | H. sapiens | Affinity Capture-Western | Lu D (2011) | Low Throughput |
| ELAVL1 | BAIT | H. sapiens | Affinity Capture-RNA | Abdelmohsen K (2009) | High Throughput |
| EPHB1 | HIT | H. sapiens | Affinity Capture-Western | Rodriguez S (2013) | Low Throughput |
| EPHB1 | BAIT | H. sapiens | Affinity Capture-Western | Rodriguez S (2013) | Low Throughput |
| ESR1 | HIT | H. sapiens | Reconstituted Complex | Lin HK (2004) | Low Throughput |
| FBN2 | HIT | H. sapiens | Affinity Capture-MS | Crockett DK (2005) | Low Throughput |
| FBXW7 | BAIT | H. sapiens | Affinity Capture-Western | Yang C (2013) | Low Throughput |
| FBXW7 | HIT | H. sapiens | Affinity Capture-Western | Yang C (2013) | Low Throughput |
| FRK | HIT | H. sapiens | Affinity Capture-MS | Yim EK (2009) | Low Throughput |
| FRK | HIT | H. sapiens | Affinity Capture-Western | Yim EK (2009) | Low Throughput |
| FRK | BAIT | H. sapiens | Affinity Capture-Western | Yim EK (2009) | Low Throughput |
| FZR1 | BAIT | H. sapiens | Affinity Capture-Western | Song MS (2011) | Low Throughput |
| FZR1 | BAIT | H. sapiens | Affinity Capture-Western | Choi BH (2014) | Low Throughput |
| FZR1 | HIT | H. sapiens | Reconstituted Complex | Song MS (2011) | Low Throughput |
| G3BP2 | HIT | H. sapiens | Affinity Capture-MS | Crockett DK (2005) | Low Throughput |
| GFRA2 | HIT | H. sapiens | Affinity Capture-MS | Crockett DK (2005) | Low Throughput |
| GPR113 | HIT | H. sapiens | Affinity Capture-MS | Crockett DK (2005) | Low Throughput |
| HBA1 | HIT | H. sapiens | Two-hybrid | Stelzl U (2005) | High Throughput |
| HDAC4 | BAIT | H. sapiens | Negative Genetic | Lin YY (2012) | High Throughput |
| INHBE | HIT | H. sapiens | Affinity Capture-MS | Crockett DK (2005) | Low Throughput |
| IRS4 | HIT | H. sapiens | Affinity Capture-MS | Crockett DK (2005) | Low Throughput |
| IRS4 | HIT | H. sapiens | Affinity Capture-Western | Crockett DK (2005) | Low Throughput |
| KAT2B | HIT | H. sapiens | Affinity Capture-Western | Okumura K (2006) | Low Throughput |
| KAT2B | BAIT | H. sapiens | Affinity Capture-Western | Okumura K (2006) | Low Throughput |
| KRT14 | HIT | H. sapiens | Affinity Capture-MS | Crockett DK (2005) | Low Throughput |
| LATS1 | BAIT | H. sapiens | Biochemical Activity | Chiyoda T (2012) | Low Throughput |
| MAGI3 | HIT | H. sapiens | Affinity Capture-Western | Wu Y (2000) | Low Throughput |
| MAGI3 | BAIT | H. sapiens | Reconstituted Complex | Wu Y (2000) | Low Throughput |
| MAGI3 | BAIT | H. sapiens | Two-hybrid | Wu Y (2000) | Low Throughput |
| MAP2K6 | HIT | H. sapiens | Affinity Capture-MS | Crockett DK (2005) | Low Throughput |
| MED12 | HIT | H. sapiens | Affinity Capture-MS | Crockett DK (2005) | Low Throughput |
| MVP | HIT | H. sapiens | Affinity Capture-Western | Yu Z (2002) | Low Throughput |
| MVP | BAIT | H. sapiens | Reconstituted Complex | Yu Z (2002) | Low Throughput |
| MVP | HIT | H. sapiens | Two-hybrid | Yu Z (2002) | Low Throughput |
| NCOA3 | BAIT | H. sapiens | Affinity Capture-Western | Yang C (2013) | Low Throughput |
| NCOA3 | HIT | H. sapiens | Affinity Capture-Western | Yang C (2013) | Low Throughput |
| NDFIP1 | BAIT | H. sapiens | Affinity Capture-Western | Mund T (2010) | Low Throughput |
| NDFIP1 | BAIT | H. sapiens | Affinity Capture-Western | Howitt J (2012) | Low Throughput |
| NDFIP1 | HIT | H. sapiens | Affinity Capture-Western | Howitt J (2012) | Low Throughput |
| NDFIP1 | HIT | H. sapiens | PCA | Li Y (2014) | Low Throughput |
| NDFIP2 | BAIT | H. sapiens | Affinity Capture-Western | Mund T (2010) | Low Throughput |
| NEDD4 | HIT | H. sapiens | Affinity Capture-Western | Yim EK (2009) | Low Throughput |
| NEDD4 | HIT | H. sapiens | Affinity Capture-Western | Wu Y (2013) | Low Throughput |
| NEDD4 | BAIT | H. sapiens | Biochemical Activity | Wang X (2008) | Low Throughput |

| | | | | | |
|---|---|---|---|---|---|
| NEDD4 | BAIT | H. sapiens | Biochemical Activity | Chung S (2011) | Low Throughput |
| NEDD4 | BAIT | H. sapiens | Biochemical Activity | Hong SW (2013) | Low Throughput |
| NEDD4 | HIT | H. sapiens | Reconstituted Complex | Wang X (2008) | Low Throughput |
| NEDD4 | HIT | H. sapiens | Reconstituted Complex | Hong SW (2013) | Low Throughput |
| P3H4 | HIT | H. sapiens | Affinity Capture-MS | Crockett DK (2005) | Low Throughput |
| PARK7 | BAIT | H. sapiens | Affinity Capture-Western | Das F (2011) | Low Throughput |
| PARK7 | HIT | H. sapiens | Affinity Capture-Western | Das F (2011) | Low Throughput |
| PARK7 | BAIT | H. sapiens | Affinity Capture-Western | Kim YC (2009) | Low Throughput |
| PARK7 | BAIT | H. sapiens | Reconstituted Complex | Kim YC (2009) | Low Throughput |
| PDGFRA | HIT | H. sapiens | Affinity Capture-MS | Crockett DK (2005) | Low Throughput |
| PINK1 | HIT | H. sapiens | Affinity Capture-MS | Crockett DK (2005) | Low Throughput |
| PKN2 | HIT | H. sapiens | Affinity Capture-MS | Crockett DK (2005) | Low Throughput |
| PPP1CA | BAIT | H. sapiens | Affinity Capture-Western | Flores-Delgado G (2007) | High Throughput |
| PPP2R4 | HIT | H. sapiens | Affinity Capture-Western | Crockett DK (2005) | Low Throughput |
| PPP3CA | BAIT | H. sapiens | Affinity Capture-Western | Mistafa O (2010) | Low Throughput |
| PTK2B | HIT | H. sapiens | Affinity Capture-MS | Crockett DK (2005) | Low Throughput |
| PTK2 | HIT | H. sapiens | Affinity Capture-Western | Tamura M (1999) | Low Throughput |
| PTK2 | HIT | H. sapiens | Affinity Capture-Western | Haier J (2002) | Low Throughput |
| PTK2 | HIT | H. sapiens | Affinity Capture-Western | Crockett DK (2005) | Low Throughput |
| PTPN14 | HIT | H. sapiens | Affinity Capture-MS | Crockett DK (2005) | Low Throughput |
| PXN | HIT | H. sapiens | Affinity Capture-Western | Haier J (2002) | Low Throughput |
| QRFPR | HIT | H. sapiens | Affinity Capture-MS | Crockett DK (2005) | Low Throughput |
| RPL14 | HIT | H. sapiens | Affinity Capture-MS | Crockett DK (2005) | Low Throughput |
| SHARPIN | BAIT | H. sapiens | Affinity Capture-Western | He L (2010) | Low Throughput |
| SHARPIN | HIT | H. sapiens | Affinity Capture-Western | He L (2010) | Low Throughput |
| SHARPIN | HIT | H. sapiens | Affinity Capture-Western | De Melo J (2014) | Low Throughput |
| SHARPIN | BAIT | H. sapiens | Affinity Capture-Western | De Melo J (2014) | Low Throughput |
| SLC9A3R1 | HIT | H. sapiens | Affinity Capture-Western | Yang L (2011) | Low Throughput |
| SLC9A3R1 | BAIT | H. sapiens | Affinity Capture-Western | Rodriguez S (2013) | Low Throughput |
| SLC9A3R1 | HIT | O. cuniculus | Reconstituted Complex | Yang L (2011) | Low Throughput |
| SLC9A3R1 | HIT | H. sapiens | Reconstituted Complex | Yang L (2011) | Low Throughput |
| SMTN | HIT | H. sapiens | Affinity Capture-MS | Crockett DK (2005) | Low Throughput |
| SMURF2 | BAIT | M. musculus | Affinity Capture-Luminescence | Narimatsu M (2009) | Low Throughput |
| STUB1 | HIT | H. sapiens | Affinity Capture-Western | Ahmed SF (2012) | Low Throughput |
| STUB1 | BAIT | H. sapiens | Affinity Capture-Western | Ahmed SF (2012) | Low Throughput |
| STUB1 | HIT | H. sapiens | Reconstituted Complex | Ahmed SF (2012) | Low Throughput |
| SUMO1 | HIT | H. sapiens | Affinity Capture-Western | Da Silva-Ferrada E (2013) | Low Throughput |
| SUMO1 | BAIT | H. sapiens | Affinity Capture-Western | Huang J (2012) | Low Throughput |
| SUMO3 | HIT | H. sapiens | Affinity Capture-Western | Da Silva-Ferrada E (2013) | Low Throughput |
| TCEB3C | HIT | H. sapiens | Affinity Capture-MS | Crockett DK (2005) | Low Throughput |
| TP53 | HIT | H. sapiens | Affinity Capture-Western | Freeman DJ (2003) | Low Throughput |
| TP53 | BAIT | H. sapiens | Affinity Capture-Western | Freeman DJ (2003) | Low Throughput |
| TP53 | HIT | H. sapiens | Affinity Capture-Western | Zhou M (2003) | Low Throughput |
| TP53 | BAIT | H. sapiens | Affinity Capture-Western | Zhou M (2003) | Low Throughput |
| TP53 | HIT | H. sapiens | Reconstituted Complex | Hong SW (2013) | Low Throughput |
| TTBK2 | HIT | H. sapiens | Affinity Capture-MS | Crockett DK (2005) | Low Throughput |
| UBC | BAIT | H. sapiens | Affinity Capture-Western | Wu W (2003) | Low Throughput |
| UBC | BAIT | H. sapiens | Affinity Capture-Western | Mund T (2010) | Low Throughput |
| UBC | HIT | H. sapiens | Affinity Capture-Western | Maddika S (2011) | Low Throughput |
| UBC | HIT | H. sapiens | Affinity Capture-Western | Yim EK (2009) | Low Throughput |

| | | | | | |
|---|---|---|---|---|---|
| UBC | BAIT | H. sapiens | Affinity Capture-Western | Howitt J (2012) | Low Throughput |
| UBC | HIT | H. sapiens | Affinity Capture-Western | Mistafa O (2010) | Low Throughput |
| UBC | HIT | H. sapiens | Affinity Capture-Western | Yang L (2011) | Low Throughput |
| UBC | HIT | H. sapiens | Affinity Capture-Western | Ahmed SF (2012) | Low Throughput |
| UBC | BAIT | H. sapiens | Affinity Capture-Western | Ahmed SF (2012) | Low Throughput |
| UBC | HIT | H. sapiens | Affinity Capture-Western | Morotti A (2013) | Low Throughput |
| UBC | HIT | H. sapiens | Affinity Capture-Western | Zhang J (2013) | Low Throughput |
| UBC | HIT | H. sapiens | Affinity Capture-Western | Hong SW (2013) | Low Throughput |
| UBC | BAIT | H. sapiens | Affinity Capture-Western | Li Y (2014) | Low Throughput |
| UBC | HIT | H. sapiens | Affinity Capture-Western | Choi BH (2014) | Low Throughput |
| UBC | BAIT | H. sapiens | Affinity Capture-Western | Choi BH (2014) | Low Throughput |
| UBC | BAIT | H. sapiens | Affinity Capture-Western | Maehama T (2014) | Low Throughput |
| UBC | HIT | H. sapiens | Affinity Capture-Western | Aronchik I (2014) | Low Throughput |
| UBC | HIT | H. sapiens | Affinity Capture-Western | De Melo J (2014) | Low Throughput |
| UBC | HIT | H. sapiens | Affinity Capture-Western | Wang X (2008) | Low Throughput |
| UBC | HIT | H. sapiens | PCA | Li Y (2014) | Low Throughput |
| UBE2I | HIT | H. sapiens | Affinity Capture-Western | Waite KA (2003) | Low Throughput |
| UBE2I | BAIT | H. sapiens | Affinity Capture-Western | Huang J (2012) | Low Throughput |
| UBE2L3 | HIT | H. sapiens | Affinity Capture-Western | Waite KA (2003) | Low Throughput |
| USP4 | HIT | H. sapiens | Affinity Capture-MS | Zhang J (2013) | Low Throughput |
| USP7 | HIT | H. sapiens | Affinity Capture-MS | Zhang J (2013) | Low Throughput |
| USP7 | HIT | H. sapiens | Affinity Capture-Western | Wu Y (2013) | Low Throughput |
| USP7 | BAIT | H. sapiens | Affinity Capture-Western | Zhang J (2013) | Low Throughput |
| USP8 | HIT | H. sapiens | Affinity Capture-MS | Zhang J (2013) | Low Throughput |
| USP8 | BAIT | H. sapiens | Affinity Capture-Western | Zhang J (2013) | Low Throughput |
| USP10 | HIT | H. sapiens | Affinity Capture-MS | Zhang J (2013) | Low Throughput |
| USP10 | BAIT | H. sapiens | Affinity Capture-Western | Zhang J (2013) | Low Throughput |
| USP13 | HIT | H. sapiens | Affinity Capture-MS | Zhang J (2013) | Low Throughput |
| USP13 | BAIT | H. sapiens | Affinity Capture-Western | Zhang J (2013) | Low Throughput |
| USP13 | BAIT | H. sapiens | Biochemical Activity | Zhang J (2013) | Low Throughput |
| USP13 | HIT | H. sapiens | Reconstituted Complex | Zhang J (2013) | Low Throughput |
| USP39 | HIT | H. sapiens | Affinity Capture-MS | Zhang J (2013) | Low Throughput |
| UTP14A | HIT | H. sapiens | Two-hybrid | Stelzl U (2005) | High Throughput |
| WNT4 | HIT | H. sapiens | Affinity Capture-MS | Crockett DK (2005) | Low Throughput |
| WWP1 | HIT | H. sapiens | Affinity Capture-Western | Maddika S (2011) | Low Throughput |
| WWP1 | HIT | H. sapiens | Reconstituted Complex | Maddika S (2011) | Low Throughput |
| WWP2 | HIT | H. sapiens | Affinity Capture-MS | Crockett DK (2005) | Low Throughput |
| WWP2 | HIT | H. sapiens | Affinity Capture-Western | Ahmed SF (2012) | Low Throughput |
| WWP2 | HIT | H. sapiens | Affinity Capture-Western | Wu Y (2013) | Low Throughput |
| XIAP | HIT | H. sapiens | Affinity Capture-Western | Van Themsche C (2009) | Low Throughput |
| XIAP | BAIT | H. sapiens | Affinity Capture-Western | Van Themsche C (2009) | Low Throughput |
| XIAP | HIT | H. sapiens | Affinity Capture-Western | Ahmed SF (2012) | Low Throughput |
| XIAP | BAIT | H. sapiens | Biochemical Activity | Van Themsche C (2009) | Low Throughput |
| ZNF787 | HIT | H. sapiens | Affinity Capture-MS | Crockett DK (2005) | Low Throughput |

# 8.5 All identified PTEN-interacting proteins

**Table 8.3** Identification and LC-MS based label-free quantification of the binding partners of reduced and 1 mM $H_2O_2$ oxidized PTEN following GSH affinity enrichment showing the protein hits with confidence score >50 and 2 unique peptides but q-values for quantification below 0.05

| Accession[1] | Peptide count[2] | Confidence score[3] | p-value[4] | q-value[4] | Fold change[4] | Highest mean condition | Protein Description |
|---|---|---|---|---|---|---|---|
| GBB4_HUMAN | 3 (2) | 162.86 | 0.0562 | 0.0507 | 4.6 | Oxidized | Guanine nucleotide-binding protein subunit beta-4 |
| RL27_HUMAN | 3 (3) | 152.87 | 0.0609 | 0.0527 | 1.3 | Oxidized | 60S ribosomal protein L27 |
| SSFA2_HUMAN | 3 (3) | 148.17 | 0.0678 | 0.0561 | 3.0 | Oxidized | Sperm-specific antigen 2 |
| DNJA1_HUMAN | 2 (2) | 130.48 | 0.0667 | 0.0561 | 1.5 | Oxidized | DnaJ homolog subfamily A member 1 |
| SPTB2_HUMAN | 2 (2) | 105.4 | 0.072 | 0.057 | 2.2 | Oxidized | Spectrin beta chain, non-erythrocytic 1 |
| LIMA1_HUMAN | 5 (5) | 316.93 | 0.0881 | 0.0627 | 3.0 | Oxidized | LIM domain and actin-binding protein 1 |
| RL22L_HUMAN | 2 (2) | 195.95 | 0.0848 | 0.0627 | 1.5 | Reduced | 60S ribosomal protein L22-like 1 |
| RLA2_HUMAN | 3 (3) | 157.14 | 0.0936 | 0.0657 | 1.6 | Reduced | 60S acidic ribosomal protein P2 |
| RL27A_HUMAN | 3 (3) | 172.46 | 0.0993 | 0.0662 | 1.7 | Oxidized | 60S ribosomal protein L27a |
| FLNB_HUMAN | 2 (2) | 79.65 | 0.0984 | 0.0662 | 2.2 | Oxidized | Filamin-B |
| MYO1D_HUMAN | 2 (2) | 72.78 | 0.1039 | 0.0682 | 1.9 | Oxidized | Unconventional myosin-Id |
| TBB5_HUMAN | 22 (2) | 1494.03 | 0.1187 | 0.0732 | 2.6 | Reduced | Tubulin beta chain |
| PLEC_HUMAN | 16 (15) | 780.03 | 0.1183 | 0.0732 | 1.7 | Oxidized | Plectin |
| MTDC_HUMAN | 3 (3) | 183.16 | 0.1174 | 0.0732 | 2.4 | Oxidized | Bifunctional methylenetetrahydrofolate dehydrogenase/ cyclohydrolase, mitochondrial |
| LDHB_HUMAN | 3 (3) | 134.03 | 0.1212 | 0.0732 | 1.6 | Oxidized | L-lactate dehydrogenase B chain |
| RS17L_HUMAN | 2 (2) | 94.73 | 0.1227 | 0.0732 | 2.3 | Oxidized | 40S ribosomal protein S17-like |
| SDC1_HUMAN | 2 (2) | 160.1 | 0.1339 | 0.0749 | 1.4 | Reduced | Syndecan-1 |
| RS25_HUMAN | 2 (2) | 126.99 | 0.1339 | 0.0749 | 2.4 | Oxidized | 40S ribosomal protein S25 |
| COF1_HUMAN | 2 (2) | 122.11 | 0.1308 | 0.0749 | 6.6 | Oxidized | Cofilin-1 |

| | | | | | | | |
|---|---|---|---|---|---|---|---|
| RCC2_HUMAN | 4 (4) | 186.66 | 0.1421 | 0.078 | 8.3 | Oxidized | Protein RCC2 |
| MYOF_HUMAN | 2 (2) | 75.41 | 0.1525 | 0.0794 | 1.7 | Oxidized | Myoferlin |
| RS6_HUMAN | 2 (2) | 119.95 | 0.1619 | 0.0818 | 1.5 | Oxidized | 40S ribosomal protein S6 |
| GPC1_HUMAN | 4 (4) | 276.71 | 0.1723 | 0.0853 | 1.8 | Oxidized | Glypican-1 |
| RL7_HUMAN | 3 (2) | 130.63 | 0.1782 | 0.0874 | 1.4 | Oxidized | 60S ribosomal protein L7 |
| TBA1B_HUMAN | 8 (8) | 612.08 | 0.1847 | 0.088 | 2.0 | Reduced | Tubulin alpha-1B chain |
| ATPG_HUMAN | 2 (2) | 76.67 | 0.1842 | 0.088 | 1.1 | Oxidized | ATP synthase subunit gamma, mitochondrial |
| PLAK_HUMAN | 2 (2) | 97.41 | 0.1902 | 0.0892 | 1.9 | Oxidized | Junction plakoglobin |
| ARF4_HUMAN | 4 (3) | 211.29 | 0.1993 | 0.0907 | 1.3 | Reduced | ADP-ribosylation factor 4 |
| PEPL_HUMAN | 2 (2) | 74.53 | 0.1993 | 0.0907 | 2.4 | Oxidized | Periplakin |
| RL13A_HUMAN | 2 (2) | 77.83 | 0.2067 | 0.0932 | 1.2 | Reduced | 60S ribosomal protein L13a |
| RL23_HUMAN | 7 (7) | 848.54 | 0.2187 | 0.0969 | 1.3 | Oxidized | 60S ribosomal protein L23 |
| NCF1_HUMAN | 2 (2) | 260.51 | 0.2238 | 0.0975 | 3.4 | Reduced | Neutrophil cytosol factor |
| RS20_HUMAN | 2 (2) | 238.72 | 0.2392 | 0.1017 | 3.5 | Oxidized | 40S ribosomal protein S20 |
| GPC4_HUMAN | 2 (2) | 113.55 | 0.2396 | 0.1017 | 1.3 | Oxidized | Glypican-4 |
| RS27_HUMAN | 4 (2) | 438.84 | 0.2545 | 0.1071 | 1.7 | Oxidized | 40S ribosomal protein S27 |
| EFTU_HUMAN | 6 (6) | 357.5 | 0.2645 | 0.1095 | 2.2 | Oxidized | Elongation factor Tu, mitochondrial |
| H2A1B_HUMAN | 2 (2) | 110.47 | 0.2833 | 0.1138 | 1.8 | Reduced | Histone H2A type 1-B/E |
| S10A8_HUMAN | 2 (2) | 81.02 | 0.2903 | 0.1141 | 1.6 | Reduced | Protein S100-A8 |
| MYH10_HUMAN | 3 (2) | 137.31 | 0.306 | 0.1171 | 1.5 | Oxidized | Myosin-10 |
| CH60_HUMAN | 2 (2) | 172.34 | 0.3299 | 0.1211 | 1.7 | Reduced | 60 kDa heat shock protein, mitochondrial |
| RL14_HUMAN | 2 (2) | 111.65 | 0.3332 | 0.1211 | 1.4 | Oxidized | 60S ribosomal protein L14 |
| ATPA_HUMAN | 5 (5) | 274.87 | 0.3643 | 0.1243 | 3.6 | Reduced | ATP synthase subunit alpha, mitochondrial |
| KBTB4_HUMAN | 3 (3) | 209.58 | 0.3589 | 0.1243 | 4.2 | Oxidized | Kelch repeat and BTB domain-containing protein 4 |
| KPYM_HUMAN | 2 (2) | 68.52 | 0.3532 | 0.1243 | 1.7 | Oxidized | Pyruvate kinase PKM |
| RS4X_HUMAN | 5 (5) | 258.56 | 0.4035 | 0.1282 | 1.2 | Reduced | 40S ribosomal protein S4, X isoform |
| ADT2_HUMAN | 3 (3) | 124.64 | 0.4005 | 0.1282 | 1.2 | Oxidized | ADP/ATP translocase 2 |
| DCA11_HUMAN | 10 (10) | 690.54 | 0.4611 | 0.1387 | 1.8 | Oxidized | DDB1- and CUL4-associated factor 11 |

| | | | | | | | |
|---|---|---|---|---|---|---|---|
| S10A9_HUMAN | 3 (3) | 163.19 | 0.5196 | 0.1535 | 5.7 | Reduced | Protein S100-A9 |
| TBB4B_HUMAN | 20 (2) | 1338.36 | 0.5478 | 0.1581 | 26.2 | Reduced | Tubulin beta-4B chain |
| RL12_HUMAN | 3 (3) | 179.33 | 0.5588 | 0.1595 | 1.1 | Oxidized | 60S ribosomal protein L12 |
| LEG1_HUMAN | 3 (3) | 110.7 | 0.5663 | 0.1607 | 1.4 | Oxidized | Galectin-1 |
| MYO1B_HUMAN | 9 (9) | 609.46 | 0.573 | 0.1617 | 1.2 | Oxidized | Unconventional myosin-Ib |
| RS3_HUMAN | 4 (4) | 184.78 | 0.5865 | 0.1637 | 1.7 | Oxidized | 40S ribosomal protein S3 |
| SDC4_HUMAN | 3 (3) | 232.89 | 0.6254 | 0.1717 | 1.1 | Reduced | Syndecan-4 |
| RS13_HUMAN | 2 (2) | 99.46 | 0.6379 | 0.1722 | 1.0 | Reduced | 40S ribosomal protein S13 |
| ML12A_HUMAN | 3 (3) | 197.71 | 0.656 | 0.1741 | 1.1 | Oxidized | Myosin regulatory light chain 12A |
| HS90B_HUMAN | 4 (2) | 277.94 | 0.7047 | 0.1825 | 1.1 | Oxidized | Heat shock protein HSP 90-beta |
| CALM_HUMAN | 4 (4) | 250.24 | 0.7046 | 0.1825 | 1.1 | Reduced | Calmodulin |
| MPCP_HUMAN | 2 (2) | 104.89 | 0.7018 | 0.1825 | 1.1 | Reduced | Phosphate carrier protein, mitochondrial |
| RL31_HUMAN | 3 (3) | 177.71 | 0.7252 | 0.186 | 1.1 | Reduced | 60S ribosomal protein L31 |
| SNTB2_HUMAN | 2 (2) | 133.42 | 0.7512 | 0.1888 | 1.2 | Oxidized | Beta-2-syntrophin |
| MYO1C_HUMAN | 11 (11) | 776.71 | 0.7577 | 0.1889 | 1.1 | Oxidized | Unconventional myosin-Ic |
| SETX_HUMAN | 2 (2) | 71.6 | 0.7684 | 0.1889 | 1.0 | Oxidized | Probable helicase senataxin |
| RL13_HUMAN | 4 (4) | 176.14 | 0.7832 | 0.1906 | 1.0 | Oxidized | 60S ribosomal protein L13 |
| RS26_HUMAN | 2 (2) | 84.7 | 0.785 | 0.1906 | 1.1 | Reduced | 40S ribosomal protein S26 |
| RS27A_HUMAN | 2 (2) | 89.07 | 0.798 | 0.192 | 1.0 | Reduced | Ubiquitin-40S ribosomal protein S27a |
| CP013_HUMAN | 2 (2) | 196.28 | 0.8487 | 0.197 | 1.0 | Reduced | UPF0585 protein C16orf13 |
| YES_HUMAN | 2 (2) | 97.43 | 0.8488 | 0.197 | 1.9 | Oxidized | Tyrosine-protein kinase Yes |
| DDB1_HUMAN | 7 (7) | 347.08 | 0.8942 | 0.2017 | 1.0 | Oxidized | DNA damage-binding protein 1 |
| SDCB1_HUMAN | 2 (2) | 68.67 | 0.948 | 0.211 | 1.0 | Oxidized | Syntenin-1 |

[1]Accession = SwissProt Protein ID

[2]Peptide count = the number of detected peptides (the number of unique peptides) used for quantification

[3]The protein confidence score was generated using Mascot as described in the experimental.

[4]The p-value, q-value and fold change were generated by Progenesis QI for proteomics as described in the experimental.

The data was obtained from the analysis of three independent GSH-affinity experiments. The list was restricted to the protein hits showing a confidence score ≥ 50, a number of unique peptides ≥ 2 and a q value >0.05. Ranking is based on q-values.

**Table 8.4** Identification and LC-MS based label-free quantification of the binding partners of reduced and 1mM $H_2O_2$ oxidized PTEN following GSH affinity enrichment showing the protein hits for which the number of unique peptides used for quantification was below 2

| Accession[1] | Peptide count[2] | Confidence score[3] | p-value[4] | q-value[4] | Fold change[4] | Highest mean condition | Protein Description |
|---|---|---|---|---|---|---|---|
| FBX3_HUMAN | 1 (1) | 49.67 | < 0.0001 | 0.0001 | 3206.7 | Oxidized | F-box only protein 3 |
| 1433T_HUMAN | 3 (1) | 175.01 | 0.0026 | 0.0215 | Infinity | Oxidized | 14-3-3 protein theta |
| RL29_HUMAN | 1 (1) | 36.25 | 0.0034 | 0.0246 | 6.6 | Oxidized | 60S ribosomal protein L29 |
| HNRPF_HUMAN | 1 (1) | 65.45 | 0.0042 | 0.0261 | 2.4 | Oxidized | Heterogeneous nuclear ribonucleoprotein F |
| RL15_HUMAN | 1 (1) | 50.24 | 0.0050 | 0.0261 | 4.7 | Reduced | 60S ribosomal protein L15 |
| NDUA4_HUMAN | 1 (1) | 54.94 | 0.0083 | 0.0301 | 2.2 | Reduced | NADH dehydrogenase [ubiquinone] 1 alpha subcomplex subunit 4 |
| CD109_HUMAN | 1 (1) | 54.14 | 0.0100 | 0.0337 | 1.6 | Oxidized | CD109 antigen |
| DSG2_HUMAN | 1 (1) | 58.22 | 0.0151 | 0.0387 | 5.7 | Oxidized | Desmoglein-2 |
| HEM6_HUMAN | 1 (1) | 56.15 | 0.0139 | 0.0387 | 23.2 | Oxidized | Coproporphyrinogen-III oxidase, mitochondrial |
| PYR1_HUMAN | 1 (1) | 39.34 | 0.0153 | 0.0387 | 1.5 | Oxidized | CAD protein |
| GNAI3_HUMAN | 4(1) | 202.98 | 0.0219 | 0.0437 | 8.5 | Oxidized | Guanine nucleotide-binding protein G(k) subunit alpha |
| CD44_HUMAN | 1 (1) | 113.75 | 0.0200 | 0.0437 | 1.7 | Reduced | CD44 antigen |
| ECHB_HUMAN | 1 (1) | 36.19 | 0.0227 | 0.0437 | 1.2 | Oxidized | Trifunctional enzyme subunit beta, mitochondrial |
| RL7A_HUMAN | 1 (1) | 74.01 | 0.0280 | 0.0448 | 1.9 | Oxidized | 60S ribosomal protein L7a |
| DEST_HUMAN | 1 (1) | 44.55 | 0.0278 | 0.0448 | 9.7 | Oxidized | Destrin |
| PCBP2_HUMAN | 1 (1) | 67.8 | 0.0302 | 0.0454 | 3.7 | Oxidized | Poly(rC)-binding protein 2 |
| GBB1_HUMAN | 2 (1) | 128.85 | 0.0335 | 0.0456 | 5.4 | Oxidized | Guanine nucleotide-binding protein G(I)/G(S)/G(T) subunit beta-1 |
| SSBP_HUMAN | 1 (1) | 53.32 | 0.0353 | 0.0456 | 6.8 | Oxidized | Single-stranded DNA-binding protein, mitochondrial |
| CRF_HUMAN | 1 (1) | 32.66 | 0.0344 | 0.0456 | 5.0 | Reduced | Corticoliberin 1 |
| RS23_HUMAN | 1 (1) | 73.79 | 0.0490 | 0.0463 | 2.3 | Oxidized | 40S ribosomal protein S23 |
| CTND1_HUMAN | 1 (1) | 63.34 | 0.0486 | 0.0463 | 6.8 | Oxidized | Catenin delta-1 |
| RL35_HUMAN | 1 (1) | 60.03 | 0.0458 | 0.0463 | 1.7 | Oxidized | 60S ribosomal protein L35 |
| RS12_HUMAN | 1 (1) | 42.03 | 0.0488 | 0.0463 | 3.1 | Oxidized | 40S ribosomal protein S12 |
| HID1_HUMAN | 1 (1) | 41.84 | 0.0412 | 0.0463 | 4.4 | Reduced | Protein HID1 |
| XRCC5_HUMAN | 1 (1) | 37.8 | 0.0556 | 0.0507 | Infinity | Oxidized | X-ray repair cross-complementing protein 5 |
| MCM3_HUMAN | 1 (1) | 34.21 | 0.0577 | 0.0511 | 1.8 | Oxidized | DNA replication licensing factor MCM3 |
| S10A7_HUMAN | 1 (1) | 38.55 | 0.0615 | 0.0527 | 6.4 | Reduced | Protein S100-A7 |
| RL5_HUMAN | 1 (1) | 47.31 | 0.0695 | 0.0566 | 3.3 | Oxidized | 60S ribosomal protein L5 |
| RL11_HUMAN | 1 (1) | 70.16 | 0.0722 | 0.0570 | 1.3 | Oxidized | 60S ribosomal protein L11 |
| ACTN4_HUMAN | 1 (1) | 39.87 | 0.0744 | 0.0577 | 2.0 | Oxidized | Alpha-actinin-4 |
| RS5_HUMAN | 1 (1) | 35.36 | 0.0754 | 0.0577 | 2.5 | Reduced | 40S ribosomal protein S5 |
| MAGI1_HUMAN | 1 (1) | 42.61 | 0.0822 | 0.0620 | 1.9 | Oxidized | Membrane-associated guanylate kinase, WW and PDZ domain-containing protein 1 |
| SMD3_HUMAN | 1 (1) | 68.52 | 0.0872 | 0.0627 | 1.6 | Oxidized | Small nuclear ribonucleoprotein Sm D3 |
| CMYA5_HUMAN | 1 (1) | 35.33 | 0.0871 | 0.0627 | 1.8 | Oxidized | Cardiomyopathy-associated protein 5 |
| HORN_HUMAN | 1 (1) | 50.25 | 0.0996 | 0.0662 | 11.1 | Reduced | Hornerin |
| MYO5B_HUMAN | 1 (1) | 32.57 | 0.0970 | 0.0662 | 2.1 | Oxidized | Unconventional myosin-Vb |
| RS3A_HUMAN | 1 (1) | 36.31 | 0.1225 | 0.0732 | 4.7 | Oxidized | 40S ribosomal protein S3a |
| RS15_HUMAN | 1 (1) | 35.11 | 0.1231 | 0.0732 | 1.5 | Oxidized | 40S ribosomal protein S15 |
| RL32_HUMAN | 1 (1) | 42.67 | 0.1325 | 0.0749 | 6.5 | Oxidized | 60S ribosomal protein L32 |
| EPCAM_HUMAN | 1 (1) | 34.34 | 0.1295 | 0.0749 | 2.9 | Oxidized | Epithelial cell adhesion molecule |
| PSMD2_HUMAN | 1 (1) | 53.25 | 0.1470 | 0.0794 | 2.0 | Oxidized | 26S proteasome non-ATPase regulatory subunit 2 |

| | | | | | | | |
|---|---|---|---|---|---|---|---|
| AGRIN_HUMAN | 1 (1) | 48.65 | 0.1513 | 0.0794 | 1.7 | Oxidized | Agrin |
| RL8_HUMAN | 1 (1) | 71.31 | 0.1586 | 0.0809 | 1.2 | Oxidized | 60S ribosomal protein L8 |
| PGAP1_HUMAN | 1 (1) | 40.02 | 0.1582 | 0.0809 | 2.4 | Reduced | GPI inositol-deacylase |
| RS7_HUMAN | 1 (1) | 42.34 | 0.1645 | 0.0823 | 3.5 | Reduced | 40S ribosomal protein S7 |
| H2B1J_HUMAN | 1 (1) | 43.08 | 0.1805 | 0.0877 | 1.2 | Reduced | Histone H2B type 1-J |
| RS24_HUMAN | 1 (1) | 41.38 | 0.1925 | 0.0892 | 6.3 | Oxidized | 40S ribosomal protein S24 |
| RUVB2_HUMAN | 1 (1) | 35.86 | 0.1925 | 0.0892 | 2.2 | Oxidized | RuvB-like 2 |
| HSPB1_HUMAN | 1 (1) | 63.42 | 0.2085 | 0.0932 | 3.9 | Reduced | Heat shock protein beta-1 |
| RL10L_HUMAN | 1 (1) | 42.32 | 0.2208 | 0.0970 | 3.5 | Oxidized | 60S ribosomal protein L10-like |
| ARF1_HUMAN | 2 (1) | 88.51 | 0.2270 | 0.0980 | 1.3 | Reduced | ADP-ribosylation factor 1 |
| P5CR1_HUMAN | 1 (1) | 51.34 | 0.2617 | 0.1093 | 1.8 | Oxidized | Pyrroline-5-carboxylate reductase 1, mitochondrial |
| 1433Z_HUMAN | 3 (1) | 184.23 | 0.2747 | 0.1128 | 2.5 | Oxidized | 14-3-3 protein zeta/delta |
| TBB3_HUMAN | 16 (1) | 1067.14 | 0.2807 | 0.1138 | 2.6 | Reduced | Tubulin beta-3 chain |
| RL18_HUMAN | 1 (1) | 76.6 | 0.2849 | 0.1138 | 1.5 | Oxidized | 60S ribosomal protein L18 |
| PKP2_HUMAN | 1 (1) | 56.03 | 0.2861 | 0.1138 | 2.5 | Oxidized | Plakophilin-2 |
| SERA_HUMAN | 1 (1) | 45.18 | 0.2914 | 0.1141 | 2.2 | Reduced | D-3-phosphoglycerate dehydrogenase |
| RS27L_HUMAN | 3 (1) | 298.09 | 0.3058 | 0.1171 | 1.6 | Oxidized | 40S ribosomal protein S27-like |
| MIF_HUMAN | 1 (1) | 44.15 | 0.3155 | 0.1198 | 1.2 | Oxidized | Macrophage migration inhibitory factor |
| GBG12_HUMAN | 1 (1) | 110.3 | 0.3184 | 0.1199 | 2.4 | Oxidized | Guanine nucleotide-binding protein G(I)/G(S)/G(O) subunit gamma-12 |
| C2TA_HUMAN | 1 (1) | 32.32 | 0.3204 | 0.1199 | 1.5 | Oxidized | MHC class II transactivator |
| RALA_HUMAN | 1 (1) | 50.68 | 0.3272 | 0.1211 | 1.4 | Oxidized | Ras-related protein Ral-A |
| LEG7_HUMAN | 1 (1) | 40.9 | 0.3315 | 0.1211 | 3.6 | Reduced | Galectin-7 |
| TIM50_HUMAN | 1 (1) | 42.37 | 0.3372 | 0.1215 | 1.3 | Oxidized | Mitochondrial import inner membrane translocase subunit TIM50 |
| APOD_HUMAN | 1 (1) | 36.11 | 0.3483 | 0.1239 | 2.9 | Oxidized | Apolipoprotein D |
| RL6_HUMAN | 1 (1) | 60.07 | 0.3705 | 0.1243 | 1.1 | Oxidized | 60S ribosomal protein L6 |
| ARL1_HUMAN | 1 (1) | 58.27 | 0.3706 | 0.1243 | 1.2 | Oxidized | ADP-ribosylation factor-like protein 1 |
| IGHG1_HUMAN | 1 (1) | 51.63 | 0.3640 | 0.1243 | 4.2 | Reduced | Ig gamma-1 chain C region |
| RFA3_HUMAN | 1 (1) | 51.1 | 0.3545 | 0.1243 | 37.2 | Oxidized | Replication protein A 14 kDa subunit |
| CECR1_HUMAN | 1 (1) | 48.1 | 0.3739 | 0.1243 | Infinity | Oxidized | Adenosine deaminase CECR1 |
| TCPH_HUMAN | 1 (1) | 40.07 | 0.3739 | 0.1243 | Infinity | Oxidized | T-complex protein 1 subunit eta |
| IGKC_HUMAN | 1 (1) | 32.28 | 0.3739 | 0.1243 | Infinity | Reduced | Ig kappa chain C region |
| PGBM_HUMAN | 4 (4) | 200.74 | 0.3856 | 0.1248 | 1.1 | Oxidized | Basement membrane-specific heparan sulfate proteoglycan core protein |
| HNRH1_HUMAN | 1 (1) | 77.91 | 0.3851 | 0.1248 | 1.6 | Reduced | Heterogeneous nuclear ribonucleoprotein H |
| FABP5_HUMAN | 1 (1) | 40.66 | 0.3816 | 0.1248 | 5.2 | Reduced | Fatty acid-binding protein, epidermal |
| OR7G3_HUMAN | 1 (1) | 35.2 | 0.4021 | 0.1282 | 1.2 | Oxidized | Olfactory receptor 7G3 |
| 1433S_HUMAN | 2 (1) | 121.66 | 0.4272 | 0.1344 | 118.0 | Reduced | 14-3-3 protein sigma |
| PDP1_HUMAN | 1 (1) | 42.99 | 0.4310 | 0.1344 | 1.3 | Oxidized | [Pyruvate dehydrogenase [acetyl-transferring]]-phosphatase 1, mitochondrial |
| ARHGH_HUMAN | 1 (1) | 40.09 | 0.4285 | 0.1344 | 1.1 | Reduced | Rho guanine nucleotide exchange factor 17 |
| HS90A_HUMAN | 3 (1) | 189.32 | 0.4363 | 0.1352 | 1.3 | Oxidized | Heat shock protein HSP 90-alpha |
| PCNA_HUMAN | 1 (1) | 34.34 | 0.4537 | 0.1381 | 1.1 | Oxidized | Proliferating cell nuclear antigen |
| SMD2_HUMAN | 1 (1) | 50.52 | 0.4576 | 0.1384 | 1.2 | Oxidized | Small nuclear ribonucleoprotein Sm D2 |
| RS8_HUMAN | 1 (1) | 40.69 | 0.4985 | 0.1490 | 1.1 | Reduced | 40S ribosomal protein S8 |
| FA47A_HUMAN | 1 (1) | 33.85 | 0.5030 | 0.1495 | 1.2 | Oxidized | Protein FAM47A |
| RL23A_HUMAN | 1 (1) | 35.01 | 0.5337 | 0.1558 | 1.1 | Oxidized | 60S ribosomal protein L23a |
| PIP_HUMAN | 1 (1) | 60.36 | 0.5464 | 0.1581 | 30.6 | Reduced | Prolactin-inducible protein |
| TBB6_HUMAN | 7 (1) | 347.18 | 0.5571 | 0.1595 | 10.4 | Reduced | Tubulin beta-6 chain |

| | | | | | | | |
|---|---|---|---|---|---|---|---|
| HS71L_HUMAN | 3 (1) | 162.95 | 0.5833 | 0.1637 | 4.5 | Oxidized | Heat shock 70 kDa protein 1-like |
| GFAP_HUMAN | 1 (1) | 79.58 | 0.6410 | 0.1722 | 1.2 | Oxidized | Glial fibrillary acidic protein |
| ZA2G_HUMAN | 1 (1) | 51.28 | 0.6326 | 0.1722 | 1.1 | Oxidized | Zinc-alpha-2-glycoprotein |
| RL26L_HUMAN | 1 (1) | 36.71 | 0.6404 | 0.1722 | 1.1 | Reduced | 60S ribosomal protein L26-like 1 |
| A16L2_HUMAN | 1 (1) | 36.12 | 0.6567 | 0.1741 | 1.0 | Reduced | Autophagy-related protein 16-2 |
| AL1A2_HUMAN | 1 (1) | 49.13 | 0.6959 | 0.1825 | 1.0 | Reduced | Retinal dehydrogenase 2 |
| ZN630_HUMAN | 1 (1) | 35.87 | 0.7144 | 0.1841 | 1.1 | Oxidized | Zinc finger protein 630 |
| USMG5_HUMAN | 2 (1) | 106.05 | 0.7307 | 0.1862 | 1.4 | Oxidized | Up-regulated during skeletal muscle growth protein 5 |
| RAE1_HUMAN | 1 (1) | 35 | 0.7335 | 0.1862 | 1.4 | Reduced | Rab proteins geranylgeranyltransferase component A 1 |
| PPIA_HUMAN | 1 (1) | 48.93 | 0.7455 | 0.1883 | 1.1 | Oxidized | Peptidyl-prolyl cis-trans isomerase A |
| RLA1_HUMAN | 1 (1) | 50.17 | 0.7633 | 0.1889 | 1.1 | Oxidized | 60S acidic ribosomal protein P1 |
| RS11_HUMAN | 1 (1) | 41.87 | 0.7702 | 0.1889 | 1.1 | Oxidized | 40S ribosomal protein S11 |
| SUCA_HUMAN | 1 (1) | 36.88 | 0.7661 | 0.1889 | 1.1 | Reduced | Succinyl-CoA ligase [ADP/GDP-forming] subunit alpha, mitochondrial |
| DTNA_HUMAN | 1 (1) | 53.11 | 0.8038 | 0.1924 | 1.2 | Oxidized | Dystrobrevin alpha |
| GSTA1_HUMAN | 1 (1) | 35.16 | 0.8160 | 0.1944 | 1.0 | Oxidized | Glutathione S-transferase A1 |
| MED23_HUMAN | 1 (1) | 34.9 | 0.8283 | 0.1955 | 2.1 | Oxidized | Mediator of RNA polymerase II transcription subunit 23 |
| RL22_HUMAN | 1 (1) | 66.32 | 0.8379 | 0.1969 | 1.1 | Oxidized | 60S ribosomal protein L22 |
| RL36_HUMAN | 1 (1) | 48.57 | 0.8646 | 0.1994 | 1.1 | Reduced | 60S ribosomal protein L36 |
| HSP71_HUMAN | 3 (1) | 199.56 | 0.8825 | 0.2010 | 1.3 | Oxidized | Heat shock 70 kDa protein 1A/1B |
| A16L1_HUMAN | 1 (1) | 35.3 | 0.8786 | 0.2010 | 1.3 | Oxidized | Autophagy-related protein 16-1 |
| MAP6_HUMAN | 1 (1) | 35.02 | 0.8835 | 0.2010 | 1.0 | Oxidized | Microtubule-associated protein 6 |
| UBE2O_HUMAN | 1 (1) | 34.08 | 0.8898 | 0.2016 | 1.0 | Reduced | Ubiquitin-conjugating enzyme E2 O |
| PHLA2_HUMAN | 1 (1) | 43.4 | 0.9245 | 0.2066 | 1.0 | Oxidized | Pleckstrin homology-like domain family A member 2 |
| RL4_HUMAN | 1 (1) | 38.89 | 0.9728 | 0.2146 | 2.3 | Reduced | 60S ribosomal protein L4 |

[1]Accession = SwissProt Protein ID

[2]Peptide count = the number of detected peptides (the number of unique peptides) used for quantification

[3]The protein confidence score was generated using Mascot as described in the experimental

[4]The p-value, q-value and fold change were generated by Progenesis QI for proteomics as described in the experimental

The data was obtained from the analysis of three independent GSH-affinity experiments. The list was restricted to the protein hits showing a number of unique peptides < 2. Ranking is based on q-values.

**Table 8.5** Identification and LC-MS based label-free quantification of the proteins bound to the untreated and oxidized PTEN-GST that were also identified in the sample eluted from the GST control and the GSH beads alone

| **Accession**[1] | **Peptide count**[2] | **Confidence score**[3] | **p-value**[4] | **q-value**[4] | **Fold change**[4] | **Highest mean condition** | **Protein Description** |
|---|---|---|---|---|---|---|---|
| LANC1_HUMAN | 2 (2) | 79.89 | 0.0081 | 0.0301 | 2.4 | Oxidized | LanC-like protein 1 |
| ACTB_HUMAN | 9 (9) | 594.1 | 0.0284 | 0.0448 | 2.6 | Oxidized | Actin, cytoplasmic 1 |
| EF1A2_HUMAN | 4 (4) | 243.3 | 0.0358 | 0.0456 | 1.9 | Oxidized | Elongation factor 1-alpha 2 |
| EF1G_HUMAN | 6 (6) | 445.16 | 0.1063 | 0.0689 | 1.7 | Oxidized | Elongation factor 1-gamma |
| H4_HUMAN | 1 (1) | 45.39 | 0.1349 | 0.0749 | 1.3 | Reduced | Histone H4 |
| GSTP1_HUMAN | 15 (15) | 2461.58 | 0.1502 | 0.0794 | 1.8 | Reduced | Glutathione S-transferase P |
| ALBU_HUMAN | 9 (9) | 736.39 | 0.1525 | 0.0794 | 1.6 | Reduced | Serum albumin |
| PTEN_HUMAN | 26 (25) | 2441.14 | 0.2968 | 0.1153 | 1.5 | Oxidized | Phosphatidylinositol 3,4,5-trisphosphate 3-phosphatase and dual-specificity protein phosphatase PTEN |
| MYH9_HUMAN | 7 (5) | 425.51 | 0.3393 | 0.1215 | 1.3 | Oxidized | Myosin-9 |
| CCD87_HUMAN | 1 (1) | 63.52 | 0.3838 | 0.1248 | 1.5 | Oxidized | Coiled-coil domain-containing protein 87 |
| RS16_HUMAN | 6 (5) | 386.86 | 0.4464 | 0.1375 | 2.2 | Oxidized | 40S ribosomal protein S16 |
| GEMI4_HUMAN | 2 (1) | 76.32 | 0.4504 | 0.1379 | 1.5 | Oxidized | Gem-associated protein 4 |
| MYL6_HUMAN | 3 (3) | 200.09 | 0.5325 | 0.1558 | 1.3 | Oxidized | Myosin light polypeptide 6 |
| DCD_HUMAN | 3 (3) | 315.14 | 0.6082 | 0.1688 | 1.1 | Reduced | Dermcidin |
| EF1B_HUMAN | 4 (4) | 369.47 | 0.6140 | 0.1695 | 1.3 | Reduced | Elongation factor 1-beta |
| EF1A1_HUMAN | 4 (2) | 224.11 | 0.6584 | 0.1741 | 1.2 | Oxidized | Elongation factor 1-alpha 1 |
| XRCC6_HUMAN | 3 (3) | 237.83 | 0.7982 | 0.1920 | 1.9 | Oxidized | X-ray repair cross-complementing protein 6 |
| RS14_HUMAN | 3 (3) | 223.82 | 0.8222 | 0.1950 | 1.1 | Oxidized | 40S ribosomal protein S14 |
| RS10_HUMAN | 3 (3) | 176.74 | 0.8503 | 0.1970 | 1.0 | Oxidized | 40S ribosomal protein S10 |
| RS18_HUMAN | 5 (5) | 305.06 | 0.9218 | 0.2066 | 1.1 | Reduced | 40S ribosomal protein S18 |

[1]Accession = SwissProt Protein ID

[2]Peptide count = the number of detected peptides (the number of unique peptides) used for quantification

[3]The protein confidence score was generated using Mascot as described in the experimental

[4]The p-value, q-value and fold change were generated by Progenesis QI for proteomics as described in the experimental.

The data was obtained from the analysis of three independent GSH-affinity experiments. Ranking is based on q-values.

**Table 8.6** Identification and LC-MS based label-free quantification of PTEN-EGFP binding proteins affinity-captured by Co-IP from HCT116 cell lysate showing the protein hits with more than 2 unique peptides

| **Accession**[1] | **Peptides**[2] | **Score**[3] | **Description** | **Average Normalized Abundances**[4] |
|---|---|---|---|---|
| NONO_HUMAN | 37 (36) | 3733.64 | Non-POU domain-containing octamer-binding protein | 546000 |
| SFPQ_HUMAN | 33 (32) | 3136.4 | Splicing factor, proline- and glutamine-rich | 112000 |
| PABP1_HUMAN | 31 (19) | 2663.77 | Polyadenylate-binding protein 1 | 201000 |
| PABP4_HUMAN | 26 (14) | 2067.69 | Polyadenylate-binding protein 4 | 39100 |
| EWS_HUMAN | 14 (13) | 1968.61 | RNA-binding protein EWS | 1030000 |
| RBM14_HUMAN | 20 (20) | 1749.49 | RNA-binding protein 14 | 162000 |
| ACTB_HUMAN | 16 (11) | 1606.03 | Actin, cytoplasmic 1 | 61800 |
| HNRPM_HUMAN | 23 (22) | 1580.56 | Heterogeneous nuclear ribonucleoprotein M | 50900 |
| ROA2_HUMAN | 15 (12) | 1480.19 | Heterogeneous nuclear ribonucleoproteins A2/B1 | 71400 |
| HS90B_HUMAN | 20 (9) | 1440.25 | Heat shock protein HSP 90-beta | 12200 |
| NUFP2_HUMAN | 16 (16) | 1398.64 | Nuclear fragile X mental retardation-interacting protein 2 | 28500 |
| PTEN_HUMAN | 16 (16) | 1252.96 | Phosphatidylinositol 3,4,5-trisphosphate 3-phosphatase and dual-specificity protein phosphatase PTEN | 233000 |
| G3BP1_HUMAN | 15 (13) | 1250.77 | Ras GTPase-activating protein-binding protein 1 | 69900 |
| FUS_HUMAN | 12 (10) | 1247.09 | RNA-binding protein FUS | 129000 |
| IF2B2_HUMAN | 17 (13) | 1186.93 | Insulin-like growth factor 2 mRNA-binding protein 2 | 14700 |
| HS90A_HUMAN | 17 (6) | 1164.28 | Heat shock protein HSP 90-alpha | 5278.25 |
| LAP2A_HUMAN | 14 (14) | 1159.21 | Lamina-associated polypeptide 2, isoform alpha | 28700 |
| PTBP1_HUMAN | 11 (10) | 1149.35 | Polypyrimidine tract-binding protein 1 | 21800 |
| G3BP2_HUMAN | 14 (11) | 1115.7 | Ras GTPase-activating protein-binding protein 2 | 32200 |
| RTCB_HUMAN | 16 (16) | 1087.16 | tRNA-splicing ligase RtcB homolog | 35300 |
| DDX1_HUMAN | 19 (19) | 1056.89 | ATP-dependent RNA helicase DDX1 | 27200 |
| WDR82_HUMAN | 14 (14) | 1054.63 | WD repeat-containing protein 82 | 50700 |
| TBB5_HUMAN | 16 (2) | 1045.15 | Tubulin beta chain | 7057.32 |
| CH60_HUMAN | 13 (13) | 1016.71 | 60 kDa heat shock protein, mitochondrial | 18800 |
| HNRPK_HUMAN | 14 (14) | 964.34 | Heterogeneous nuclear ribonucleoprotein K | 18600 |
| TOX4_HUMAN | 12 (12) | 963.19 | TOX high mobility group box family member 4 | 63400 |
| PP1A_HUMAN | 10 (4) | 907.32 | Serine/threonine-protein phosphatase PP1-alpha catalytic subunit | 26800 |
| YBOX1_HUMAN | 10 (9) | 868.78 | Nuclease-sensitive element-binding protein 1 | 15200 |
| ROA1_HUMAN | 9 (5) | 868.23 | Heterogeneous nuclear ribonucleoprotein A1 | 16800 |

| | | | | |
|---|---|---|---|---|
| FXR1_HUMAN | 13 (12) | 861.41 | Fragile X mental retardation syndrome-related protein 1 | 13400 |
| IF2B3_HUMAN | 12 (9) | 830.68 | Insulin-like growth factor 2 mRNA-binding protein 3 | 9327.45 |
| ACTC_HUMAN | 10 (2) | 829.97 | Actin, alpha cardiac muscle 1 | 952.84 |
| HSP7C_HUMAN | 13 (11) | 809.93 | Heat shock cognate 71 kDa protein | 9336.89 |
| PP1B_HUMAN | 8 (3) | 801.35 | Serine/threonine-protein phosphatase PP1-beta catalytic subunit | 6561.29 |
| CAPR1_HUMAN | 11 (11) | 787.7 | Caprin-1 | 48200 |
| PSPC1_HUMAN | 10 (10) | 744.37 | Paraspeckle component 1 | 23300 |
| ALBU_HUMAN | 11 (11) | 712.88 | Serum albumin | 71400 |
| ENOA_HUMAN | 11 (8) | 676.74 | Alpha-enolase | 8437.81 |
| TBA1A_HUMAN | 10 (10) | 676.11 | Tubulin alpha-1A chain | 22100 |
| RS18_HUMAN | 10 (10) | 675.69 | 40S ribosomal protein S18 | 36600 |
| ELAV1_HUMAN | 7 (7) | 667.51 | ELAV-like protein 1 | 18100 |
| HNRH1_HUMAN | 7 (3) | 665.39 | Heterogeneous nuclear ribonucleoprotein H | 2594.4 |
| EF1A1_HUMAN | 10 (10) | 645.25 | Elongation factor 1-alpha 1 | 57700 |
| ROA3_HUMAN | 8 (6) | 635.15 | Heterogeneous nuclear ribonucleoprotein A3 | 4215.62 |
| RS4X_HUMAN | 11 (11) | 625.81 | 40S ribosomal protein S4, X isoform | 8836.6 |
| PP1RA_HUMAN | 12 (12) | 612.77 | Serine/threonine-protein phosphatase 1 regulatory subunit 10 | 16200 |
| FA98A_HUMAN | 6 (6) | 605.38 | Protein FAM98A | 12000 |
| TRAF3_HUMAN | 10 (8) | 602.59 | TNF receptor-associated factor 3 | 8877.83 |
| CPSF5_HUMAN | 8 (8) | 594.47 | Cleavage and polyadenylation specificity factor subunit 5 | 23300 |
| G3P_HUMAN | 9 (9) | 586.96 | Glyceraldehyde-3-phosphate dehydrogenase | 26400 |
| GRP78_HUMAN | 10 (8) | 577.61 | 78 kDa glucose-regulated protein | 4156.06 |
| RS3_HUMAN | 12 (12) | 542.64 | 40S ribosomal protein S3 | 9871.58 |
| ATX2L_HUMAN | 9 (9) | 540.04 | Ataxin-2-like protein | 6964.24 |
| DDX17_HUMAN | 9 (7) | 522.73 | Probable ATP-dependent RNA helicase DDX17 | 6588.78 |
| DDX5_HUMAN | 9 (7) | 520.88 | Probable ATP-dependent RNA helicase DDX5 | 16800 |
| LDHA_HUMAN | 9 (7) | 500.74 | L-lactate dehydrogenase A chain | 5675.55 |
| ALDOA_HUMAN | 8 (8) | 488.84 | Fructose-bisphosphate aldolase A | 10700 |
| FXR2_HUMAN | 7 (6) | 484.17 | Fragile X mental retardation syndrome-related protein 2 | 1889.51 |
| RS3A_HUMAN | 9 (9) | 483.39 | 40S ribosomal protein S3a | 16300 |
| CPSF6_HUMAN | 6 (6) | 471.3 | Cleavage and polyadenylation specificity factor subunit 6 | 8978.42 |
| CN166_HUMAN | 8 (8) | 464.72 | UPF0568 protein C14orf166 | 8573.82 |
| RS2_HUMAN | 10 (10) | 462.57 | 40S ribosomal protein S2 | 6503.36 |
| HNRPF_HUMAN | 6 (4) | 451.49 | Heterogeneous nuclear ribonucleoprotein F | 4354.05 |

| | | | | |
|---|---|---|---|---|
| RS19_HUMAN | 7 (7) | 447.67 | 40S ribosomal protein S19 | 15600 |
| 1433Z_HUMAN | 6 (5) | 404.01 | 14-3-3 protein zeta/delta | 3038.04 |
| LDHB_HUMAN | 6 (4) | 392.69 | L-lactate dehydrogenase B chain | 2189.7 |
| KPYM_HUMAN | 6 (6) | 390.12 | Pyruvate kinase PKM | 9366.31 |
| PDIA1_HUMAN | 5 (5) | 373.86 | Protein disulfide-isomerase | 2129.2 |
| HSP71_HUMAN | 6 (2) | 348.07 | Heat shock 70 kDa protein 1A/1B | 752.57 |
| RS14_HUMAN | 5 (5) | 347.56 | 40S ribosomal protein S14 | 12600 |
| RS16_HUMAN | 6 (6) | 343.87 | 40S ribosomal protein S16 | 22500 |
| RS13_HUMAN | 5 (5) | 343.18 | 40S ribosomal protein S13 | 11200 |
| H4_HUMAN | 5 (5) | 341.44 | Histone H4 | 19300 |
| EZRI_HUMAN | 6 (6) | 338.63 | Ezrin | 3617.36 |
| ODB2_HUMAN | 6 (5) | 321.92 | Lipoamide acyltransferase component of branched-chain alpha-keto acid dehydrogenase complex, mitochondrial | 2972.01 |
| ANXA2_HUMAN | 6 (6) | 320.89 | Annexin A2 | 5482.44 |
| RS8_HUMAN | 5 (5) | 317.28 | 40S ribosomal protein S8 | 7365.08 |
| ROA0_HUMAN | 5 (3) | 306.56 | Heterogeneous nuclear ribonucleoprotein A0 | 1627.76 |
| TERF2_HUMAN | 5 (5) | 290.93 | Telomeric repeat-binding factor 2 | 6372.84 |
| RL26_HUMAN | 5 (5) | 289.56 | 60S ribosomal protein L26 | 7321.72 |
| ILF2_HUMAN | 5 (5) | 281.64 | Interleukin enhancer-binding factor 2 | 2023.3 |
| RBMX_HUMAN | 4 (4) | 280.68 | RNA-binding motif protein, X chromosome | 6944.56 |
| PGK1_HUMAN | 5 (5) | 280.26 | Phosphoglycerate kinase 1 | 3479.27 |
| SSBP_HUMAN | 4 (4) | 273.25 | Single-stranded DNA-binding protein, mitochondrial | 14100 |
| ATX2_HUMAN | 4 (4) | 266.34 | Ataxin-2 | 37.48 |
| TCP4_HUMAN | 4 (4) | 263 | Activated RNA polymerase II transcriptional coactivator p15 | 2449.55 |
| HNRL1_HUMAN | 5 (4) | 262.77 | Heterogeneous nuclear ribonucleoprotein U-like protein 1 | 1198.33 |
| RS11_HUMAN | 5 (5) | 260.03 | 40S ribosomal protein S11 OS | 8592.37 |
| IF4A3_HUMAN | 5 (4) | 252.89 | Eukaryotic initiation factor 4A-III | 11900 |
| RL8_HUMAN | 4 (4) | 250.56 | 60S ribosomal protein L8 | 3000.68 |
| CTF8A_HUMAN | 4 (4) | 249.73 | Chromosome transmission fidelity protein 8 homolog isoform 2 | 529.59 |
| XRCC6_HUMAN | 4 (4) | 247 | X-ray repair cross-complementing protein 6 | 2457.96 |
| HNRPQ_HUMAN | 4 (4) | 243.26 | Heterogeneous nuclear ribonucleoprotein Q | 4158.69 |
| ATPA_HUMAN | 3 (3) | 237.85 | ATP synthase subunit alpha, mitochondrial | 1023.53 |
| RL23A_HUMAN | 3 (3) | 236.89 | 60S ribosomal protein L23a | 12600 |
| RL31_HUMAN | 4 (4) | 235.43 | 60S ribosomal protein L31 1 | 8672.43 |
| DDX3X_HUMAN | 4 (4) | 235.08 | ATP-dependent RNA helicase DDX3X | 1984.26 |

| | | | | |
|---|---|---|---|---|
| GRP75_HUMAN | 4 (3) | 231.34 | Stress-70 protein, mitochondrial | 1090.02 |
| FUBP3_HUMAN | 5 (4) | 231.1 | Far upstream element-binding protein 3 | 1298.86 |
| FMR1_HUMAN | 3 (2) | 230.5 | Fragile X mental retardation protein 1 | 496.76 |
| RL22L_HUMAN | 2 (2) | 225.37 | 60S ribosomal protein L22-like 1 | 2308.21 |
| RL18_HUMAN | 3 (3) | 221.47 | 60S ribosomal protein L18 | 1513.43 |
| CPSF7_HUMAN | 3 (3) | 219.58 | Cleavage and polyadenylation specificity factor subunit | 1328.44 |
| RL7A_HUMAN | 4 (4) | 217.16 | 60S ribosomal protein L7a | 1820.11 |
| RS27_HUMAN | 4 (4) | 213.66 | 40S ribosomal protein S27 | 2608.79 |
| MOV10_HUMAN | 3 (3) | 213.21 | Putative helicase MOV-10 | 400.88 |
| RS7_HUMAN | 5 (5) | 211.75 | 40S ribosomal protein S7 | 8403.72 |
| VDAC1_HUMAN | 3 (2) | 210.89 | Voltage-dependent anion-selective channel protein 1 | 191.46 |
| TE2IP_HUMAN | 3 (3) | 205.14 | Telomeric repeat-binding factor 2-interacting protein 1 | 3541.28 |
| NDKA_HUMAN | 4 (4) | 203.91 | Nucleoside diphosphate kinase A | 2765.63 |
| DCD_HUMAN | 2 (2) | 203.9 | Dermcidin | 40500 |
| THOC4_HUMAN | 2 (2) | 200.5 | THO complex subunit 4 | 2962.22 |
| LSM12_HUMAN | 3 (3) | 199.11 | Protein LSM12 homolog | 8904.1 |
| RS9_HUMAN | 5 (5) | 198.54 | 40S ribosomal protein S9 | 6700.77 |
| RS10_HUMAN | 3 (3) | 197.36 | 40S ribosomal protein S10 | 5380.03 |
| NUCL_HUMAN | 4 (4) | 194.83 | Nucleolin | 1237.99 |
| RL10_HUMAN | 3 (3) | 192.94 | 60S ribosomal protein L10 | 3265.33 |
| RL12_HUMAN | 3 (3) | 192.92 | 60S ribosomal protein L12 | 3199.86 |
| RS15_HUMAN | 3 (3) | 192.89 | 40S ribosomal protein S15 | 4127.64 |
| RL17_HUMAN | 3 (3) | 189.6 | 60S ribosomal protein L17 | 8023.17 |
| ANXA1_HUMAN | 2 (2) | 184.77 | Annexin A1 | 348.36 |
| RBM8A_HUMAN | 3 (3) | 182.28 | RNA-binding protein 8A | 930.43 |
| RLA0_HUMAN | 4 (4) | 181.26 | 60S acidic ribosomal protein P0 | 3571.97 |
| TRI25_HUMAN | 4 (4) | 181.02 | E3 ubiquitin/ISG15 ligase TRIM25 | 1569.3 |
| RL23_HUMAN | 2 (2) | 180.3 | 60S ribosomal protein L23 | 2284.74 |
| RS15A_HUMAN | 4 (4) | 180.29 | 40S ribosomal protein S15a | 12000 |
| TCPQ_HUMAN | 3 (3) | 179.53 | T-complex protein 1 subunit theta | 856.81 |
| IF4A1_HUMAN | 3 (2) | 177.05 | Eukaryotic initiation factor 4A-I | 258.23 |
| TPIS_HUMAN | 3 (3) | 176.45 | Triosephosphate isomerase | 553.56 |
| LASP1_HUMAN | 3 (3) | 174.98 | LIM and SH3 domain protein 1 | 1261.95 |
| PRDX1_HUMAN | 4 (4) | 173.27 | Peroxiredoxin-1 | 3012.07 |
| RL13_HUMAN | 2 (2) | 170.55 | 60S ribosomal protein L13 | 2201.69 |
| TIAR_HUMAN | 3 (3) | 170.3 | Nucleolysin TIAR | 1696.6 |

| | | | | |
|---|---|---|---|---|
| 1433G_HUMAN | 3 (2) | 169.91 | 14-3-3 protein gamma | 239.88 |
| HNRPD_HUMAN | 3 (3) | 169.8 | Heterogeneous nuclear ribonucleoprotein D0 | 3063.46 |
| YTHD2_HUMAN | 3 (3) | 166.86 | YTH domain family protein 2 | 1961.4 |
| RS25_HUMAN | 3 (3) | 160.46 | 40S ribosomal protein S25 | 5004.7 |
| RL22_HUMAN | 2 (2) | 160.01 | 60S ribosomal protein L22 | 3897.91 |
| PURB_HUMAN | 3 (2) | 159.62 | Transcriptional activator protein Pur-beta | 147.53 |
| RS17L_HUMAN | 3 (3) | 158.9 | 40S ribosomal protein S17-like | 3100.06 |
| BCKD_HUMAN | 3 (3) | 156.37 | [3-methyl-2-oxobutanoate dehydrogenase [lipoamide]] kinase, mitochondrial | 2220.07 |
| PDIA3_HUMAN | 3 (3) | 155.37 | Protein disulfide-isomerase A3 | 1118.81 |
| G6PI_HUMAN | 3 (3) | 155.28 | Glucose-6-phosphate isomerase | 567.04 |
| RS6_HUMAN | 2 (2) | 152.91 | 40S ribosomal protein S6 | 2371.51 |
| H2B1L_HUMAN | 2 (2) | 152.33 | Histone H2B type 1-L | 2083.43 |
| TCPB_HUMAN | 3 (2) | 152.11 | T-complex protein 1 subunit beta | 365.5 |
| HNRPC_HUMAN | 3 (3) | 150.42 | Heterogeneous nuclear ribonucleoproteins C1/C2 | 4683.06 |
| PPIA_HUMAN | 3 (3) | 149.59 | Peptidyl-prolyl cis-trans isomerase A | 1984.15 |
| RL11_HUMAN | 2 (2) | 149.3 | 60S ribosomal protein L11 | 6584.62 |
| ATPB_HUMAN | 3 (3) | 148.48 | ATP synthase subunit beta, mitochondrial | 976.72 |
| PGAM5_HUMAN | 3 (3) | 143.29 | Serine/threonine-protein phosphatase PGAM5, mitochondrial | 1314.32 |
| KHDR1_HUMAN | 3 (3) | 142.98 | KH domain-containing, RNA-binding, signal transduction-associated protein 1 | 5694.65 |
| THIL_HUMAN | 2 (2) | 141.03 | Acetyl-CoA acetyltransferase, mitochondrial | 167.19 |
| PCBP1_HUMAN | 2 (2) | 138.87 | Poly(rC)-binding protein 1 | 684.04 |
| VDAC2_HUMAN | 2 (2) | 138.41 | Voltage-dependent anion-selective channel protein 2 | 1095.65 |
| CIRBP_HUMAN | 2 (2) | 132.57 | Cold-inducible RNA-binding protein | 969.66 |
| RL19_HUMAN | 2 (2) | 131.63 | 60S ribosomal protein L19 | 537.15 |
| HSPB1_HUMAN | 2 (2) | 130.74 | Heat shock protein beta-1 2 | 2017.14 |
| DHX15_HUMAN | 3 (3) | 130.55 | Putative pre-mRNA-splicing factor ATP-dependent RNA helicase DHX15 | 1591.68 |
| UBP10_HUMAN | 3 (3) | 130.53 | Ubiquitin carboxyl-terminal hydrolase 10 | 1137.74 |
| PROF1_HUMAN | 2 (2) | 129.17 | Profilin-1 | 1322.26 |
| RAB1B_HUMAN | 3 (3) | 126.3 | Ras-related protein Rab-1B | 879.2 |
| SMD2_HUMAN | 3 (3) | 126.03 | Small nuclear ribonucleoprotein Sm D2 | 1232.19 |
| PCNA_HUMAN | 3 (3) | 126.02 | Proliferating cell nuclear antigen | 512.16 |
| RB11A_HUMAN | 3 (2) | 125.18 | Ras-related protein Rab-11A | 521.65 |
| EFTU_HUMAN | 2 (2) | 123.01 | Elongation factor Tu, mitochondrial | 1190.6 |
| MSI2H_HUMAN | 2 (2) | 122.35 | RNA-binding protein Musashi homolog 2 | 828.59 |

| | | | | |
|---|---|---|---|---|
| RL7_HUMAN | 3 (3) | 121.45 | 60S ribosomal protein L7 | 2622.87 |
| RS5_HUMAN | 3 (3) | 120.46 | 40S ribosomal protein S5 | 3132.03 |
| CH10_HUMAN | 2 (2) | 120.25 | 10 kDa heat shock protein, mitochondrial | 664.46 |
| TRAF4_HUMAN | 2 (2) | 117.22 | TNF receptor-associated factor 4 | 296.79 |
| RS26_HUMAN | 2 (2) | 116.95 | 40S ribosomal protein S26 | 2290.79 |
| SRSF9_HUMAN | 2 (2) | 115.35 | Serine/arginine-rich splicing factor 9 | 473 |
| RFA2_HUMAN | 2 (2) | 114.57 | Replication protein A 32 kDa subunit | 1928.12 |
| EF1D_HUMAN | 2 (2) | 112.88 | Elongation factor 1-delta | 144.2 |
| TMEDA_HUMAN | 2 (2) | 107.14 | Transmembrane emp24 domain-containing protein 10 | 1535.22 |
| H31T_HUMAN | 2 (2) | 105.38 | Histone H3.1t | 10900 |
| EF2_HUMAN | 2 (2) | 104.32 | Elongation factor 2 | 125.38 |
| FUBP2_HUMAN | 2 (2) | 100.96 | Far upstream element-binding protein 2 | 378.37 |
| CASPE_HUMAN | 2 (2) | 100.85 | Caspase-14 | 1171.88 |
| EMD_HUMAN | 2 (2) | 100.65 | Emerin | 362.35 |
| RL13A_HUMAN | 2 (2) | 99.28 | 60S ribosomal protein L13a | 1881.3 |
| FKBP4_HUMAN | 2 (2) | 98.96 | Peptidyl-prolyl cis-trans isomerase FKBP4 | 549.77 |
| PA2G4_HUMAN | 2 (2) | 97.82 | Proliferation-associated protein 2G4 | 1315.58 |
| PCBP2_HUMAN | 2 (2) | 96.35 | Poly(rC)-binding protein 2 | 929 |
| RENT1_HUMAN | 2 (2) | 96.28 | Regulator of nonsense transcripts 1 | 556.83 |
| U2AF2_HUMAN | 2 (2) | 95.89 | Splicing factor U2AF 65 kDa subunit | 1251.54 |
| RAN_HUMAN | 2 (2) | 95.84 | GTP-binding nuclear protein Ran | 1849.87 |
| H2A1B_HUMAN | 2 (2) | 95.17 | Histone H2A type 1-B/E | 2908.23 |
| MDHM_HUMAN | 2 (2) | 94.92 | Malate dehydrogenase, mitochondrial | 350.27 |
| CALR_HUMAN | 2 (2) | 93.89 | Calreticulin | 272.61 |
| ALDOC_HUMAN | 2 (2) | 93.49 | Fructose-bisphosphate aldolase C | 583.51 |
| ZC3H4_HUMAN | 2 (2) | 92.33 | Zinc finger CCCH domain-containing protein 4 | 627.54 |
| AGO2_HUMAN | 2 (2) | 91.58 | Protein argonaute-2 | 131.94 |
| RFA1_HUMAN | 2 (2) | 91.29 | Replication protein A 70 kDa DNA-binding subunit | 1962.12 |
| SRSF1_HUMAN | 2 (2) | 91.29 | Serine/arginine-rich splicing factor 1 | 2102.53 |
| TFAM_HUMAN | 2 (2) | 90.7 | Transcription factor A, mitochondrial | 516.49 |
| HNRH3_HUMAN | 2 (2) | 90.35 | Heterogeneous nuclear ribonucleoprotein H3 | 612.3 |
| RL27_HUMAN | 2 (2) | 89.54 | 60S ribosomal protein L27 | 1182 |
| PARK7_HUMAN | 2 (2) | 87.02 | Protein DJ-1 | 201.31 |
| TMED9_HUMAN | 2 (2) | 86.55 | Transmembrane emp24 domain-containing protein 9 | 1134.77 |
| RL9_HUMAN | 2 (2) | 77.52 | 60S ribosomal protein L9 | 1136.15 |
| PGAM1_HUMAN | 2 (2) | 77.44 | Phosphoglycerate mutase 1 | 778.04 |
| DEF1_HUMAN | 2 (2) | 77.42 | Neutrophil defensin 1 | 52.18 |

| | | | | |
|---|---|---|---|---|
| ABC3F_HUMAN | 2 (2) | 77.35 | DNA dC->dU-editing enzyme APOBEC-3F | 1268.22 |
| DEFM_HUMAN | 2 (2) | 77.03 | Peptide deformylase, mitochondrial | 1501.04 |
| XRCC5_HUMAN | 2 (2) | 76.07 | X-ray repair cross-complementing protein 5 | 1987.86 |
| RL28_HUMAN | 2 (2) | 76.06 | 60S ribosomal protein L28 | 624.03 |
| PSB5_HUMAN | 2 (2) | 74.96 | Proteasome subunit beta type-5 | 87.99 |
| PHB_HUMAN | 2 (2) | 74.75 | Prohibitin | 99.47 |
| PKP3_HUMAN | 2 (2) | 72.92 | Plakophilin-3 | 545.32 |
| RSMN_HUMAN | 2 (2) | 72.64 | Small nuclear ribonucleoprotein-associated protein N | 952.79 |
| SBSN_HUMAN | 2 (2) | 72.09 | Suprabasin | 746.66 |
| NSUN4_HUMAN | 2 (2) | 70.17 | 5-methylcytosine rRNA methyltransferase NSUN4 | 5655.63 |

[1]Accession = SwissProt Protein ID
[2]Peptide count = the number of detected peptides (the number of unique peptides) used for quantification
[3]The protein confidence score was generated using Mascot as described in the experimental.
[4]Average normalized abundance of the protein calculated by label-free quantification.
Ranking is based on Confidence score.

**Table 8.7** Identification and LC-MS based label-free quantification of PTEN-EGFP binding proteins affinity-captured by Co-IP from HCT116 cell lysate showing the protein hits with less than 2 unique peptides

| Accession[1] | Peptides[2] | Score[3] | Description | Average Normalized Abundance[4] |
|---|---|---|---|---|
| TBB4B_HUMAN | 17 (1) | 1040.73 | Tubulin beta-4B chain | 1992.29 |
| TBB4A_HUMAN | 14 (0) | 848.64 | Tubulin beta-4A chain | 0 |
| TBB2A_HUMAN | 13 (0) | 794.9 | Tubulin beta-2A chain | 0 |
| PP1G_HUMAN | 8 (1) | 753.57 | Serine/threonine-protein phosphatase PP1-gamma catalytic subunit | 4357.34 |
| TBB3_HUMAN | 10 (0) | 710.23 | Tubulin beta-3 chain | 0 |
| HNRH2_HUMAN | 4 (1) | 508.27 | Heterogeneous nuclear ribonucleoprotein H2 | 59.33 |
| YBOX3_HUMAN | 4 (1) | 361.03 | Y-box-binding protein 3 | 797.79 |
| HS71L_HUMAN | 5 (0) | 306.99 | Heat shock 70 kDa protein 1-like | 0 |
| TBB6_HUMAN | 6 (0) | 301.08 | Tubulin beta-6 chain | 0 |
| RBP56_HUMAN | 3 (1) | 257.03 | TATA-binding protein-associated factor 2N | 3596.86 |
| MAGB2_HUMAN | 1 (1) | 178.83 | Melanoma-associated antigen B2 | 547.58 |
| ENOG_HUMAN | 2 (0) | 178 | Gamma-enolase | 0 |
| RS20_HUMAN | 1 (1) | 146.03 | 40S ribosomal protein S20 | 3920.28 |
| PAP1M_HUMAN | 2 (0) | 127.48 | Polyadenylate-binding protein 1-like 2 | 0 |
| IF4E_HUMAN | 1 (1) | 120.67 | Eukaryotic translation initiation factor 4E | 2804.52 |
| VDAC3_HUMAN | 2 (1) | 114.71 | Voltage-dependent anion-selective channel protein 3 | 37.53 |
| CPNS1_HUMAN | 1 (1) | 103.02 | Calpain small subunit 1 | 195.69 |
| S10A9_HUMAN | 1 (1) | 102.68 | Protein S100-A9 | 3545.53 |
| RS29_HUMAN | 1 (1) | 101.88 | 40S ribosomal protein S29 | 3013.03 |
| 1433B_HUMAN | 2 (1) | 101.35 | 14-3-3 protein beta/alpha | 429.28 |
| TCPA_HUMAN | 2 (1) | 97.29 | T-complex protein 1 subunit alpha | 223.89 |
| TRY3_HUMAN | 1 (1) | 94.79 | Trypsin-3 | 817.83 |
| RL21_HUMAN | 1 (1) | 89.79 | 60S ribosomal protein L21 | 1839.78 |
| PURA_HUMAN | 2 (1) | 87.17 | Transcriptional activator protein Pur-alpha | 1442.04 |
| SC61B_HUMAN | 1 (1) | 86.94 | Protein transport protein Sec61 subunit beta | 365.15 |
| RS23_HUMAN | 1 (1) | 84.65 | 40S ribosomal protein S23 | 829.21 |
| RAB5C_HUMAN | 1 (1) | 84.52 | Ras-related protein Rab-5C | 247.53 |
| TFCP2_HUMAN | 1 (1) | 84.41 | Alpha-globin transcription factor CP2 | 1260.22 |
| PSA3_HUMAN | 1 (1) | 82.65 | Proteasome subunit alpha type-3 | 122.89 |
| FILA2_HUMAN | 1 (1) | 79.56 | Filaggrin-2 | 233.88 |
| SMD3_HUMAN | 1 (1) | 79.03 | Small nuclear ribonucleoprotein Sm D3 | 687.63 |
| TRIP6_HUMAN | 2 (1) | 78.87 | Thyroid receptor-interacting protein 6 | 1656.89 |
| ZAGL1_HUMAN | 1 (1) | 78.8 | Putative zinc-alpha-2-glycoprotein-like 1 | 927.93 |
| 1433S_HUMAN | 2 (1) | 78.51 | 14-3-3 protein sigma | 97.36 |
| MIF_HUMAN | 1 (1) | 77.83 | Macrophage migration inhibitory factor | 655.62 |
| RS24_HUMAN | 1 (1) | 77.01 | 40S ribosomal protein S24 | 1508.15 |
| DAZP1_HUMAN | 1 (1) | 76.61 | DAZ-associated protein 1 | 279.28 |
| RU1C_HUMAN | 1 (1) | 76.22 | U1 small nuclear ribonucleoprotein C | 431.29 |
| CYB5B_HUMAN | 1 (1) | 76.06 | Cytochrome b5 type B | 147.04 |
| 1433E_HUMAN | 2 (1) | 75.72 | 14-3-3 protein epsilon | 330.08 |
| RL27A_HUMAN | 1 (1) | 75.69 | 60S ribosomal protein L27a | 2669.13 |

| | | | | |
|---|---|---|---|---|
| C1QBP_HUMAN | 1 (1) | 75.4 | Complement component 1 Q subcomponent-binding protein, mitochondrial | 199.12 |
| S10A8_HUMAN | 1 (1) | 73.8 | Protein S100-A8 | 525.2 |
| UBE2N_HUMAN | 1 (1) | 72.88 | Ubiquitin-conjugating enzyme E2 N | 132.77 |
| MGN_HUMAN | 1 (1) | 72.35 | Protein mago nashi homolog | 420.71 |
| EF1G_HUMAN | 1 (1) | 71.15 | Elongation factor 1-gamma | 1086.59 |
| TOM22_HUMAN | 1 (1) | 69.93 | Mitochondrial import receptor subunit TOM22 homolog | 48.26 |
| SRSF3_HUMAN | 1 (1) | 68.84 | Serine/arginine-rich splicing factor 3 | 1440.7 |
| ROAA_HUMAN | 1 (1) | 68.81 | Heterogeneous nuclear ribonucleoprotein A/B | 144.66 |
| RL29_HUMAN | 1 (1) | 68.72 | 60S ribosomal protein L29 | 565.93 |
| HNRPL_HUMAN | 1 (1) | 67.73 | Heterogeneous nuclear ribonucleoprotein L | 265.11 |
| GLU2B_HUMAN | 1 (1) | 67.28 | Glucosidase 2 subunit beta | 9.29 |
| HELZ_HUMAN | 1 (0) | 65.68 | Probable helicase with zinc finger domain | 0 |
| PSA5_HUMAN | 1 (1) | 62.69 | Proteasome subunit alpha type-5 | 179.69 |
| RL24_HUMAN | 1 (1) | 62.42 | 60S ribosomal protein L24 | 249.71 |
| SMN_HUMAN | 1 (1) | 61.24 | Survival motor neuron protein | 155.29 |
| SMD1_HUMAN | 1 (1) | 60.42 | Small nuclear ribonucleoprotein Sm D1 | 119.05 |
| RL35_HUMAN | 1 (1) | 59.67 | 60S ribosomal protein L35 | 1183.18 |
| COF1_HUMAN | 1 (1) | 59.14 | Cofilin-1 | 939.69 |
| PNKP_HUMAN | 1 (1) | 58.85 | Bifunctional polynucleotide phosphatase/kinase | 168.05 |
| AIFM2_HUMAN | 1 (0) | 58.3 | Apoptosis-inducing factor 2 | 0 |
| SAHH_HUMAN | 1 (1) | 58.12 | Adenosylhomocysteinase | 201.19 |
| RUXF_HUMAN | 1 (1) | 57.58 | Small nuclear ribonucleoprotein F | 3.21 |
| PHB2_HUMAN | 1 (1) | 57.44 | Prohibitin-2 | 174.98 |
| HNRDL_HUMAN | 1 (1) | 56.58 | Heterogeneous nuclear ribonucleoprotein D-like | 430.04 |
| DRG1_HUMAN | 1 (1) | 56.27 | Developmentally-regulated GTP-binding protein 1 | 167.9 |
| RL15_HUMAN | 1 (1) | 55.83 | 60S ribosomal protein L15 | 635.15 |
| MDHC_HUMAN | 1 (1) | 55.46 | Malate dehydrogenase, cytoplasmic | 35.71 |
| TFG_HUMAN | 1 (1) | 55.11 | Protein TFG | 1369.61 |
| TBP_HUMAN | 1 (1) | 53.01 | TATA-box-binding protein | 700.48 |
| ILF3_HUMAN | 1 (0) | 52.69 | Interleukin enhancer-binding factor 3 | 0 |
| SET_HUMAN | 1 (1) | 51.91 | Protein SET | 112.79 |
| IDHP_HUMAN | 1 (1) | 51.63 | Isocitrate dehydrogenase [NADP], mitochondrial | 103.71 |
| CLIC1_HUMAN | 1 (1) | 51.61 | Chloride intracellular channel protein 1 | 54.02 |
| DHSO_HUMAN | 1 (1) | 51.2 | Sorbitol dehydrogenase | 218.78 |
| RT07_HUMAN | 1 (1) | 50.67 | 28S ribosomal protein S7, mitochondrial | 110 |
| LMNA_HUMAN | 1 (1) | 50.64 | Prelamin-A/C | 214.76 |
| FEN1_HUMAN | 1 (1) | 49.83 | Flap endonuclease 1 | 86.84 |
| T2FB_HUMAN | 1 (1) | 49.81 | General transcription factor IIF subunit 2 | 190.01 |
| RL38_HUMAN | 1 (1) | 49.73 | 60S ribosomal protein L38 | 10400 |
| ERH_HUMAN | 1 (1) | 48.89 | Enhancer of rudimentary homolog | 472.72 |
| PSA6_HUMAN | 1 (1) | 48.61 | Proteasome subunit alpha type-6 | 85.81 |
| MPCP_HUMAN | 1 (1) | 48.46 | Phosphate carrier protein, mitochondrial | 91.38 |
| GRSF1_HUMAN | 1 (1) | 47.96 | G-rich sequence factor 1 | 298.5 |
| RANG_HUMAN | 1 (1) | 47.52 | Ran-specific GTPase-activating protein | 120 |
| CDC37_HUMAN | 1 (1) | 47.29 | Hsp90 co-chaperone Cdc37 | 27.07 |

| | | | | |
|---|---|---|---|---|
| RLA1_HUMAN | 1 (1) | 47.13 | 60S acidic ribosomal protein P1 | 1296.3 |
| SRP14_HUMAN | 1 (1) | 46.93 | Signal recognition particle 14 kDa protein | 549.54 |
| F195A_HUMAN | 1 (1) | 46.31 | Protein FAM195A | 0 |
| PDCD6_HUMAN | 1 (1) | 46.05 | Programmed cell death protein 6 | 325.48 |
| HMGA1_HUMAN | 1 (1) | 45.97 | High mobility group protein HMG-I/HMG-Y | 505.11 |
| PRDX3_HUMAN | 1 (1) | 45.78 | Thioredoxin-dependent peroxide reductase, mitochondrial | 50.93 |
| RLA2_HUMAN | 1 (1) | 45.53 | 60S acidic ribosomal protein P2 | 534.58 |
| S10A6_HUMAN | 1 (1) | 45.46 | Protein S100-A6 | 70.59 |
| PRKRA_HUMAN | 1 (1) | 45.44 | Interferon-inducible double stranded RNA-dependent protein kinase activator A | 224.79 |
| TCPZ_HUMAN | 1 (1) | 45.14 | T-complex protein 1 subunit zeta | 208.59 |
| BAF_HUMAN | 1 (1) | 45.03 | Barrier-to-autointegration factor | 356.67 |
| BASI_HUMAN | 1 (1) | 44.85 | Basigin | 704.93 |
| RS12_HUMAN | 1 (1) | 44.38 | 40S ribosomal protein S12 | 948.56 |
| NPM_HUMAN | 1 (1) | 44 | Nucleophosmin | 356.12 |
| LAT1_HUMAN | 1 (1) | 43.69 | Large neutral amino acids transporter small subunit 1 | 189.41 |
| NOLC1_HUMAN | 1 (1) | 43.66 | Nucleolar and coiled-body phosphoprotein 1 | 223.89 |
| CSK2B_HUMAN | 1 (1) | 43.09 | Casein kinase II subunit beta | 73.7 |
| GBLP_HUMAN | 1 (1) | 42.78 | Guanine nucleotide-binding protein subunit beta-2-like 1 | 168.56 |
| PEBP1_HUMAN | 1 (1) | 42.69 | Phosphatidylethanolamine-binding protein 1 3 | 89.43 |
| RSSA_HUMAN | 1 (1) | 42.39 | 40S ribosomal protein SA | 897.73 |
| SPAT7_HUMAN | 1 (1) | 42.38 | Spermatogenesis-associated protein 7 | 253.46 |
| PEBB_HUMAN | 1 (1) | 41.95 | Core-binding factor subunit beta | 312.74 |
| RUXE_HUMAN | 1 (1) | 41.83 | Small nuclear ribonucleoprotein E | 557.41 |
| TADBP_HUMAN | 1 (1) | 41.62 | TAR DNA-binding protein 43 | 584.43 |
| MYL6_HUMAN | 1 (1) | 41.59 | Myosin light polypeptide 6 | 99.77 |
| STAU2_HUMAN | 1 (1) | 41.44 | Double-stranded RNA-binding protein Staufen homolog 2 | 398.36 |
| LRC59_HUMAN | 1 (1) | 41.39 | Leucine-rich repeat-containing protein 59 | 379.93 |
| HEM6_HUMAN | 1 (1) | 41.17 | Coproporphyrinogen-III oxidase, mitochondrial | 78.35 |
| PEX1_HUMAN | 1 (1) | 41.16 | Peroxisome biogenesis factor 1 | 54.99 |
| NC2B_HUMAN | 1 (1) | 41.06 | Protein Dr1 | 158.2 |
| RAB10_HUMAN | 1 (1) | 40.75 | Ras-related protein Rab-10 | 134.63 |
| STAU1_HUMAN | 1 (1) | 40.43 | Double-stranded RNA-binding protein Staufen homolog 1 | 189.77 |
| SLBP_HUMAN | 1 (1) | 39.85 | Histone RNA hairpin-binding protein | 65.97 |
| ADT2_HUMAN | 1 (1) | 39.76 | ADP/ATP translocase 2 | 296000 |
| TMED2_HUMAN | 1 (1) | 39.61 | Transmembrane emp24 domain-containing protein 2 | 268.5 |
| ADT1_HUMAN | 1 (1) | 39.08 | ADP/ATP translocase 1 | 41.13 |
| SPTN5_HUMAN | 1 (1) | 39.02 | Spectrin beta chain, non-erythrocytic 5 | 366.57 |
| DHX30_HUMAN | 1 (1) | 38.93 | Putative ATP-dependent RNA helicase DHX30 | 69.72 |
| RL36_HUMAN | 1 (1) | 38.85 | 60S ribosomal protein L36 | 164.81 |
| CDC20_HUMAN | 1 (1) | 38.81 | Cell division cycle protein 20 homolog | 59.46 |
| RUVB2_HUMAN | 1 (1) | 38.77 | RuvB-like 2 | 155.57 |
| RL18A_HUMAN | 1 (1) | 38.22 | 60S ribosomal protein L18a | 394.02 |
| PM14_HUMAN | 1 (1) | 37.94 | Pre-mRNA branch site protein p14 | 191.92 |
| ARF5_HUMAN | 1 (1) | 37.84 | ADP-ribosylation factor 5 | 88800 |

| | | | | |
|---|---|---|---|---|
| KCRB_HUMAN | 1 (1) | 37.8 | Creatine kinase B-type | 223.07 |
| LPIN2_HUMAN | 1 (0) | 37.38 | Phosphatidate phosphatase LPIN2 | 0 |
| ARF1_HUMAN | 1 (1) | 37.14 | ADP-ribosylation factor 1 | 209.35 |
| SPB4_HUMAN | 1 (1) | 37.06 | Serpin B4 | 243.67 |
| HS74L_HUMAN | 1 (1) | 36.9 | Heat shock 70 kDa protein 4L | 783.48 |
| LS14A_HUMAN | 1 (1) | 36.68 | Protein LSM14 homolog A | 545.87 |
| LEKR1_HUMAN | 1 (1) | 36.45 | Leucine-, glutamate- and lysine-rich protein 1 | 51.2 |
| GAR1_HUMAN | 1 (1) | 36.29 | H/ACA ribonucleoprotein complex subunit 1 | 692.14 |
| RL10A_HUMAN | 1 (1) | 36.09 | 60S ribosomal protein L10a | 3118.37 |
| CYTA_HUMAN | 1 (1) | 35.87 | Cystatin-A | 563.08 |
| RAB21_HUMAN | 1 (1) | 35.8 | Ras-related protein Rab-21 | 54.87 |
| TAGL2_HUMAN | 1 (1) | 35.62 | Transgelin-2 | 64.6 |
| BUB3_HUMAN | 1 (1) | 35.57 | Mitotic checkpoint protein BUB3 | 349.19 |
| PLAK_HUMAN | 1 (1) | 35.43 | Junction plakoglobin | 56.92 |
| ISG15_HUMAN | 1 (1) | 35.38 | Ubiquitin-like protein ISG15 | 21.61 |
| PRDX2_HUMAN | 1 (1) | 35.38 | Peroxiredoxin-2 | 13700 |
| ARHGH_HUMAN | 1 (1) | 35.21 | Rho guanine nucleotide exchange factor 17 | 5844.16 |
| TSN10_HUMAN | 1 (0) | 35.02 | Tetraspanin-10 | 0 |
| RL3_HUMAN | 1 (1) | 34.82 | 60S ribosomal protein L3 | 288.86 |
| PAIRB_HUMAN | 1 (1) | 34.76 | Plasminogen activator inhibitor 1 RNA-binding protein | 313.65 |
| FBRL_HUMAN | 1 (1) | 34.66 | rRNA 2'-O-methyltransferase fibrillarin | 239.72 |
| ATPO_HUMAN | 1 (1) | 33.48 | ATP synthase subunit O, mitochondrial | 36.08 |
| MIO_HUMAN | 1 (1) | 33.43 | WD repeat-containing protein mio | 1401.25 |
| RL36A_HUMAN | 1 (1) | 33.17 | 60S ribosomal protein L36a | 127.58 |
| RS27A_HUMAN | 1 (1) | 32.95 | Ubiquitin-40S ribosomal protein S27a | 319.89 |
| SF01_HUMAN | 1 (1) | 32.64 | Splicing factor 1 | 422.06 |
| CLP1_HUMAN | 1 (1) | 32.15 | Polyribonucleotide 5'-hydroxyl-kinase Clp1 | 51.96 |

[1]Accession = SwissProt Protein ID
[2]Peptide count = the number of detected peptides (the number of unique peptides) used for quantification
[3]The protein confidence score was generated using Mascot as described in the experimental
[4]Average normalized abundance of the protein calculated by label-free quantification
Ranking is based on Confidence score.

# 8.6 Uncropped Western blot scans

For all the uncropped Western blot scans shown in this section, the dashed red boxes mark the borders of cropped area used to generate the corresponding figure shown in the main body of the thesis. The molecular weight markers are shown on the left. The detected protein is indicated on the right, and the antibody used is indicated at the bottom.

## 8.6.1 Uncropped scans of Western blots presented in Figure 4.6

Along the top of each Western blot scan shown are indicated the bait protein(s) and any oxidizing and/or reducing treatments performed on the PTEN-GST bait.

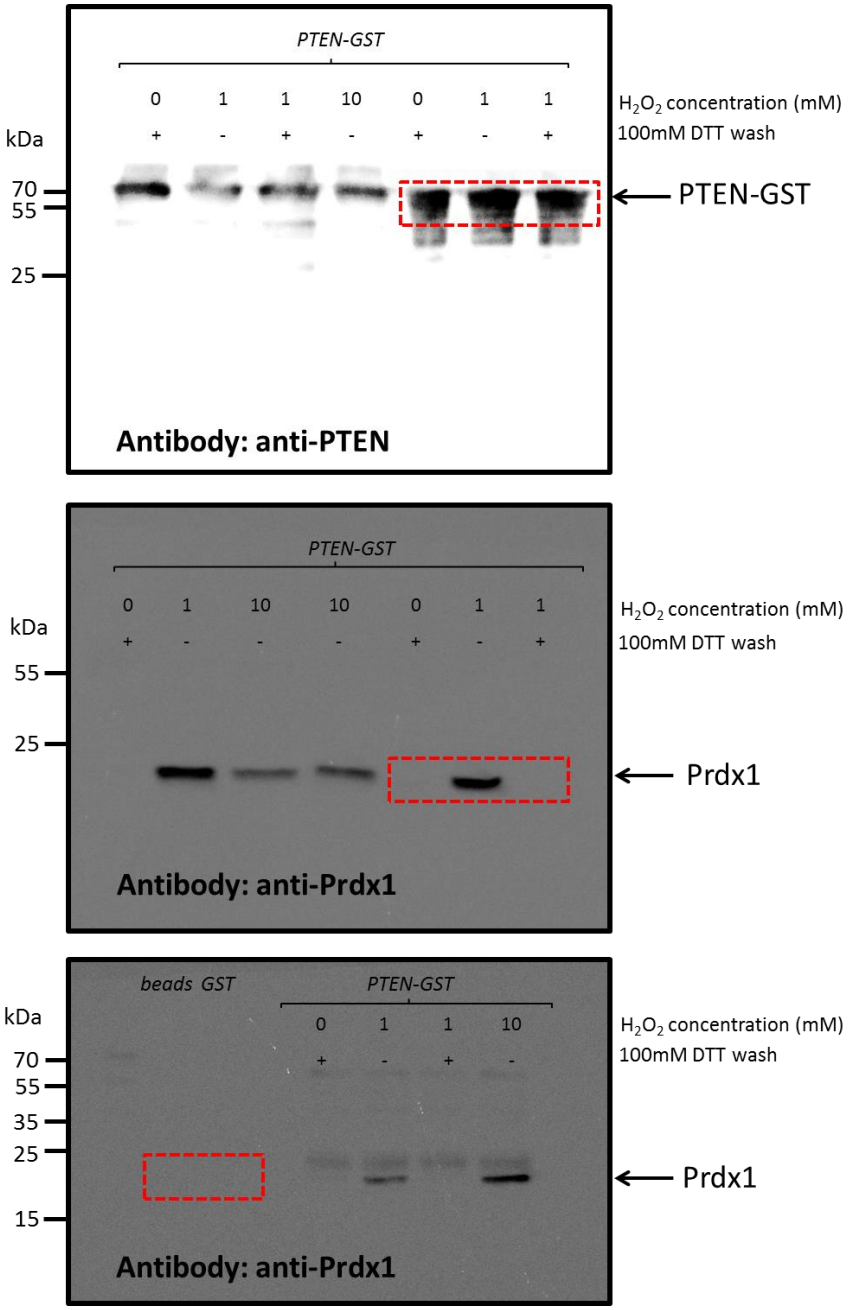


**Figure 8.3 Uncropped scans of the Western Blots presented in Figure 4.6 (A).**

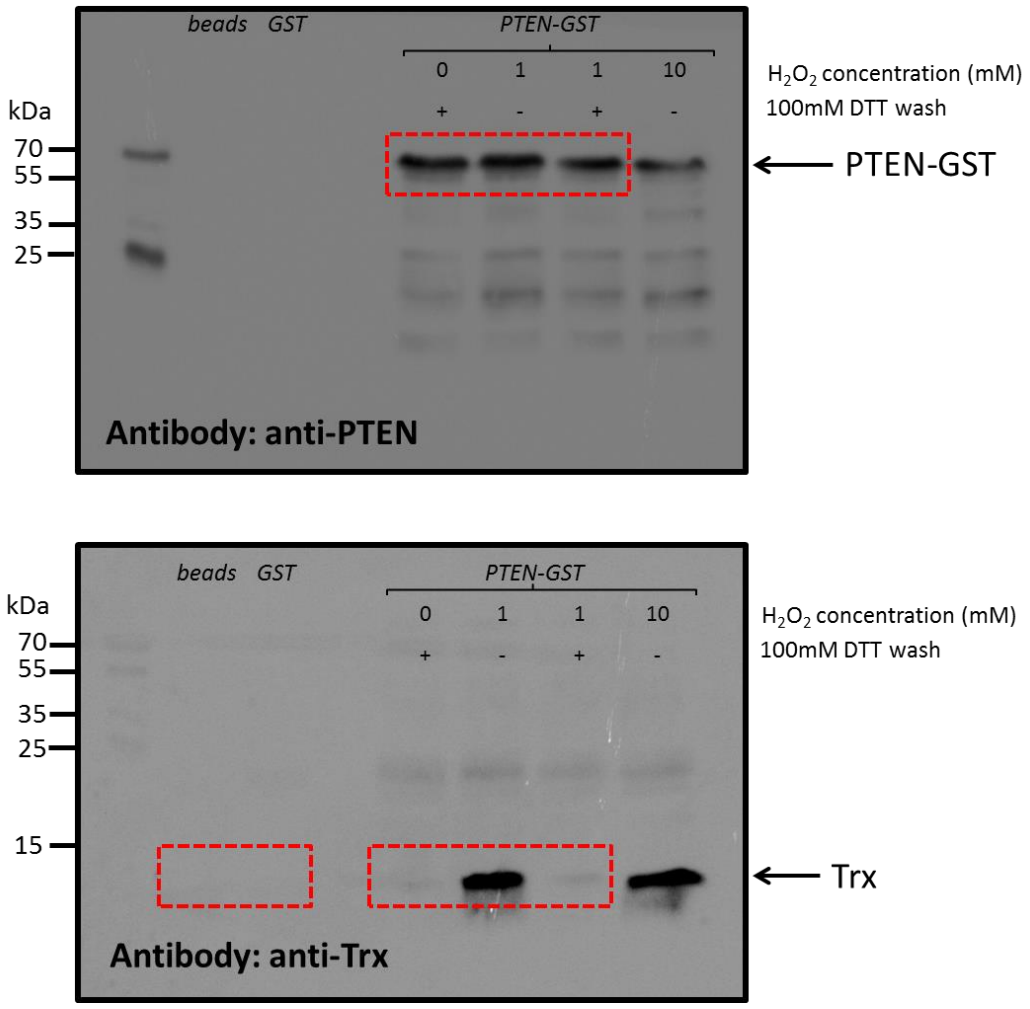


**Figure 8.4 Uncropped scans of the Western Blots presented in Figure 4.6 (B).**

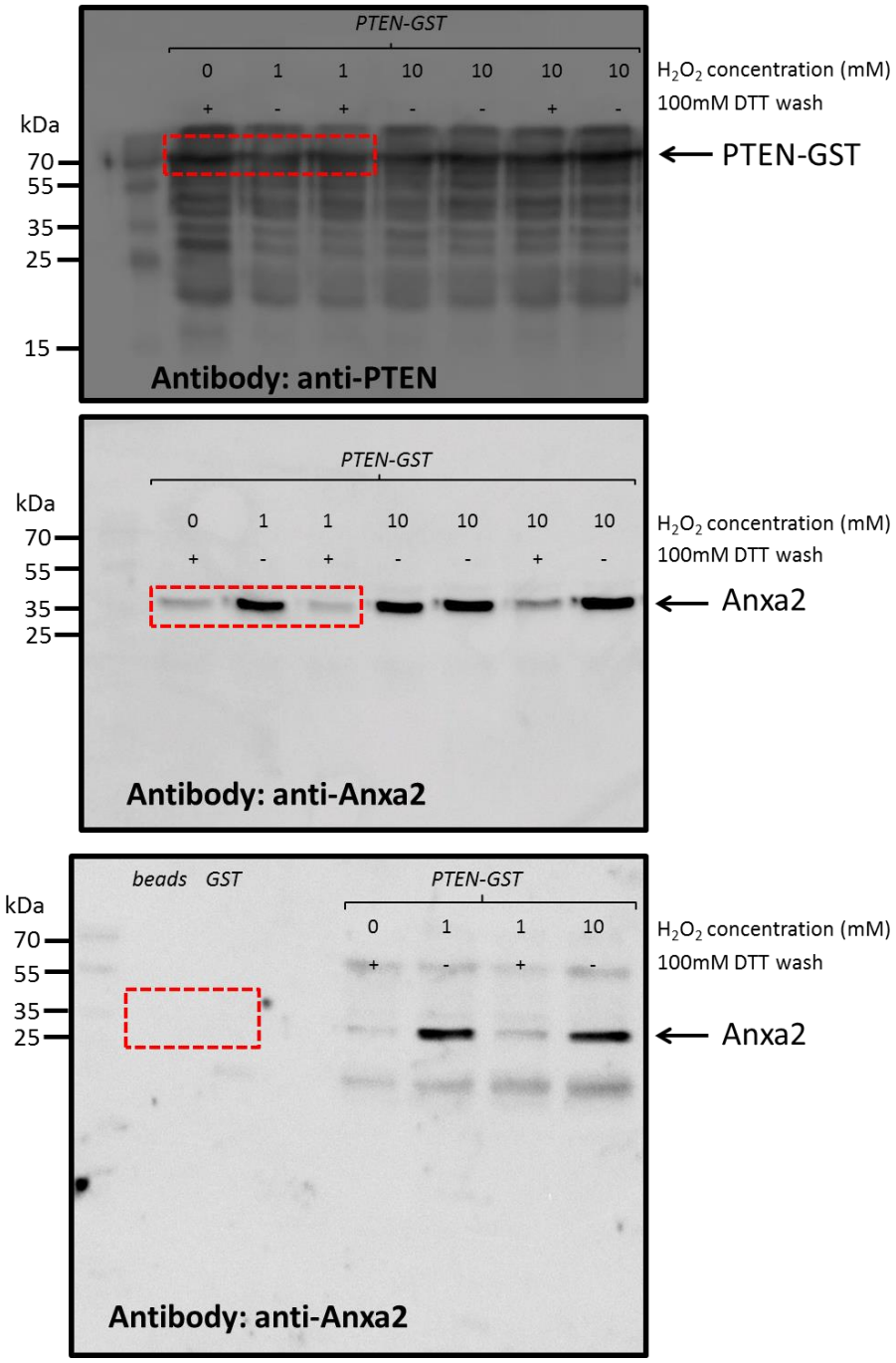


**Figure 8.5 Uncropped scans of the Western Blots presented in Figure 4.6 (C).**

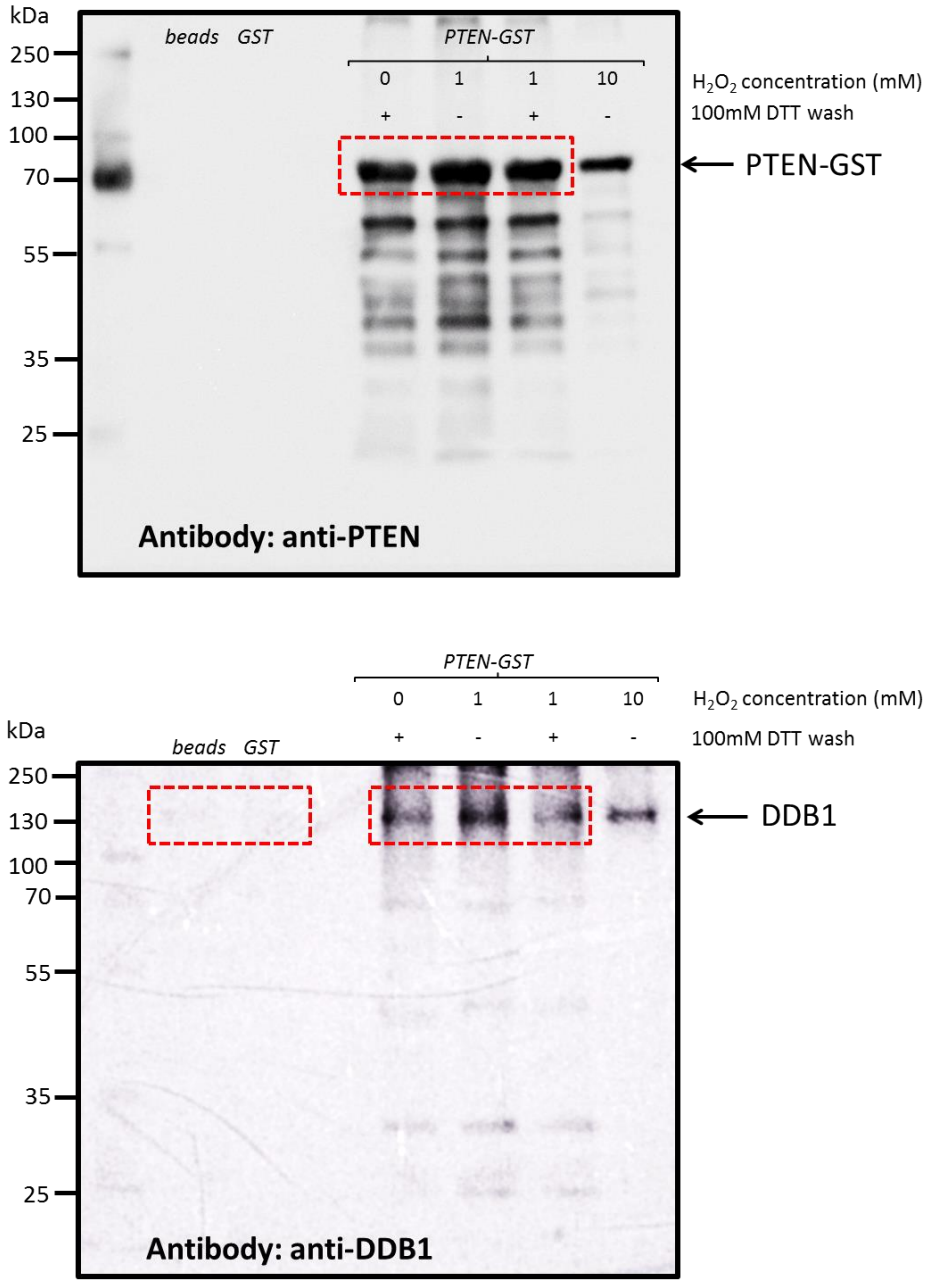


**Figure 8.6 Uncropped scans of the Western Blots presented in Figure 4.6 (D).**

### 8.6.2 Uncropped scans of Western blots presented in Figure 5.2 and Figure 5.4

Along the top of each Western blot scan shown are indicated the sample type and any oxidizing and/or reducing treatments performed on the HCT116 cells.

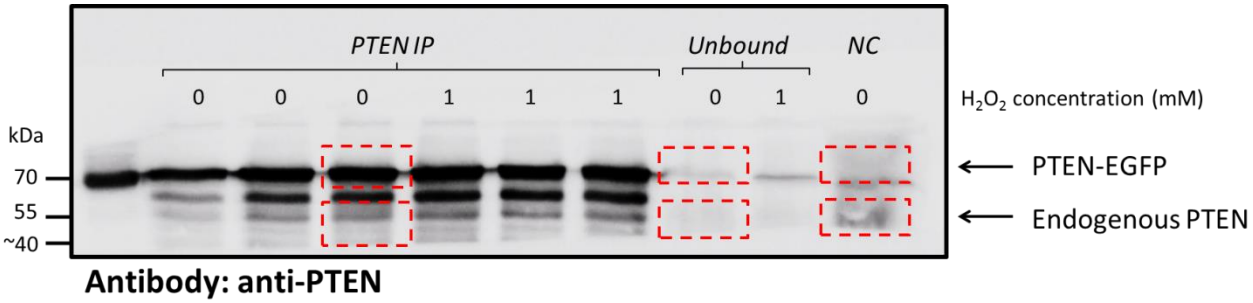


**Figure 8.7 Uncropped scan of the Western blot presented in Figure 5.2.**

IP = immunoprecipitation**.** NC = negative control.

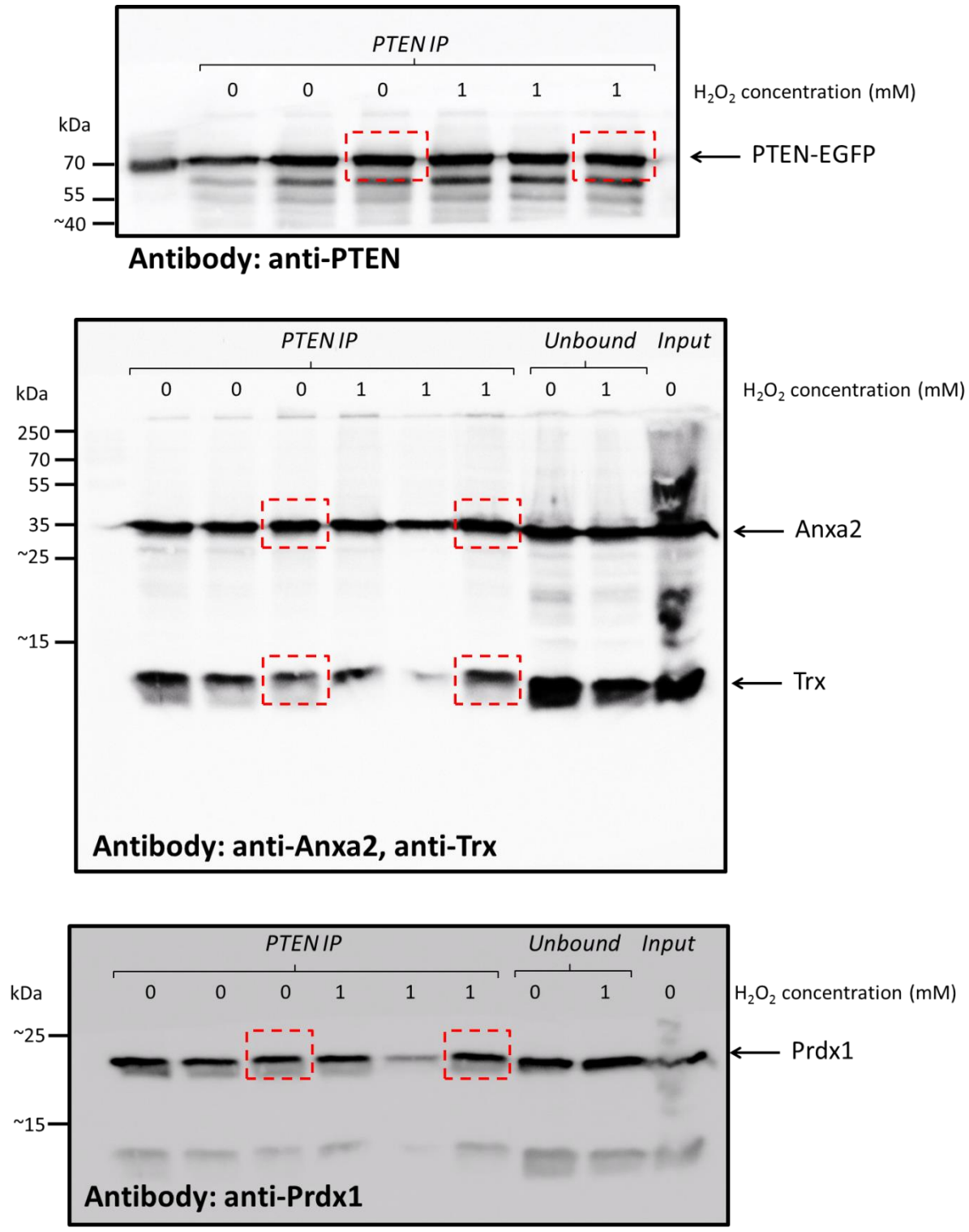


**Figure 8.8 Uncropped scans of Western blots presented in Figure 5.4 (A).**

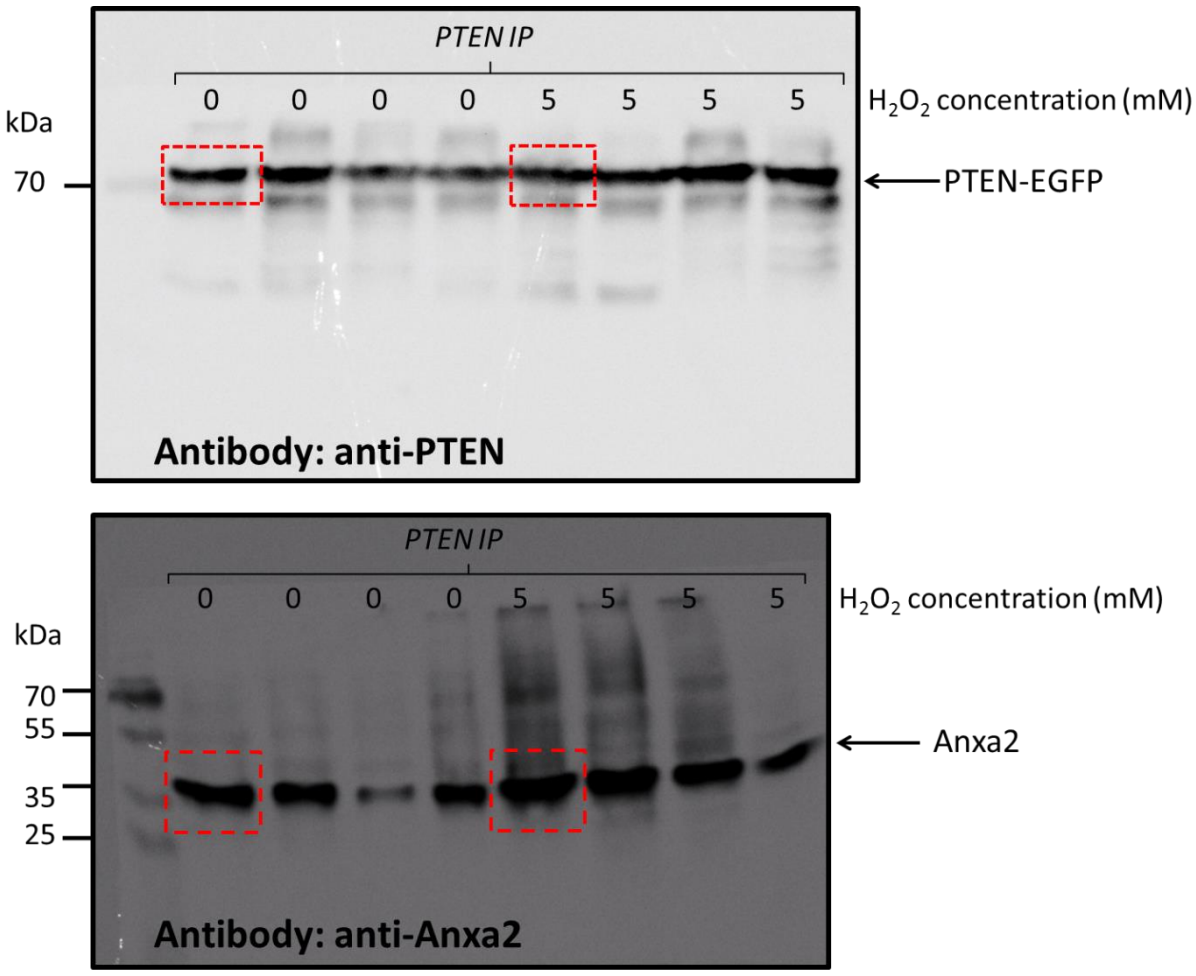


**Figure 8.9 Uncropped scans of Western blots presented in Figure 5.4 (B).**

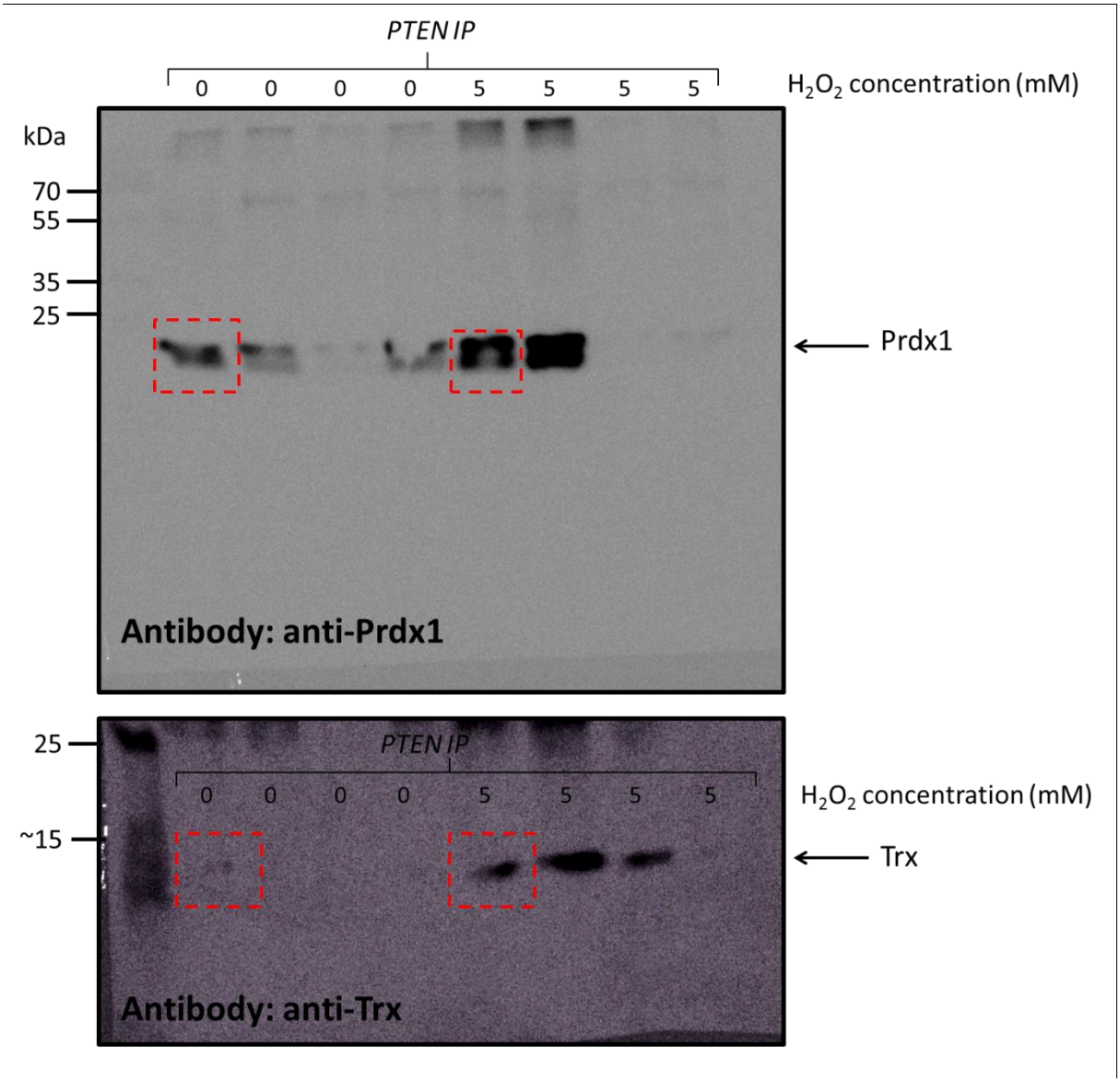


**Figure 8.10 Uncropped scans of Western blots presented in Figure 5.4 (B, continued).**